PULKOVO OBSERVATORY

OBSERVATOIRE DE PARIS

SYSTÈMES DE RÉFÉRENCE TEMPS-ESPACE

UMR8630 / CNRS

Recent developments and prospects in ground-based and space astrometry

Développements récents et perspectives en astrométrie au sol et en astrométrie spatiale

JOURNÉES 2014 ☆

SYSTÈMES DE RÉFÉRENCE SPATIO - TEMPORELS

☆ ST. PETERSBURG, 22-24 SEPTEMBER

PULKOVO OBSERVATORY

Pulkovskoe sh. 65, 196140 St. Petersburg, RUSSIA

OBSERVATOIRE DE PARIS

SYSTÈMES DE RÉFÉRENCE TEMPS-ESPACE

UMR 8630 / CNRS

61 avenue de l'Observatoire, F-75014 Paris, FRANCE

Recent developments and prospects in ground-based and space astrometry

Développements récents et perspectives en astrométrie au sol et en astrométrie spatiale

Edited by

Actes publiés par

Z. MALKIN and N. CAPITAINE

JOURNÉES 2014 ☆

SYSTÈMES DE RÉFÉRENCE SPATIO - TEMPORELS

☆ ST. PETERSBURG, 22-24 SEPTEMBER

Participants of the Journées 2014 at the portico of the main Pulkovo Observatory building

The Journés 2014 were organized in cooperation with Paris Observatory and co-sponsored by the International Astronomical Union, the International Association of Geodesy, the Government of St. Petersburg, Dynasty Foundation, and Russian Foundation for Basic Research (project 14-02-20253-g).

ISBN 978-5-9651-0873-2 **ISBN 978-2-901057-70-3**

TABLE OF CONTENTS

PREFACE

The Journées 2014 "Systèmes de référence spatio-temporels", with the sub-title "Recent developments and prospects in ground-based and space astrometry", were organized at Pulkovo Observatory, from 22 to 24 September 2014, and were included in the program of celebrating of the 175th anniversary of the Pulkovo observatory. They were organized in cooperation with the Paris Observatory ("Systèmes de Référence Temps Espace" (SYRTE) Department) and were co-sponsored by the International Astronomical Union (IAU), the International Association of Geodesy (IAG), the Government of St. Petersburg, Dynasty Foundation, and Russian Foundation for Basic Research.

The Journées 2014 were the 23rd meeting in this series of international meetings, whose main purpose is to provide an international forum for advanced discussion in the fields of space and time reference systems, Earth rotation, astrometry and time. The Journées were organized in Paris each year from 1988 to 1992, and then, since 1994, alternately in Paris (in 1994, 1996, 1998, 2000, 2004, 2007, 2010 and 2013) and other European cities, namely Warsaw in 1995 and 2005, Prague in 1997, Dresden in 1999 and 2008, Brussels in 2001, Bucharest in 2002, St. Petersburg in 2003 and Vienna in 2011. Such an organization has been the result of an active and continuing cooperation between the SYRTE Department of Paris Observatory and other institutions in Europe.

The scientific programme of the Journées 2014 was focused on the issues related to the recent developments and new challenges in astronomical space and time reference systems and their relativistic aspects, realization of the next ICRF, astrometric catalogs, Earth rotation and geodynamics, astronomical almanacs and software, and planetary ephemerides. A special session was devoted to the history of the Pulkovo observatory.

There were 87 participants, coming from 16 different countries. The scientific programme included 7 invited talks, 44 oral presentations and 34 posters; it was composed of the following sessions:

Session 1: Celestial reference system and frame
Session 2: Relativity and time scales
Session 3: Solar and extrasolar systems dynamics
Sub-Session on the "IAU/IAG Joint Working Group on Theory of Earth Rotation"
Session 4: Earth's rotation and geodynamics
Session 5: Astronomical almanacs and software

The sessions included several discussions on issues related to e.g. the Working Group on "Theory of Earth Rotation" and the future of almanac services. A general discussion was devoted to the reorganization of the IAU structure. Business meetings of the IAU Commission 19 and of the SOFA IAU Working Group were also organized in association with these Journées.

In addition to these scientific activities, the participants met for a cocktail and a conference dinner in the Pulkovo Observatory on Monday and Tuesday evening 22 and 23 September, respectively. A special excursion on the Pulkovo Observatory took place on 24 September after the closing of the meeting. PDF version of the presentations made at the Journées 2014, as well as other information related to the meeting are available at `http://www.gao.spb.ru/english/as/j2014/home.htm`.

These Proceedings are divided into six sections corresponding to the sessions of the meeting. The Table of Contents is given on pages iii to v, the list of participants on pages vii and viii, the detailed scientific programme on pages ix to xiv.

The electronic version of the volume is available at `http://syrte.obspm.fr/jsr/journees2014/pdf/`. According to the SOC decision it is the last Journées Proceedings published in paper form.

We thank here all the participants in the Journées 2014. We are very grateful to the Scientific Organizing Committee for its active role in the elaboration of the scientific programme and to all the authors of the papers for their valuable contributions. We are also grateful to Olivier Becker for his help for the preparation of the web site for the meeting and the on-line proceedings. On behalf of the SOC, we express our thanks to the Director of the Pulkovo Observatory and Local Organizing Committee for the very efficient preparation of the meeting and the very good local conditions and organization.

Nicole CAPITAINE and Zinovy MALKIN
Co-Chairs of the SOC
30 March 2015

List of Participants

ANDREI Alexandre Humberto, Observatorio Nacional, MCTI, Brasil
AVRAMENKO Arkady, Physical Institute RAS, Russia
BELL Steven, HM Nautical Almanac Office, United Kingdom
BIZOUARD Christian, SYRTE - Observatoire de Paris, CNRS/UPMC, France
BORUKHA Maria, St. Petersburg State University, Russia
BOURGOIN Adrien, SYRTE - Observatoire de Paris, CNRS/UPMC, France
BRATTSEVA Olga, Institute of Applied Astronomy RAS, Russia
BRZEZIŃSKI Aleksander, Space Research Center PA S, Poland
CAPITAINE Nicole, SYRTE - Observatoire de Paris, CNRS/UPMC, France
CHUVASHOV Ivan, Tomsk State University, Russia
DAMLJANOVIĆ Goran, Belgrade Astronomical Observatory, Serbia
DEHANT Véronique, Royal Observatory of Belgium, Belgium
DEVYATKIN Alexander, Pulkovo Observatory RAS, Russia
DING Ping-Jie, Nanjing University, China
ESCAPA Alberto, University of Leon, Spain
FERRÁNDIZ Jose, University of Alicante, Spain
FILIPPOVA Alexandra, Moscow Aviation Institute, Russia
GALUSHINA Tatyana, Tomsk State University, Russia
GAYAZOV Iskandar, Institute of Applied Astronomy RAS, Russia
GIRDIUK Anastasiia, Institute of Applied Astronomy RAS, Russia
GORSHANOV Denis, Pulkovo Observatory RAS, Russia
GORSHKOV Victor, Pulkovo Observatory RAS, Russia
GROSS Richard, Jet Propulsion Laboratory, Caltech, USA
GUSEVA Irina, Pulkovo Observatory RAS, Russia
HEES Aurelien, Rhodes University, South Africa
HEINKELMANN Robert, GFZ Potsdam, Germany
HESTROFFER Daniel, IMCCE - Observatoire de Paris, France
HOHENKERK Catherine, HM Nautical Almanac Office, United Kingdom
HUANG Chengli, Shanghai Astronomical Observatory, China
IDDINK Andreas, IGG, University of Bonn, Germany
KAUTS Vladimir, Physical Institute RAS, Russia
KLIONER Sergei, Dresden University of Technology, Germany
KOVALENKO Irina, IMCCE - Observatoire de Paris, France
KUDRYASHOVA Maria, Royal Observatory of Belgium, Belgium
KURDUBOV Sergey, Institute of Applied Astronomy RAS, Russia
KUZNETSOV Eduard, Ural Federal University, Russia
LASSAILLY Corinne, French Embassy in Russia, France
LE PONCIN-LAFITTE Christophe, SYRTE - Observatoire de Paris, CNRS/UPMC, France
LIPOVKA Neonila, Special Astrophysical Observatory RAS, Russia
LITVINOV Dmitry, Moscow State University, Russia
LIU Jia-Cheng, Nanjing University, China
LUKASHOVA Marina, Institute of Applied Astronomy RAS, Russia
MALKIN Zinovy, Pulkovo Observatory RAS, Russia
MEDVEDEV Yurii, Institute of Applied Astronomy RAS, Russia
MILLER Natalia, Pulkovo Observatory RAS, Russia
MOHNATKIN Artem, St. Petersburg State University, Russia
MOSENKOV Aleksandr, Pulkovo Observatory RAS, Russia
NASTULA Jolanta, Space Research Center PAS, Poland
NELMES Susan, HM Nautical Almanac Office, United Kingdom
PASHKEVICH Vladimir, Pulkovo Observatory RAS, Russia
PASYNOK Sergey, VNIIFTRI, Russia
PAVLOV Dmitry, Institute of Applied Astronomy RAS, Russia
PEREPELKIN Vadim, Moscow Aviation Institute, Russia

PERMINOV Alexander, Ural Federal University, Russia
PETROV Sergey, St. Petersburg State University, Russia
PITJEVA Elena, Institute of Applied Astronomy RAS, Russia
POPADYOV Victor, CNIIGAiK, Russia
POPOVA Elena, Pulkovo Observatory RAS, Russia
RAPOSO-PULIDO Virginia, IGN / GFZ Potsdam, Germany
RON Cyril, Astronomical Institute ASCR, Czech Republic
SCHINDELEGGER Michael, Vienna University of Technology, Austria
SHAH Ekta, Indian Institute of Technology Bombay, India
SHEN Wenbin, Wuhan University, China
SHEVCHENKO Ivan, Pulkovo Observatory RAS, Russia
SIDORENKOV Nikolay, Hydrometcenter of Russia, Russia
SKRIPNICHENKO Pavel, Ural Federal University, Russia
SKRIPNICHENKO Vladimir, Institute of Applied Astronomy RAS, Russia
SKURIKHINA Elena, Institute of Applied Astronomy RAS, Russia
SMIRNOV Sergey, St. Petersburg State University, Russia
SOFFEL Michael, Dresden University of Technology, Germany
SOKOV Eugene, Pulkovo Observatory, Russia
SPIRIDONOV Eugene, Institute of Physics of the Earth RAS, Russia
SUVORKIN Vladimir, Institute of Applied Astronomy RAS, Russia
TANG Kai, Shanghai Astronomical Observatory, China
TERCJAK Monika, Warsaw University of Technology, Poland
TITOV Oleg, Geoscience Australia, Australia
TROFIMOV Dmitrii, St. Petersburg State University, Russia
TSURKIS Ilya, Institute of Physics of the Earth RAS, Russia
TSVETKOV Alexander, St. Petersburg State University, Russia
TSYBA Efim, VNIIFTRI, Russia
VASILYEV Mikhail, Institute of Applied Astronomy RAS, Russia
VAVILOV Dmitrii, Institute of Applied Astronomy RAS, Russia
VITYAZEV Veniamin, St. Petersburg State University, Russia
YAGUDINA Eleonora, Institute of Applied Astronomy RAS, Russia
ZAKHAROVA Polina, Ural Federal University, Russia
ZHAROV Vladimir, Moscow State University, Russia
ZOTOV Leonid, Moscow State University, Russia

SCIENTIFIC PROGRAMME

Scientific Organising Commitee: A. Brzeziński, Poland; N. Capitaine, France (Co-Chair); V. Dehant, Belgium; A. Escapa, Spain; C. Hohenkerk, UK; C. Huang, China; I. Kumkova, Russia; Z. Malkin, Russia (Co-Chair); D.D. McCarthy, USA; M. Soffel, Germany; J. Souchay, France; J. Vondrák, Czech Republic; Ya. Yatskiv, Ukraine.

Local Organising Commitee: A. Devyatkin (Chair), T. Borisevich, A. Vershkov, Z. Malkin, K. Maslennikov, N. Miller, V. Pashkevich, V. Pleshakov, I. Shevchenko.

Monday 22 September 2014

9:00–9:20: Opening of the Journées 2014
Welcome from A. Stepanov, Director of the Pulkovo Observatory
Welcome from C. Lassailly, Coordinator on the scientific cooperation, French embassy in Russia
Introduction to the Journées 2014 by N. Capitaine, Co-Chair of the SOC

09:20–09:50: Special session on the History of the Pulkovo Observatory

Stepanov A. *175 years of the Pulkovo Observatory.*

09:50–10:10: Session 1. Celestial reference system and frame
(Chair: N. Capitaine)

Malkin Z., Jacobs C., and IAU ICRF3 Working Group. (invited) *The ICRF-3: Status, plans, and progress on the next generation International Celestial Reference Frame.*

10:10–10:40: Coffee break

10:40–13:00: Session 1. (continuation)
(Chair: A. Andrei)

Raposo-Pulido V., Lambert S., Capitaine N., Nilsson T., Heinkelmann R., Schuh H. *On the systematics in apparent proper motions of radio sources observed by VLBI.*
Andrei A., Coelho B., Anton S. *Morphology of QSO host galaxies — a look at the SED.*
Damljanović G., Taris F., Boeva S. *Some preliminary photometric results of QSOs useful for the link between future Gaia CRF and ICRF.*
Iddink A., Jacobs C., Artz T., Nothnagel A. *First results of X/S and X/Ka-band catalog combinations with full covariance information.*
Tsvetkov A., Vityazev V. *Comparison of astrometric catalogues UCAC4, XPM, PPMXL.*
Popadyov V., Tolchelnikova S. *Some common problems in geodesy and astrometry after establishing ICRF.*
Ding P.-J., Liu J.-C., Zhu Z. *Galactic coordinate system based on multi-wavelength catalogues.*
Discussion *(Chair: Z. Malkin)*

13:00–13:45: Lunch-break

13:45–14:00: Group photo at the portico in the center of the Observatory building

14:00–15:30: Session 2. Relativity and time scales
(Chair: M. Soffel, O. Titov)

Hees A., Bertone S., Le Poncin-Lafitte C., Teyssandier P. (invited) *The Time Transfer Function as a tool to compute range, Doppler and astrometric observables.*
Klioner S. (invited) *Relativistic aspects of Gaia mission.*
Capitaine N., Soffel M. *On the definition and use of the ecliptic in modern astronomy.*
Tang K., Soffel M., Tao J.-H., Tang Z.-H. *Relativistic precession model of the Earth for long time interval.*

Soffel M. *Work related with IAU C52: RIFA.*
Litvinov D., Bartel N., Biriukov A., Kauts V., Kulagin V., Rudenko V. *Gravitational redshift experiment with the space radio telescope RadioAstron.*

15:30–16:00: Coffee break

16:00–16:40: Session 2. (continuation)
(Chair: M. Soffel)

Titov O., Girdiuk A. *Deflection of light induced by the Sun gravity field and measured with geodetic VLBI.*
Le Poncin-Lafitte C., Delva P., Meynadier F., Guerlin C., Wolf P., Laurent P. *Time and frequency transfer with a microwave link in the ACES PHARAO mission.*
Discussion *(Chair: S. Klioner)*

16:40–18:00: POSTER SESSION

18:00–19:30: WELCOME DRINK

Tuesday 23 September 2014

09:00–10:30: Session 3. Solar and extrasolar systems dynamics
(Chair: V. Dehant)

Shevchenko I. (invited) *Resonances in the Solar and exoplanetary systems.*
Devyatkin A., Gorshanov D., L'vov V., Tsekmeister S., Petrova S., Martyusheva A., Slesarenko V., Naumov K., Sokova I., Sokov E., Zinoviev S., Karashevich S., Ivanov A., Lyashenko A., Rusov S., Kouprianov V., Bashakova E., Melnikov A. *Investigation of asteroids in Pulkovo Observatory.*
Sokova I., Sokov E., Roschina E., Rastegaev D., Gorshanov D., Balega Yu., Dyachenko V. *The binary asteroid 22 Kalliope: Linus orbit determination on the basis of speckle interferometric observations.*
Pitjeva E. *Evolution of EPM ephemerides of IAA RAS.*
Girdiuk A. *Improvement of the Pluto orbit using additional new data.*
Kudryashova M., Rosenblatt P., Marty J.-Ch. *Phobos mass estimations from MEX and Viking1 data: influence of different noise sources and estimation strategies.*

10:30–11:00: Coffee break

11:00–12:00: Session 3. (continuation)
(Chair: A. Escapa, D. Hestroffer)

Perminov A., Kuznetsov E. *Expansion of the Hamiltonian of a planetary system into the Poisson series in all elements.*
Guseva I. *Some peculiarities of orbits of observed comets.*
Kuznetsov E., Zakharova P. *Long time dynamical evolution of highly elliptical satellites orbits.*
Vasilyev M., Yagudina E., Torre J.-M., Feraudy D. *Planned LLR station in Russia and its impact on the lunar ephemeris accuracy.*

12:00–13:00: Sub-Session on the IAU/IAG Joint Working Group "Theory of Earth Rotation"
(Chair: J. Ferrándiz, R. Gross)

Ferrándiz J., Gross R. *Report on the activities of the IAU/IAG Joint Working Group on Theory of Earth Rotation.*
Getino J., Escapa A. *Report on activities of the Sub-Working Group 1 "Precession/Nutation" of the IAU/IAG Joint Working Group on Theory of Earth Rotation.*
Brzeziński A. *Report on activities of the IAU/IAG Joint Working Group on Theory of Earth Rotation, Sub-WG 2 "Polar motion and UT1".*

Heinkelmann R. *IAU/IAG Joint Working Group on the Theory of Earth Rotation. Sub Working Group 3: Numerical solutions and validation.*
Discussion *(Chair: J. Ferrándiz, R. Gross)*

13:00–14:00: Lunch-break

14:00–15:30: Session 4. Earth's rotation and geodynamics
(Chair: C. Ron, R. Heinkelmann)

Schindelegger M., Böhm J., Salstein D. (invited) *The global S1 tide and Earth's nutation.*
Dehant V. *Refinements on precession, nutation, and wobble of the Earth.*
Liu J.-C., Capitaine N. *Possible improvements of the IAU 2006 precession. The preliminary results.*
Zharov V. *Towards new nutation theory.*
Bizouard C., Zotov L., Sidorenkov N. *Lunar influence on equatorial atmospheric angular momentum and consequences for nutation.*
Tercjak M., Böhm J., Brzeziński A., Gebauer A., Klügel T., Schreiber U., Schindelegger M. *Estimation of nutation rates from combination of ring laser and VLBI data.*
Brzeziński A., Wielgosz A., Böhm S. *On application of the complex demodulation procedure for monitoring Earth rotation: comparison with the standard approach using the long periodic EOP components estimated from VLBI data analysis by the VieVS CD software.*

15:30–16:00: Coffee break

16:00–17:40: Session 4. (continuation)
(Chair: A. Brzeziński, V. Zharov)

Baenas T., Ferrándiz J., Escapa A., Getino J. *Effects of the tidal mass redistribution on the Earth rotation.*
Pashkevich V. *New high-precision Earth and Moon rotation series at long time intervals.*
Markov Yu., Filippova A. *Numerical-analytical modeling of the Earth's pole oscillations.*
Nastula J., Wińska M., Biryło M. *Comparison of polar motion excitation functions computed from different sets of gravimetric coefficients.*
Ron C., Vondrák J. *Geomagnetic excitation of nutation.*
Sidorenkov N. *The Chandler wobble of the poles and its amplitude modulation.*
Zotov L., Bizouard C. *Prediction of the Chandler wobble.*
Pasynok S., Bezmenov I., Kaufman M. *Operative EOP activities in VNIIFTRI.*

18:00–20:00: CONFERENCE DINNER

Wednesday 24 September 2014

09:00–10:20: Session 4. (continuation)
(Chair: C. Huang, Ch. Bizouard)

Huang C., Zhang M. (invited) *Do we need various assumptions to get a good FCN? — A new multiple layer spectral method.*
Gorshkov V., Shcherbakova N., Mohnatkin A., Smirnov S., Petrov S., Trofimov D., Guseva T., Perederin V., Rosenberg N. *Deformation of the South-Eastern Baltic Shield from GNSS observations.*
Discussion *(Chair: C. Huang)*

10:20–10:50: Coffee break

10:50–12:00: Session 5. Astronomical almanacs and software
(Chair: C. Hohenkerk, E. Pitjeva)

Bell S., Nelmes S., Prema P., Whittaker J. (invited) *The future of almanac services. An HMNAO perspective ...*

Pavlov D., Skripnichenko V. *Rework of the ERA software system: ERA-8.*
Galushina T., Bykova L., Letner O., Baturin A. *The software "IDA" for investigation of asteroid dynamics and its use for study of some asteroid motion.*
Discussion *(Chair: S. Bell)*

12:00–13:00: General discussion and closing the Journées 2014
(Chair: N. Capitaine, Z. Malkin)

13:00–13:45: Lunch-break

13:45–14:25: SOFA Business meeting
IAU Commission 19 Business Meeting

14:30–16:00: Excursion on the Pulkovo Observatory

LIST OF POSTERS

Session 1: Celestial reference system and frame

Kurdubov S., Skurikhina E. *Core sources set selection.*
Lipovka A., Lipovka N. *On the transition to the radio system coordinates ICRF.*
Medvedev Y., Kuznetsov V. *Using positional observations of numbered minor planets for determination of star catalog errors.*
Taris F., Damljanović G., Andrei A., Klotz A., Vachier F. *Optical monitoring of QSOs in the framework of the Gaia space mission.*
Vityazev V., Tsvetkov A. *Kinematics derived from Northern and Southern hemispheres of huge ICRS astrometric catalogues.*

Session 2: Relativity and time scales

Avramenko A. *Parametric invariance of the relativistic pulsar time scales.*
Heinkelmann R., Soja B., Schuh H. *Gravitational effects from a series of IVS R&D VLBI-sessions with observations close to the Sun.*

Session 3: Solar and extrasolar systems dynamics

Hestroffer D., David P., Hees A., Le Poncin Lafitte C. *Local test of general relativity with Solar system objects.*
Hestroffer D., Arlot J.-E., Lainey V., Robert V. *Taking the opportunity of the Gaia reference star catalogue for observing the Solar system in the past.*
Kovalenko I., Hestroffer D., Doressoundiram A. *Statistical inversion method for binary asteroids' orbit determination.*
Popova E. *Diagrams of stability of circumbinary planetary systems.*
Sigismondi C., Regoli V., Andrei A. *Measures of the Earth obliquity during 1701 winter solstice at the Clementine meridian line in Rome.*
Vavilov D., Medvedev Y. *Method of determining the orbits of the small bodies in the Solar system based on an exhaustive search of orbital planes.*

Session 4: Earth's rotation and geodynamics

Bezmenov I., Pasynok S. *GLONASS orbit/clock combination in VNIIFTRI.*
Escapa A., Baenas T., Ferrándiz J., Getino J. *On the minimization properties of the Tisserand systems.*
Gorshkov V. *Pole tide triggering of seismicity.*
Gross R., Nastula J. *Estimating the period and Q of the Chandler Wobble from observations and models of its excitation.*
Heinkelmann R., Belda-Palazon S., Ferrándiz-Leal J., Schuh H. *The consistency of the current conventional celestial and terrestrial reference frames and the conventional EOP series.*
Hu H., Wang R., Malkin Z. *Application of Titius-Bode law in earthquake study.*
Miller N. *Periodical regularities of polar motion in the Pulkovo latitude variations.*
Perepelkin V., Bondarenko V. *Irregular effects in the oscillatory process of the Earth's pole and temporal variations of the geopotential.*
Skurikhina E., Ipatov A., Smolentsev S., Diakov A., Olifirov V. *High-frequency Earth rotation variations from VLBI observations CONT14.*
Spiridonov E., Tsurkis I., Kuchay M., Sinyukhina S. *The probabilistic approach to the description of the Chandler wobble.*
Sun R., Shen W. *Triaxial Earth's rotation: Chandler wobble, free core nutation and diurnal polar motion.*
Tsyba E., Kaufman M. *Improvement of the software Bernese for calculation of the Earth rotation parameters according to the data of satellite laser ranging (Lageos 1, Lageos 2) in the Main Metrological Centre of the State Time and Frequency Service.*

Session 5: Astronomical almanacs and software

Session 1

CELESTIAL REFERENCE SYSTEM AND FRAME

SYSTÈME ET REPÈRE DE RÉFÉRENCE CÉLESTES

THE ICRF-3: STATUS, PLANS, AND PROGRESS ON THE NEXT GENERATION INTERNATIONAL CELESTIAL REFERENCE FRAME

Z. MALKIN[1], C.S. JACOBS[2], F. ARIAS[3], D. BOBOLTZ[4], J. BÖHM[5], S. BOLOTIN[6], G. BOURDA[7,8], P. CHARLOT[7,8], A. DE WITT[9], A. FEY[10], R. GAUME[10], D. GORDON[6], R. HEINKELMANN[11], S. LAMBERT[12], C. MA[13], A. NOTHNAGEL[14], M. SEITZ[15], E. SKURIKHINA[16], J. SOUCHAY[12], O. TITOV[17]

[1] Pulkovo Observatory, Pulkovskoe Sh. 65, St. Petersburg 196140, Russia
e-mail: malkin@gao.spb.ru

[2] Jet Propulsion Laboratory, California Institute of Technology/NASA, Pasadena CA, USA
e-mail: Christopher.S.Jacobs@jpl.nasa.gov

[3] Bureau International des Poids et Mesures (BIPM), Paris, France

[4] Astronomical Sciences, National Science Foundation, Arlington, VA

[5] Technische Universität Wien, Austria

[6] NVI, Inc./NASA Goddard Space Flight Center, Greenbelt, MD, USA

[7] Université de Bordeaux, LAB, UMR 5804, Floirac, France

[8] CNRS, LAB, UMR 5804, Floirac, France

[9] Hartebeesthoek Radio Astronomy Observatory, South Africa

[10] U.S. Naval Observatory, Washington D.C., USA

[11] Deutsches GeoForschungsZentrum Potsdam, Germany

[12] Observatoire de Paris, SYRTE, CNRS, UPMC, Paris, France

[13] NASA Goddard Space Flight Center, Greenbelt, MD, USA

[14] Institute of Geodesy and Geoinformation, University Bonn, Germany

[15] Deutsches Geodätisches Forschungsinstitut (DGFI), Munich, Germany

[16] Institute of Applied Astronomy, St. Petersburg, Russia

[17] Geoscience Australia, Canberra, Australia

ABSTRACT. The goal of this presentation is to report the latest progress in creation of the next generation of VLBI-based International Celestial Reference Frame, ICRF3. Two main directions of ICRF3 development are improvement of the S/X-band frame and extension of the ICRF to higher frequencies. Another important task of this work is the preparation for comparison of ICRF3 with the new generation optical frame GCRF expected by the end of the decade as a result of the Gaia mission.

1. INTRODUCTION

In 1997, the International Celestial Reference Frame (ICRF) based on the positions of 608 extragalactic radio sources derived from the VLBI observations at S/X bands has been adopted by the IAU as the fundamental celestial reference frame, replacing the FK5 optical frame (Ma et al., 1998). The first ICRF, hereafter referred to as ICRF1, was replaced in 2009 by ICRF2 also based on S/X observations (Ma et al., 2009), the current IAU standard celestial reference frame. The ICRF2 is very much improved with respect to ICRF1 in the sense of both number of sources included and position accuracy. However, it still has serious problems discussed in Section 2. To mitigate these problems, a new generation frame, the ICRF3, is currently under development making use of both new VLBI observations and new developments in data analysis. This work is coordinated by the IAU Division A Working Group Third Realization of International Celestial Reference Frame (Chair Christopher Jacobs). We present here the current status of the ICRF3 as of September 2014 and prospects for the near future.

There are three primary tasks of the ICRF3 activity. The first goal is a substantial improvement of ICRF2 in S/X band. The progress in this direction is described in Section 3. The second task is to extend the ICRF to higher frequencies, such as Ka, K, and Q bands, which is crucial for many important practical applications. The third goal is to prepare the link of the new generation Gaia-based optical frame GCRF to ICRF3 by the end of the decade. This problem is discussed in Section 5.

2. CURRENT ICRF STATUS

The ICRF2 catalog was computed using nearly 30 years of VLBI observations and provides accurate positions of 295 "defining" sources and generally less accurate positions of 3119 other radio sources (Fig. 1). The advantages of the ICRF2 with respect to the ICRF1 are manyfold:

- increasing total number of sources from 608 (717 with two extensions) to 3414;
- increasing number of the defining sources from 212 to 295 and improving their sky distribution;
- more uniform distribution of the defining sources;
- improving the source position uncertainty; decreasing the noise floor from 250 μas to 40 μas;
- elimination of large ICRF1 systematic error at the level of ≈0.2 mas (Fig. 2);
- improving axes stability from ≈20 μas to ≈10 μas.

However, ICRF2 still has several serious deficiencies, the main of which are:

- Very non-uniform distribution of the position accuracy. About 2/3 of the sources are from the VCS survey (Beasley et al., 2002) and have about 5 times worse median precision as compared with non-VCS ICRF2 sources. Besides, 39 special handling unstable sources processed in *arc* mode have position uncertainties much large than other sources having similar number of observations (Fig. 3).
- Both, distribution of the ICRF2 sources and their position errors over the sky, are not uniform. Most of the sources are north of −45°, i.e. within VLBA sky coverage limits. Due to the relatively small number of stations in the southern hemisphere (particularly a lack of large antennas), position errors of the southern sources are generally substantially worse (Fig. 1). In spite of putting into operation four new stations in Australia and New Zealand, the percentage of observations of southern sources, especially in the southern polar cap region remains practically the same as for ICRF1 (Fig. 4).
- As follows from theoretical considerations (Liu et al., 2012) and analysis of the latest source position catalogs (Malkin, 2014; Sokolova & Malkin, 2014; Lambert, 2014), ICRF2 may have residual systematics at a level of ≈20 μas and rotations at a level of a few μas per decade (Figs. 5, 6).
- Official ICRF2 catalog is defined for S/X bands only, whereas many scientific and practical applications require the CRF realization of similar quality for other frequencies.

The ICRF3 activity is aims at elimination of these ICRF2 problems taking advantage of gradually increasing total number of observations (on average about 0.6 million observations per year during the last years), more active observations at southern stations, and new developments in VLBI technology and data analysis.

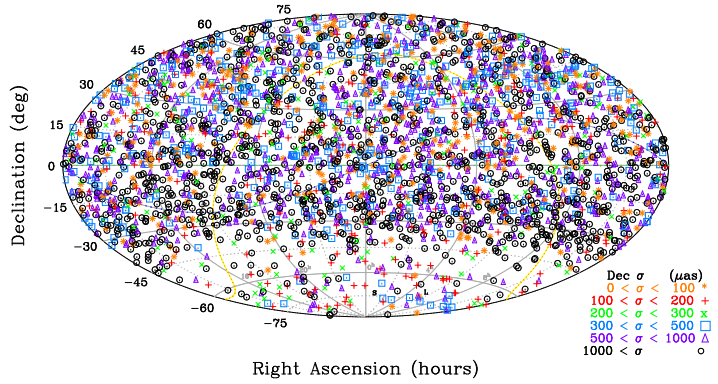

Figure 1: ICRF2: the current IAU standard frame consists of 3414 sources (Ma et al., 2009). Note the lower spatial density of sources south of −30°. About 2/3 of the sources (2197) originating from the VCS survey have 5 times lower precision than the well observed sources.

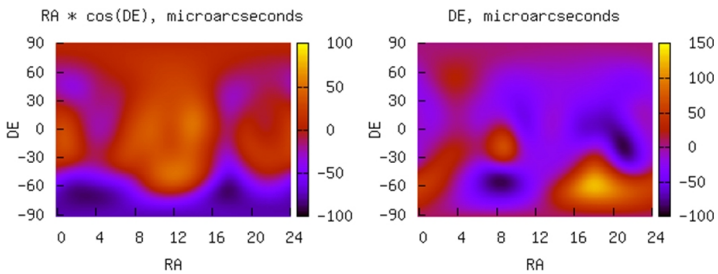

Figure 2: ICRF2 minus ICRF1 smoothed differences, μas.

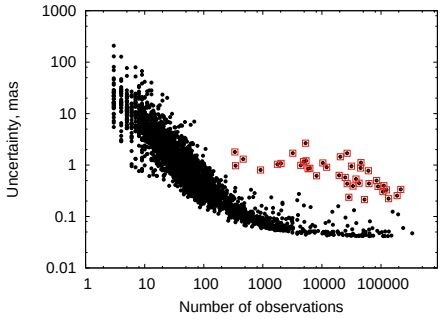

Figure 3: Uncertainties of the ICRF2 source positions vs. number of observations. Note that the arc sources (highlighted) do not follow the general law.

Number of observations, thousand

Epoch	–90... –60	–60... –30	–30...0	0...+30	+30...+60	+60– ...+90
ICRF1	9 (**0.5%**)	13 (**0.7%**)	296 (**16.6%**)	617 (**34.7%**)	632 (**35.5%**)	213 (**11.9%**)
ICRF2	23 (**0.3%**)	136 (**2.0%**)	1163 (**16.8%**)	1949 (**28.2%**)	2668 (**38.6%**)	965 (**14.0%**)
Current	60 (**0.6%**)	279 (**2.9%**)	1653 (**17.1%**)	2673 (**27.6%**)	3569 (**36.9%**)	1446 (**14.9%**)

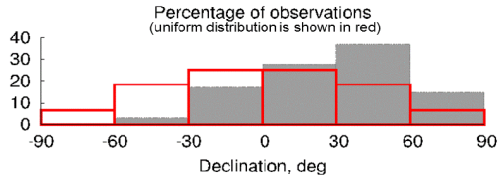

Figure 4: Number of observations by declination bands. Note that the percentage of observations in the south polar cup region is not improved w.r.t. ICRF1.

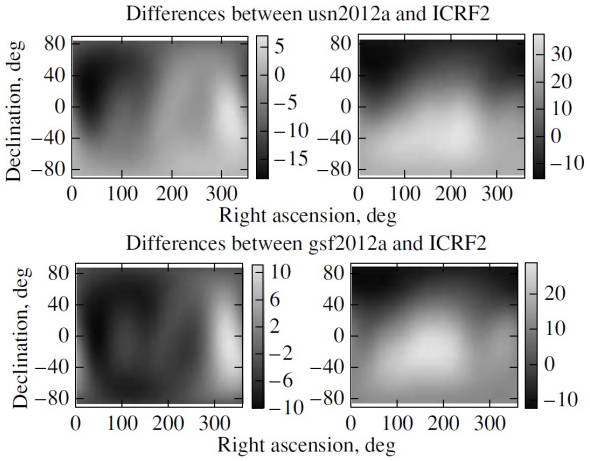

Figure 5: Differences between recent VLBI catalogues and ICRF2, μas (Sokolova, Malkin, 2014).

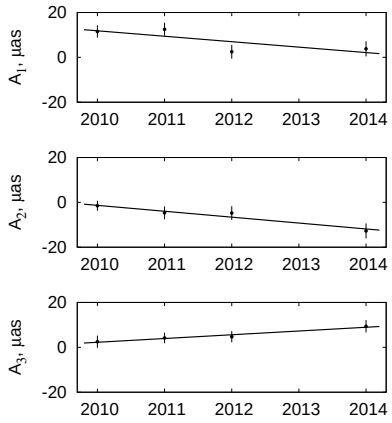

Figure 6: Rotation of GSFC astrometric catalogues w.r.t. ICRF2 (Malkin, 2014).

3. IMPROVING S/X ICRF

The first problem to be solved for improving ICRF2 in S/X band is to achieve a more uniform distribution of the source position uncertainty. Figure 3 shows how it depends on the number of observations (dependence on the number of sessions is weaker). Two main steps in this direction are now underway.

The VCS2 project was proposed and accepted by NRAO in 2014 (P.I. David Gordon). Eight 24 h observing sessions are planned, and five of them have been observed, correlated, and analyzed at the GSFC VLBI group. The first results of the analysis have shown manyfold improvement in the position uncertainty for re-observed VCS sources (Fig. 7).

Improving the ICRF in the southern hemisphere in the sense of both the number of sources and their position accuracy is another primary task of the ICRF3. A giant step in this direction was made with the inclusion of new VLBI antennas in Australia (Hobart, Katherine, Yarragadee), New Zealand (Warkworth), and S. Africa (HartRao) in the IVS observing programs. Because the new stations are equipped with relatively small antennas (12 m in Australia and New Zealand, and 15 m in S. Africa), larger antennas such as Parkes 64 m, DSS45 34 m, Hobart 26 m, and HartRAO 26 m will need to be added in order to detect weaker sources (Titov et al., 2013). Further improvement in the number of observations of southern sources can be achieved through inclusion of CRF sources in the regular IVS EOP observing programs (Malkin et al., 2013).

Important factors limiting the source position precision and accuracy are source structure and the core-shift effect. They are most significant in S/X band. Both increasing of the number of many-baseline observations and developments in VLBI technology and analysis are needed to mitigate these effects.

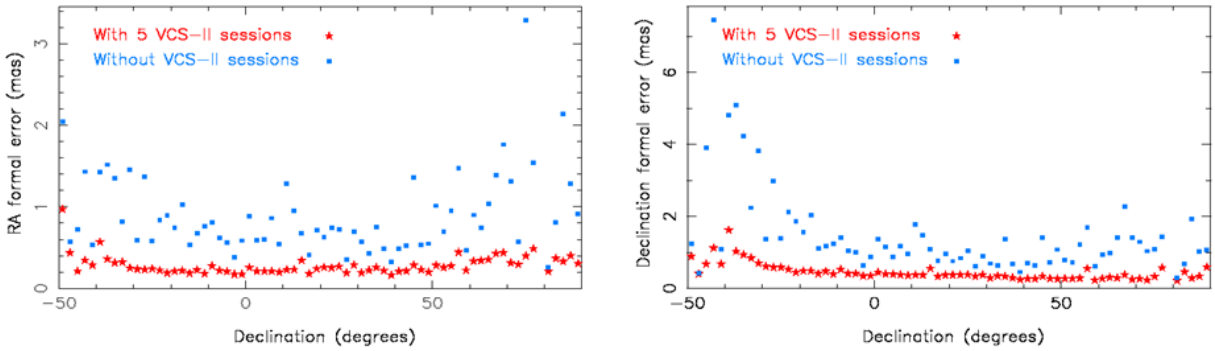

Figure 7: VCS2: Average uncertainties in 2-degree bins for 1309 re-observed VSC sources. Note ≈3 times improvement in precision and much more uniform distribution of the position uncertainties over declination.

4. EXTENDING ICRF TO HIGHER FREQUENCY BANDS

As radio frequencies increase, sources tend to become more core dominated as the extended structure in the jets tends to fade away with increasing frequency. Also the spatial offset of the radio emissions from the AGN's central black hole due to opacity effects (core shift) is reduced with increasing observing frequency.

On the other hand, observations at K and Ka bands are more weather sensitive, which combined with the shorter wavelengths leads to shorter coherence times. Furthermore, sources are often weaker and antenna pointing is more difficult. The combined effect is lower sensitivity, but advances in recording technology are rapidly compensating with higher data rates. Currently, the IVS, the VLBA and JPL's Deep Space Network are moving to 2 Gbps operations.

Currently, active CRF works are underway at K (22–24 GHz), Ka (32 GHz), and to a lesser extent Q (43 GHz) bands.

Lanyi et al. (2010) and Charlot et al. (2010) did pioneering work to develop high precision celestial frames at 24 GHz. Currently, the K-band CRF includes 275 sources (Fig. 8). Most sources have a position precision better than 200 μas. Further development is expected in the framework of activity of a new K-band full sky coverage collaboration (de Witt et al., 2014). Accurate positions of more than 500 K-band sources are expected in the near future.

Since 2005, the two baselines of NASA's Deep Space Network have been making observations at X/Ka-band of about 500 sources down to −45°. Recently they have been joined by ESA's DSA03 35 m antenna in Malargüe, Argentina resulting in full sky coverage at Ka-band (Horiuchi et al., 2013). Now, the regularly observed Ka network consists of four stations: Goldstone (CA, USA), Tidbinbilla (A.C.T., Australia), Malargüe (Mendoza, Argentina), and Robledo de Chavela (Spain). The current X/Ka-band CRF includes 644 sources (Fig. 9), 700+ sources are expected in the near future.

It should be noted that, as with S/X, high frequency CRFs are still weak in the south.

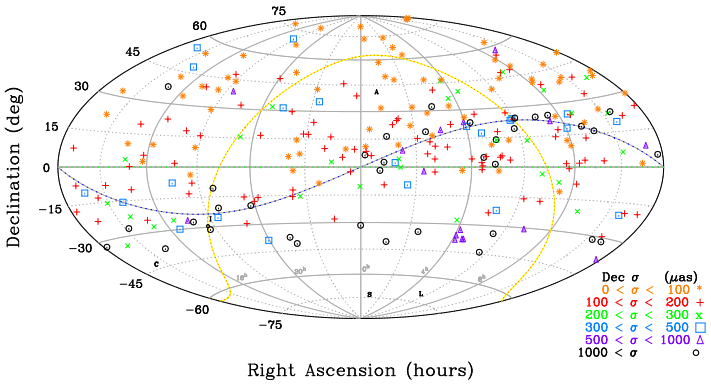

Figure 8: K-band CRF: 268 sources, still weak in the south.

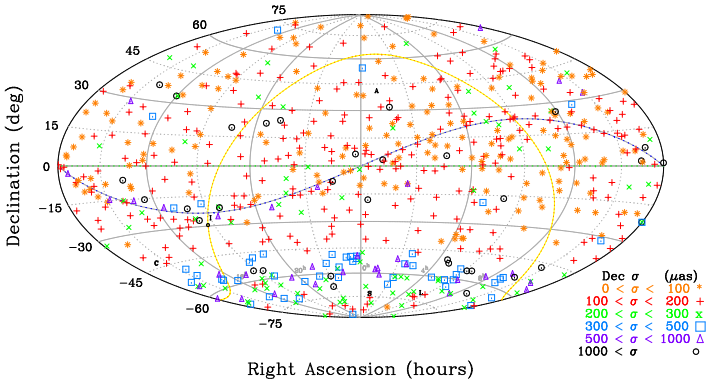

Figure 9: X/Ka-band CRF: 654 sources, still weak in the south.

5. OPTICAL–RADIO FRAMES LINK

Launched in December 2013, ESA's Gaia mission is designed to make state-of-the-art astrometric measurements (positions, proper motions and parallaxes) of a billion objects as well as photometric and radial velocity measurements (Lindegren, 2008; Mignard, 2014). Gaia's observations will include approximately 500,000 AGN of which ≈20,000 will be optically bright ($V < 18$ mag) thus enabling very high expected precisions of 70–150 μas at $V = 18^m$ and 25–50 μas at $V = 16^m$.

Gaia Celestial Reference Frame (GCRF) will be created in two steps. First an internally consistent solution will be computed from the data collected during the Gaia mission by the end of the decade. Then this solution should be oriented in such a way to be consistent with the VLBI-based ICRF.

To provide the ICRF-GCRF link with the highest accuracy, dedicated efforts are underway in the framework of the ICRF3 activity. First it is necessary to identify a sufficient number of optically and radio bright objects, whose positions can be reliably determined from both VLBI and Gaia observations with accuracy better than 100 μas. Bourda et al. (2010) estimated that 300+ AGN are optically bright while also strong and compact in radio thus enabling both Gaia and VLBI to make very precise position measurements. This common set of sources should allow the GCRF and ICRF radio frames to be rotationally aligned to better than 10 μas precision. After making the optical-radio alignment, position offsets between the two techniques can be studied to characterize systematic errors. Having multiple radio frames (S/X, K, X/Ka) should be of great value in characterizing frequency dependent effects e.g. core shift.

The work to extend the list of common Gaia-VLBI sources through the optical photometry of the current and prospective ICRF sources is underway (Taris et al., 2013).

6. CONCLUSIONS

Our goals are to improve the precision, spatial and frequency coverage relative to the ICRF2 by 2018. This date is driven by the desire to create radio frames that are ready for comparison with the Gaia optical frame. Several specific actions are underway. The VCS2 project is aimed at substantial improvement in S/X-band precision of about 2200 VCS sources. Five sessions (of eight planned) are completed, and the first results are very encouraging. S/X-band southern precision improvements are planned from observations with five new southern antennas, such as AuScope and HartRAO. Both these factors: completion of the VCS2 and substantial increase of the number of astrometric VLBI observations (currently about 9.8 million delays compared to 6.5 million delays used to derive ICRF2), especially in the south, makes it possible to publish an intermediate ICRF version in 2015, which can be substantially improved with respect to ICRF2 and may be very useful for different applications.

Large progress is also being achieved in developing the CRF at Ka and K bands. New improvements are expected, in particular, from adding a new ESA station in Malargüe, Argentina thus providing three additional baselines to Australia, California and Spain.

On the analysis front, special attention will be given to combination techniques both of VLBI catalogs and of multiple data types (Iddink et al., 2014, 2015; Seitz et al., 2014; Sokolova & Malkin 2014). Consistency of CRF, TRF, and EOP is another area of concern, see, e.g., Seitz et al. (2014).

The creation of a next generation VLBI-based ICRF and the Gaia-based new-generation optical GCRF

are main projects in fundamental astrometry for this decade. Both frames are intended to provide ICRS realizations with systematic accuracy better than 10 μas. It is anticipated that further comparison and merging of both the radio ICRF and the optical GCRF will allow construction of a new highly accurate multiband and systematically uniform ICRF.

Acknowledgements. The authors thank the International VLBI Service for Geodesy and Astrometry (IVS, Schuh & Behrend, 2012) and its members for decades of dedication to the collection of the data used in this research. This work is done in part under NASA contract. Sponsorship by U.S. Government, as well as other respective institutes and funding agencies is acknowledged.

7. REFERENCES

Beasley, A.J., et al., 2002, "VLBA Calibrator Survey—VCS1", ApJS, 141, pp. 13–21.

de Witt, A., et al., 2014, "Extending the K-band celestial frame emphasizing Southern hemisphere", In: Proc. Journées 2013 "Systèmes de Référence Spatio-Temporels", N. Capitaine (ed.), Observatoire de Paris, pp. 61–64.

Bourda, G., et al., 2010, "VLBI observations of optically-bright extragalactic radio sources for the alignment of the radio frame with the future Gaia frame", A&A, 520, A113.

Charlot, P., et al., 2010, "The Celestial Reference Frame at 24 and 43 GHz. II. Imaging", AJ, 139, pp. 1713–1770 .

Horiuchi, S., et al., 2013, "The X/Ka Celestial Reference Frame: Results from combined NASA-ESA baselines", Asia-Pacific Radio Astronomy Conference 2013, ADS: 2013apra.confE...1H.

Iddink, A., et al., 2014, "Rigorous VLBI intra-technique combination strategy for upcoming CRF realizations", , In: Proc. Journées 2013 "Systèmes de Référence Spatio-Temporels", N. Capitaine (ed.), Observatoire de Paris, pp. 81–83.

Iddink, A., et al., 2015, "First results of S/X and X/Ka-band catalogue combinations with full covariance information", this volume, pp. 20–23.

Lambert, S., 2014, "Comparison of VLBI radio source catalogs", A&A, 570, A108.

Lanyi, G., et al., 2010, "The Celestial Reference Frame at 24 and 43 GHz. I. Astrometry", AJ, 139, pp. 1695–1712.

Lindegren, L., et al., 2008, "The Gaia Mission: Science, Organization and Present Status", IAU Symp. 248, pp. 217–223.

Liu, J.-C., et al. 2012, "Systematic effect of the Galactic aberration on the ICRS realization and the Earth orientation parameters", A&A, 548, A50.

Ma, et al., 1998, "The International Celestial Reference Frame as Realized by Very Long Baseline Interferometry", AJ, 116, pp. 516–546.

Ma, et al., 2009, "The second realization of the International Celestial Reference Frame by Very Long Baseline Interferometry", IERS Technical Note 35, Fey, A.L., Gordon, D., Jacobs, C.S. (eds.).

Malkin, Z., et al., 2013, "Searching for an Optimal Strategy to Intensify Observations of the Southern ICRF sources in the framework of the regular IVS observing programs", In: Proc. 21st Meeting of the EVGA, N. Zubko, M. Poutanen (eds.), Rep. Finn. Geod. Inst., 2013:1, pp. 199–203.

Malkin, Z., 2014, "On the implications of the Galactic aberration in proper motions for the Celestial Reference Frame", MNRAS, 445, pp. 845–849.

Mignard, F., 2014, "Gaia status and early mission", In: Proc. Journées 2013 "Systèmes de Référence Spatio-Temporels", N. Capitaine (ed.), Observatoire de Paris, pp. 57–60.

Schuh, H., Behrend, D., 2012, "VLBI: A fascinating technique for geodesy and astrometry", J. Geodyn., 61, pp. 68–80.

Seitz, M., et al., 2014, "Consistent adjustment of combined terrestrial and celestial reference frames", In: Rizos C., Willis P. (eds.), IAG Symposia, 139, pp. 215–221.

Sokolova, Y., Malkin, Z., 2014, "Pulkovo combined catalogue of radio source positions PUL 2013", Astron. Lett., 40, pp. 268–277.

Taris, F., et al., 2013, "Optical monitoring of extragalactic sources for linking the ICRF and the future Gaia celestial reference frame. I. Variability of ICRF sources", A&A, 552, A98.

Titov, O., et al., 2013, "International collaboration for improvement of the Celestial Reference Frame in the southern hemisphere", IAG Symposium, Potsdam.
`http://www.iag2013.org/IAG_2013/Publication_files/abstracts_iag_2013_2808.pdf`

ON THE SYSTEMATICS IN APPARENT PROPER MOTIONS OF RADIO SOURCES OBSERVED BY VLBI

V. RAPOSO-PULIDO[1,2], S. LAMBERT[3], N. CAPITAINE[3], T. NILSSON[1], R. HEINKELMANN[1], H. SCHUH[1]
[1] Helmholtz Centre Potsdam, GFZ German Research Centre for Geosciences
Department 1: Geodesy and Remote Sensing, 14473 Potsdam, Germany
e-mail: raposo@gfz-potsdam.de
[2] IGN, Instituto Geográfico Nacional, Madrid, Spain
[3] SYRTE, Observatoire de Paris, CNRS, UPMC
61, avenue de l'Observatoire, 75014 Paris, France

ABSTRACT. For about twenty years, several authors have been investigating the systematics in the apparent proper motions of radio source positions. In some cases, the theoretical work developed (Pyne et al., 1996) could not be assessed due to the few number of VLBI observations. In other cases, the effects attributed to apparent proper motion could not be related successfully because there were no significant evidences from a statistical point of view (MacMillan, 2005). In this work we provide considerations about the estimation of the coefficients of spherical harmonics, based on a three-step procedure used by Titov et al. (2011) and Titov and Lambert (2013). The early stage of this work has been to compare step by step the computations and estimation processes between the Calc/Solve (http://gemini.gsfc.nasa.gov/solve/) and VieVS software (Böhm et al., 2012). To achieve this, the results were analyzed and compared with the previous study done by Titov and Lambert (2013).

1. INTRODUCTION

The acceleration of the Solar System Barycenter (SSB) in the Universe, which is due, for a large part, to the rotation of the SSB about the Galactic center in 250 Myr, produces a dipolar anisotropy of the extragalactic body proper motion field. Several works analyzed geodetic VLBI observations (Pyne et al., 1996; MacMillan, 2005) and failed to isolate this effect from VLBI noise mainly because of a too small number of observations. Finally, the effect was first detected by Titov et al. (2011) and confirmed in Titov and Lambert (2013). However, other parallel studies led with different methods found a drastically different orientation of the dipole (Xu et al., 2012). In order to understand the possible reasons of these differences and to improve the determination of the SSB acceleration, we reproduce in this study the computation of Titov and Lambert (2013) using an independent geodetic VLBI analysis software package (VieVS). Especially, we focus on the value of constraint on source position, which was identified as a key point by Titov et al. (2011).

2. THE STUDY

Different methods have been applied to estimate the systematics in apparent proper motions. One of them is the three-step procedure applied by Titov et al. (2011) and Titov and Lambert (2013). It has the advantage that almost everything is estimated after the VLBI analysis, thus we have the possibility to check the different steps:

1. Radio source time series are estimated from VLBI analysis
2. Apparent proper motions are fitted to their coordinate time series
3. Spherical harmonics are fitted to the proper motion field

To compare VieVS (1979-Dec/2013) results against results of Calc/Solve (1979-Feb/2013), and assess the consistency of both VLBI softwares, we use the same a priori configuration and parameterization chosen by Titov and Lambert (2013) to analyse the VLBI sessions. In the present study we also

excluded sessions which are not suitable for reliable Earth Orientation Parameters (EOP) determination (http://lupus.gsfc.nasa.gov/files_IVS-AC/eop_exclusion.txt), decreasing the initial number of sessions from 5812 to 4677, while the previous study (Titov and Lambert, 2013) provides 5632. For both studies the models followed the IERS Conventions (2010) (Petit and Luzum, 2010).

Radio sources with less than three observations per sessions were excluded, choosing a cut-off elevation angle of 5°. The celestial frame was tied to the current International Celestial Reference Frame (ICRF2, Fey et al., 2009) by applying individual constraint on each source. We estimated four different solutions with VieVS, depending on the weights: $\sigma = 10^{-5}$ rad ($\sim$ 2 as), $\sigma = 10^{-6}$ rad ($\sim$ 200 mas), $\sigma = 10^{-7}$ rad ($\sim$ 20 mas), $\sigma = 10^{-8}$ rad ($\sim$ 2 mas). Titov, et al. (2011) showed that constraining each source using very loose constraint (σ = 2 as) is equivalent to apply loose NNR constraint with the same weight.

3. THREE-STEP PROCEDURE

After time series of the radio sources have been estimated with VieVS, we proceed to compute the proper motions. First, we exclude sessions with RMS larger than 100 ps as well as the 39 special handling sources, whose large structure could affect the harmonics estimation. After that, we apply an outlier elimination algorithm for each time series, that is, data points with distances from the mean larger than T_1 times the uncertainties are removed (where $T_1 = 90$ is the value provided by Titov and Lambert, 2013). Only radio sources with more than ten sessions are chosen for velocity estimation, reducing the number by one-sixth of the total before the iteration ($\sim$ 545 out of $\sim$ 3200). The velocities are estimated by a linear fit to the source positions, weighting the equations by using the inverse of the variance of the offsets ($\sigma^2_{d\alpha cos\delta}, \sigma^2_{d\delta}$). Comparing the velocities of the 49 most observed sources for both softwares, the results are the closest to Titov and Lambert (2013) study when tighter constraints are applied in VieVS ($\sigma = 10^{-7}$ rad). In Calc/Solve we found a stability of the velocities for $\sigma = 10^{-6}$ rad or looser, while in VieVS the singularity level is achieved by $\sigma = 10^{-5}$ rad or looser, that is, strength of the constraint is loose enough to cannot remove the degeneracy.

To estimate the spherical harmonics by fitting to the proper motion field, we apply the equations developed by Mignard and Klioner (2012) to decompose the systematic part of the proper motion field into different harmonics:

$$\Delta\mu_\alpha \cos\delta = -d_1 \sin\alpha + d_2 \cos\alpha + r_1 \cos\alpha \sin\delta + r_2 \sin\alpha \sin\delta - r_3 \cos\delta$$

$$\Delta\mu_\delta = -d_1 \cos\alpha \sin\delta - d_2 \sin\alpha \sin\delta + d_3 \cos\delta - r_1 \sin\alpha + r_2 \cos\alpha$$

where ($\Delta\mu_\alpha \cos\delta$, $\Delta\mu_\delta$) is the systematic part of the proper motion field, (d_1, d_2, d_3) the electric harmonics of degree one (acceleration of the SSB) and (r_1, r_2, r_3) the magnetic harmonics of degree one (global rotations).

To estimate the Vector Spherical Harmonics (VSH), we do a second iterative process to exclude the unstable radio sources, i.e., radio sources with residual velocities larger than T_2 times the residual rms were excluded from the set (where $T_2 = 7$ is the value provided by Titov and Lambert, 2013). Table 1 shows the values estimated for the systematics using the constraints $\sigma = 10^{-6}$ rad, 10^{-7} rad and 10^{-8} rad. The dipole values provided by $\sigma = 10^{-6}$ rad and 10^{-7} rad are the closest to the Titov and Lambert (2013) study for the first two components. However, we obtain strong discrepancies for the third component (that traduces the declination of the dipole) (see Table 1).

VSH [μas/yr]	10^{-6} rad (407 sour.)	10^{-7} rad (388 sour.)	10^{-8} rad (425 sour.)	T and L, 2013 (427 sour.)
d_1	-0.2 ± 1.9	-0.6 ± 0.6	0.0 ± 0.4	-0.4 ± 0.7
d_2	-5.8 ± 1.6	-5.7 ± 0.7	-4.5 ± 0.4	-5.7 ± 0.8
d_3	0.8 ± 1.3	1.1 ± 0.7	0.8 ± 0.4	-2.8 ± 0.9
r_1	0.31 ± 1.5	2.8 ± 0.7	2.5 ± 0.4	-1.1 ± 0.9
r_2	-2.4 ± 1.8	0.6 ± 0.7	0.4 ± 0.4	1.4 ± 0.8
r_3	-20.9 ± 1.5	-2.0 $\pm$ 0.5	0.6 ± 0.3	0.7 ± 0.6

Table 1: VSH values depending on the constraint applied.

4. CONCLUSIONS

Using a constraint of 10^{-7} rad leads to a dipole amplitude quite similar to Titov and Lambert (2013). However, though the agreement is good for the amplitude, the orientation of the dipole significantly differs. The present study provides a dipole of amplitude 5.85 $\pm$ 0.91, oriented towards $\alpha = 263.82 \pm 6.66°$ and $\delta = 5.85 \pm 7.12°$. Titov and Lambert (2013) provides a dipole of amplitude 6.4 $\pm$ 1.1, oriented towards $\alpha = 266 \pm 7°$ and $\delta = -26 \pm 7°$. At this stage, we need a deeper study to find out the reason.

A comparison between different software and approaches for the estimation of very small effects, such as the galactic aberration effect, from VLBI observations is essential. This aims at providing a better understanding of the scientific results. This work has provided such a detailed comparison. Further tests are still necessary.

Acknowledgements. We acknowledge the Local Organizing Committee (LOC) for travel funding and DFG for supporting our project ECORAS out of which the conference participation was partly covered.

This work was performed during a stay by V. Raposo-Pulido at the Paris Observatory, financed by Paris Observatory and GFZ.

5. REFERENCES

Böhm, J., Böhm, S., Nilsson, T., Pany, A., Plank, L., Spicakova, H., Teke, K., Schuh, H., 2012, In: "The New Vienna VLBI Software VieVS", S. Kenyon et al. (eds.), IAG Symposia, 136, pp. 1007–1011, doi:10.1007/978-3-642-20338-1_126.

Fey, A.L., Gordon, D., Jacobs, C.S. (eds.), 2009, "The Second Realization of the International Celestial Reference Frame by Very Long Baseline Interferometry", Presented on behalf of the IERS/IVS Working Group, IERS Technical Note 35, Frankfurt am Main: Verlag des Bundesamts für Kartographie und Geodäsie.

MacMillan, D.S., 2005, "Quasar Apparent Proper Motion Observed by Geodetic VLBI Networks", ASP Conference Series, 340, pp. 477–481.

Mignard, F., Klioner, S., 2012, "Analysis of astrometric catalogues with vector spherical harmonics", arXiv: 1207.0025v3.

Petit, G., Luzum, B. (eds.), 2010, IERS Conventions (2010), IERS Technical Note 36, Frankfurt am Main: Verlag des Bundesamts für Kartographie und Geodäsie.

Pyne, T., Gwinn, C.R., Birkinshaw, M., Eubanks, T.M., Matsakis, D.N., 1996, "Gravitational radiation and Very Long Baseline Interferometry", ApJ, 465, pp. 566-577.

Titov, O., Lambert, S., Gontier, A.-M., 2011, "VLBI measurement of the secular aberration drift", A&A, 529, A91.

Titov, O., Lambert, S., 2013, "Improved VLBI measurement of the solar system acceleration", A&A, 559, A95.

Xu, M.H., Wang, G.L., Zhao, M., 2012, "The solar acceleration obtained by VLBI observations", A&A, 544, A135.

MORPHOLOGY OF QSO HOST GALAXIES — A LOOK AT THE SED

A.H. ANDREI[1,2,3,4], B. COELHO[3], S. ANTÓN[5,6]
[1] Observatório Nacional/MCTI
Rua Gal. José Cristino 77, Rio de Janeiro, RJ CEP 20921-400, Brasil
e-mail: oat1@ov.ufrj.br
[2] SYRTE/Observatoire de Paris
Avenue de l'Observatoire 61, Paris 75014, France
[3] Observatório do Valongo/UFRJ
Ladeira do Pedro Antônio 43, Rio de Janeiro, RJ CEP 20080-090, Brasil
[4] Osservatorio Astrofisico di Torino/INAF
Strada Osservatorio 20, Pino Torinese, TO 10025, Italia
[5] Instituto de Astrofísica de Andalucía/CSIC
Glorieta de la Astronomia s/n, 18008, Granda, España
[6] Faculdade de Ciências/Universidade de Lisboa
Tapada da Ajuda 1349-018, Lisboa, Portugal

ABSTRACT. The Gaia Initial QSO Catalogue presents several characteristics of its 1,248,372 listed objects, among which the optical morphological type. From this a program studies the host galaxies of QSOs present in the SDSS up to its 8th release, based on retrieving a data bank of images in the five *ugriz* colors for the 105,783 objects spectroscopically found as QSOs. The first scope of this program is to study QSOs for which the isophotes of the host galaxy are not pronounced, so that the centroid determination is not affected for those fundamental grid-points of the Gaia Celestial Reference Frame. Since the target images come from relatively short exposures, we developed an approach to access disturbances of the target PSF relatively to the nearby stars. Here we focus on the first results for absolute magnitude of QSOs combining the SDSS colors and the SED library from Gaia.

1. INTRODUCTION

The latest, updated, and fully corrected version of the Gaia Initial QSO Catalog (GIQC, Andrei et al., 2014), produced by the CU3 GWP-S-335-13000 contains 1,248,372 objects, of which 191,372 are considered and marked as Defining ones, because of their observational history and existence of spectroscopic redshift. Also objects with strong, calibrator-like radio emission are included in this category. The Defining objects represent a clean sample of quasars. The remaining objects aim to bring completeness to the GIQC at the time of its compilation. For the whole GIQC the average density is 30.3 sources per sq.deg., practically all sources have an indication of magnitude and of morphological indexes, and 90% of the sources have an indication of redshift and of variability indexes (Fig. 1). QSOs are crucial targets to define the Gaia Celestial Reference Frame (GCRF), and accordingly on board means are capable of classifying them. The QSO classification contains three major orientations: getting a zero-contaminants QSO sample to determine the GCRF; deriving the most complete QSO sample based on the full Gaia data; and determining astrophysical parameters for each QSO. The determination itself of a Gaia source as a QSO is planned to rely primarily on comparison of the photometric output against a template of spectral energy distributions (SED), and secondarily on astrometric observables, variability analysis and a reliable initial list of known QSOs.

It is now largely accepted that depending on whether the jets from where the radio emission emanates are seen head-on or face-on the disagreement between the radio and optical centroids can reach several milliarcseconds. Since the GCRF will define the Celestial Reference Frame to sub-μas level and the number of sources tying it to the current ICRF is of less than 100, these outliers must be flagged off the soonest. And the situation can be still more adverse, noticing that most of Gaia quasars are at redshift smaller than 1 and that those belonging to the current ICRF are much closer yet. Coherently with the findings of the Gaia WP Initial QSO Catalog, in the Gaia data treatment all QSOs will be handled as

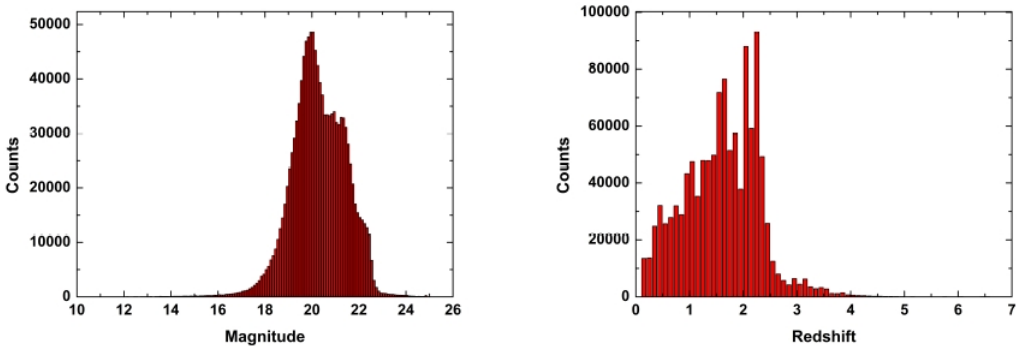

Figure 1: Magnitude and redshift counts of the GIQC sources.

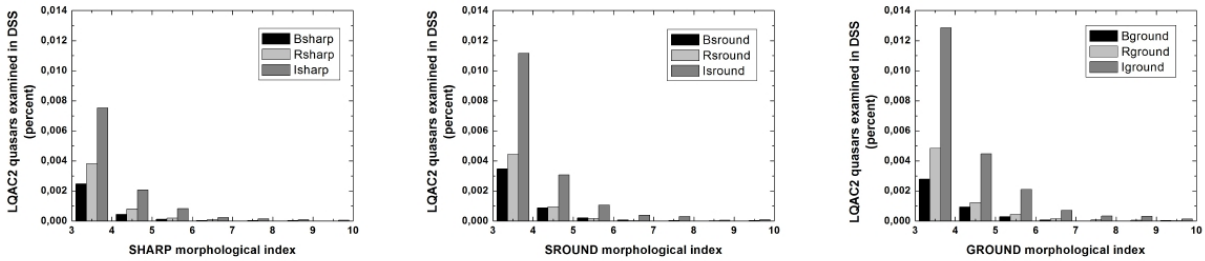

Figure 2: Binned distribution of the morphological indexes, for quasars that are markedly non-pointlike. Data from the LQAC2 catalogue (Souchay et al., 2012) and B, R, I plates from the DSS (The Digitized Sky Survey was produced at the Space Telescope Science Institute under U.S. Government grant NAG W-2166).

extended sources in order to model for the host galaxy isophotes. Yet, there is a loss of astrometric precision in both extremes, when the host galaxy is very bright and extensive, and when the source is not pointlike but there aren't enough photons to properly fit the structure underneath (Fig. 2). Thus in the GIQC the morphological classification derives from comparing the target PSF characteristics against the local PSF characteristics, as given by the average from nearby stars of similar magnitude (Andrei et al., 2010).

The absolute magnitude of quasars is used in the GIQC as starting point to calculate the variability indexes and to interpret the morphological indexes. From the absolute magnitude the luminosity and mass are worked out, and hence the radius of the accretion disk is calculated (Morgan et al., 2010; Shen et al., 2008). From these the probability of accretion disk or torus instabilities to induce optical variability are derived (Popovic et al., 2012). It is also from the absolute magnitude of the quasar that features of the host galaxy can be estimated (Serjeant et al., 2009), from which the morphological indexes are understood.

2. THE DETERMINATION OF QSOs' ABSOLUTE MAGNITUDE

The determination of the absolute magnitude is fundamental to discuss the QSOs and host galaxies properties from the astrophysical and cosmological points of view. Usually in the literature the absolute magnitude of QSOs is simplified by a power law continuum. A complete description, allowing for the blue-bump and the presence of emission lines will give a more reliable measure of the light coming from the AGN, thus improving a separate discussion of the central engine and extended environment, and a better characterization of the QSO itself.

We develop a program to study the host galaxies of QSOs present in the SDSS up to its 8th release. The main observational data thus comprises a large retrieved data bank of images in the five *ugriz* colors for the 105,783 objects spectroscopically found as QSOs, within frames large enough to contain tens of comparison stars and several field galaxies. From it the *ugriz* magnitudes are combined with the Gaia

Quasar Synthetic Spectra library (QSSL, Claeskens et al., 2006) to derive the absolute magnitudes.

Initially we de-convolve the apparent magnitudes from the bandpass and integrated efficiency of the *ugriz* filters (Fukugita et al., 1996) to re-construct the incoming flux density.

Next the absorption and reddening are taken into account. For the galactic absorption the Schlegel et al. (1998) high resolution ($\sim$ few arc-minute) 100μ intensity map is used from the equatorial coordinates. The tables return the V band extinction as function (B-V), which can be extended to other bands and passbands. After that the Lyman-α forest absorption must be accounted for. The models are controversial, because the size and density of hydrogen clouds and blobs vary in redshift. We adopted the model of Meiksin (2006) that computes the attenuation for different system of astronomy filters, including the SDSS *ugriz*.

Intergalactic dust includes from micro particles to large molecules. There are models and examples of increasing dust column density along the line of site. However, for most cases the amount of reddening is uncorrelated to the amount of extinction due to the Lyman-α forest. And the lines associated to gas accompanying the dust are better explained at the rest frame. This is adopted the model of Hopkins et al. (2004). This model assumes the reddening toward quasars as dominated by SMC-like dust at the quasar redshift. It computes the color attenuation based of a large sample of SDSS QSOs. Following this model we calculated the modal values – or mean value where the samples are too small – that correspond to the intrinsic colors of QSOs at a given redshift; the excess to it must be corrected to the obtained rest-frame color (hence absolute magnitude).

Finally, at the rest frame, we combine the redshift from the SDSS with knowledge of the Spectral Energy Distribution (SED) to derive the absolute magnitudes in different bands and passbands. The QSSL coverage is complemented by the SWIRE template library (Polletta et al., 2006). Their extent are as bellow.

- QSSL: wavelength – λ from 2,500.5Å to 10,499.5Å, step 0.5Å; spectral index – α from -4 to $+3$, step 1; flux – W (arbitrary units) from 10^2 to 10^6, step $\times$ 1.58489; redshift – z from 0.0 to 5.5, step 0.1019.
- SWIRE: wavelength – λ from 1,000.5Å to 1,000 μ, step $20\times\log(\lambda)$ Å; spectral index – α for QSO type 1 (face on) and QSO type 2 (edge on); flux – W (arbitrary units) from 1 to 20; redshift – z on the rest frame.

3. RESULTS

The obtained absolute magnitudes follow well what is expected from the current astrophysical models (Fig. 3). Both the effects of the blue-bump and of the cosmological increase of brightness are well recovered. Also the variation of the spectral indexes is in agreement with the unified model (Fig. 4).

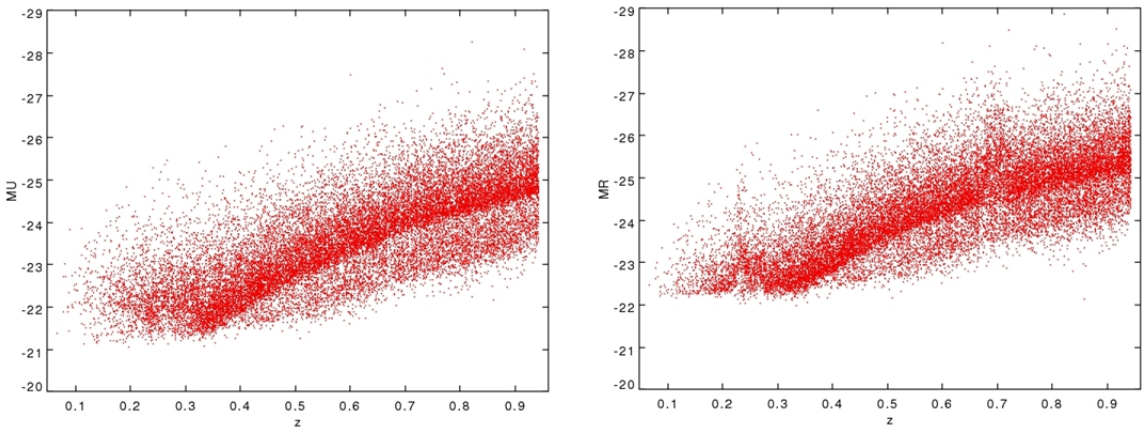

Figure 3: Calculated absolute magnitudes. The cosmological increase towards a maximum around z=2 is clear. The absolute magnitudes are generally brighter than those in the literature because the SED and emission lines are included.

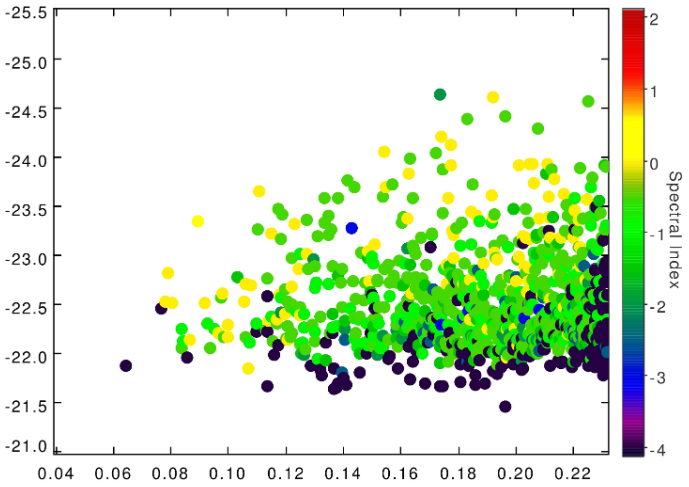

Figure 4: Spectral index distribution resulting from the fitting of the best SED for the calculation of the absolute magnitudes.

These results are being continued to discuss the morphological output in Gaia observations along different LSFs (line spread function), in special for the ICRF quasars that will contribute to the radio-to-optical link of the GCRF, in which the reconciliation of the centroids is of paramount importance.

Acknowledgements. A.H.A. thanks the CNPq/BR Bolsa de Pesquisa and the CAPES/BR AEX grant. Funding for the SDSS has been provided by the Alfred P. Sloan Foundation, the Participating Institutions, the N.S.F. and the U.S. Dept. of Energy Office of Science.

4. REFERENCES

Andrei, A.H., et al., 2010, "Gaia Initial QSO Catalogue for Gaia — The MDB version", Gaia Research Note GAIA-C3-SP-GPA-AA-002-1.

Andrei, A.H., et al., 2014, "The Gaia Initial Quasar Catalog", In: Proc. Journées 2013 "Systèmes de Référence Spatio-Temporels", N. Capitaine (ed.), Observatoire de Paris, pp. 84–87.

Souchay, J., et al., 2012, "The Second Release of the Large Quasar Astrometric Catalog", A&A, 537, 99.

Claeskens, J.-F., et al., 2006, "Identification and Redshift Determination of Quasi-stellar Objects with Medium-band Photometry: Application to Gaia", MNRAS 367, 879.

Fukugita, M., et al., 1996, "The Sloan Digital Sky Survey Photometric System", AJ, 111, 174.

Hopkins, P.F., 2004, "Dust Reddening in Sloan Digital Sky Survey Quasars", AJ, 128, 1112.

Meiksin, A., 2006, "Colour Corrections for High-redshift Objects Due to Intergallactic Attenuation", MNRAS, 365, 833.

Morgan, C.W., et al., 2010, "The Quasar Accretion Disk Size-black Hole Mass Relation", ApJ, 712, 1129.

Polletta, M. del Carmen, 2006, "Chandra and Spitzer unveil Heavily Obscured Quasars in the Chandra/SWIRE Survey", ApJ, 642, 673.

Popovic, L.C., et al., 2012, "Photocentric Variability of Quasars caused by Variations in their Inner Structure: Consequences for Gaia Measurements", A&A, 538, 107.

Schlegel, D.J., et al., 1998, "Maps of Dust Infrared Emission for Use in Estimation of Reddening and Cosmic Microwave Backgrouns Radiation Foregrounds", ApJ, 500, 525.

Serjeant, S., et al., 2009, "The Evolution of Star Formation in Quasar Host Galaxies", MNRAS, 397, 265.

Shen, Y., et al., 2008, "Biases in Virial Black Hole Masses: An SDSS Perspective", ApJ, 680, 169.

SOME PRELIMINARY PHOTOMETRIC RESULTS OF QSOs USEFUL FOR THE LINK BETWEEN FUTURE GAIA CRF AND ICRF

G. DAMLJANOVIĆ[1], F. TARIS[2], S. BOEVA[3]
[1] Belgrade Astronomical Observatory
Volgina 7, 11060 Belgrade 38, Serbia
e-mail: gdamljanovic@aob.rs
[2] SYRTE, Observatoire de Paris, CNRS/UPMC
75014 Paris, France
e-mail: francois.taris@obspm.fr
[3] Institute of Astronomy with NAO, BAS
BG-1784, Sofia, Bulgaria
e-mail: sboeva@astro.bas.bg

ABSTRACT. Gaia was launched in December 2013 as cornerstone mission of the European Space Agency (ESA). It is going to map the entire sky (over one billion stars) and more than 500,000 quasars (QSOs); all objects with apparent V band magnitudes in the range $5.6 < V < 20$ (Mignard 2014). During its 5-year lifetime it will produce a unique time-domain space survey. The main result will be a dense optical QSO-based Gaia Celestial Reference Frame (Gaia CRF). So, the high accuracy link between future Gaia CRF and International CRF (ICRF) will be of importance. About 90% of the ICRF sources are not suitable for that link (they are not bright enough in optical domain, they have significant extended radio emission, etc.), but there are other (candidate) sources – weak extragalactic radio sources (ERS) with bright optical counterparts which we need to investigate. Some candidate sources were already imaging by VLBI, and some sources were detected as useful ones on VLBI scales. Also, the astrophysical processes could produce displacements of the optical photocenter of these objects, and because of it the variations of their light curves are important first information to check candidate sources for establishing the link of reference systems. Our observations of 47 candidate objects were carried out more than one year in the B, V and R bands using the $D = 0.6$ m new telescope at the Astronomical Station Vidojevica (ASV, of Astronomical Observatory in Belgrade, Serbia). Some preliminary photometric results are presented as a part of astrophotometric and astrophysical investigations of ERS in the framework of the reference systems. Also, some photometric results following from the data obtained by using the TJO (Telescopi Juan Oró, $D = 0.8$ m) in OAdM (Observatori Astronòmic del Montsec, Spain) are presented.

1. INTRODUCTION

After the Hipparcos (ESA 1997, van Leeuwen 2007), Gaia is the next European space astrometric mission. One of the main results of the Gaia mission (of the European Space Agency – ESA) will be a new optical Gaia Celestial Reference Frame (Gaia CRF). The Gaia CRF will be based on bright quasars (QSOs) with the most accurate coordinates, and will supersede the current International CRF (ICRF) which is based on Very Long Baseline Interferometry (VLBI) radio data. For the high accuracy link (until a few tens of μas,) between two mentioned frames, the extragalactic radio sources (ERS) with optical counterparts are of importance, but only 10% of the ICRF objects are suitable for that link. This means a new set of sources should be defined and tested (Bourda et al. 2010, 2011; Taris et al. 2011, 2013; Petrov 2011, 2013). Good candidates are: the distant ERS, with negligible proper motions, bright enough in the optical domain (with V magnitudes up to about 18), compact structures, etc. For now, the optical – radio shift (about 150 μas at X-band) is nearly ten times larger than VLBI and Gaia position accuracies (a few tens of μas at V magnitudes 15–18).

The photometric monitoring of candidates (mostly QSOs) is the first step for their testing, because the flux variability is one of the most important properties of QSOs. The relationship between QSO's morphology, magnitude variability and astrometry is described in the paper (Popović et al. 2012). So, the morphology and photometry variations of common QSOs (visible in optical and radio domains) could make displacement of their optical photocenters. Because of that, since 2010 a set of 47 objects has

been already monitored to measure their flux variability. Here, we present some preliminary photometric results of the ASV (Astronomical Station Vidojevica, Astronomical Observatory in Belgrade, $D = 0.6$ m, Serbia) data from mid-2013 and TJO (Telescopi Juan Oró, Observatori Astronòmic del Montsec, 0.8m, Spain) ones.

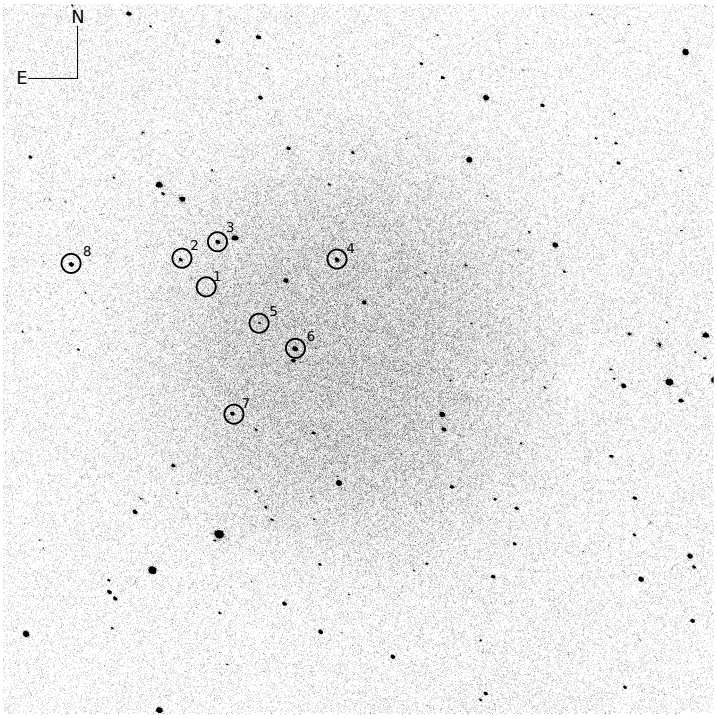

Figure 1: Object 1535+231 (number 1) and calibration stars (2-8); FoV=16′, the 60 cm ASV telescope.

2. OBSERVATIONS AND RESULTS

It has been noted that ERS are not point-like objects and that their morphology and photometry are changing with time; that fact is of importance for Gaia astrometry. So, it is necessary to monitor the ICRF sources at both optical and radio wavelengths. Also, to check the candidate sources (first of all to do it via photometric monitoring).

That photometric monitoring of mentioned 47 objects is under progress using a few telescopes. From mid-2013 we have done it with the 60 cm ASV instrument ($D/F = 0.6m/6m$, long.=21.5°, lat.=43.1°, h=1150 m) and the CCD camera Apogee Alta U42 (2048x2048 pixels, pixel size is 13.5x13.5 μm, scale is 0.″46 per pixel, FoV=15.8′x15.8′). We present particularly some photometric results for the object 1535+231, obtained with the ASV telescope, in Fig. 2 (usually, one point per a few months). The seeing is in general about 1.″5, but during our observations in July and September 2013 it was better than 1″. The filters Johnson BV and Cousins R were used, and we made 3 frames per filter. All frames were reduced individually (dark, bias, flat, hot/death pixels), and the MaxIm DL image processing packages were used for reduction and photometry (relative to the available reference stars, see Fig. 1). Because of very close relationship between astrophysics and astrometry of QSOs (for Gaia mission), we apply the differential photometry and use the secondary standard stars to get small error (about 0.1 mag) of B, V, R magnitudes of object. The calibration stars are from SDSS catalogue (Abazajian et al. 2009), because there is a lack of standard stars with BVRI magnitudes for differential photometry of mentioned QSOs. And to calculate the BVRI magnitudes from *ugriz* ones, the Chonis and Gaskell (2008) transformations were used, within a magnitude range $14.5 < g, r, i < 19.5$:

$B = g + (0.327 \pm 0.047)(g - r) + (0.216 \pm 0.027)$
$V = g - (0.587 \pm 0.022)(g - r) - (0.011 \pm 0.013)$
$R = r - (0.272 \pm 0.092)(r - i) - (0.159 \pm 0.022)$
$I = i - (0.337 \pm 0.191)(r - i) - (0.370 \pm 0.041)$.

We found about 60% of 47 objects in SDSS DR10. For other objects we plan to use the Two Micron All Sky Survey (2MASS) catalogue. The systematic errors of these calibrations stars (local errors, instrumental ones, their flux variability, etc.) were checked via our own data (3 or 4 epochs during about one year observations) in accordance with the rejection criterion that we set to 3σ value; σ is in line with dispersion of our data.

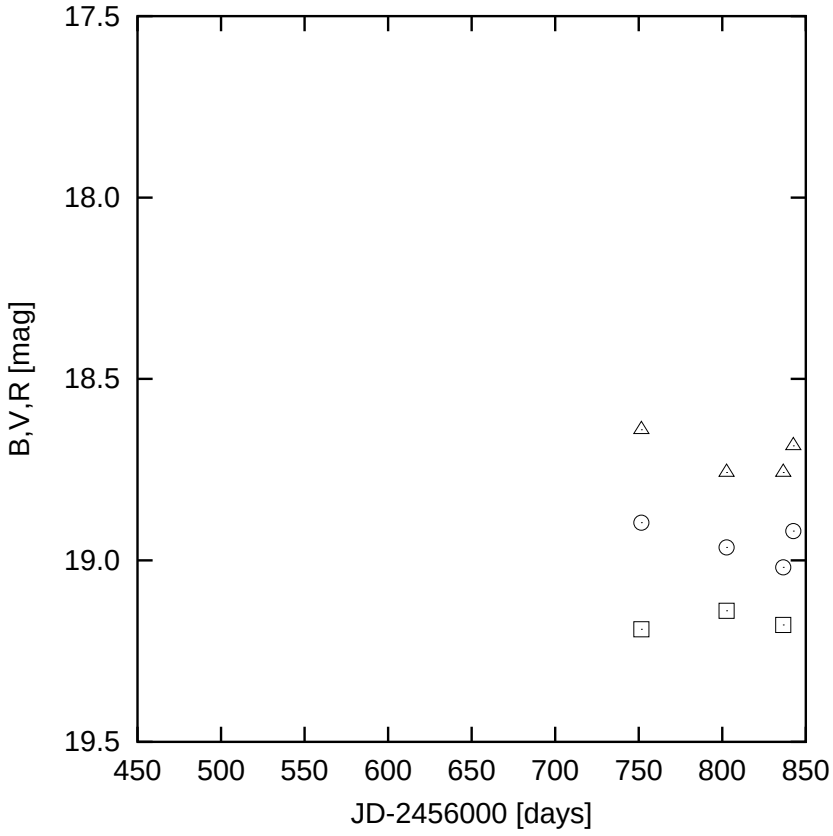

Figure 2: The values of B(square), V(circle), R(triangle) magnitudes of object 1535+231; the 60 cm ASV telescope (April 3^{rd} – July 3^{rd} 2014).

Also, the flux variability of QSOs can be simply checked by comparison to other stars which are close to the object. The differences of magnitudes in R filter between the object 1535+231 and stars (relative to the star A and to the star B) using TJO observations are presented in Fig. 3 (one point per day). From both data sets (ASV and TJO), there are some photometric changes of object 1535+231 during the time, but we need more data for final conclusion about the flux stability of that object.

3. CONCLUSION

Since 2010, the optical observations of 47 objects, mostly QSOs, are going on for their photometry monitoring (to check the flux variability of QSOs) using several telescopes. These QSOs could be useful for an accurate link between the future Gaia CRF and ICRF. Some results obtained with the 0.6 m ASV and 0.8 m TJO instruments are presented. With the 60 cm ASV telescope, we joined that monitoring since mid-2013.

Using the transformations (Chonis and Gaskell 2008) and *ugriz* magnitudes from SDSS we get the BVR ones for calibration stars near QSO (for about 60% of mentioned objects). From our data, these input BVR magnitudes of secondary comparison stars were checked for some systematics (flux variability of stars, local errors, instrumental ones, etc.), and used to determine the BVR magnitudes of QSOs via differential photometry (see Figs. 1 and 2 for the object 1535+231, one ASV point per few months). In Fig. 3 (one TJO point per day), the flux variability in R filter of QSOs is presented; it was simply checked by comparison to other stars which are close to the object. From both sets of data (ASV and TJO), some

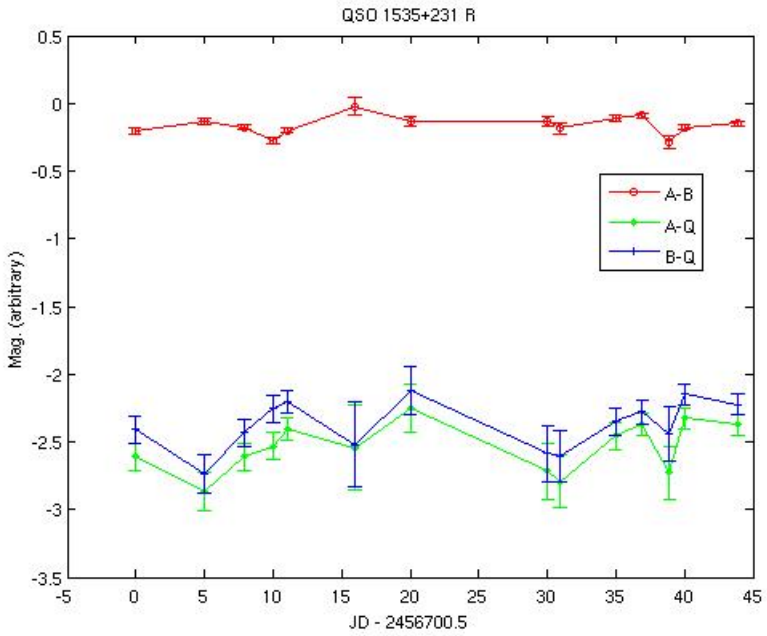

Figure 3: Photometry results (in R filter) for object 1535+231 using data of the 0.8 m TJO.

photometric changes for object 1535+231 during the time are noticeable, and we continue monitoring of that object.

Even some problems during observations of QSOs (optical faintness of QSOs, atmospheric influences, technical problems, etc.), with both instruments we could produce the data which are good enough for photometry investigation and in line with the link between the future Gaia CRF (optical) and ICRF (radio) frames.

Acknowledgements. G. Damljanović performed this work as a part of Project No. 176011 "Dynamics and kinematics of celestial bodies and systems" supported by the Ministry of Education, Science and Technological Development of the Republic of Serbia. Also, G. Damljanović gratefully acknowledges the observing grant support from the Institute of Astronomy and Rozhen National Astronomical Observatory, Bulgarian Academy of Sciences.

4. REFERENCES

Abazajian, K.N., et al., 2009, AJ Suppl., 182, 543.
Bourda, G., et al., 2010, A&A, 520, A113.
Bourda, G., et al., 2011, A&A, 526, A102.
Chonis, T.S., Gaskell, C.M., 2008, AJ, 135, 264.
ESA, 1997, "The Hipparcos and Tycho Catalogues", ESA SP-1200, ESA Publications Division, Noordwijk.
Mignard, F., 2014, In: Proc. Journées 2013 "Systèmes de Référence Spatio-Temporels", N. Capitaine (ed.), Observatoire de Paris, pp. 57–60.
Petrov, L., 2011, AJ, 142, 105.
Petrov, L., 2013, AJ, 146, 5.
Popović, L., et al., 2012, A&A, 538, A2107.
Taris, F., et al., 2011, A&A, 526, A25.
Taris, F., et al., 2013, A&A, 552, A98.
van Leeuwen, F., 2007, "Hipparcos, the new reduction of the raw data", Dordrecht: Springer.

FIRST RESULTS OF S/X AND X/KA-BAND CATALOGUE COMBINATIONS WITH FULL COVARIANCE INFORMATION

A. IDDINK[1], C. JACOBS[2], T. ARTZ[1], A. NOTHNAGEL[1]
[1] Institute of Geodesy and Geoinformation, University of Bonn
Nußallee 17, 53115 Bonn, Germany
e-mail: aiddink@uni-bonn.de, artz@igg.uni-bonn.de, nothnagel@uni-bonn.de
[2] Jet Propulsion Laboratory, California Institute of Technology
4800 Oak Grove Dr., Pasadena, CA 91109, USA
e-mail: Christopher.S.Jacobs@jpl.nasa.gov

ABSTRACT. The currently existing realizations of the International Celestial Reference System (ICRS), the ICRF1 and ICRF2, are based on solutions estimated by a single VLBI group. All sessions used were dual frequency S/X-band (2.3/8.4 GHz) VLBI sessions. In addition to an improved precision one of the main goals for the upcoming realization of the ICRF3 is an enhanced frequency coverage compared to the ICRF2. By including solutions with full variance-covariance information based on X/Ka-band (8.4/32 GHz) observations in a rigorous VLBI intra-technique combination, an improved frequency coverage can be realized. In this paper, we present a method to mix the combination on the level of datum free normal equation systems (NEQ) and on the solution level with full covariance information. We show preliminary results of a combined S/X- and X/Ka-band catalogue and discuss the prerequisites and the limitations of this approach.

1. INTRODUCTION

The last two versions of the International Celestial Reference Frame (ICRF) had been generated by the VLBI group at the NASA Goddard Space Flight Center (GSFC) with the software package Calc/Solve. Despite the fact that several other catalogues of different analysis centers existed, only comparisons between these solutions had been made (Fey et al. 2009). The primary reason for this procedure was the missing machinery which permits a rigorous combination of radio source position catalogues including a full propagation of the variance-covariance information. To overcome this deficit in the upcoming generation of the ICRF3, a combination procedure for celestial reference frame determinations has been proposed in Iddink et al. (2014a, 2014b). The developed procedure is based on the combination at the level of datum-free normal equations (NEQs), which enables the rigorous transfer of the full variance-covariance information of all parameters and all individual input contributions. In general, these contributions are based on dual frequency S/X-band (2.3/8.4 GHz) sessions, which are being analysed and provided by different analysis centers. Up to now over 5000 sessions were observed and analysed by each of the contributing analysis centers and all information is freely available on the server of the International VLBI Service (IVS) on a session by session basis. The delivery and exchange of these analysis results is performed with the Solution Independent Exchange Format (SINEX).

In addition to this, today a remarkable number of observations at X/Ka-band (8.4/32 GHz) exists, mainly observed on the intercontinental baselines of NASA's Deep Space Network (DSN). The results of these observations are presently realized in a single X/Ka-band catalogue and consist of 631 X/Ka sources (Jacobs et al. 2012). Compared to S/X-band catalogues, X/Ka-band permits access to more compact radio sources. It is important to highlight, that the provided X/Ka contribution is composed of a monolithic X/Ka-band solution vector plus the corresponding full variance-covariance matrix. This contrasts with the S/X-band contributions which are based on session-wise datum-free NEQs. Hence, in order to fulfill the main objectives of the upcoming realization of the ICRF3 (Jacobs et al. 2014), to get an improved frequency coverage and a combined product of multiple VLBI contributions, a suitable methodology and software to combine these different types of contributions need to be focused on.

2. COMBINATION APPROACH

Motivated by the need for a combined multi-frequency CRF, the underlying combination mechanism needs to be structured and divided into several sections. In order to guarantee that the contributions of the combination are not distorted by any constraints before combining them, the combination itself is performed at the level of datum-free NEQs.

In case of the given X/Ka-band solution with full variance-covariance information, the complete datum definition on Earth and in space is already fixed. While the terrestrial reference frame (TRF) is constrained to results from previous solutions, the CRF is aligned to the ICRF2. This is done by an NNR condition based on the positions of a number of selected sources. Hence, in order to be able to include the X/Ka-band solution in the common combination procedure, the datum-free NEQ needs to be reconstructed using information about the applied constraints, illustrated in Fig. 1. The provided X/Ka-band contribution consists of a solution vector x, containing only the source position parameters, and the corresponding full variance-covariance matrix Q_{xx}. All the other system components like the TRF and EOPs have been already removed in previous analysis steps and are not available in the provided dataset. As a consequence, only the applied NNR condition in the context of the CRF can be removed to obtain the datum-free X/Ka-band NEQ system.

It is essential to know, which sources and which weights were used for the applied NNR condition. Based on this information, the constraint matrix C can be generated and subtracted from the inverted full covariance matrix Q_{xx}^{-1}. Assuming that all information about the applied NNR constraints is given entirely, a fully datum-free NEQ should be obtained. Due to remaining datum-defining impacts like troposphere and the tidal effects which are sensitive to absolute orientation of the catalogue, the resulting NEQ N_{free} is not strictly rank 3 deficient. For our first initial combination approach in context of a multi-frequency band CRF, we neglect this less than ideal situation.

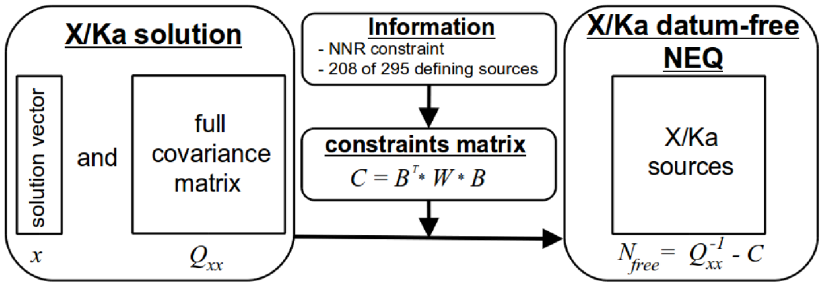

Figure 1: Reconstruction of datum-free NEQ based on given X/Ka-band solution.

In contrast to the monolithic X/Ka-band solution, the S/X-band contribution relies on several thousand datum-free single session NEQs. Based on these NEQs, we are able to generate one monolithic datum-free NEQ, containing all CRF, Earth orientation parameters (EOPs) and TRF components with respect to S/X-band observing sessions, as shown in Fig. 2. Due to the fact that the X/Ka-band contribution only contains the CRF component, only the sources can be used to link the contributions to each other within the combination. Fortunately, a significant number of sources in the X/Ka-band catalogue corresponds to those of S/X-band. These sources can be used as link sources for the datum transfer. Applying an NNR condition to a number of selected linking sources, automatically aligns the remaining non-corresponding sources to eachother and defines their positions. Consequently this leads to a combined S/X and X/Ka catalogue. It needs to be mentioned that combining source positions of different observing frequencies may lead to systematic effects and should not be performed with every possible link source. Hence, in upcoming studies it needs to be investigated if different emitting cores, respectively core shifts, need to be considered in the CRF combination. Due to the physics of quasars a parameterization of some kind of source tie might become indispensable when trying to combine source position parameters of different frequency bands.

Furthermore, even if the TRF component would be existent in the provided X/Ka-band dataset, no direct combination of the station coordinates would be possible. This is due to the fact that the observing sites are completely different to the ones which are used in the regular IVS S/X-band observing sessions. Because we focus on the multi-frequency combination mechanism, we currently simplify the combination by using S/X-band analysis results provided by only one analysis centers (GSFC).

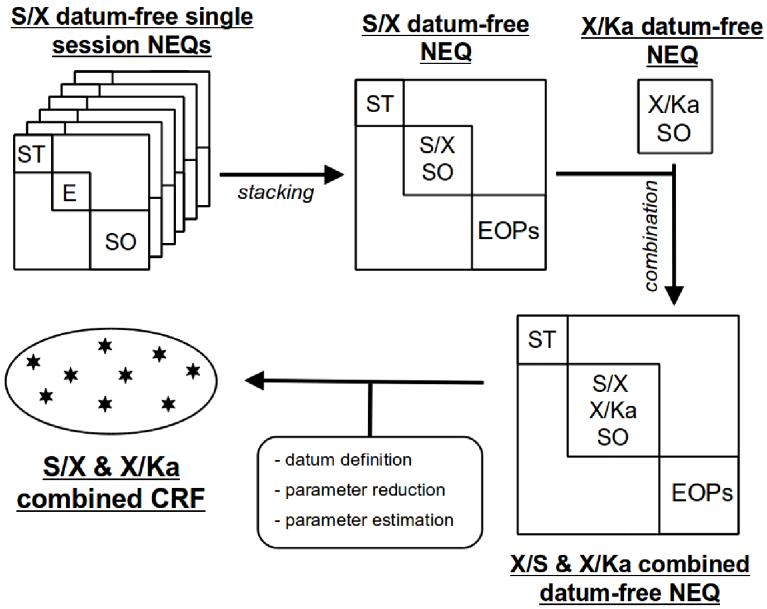

Figure 2: General combination approach after reconstruction at the level of datum-free NEQs for a multi-frequency band CRF. ST = station coordinates, E/EOPs = Earth orientation parameters, SO = source positions.

3. RESULTS AND OUTLOOK

In a first step, a datum-free monolithic NEQ system based on daily sessions data from GSFC was generated. About 4000 single SINEX files were used and stacked together. The resulting monolithic NEQ system contained 1682 global source positions including all 295 ICRF2 defining sources. The small number of sources is owed to the fact that only sources with at least 3 good observations in each session were set up. Furthermore, to facilitate our intial combination investigations, the special handling sources had been parameterized as global parameters as well. In a next step the properties of the reconstructed monolithic X/Ka-band NEQ was analysed. The contribution is composed of 631 sources including 208 of 295 defining sources. Consequently, all 208 defining sources can be used as link sources. All in all, 443 of the 631 X/Ka-band sources are existent in the generated S/X-band contribution and can be used as link sources. Approximately 65% of the 188 sources which are only existing in the X/Ka-band contribution are located in the southern celestial hemisphere. For our initial combination results we fixed the S/X-band station coordinates and applied an NNR condition to all 208 linking defining sources. Finally we obtained a combined S/X and X/Ka catalogue with 1870 sources and calculated the residuals by subtracting the combined catalogue minus the original X/Ka catalogue. In Fig. 3 the residuals of the 208 linking defining sources are illustrated. The results should only demonstrate the proper function of our initial multi-frequency CRF combination. The variations of the residuals match the expectations with no significant systematics recognizable except for the far southern sources. Here we can see some slightly bigger residuals pointing in similar directions.

Summarizing, a combination approach for a S/X and X/Ka dual frequency CRF generation has been presented in this paper. The underlying combination mechanism and the most important steps have been described and illustrated. Based on the gained achievements further investigations need to be focused on. For example, the non-ITRF observing sites, the core shift and the parameterization of special handling sources as arc parameters need to be looked at.

4. REFERENCES

Iddink, A., Nothnagel, A., Artz, T., 2014a, "Rigorous VLBI Intra-Technique Combination For Upcoming CRF Realizations", In: Proc. Journées 2013 "Systèmes de Référence Spatio-Temporels", N. Capitaine (ed.), Observatoire de Paris, pp. 81–83.

Iddink, A., Artz, T., Nothnagel, A., 2014b, "Development of a Combination Procedure for Celestial Reference Frame Determination", In: IAG Symposia, 143, in print.

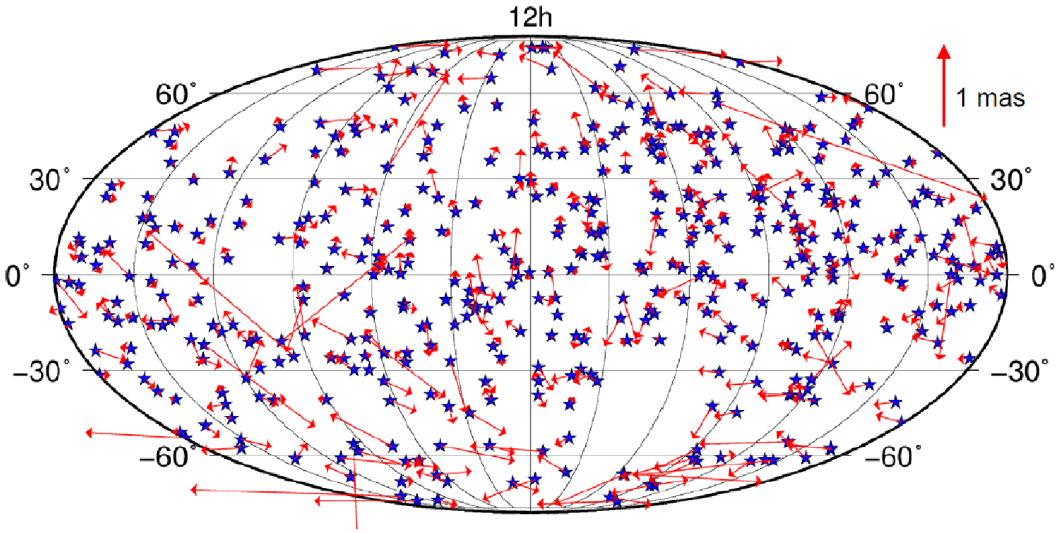

Figure 3: Initial results of a combined S/X and X/Ka catalogue. Residuals of the combined catalogue minus the original X/Ka catalogue of all linking defining sources.

Jacobs, C.S., Bach, U., Colomer, F., Garcia-Miro, C., Gomez Gonzalez, J., Gulyaev, S., Horiuchi, S., Ichikawa, R., Kraus, A., Kronschnabl, G., Lopez-Fernandez, J.A., Lovell, J., Majid, W., Natusch, T., Neidhardt, A., Phillips, C., Porcas, R., Romero-Wolf, A., Saldana, L., Schreiber, U., Sotuela, I., Takeuchi, H., Trinh, J., Tzioumis, A., de Vincente, P., Zharov, V., 2012, "The Potential for a Ka-band (32 GHz) Worldwide VLBI Network", IVS 2012 General Meeting Proc., pp. 194–198.

Jacobs, C.S., et al., 2014, "ICRF-3: Roadmap to the Next Generation ICRF", In: Proc. Journées 2013 "Systèmes de Référence Spatio-Temporels", N. Capitaine (ed.), Observatoire de Paris, pp. 51–56.

Fey, A.L., Gordon, D., Jacobs, C.S. (eds.), 2009. "The second realization of the international celestial reference frame by very long baseline interferometry: Presented on behalf of the IERS/IVS Working Group", A.L. Fey, D. Gordon, C.S. Jacobs (eds.), IERS Technical Note 35, Verlag des Bundesamtes für Geodäsie und Kartographie, Frankfurt am Main.

COMPARISON OF ASTROMETRIC CATALOGUES UCAC4, XPM, PPMXL

V. VITYAZEV, A. TSVETKOV
Saint-Petersburg State University
198504 Petrodvorets, Universitetsky pr., 28., St. Petersburg, Russia
e-mail: vityazev@list.ru, A.S.Tsvetkov@inbox.ru

ABSTRACT. We declare the first results of the representation of the differences between the proper motions UCAC4-PPMXL, XPM-UCAC4 and XPM-PPMXL by vector spherical harmonics in the 10 to 16 J mag range (2MASS photometric system). It was found that the PM systematic differences vary from - 15 to 15 mas/y. The proper motion XPM catalogue has the least systematic deviation from the PPMXL and UCAC4 for stars fainter J=13. The values of spin for UCAC4 on PPMXL are 5 times less than values for XPM on PPMXL and UCAC4. Magnitude equation is clearly seen through dependence of the decomposition coefficients and mutual spins on J magnitude. The influence of low order vector spherial harmonics on the determination of the Ogorodnikov-Milne coefficients is clarified.

1. INTRODUCTION

The pre-GAIA modern astrometric catalogues UCAC4 (Zacharias, et al., 2013), PPMXL (Roeser, et al., 2010) and XPM (Fedorov, et al., 2009) with full coverage of the sky provide a qualitatively new material for investigations in various fields of astronomy. At present, the largest catalogue of positions and proper motions is PPMXL. It contains about 900 million objects and is full from the brightest stars down to magnitude V=20 with absolute proper motions in the ICRS reference frame. The mean errors of the proper motions range from 4 mas/y to 10 mas/y. The accuracies of positions are estimated to be 80-120 mas (at epoch 2000.0). The UCAC4 is an all-sky catalogue containing about 113 million stars covering the 8 to 16 magnitude range in a single bandpass between V and R. The positional accuracy of stars in UCAC4 at mean epoch is about 15-100 mas per coordinate, the formal errors in PMs range from about 1 to 10 mas/y depending on magnitude. Systematic errors in PMs are estimated to be about 1-4 mas/y. The UCAC4 may be considered complete to R=16. It contains accurate positions and proper motions on the ICRS at a mean epoch 2000. The XPM catalogue (2009) combines data from the 2MASS and USNO-A2.0 catalogues in order to derive the absolute proper motions of about 280 million stars distributed all over the sky excluding a small region near the galactic centre, in the magnitude range $12^m < B < 19^m$. The proper motions were derived from the 2MASS Point Sources and USNO-A2.0 catalogue positions with a mean epoch difference of about 45 years for the Northern hemisphere and about 17 years for the Southern one. The generated catalogue contains the ISRS positions of stars for the J2000 epoch, original absolute proper motions, as well as B, R, J, H and K magnitudes. The proper motion errors vary from 3 to 10 mas/y, depending on a specific field. The zero-point of the absolute proper motion frame (the absolute calibration) was specified with more than 1 million galaxies from 2MASS and USNO-A2.0

The PPMXL and UCAC4 realize the reference frames which do not rotate with respect to the quasars, whereas the XPM frame is claimed to be free of rotation with respect to galaxies. Theoretically, both quasars and galaxies form the quasi-inertial reference systems but due to different techniques of measurement the resulting reference frames may differ systematically. The main goal of this paper is to calculate the systematic differences in proper motions and to evaluate the mutual rotation of the frames under consideration.

2. MODELING AND ANALYSIS OF THE SYSTEMATIC DIFFERENCES

For the first time, the representation of systematic differences in positions and proper motions of stars by orthogonal functions was proposed by Brosche (1966). The modification of this approach based on functions “Legendre-Hermite-Fourier” (Bien, et al., 1978) became the standard tool for the coomparison

the RA and DEC systems of astrometric catalogues prior to Hipparcos. The two-dimensional vector spherical harmonics (henceforth VHS) were proposed by Mignard (Mignard and Morando, 1990; Mignard and Froeschle, 2000) to derive the systematic differences between Hipparcos and FK5. Further extensive study of this technique aiming at its application in the GAIA project may be found in (Mignard and Klioner, 2012). The three-dimensional kinematic study of proper motions and radial velocities with vector spherical harmonics was developed by Vityazev and Tsvetkov (2014).

In this paper we calculate the systematic differences using the notations of our works on kinematic study of the proper motions with vector spherical harmonics (Vityazev and Tsvetkov, 2009, 2014). The following steps have been done. First of all, by the cross identification of stars within J photometric band (2MASS photometric system) the list of 41 316 676 common stars in the J 10-16 range have been compiled for our catalogues. After that the differences $\Delta\mu_l \cos b$ and $\Delta\mu_b$ for stars belonging to each of 1200 HealPix (Gorski, et al., 2005) areas have been calculated and their means were assigned to the centers of the areas. In this way the differences PPMXL-UCAC4, XPM-UCAC4 and XPM-PPMXL were formed in the J magnitude bins 10-12, 12-14 and 14-16. The ranges of the mean values $\Delta\mu_l \cos b$ and $\Delta\mu_b$ are shown in Fig. 1 from which we may conclude that for stars fainter 13^m the differences of all the catalogues vary within almost the same range, whereas for brighter stars the deviation of the XPM from PPMXL and UCAC4 exceeds the range of PPMXL–UCAC4 by factor 2 or 3.

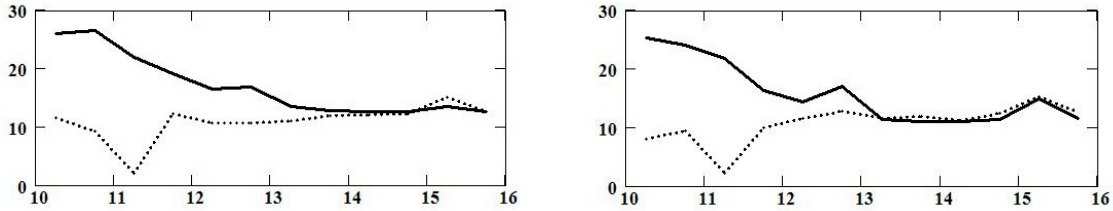

Figure 1: Range of the systematic differences $\Delta\mu_l \cos b$ (left) and $\Delta\mu_b$ (right) as function of magnitude. Solid line – ((XPM-UCAC4)+(XPM-PPMXL))/2; dots – (PPMXL-UCAC4). Units mas/y.

At the second step the representation of the pixel's mean values with vector spherical harmonics was done according to equation

$$\Delta\mu_l \cos b\mathbf{e}_l + \Delta\mu_b\mathbf{e}_b, = \sum_{nkp} t_{nkp}\mathbf{T}_{nkp} + \sum_{nkp} s_{nkp}\mathbf{S}_{nkp}, \tag{1}$$

where $\mathbf{e}_l$ and $\mathbf{e}_b$ are the unit vectors in the directions of the longitude and latitude in a plane tangential to the sphere. Consequently, the toroidal (magnetic) $\mathbf{T}_{nkp}$ and spheroidal (electric) $\mathbf{S}_{nkp}$ vector harmonics are derived from the scalar vector harmonic $K_{nkp}(l, b)$ according to formulae

$$\mathbf{T}_{nkp} = \frac{1}{\sqrt{n(n+1)}}\left(\frac{\partial K_{nkp}(l,b)}{\partial b}\mathbf{e}_l - \frac{1}{\cos b}\frac{\partial K_{nkp}(l,b)}{\partial l}\mathbf{e}_b\right), \tag{2}$$

$$\mathbf{S}_{nkp} = \frac{1}{\sqrt{n(n+1)}}\left(\frac{1}{\cos b}\frac{\partial K_{nkp}(l,b)}{\partial l}\mathbf{e}_l + \frac{\partial K_{nkp}(l,b)}{\partial b}\mathbf{e}_b\right). \tag{3}$$

The expansion coefficients t_{nkp} and s_{nkp} and their root-mean-square errors (rmse) can be derived from the equation (1) by the standard least-squares procedure. The total number of decomposition terms can be chosen with statistical criteria (Brosche, 1966; Mignard and Klioner, 2012). The full description of the VSH notations may be found in (Mignard and Morando, 1990).

We calculated the expansion coefficients for the PM differences in J mag bins 10-12, 12-14, 14-16. The results up to n=2 are shown in Table1 for PPMXL-UCAC4 and XPM-PPMXL. Obviously, to compare XPM and UCAC4 one may calculate (XPM-UCAC4)=(XPM-PPMXL)+(PPMXL-UCAC4).

To see how different the proper motions tied to quasars or galaxies may be, we introduce the mutual spin $\Omega = \sqrt{\omega_x^2 + \omega_y^2 + \omega_z^2}$, where the components of the spin $\omega_x, \omega_y, \omega_z$, of one reference frame on another are connected with the first order coefficients of their systematic differences expansion on VSH by the relations (Mignard and Morando, 1990; Vityazev and Tsvetkov, 2009): $t_{101} = 2.89\omega_z$, $t_{110} = 2.89\omega_y$, $t_{111} = 2.89\omega_x$. The dependence of the coefficients t_{101}, t_{110}, t_{111} on magnitude is shown in Fig. 2. Here

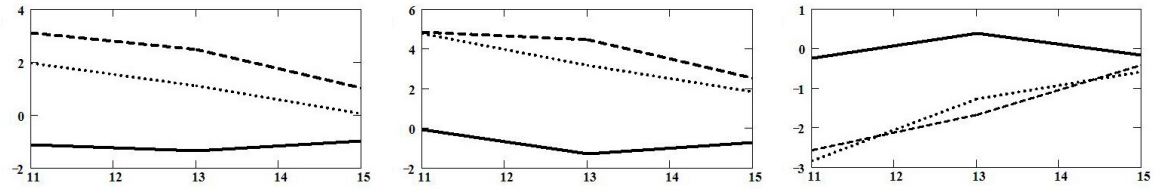

Figure 2: Toroidal coefficients via magnitude. Left to right: t_{101}, t_{110}, t_{111}. Solid line – (PPMXL-UCAC4); dots – (XPM-UCAC4); dashes – (XPM-PPMXL). Units: mas/y.

	$10-12^m$	$10-12^m$	$12-14^m$	$12-14^m$	$14-16^m$	$14-16^m$
	$PPMXL-$ $-UCAC4$	$XPM-$ $-PPMXL$	$PPMXL-$ $-UCAC4$	$XPM-$ $-PPMXL$	$PPMXL-$ $-UCAC4$	$XPM-$ $-PPMXL$
t_{101}	$-1,13$	$3,09$	$-1,37$	$2,48$	$-0,98$	$1,02$
t_{110}	$-0,07$	$4,85$	$-1,29$	$4,47$	$-0,72$	$2,53$
t_{111}	$-0,25$	$-2,58$	$0,39$	$-1,67$	$-0,18$	$-0,41$
t_{201}	$-0,32$	$0,08$	$0,23$	$-0,37$	$0,38$	$-0,29$
t_{210}	$-0,35$	$-0,03$	$-1,40$	$0,89$	$-1,54$	$0,38$
t_{211}	$0,21$	$0,64$	$0,56$	$0,15$	$0,01$	$0,51$
t_{220}	$1,39$	$-0,88$	$2,38$	$-1,81$	$2,39$	$-1,20$
t_{221}	$0,19$	$-0,72$	$0,76$	$-0,62$	$0,65$	$-0,40$
s_{101}	$-1,26$	$2,15$	$-1,44$	$1,10$	$-2,29$	$1,37$
s_{110}	$-2,58$	$0,64$	$-2,90$	$0,96$	$-4,17$	$1,94$
s_{111}	$-0,89$	$0,72$	$-1,05$	$1,57$	$-0,18$	$1,35$
s_{201}	$-0,22$	$-0,66$	$0,45$	$-0,66$	$0,44$	$-0,79$
s_{210}	$-0,67$	$1,42$	$-1,32$	$1,67$	$-1,31$	$1,62$
s_{211}	$-0,50$	$0,57$	$-0,78$	$0,37$	$-0,63$	$0,12$
s_{220}	$0,51$	$-1,39$	$0,81$	$-1,40$	$0,94$	$-1,49$
s_{221}	$0,19$	$-0,26$	$0,88$	$-0,88$	$1,24$	$-0,98$
σ	$\pm 0,10$	$\pm 0,21$	$\pm 0,12$	$\pm 0,14$	$\pm 0,14$	$\pm 0,15$

Table 1: Toroidal and spheroidal coefficients of the proper motion systematic differences representation on VSH. Units: mas/y. The last row - rmse of the coefficients.

	10-12	12-14	14-16
PPMXL-UCAC4	0.40 ± 0.04	0.67 ± 0.04	0.43 ± 0.05
XPM-PPMXL	2.18 ± 0.07	1.86 ± 0.05	0.95 ± 0.05
XPM-UCAC4	2.04 ± 0.07	1.25 ± 0.04	0.66 ± 0.05

Table 2: Spin of mutual rotation. Units: mas/y.

one can see that the XPM does rotate on the PPMXL and UCAC4 faster than the UCAC4 rotates on the PPMXL. Moreover, using our VSH coeficients we can estimate the value of mutual spin of our catalogues (Table 2). From this Table we see that small mutual spin may be found for UCAC4 and PPMXL. In other words, the proper motions of both the catalogues being tied to quasars have but small mutial rotation. Quite opposite situation we see for XPM with respect to PPMXL and UCAC4 since the mutual spins XPM-PPMXL and XPM-UCAC4 are sufficiently large. Naturally, this is a consequance of the different obervational techniques used to derive the absolute proper motions by tying them to galaxies and quasars.

3. STELLAR KINEMATICS

The connection of low order VSH coefficients of the PMs decomposition with the Ogorodnikov-Milne coefficients is clarified in (Vityazev and Tsvetkov, 2009). In particular, the coefficients s_{210}, s_{211}, s_{220} (Fig. 3) are connected with the elements of the deformation tensor by expressions $s_{210} = 2.24 M_{23}^{+}$,

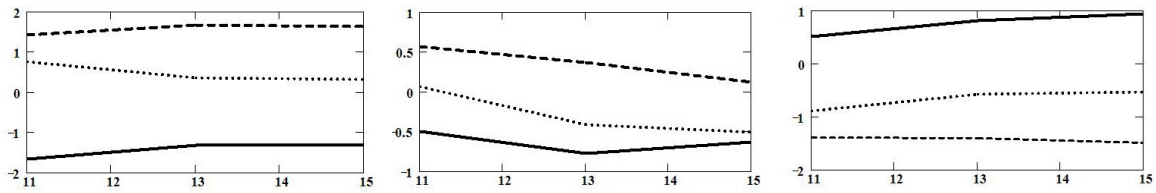

Figure 3: Spheroidal coefficients via magnitude. Left to right: s_{210}, s_{211}, s_{220}. Solid line – (PPMXL-UCAC4); dots – (XPM-UCAC4); dashes – (XPM-PPMXL). Units: mas/y.

$s_{211} = 2.24M_{13}^{+}$, $s_{220} = 2.24M_{12}^{+}$. For this reason, the VSH coefficients of the PM systematic differences may be used for directly reducing a kinematic parameter from the system of one catalogue to the system of another catalogue. For example, the mean PPMXL-UCAC4 coefficients $t_{101} = -1.16 \pm 0.07$ and $s_{220} = 0.75 \pm 0.07$ mas/y yield the differences of the Oort constants $\Delta B = -1.90 \pm 0.11$ and $\Delta A = 1.59 \pm 0.15$ km/s/kpc, which is confirmed by direct evaluation of these parameters provided the same list of stars was used.

4. MAGNITUDE EQUATION

General analysis of the VSH coefficients in proper motions reveals rather strong magnitude equation. It may be seen, for example, in Figs. 1–3. The rigorous description of the magnitude equation requires introduction of additional basic functions which will be done elsewhere.

Acknowledgements. This work was done with support of the St. Petersburg University Grant 6.0.161.2010.

5. REFERENCES

Bien, R., Fricke, W., Lederle, T., Schwan, H., 1978, "Methods for the Comparison of Systems of Star Positions to BE Applied in the Construction of the FK5", Veröf. des Astron. Rechen-Inst. Heidelberg, Nr. 29.

Brosche P., 1966, "Representation of systematic differences in positions and proper motions of stars by spherical harmonics", Veröf. des Astron. Rechen-Inst. Heidelberg, Nr. 17.

Fedorov, P.N., Myznikov, A.A, Akhmetov, V.S., 2009, "The XPM Catalogue: absolute proper motions of 280 million stars", MNRAS, 393, pp. 133–138.

Gorski, K.M., Hivon, E., Banday, A.J., Wandelt, B.D., Hansen, F.K., Reinecke, M., Bartelmann, M., 2005, "HEALPix: A Framework for High-Resolution Discretization and Fast Analysis of Data Distributed on the Sphere", ApJ, 622(2), pp. 759–771.

Mignard, F., Froeschle, M., 2000, "Global and local bias in the FK5 from the Hipparcos data", A&A, 354, p. 732–739.

Mignard, F., Morando, B., 1990, "Analyse de catalogues stellaires au moyen des harmoniques vectorielles". Journées 1990: Systemes de reference spatio-temporels, pp. 151–158.

Mignard, F., Klioner, S., 2012, "Analysis of astrometric catalogues with vector spherical harmonics", A&A, 547, A59.

Roeser, S., et al., 2010, "The PPMXL Catalog of positions and proper motions on the ICRS. Combining USNO-B1.0 and 2MASS", AJ, 139(6), pp. 2440–2447.

Vityazev, V.V., Tsvetkov, A.S., 2009, "Analysis of the three-dimensional stellar velocity field using vector spherical functions", Astron. Lett., 35(2), pp. 100–113.

Vityazev, V.V., Tsvetkov, A.S., 2014, "Intercomparison of kinematics derived from catalogues UCAC4, PPMXL and XPM with vector spherical harmonics", MNRAS, 442, pp. 1249–1264.

Zacharias, N., et al., 2013, "The Fourth US Naval Observatory CCD Astrograph Catalog (UCAC4)", AJ, 145, 44.

SOME COMMON PROBLEMS IN GEODESY AND ASTROMETRY AFTER ESTABLISHMENT OF ICRF

V.V. POPADYOV[1], S.A. TOLCHELNIKOVA[2]
[1] Centre de géodésie et cartographie (CNIIGAiK)
Onezhkaya, 26, Moscow, Russia
e-mail: azyas@mail.ru
[2] Central Astronomical Observatory at Pulkovo of the Russian Academy of Sciences
Pulkovskoe shosse, 65, 196140 St. Peterburg, Russia
e-mail: stolchelnikova@gmail.ru

ABSTRACT. After the "revolution in astrometry" on the eve of XXI century radio frame ICRF and triad ICRS were established as the main reference for astronomy and sciences connected to it, e.g. geodesy and gravimetry. During previous years stars were used as reference points and unity of the sciences was achieved by means of using the plumb lines as terrestrial reference. The expansion of this terrestrial frame to vertical lines at many places has been one of the purposes of geodetic measurements. We consider very useful empirical unity of three branches of the one indivisible science should be preserved. Mutual dependence to each other is secured in modern geodesy and gravimetry, and up to now some parameters used or got in geodesy, are common with those used in gravimetry, astronomy and geodynamics. We discuss several problems in connecting geodetic and gravimetric observations with radio observations used for the compilation of the ICRF in order to attract the attention of experts in optical and radio astrometry.

1. INTRODUCTION

Proving the necessity of recognizing radiosystem as the International reference system, astronomers used the following arguments:

(i) the accuracy of the measurements in the radio range already achieved, is unattainable to optical observations;

(ii) the use of reference radioobjects are located at extragalactic distances, therefore the possibility to find the proper motions of reference radiosources will be unnoticed for a long time. (Walter and Sovers, 2000, p. 137). Some authors even suggest the epoch of observations of reference radiocatalogues might be not fixed in future (Feissell and Mignar, 1998, p. L35; Walter and Sovers, 2000, p. 137);

(iii) the possibility of observations in any weather and low value of radiorefraction in the Earth's atmosphere (in the opinion of the authors of the monograph (Gubanov et al., 1983, pp. 30–38) it does not exceed $0.01''$ and will decrease with the increase of the interferometer base), is also the privilege of the point like extragalactic sources.

The consequences of displacing the traditional optical frame for the radio one are not widely discussed. We believe that it is advisable to consider the influence of the transition to the geodesy and gravimetry, where the unsolved problems and questions have already appeared. At first we remained the method of the radio reference frame establishing and the new distribution of problems between the optical and radio astrometry.

2. ON THE METHOD OF ICRF ESTABLISHING AND THE NEW DISTRIBUTION OF PROBLEMS IN ASTROMETRY

The measurements of angular differences between radiosources are not sufficient for deriving their spherical coordinates, two points with already known spherical coordinates, are needed as the zero-points of a frame. As soon as the large circle passing through one of the points, is obtained the pole in 90 degree from it is found. The third point on the sphere will appear when the required center of the triad is found, it gives the origin of directions to the objects with the known distances as well as to the images of infinitely distant bodies.

On the necessity to distinguish the spherical coordinate system with an uncertain position of center from Cartesian system with fixed position of its origin center is written in Tolchelnikova (2009). Triad may be associated with the Sun or planet's centers, of the places of observation on the Earth's surface and in the future also the instruments' places on the Moon, Mars, etc. When the origin is changed the spherical coordinates of the stars will change, but the changes of the distances to the origin of celestial sphere is impossible to consider.

Although historically the solution of the coordinate problem began with the establishment the two spherical coordinate systems (frames), with one common zero-point, the spherical radiosystem ICRF was established simultaneously with the Cartesian triad ICRS with the origin at the barycenter of the Solar system. Since the information obtained from arc observations is not sufficient, to establish radioframe two the zero-points were accepted: equator of the catalog FK5 (mean observation epoch 1991.25) and dynamic equinox (standard epoch J2000.0). Three axes of ICRS were defined: x axis is directed to a point with coordinates $\alpha = 0^h$, $\delta = 0^\circ$, y axis is directed to point $\alpha = 6^h$, $\delta = 0^\circ$, and z axis is directed to the pole $\delta = 90^\circ$. There is neither star nor quasar in these points.

Walter and Sovers (2000) write that "other designations should be taken in the ICRS to distinguish these coordinates from the standard catalog FK5. Such a change of notation, of course, was not held to preserve continuity in the customary practice" (Walter and Sovers, 2000, p. 142). Saving of the names cannot guarantee continuity, but we agree that the continuity with the fundamental catalog has been achieved for the epoch of the establishment of the radioframe.

The point of view on the "longevity" of quasar coordinate system became the common opinion, and therefore the solution of fundamental problems has been entrusted with the positional radioastronomy (radioastometry). Absolute concord in some questions is not achieved. For example, V.V. Vityazev writes about the system ICRS, which the directions of the coordinate axes fixed in space once and for ever and no changes will be allowed (Finkelstein et al., 2001, p. 95). Walter and Sovers (2000) believe that soon or later some small corrections might be need for "maintaining" of directions of the axes of established radiosystem. They call the coordinate system ICRS revolutionary because "for the first time in the history of a common celestial coordinate system is no longer connected with equinox and ecliptic plane" (Walter and Sovers, 2000, p. 165).

Based on the fact that the radiosystem is recognized as the main reference, which has international status, new distribution of problems is discussed in the papers of our fellow citizens as the perspectives for the development of astrometry designed by IAU. Their plenary papers presented to the conference "Astrometry, geodynamics and celestial mechanics on the threshold of the XXI century" were published in Finkelstein et al. (2001).

3. THE INFLUENCE OF DISPLACING THE OPTICAL REFERENCE COORDINATE SYSTEM FOR RADIOSYSTEM ON GEODESY AND GRAVIMETRY

As is known, in the XX century we distinguished three relatively independent sciences of the indivisible one: astrometry, geodesy and gravimetry. They solved their own and common fundamental problems, e.g. determination of terrestrial coordinate system and the Earth rotation.

Using the coordinates of International catalog of stars and now quasars does not solve the problem of establishing terrestrial system. In the traditional method the solution was provided that astrometry, geodesy and gravimetry had the common empirical foundation – their observations were based on vertical directions in the places of observations. Astronomers performed fundamental (absolute) observations and the observers of Earth rotation services, beginning with the ILS and BIH, were tied to plumb line, or to mercury horizon depending on the instrument they used. The coordinate system of fundamental star catalogs FK5 was expanded by relative method to larger number of stars, including those of the Catalog of geodetic stars.

The established optical frame CRF with the coordinates of over one hundred thousand stars was used as a celestial reference in astro-geodetic observations and plumb-lines in many points of the Earth as the terrestrial reference. The CRF with the moving equator and equinox was of practical importance e.g. for navigation up to XX century.

On the eve of the XX century the zero-points of terrestrial reference were accepted: the prime meridian of Greenwich observatory and the mean pole of the epoch, later replaced by Conventional International Origin (CIO). The new zero-points for longitude λ and latitude ϕ were needed for practice and to obtain the rotation of the Earth axis relative to CRF. The terrestrial reference based on the vertical directions has no center since the plumb-lines do not intersect in one point. Therefore to complete the foundation

of the triad TRS is impossible without geodetic and gravimetric observations.

Studies of the figure of the Earth are performed in geodesy. Plumb-lines were used in order to measure their deviations from the normal directions to reference-ellipsoid for the purpose of obtaining the orientation of reference-ellipsoid and to establish geoid. Besides the two coordinates on the surface, one altitude coordinate is measured in many points to establish geoid.

For studies by means of dynamic methods we need the centers of masses of bodies. The methods of gravimetry permit to measure the gravitational deviations from vertical lines in the direction of the lines and from normals to reference ellipsoid to obtain the center of the Earth mass. It became the origin of TRS with terrestrial zero-points. Directions of the plumb-lines were common with those of the celestial frame CRF.

Thus the empirical unity of astrometry, geodesy and gravimetry was achieved by means of common celestial and terrestrial reference for observations of stars, the Sun, the Motion and planets. The results of geodesy and gravimetry, in turn, were used in astronomy, celestial mechanics, geodynamics, astrophysics and geology.

Radical changes during the "revolution in astrometry" (Walter and Sovers, 2000) were due to technical achievements, new techniques of observations and atomic clocks. Technology of GPS/GLONASS with the support of calculated ephemerides of satellites permits to obtain the coordinates and velocities of terrestrial points with precision, satisfying the civil users "within a certain period". The positions of points are connected to the Earth mass center, thereby the possibility of using dynamic methods is provided now.

When the GNSS (Global Navigation Satellite Systems) methods have appeared geodesy became less dependent on astrometry: the methods of geometrical positioning solved the Earth figure determination. The problem remains of verifying the appropriate physical characteristics of gravitation field, in particular the deflection of plumb-lines anomalies. A plumb-lines rotation ($\Delta\xi$, $\Delta\eta$) should be monitored by independent physical methods. Since astronomical latitude and longitude are not available any more no variations of plumb lines $\Delta\xi$ag, $\Delta\eta$ag are fixed to control gravity variations $\Delta\xi$gr, $\Delta\eta$gr and unless the updating of gravimetric field near the Earth surface is possible, technology of satellite gradiometry cannot submit a detailed field near the Earth surface. There are no clear solutions of astroorientation for areal and satellite surveys and determination of astronomical azimuths for ballistics starts.

Taking into account the impossibility to mount radio telescopes at the points of astro–geodetic net or points of GPS/GLONASS observations, we must ask: How should geodesy use ICRF?

The three mentioned sciences still need periodic reference to the celestial coordinate to ensure the possibility of obtaining secular and long periodic motions. Is it available in the case when celestial observations are not related to vertical lines? It seems that modern astronomers do not foresee mutual benefits of cooperation with geodesy and gravimetry. TRF with the new zero points on celestial sphere has neither origin, no directions to terrestrial points, nevertheless it is supposed to be used for establishment of the ITRF with the origin in center of the Sun or barycenter. Of cause, there is no possibility to observe from these points and from the Earth center, but evidently neither geodetic nor gravimetric methods could be ever used in measurements of the Sun or barycenter. Only the Solar disk is observable, to obtain the barycenter one needs the theory of orbital motions of planets.

The difficulties in linking of ITRS to ICRS using the modern numeral models reflected in IAU resolutions, are shown in Tolchelnikova (2009). The link is more complicated now due to increasing number of parameters in dynamic models, as a result the number of independent equations of conditions became less than the number of unknowns. In this case the system of equations is insoluble i.e. the solution of the system by means of precise methods of mathematics is impossible.

4. ON ESTIMATING ERRORS OF RADIOSYSTEM ICRF

Since ICRF is suggested as a reference for geodetic measurements we are interested in the precisions of radio coordinates. The process of compilation of radiocatalogues and the sources of their errors are described in several papers published by A.A. Lipovka and N.M. Lipovka, e.g., in Lipovka and Lipovka (2013a, 2013b). One of conclusions of the authors is that there are more radiostars in comparison with those, already known. It becomes evident that the "problem of empty fields" would have been eliminated if the experience of optical catalogues compilations were taken into account.

The author reduced the coordinates of radiosources to the system of star catalogue of Palomar Sky Survey and constellations of radiosources coincidences with the bright star images on the fields of $1^\circ \times 1^\circ$, was evident and analyzed by the authors. Previously it was supposed that there are no stars on the fields

or 1–2 coincidences of stellar and radio images, which might be the accidental ones.

We have no place in this presentation for explanations of the results and several sources of errors. One of the new suggestions is eliminated since it became evident that it is not only our Sun but the other "yellow dwarfs" also emit radio waves. We should say that theoretical astrophysicists and physicists are reviled from explanations of the one more "paradox of Nature". The large errors in radiocatalogues shown by the authors might be regarded as the local errors of radiocatalogues due to the impossibility of achieving the same stability of mounting the radiotelescopes as optical instruments. In the last case the continual daily check on orientation of the optical axis of the telescope was provided.

To astrometry is important that some of the radiosources analyzed by the authors, previously considered as quasars, appear to be the bright stars. If it will be confirmed from analysis of more fields, we might ask: What preference remains for the quasars in comparison to the stars if the former are situated in our Galaxy?

5. CONCLUSIONS

Some experts in geodesy take care for preserving the empirical unity not only with gravimetry but also with astronomy as it becomes clear from the their papers in Brovar (2010). B.V. Brovar writes about coming years when geodesy should master the new scientific gift from astronomy and connect the created geodetic net to ICRS which is eager to break off the connection with equator and ecliptic (Brovar, 2010, p. 13).

The former empirical unity of the mentioned sciences was destroyed during the "revolution in astrometry" (Walter and Sovers, 2000), and we may ask whether something equivalent to it has been proposed.

It is well known separation of sciences is not fruitful for their development (Tolchelnikova, 2011). Remember the IAU Resolution about unification of several commissions which was realized. We suppose the Journées will give opportunity for discussion of many problems in scientific field of sciences about the measurements on the Earth and from our planet together with the historians of science interested in the topic.

6. REFERENCES

Brovar, B.V. (ed.), 2010, "Gravimetry and geodesy", Moscow: Nauchny Mir, 570 pp. (in Russian)

Feissell, M., Mignar, F., 1998, "The adoption of ICRS on 1 January 1998: meaning and consequences", A&A, 331, pp. L33–L136.

Finkelstein, A.M., et al. (eds.), 2001, "Astrometry, geodynamics and celestial mechanics on the threshold of XXI century", Transactions of IAA, v. 6. (in Russian)

Gubanov, V.S., Finkelshtein, A.M., Fridman P.A., 1983, "Introduction to radioastrometry", Moscow: Nauka, 280 pp. (in Russian)

Lipovka, A.A., Lipovka, N.M., 2013a, "Radio emission from the galactic cluster A1716 and a group of stars", Astrophysics, 56(2), pp. 221–228.

Lipovka, A.A., Lipovka, N.M., 2013b, "Problem of connecting the radio and optical systems. History and perspectives". Geodesy and cartography, No. 10, pp. 2–7. (in Russian)

Tolchelnikova, S.A., 2009, "On collaboration of astrometry and geodesy in studies of Earth rotations". Geodesy and Cartography, No. 8, pp. 24–29. (in Russian)

Tolchelnikova, S.A., 2011, "The role of classical heritage for fundamental studies". Geodesy and Cartography, No. 8, pp. 2–8. (in Russian)

Walter, H.G., Sovers, O.J., 2000, "Astrometry of Fundamental Catalogues: The Evolution from Optical to Radio Reference Frames", Heidelberg: Springer–Verlag, 232 pp.

GALACTIC COORDINATE SYSTEM BASED ON MULTI-WAVELENGTH CATALOGUES

P.-J. DING[1,2], J.-C. LIU[1,2], Z. ZHU[1,2]
[1] School of Astronomy and Space Science, Nanjing University, Nanjing 210046, China
[2] Key Laboratory of Modern Astronomy and Astrophysics (Nanjing University), Ministry of Education, Nanjing 210046, China
e-mail: dingpjlcj@163.com, jcliu@nju.edu.cn, zhuzi@nju.edu.cn

ABSTRACT. The currently used Galactic Coordinate System (GalCS) is based on the FK5 system at J2000.0, which was transformed from the FK4 system at B1950.0. The limitations and misunderstandings for this transformed GalCS is necessarily be avoided by defining a new GalCS connecting directly to the International Celestial Reference System (ICRS). We try to find the best orientation of the GalCS using data from two all-sky surveys: AKARI and WISE at six wavelengths between 3.4 μm to 90 μm, and synthesize results obtained at various wavelengths to define an improved GalCS in the framework of the ICRS. The revised GalCS parameters for defining the new GalCS in the ICRS are summarized as: $\alpha^{\rm p} = 192\overset{\circ}{.}777$, $\delta^{\rm p} = 26\overset{\circ}{.}9298$, for the equatorial coordinates of the north Galactic pole and $\theta = 122\overset{\circ}{.}95017$ for the position angle of the Galactic center. As one of the Galactic sub-structures, the Galactic warp presents different forms in different GalCS that are constructed with various data and methods, which shows the importance of re-defining a Galactic coordinate system by the IAU for better study of the Galactic structure and kinematics.

1. INTRODUCTION

The Galactic coordinate system (hereafter GalCS) is a practical coordinate system for studies of the Galactic structure, kinematics, and dynamics. The current GalCS adopted by the Hipparcos team is related to the J2000.0 FK5-based reference system (Murray 1989) which was transformed from its original IAU 1958 definition based on the FK4 reference system (Blaauw et al. 1960). Liu et al. (2011a) found that this transformed coordinate system is not an optimal one and it can also lead to misunderstandings. So a new GalCS directly related to the International Celestial Reference System (ICRS) is necessary. More recently, by adopting all-sky survey data from 2MASS in near-infrared band and SPECFIND v2.0 in radio band, Liu et al. (2011b, hereafter L11b) have updated the three parameters used to define the directions of axes of the GalCS in the equatorial system, namely $\alpha^{\rm p}$, $\delta^{\rm p}$, and θ, where ($\alpha^{\rm p}$, $\delta^{\rm p}$) is the equatorial coordinate of the north Galactic pole (NGP) and θ is the position angle of the Galactic center (GC). We note that there remains room for improvement in establishing a more proper GalCS. In this work, we use catalogues from latest all-sky surveys to revise the GalCS parameters.

2. DATA

As described in L11b, a well-defined GalCS should coincide with the feature of the Milky Way. An optimal GalCS means that the distribution of the Galactic sources on the celestial sphere is symmetric about the basic plane (i.e. $x - y$ plane) of the GalCS. It should be noted that the interstellar extinction prevents us to obtain a complete distribution of stars in the optical band. Thus large infrared catalogues are the most suitable data to find the position of the basic plane because the effect of extinction in long band is relatively weak. In this work, we use catalogues from the AKARI infrared all-sky survey (Murakami et al. 2007) and catalogues from Wide-field Infrared Survey Explorer (WISE) (Wright et al. 2010) to carry out following computations.

The AKARI survey provided catalogues in two bands centered at 9 μm and 90 μm respectively. We need to reject sources near the Sun by removing sources with high fluxes and abandon extragalactic sources with low fluxes or staying away from the Milky Way belt (e.g. the Large and Small Magellanic Cloud). Therefore we only selected sources between $\pm 15^\circ$ of latitude in the flux range from 0.101 Jy to 45 Jy in 9 μm band and sources within $\pm 6^\circ$ of latitude with fluxes between 0.46 Jy and 120 Jy in 90 μm

band. Figure 1 shows the distribution of selected sources observed at the two bands respectively. We can see clearly the Milky Way belt on the celestial sphere.

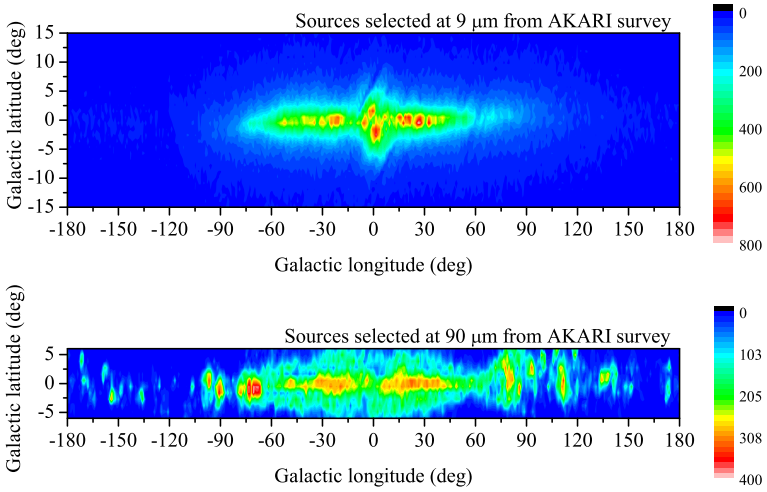

Figure 1: The distribution of sources selected from 9 μm and 90 μm observations of AKARI, respectively.

The WISE all-sky catalog contains positions and four-band (centered at 3.4 μm, 4.6 μm, 12 μm, 22 μm respectively) information of photometry. Like what we have done for AKARI data, we determine the magnitude ranges of selected WISE sources, which are such that $10 < m_{3.4\mu\mathrm{m}} < 14.8$, $9 < m_{4.6\mu\mathrm{m}} < 14.5$, $8.5 < m_{12\mu\mathrm{m}} < 12.4$, $5.5 < m_{22\mu\mathrm{m}} < 8.8$. We retain the data with $|b| < 25°$ in 3.4 μm band, $|b| < 20°$ in 4.6 μm band, $|b| < 4°$ in 12 μm band and $|b| < 3°$ in 22 μm band. For 12 μm and 22 μm bands, the selected sources are restricted within the longitude range from $-60°$ to $60°$.

3. CALCULATING GALCS PARAMETERS WITH DIFFERENT METHODS

Our purpose is to calculate the three parameters $(\alpha^{\mathrm{p}}, \delta^{\mathrm{p}}, \theta)$ for the GalCS orientation in the equatorial coordinate system. We can obtain the direction of NGP, the z-axis, by fitting the equation for the position of the basic plane of GalCS, to the distribution of chosen data. We can also adopt the direction of GC, i.e. the direction of the x-axis of the GalCS, using results from direct observations for the Sgr A*. To keep the orthogonality of the GalCS, we used two methods to find the orientation of the GalCS. The first method is to fix the z-axis of the GalCS from the LSQ method, and then to find the direction of the x-axis by adopting the position of Sgr A* at the GC (hereafter the z-fixed method). The second method, called x-fixed method is to fix the direction of the x-axis to the observed position of Sgr A* and then to determine the direction of the z-axis perpendicular to the x-axis with the survey data.

In the z-fixed method, we first fit the position of NGP. Figure 2 presents values for α^{p} and δ^{p} in six bands, associated with the results from the 2MASS (1.25 μm band) and the SPECFIND v2.0 catalogues (radio band) as provided by L11b. The differences between the values for both α^{p} and δ^{p} derived from different bands are at an order of 0.1°.

After calculating the mean values of α^{p} and δ^{p}, we obtain the position angle θ of GC (Sgr A*). The position of Sgr A* can be found in Reid & Brunthaler (2004). The new parameters based on the z-fixed method that define the orientation of the new GalCS in the ICRS are such that

$$\begin{aligned} \alpha^{\mathrm{p}}_{\mathrm{z-fixed}} &= 192\overset{\circ}{.}582, \\ \delta^{\mathrm{p}}_{\mathrm{z-fixed}} &= 26\overset{\circ}{.}8935, \\ \theta_{\mathrm{z-fixed}} &= 122\overset{\circ}{.}86216. \end{aligned} \tag{1}$$

In the x-fixed method, we fit the position angle η of the NGP (see Fig. 5 of L11b) to find an optimal z-axis. We obtained the best results for η for six wavelengths as shown in Fig. 3, associated with the values from 2MASS and SPECFIND provided by L11b.

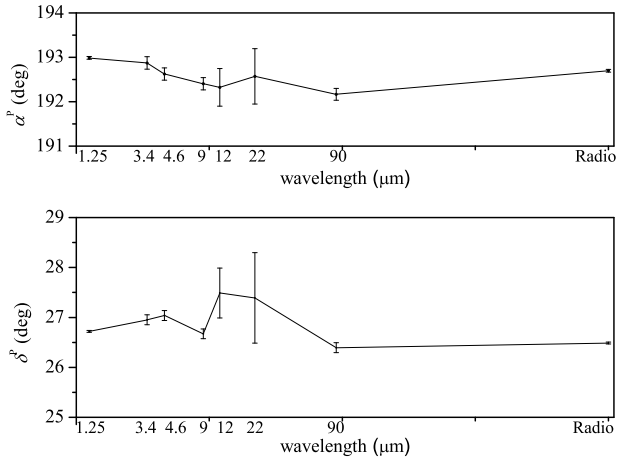

Figure 2: The values of $\alpha^{\rm p}$ and $\delta^{\rm p}$ fitted at different wavelengths with the z-fixed method.

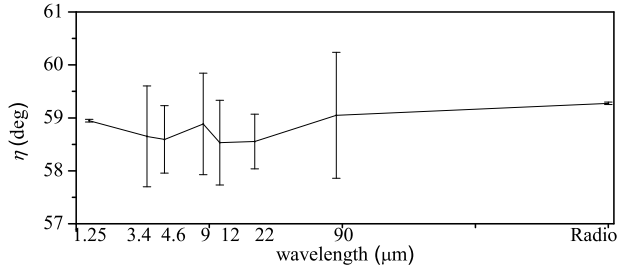

Figure 3: Values of η fitted in different bands with the x-fixed method.

We apply the mean value of η and the position of Sgr A* to obtain the revised values for GalCS parameters:

$$\begin{aligned} \alpha^{\rm p}_{\rm x-fixed} &= 192\overset{\circ}{.}777, \\ \delta^{\rm p}_{\rm x-fixed} &= 26\overset{\circ}{.}9298, \\ \theta_{\rm x-fixed} &= 122\overset{\circ}{.}95017. \end{aligned} \tag{2}$$

4. THE GALACTIC WARP IN DIFFERENT GALCS

The study of the typical form of the Galactic warp, a famous Galactic sub-structure, is closely related to the GalCS. We can analyze the effect of different GalCS on the study of the structure of the Milky Way by comparing the fitted warp parameters, the inclination angle $b_{\rm w}$ of the warp plane with respect to the Galactic plane and the Galactic longitude $l_{\rm w}$ of the intersecting line of two planes.

The data used to fit the warp plane is selected from Hipparcos O-B5 stars (Miyamoto & Zhu 1998). The results (in the GalCS derived from the x-fixed method) are shown in Fig. 4. (The GalCS related to 2MASS and SPECFIND are from L11b.) Both $b_{\rm w}$ and $l_{\rm w}$ change evidently with the Galactic wavelengths. This shows that an explicit and unitive definition of the GalCS is important for study the Galactic structures.

5. RECOMMENDATION ON THE NEW GALCS

The GalCS parameters derived from the z-fixed and x-fixed methods differ in an order of 0.1°. By comparing the two methods, we recommend results derived from the x-fixed method to be the new GalCS parameters, taking consideration of its lower uncertainty. The inclination of the revised basic plane with

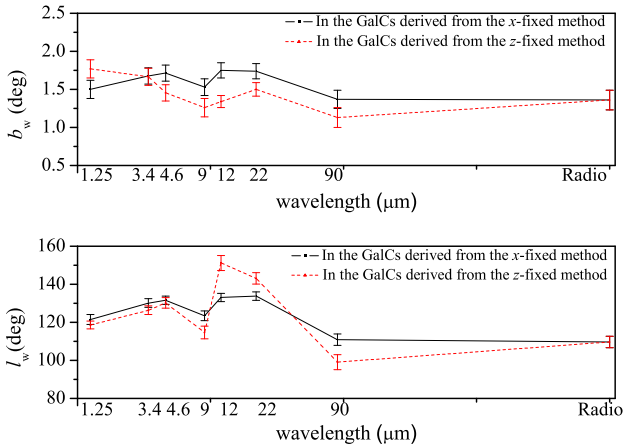

Figure 4: The warp parameters fitted in the GalCS in eight bands. Results in the GalCS derived from the x-fixed and z-fixed methods in each band are provided for comparison.

respect to the original basic plane is 0.2°. The numerical transformation matrix $\mathcal{N}$ from the equatorial to the Galactic coordinate system can be written as:

$$\mathcal{N} = \begin{pmatrix} -0.0546533401 & -0.8728440988 & -0.4849290583 \\ +0.4909257965 & -0.4463911532 & +0.7481489161 \\ -0.8694854080 & -0.1971753470 & +0.4528984519 \end{pmatrix}. \quad (3)$$

Though there exist several uncertainties, the newly established GalCS is closer to the feature of the Milky Way than the traditional one. The transformation definition based on IAU 1958 GalCS should be dropped and the new definition of the GalCS based on modern observations is possible.

6. REFERENCES

Blaauw, A., Gum, C.S., Pawsey, J.L., Westerhout, G., 1960, "The new I. A. U. system of galactic coordinates (1958 revision)", MNRAS, 121, 123.

Liu, J.-C., Zhu, Z., Zhang, H., 2011a, "Reconsidering the Galactic coordinate system", A&A, 526, A16.

Liu, J.-C., Zhu, Z., Hu, B., 2011b, "Constructing a Galactic coordinate system based on near-infrared and radio catalogs", A&A, 536, A102.

Miyamoto, M., Zhu, Z., 1998, "Galactic Interior Motions Derived from HIPPARCOS Proper Motions. I. Young Disk Population", AJ, 115, 1483.

Murakami, H., Baba, H., Barthel, P., et al., 2007, "The Infrared Astronomical Mission AKARI", PASJ, 59, 369.

Murray, C.A., 1989, "The transformation of coordinates between the systems of B1950.0 and J2000.0, and the principal galactic axes referred to J2000.0", A&A, 218, 325

Reid, M.J., Brunthaler, A., 2004, "The Proper Motion of Sagittarius A*. II. The Mass of Sagittarius A*", ApJ, 616, 872.

Wright, E.L., Eisenhardt, P.R.M., Mainzer, A.K., et al., 2010, "The Wide-field Infrared Survey Explorer (WISE): Mission Description and Initial On-orbit Performance", AJ, 140, 1868.

CORE SOURCES SET SELECTION

S.L. KURDUBOV, E.A. SKURIKHINA
Institute of Applied Astronomy of RAS
Kutuzov Quay 10, 191187 St.-Petersburg, Russia
e-mail: ksl@ipa.nw.ru, sea@ipa.nw.ru

ABSTRACT. In earlier work (Kurdubov & Skurikhina, 2009) we had suggested ranking method of sources sets in order to select the list of sources that better define the orientation parameters of rigid rotation transformation from one system to another. The transformation parameters formal errors were selected as characteristic of sources set. For all catalogues IVS WG2 was selected special order in the sources list and obtained transformation parameters accuracy as function of the number of sources. For all catalogues that function has a minimum between 300 and 400 sources, adding the sources after the minimum leads to increasing formal errors of orientation parameters. After that we selected the common sources which placed before minimum of functions and obtained the "optimal set".

The aim of this study is to select the set of sources that minimize formal errors of the orientation parameters of rigid rotation transformation model. Instead of over investigators we don't use ranking of sources. We construct ranking parameter that can characterize the list of sources. Then we can compare not individual sources but set of them. Main advantage of our method is that it take into account both geometrical distribution of the sources in the set and source positions accuracy.

Lets set some definitions. Let we have two catalogues (RA,DE) and (ra,de) then we can represent the differences $dRA = RA - ra$ and $dDE = DE - de$ between them in form

$$dRA = A1\tan(DE)\cos(RA) + A2\tan(DE)\sin(RA) - A3,$$

$$dDE = A1\sin(RA) + A2\cos(RA),$$

where A_1, A_2, A_3 are transformation parameters. If we select the set of common sources in the two catalogues then we can calculate parameters $\mathbf{A} = (A1, A2, A3)$ and formal errors σ_{A1}, σ_{A2}, σ_{A3} by the Least Square method:

$$\mathbf{A} = \mathbf{N}^{-1}\mathbf{b}, \quad \sigma_{A1} = \sigma_0\mathbf{N}^{-1}[0,0], \quad \sigma_{A2} = \sigma_0\mathbf{N}^{-1}[1,1], \quad \sigma_{A3} = \sigma_0\mathbf{N}^{-1}[2,2].$$

We form normal equation matrix $\mathbf{N} = \mathbf{C^T P C}$, where $\mathbf{C} = \partial(dRA, dDE)/\partial A$ with the $\mathbf{P} = \mathbf{E}$ unitary matrix. The diagonal elements of inverted normal matrix $\mathbf{N}^{-1}[0,0]$, $\mathbf{N}^{-1}[1,1]$, $\mathbf{N}^{-1}[2,2]$ not affected by the differences between two catalogues and depend only from the set of sources. For calculation σ_0 we use the formal errors of the selected set of sources

$$\sigma_0 = \frac{\sum(\sigma_{RA})^2 + \sum(\sigma_{DE})^2}{N-3}. \tag{1}$$

Thus we calculate σ_{A1}, σ_{A2}, σ_{A3} what not affected by the differences between two catalogues and depend only from the geometrical distribution of the sources in the set and formal errors of source coordinates. We don't use for σ_0 standard formula

$$\hat{\sigma_0} = \frac{\sum(r_{RA})^2 + \sum(r_{DE})^2}{N-3} \tag{2}$$

where r_{RA} and r_{DE} - residuals after transformation, because all CRF catalogues obtained from the same data and using σ_{RA} and σ_{DE} gives more adequate results.

For source list ranking parameter q we select maximum of the orientation parameters formal errors:

$$q = MAX(\sigma_{A1}, \sigma_{A2}, \sigma_{A3}). \tag{3}$$

If we want to define the orientation of the catalogue by the best way we need select the set of sources that minimize parameter q. The obtained set of sources can be considered as set of "defining" sources. We take into account only sources presented in the ICRF-Ext.2 catalogue and have more than 10 session in the gsf008a catalogue. We use next algorithm for the selection that set of sources:

1. Triple loop over all sources to select three sources that gives minimum of q. At this step we have optimal set for $N_{sources} = 3$.
2. Search over all remaining sources in order to minimize q for $N + 1$ sources Remove the founded source from the list of remaining sources and add it to the final set.
3. Repeat step 2 for all remaining sources.

After that we have sequence of the lists then contains optimal set of sources for given $N_{sources}$ (see the bottom line on the Fig. 1, left side). We obtained for all catalogues MAX(σ_{A1}, σ_{A2}, σ_{A3}) as a function of the number of sources. For all catalogues it has a minimum between 300 and 500 sources, adding the sources after the minimum leads to increasing formal errors of orientation parameters.

The first three sources in set after step 1 were: 0851+202, 0955+476, and 2037+511.

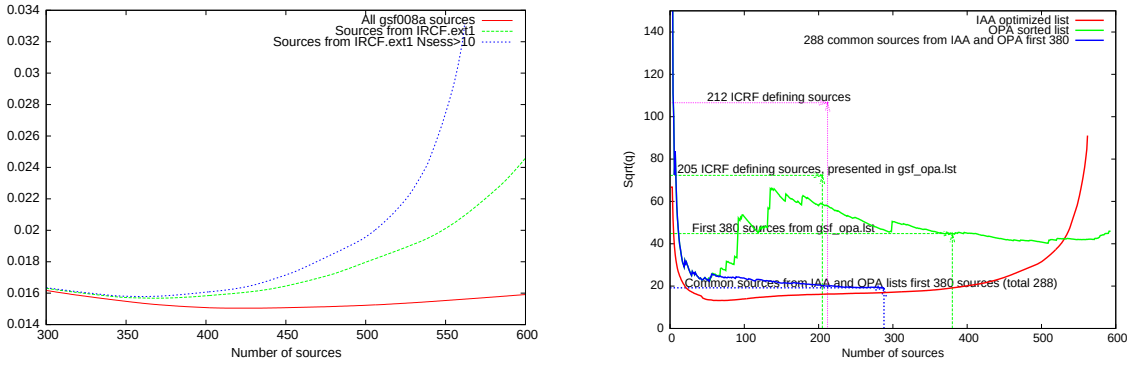

Figure 1: Normalized MAX(σ_{A1}, σ_{A2}, σ_{A3}) vs. number of sources for different catalogues (left) and MAX(σ_{A1}, σ_{A2}, σ_{A3}) vs. number of sources for different subset of gsf2008a catalogue (right).

We have compared our optimized list with the OPA ranked list. Also we calculated parameter q for ICRF 212 defining sources list and for some lists of common sources. The results are presented at the right side of Fig. 1. The $\sqrt{q}$ plotted on the graph can be considered as the maximum formal error of the orientation parameters for the given set of sources. The ICRF 212 defining list gives worse result than subset of the first sources from OPA or IAA lists. Excluding from it 7 sources not presented in OPA list gives significant improvement. First 380 sources from the OPA list (Lambert & Gontier, 2009) shows much better result than the 205 ICRF defining sources. But if we take common sources from first 380 OPA list and first 380 IAA list we obtain almost two times better result by our criteria. The common set contains 288 sources. It seems that transformation parameters for ICRF2 by the first 380 sources of OPA ranked list will be not estimated with the best accuracy. We suppose it would be better to use part of our optimized list or common part of the N sources from our list and OPA for transformation parameters calculation. The function $q(N)$ for our optimized list rapidly increases only after $N = 400$ sources. Thus if one takes the common part of any list of sources with our list for $N \leq 400$ it will increase accuracy of transformation parameters. The presented algorithm can be used for selection of core sources for new catalogues. We plan to use selected sources for actual computing transformation parameters between catalogues for ICRF3. The algorithm need to be reviewed in case of upcoming of multi wavelength reference frame.

REFERENCES

Lambert, S., Gontier, A.-M., 2009, "On radio source selection to define a stable celestial frame", A&A, 493(1), pp. 317–323.

Kurdubov, S.L., Skurikhina, E.A., 2009, "Dependence of Catalogue Orientation Parameters Accuracy from Sources Set Selection", In: Proc. 19th European VLBI for Geodesy and Astrometry Working Meeting, G. Bourda, P. Charlot, A. Collioud (eds.), pp. 5–8.

ON THE PROBLEM OF USING OF THE ICRF RADIO COORDINATES REFERENCE SYSTEM

A.A. LIPOVKA[1], N.M. LIPOVKA[2].
[1] Center of research for physics, Sonora State University
Centro de Investigacion en Fisika, Universidad se Sonora. Rosales y Blvd. Transversal, Col. Centro, Edif. 3-1. 83000, Hermosillo, Sonora, Apdo. Postal: 5-88, Mexico
e-mail: aal@cifus.uson.mx
[2] Retired
e-mail: nila_lip@mail.ru

ABSTRACT. In present paper we show that identification of the optical and radio sky must be proved and confirmed by an independent technique based on the coincidence of several objects in radio and optic wavelength in the field under investigation, within the first lobe of the radio interferometer. Paradox of mismatching of main part of radio objects with the optical ones, should be resolved by using the correct method of the identification of the radio sources with the optical ones.

Radio catalog ICRF2 was recommended by IAU in 2009 as the main radio coordinates reference system, with which the results of all observations within the optical range of wave lengths should be should be agreed. But on the one hand, it should be noted that ICRF2 catalog includes radio sources, with the coordinates measurement accuracy to be significantly worse than those in optical range. On the other hand, fraction of the formally identified sources by the coordinate coincidence is dramatically small. For this reason declared millisecond accuracy of radio coordinates for the ICRF2 catalog should be confirmed by an independent method of optical identification.

Our optical identification carried out with method described in our previous paper (Lipovka & Lipovka, 2011), showed that the main part of radio sky was identified with optical sky incorrectly. Besides that we had discovered radio refraction in interstellar matter, which can exceed several arcseconds in the fields characterized by high density of interstellar gas, see Lipovka & Lipovka (2007).

In the present work it is shown that reasonable identifications of optical and radio sky should be substantiated and confirmed by the fact of matching of several radio and optical objects at the investigated area within the first lobe of radio interferometer diagram. Only in this case the paradox of mismatch of main part of radio sources with the optical celestial objects could be solved.

The optical identifications were made for 10 plates of one square degree each. For these plates 96 radio sources were identified with stars brighter than 15^m and 17 radio sources were identified with diffuse objects in optics (see for details Lipovka & Lipovka, 2013a). On three plates appeared three radio sources from ICRF2 catalog (Fig. 1, upper plots), and we identified them with the stars (Fig. 1, bottom plots) using our identifications method (Lipovka & Lipovka, 2011). One can see an these figures contours of snapshot images of NVSS radiosurvey of NRAO observatory. It is clear, due to their large dimensions this radio sources can not be used as the reference objects to identify celestial radio objects with optical ones. The errors of initial identification of radio sky with the optical one are considered in Lipovka & Lipovka (2013b). In Table 1 the coordinates of these radio objects (columns 2, 3) are suggested in accordance with ICRF2 catalog. Columns 8, 9 are corrections to right ascension and declination, which should be added to coordinates of ICRF2 radio sources, to obtain coordinates of optical objects, with which these radio sources are identified. Star names are presented in column 10 of Table 1. As a result of correct identification 25 stars and 2 objects with diffuse image were identified at three single-degree areas.

Developed method of matching radio sky with optical objects, showed that the bright radio sources are identified mainly with stars in optics. This fact has a great importance for theoretical astrophysics, opening the way to study the stars radiation mechanisms, their evolution and investigation of interstellar matter properties by using revealed radio refraction in interstellar medium.

Suggested high precision catalog ICRF2 should be revised and cannot be used immediately for identifications of radio and optical sky.

No	RA h m s	Decl. o ’ ”	z	m	Type	fig.	Δ RA m s	Δ Decl. ’ ”	name	fig.
1	00 26 51.44	-11 12 52.42	1.115	19.4	Q	1	01 09.3	-27 25.0	HD2438	1a
2	00 29 14.24	+34 56 32.24	0.517	20.4	G	2	-03 22.2	+21 47.0	HD2154	2a
3	21 15 29.41	+29 33 38.36	1.514	19.5	Q	3	-02 32.4	+38 39.4	zet Cyg	3a

Table 1: Results of identification. See text for detail.

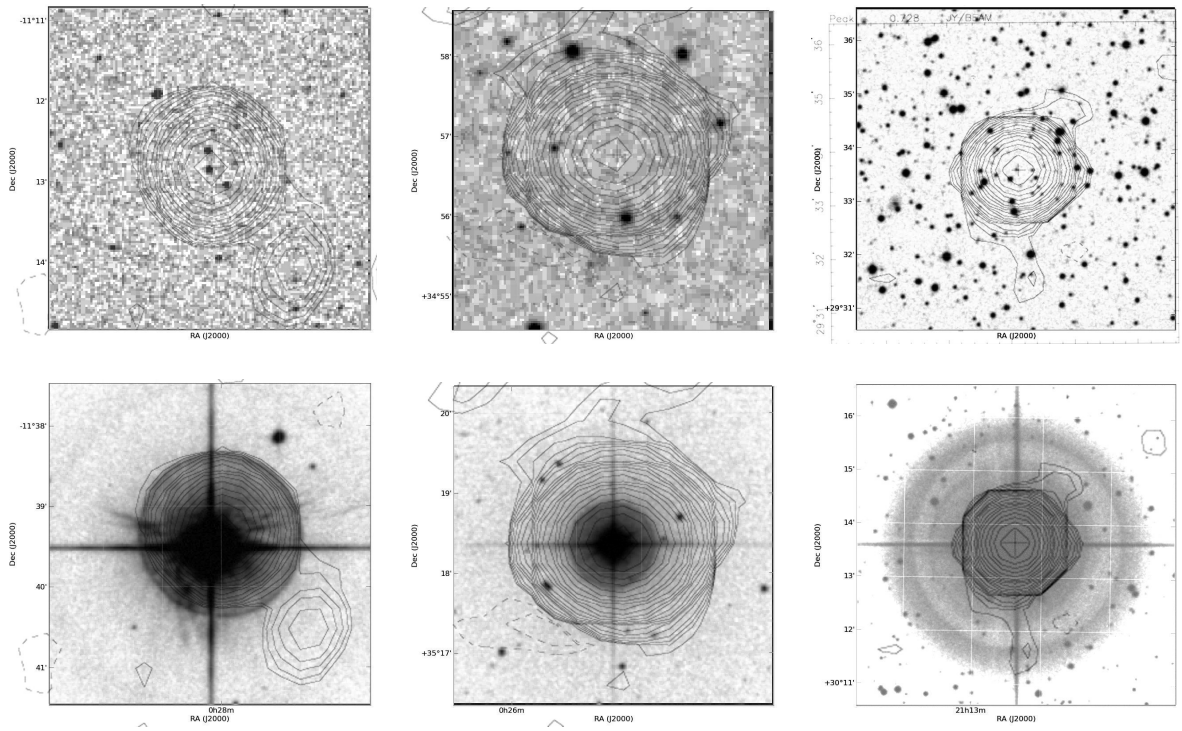

Figure 1: Identification suggested by ICRF (upper plots), and identification obtained by the authors (bottom plots).

REFERENCES

Lipovka, A.A., Lipovka, N.M., 2007, “The end of the “Empty Field” epoch in optical identifications”, “Molecules in Space and Laboratory”, the meeting held in Paris, France, May 14–18, 2007, J.L. Lemaire, F. Combes (eds.), Publisher: S. Diana., p. 26.

Lipovka, A.A., Lipovka, N.M., 2011, “Method of identifications of celestial radio sources coordinates to optical astronomical coordinate system LIPOVKA-KOSTKO-LIPOVKA (LKL)”, Patent No. 2447641.

Lipovka, A.A., Lipovka, N.M., 2013a, “Radio emission from the galactic cluster A1716 and a group of stars”, Astrophysics, 56(2), pp. 221–228.

Lipovka, A.A., Lipovka N.M., 2013b, “The problems of identifications of radio sky with the optical ones. History and Perspectives”, Geodesy and Cartography, No. 10, pp. 2–7. (in Russian)

USING POSITIONAL OBSERVATIONS OF NUMBERED MINOR PLANETS FOR DETERMINATION OF STAR CATALOG ERRORS

Y.D. MEDVEDEV, V.B. KUZNETSOV
Institute of Applied Astronomy RAS
St. Petersburg, Russia
e-mail: medvedev@ipa.nw.ru, v.kuznetsov@ipa.nw.ru

ABSTRACT. The systematic errors of star catalogs have been defined by the O-C of the asteroid positional observations. 102 760 633 positional observations for 404 941 numbered asteroids were used. The considerable systematic errors for the USNO A2.0 catalog are founded. For this catalogue we can estimated also the value of variation of systematic errors for some areas on the celestial sphere.

1. INTRODUCTION

The Ephemerides of minor planet are calculated by Institute of Applied Astronomy of Russian Academy of Science. For this Ephemerides the elements of minor planet are improved by the differential method using all available observations.The O-C of asteroid positional observations ("observed-calculated" residuals) are calculated.These values of O-C are used for estimation of the systematic errors of star catalogs. Improvement of asteroid orbits was conducted in two steps. At the first step the orbital elements of Ceres, Pallas and Vesta were improved, taking into account the perturbations from the major planets, the Moon, Pluto using DE405 and their mutual perturbations. Then we calculated ephemerides of these three planets. To calculate the orbital elements of other numbered asteroids we used obtained ephemerides and all available positional observations. 102 760 633 values of O-C for 404 941 numbered asteroids were chosen. We chosen observations made after 2001. The greatest number of observations after 2001 refers to the following catalogs: USNO A2.0 (37 732 050 observations), UCAC-2 and 3 (27 529 078 observations), USNO B1.0 (11 778 775 observations) and UCAC-4 (4 501 387 observations).

2. PROCEDURE OF CALCULATION OF CATALOGUE BIASES

The celestial sphere is split into 10212 about equal areas. Then each O-C value was associated with the corresponding area. The mean value of O-C of the basic star catalog was calculated for each areas and interpreted as a star catalog systematic bias of the area. Then larger number of O-C for different planets we used to calculate the mean value for each area then smaller its error is obtained. Our results shows that a few thousand observations for hundred different planets are needed for reliable determination of catalogue bias in the area.

We calculated the star systematic biases for 4 catalogs. The greatest errors have been obtained for the USNO A2.0. We can calculated also the variation of the systematic errors for this catalog for some areas on the celestial sphere. The the variation of the systematic errors is calculated by the following way.The mean values of individual areas were calculated using O-C referred to six different time intervals:$(2001-2002), (2003-2004), (2005-2006), (2007-2008), (2009-2010), (2011-2014)$. The obtained values were approximated by the linear equations:

$$\begin{cases} \Delta\dot{\alpha}(t_i - 2011.5) + \Delta\alpha_0 = \Delta\alpha_i \\ \Delta\dot{\delta}(t_i - 2011.5) + \Delta\delta_0 = \Delta\delta_i \end{cases} \tag{1}$$

where $t_i = 2001.5, 2003.5, \ldots, 2011.5$ – the middle of the intervals. Then the overdetermined (1) system was solved by MLS. Using the obtained values the error of USNO A2.0 catalog for some areas at various epochs are calculated.

3. CALCULATION AND COMPARISON

We calculated the errors of right ascensions and declinations at 2011 and 2014 $\Delta\alpha_{2011}$, $\Delta\delta_{2011}$, $\Delta\alpha_{2014}$ and $\Delta\delta_{2014}$ and compared them with the results in (Chesley, et al., 2010). The results of comparison for some areas are given in the Table 1, where: α, δ (in terms of hours and degrees) are the coordinates of an area center ; $\Delta\alpha, \Delta\delta$ (in terms of arcseconds) are the systematic errors of right ascensions and declinations of the USNO A2.0 catalog (in terms of arcseconds) given in (Chesley, et al., 2010). The next columns contain $\Delta\alpha_{2011}$, $\Delta\delta_{2011}$, $\Delta\alpha_{2014}$ and $\Delta\delta_{2014}$ – right ascensions and declinations at 2011 and 2014. The values $\Delta\alpha_{2014}$ and $\Delta\delta_{2014}$ are shown with its errors. The data of Table 1 are shown that the variations of the systematic errors for the USNO A2.0 catalog are not large. It should be noted that jumps of systematic errors of the USNO A2.0 catalog for certain areas in (Chesley, et al., 2010) are revealed. In particular for the area with coordinates $(0^h.753, 3^\circ.21)$ the bias of declination obtained in (Chesley, et al., 2010) differs from the other in neighboring areas. Systematic errors that are defined by us vary more smoothly from area to area, but we calculated star errors for areas contained sufficient number of observations of different planets. Therefore the catalog biases of USNO A2 are not estimated by us for all areas on the celestial sphere as it were done in (Chesley, et al., 2010).

α	δ	$\Delta\alpha$	$\Delta\delta$	$\Delta\alpha_{2011}$	$\Delta\delta_{2011}$	$\Delta\alpha_{2014}$	$\Delta\delta_{2014}$
$23^h.914$	$4^\circ.82$	-0.08	0.33	-0.01	0.34	0.02±0.02	0.39±0.03
0.082	4.82	-0.02	0.27	-0.01	0.44	0.02±0.01	0.49±0.05
0.250	3.21	-0.05	0.35	-0.21	0.48	-0.21±0.01	0.53±0.05
0.418	3.21	-0.03	0.46	0.17	0.54	0.21±0.01	0.60±0.03
0.586	3.21	-0.01	0.47	-0.03	0.49	-0.01±0.01	0.56±0.03
0.753	3.21	-0.09	0.01	-0.02	0.41	0.02±0.00	0.47±0.03
0.921	3.21	-0.12	0.24	-0.07	0.31	-0.05±0.02	0.36±0.02
1.089	3.21	-0.04	0.44	-0.06	0.41	-0.03±0.02	0.45±0.03
1.257	3.21	-0.14	0.32	0.14	0.59	0.18±0.04	0.67±0.04
1.425	3.21	-0.11	0.33	-0.18	0.49	-0.16±0.03	0.55±0.04

Table 1: Catalog biases of USNO A2 at Epoch 2011 and 2014.

4. CONCLUSION

The accuracy and number of new positional observations of asteroids allow to estimate the accuracy of reference star catalogs.

The variation of the systematic errors for the USNO A2.0 catalog are shown.

The values of the systematic errors for USNO A2.0 catalog vary from area to area as well as with time.

Using our calculation the observations based on this catalog can be corrected not only depending on the different areas, but the different epochs as well.

5. REFERENCES

Chesley, S.R., Baer, J., Monet, D.G., 2010, "Treatment of star catalog biases in asteroid astrometric observations", Icarus, 210, pp. 158–181.

OPTICAL MONITORING OF QSO IN THE FRAMEWORK OF THE GAIA MISSION

F. TARIS[1], G. DAMLJANOVIĆ[2], A. ANDREI[1,3,4], A. KLOTZ[5,6], F. VACHIER[7]
[1] Observatoire de Paris - SYRTE, CNRS, UPMC
61, Av. de l'observatoire 75014 Paris, France
e-mail: francois.taris@obspm.fr
[2] Astronomical observatory, Belgrade, Serbia
[3] ON/MCT - Observatorio Nacional, Brazil
[4] OV/UFRJ - Observatorio do Valongo, Brazil
[5] Université de Toulouse, UPS-OMP, IRAP, Toulouse, France
[6] CNRS, IRAP, Toulouse, France
[7] Observatoire de Paris - IMCCE

ABSTRACT. The Gaia astrometric mission of the European Space Agency has been launched the 19th December 2013. It will provide an astrometric catalogue of 500.000 extragalactic sources that could be the basis of a new optical reference frame. On the other hand, the current International Celestial Reference Frame (ICRF) is based on the observations of extragalactic sources at radio wavelength. The astrometric coordinates of sources in these two reference systems will have roughly the same uncertainty. It is then mandatory to observe a set of common targets at both optical and radio wavelength to link the ICRF with what could be called the GCRF (Gaia Celestial Reference Frame). We will show in this paper some results obtained with the TJO, Telescopi Juan Oro, from Observatori Astronomic del Montsec in Spain. It also presents some results obtained with the Lomb-Scargle and CLEAN algoritm methods applied to optical magnitude obtained with the TAROT telescopes.

1. THE TELESCOPES USED

A set of optical telescopes is currently used both for morphology (large facilities) and for photometry (robotic/manual and small/medium telescopes). This paper is more particularly dedicated to the photometry aspect, the morphology being currently under study and will be presented elsewhere. The photometric program (magnitude monitoring) has begun in 2010 and is currently under progress. Among all the telescopes used, three of them, The Telescopi Joan Oró (TJO)[1] from the Observatori Astronòmic del Montsec (OAdM, Spain) and the two twin TAROT telescopes from Observatoire de la Côte d'Azur (OCA, France)[2] and European Southern Observatory (ESO, Chile), provide light curves that are presented and used in the frame of this work (Fig. 1). The data obtained with the TJO are differential magnitudes against two reference stars while the data obtained with the TAROT telescope are direct magnitudes. Both of them are shown here in R Cousins filter.

2. LOMB-SCARGLE AND CLEAN PERIODOGRAMS

The Lomb-Scargle periodogram is a very common tool for spectral analysis of time series with unequally spaced data (Scargle, 1982; Press & Rybicky, 1989). It is equivalent to the least-squares fitting of sine wave. An independent method has been chosen to confirm the frequencies obtained by the Lomb-Scargle method (to avoid misinterpretation of frequency peaks). This method, the CLEAN algorithm, has been described by Roberts et al. (1987) and, in our case, implemented by Jablonski (1991). The Table 1 gives the comparison of the detected periods obtained by the two previously mentioned methods in the case of the TAROT light curves.

[1] see http://www.oadm.cat/en/home.htm
[2] see http://tarot.obs-hp.fr/tarot

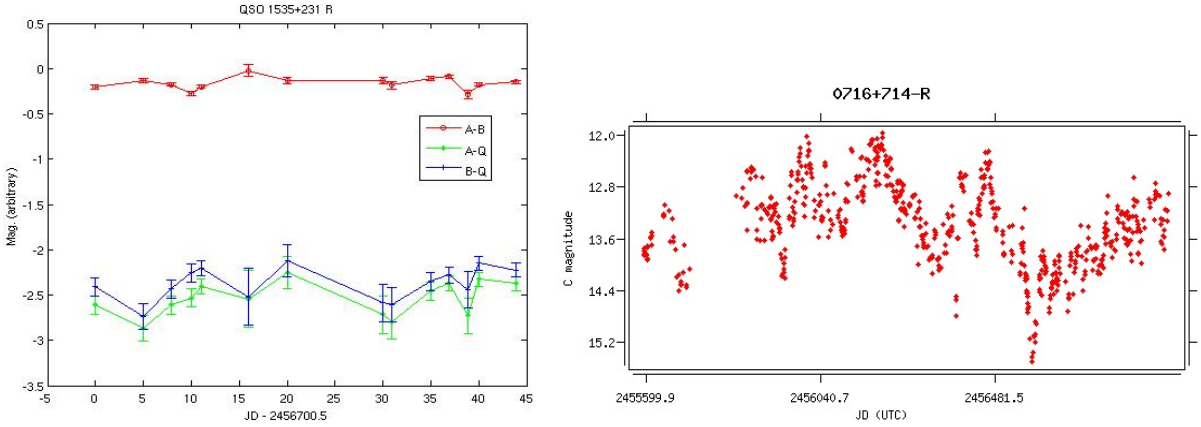

Figure 1: On the left panel, R light curve for QSO 1535+231 obtained with the TJO. On the right panel IERS B0716+714 R light curve obtained with TAROT telescope (OCA).

IERS Name	Lomb-Scargle	CLEAN	IERS Name	Lomb-Scargle	CLEAN
B0405-123	1228	1169	B1101-325	1759	2050
	277			262	
	84	87		655	603
	201			359	366
B0716+714	1000	1055	B1424+240	423	442
	316	310		816	847
	235	215		214	216
	163			99	
	68	68		151	159
				76	76

Table 1: Comparison of the detected periods (in days) by the Lomb-Scargle and CLEAN methods.

3. CONCLUSION

Binary central compact objects are not part of the current unified model of AGN. But it must be noted that supermassive binary black holes are predicted to be at an inevitable late stage in the evolution of the galaxy mergers (Beckmann & Shrader, 2012). Despite this fact, one could reasonably suspect that the rotation of the accretion disk and the dynamic of the accretion flow produce some periodic or quasi-periodic phenomena. Many objects are well known to exhibit one or more (quasi-)periodicity, such as for example B0109+224 (Ciprini et al., 2003), B0716+714 (Zhang, et al., 2009), B0735+178 (Qian & Tao, 2004), B1253-055 (Li et al., 2009). This work confirms some periods already known for B0716+714. These periods are the signature of some underlying astrophysical phenomena that could modify the photocenter of this target. This could be an issue for the link of reference systems.

4. REFERENCES

Beckmann, V., Shrader, C., 2012, "Active Galactic Nuclei", Wiley-VCH Verlag GmbH & Co.
Ciprini, S., Tosti, G., Raiteri, C., et al., 2003, A&A, 400, 487.
Jablonski, F., 1991, Private communication.
Li, H., Xie, G., Chen, L., et al., 2009, PASP, 121, 1172.
Press, W., Rybicki, G., 1989, ApJ., 338, 277.
Qian, B., Tao, J., 2004, PASP, 116, 161.
Roberts, D.H., Lehar, J., Dreher, J.W., 1987, AJ, 93, 968.
Scargle, J.D., 1982, ApJ, 263, 835.
Zhang, H., Zhang, X., Dong, F., et al., 2009, ChA&A, 33, 373.

KINEMATICS DERIVED FROM NORTHERN AND SOUTHERN HEMISPHERES OF HUGE ASTROMETRIC CATALOGUES

V. VITYAZEV, A. TSVETKOV
Saint-Petersburg State University
198504 Petrodvorets, Universitetsky pr., 28., St. Petersburg, Russia
e-mail: vityazev@list.ru, A.S.Tsvetkov@inbox.ru

ABSTRACT. It is shown that the kinematic analysis of the UCAC4, PPMXL and XPM proper motions in northern and southern Galactic hemispheres detects retardation of the Galaxy's rotational velocity and acceleration of the expansion velocity of the stellar system with increasing the distance from the principal Galactic plane. The estimates of the vertical gradient of the Galactic rotation are UCAC4: 40.1 ± 0.2; PPMXL: 36.2 ± 0.4; XPM: 37.7 ± 0.1 $\mathrm{km \cdot s^{-1} \cdot kpc^{-1}}$, while the values of the vertical gradient of the expansion velocity turned out to be UCAC4: 11.9 ± 0.2; PPMXL: 19.0 ± 1.1; XPM: 10.9 ± 0.3 $\mathrm{km \cdot s^{-1} \cdot kpc^{-1}}$.

1. INTRODUCTION

Modern astrometric catalogues realizing the ICRS in optical waves with full coverage of the sky provide a qualitatively new material, in particular, for investigating the kinematics of nearby stars in both Galactic hemispheres separately. In case of the Ogorodnikov–Milne model (Du Mont, 1997) the stellar velocity field is given by expression

$$\vec{V} = \vec{V}_0 + M^+ \vec{r} + M^- \vec{r}, \tag{1}$$

where: $\vec{V}_0$ — the velocity of the Sun with respect to given centroid of stars; M^+ — the diverging matrix with the dilation coefficients M^+_{11}, M^+_{22}, M^+_{33}, and M^+_{12}, M^+_{13} M^+_{23} standing for shears in the galactic planes (x, y), (x, z), (y, z); M^- — the rotation matrix with the components Ω_1, Ω_2, Ω_3 about axes x, y, z.

Unfortunately, due to high correlations of the parameters the standard LS solutions of the Ogorodnikov-Milne equations on hemispheres are hardly to be trusted. To remedy this we use an approach the first step of which is the expansion of proper motions on a system of vector spherical harmonics which are orthonormal on a hemisphere. At the second step, the kinematical parameters are derived from the coefficients of the expansion. For more detail of the method the reader is referred to (Vityazev and Tsvetkov, 2014).

2. NUMERICAL RESULTS

We applied our method to proper motions of stars listed in the catalogues UCAC4 (Zacharias, et al., 2013), PPMXL (Roeser, et al., 2010) and XPM (Fedorov, et al., 2009). The full description of the results may be found in (Vityazev and Tsvetkov, 2014). The present paper is devoted to the "northern" and "southern" solutions only, since all the tree catalogues gave evidence that the parameters Ω_1, $M^+_{2,3}$, Ω_2, $M^+_{1,3}$ have different signs in different hemispheres.

Now, in the galactocentric cylindrical coordinate system (Miyamoto and Soma, 1993) we have $\Omega_1 - M^+_{32} = -\frac{\partial V_S}{\partial z}$, where V_S is the circular velocity of the local reference frame around the galactic center. This quantity is identified with the Galaxy's rotational velocity in the solar neighborhood. From Table which gives the numerical values for the values $\Omega_1 - M^+_{32}$ that we obtained from different samples of our catalogues, we see that the vertical gradient of the Galaxy's rotational velocity $\frac{\partial V_S}{\partial z}$ has different signs in the northern and southern galactic hemispheres, with the velocity itself decreasing with increasing distance from the principal galactic plane. Again, from the Table for the the vertical gradient of the expansion velocity of the stellar system $\Omega_2 + M^+_{13} = -\frac{\partial V_R}{\partial z}$ we may conclude that the expansion velocity increases with increasing distance from the principal galactic plane. The estimates of both the gradients $\left|\frac{\partial V_S}{\partial z}\right|$ and $\left|\frac{\partial V_R}{\partial z}\right|$ derived from all the catalogues under consideration are in good agreement.

	11^m	12^m	13^m	14^m	15^m	16^m
Catalogue UCAC4						
$(\Omega_1 - M_{32}^+)_N$	$42,4 \pm 0,8$	$39,6 \pm 0,7$	$36,9 \pm 0,5$	$35,7 \pm 0,4$	$35,2 \pm 0,3$	$36,0 \pm 0,3$
$(\Omega_1 - M_{32}^+)_S$	$-41,5 \pm 0,9$	$-42,1 \pm 1,1$	$-44,6 \pm 0,8$	$-43,2 \pm 0,7$	$-42,3 \pm 0,4$	$-41,9 \pm 0,3$
$\left\lvert\frac{\partial V_S}{\partial z}\right\rvert$	42.0 ± 0.6	$40,8 \pm 0,7$	$40,8 \pm 0,5$	$39,4 \pm 0,4$	$38,7 \pm 0,3$	$39,0 \pm 0.2$
$(\Omega_2 + M_{31}^+)_N$	$-15,6 \pm 0,8$	$-19,7 \pm 0,7$	$-16,3 \pm 0,5$	$-10,9 \pm 0,4$	$-7,8 \pm 0,3$	$-6,6 \pm 0,3$
$(\Omega_2 + M_{31}^+)_S$	$11,3 \pm 0,9$	$13,6 \pm 1,1$	$11,8 \pm 0,8$	$12,6 \pm 0,7$	$9,5 \pm 0,4$	$7,3 \pm 0,3$
$\left\lvert\frac{\partial V_R}{\partial z}\right\rvert$	$13,5 \pm 0,6$	$16,7 \pm 0,7$	$14,0 \pm 0,5$	$11,7 \pm 0,4$	$8,6 \pm 0,3$	$6,8 \pm 0,2$
Catalogue PPMXL						
$(\Omega_1 - M_{32}^+)_N$	51.3 ± 1.8	40.2 ± 1.6	45.1 ± 1.7	47.8 ± 1.0	$47.3 \pm 0,7$	$43.9 \pm 0,6$
$(\Omega_1 - M_{32}^+)_S$	-45.6 ± 2.8	$-47,0 \pm 1,7$	$-40,5 \pm 1.7$	-35.4 ± 1.2	$-33,2 \pm 0,8$	$-29,4 \pm 0,7$
$\left\lvert\frac{\partial V_S}{\partial z}\right\rvert$	48.4 ± 1.7	43.6 ± 1.2	42.8 ± 1.2	41.6 ± 0.8	40.3 ± 0.5	36.7 ± 0.5
$(\Omega_2 + M_{31}^+)_N$	$-20,8 \pm 1,8$	$-17,3 \pm 1,7$	$-21,1 \pm 1,7$	$-18,1 \pm 1,0$	$-16,5 \pm 0,7$	$-11,9 \pm 0,6$
$(\Omega_2 + M_{31}^+)_S$	$16,2 \pm 2,8$	$21,6 \pm 1,7$	$23,4 \pm 1,7$	$25,3 \pm 1,2$	$18,9 \pm 0,8$	$17,9 \pm 0,7$
$\left\lvert\frac{\partial V_R}{\partial z}\right\rvert$	$18,5 \pm 1,6$	$19,4 \pm 1,2$	$22,2 \pm 1,2$	$21,7 \pm 0,8$	$17,7 \pm 0,5$	$14,9 \pm 0,4$
Catalogue XPM						
$(\Omega_1 - M_{32}^+)_N$	34.4 ± 1.4	33.3 ± 0.8	34.6 ± 0.5	37.7 ± 0.4	38.1 ± 0.3	36.4 ± 0.2
$(\Omega_1 - M_{32}^+)_S$	-63.0 ± 1.4	-62.3 ± 0.9	-56.6 ± 0.6	-49.1 ± 0.4	-42.1 ± 0.4	-39.8 ± 0.3
$\left\lvert\frac{\partial V_S}{\partial z}\right\rvert$	48.7 ± 1.0	47.8 ± 0.6	45.6 ± 0.4	43.4 ± 0.3	40.1 ± 0.2	38.1 ± 0.2
$(\Omega_2 + M_{31}^+)_N$	$-6,8 \pm 1,4$	$-9,7 \pm 0,8$	$-8,6 \pm 0,5$	$-6,0 \pm 0,3$	$-4,7 \pm 0,3$	$-3,9 \pm 0,2$
$(\Omega_2 + M_{31}^+)_S$	$19,9 \pm 1,4$	$19,6 \pm 1,0$	$17,0 \pm 0,7$	$14,3 \pm 0,4$	$11,5 \pm 0,4$	$8,6 \pm 0,3$
$\left\lvert\frac{\partial V_R}{\partial z}\right\rvert$	$13,3 \pm 1,0$	$14,6 \pm 0,6$	$12,8 \pm 0,4$	$10,2 \pm 0,3$	$8,1 \pm 0,2$	$6,3 \pm 0,2$

Table 1: Values $\Omega_1 - M_{32}^+$ and $\Omega_2 + M_{31}^+$ obtained from northern and southern galactic hemispheres of the UCAC4, PPMXL and XPM. Units: $\mathrm{km} \cdot \mathrm{s}^{-1} \cdot \mathrm{kpc}^{-1}$.

The values $\Omega_1 + M_{32}^+ = -\frac{1}{R}\frac{\partial V_z}{\partial \theta}$ which are associated with the local Galactic warp, and the radial gradient of the vertical velocity field $\Omega_2 - M_{13}^+ = \frac{\partial V_z}{\partial R}$ turned out to be unreliable.

3. CONCLUSIONS

The success of this paper is based on the vector spherical harmonics solutions of the Ogorodnikov-Milne equations on hemispheres which permitted to obtain the uncorrelated values of the kinematical parameters and to show that some of them have different signs in both hemispheres. The transition to the Galactocentric cylinder coordinate system immediately made it clear that the change of signs is connected with the retardation of the Galaxy's rotational velocity and acceleration of the expansion velocity of the stellar system with increasing the distance from the principal Galactic plane.

Acknowledgements. This work was done with support of the St. Petersburg University Grant 6.0.161.2010.

4. REFERENCES

Du Mont, B., 1997, "A three-dimensional analysis of the kinematics of 512 FK4 Sup. stars", A&A, 61(1), pp. 127–132.

Fedorov, P.N., Myznikov, A.A, Akhmetov, V.S., 2009, "The XPM Catalogue: absolute proper motions of 280 million stars", MNRAS, 393, pp. 133–138.

Miyamoto, M., Soma, M., 1993, "Is the vorticity vector of the Galaxy perpendicular to the Galactic plane? I. Precessional corrections and equinoctial motion correction to the FK5 system", AJ, 105, pp. 691–701.

Roeser, S., et al., 2010, "The PPMXL Catalog of positions and proper motions on the ICRS. Combining USNO-B1.0 and 2MASS", AJ, 139(6), pp. 2440–2447.

Vityazev, V.V., Tsvetkov, A.S., 2014, "Intercomparison of kinematics derived from catalogues UCAC4, PPMXL and XPM with vector spherical harmonics", MNRAS, 442, pp. 1249–1264.

Zacharias, N., et al., 2013, "The Fourth US Naval Observatory CCD Astrograph Catalog (UCAC4)", AJ, 145, 44.

Session 2

RELATIVITY AND TIME SCALES

RELATIVITÉ ET ÉCHELLES DE TEMPS

RANGE, DOPPLER AND ASTROMETRIC OBSERVABLES COMPUTED FROM TIME TRANSFER FUNCTIONS: A SURVEY

A. HEES[1], S. BERTONE[2,3], C. LE PONCIN-LAFITTE[2], P. TEYSSANDIER[2]
[1] Department of Mathematics, Rhodes University, Grahamstown 6140, South Africa
e-mail: A.Hees@ru.ac.za
[2] Observatoire de Paris, SYRTE, CNRS/UMR 8630, LNE, UPMC
61, avenue de l'Observatoire, F-75014 Paris, France
e-mail: {stefano.bertone,christophe.leponcin,pierre.teyssandier}@obspm.fr
[3] currently at Astronomical Institute, University of Bern

ABSTRACT. Determining range, Doppler and astrometric observables is of crucial interest for modelling and analyzing space observations. We recall how these observables can be computed when the travel time of a light ray is known as a function of the positions of the emitter and the receiver for a given instant of reception (or emission). For a long time, such a function–called a reception (or emission) time transfer function–has been almost exclusively calculated by integrating the null geodesic equations describing the light rays. However, other methods avoiding such an integration have been considerably developped in the last twelve years. We give a survey of the analytical results obtained with these new methods up to the third order in the gravitational constant G for a mass monopole. We briefly discuss the case of quasi-conjunctions, where higher-order enhanced terms must be taken into account for correctly calculating the effects. We summarize the results obtained at the first order in G when the multipole structure and the motion of an axisymmetric body is taken into account. We present some applications to on-going or future missions like Gaia and Juno. We give a short review of the recent works devoted to the numerical estimates of the time transfer functions and their derivatives.

1. OBSERVABLES COMPUTABLE FROM TIME TRANSFER FUNCTIONS

Many observations in the Solar System rest on the measurement of the travel time of light rays. Modelling the light propagation requires a mathematical tool defined as follows. Assume that space-time is covered by a single system of coordinates $x^0 = ct, \boldsymbol{x} = (x^i)$, where $i = 1, 2, 3$. Consider a light ray emitted at time t_A at a point of spatial coordinates $\boldsymbol{x}_A$ and received at time t_B at a point of spatial coordinates $\boldsymbol{x}_B$. Here, light rays are null geodesic paths (light propagating in a vacuum). The light travel time $t_B - t_A$ may be regarded as a function of the variables $\boldsymbol{x}_A, t_B, \boldsymbol{x}_B$, so that one can write

$$t_B - t_A = \mathcal{T}_r(\boldsymbol{x}_A, t_B, \boldsymbol{x}_B). \tag{1}$$

$\mathcal{T}_r$ may be called the "(reception) time transfer function" (TTF)[1]. As we shall see below, the interest of this function is not confined to the range experiments: knowing $\mathcal{T}_r$ is sufficient for modelling observations based on the Doppler-tracking or the gravitational bending of light (astrometry).

1. Suppose that the above-mentioned signal is exchanged between two observers $\mathcal{O}_A$ and $\mathcal{O}_B$. Let ν_A and ν_B be the frequencies of the signal as measured at $(ct_A, \boldsymbol{x}_A)$ by $\mathcal{O}_A$ and at $(ct_B, \boldsymbol{x}_B)$ by $\mathcal{O}_B$, respectively. The ratio ν_B/ν_A is given by (see, e.g., Teyssandier et al. 2008b and references therein)

$$\frac{\nu_B}{\nu_A} = \frac{[(g_{00} + 2g_{0i}\beta^i + g_{ij}\beta^i\beta^j)^{1/2}]_{x_A}}{[(g_{00} + 2g_{0i}\beta^i + g_{ij}\beta^i\beta^j)^{1/2}]_{x_B}} \frac{(k_0)_{x_B}}{(k_0)_{x_A}} \frac{1 + (\beta^i \widehat{k}_i)_{x_B}}{1 + (\beta^i \widehat{k}_i)_{x_A}}, \tag{2}$$

where the quantities $g_{\alpha\beta}$ are the components of the metric, $\beta^i_{x_A} = [dx^i_A/cdt]_{t_A}$ and $\beta^i_{x_B} = [dx^i_B/cdt]_{t_B}$ are the coordinate velocities divided by c of $\mathcal{O}_A$ at time t_A and $\mathcal{O}_B$ at time t_B, respectively. The quantities $\widehat{k}_i$ are defined by $\widehat{k}_i = k_i/k_0$, where the k_α are the covariant components of the vector k^μ tangent to the

[1] In this communication, we generally omit the term "reception" for the sake of brevity. Note that similar results can be derived from the "(emission) time transfer function" $\mathcal{T}_e$ defined by $t_B - t_A = \mathcal{T}_e(t_A, \boldsymbol{x}_A, \boldsymbol{x}_B)$.

light ray described by affine parametric equations. One has (see Le Poncin-Lafitte et al. 2004)

$$\left(\widehat{k}_i\right)_{A} = c\frac{\partial \mathcal{T}_r}{\partial x^i_{A}}, \qquad \left(\widehat{k}_i\right)_{B} = -c\frac{\partial \mathcal{T}_r}{\partial x^i_{B}}\left[1-\frac{\partial \mathcal{T}_r}{\partial t_{B}}\right]^{-1}, \qquad \frac{(k_0)_{B}}{(k_0)_{A}} = 1-\frac{\partial \mathcal{T}_r}{\partial t_{B}}. \tag{3}$$

Substituting these relations in (2) yields ν_{B}/ν_{A} in terms of the derivatives of the TTF as follows

$$\frac{\nu_{B}}{\nu_{A}} = \frac{[(g_{00}+2g_{0i}\beta^i+g_{ij}\beta^i\beta^j)^{1/2}]_{x_A}}{[(g_{00}+2g_{0i}\beta^i+g_{ij}\beta^i\beta^j)^{1/2}]_{x_B}}\,\frac{1-\frac{\partial \mathcal{T}_r}{\partial t_B}-c\beta^i_{x_B}\frac{\partial \mathcal{T}_r}{\partial x^i_B}}{1+c\beta^i_{x_A}\frac{\partial \mathcal{T}_r}{\partial x^i_A}}, \tag{4}$$

a formula which can also be inferred without using (2), as it is shown in Hees et al. 2012.

2. Let $\{\lambda_{\underline{\alpha}}, \underline{\alpha}=0,1,2,3\}$ be an orthonormal comoving tetrad attached to $\mathcal{O}_{B}$ ($\lambda_{\underline{0}}$ coincides with the unit 4-velocity vector of $\mathcal{O}_{B}$). The direction of the light ray as measured by $\mathcal{O}_{B}$ is defined by a unit vector proportional to the orthogonal projection of k^μ on the rest frame of $\mathcal{O}_{B}$ at x_{B}. The spatial components $n^{\underline{i}}$ of this vector in the basis $\{\lambda_{\underline{i}}\}$ is given by (see, e.g., Brumberg 1991)

$$n^{\underline{i}} = -\left(\frac{\lambda^0_{\underline{i}}+\lambda^j_{\underline{i}}\,\widehat{k}_j}{\lambda^0_{\underline{0}}+\lambda^j_{\underline{0}}\,\widehat{k}_j}\right)_{x_B}, \tag{5}$$

where $\lambda^\mu_{\underline{\alpha}}$ denote the components of the 4-vector $\lambda_{\underline{\alpha}}$ in the natural basis associated to the coordinates (x^μ). It follows from (3) that each $n^{\underline{i}}$ can be expressed in terms of the derivatives of the TTF.

An analogous conclusion can be drawn for the angular separation ϕ between two point-like sources S and S' as measured by $\mathcal{O}_{B}$ at x_{B}. Indeed, one has (Teyssandier & Le Poncin-Lafitte 2006)

$$\sin^2\frac{\phi}{2} = -\frac{1}{4}\left[\frac{\left(g_{00}+2g_{0k}\beta^k+g_{kl}\beta^k\beta^l\right)g^{ij}(\widehat{k}_i-\widehat{k}'_i)(\widehat{k}_j-\widehat{k}'_j)}{(1+\beta^m\widehat{k}_m)(1+\beta^l\widehat{k}'_l)}\right]_{B}, \tag{6}$$

where the quantities $\widehat{k}_i$ and $\widehat{k}'_i$ are related to the light rays arriving from S and S', respectively.

2. A SURVEY OF THE METHODS PROPOSED FOR CALCULATING THE TTFs

Two approaches exist to determine the light propagation in metric theories of gravity. The most widespread method consists in solving the null geodesic equations. Analytical solutions have been developed within the first post-Newtonian (1pN) or first post-Minkowksian (1pM) approximation dealing with static monopoles (Shapiro 1964), static mass multipole moments (Kopeikin 1997), moving monopoles (Kopeikin & Schäffer 1999 and Klioner 2003a), moving multipole moments (Kopeikin & Makarov 2007),... After the pioneering papers by Richter & Matzner 1983 and Brumberg 1987, an analytical solution has been derived within the 2pM approximation for a static monopole, with a metric containing three arbitrary post-Newtonian parameters (Klioner & Zschocke 2010). Finally, the gravitational deflection of the image of a star when observed at a finite distance from a static monopole has been obtained up to the 2pM order in Ashby & Bertotti 2010. On the other hand, a numerical treatment based on a shooting method has been proposed in San Miguel 2007.

The other approach enables to determine the TTFs without integrating the null geodesic equations. Initially grounded on Synge's world function (see John 1975 for the Schwarzschild space-time, and then Linet & Teyssandier 2002, Le Poncin-Lafitte et al. 2004 for much more general cases), this approach is now based on the direct determination of the TTFs (Teyssandier & Le Poncin-Lafitte 2008a).

3. POST-MINKOSWKIAN EXPANSION OF THE TTF

We assume that the metric may be expanded in a series in powers of the gravitational constant G:

$$g_{\mu\nu}(x,G) = \eta_{\mu\nu}+\sum_{n=1}^{\infty} g^{(n)}_{\mu\nu}(x,G), \tag{7}$$

where $\eta_{\mu\nu}=\text{diag}\,\{1,-1,-1,-1\}$ is the Minkowski metric and $g^{(n)}_{\mu\nu}(x,G)$ stands for the term of order G^n. Then, it may be supposed that $\mathcal{T}_r$ is represented by an asymptotic expansion in a series in powers of G:

$$\mathcal{T}_r(\boldsymbol{x}_{A},t_{B},\boldsymbol{x}_{B}) = \frac{R_{AB}}{c}+\sum_{n=1}^{\infty}\mathcal{T}_r^{(n)}(\boldsymbol{x}_{A},t_{B},\boldsymbol{x}_{B}), \tag{8}$$

where $R_{AB} = |\boldsymbol{x}_B - \boldsymbol{x}_A|$ and $\mathcal{T}_r^{(n)}$ stands for the perturbation term of order G^n. It is shown in Teyssandier & Le Poncin-Lafitte 2008a that each $\mathcal{T}_r^{(n)}$ can be expressed by an iterative procedure as a line integral whose the integrand involves only the terms $g_{\mu\nu}^{(k)}$ and $\mathcal{T}_r^{(l)}$ such that $k \leq n-1$, $l \leq n-1$, with an integration taken along the straight line passing through x_B defined by

$$x^\alpha = z^\alpha(\lambda), \quad z^0(\lambda) = x_B^0 - \lambda R_{AB}, \quad z^i(\lambda) = x_B^i - \lambda(x_B^i - x_A^i), \quad 0 \leq \lambda \leq 1. \tag{9}$$

So, computing the TTFs never requires the knowledge of the real null geodesics followed by the photons.

4. APPLICATION TO STATIC, SPHERICALLY SYMMETRIC SPACE-TIMES

The procedure outlined in section 3 allows the determination of the TTF and the direction of light propagation in a static spherically symmetric space-time at any order in G (Teyssandier 2014). This determination can also be obtained by an iterative solution of an integro-differential equation derived from the null geodesic equations (Linet & Teyssandier 2013). Denoting by M the mass of the central body and assuming the metric to be a generalization of the Schwarzschild ds^2 written in the form

$$ds^2 = \left(1 - \frac{2m}{r} + 2\beta\frac{m^2}{r^2} - \frac{3}{2}\beta_3\frac{m^3}{r^3} + \cdots\right)(dx^0)^2 - \left(1 + 2\gamma\frac{m}{r} + \frac{3}{2}\epsilon\frac{m^2}{r^2} + \frac{1}{2}\gamma_3\frac{m^3}{r^3} + \cdots\right)d\boldsymbol{x}^2, \tag{10}$$

where $r = |\boldsymbol{x}|$, $m = GM/c^2$ and the coefficients $\beta, \beta_3, \gamma, \epsilon, \gamma_3$, are post-Newtonian parameters equal to 1 in general relativity, the two methods lead to expressions[2] as follow for the first three terms in Eq. (8):

$$\mathcal{T}^{(1)}(\boldsymbol{x}_A, \boldsymbol{x}_B) = \frac{(1+\gamma)m}{c}\ln\left(\frac{r_A + r_B + R_{AB}}{r_A + r_B - R_{AB}}\right), \tag{11a}$$

$$\mathcal{T}^{(2)}(\boldsymbol{x}_A, \boldsymbol{x}_B) = \frac{m^2}{r_A r_B}\frac{R_{AB}}{c}\left[\kappa\frac{\arccos \boldsymbol{n}_A.\boldsymbol{n}_B}{|\boldsymbol{n}_A \times \boldsymbol{n}_B|} - \frac{(1+\gamma)^2}{1 + \boldsymbol{n}_A.\boldsymbol{n}_B}\right], \tag{11b}$$

$$\mathcal{T}^{(3)}(\boldsymbol{x}_A, \boldsymbol{x}_B) = \frac{m^3}{r_A r_B}\left(\frac{1}{r_A} + \frac{1}{r_B}\right)\frac{R_{AB}}{c(1 + \boldsymbol{n}_A.\boldsymbol{n}_B)}\left[\kappa_3 - (1+\gamma)\kappa\frac{\arccos \boldsymbol{n}_A.\boldsymbol{n}_B}{|\boldsymbol{n}_A \times \boldsymbol{n}_B|} + \frac{(1+\gamma)^3}{1 + \boldsymbol{n}_A.\boldsymbol{n}_B}\right], \tag{11c}$$

where $\boldsymbol{n}_A = \boldsymbol{x}_A/r_A$, $\boldsymbol{n}_B = \boldsymbol{x}_B/r_B$ and $\kappa = 2(1+\gamma) - \beta + 3/4\varepsilon$, $\kappa_3 = 2\kappa - 2\beta(1+\gamma) + (3\beta_3 + \gamma_3)/4$.

Equation (11a) is equivalent to the well-kown formula due to Shapiro and (11b) recovers the expression already obtained in Teyssandier & Le Poncin-Lafitte 2008a, and then in Klioner & Zschocke 2010. On the other hand, (11c) is a recent result and shows the fecondity of the new procedures.

It follows from Eqs. (11a)-(11c) that at least for $n \leq 3$, an enhancement of the contribution proportional to $(1+\gamma)^n$ appears in configurations of quasi-conjunction, i.e. when the unit 3-vectors $\boldsymbol{n}_A$ and $\boldsymbol{n}_B$ are almost opposite ($1 + \boldsymbol{n}_A.\boldsymbol{n}_B \sim 0$). A result inferred in Ashby & Bertotti 2010 by an 'asymptotic reasoning' is thus rigorously confirmed. The 2pM enhanced term in (11b) will be required for analyzing data in future missions like for example BepiColombo (Iess et al. 2009), as it may be seen on Figs. 2 and 3 in Hees et al. 2014a. The 3pM enhanced contribution from the Sun may reach 30 ps for a light ray grazing the Sun (see Table 1 in Linet & Teyssandier 2013). Taking this contribution into account will therefore be necessary for modelling space mission proposals like ODYSSEY (Christophe 2009), LATOR (Turyshev 2009) or ASTROD (Braxmaier et al. 2012), designed to measure the 1pN parameter γ at the level of 10^{-7}-10^{-8}.

The light deflection has been calculated and discussed within the 2pM approximation in Klioner & Zschocke 2010, Ashby & Bertotti 2010 and Teyssandier 2012. The enhanced 2pM term, proportional to $(1+\gamma)^2$, can reach 16 microarcsecond (μas) for a ray grazing Jupiter (see right of Fig. 2) and is therefore required in the analysis of Gaia data (see, e.g., de Bruijne 2012). In Teyssandier & Linet 2014 and Hees et al. 2014a, it is noted that for a ray grazing the Sun, the 2pM and 3pM enhanced contributions amount to 3 milliarcsecond (mas) and 12 μas, respectively. The last value is to be compared with the 2pM contribution due to the 2pN parameter κ, as illustrated on the left of Fig. 2.

5. EFFECTS DUE TO THE ASPHERICITY AND/OR THE MOTION OF BODIES

The gravitational potential of an axisymmetric body is parametrized amongst others by its mass multipole moments J_n. Using a property previously established in Kopeikin 1997 and recovered later

[2]Note that owing to the static character of the metric, $\mathcal{T}_r$ does not depend on t_B. So we may remove the index r.

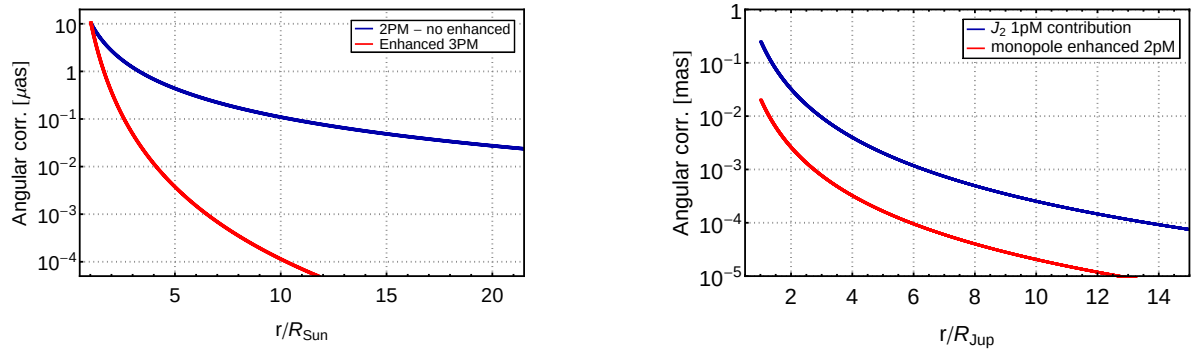

Figure 1: Left: Contribution of the 2pM term proportional to κ and the 3pM enhanced term on the light deflection for a Sun grazing ray. – Right: Contribution of Jupiter J_2 at 1pM order and contribution of the enhanced 2pM Jupiter monopole term on the deflection of a Jupiter grazing light ray.

(see Teyssandier et al. 2008b and references therein), explicit formulas for the contributions of each J_n to the TTF and its first derivatives have been given in Le Poncin-Lafitte & Teyssandier 2008. Thus, it becomes possible to calculate the influence of any J_n on the gravitational light deflection. These results generalize the expressions previously obtained in various papers for $n = 1$ and $n = 2$ (see, e.g., Klioner 2003b, Kopeikin & Makarov 2007, and references therein). Recall that the Jupiter J_2 must be taken into account in the analysis of Gaia (see Crosta & Mignard 2006 and references therein) or VLBI observations (see the right of Fig. 1) since it produces a deflection amounting to 240 μas for a grazing light ray. A similar conclusion holds for the Juno mission (see Anderson et al. 2004) since it is shown in Hees et al. 2014b that the influence of the quadrupole moment of Jupiter reaches the level of the cm for the range and the level of 10 μm/s for the Doppler (see left of Fig. 2). Some of these effects will be relevant in the data reduction since the expected accuracies for Juno are of 10 cm on the range and 1 μm/s on the Doppler.

The procedure outlined in section 3 noticeably facilitates the determination of the TTF of a uniformly moving axisymmetric body within the 1pM approximation. Denote by $\tilde{\mathcal{T}}_r^{(1)}$ the 1pM TTF corresponding to the body at rest. When this body is uniformly moving with a coordinate velocity $\boldsymbol{v} = c\boldsymbol{\beta}$, it is shown in Hees et al. 2014b that the 1pM TTF can be written as

$$\mathcal{T}_r^{(1)}(\boldsymbol{x}_A, t_B, \boldsymbol{x}_B) = \Gamma(1 - \boldsymbol{N}_{AB}.\boldsymbol{\beta})\tilde{\mathcal{T}}_r^{(1)}(\boldsymbol{R}_A + \Gamma R_{AB}\boldsymbol{\beta}, \boldsymbol{R}_B) \,, \tag{12}$$

where $\Gamma = (1 - \beta^2)^{-1/2}$ is the Lorentz factor and

$$\boldsymbol{R}_X = \boldsymbol{x}_X - \boldsymbol{x}_p(t_0) + \frac{\Gamma^2}{1+\Gamma}\boldsymbol{\beta}\left[\boldsymbol{\beta}.(\boldsymbol{x}_X - \boldsymbol{x}_p(t_0))\right] - \Gamma\boldsymbol{v}(t_B - t_0) \,, \tag{13}$$

with $\boldsymbol{x}_p(t_0)$ being the position of the deflecting body at an arbitrary time t_0 usually chosen between $t_B - R_{AB}/c$ and t_B. This recent and general result is particularly simple. The first derivatives of the right-hand side of (12) are easily calculated. For a moving monopole, using Eq. (11a) for $\tilde{\mathcal{T}}_r^{(1)}$ and Eq. (12) gives

$$\mathcal{T}_r^{(1)}(\boldsymbol{x}_A, t_B, \boldsymbol{x}_B) = (1+\gamma)m\Gamma(1 - \boldsymbol{\beta}.\boldsymbol{N}_{AB}) \ln \frac{|\boldsymbol{R}_A + \Gamma R_{AB}\boldsymbol{\beta}| + R_B + \Gamma R_{AB}(1 - \boldsymbol{\beta}.\boldsymbol{N}_{AB})}{|\boldsymbol{R}_A + \Gamma R_{AB}\boldsymbol{\beta}| + R_B - \Gamma R_{AB}(1 - \boldsymbol{\beta}.\boldsymbol{N}_{AB})}. \tag{14}$$

This formula recovers the expression obtained in Kopeikin & Schäffer 1999 and Klioner 2003a using longer calculations. A low velocity expansion of this result is obtained in Bertone et al. 2014. To finish, let us mention that using a similar method but a symmetric trace free (STF) decomposition of the gravitational potential, Soffel & Han 2014 have also determined the expression of the TTF produced by a moving body with arbitrary static multipoles, but their result is only valid in the slow velocity approximation.

In Hees et al. 2014b, these results are applied in the context of the Juno mission to discuss the effects of the mass and the quadrupole moment of Jupiter when the motion of this planet is taken into account. The effect of the motion of Jupiter's monopole is represented on the right of Fig. 2. This contribution is smaller than the expected Juno Doppler accuracy and can safely be ignored in the reduction of the

observations. Nevertheless, it is important to point out that this numerical estimate depends highly on the geometry of the probe orbit and should be reassessed in the context of other space missions. In particular, this contribution depends on the quantity $\boldsymbol{\beta}.\boldsymbol{N}_{AB}$ and on the presence of conjunctions (which is not the case for Juno owing its polar orbit, but will be the case in other missions). The deflection of light produced by the motion of Jupiter monopole is of the order of 0.04 μas for a grazing light ray and can safely be ignored for current observations.

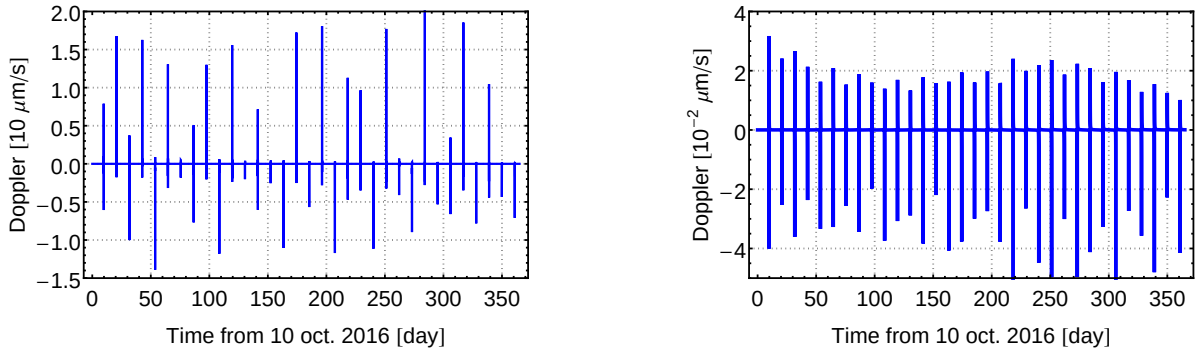

Figure 2: Left: Effect of Jupiter J_2 on a Doppler link between Juno and Earth. Right: Effect of Jupiter's velocity on a Doppler link between Juno and Earth.

6. NUMERICAL DETERMINATION OF THE TTFs AND THEIR DERIVATIVES

The TTF formalism lends itself well to the numerical simulations of the light propagation in curved space-time. This is useful when no analytical expressions can be found or when systematic comparisons of the propagation of light in different space-times are discussed. This approach is fully developed within the 2pM approximation in Hees et al. 2014a. The iterative procedure mentioned in Sect. 3 gives

$$\mathcal{T}_r^{(1)} = \int_0^1 n\left[z^\alpha(\lambda); g^{(1)}_{\alpha\beta}, R_{AB}\right] d\lambda, \tag{15a}$$

$$\frac{\partial \mathcal{T}_r^{(1)}}{\partial x^i_{A/B}} = \int_0^1 n_{A/B}\left[z^\alpha(\lambda); g^{(1)}_{\alpha\beta}, g^{(1)}_{\alpha\beta,\sigma}, \boldsymbol{x}_A, \boldsymbol{x}_B\right] d\lambda, \tag{15b}$$

for $\mathcal{T}_r^{(1)}$ and its first derivatives, and then

$$\mathcal{T}_r^{(2)} = \int_0^1\int_0^1 l\left[z^\alpha(\mu\lambda); g^{(2)}_{\alpha\beta}, g^{(1)}_{\alpha\beta}, g^{(1)}_{\alpha\beta,\sigma}, \boldsymbol{x}_A, \boldsymbol{x}_B\right] d\mu\, d\lambda\,, \tag{16a}$$

$$\frac{\partial \mathcal{T}_r^{(2)}}{\partial x^i_{A/B}} = \int_0^1\int_0^1 l_{A/B}\left[z^\alpha(\mu\lambda); g^{(2)}_{\alpha\beta}, g^{(2)}_{\alpha\beta,\sigma}, g^{(1)}_{\alpha\beta}, g^{(1)}_{\alpha\beta,\sigma}, g^{(1)}_{\alpha\beta,\sigma\delta}, \boldsymbol{x}_A, \boldsymbol{x}_B\right] d\mu\, d\lambda\,, \tag{16b}$$

for $\mathcal{T}_r^{(2)}$ and its first derivatives, where the functions n, n_A, n_B, l, l_A and l_B can be explicitly written (see Hees et al. 2014a). All the integrations are taken over the straight line defined by Eqs. (9).

This kind of procedure avoids the numerical integration of the full set of geodesic equations, which is unnecessarily time consuming since we are only concerned by a single 'time function'. It has been successfully applied to simulate range, Doppler and astrometric observations within some alternative theories of gravity in order to find signatures differing from the predictions of general relativity (Hees et al. 2012, Hees et al. 2014c), and more recently to compute the propagation of light in the field of arbitrarily moving monopoles, when no analytical solution is available (Hees et al. 2014b).

7. CONCLUSION

This survey shows that the TTF formalism is a powerful tool for computing the range, Doppler and astrometric (VLBI) observables involved in Solar System experiments. The iterative method summarized

in section 3 is very effective in deriving analytical and numerical solutions. The simplicity of this method relies mainly on the fact that one never has to determine the real trajectory of the photon in order to perform an explicit calculation of the TTF. We have reviewed some of the analytical expressions derived using this formalism. This method has been successfully applied to determine the light propagation in a static spherically symmetric space-time up to the 3pM order and a generic procedure enabling to compute higher order terms has been developed. It has also been applied to determine the influence of the motion and asphericity of bodies on the light propagation. The result is obtained by simple calculations. We have assessed the influence of different terms in the observation of space missions like Gaia or Juno. Finally, the TTF formalism turns out to be very well adapted to the numerical simulations of the effects observable in the Solar System.

Acknowledgements. A.H. thanks the organizers for financial support to attend this meeting. The authors are grateful for the financial support of CNRS/GRAM and Observatoire de Paris/GPHYS.

8. REFERENCES

Anderson, J.D., Lau, E.L., Schubert, G., Palguta, J.L., 2004, Bull. Am. Astron. Soc., 36, 1094.
Ashby, N., Bertotti, B., 2010, Class. and Quantum Grav., 27, 145013.
Bertone S., et al., 2014, Class. and Quantum Grav., 31, 015021.
Braxmaier, C., et al., 2012, Exp. Astron., 34, 181.
Brumberg, V.A., 1987, Kinematics Phys. Celest. Bodies, 3, pp. 6–12.
Brumberg, V., 1991, "Essential relativistic celestial mechanics", Adam Hilger.
Christophe, B., et al., 2009, Exp. Astron., 23, 529.
Crosta, M.T., Mignard, F., 2006, Class. Quantum Grav., 23, 4853.
de Bruijne, J.H.J., 2012, "Science performance of Gaia, ESA's space astrometry mission", arXiv:1201.3238.
Hees, A., Lamine, B., Reynaud, S., et al., 2012, Class. and Quantum Grav., 29, 235027.
Hees, A., Bertone, S., Le Poncin-Lafitte, C., 2014a, Phys. Rev. D, 89, 064045.
Hees, A., Bertone, S., Le Poncin-Lafitte, C., 2014b, Phys. Rev. D, 90, 084020.
Hees, A., Folkner, W., Jacobson, R., Park, R., 2014c, Phys. Rev. D, 89, 102002.
Iess, L., Asmar, S., Tortora, P., 2009, Acta Astronaut., 65, 666.
John, R.W., 1975, Exp. Tech. Phys., 23, pp. 127–140.
Klioner, S., 2003a, A&A, 404, 783.
Klioner, S., 2003b, AJ, 125, 1580.
Klioner, S., Zschocke, S., 2010, Class. and Quantum Grav., 27, 075015.
Kopeikin, S., 1997, J. of Math. Physics, 38, 2587.
Kopeikin, S., Schäffer, G., 1999, Phys. Rev. D, 60, 124002.
Kopeikin, S., Makarov, V., 2007, Phys. Rev. D, 75, 062002.
Le Poncin-Lafitte, C., Linet, B., Teyssandier, P., 2004, Class. and Quantum Grav., 21, 4463.
Le Poncin-Lafitte, C., Teyssandier, P., 2008, Phys. Rev., D 77, 044029.
Linet, B., Teyssandier, P., 2002, Phys. Rev., D 66, 024045.
Linet, B., Teyssandier, P., 2013, Class. and Quantum Grav., 30, 175008.
Richter, G., Matzner, R., 1983, Phys. Rev., D 28, 3007.
San Miguel, A., 2007, Gen. Rel. and Grav., 39, 2025.
Shapiro, I., 1964, Phys. Rev. Letters, 13, 789.
Soffel, M., Han, W.-B., 2014, arXiv:1409.3743.
Teyssandier, P., Le Poncin-Lafitte, C., 2006, arXiv:gr-qc/0611078.
Teyssandier, P., Le Poncin-Lafitte, C., 2008a, Class. and Quantum Grav., 25, 145020.
Teyssandier, P., Le Poncin-Lafitte, C., Linet, B., 2008b, In: Lasers, Clocks and Drag-Free Control: Exploration of Relativistic Gravity in Space, p. 153, Springer.
Teyssandier, P., 2012, Class. and Quantum Grav., 29, 245010.
Teyssandier, P., 2014, In: Frontiers in Relativistic Celestial Mechanics, S.M. Kopeikin (ed.), vol. 2, p. 1, De Grutyer, Berlin; arXiv:1407.4361.
Teyssandier, P., Linet, B., 2014, In: Proc. Journées 2013 "Systèmes de Référence Spatio-Temporels", N. Capitaine (ed.), Observatoire de Paris, pp. 24–27.
Turyshev, S.G., et al., 2009, Exp. Astron., 27, 27.

HIGH-ACCURACY TIMING FOR GAIA DATA FROM ONE-WAY TIME SYNCHRONIZATION

S.A. KLIONER
Lohrmann-Observatorium, Technische Universität Dresden,
01062 Dresden, Germany
e-mail: Sergei.Klioner@tu-dresden.de

ABSTRACT. This work contains a brief description of the algorithms behind the timing subsystem of the Gaia data processing. The reading of the free-running atomic clock on board of Gaia should be related to the widely used time scales like TCB. The accuracy requirements for the data timing for Gaia are summarized. To monitor the synchronization between TCB and the on-board clock Gaia implements the one-way clock synchronization scheme. The available data and the algorithms used for the time synchronization are discussed.

1. REQUIREMENTS FOR THE GAIA DATA TIMING

The second ESA astrometry mission Gaia launched on 19 December 2013 successfully passed the scrutiny of the commissioning phase and delivers scientific data since July 2014. This paper is devoted to one particular aspect of the Gaia data processing: expressing the Gaia-internal time tags of each observation in terms of widely-used time scales like TCB, which can be used e.g. to interrogate solar system ephemerides or to link Gaia observations with observations performed by other instruments.

Each observation of Gaia is internally tagged with the corresponding reading of the Gaia clock latched at some fiducial event defined within the time span taken by that individual observation. A free-running clock is installed on board of Gaia and produces time tags which are called On-Board Time (OBT). OBT is a technical time scale which reflects all the imperfections of the particular clock. OBT can also have jumps related to the resets of the clock (in some technical conditions the Gaia clock can be automatically switched off before being switched on again). In this way OBT remains a purely technical time scale with no a priori relation to the widely-used time scales like TCB that are realized by Earth-based ensembles of clocks via TAI or TT.

The timing requirements for Gaia are tricky and represent a source of confusion even within the Gaia Data Processing and Analysis Consortium (DPAC). As usual in the time science, one should carefully distinguish between *stability* and *accuracy* of the timing information.

All the digital electronics on board of Gaia (e.g., the CCDs) must be driven by some frequency standard. Many space missions use a sort of quartz (crystal) oscillator to drive the on-board electronics. A space-qualified crystal oscillator has a stability of typically 5×10^{-5} in a very large range of temperature. This stability can improve to about 5×10^{-7} in the thermally stable environment of Gaia, but it is still very far from the Gaia requirements. Indeed, Gaia rotates with angular velocity of $60''$/sec or 0.6 microarcsecond in 10 nanoseconds. The ultimate accuracy of centroiding for one observation is expected to be at the order of ten microarcseconds. No systematic errors over the rotational period (6 hours = 21600) should be introduced by the clock performance. This means that the timing error should be below 10 nanoseconds over the period of 21600 seconds, which implies the frequency stability of the on-board clock below 10^{-12}. For this reason Gaia spacecraft has got an atomic (Rb) clock with the stability reaching $\sim 10^{-13}$ over the Gaia rotational period of 21600 seconds.

The accuracy requirements for the OBT tags are very different in their nature and origin. A shift in the Gaia clock phase or in its frequency would be no problem in a purely Gaia-internal data processing (as long as the frequency stability remains at the level discussed above). The relation between the OBT readings and some Gaia-external time scales becomes important as soon as some auxiliary data are used in the data processing. Those auxiliary data (e.g. Gaia or solar system ephemerides) are usually parametrized using some TAI/TT-based time scale (TT, UTC, TCG, TCB, etc.) and the relation between OBT and, say, TCB is needed to interrogate the auxiliary data with the correct argument. Similarly, analyzing some time-dependent phenomena or predicting some astronomical events one wishes to express the analysis in

terms of generally available time scales. One can think of several different sources of requirements coming from different types of time-dependent astronomical phenomena: variability of stars, motion of binary stars, motion of asteroids, etc. On the other hand, the *model* describing Gaia observations uses time-dependent positions and velocities of Gaia and massive solar system bodies and they should be computed at the correct moments of time. Taking into account all these applications, the official goal for the timing accuracy for Gaia was taken to be 1.7 microseconds. This number resulted from an assessment of the level of accuracy achievable without any upgrade of the timing hardware available at the ESA ground stations.

It is clear that at the level of accuracy better than a few milliseconds the modeling of the Gaia clock must be relativistically meaningful. This means in turn that the atomic clock of Gaia could be used to test tentative violations of the Local Positional Invariance. From this point of view, it is useful to model the timing data as careful as possible to reach maximal possible accuracy. It should be stressed that further increase of the accuracy can be reached only by improving the data processing algorithms and careful assessment of the input data. No additional observational efforts are required.

2. ONE-WAY CLOCK SYNCHRONIZATION DATA

There are many technical ways to synchronize remote clocks (see, e.g. Klioner, 1992). In principle, for a microsecond accuracy with a pair of clocks separated by 1.5 million kilometers, one would think of the so-called two-way clock synchronization as the most appropriate method. In this method a special signal generated on a reference station is sent to the remote clock (to Gaia), where it is received and, after some well-calibrated delay, re-transmitted back to the reference station together with the time reading of the remote clock at which the signal was received. The well-known advantage of this method is that the errors in the position of the remote clock don't directly deteriorate the resulting accuracy. This is also true for the tropospheric delay: the delays on the way from the ground station to the remote clock and back largely cancel out.

However, the hardware readily available on the ESA Tracking Stations (ESTRACK) is not prepared for the two-way clock synchronization and this option was dropped early at the design stage of Gaia. A straightforward one-way clock synchronization scheme was implemented instead. In the application to Gaia this scheme can be summarized as follows:

(1) a signal is generated on board of Gaia that contains the momentary (latched) OBT value – we denote it by OBT_k – and initiates the process of transmission of a special data packet, called "time packet" to the ground station;
(2) after some on-board delay the time packet is emitted from Gaia to the ground station;
(3) the time packet propagates all the way from Gaia to the phase center of the ESTRACK station antenna;
(4) after some ground-station delay the content of the time packet (in particular, the value of OBT_k) is registered by the ESTRACK station hardware by assigning the corresponding value of UTC – we denote it by UTC_k – and storing the time couple $(\mathrm{OBT}_k, \mathrm{UTC}_k)$ in the database.

Thus the raw data for the time synchronization is a series of the time couples $(\mathrm{OBT}_k, \mathrm{UTC}_k)$. These time couples are obtained at irregular intervals of time with a typical interval of 1.5 sec between the subsequent time couples within the visibility periods, that is, the periods of time during which Gaia communicates with one of the ESTRACK stations. The visibility periods range between about 3 and 16 hours depending on the data volume that needs to be transmitted from Gaia to the ground.

3. LOW-ACCURACY TIME TRANSFORMATIONS

Beside the purely scientific use summarized above, the relation of OBT and, say, UTC is required for the technical control of the spacecraft. All the control commands to be sent from the European Space Operation Center (ESOC) to the Gaia spacecraft must be time-tagged in OBT since it is the only timing information that is available on board for the Gaia hardware and software. The required accuracy of this time transformation is at most 1 millisecond (even 0.1 sec can be often tolerated). The ESOC team generates this lower-accuracy time transformation between UTC and OBT independently of Gaia DPAC. This is termed "time correlation" and is done by fitting a straight line to the moment $\mathrm{UTC}_k^{\mathrm{em}}$ as function of OBT_k using some selected number of time couples. Here $\mathrm{UTC}_k^{\mathrm{em}}$ is the computed UTC moment of emission of the signal, which was received at the moment UTC_k. The moment $\mathrm{UTC}_k^{\mathrm{em}}$ is

computed by subtracting the light travel time from UTC_k. The light travel time is computed used a predicted orbit of Gaia and neglecting tropospheric delay. The deviation of newly coming time couple data from the last computed linear relation between UTC and OBT is automatically checked. As soon as the deviation exceeds some limit, the operator is supposed to initiate the computation of the new linear relation. In this way one gets a piecewise linear relation between UTC and OBT. The validity intervals of individual linear functions range from a few hours to several weeks. The overall accuracy of the OBT synchronization obtained in this way reaches a few milliseconds.

Within the Gaia DPAC this ESOC product is used to generate the so-called Low Accuracy Time Transformation (LATT), which still uses a piecewise-linear fit between OBT and UTC, but is optimized in a number of ways to minimize the deviation from the timing data (time couples). The generation of the LATT is done immediately after the end of each visibility period of Gaia. The accuracy of the LATT is usually about 0.5 millisecond, but can vary depending on the operational circumstances. This level of accuracy is enough for the daily operations of Gaia (for all the tasks in the Gaia data processing chain that are performed immediately after receiving the next potion of the data). Since the LATT can also be generated immediately after the data become available, the LATT is used by the Gaia DPAC for daily operations.

However, the accuracy of LATT is not sufficient for the final data processing where a substantially higher accuracy is required. To improve the accuracy further, one needs to improve the model used to interpret the timing data. The deficiencies of the LATT modeling are obvious. The idea to directly correlate "UTC of emission" and OBT ignores all relativistic effects and mixes the errors of the Gaia clock with the relativistic effects between the proper time of Gaia and UTC. The latter effects are substantially non-linear and directly deteriorate the validity intervals and accuracy of the LATT.

For this reasons, a more rigorous high-accuracy approach for the Gaia clock synchronization was developed. This approach is called High Accuracy Time Transformation (HATT) The accuracy of HATT is supposed to reach the level of about 1 microsecond matching the accuracy requirements discussed above.

4. HIGH-ACCURACY TIME TRANSFORMATIONS

The HATT algorithm is a rigorous and straightforward relativistic model for the one-way clock synchronization data described in Section 2 above. The algorithm explicitly introduces the proper time of Gaia, which is denoted TG and represents an ideal clock located at the Gaia center of mass. The displacement of the Gaia's atomic clock from the Gaia center of mass is fully negligible in the current context. This means that the deviation between OBT and TG solely reflects the errors of the Gaia Rb clock.

TG can be computed as function of TCB using the ephemerides of Gaia and massive solar system bodies. The relation between the proper time of Gaia $\tau = \mathrm{TG}$ and $t = \mathrm{TCB}$ is given by the basic relation of metric gravity theories:

$$\frac{\tau}{dt} = 1 + f(t), \tag{1}$$

$$f = \frac{1}{c^2}\,\alpha(t) + \frac{1}{c^4}\,\beta(t) + \mathcal{O}(c^{-5}), \tag{2}$$

where $\alpha(t)$ and $\beta(t)$ are defined by the metric tensor of the BCRS and the usual relations of General Relativity:

$$\alpha(t) = -\frac{1}{2}\,v_o^2 - \sum_A \frac{GM_A}{r_{oA}}, \tag{3}$$

$$\begin{aligned}\beta(t) = {} & -\frac{1}{8}\,v_o^4 + \left(\beta - \frac{1}{2}\right)\left(\sum_A \frac{GM_A}{r_{oA}}\right)^2 + (2\beta - 1)\sum_A \left(\frac{GM_A}{r_{oA}} \sum_{B\neq A} \frac{GM_B}{r_{AB}}\right) \\ & + \sum_A \frac{GM_A}{r_{oA}}\left(2(1+\gamma)v_A^i v_o^i - \left(\gamma + \frac{1}{2}\right)\,v_o^2 - (1+\gamma)v_A^2 + \frac{1}{2}a_A^i r_{oA}^i \right. \\ & \left. + \frac{1}{2}(v_A^i r_{oA}^i / r_{oA})^2\right).\end{aligned} \tag{4}$$

Here $\mathbf{r}_{oA} = \mathbf{x}_o - \mathbf{x}_A$, $\mathbf{x}_o$ and $\mathbf{v}_o$ are the BCRS position and velocity of Gaia, index A enumerated gravitating bodies of the solar system, $\mathbf{x}_A$ and $\mathbf{v}_A$ are the BCRS position and velocity of body A, and GM_A is the mass parameter of that body. Similar to the treatment in (Klioner et al. 2010) we introduce here functions $\delta t(t)$ and $\delta\tau(\tau)$ as

$$\tau = t + \delta t(t), \tag{5}$$
$$t = \tau - \delta\tau(\tau). \tag{6}$$

Substituting these definitions in (1) one gets

$$\frac{d\delta t}{dt} = f(t), \tag{7}$$
$$\frac{d\delta\tau}{d\tau} = \frac{f(\tau - \delta\tau(\tau))}{1 + f(\tau - \delta\tau(\tau))}. \tag{8}$$

These relations are exact. The expression for $f(t)$ given above is approximate. The initial conditions for these differential equations come from the condition that τ = TG is numerically equal to t = TCB at some moment $t = t_0$: $\tau(t_0) = \tau_0 = t_0$. This condition is equivalent to

$$\delta t(t_0) = 0, \tag{9}$$
$$\delta\tau(\tau_0) = 0. \tag{10}$$

The initial condition for TG is in principle arbitrary and is fixed as $\tau_0 = t_0$ =JD2457023.5 TCB (2015 January 01 00:00:00.0 TCB). With these initial conditions, Eqs. (7)–(8) are integrated numerically using the solar system and Gaia ephemerides. The results of numerical integration are represented as Chebyshev polynomials (Newhall, 1989; Klioner, 2010) thus giving time ephemerides for the transformations between TG and TCB in both directions. As solar system ephemeris a special TCB-based ephemeris INPOP10e is used. Gaia ephemeris is updated once per week by the flight dynamics team of ESOC. The TG–TCB transformation is updated as soon as a new version of Gaia ephemeris is received. All time transformations relevant for Gaia data processing and the details of their implementation are summarized in (Klioner, 2010).

The overall idea of the HATT modeling is to construct a smooth relation between OBT and TG. As it was already pointed out, this relation reflects only the imperfection of the Gaia Rb clock. Since the Rb clock is of very high quality one can expect a simple relation between OBT and TG. On the other hand, the OBT–TG relation represents physical model of the Gaia clock as if the clock would be monitored in a laboratory. In this way the health status of the clock and its performance can be directly assessed.

As a mathematical model for the relation between OBT and TG one can choose piecewise linear or piecewise quadratic function to account for frequency offset and frequency drift that are typical for a Rb clock. Because of the rotation of Gaia, one should expect certain temperature variations in the service module of Gaia, where the clock is located. Those temperature variations can lead to periodic variations of the clock frequency. If the data show periodic variations of OBT with respect to TG with a period of 6 hours, this variation can be easily fitted in the model together with the quadratic or linear polynomial.

Before the clock model between TG and OBT can be constructed, one needs to recompute the raw time couples $(\mathrm{OBT}_k, \mathrm{UTC}_k)$ into the couples of OBT and TG corresponding to one and the same physical event. Various physical events can be chosen, but the most natural choice seems to be the event of the emission of the signal corresponding to the time couple $(\mathrm{OBT}_k, \mathrm{UTC}_k)$. The HATT modeling scheme is depicted on Fig. 1. The scheme can be summarized as follows:

(A) The on-board delay $\Delta_{\mathrm{on-board}}$ is added to the latched OBT value OBT_k to get the OBT moment of emission:

$$\mathrm{OBT}_k^{\mathrm{emission}} = \mathrm{OBT}_k + \Delta_{\mathrm{on-board}}\,. \tag{11}$$

The on-board delay $\Delta_{\mathrm{on-board}}$ depends on the particular telemetry mode used at the moment of observation.

(B) The corresponding value of TG at the moment of emission $\mathrm{TG}_k^{\mathrm{emission}}$ is computed from the registered UTC value UTC_k in several steps:

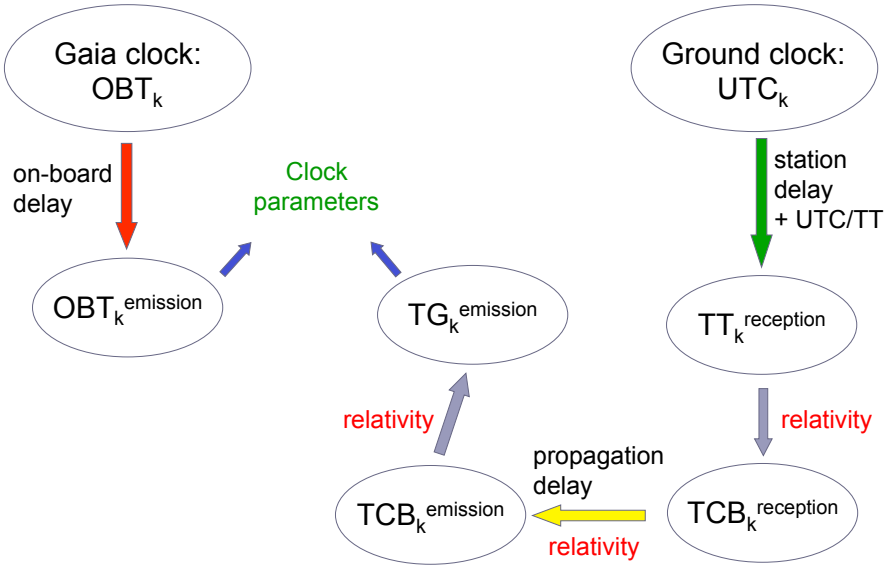

Figure 1: The HATT modeling scheme (see text for further details)

(a) The ground-station delay $\Delta_{\rm gs}$ is subtracted from the recorded UTC value UTC_k to get the UTC moment of reception:

$$\mathrm{UTC}_k^{\rm reception} = \mathrm{UTC}_k - \Delta_{\rm gs}\,. \tag{12}$$

The ground-station delay $\Delta_{\rm gs}$ again depends on the particular telemetry mode used at the moment of observation.

(b) The moment of reception in $\mathrm{TCB}_k^{\rm reception}$ is computed using the relativistic time transformations (Klioner, 2010):

$$\mathrm{UTC}_k^{\rm reception} \longrightarrow \mathrm{TAI}_k^{\rm reception} \longrightarrow \mathrm{TT}_k^{\rm reception} \longrightarrow \mathrm{TDB}_k^{\rm reception} \longrightarrow \mathrm{TCB}_k^{\rm reception} \tag{13}$$

Note that the transformation between TT and TDB is 4-dimensional and requires the position of the ground station in BCRS (this implies the use of the Earth orientation in space).

(c) The TCB moment of reception $\mathrm{TCB}_k^{\rm reception}$ is used to compute the TCB moment of emission of the corresponding signal by Gaia $\mathrm{TCB}_k^{\rm emission}$. Here one should account for the tropospheric delay $\Delta_{\rm tropo}$ and compute the TCB time interval that the signal needs to propagate from Gaia to the ground station in BCRS. This includes an solution of the implicit equation:

$$\mathrm{TCB}_k^{\rm emission} - \mathrm{TCB}_k^{\rm vacuum} = c^{-1}\,R + \Delta_{\rm pN}\,, \tag{14}$$

$$\mathrm{TCB}_k^{\rm vacuum} = \mathrm{TCB}_k^{\rm reception} - \Delta_{\rm tropo}\,, \tag{15}$$

$$R = \left|\mathbf{x}_o(\mathrm{TCB}_k^{\rm emission}) - \mathbf{x}_{\rm gs}(\mathrm{TCB}_k^{\rm vacuum})\right|\,, \tag{16}$$

$$\Delta_{\rm pN} = \sum_A \frac{2GM_A}{c^3}\,\log\frac{r_A + r_{A0} + R}{r_A + r_{A0} - R}\,, \tag{17}$$

$$r_A = \left|\mathbf{x}_o(\mathrm{TCB}_k^{\rm emission}) - \mathbf{x}_A(t_A^*)\right|\,, \tag{18}$$

$$r_{A0} = \left|\mathbf{x}_{\rm gs}(\mathrm{TCB}_k^{\rm vacuum}) - \mathbf{x}_A(t_A^*)\right|\,, \tag{19}$$

where $\mathbf{x}_o(t)$ is again the BCRS position of Gaia, $\mathbf{x}_{\rm gs}(t)$ is the BCRS position of the relevant ESTRACK station (both are computed as functions of TCB), and $\Delta_{\rm pN}$ is the relativistic (Shapiro) light propagation delay in BCRS. In (17) at least the Sun must be taken into account here, but the Earth and Jupiter may also play a role. The TCB moment t_A^* is given by the implicit equation

$$c\,(\mathrm{TCB}_k^{\rm vacuum} - t_A^*) = \mathbf{r}_{A0}\,. \tag{20}$$

The latter equation can be solved by iterations (one Newton-like iteration is sufficient here).

(d) The TCB moment of emission $\mathrm{TCB}_k^{\mathrm{emission}}$ is recomputed into the corresponding moment of the Gaia proper time TG_k:

$$\mathrm{TCB}_k^{\mathrm{emission}} \longrightarrow \mathrm{TG}_k \tag{21}$$

This is done using the TG–TCB time ephemeris described above (Klioner, 2010).

From this description, it is obvious that the HATT data processing requires a number of additional data. First, four sorts of constants are required for each ESTRACK station:

(i) the ITRS coordinates (this includes the Cartesian coordinates as well as the height above the horizon);
(ii) the coefficients of the mapping function for the tropospheric delay (the dry and wet Niell mapping functions are used; a total of 9 coefficients per station);
(iii) the adjustment of the dry delay due to the altitude difference of the barometer and the intersection of the azimuth and elevation axis of the antenna (used to compute the zenith delay from the Saastamoinen model);
(iv) the ground-station delays Δ_{gs} for each telemetry mode.

All these constants were provided by ESOC. They were known previously (from the data processing of previous missions) or determined specially for Gaia using dedicated measurements. The manufacturer of the Gaia spacecraft (Airbus DS) has provided another type of constants:

(v) the on-board delays $\Delta_{\mathrm{on-board}}$ for each telemetry mode.

In addition to these constants the following data series are needed:

(vi) Gaia orbit (updated once per week by the ESOC flight dynamics team);
(vii) meteorological data – temperature, pressure and humidity – at the relevant ESTRACK station sampled once per minute (used to compute dry and wet tropospheric delays at zenith);
(viii) information on the telemetry modes used at the time of transmission of each time couple;
(ix) the Earth orientation parameters from the IERS (C04 series from `http://datacenter.iers.org/eop/-/somos/5Rgv/latest/214`; used to compute the BCRS positions of the ground stations).

The overall modeling accuracy of this algorithm is better than 30 nanoseconds and is limited by the error of the distance between Gaia and ground stations. This error can reach 10 meters. This accuracy is more than enough for all tasks in Gaia processing. The HATT data can be updated as soon as a new potion of the timing data and the auxiliary data becomes available. Typically, the auxiliary data are updated with a delay of about one month.

As it was announced earlier, all Gaia products will be parametrized by TCB, which is the most natural coordinate time for both stellar motions and solar system dynamics and does not require any ad-hoc re-scaling of astronomical constants and coordinates.

Let us stress that UTC in its current definition plays a negative role for Gaia. UTC is traditionally used in the ESA ground segment (e.g. as master time on the ground stations) and it is hardly possible to change this tradition. However, non-physical nature of UTC (its unpredictable discontinuity because of the leap seconds) directly implies a loss of precious observational data in a significant interval of time around the newly introduced leap seconds. One can only hope that the definition of UTC will be changed and no further leap seconds will be introduced starting from some time in the future.

Acknowledgements. The author was partially supported by the BMWi grant 50QG1402 awarded by the Deutsche Zentrum für Luft- und Raumfahrt e.V. (DLR).

5. REFERENCES

Klioner, S.A., 1992, "The problem of clock synchronization: a relativistic approach", Celestial Mechanics, 53, pp. 81–109.

Klioner, S.A., 2010, "Relativistic time scales and time transformations for Gaia", Gaia internal report GAIA-CA-TN-LO-SK-012, available from the Gaia Livelink document archive `http://www.rssd.esa.int/cs/livelink/open/3042112`

Klioner, S.A., Gerlach, E., Soffel, M., 2010, "Relativistic aspects of rotational motion of celestial bodies", In: Relativity in Fundamental Astronomy, Proc. IAU Symposium 261, S. Klioner, K. Seidelmann, M. Soffel (eds.), Cambridge University Press, pp. 112–123.

Newhall, XX, 1989, "Numerical representation of planetary ephemerides", Celest. Mech., 45, pp. 305–310

ON THE DEFINITION AND USE OF THE ECLIPTIC IN MODERN ASTRONOMY

N. CAPITAINE[1], M. SOFFEL[2]

[1] SYRTE, Observatoire de Paris, CNRS, UPMC, 61, av. de l'Observatoire, 75014 Paris, France
e-mail: n.capitaine@obspm.fr

[2] Lohrmann Observatory, Dresden Technical University, 01062 Dresden, Germany
e-mail: michael.soffel@tu-dresden.de

ABSTRACT. The ecliptic was a fundamental reference plane for astronomy from antiquity to the realization and use of the FK5 reference system. The situation has changed considerably with the adoption of the International Celestial Reference system (ICRS) by the IAU in 1998 and the IAU resolutions on reference systems that were adopted from 2000 to 2009. First, the ICRS has the property of being independent of epoch, ecliptic or equator. Second, the IAU 2000 resolutions, which specified the systems of space-time coordinates within the framework of General Relativity, for the solar system (the Barycentric Celestial Reference System, BCRS) and the Earth (the Geocentric Celestial Reference System, GCRS), did not refer to any ecliptic and did not provide a definition of a GCRS ecliptic. These resolutions also provided the definition of the pole of the nominal rotation axis (the Celestial intermediate pole, CIP) and of new origins on the equator (the Celestial and Terrestrial intermediate origins, CIO and TIO), which do not require the use of an ecliptic. Moreover, the models and standards adopted by the IAU 2006 and IAU 2009 resolutions are largely referred to the ICRS, BCRS, GCRS as well as to the new pole and origins. Therefore, the ecliptic has lost much of its importance. We review the consequences of these changes and improvements in the definition and use of the ecliptic and we discuss whether the concept of an ecliptic is still needed for some specific use in modern astronomy.

1. INTRODUCTION

The ecliptic was a fundamental reference plane for astronomy (astrometry, solar system dynamics and measurements) from antiquity unto the realization and use of the FK5 reference system. This plane has been chosen because the equinox has historically provided a convenient fiducial point in the observation of the heavens and the passage of time. The situation has changed considerably with the adoption of the International Celestial Reference system (ICRS) by the IAU since 1998 and with the IAU resolutions on reference systems that were adopted between 2000 and 2009. These correspond to major improvements in concepts and realizations of astronomical reference systems, in the use of observational data and the accuracy of the models for the motions of the solar system objects and Earth's rotation[1]. In that modern context, which is consistent with General relativity (GR), the ecliptic is no more a fundamental plane and the concept of an ecliptic is not as clear as those of the other modern astronomical references.

It is therefore necessary to review the consequences of these changes and improvements in the definition and use of the ecliptic and to discuss whether the concept of an ecliptic is still needed for some specific use in modern astronomy and whether a definition of the ecliptic in the GR framework is needed.

2. THE ASTRONOMICAL REFERENCE SYSTEMS AND RELATED PARAMETERS

The IAU astronomical reference systems

The International Celestial Reference System (ICRS) based on Very Long Baseline Interferometry (VLBI) observations of extragalactic radiosources has been adopted by the International Astronomical Union (IAU) since 1st January 1998 (IAU 1997 Resolution B2). The ICRS and the corresponding frame, the International Celestial Reference Frame (ICRF), replaced the FK5 system and the fundamental catalogue of stars FK5 (based on the determination of the ecliptic, the equator and the equinox), the Hipparcos

[1]The nomenclature associated with the new concepts and models has been provided by the IAU Working Group on "Nomenclature for Fundamental Astronomy" (Capitaine et al. 2007; `http://syrte.obspm.fr/iauWGnfa`).

catalogue being adopted as the primary realization of the ICRS in optical wavelengths. According to its definition, the ICRS is kinematically non-rotating with respect to the ensemble of distant extragalactic objects. It has no intrinsic orientation but was aligned close to the mean equator and dynamical equinox of J2000.0 for continuity with previous fundamental reference systems. Its orientation is independent of epoch, ecliptic or equator and is realized by a list of adopted coordinates of extragalactic sources. The current best realization of the ICRS is the second version of the ICRF, called ICRF2 (IAU 2009 Resolution B2), to which a number of catalogues of celestial objects have been linked in order to densify it and make it accessible to astronomical observations at different wavelengths. This provides an idealized (quasi-inertial) barycentric coordinate system for measuring the positions and angular motions of the celestial objects, which is totally independent of the ecliptic.

The IAU 2000 resolutions specified the systems of space-time coordinates for the solar system and the Earth within the framework of General Relativity and provided clear procedures for the transformation between them. The Barycentric Celestial Reference System (BCRS), with its origin at the solar system barycenter and its axes oriented to match the ICRS (IAU 2006 Resolution B2) can be considered as being inertial if neglecting external galactic and extragalactic matter. It is is used for solar system ephemerides, for interplanetary spacecraft navigation, for defining the positions of remote and moving objects, etc. The Geocentric Celestial Reference System (GCRS), with its origin at the center of mass of the Earth, might be called quasi-inertial, since the spatial axes are kinematically non-rotating with respect to the spatial BCRS-axes, whereas the geocenter is accelerated (Soffel et al. 2003). It is employed for the description of physical processes in the vicinity of Earth, for satellite theory, the dynamics of Earth (including Earth's rotation), as well as for the introduction of concepts such as the equator and the International Terrestrial Reference System (ITRS), etc. Such concepts and definitions do not refer to an ecliptic and do not provide a definition of a GCRS ecliptic (e.g., the J2000 GCRS ecliptic of Fig. 1 is not defined precisely).

The Earth orientation parameters

The transformation between the GCRS (the transformed BCRS/ICRS) and the ITRS depends on Earth's rotation, that can be represented by the time-dependent Earth orientation parameters (EOP), for precession-nutation, polar motion and the rotation angle. The IAU 2000 and IAU 2006 resolutions provided accurate definitions for the pole (the Celestial intermediate pole, CIP) and for new origins on the equator (the Celestial and Terrestrial intermediate origins, CIO and TIO) defining the EOP (see Fig. 1) as well as the celestial and terrestrial intermediate reference systems (CIRS and TIRS, respectively). These concepts and definitions do not require the use of an ecliptic.

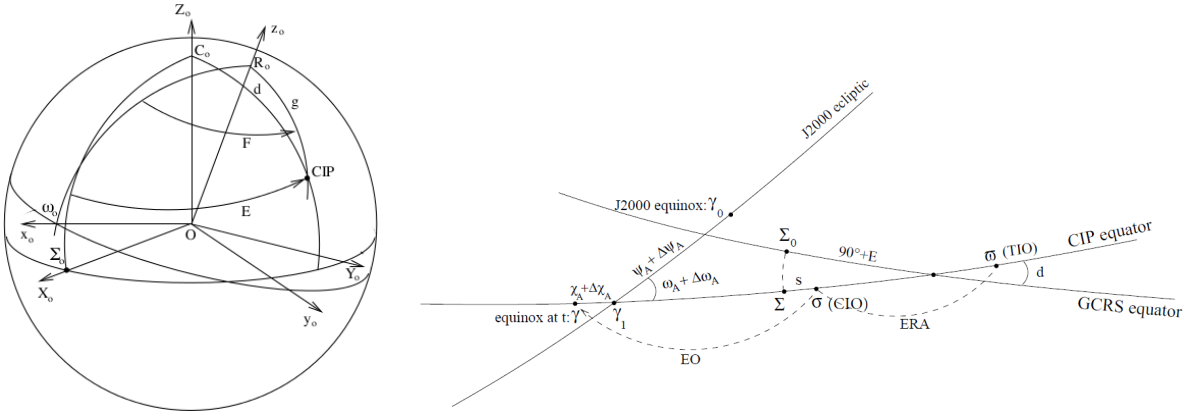

Figure 1: **left** – Orientation of the CIP unit vector: E and d are the GCRS polar coordinates (with $X = \sin d \cos E$; $Y = \sin d \sin E$); F and g are the ITRS polar coordinates (with $x = \sin g \cos F$, $y = \sin g \sin F$); **right** – ERA is the Earth Rotation Angle along the CIP equator; EO is the "equation of the origins" that links the CIO and the equinox γ; γ_0 and γ_1 are the intersections of the J2000 ecliptic (see above) with the J2000 and CIP equators, respectively; ψ_A and $\Delta\psi_A$, and ω_A and $\Delta\omega_A$ are the precession and nutation quantities in longitude and obliquity referred to the J2000 ecliptic; $\chi_A + \Delta\chi_A$ is for the ecliptic motion along the CIP equator.

In that context, right ascension and declination are considered as being generic terms which can refer to any equator and any origin on that equator (equinox, CIO, ICRS origin, etc.), with the consequence that the equinox, and therefore the ecliptic, is no longer required for expressing coordinates of celestial

objects. The IAU NFA Working Group (cf.[1]) has provided a chart explaining the CIO based reduction process from ICRS to ITRS coordinates of the directions of stars that specifies the successive celestial reference systems, i.e. ICRS, BCRS, GCRS, CIRS, TIRS and ITRS, to which the coordinates are referred and the time scale to use. This does not require the use of an ecliptic.

3. PRECESSION-NUTATION AND SOLAR SYSTEM EPHEMERIDES

IAU Precession-nutation

The current IAU precession-nutation model is composed of the IAU 2000A nutation and the IAU 2006 precession. The IAU 2000 nutation, denoted MHB2000, was obtained by Mathews et al. (2002) from the REN2000 rigid Earth nutation series of Souchay et al. (1999) for the axis of figure and the MHB2000 "transfer function" to transform from rigid to non-rigid Earth. The series for nutation in longitude and obliquity with their time variations, include 1365 terms of luni-solar and planetary origins, with "in-phase" and "out-of-phase" components and arguments that are functions of the fundamental arguments of the nutation theory, all these parameters referring to a time-dependent (i.e. moving) ecliptic.

The IAU 2006 precession (Capitaine et al. 2003) provides polynomial expressions up to the 5th degree in time t, both for the precession of the ecliptic and the precession of the equator. The precession of the ecliptic (i.e. the P_A and Q_A parameters with respect to the ecliptic and equinox of J2000.0) was computed as the part of the motion of the ecliptic covering periods longer than 300 centuries, while shorter ones are presumed to be included in the periodic component of the ecliptic motion (VSOP87 + fit to DE406). The precession of the equator was derived from the dynamical equations expressing the motion of the mean pole about the ecliptic pole. The solution includes the geodesic precession due to the relativistic rotation of the "dynamically non-rotating" geocentric frame in which the precession equations are solved with respect to the GCRS in which precession-nutation is actually observed. The convention for separating precession from nutation, as well as the integration constants used in solving the equations, have been chosen in order to be consistent with the IAU 2000A nutation. For continuity reasons, the choice of precession parameters has been left to the user. Therefore, the IAU precession for the equator provides polynomial developments for a number of quantities for use in both the equinox based and CIO based paradigms. The series for the X, Y GCRS CIP coordinates (cf. Fig. 1) consistent with the IAU 2006 precession and IAU 2000 nutation are provided in the IERS Conventions (2010) (Petit & Luzum, 2010).

Definition of the ecliptic

IAU 2006 Resolution B1 that adopted the new precession, also clarified some aspects of the definition of the ecliptic. First, it recommended that the terms *lunisolar precession* and *planetary precession* be replaced by *precession of the equator* and *precession of the ecliptic*, respectively, in order to make clear that they are due to different physical phenomena. Second, it recommended that the ecliptic pole be explicitly defined by the mean orbital angular momentum vector of the Earth-Moon barycenter (EMB) in the Barycentric Celestial Reference System (BCRS). However, even with that improvement, the concept of an ecliptic is not as clear as those of the other astronomical references introduced by the IAU 2000-2009 resolutions (cf. Section 2), e.g., for defining the "mean" of the orbital angular momentum vector, or, as already noted in Section 2, for defining the GCRS ecliptic.

The use of the ecliptic in the theory of precession-nutation

Semi-analytical solutions for the precession-nutation of the CIP equator in the GCRS can be obtained by solving the differential equations for the Euler angles ψ_A, and ω_A (cf. Bretagnon et al. 1997), or for the X and Y GCRS CIP coordinates (cf. Capitaine et al. 2005), given the semi-analytical developments of the luni-solar and planetary torques acting on the oblate Earth and integration constants; those are estimated by VLBI observations, which are only sensitive to the equator and insensitive to the ecliptic. Such solutions do not need the use of a time-dependent (i.e. moving) ecliptic.

However, the IAU 2006 precession computations followed the traditional way in which a time-dependent "ecliptic" (i.e. a kind of GCRS representation of the mean EMB orbital motion) was used as an intermediate plane for expressing the contributions to the precession rates[2] resulting from the external torque. The values that were the best compatible with the IAU 2000 nutation, were, at the time of the computation, the components in longitude and obliquity respectively, expressed in an equatorial frame linked to the moving equinox. Therefore, the integration of the equations with respect to a fixed ecliptic, required

[2]Note that the semi-analytical expressions of these rates referring to this intermediate frame are reduced as compared to expressions referred to the fixed ecliptic.

to apply a rotation by the angle χ_A that expresses the precession of the ecliptic (see Fig. 1). Such an approach, although being still quite correct at a certain level of accuracy, should be considered as belonging to the past, i.e. to a transition step where there was the need of providing consistent developments for all the precession parameters, some of them mixing equator and ecliptic for continuity reasons. It should be clear that the use of an ecliptic will not be required for providing a future semi-analytical precession-nutation solution. The precession of the ecliptic is not necessary any longer.

Modern Solar System ephemerides

Solar system ephemerides provide the positions and motions of the major planetary bodies in the solar system, including the Earth, Moon and Sun, to very high precision. The 3 state-of-the-art numerical solar system ephemerides, namely the American one, DE (Development Ephemeris; JPL), the Russian one, EPM (Ephemerides of Planets and the Moon; IPA, St.Petersburg) and the French one, INPOP (Intégrateur Numérique Planétaire de l'Observatoire de Paris) are based on the post-Newtonian equations of motion for a set of "point-masses", the Einstein-Infeld-Hoffmann (EIH) equations and the consideration of various dynamical effects such as figure effects, Earth tides, Earth rotation, lunar librations and tidal dissipation (Soffel & Langhans 2013). These equations are integrated numerically for the whole solar system including a set of selected minor planets. While the DE100-series ephemeris and the DE200 one were in the B1950 and the J2000 coordinate systems respectively (which referred to the equinox of epoch), the DE400 series (Folkner et al. 2014), as well as the recent EPM (Pitjeva & Pitjev 2013) and INPOP (Fienga et al. 2011) solutions, are oriented to the ICRF system using ICRF-based VLBI measurements of spacecrafts near planets; therefore, theses ephemerides can be considered as being dynamical realizations of the ICRF without the need of any ecliptic.

4. CONCLUDING REMARKS

The role of the ecliptic in modern astronomy

We can conclude from the previous sections that (i) no ecliptic is needed for the realization of the reference systems currently used in astronomy, (ii) the ecliptic is no more needed as a reference for the astronomical coordinates, (iii) the modern numerical barycentric ephemerides are referred to the ICRF, (iv) the modern description of precession-nutation of the equator is the motion of the CIP in the GCRS without reference to the ecliptic, (v) numerical integration, as well as modern semi-analytical integration, of precession-nutation do not use an ecliptic. However, for continuity with the traditional approach, it may be useful to define a conventional BCRS fixed ecliptic frame as realized by rotating the BCRS by a constant rotation according to some mean ecliptic and equinox J2000; note that additional conventions would then be necessary for defining its GCRS counterpart.

Therefore, while the equinox (and the tropical year) will always have some value for the seasons, the organisation of everyday life and the calendar, the geometric, kinematical and dynamical uses of ecliptic in modern astronomy are now limited to uses for continuity with historical references and parameters.

Is a definition of the ecliptic in the framework of GR necessary?

In relativity, it is necessary to carefully distinguish between barycentric and geocentric quantities, so the calculation of a moving ecliptic presents a serious problem when it is used in the GCRS. Due to the loss of the importance of the ecliptic, the definition of the time-dependent ecliptic in GR is not required.

5. REFERENCES

Bretagnon, P., Rocher, P., Simon, J.-L., 1997, A&A, 319, 305.
Capitaine, N., Wallace, P.T., Chapront, J., 2003, A&A, 412, 567.
Capitaine, N., Folgueira, M., Souchay, J., 2005, A&A, 445, 347.
Capitaine N. & the IAU NFA WG, 2007, IAU Transactions 26B, 3, K. van der Hucht (ed.), 14, pp. 74–75.
Fienga, A., Laskar, J., Kuchynka, P., et al., 2011, Celest. Mech. Dyn. Astr., 111, 363.
Folkner, W., et al., 2009, The planetary and lunar ephemeris DE421, IPN Progress Report 42–178.
IERS Conventions, 2010, G. Petit, B. Luzum (eds.), IERS Technical Note 36.
Mathews, P.M., Herring, T., Buffett, B.A., 2002, J. Geophys. Res., 107(B4), 2068.
Pitjeva, E.V., Pitjev, N.P., 2013, MNRAS, 432, 3431.
Soffel, M., Klioner, S.A., Petit, G., et al., 2003, AJ, 126, 6, 2687.
Soffel, M., Langhans, R., 2013, "Space-Time Reference Systems", Springer-Verlag, Berlin, Heidelberg.
Souchay, J., Loysel, B., Kinoshita, H., Folgueira, M., 1999, A&A Supp. Ser., 135, 111.

RELATIVISTIC PRECESSION MODEL OF THE EARTH FOR A LONG TIME INTERVAL

K. TANG[1], M.H. SOFFEL[2], J.-H. TAO[1], Z.-H. TANG[1]
[1] Shanghai Astronomical Observatory, Chinese Academy of Sciences
80 Nandan Road, Shanghai 200030, China
e-mail: tangkai@shao.ac.cn
[2] Lohrmann Observatory, TU Dresden
Mommsenstr 13, Dresden 01062, Germany

ABSTRACT. Tang et al. (2015) provided a numerical solution of the Earth's precession in the relativistic framework for a long time span. The motion of the solar system is calculated in the BCRS by numerical integration with a symplectic integrator. The part of Earth's rotation is obtained in the GCRS by integrating the post-Newtonian equations of motion published by Klioner et al. (2003). All the main relativistic effects are included following Klioner et al. (2010), especially we considered several relativistic reference systems with corresponding time scales, scaled constants and parameters. Now we improve this work to give new parameters to represent the precession of the equator, in order to avoid the problem from the calculation of a moving ecliptic in relativity. The results are still consistent with other long-term precession theories. The relativistic influences are obtained and analyzed here.

1. INTRODUCTION

The long-term precession expressions of the Earth have been developed by Vondrák et al. (2011) in the Newtonian framework. They provided an extension of the IAU 2006 (Capitaine et al., 2003) to scales of several thousand centuries. Later Tang et al. (2015) improved this work and gave a long time span relativistic precession model of the Earth. This model has very small discrepancies with respect to the IAU 2006 precession around J2000.0, with differences being only several arcseconds, and is also consistent with other long-term precession theories. However this work used the general precession $p_{\rm A}$ and the obliquity $\epsilon_{\rm A}$ as the precession parameters for the equator. It's known that these two parameters mix the motion of the the equator in the Geocentric Celestial Reference System (GCRS) and the motion of the ecliptic of date, and the calculation of a moving ecliptic would present a serious problem in the GCRS. Here we give other parameters to represent the precession of the equator to avoid this problem.

The purpose of this paper is to provide a development for the precession of the equator, while the calculation of the precession of the ecliptic is the same as Tang et al. (2015). We use our new integrator to calculate the motion of the Earth's spin axis, and to obtain the luni-solar precession in longitude $\psi_{\rm A}$, the inclination of moving equator on a fixed ecliptic ω_A directly, which are the orientation parameters of the mean equator of date in the mean ecliptic frame at epoch (Lieske et al., 1977). Details about the precession of the ecliptic can be found in Tang et al. (2015). Here we only give our result about the precession of the equator.

2. THE PRECESSION OF THE EQUATOR

The model of Earth's rotation which is used here is referred to Klioner et al. (2010). The Earth's rotation is modelled in the GCRS which is kinematically non-rotating with respect to Barycentric Celestial Reference System (BCRS). The model of the Earth's gravity field is defined in the terrestrial reference system that is obtained by rotating the GCRS spatial coordinates with a time-dependent matrix. After integrating the post-Newtonian equation of Earth's rotation given by Klioner et al. (2003), the motion of the Earth's spin axis is obtained. The post-Newtonian equations of motion are numerically integrated by the Runge-Kutta-Fehlberg (RKF) 7(8) method (Fehlberg 1968). All the initial conditions and constants are the same as in Tang et al. (2015).

By numerical analysis (Laskar et al., 1992), the basic quantities for the precession of the equator $\psi_{\rm A}$ and $\omega_{\rm A}$ can be derived from the Euler angles directly (Bretagnon et al., 1997). The approximations for

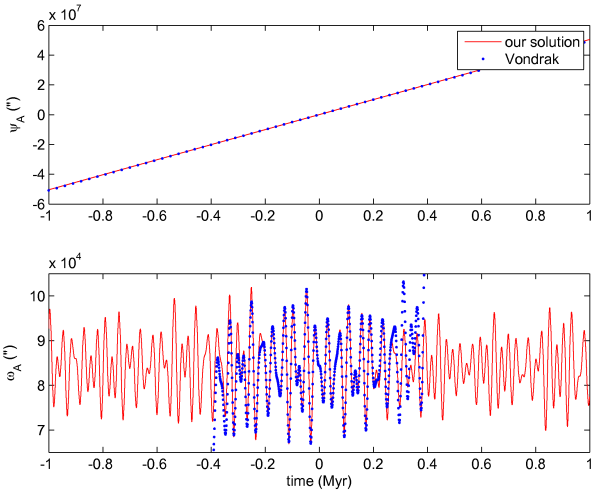

Figure 1: Comparison of our solution (solid line) and the Vondrák's solution (dotted line) for $\psi_{\rm A}$ (top), $\omega_{\rm A}$ (bottom).

the precession of the equator read:

$$\begin{aligned}\psi_{\rm A} &= 5773'' + 50''.4476T \\ &\quad + \sum_{i=1}^{30} C_i \cos(2\pi T/P_i) + S_i \sin(2\pi T/P_i), \\ \omega_{\rm A} &= 83922'' - 1''.07 \times 10^{-4} T \\ &\quad + \sum_{i=1}^{30} C_i \cos(2\pi T/P_i) + S_i \sin(2\pi T/P_i), \quad (1)\end{aligned}$$

where T is in TT year from J2000.0, and the periods P_i with the amplitudes C_i, S_i are given in Table. 1. In the second column, the name of some special frequencies s_i and p are from Laskar (1985) and Laskar et al. (2004). The comparisons of our long-term model of the precession of the equator and the Vondrák's model are shown in Fig. 1. The difference are less than one degree within the interval ±200 millennia from J2000.0.

		$\psi_{\rm A}$		$\omega_{\rm A}$			
i	Term	$C_i['']$	$S_i['']$	C_i $['']$	S_i $['']$	$P[yr]$	$f_i[''/yr]$
1	$p+s_3$	1829	-6033	-15571	-4737	40930	31.663632
2	p	1867	5362	12475	-4340	25691	50.444711
3	$p+s_4$	-541	-3209	-8199	1402	39799	32.563959
4	$p+s_1$	-2791	780	1840	6631	28839	44.938522
5	$p+s_6$	722	898	2532	-2027	53778	24.099094
6	$p+s_2$	-672	-974	-2346	1602	29649	43.711841
7		431	460	1193	-1087	41509	31.221854
8		151	-95	3445	-2438	1309223	0.9899
9		-61	26	-2992	1824	994480	1.303194
10		31	-31	2130	-619	718968	1.802584
11		-521	268	677	1320	42165	30.736352
12		29	-14	827	-911	417797	3.101988
13		-138	-363	-943	349	38904	33.313065
14		-223	-3	2	1091	15787	82.095307
15		286	234	542	-680	27332	47.41778
16		120	-330	-796	-288	30165	42.963876
17		-23	17	-803	173	556286	2.329735
18		207	-17	-15	-510	42839	30.252966
19		14	-119	-579	-66	16925	76.57474
20		-225	90	199	517	26037	49.774741
21		-96	50	254	467	15613	83.009872
22		97	76	369	-433	20466	63.323731
23		123	17	107	-557	20168	64.25881
24		53	84	415	-262	13587	95.382033
25		-24	32	-652	-150	372318	3.480894
26		-307	-75	-227	782	40303	32.156499
27		156	-49	-101	-358	28556	45.384613
28		13	-29	395	19	325726	3.978803
29		-24	100	260	71	29207	44.3731
30		-24	-46	-212	134	16729	77.47157

Table 1: The Periodic Terms in $\psi_{\rm A}$, $\omega_{\rm A}$.

3. RELATIVISTIC EFFECTS

The relativistic effects on the precession can be obtained from our program which calculates the precession both for the Newtonian and the post-Newtonian case. The relativistic influences on the precession of the ecliptic were discussed and published by Tang et al. (2015). Here we discuss the relativistic effects on the precession of the equator.

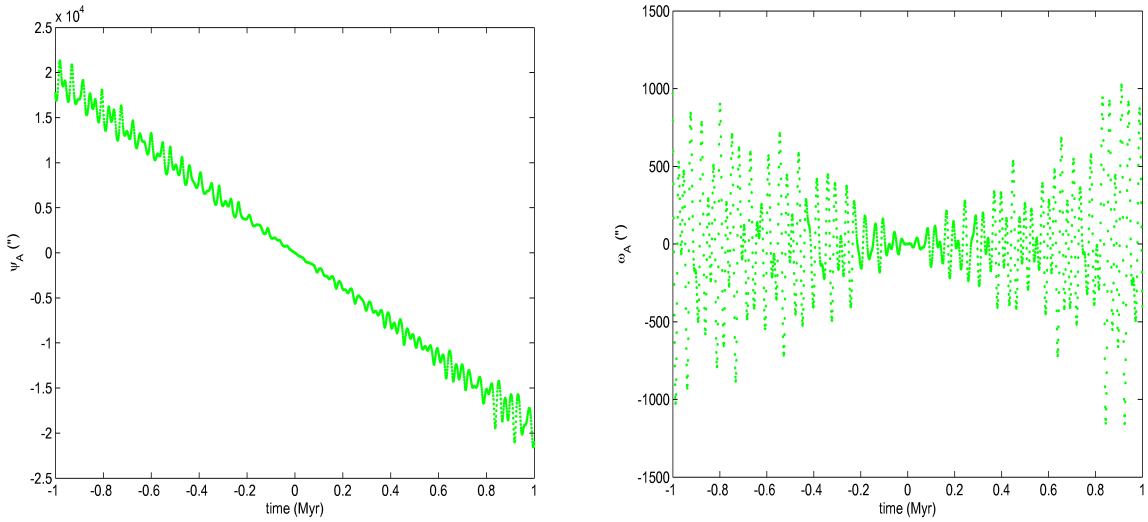

Figure 2: The effects of the geodetic precession on the precession parameter $\psi_{\rm A}$ (left) and $\omega_{\rm A}$ (right) from -1 Myr to 1 Myr.

For the rotation of the Earth, the geodetic precession is the most important one and considered by all previous works. The traditional way to account for geodetic precession is to add a precomputed geodetic precession to a purely Newtonian solution which has been already shown to be incorrect (Klioner et al. 2010). Whereas our result is integrated in a more rigorous relativistic framework, with Klioner et al. (2010). The relativistic features considered by our work are: (1) rigorous treatment of geodetic precession/nutation as an additional torque in the equations of motion, (2) four time scales, TDB, TCB, TT, TCG, which are all evaluated at the geocenter, (3) correct relativistic scaling of constants and parameters. Fig. 2 shows the relativistic effects on the precession of the equator parameters $\psi_{\rm A}$ and $\omega_{\rm A}$ due to the geodetic precession. The slope of the curve in Fig. 2 (left) related with the geodetic precession amounts to the well-known $2''$ per century. The influences accumulate with time and reach about $25\,000''$ and $1\,000''$ in ±1 Myr respectively. The influence on $\omega_{\rm A}$ leads to large obvious periodical parts, and the main period is about 25 920 yr.

The effects of the post-Newtonian inertial torque, the relativistic scaling and time scales (except for the geodetic precession) are depicted in Fig. 3. All these relativistic effects are increasing with time, but they are still too small to be considered in most cases within ±1 Myr. The amplitude of these effects for the precession parameters $\psi_{\rm A}$ and $\omega_{\rm A}$ is less than three arcsecond over this time span.

4. CONCLUSIONS

The model of the Earth's long-term precession is given above. It is consistent with the relativistic framework. The part of the precession of the ecliptic is discussed in Tang et al. (2015). The precession of the equator in the interval $\pm\,1$ Myr is calculated by using the RKF7(8) integrator, and the approximations for the precession parameters $\psi_{\rm A}$ and $\omega_{\rm A}$ are provided. Our solutions have small discrepancies with respect to the IAU 2006 precession near J2000.0, and display good consistency with other long-term precession theories.

Our model of the Earth's precession is obtained in a relativistic framework. For the precession of the equator, we consider the relativistic features including: (1) the geodetic precession/nutation, (2) the post-Newtonian inertial torque, (3) several relativistic reference systems with corresponding times scales and relativistic scaling of parameters. The relativistic effects on the precession parameters $\psi_{\rm A}$ and $\omega_{\rm A}$ are obtained and discussed.

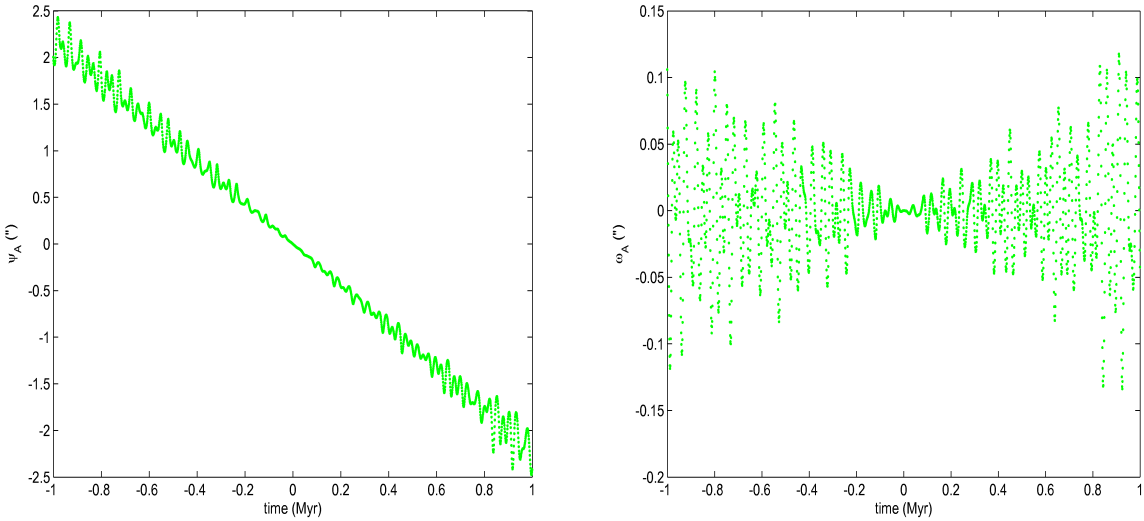

Figure 3: Other relativistic effects (except for the geodetic precession) on the precession parameter ψ_{A} (left) and ω_{A} (right) from -1 Myr to 1 Myr.

Acknowledgements. We thank Dr. Vondrák for his advices on the long-term precession and numerical analysis, and Dr. Gerlach for his help in numerical calculations. This work was supported by the National Natural Science Foundation of China under No. 11273044.

5. REFERENCES

Bretagnon, P., Rocher, P., Simon, J., 1997, "Theory of the rotation of the rigid earth", A&A, 319, pp. 305–317.

Capitaine, N., Wallace, P.T., Chapront, J., 2003, "Expressions for IAU 2000 precession quantities", A&A, 412, pp. 567–586.

Fehlberg, E., 1968, "Classical Fifth-, Sixth-, Seventh-, and Eighth-Order Runge-Kutta Formulas with Stepsize Control", NASA Tech. Rep. R-287.

Klioner, S.A., Soffel, M., Xu, C., Wu, X., 2003, "Earth's rotation in the framework of general relativity: rigid multipole moments", Journées 2001 - systèmes de référence spatio-temporels. Influence of geophysics, time and space reference frames on Earth rotation studies, pp. 232–238.

Klioner, S.A., Gerlach, E., Soffel, M., 2010, "Relativistic aspects of rotational motion of celestial bodies", In: Proc. International Astronomical Union 5, S261, pp. 112–123.

Laskar, J., 1985, "Accurate methods in general planetary theory.", A&A, 144, pp. 133–146.

Laskar, J., Froeschlé, C., Celletti, A., 1992, "The measure of chaos by the numerical analysis of the fundamental frequencies. Application to the standard mapping", Physica D: Nonlinear Phenomena, 56(2-3), pp. 253–269.

Laskar, J., Robutel, P., Joutel, F., Gastineau, M., Correia, A., Levrard, B., et al., 2004, "A long-term numerical solution for the insolation quantities of the earth", A&A, 428, pp. 261–285.

Lieske, J.H., Lederle, T., Fricke, W., Morando, B., 1977, "Expressions for the precession quantities based upon the IAU (1976) system of astronomical constants", A&A, 58, pp. 1–16.

Tang, K., Soffel, M.H., Tao, J.-H., Han, W.-B., Tang, Z.-H., 2015, "A long time span relativistic precession model of the Earth", Research in Astronomy and Astrophysics, 15(4), pp. 583–596.

Vondrák, J., Capitaine, N., Wallace, P., 2011, "New precession expressions, valid for long time intervals", A&A, 534, A22.

WORK RELATED WITH IAU C52: RIFA

M.H. SOFFEL[1], W.-B. HAN[2]

[1] Lohrmann Observatory
Dresden Technical University, 01062 Dresden, Germany
e-mail: michael.soffel@tu-dresden.de
[2] Shanghai Astronomical Observatory
80 Nandan Road, Shanghai, 200030 China
e-mail: wbhan@shao.ac.cn

ABSTRACT. Work within IAU Commission 52 RIFA (Relativity in Fundamental Astronomy) and work indirectly related with that commission is reported. The main work concentrated upon two issues: the role of an ecliptic in a relativistic framework, i.e., BCRS and GCRS, and work towards an improved and fully documented relativistic VLBI model. Related work concerned progress in the derivation of the post-linear metric for a system of bodies, body models with exterior gravitational fields with higher spin multipoles and physics in such fields.

1. MAIN WORK

The main work within IAU Commission 52 (RIFA) focussed on two issues. The first one being the role of the ecliptic within a relativistic framework and the second one is related with an improved and completely documented relativistic VLBI theory.

According to IAU2000-Resolution B1.3 (Soffel et al., 2003) the Barycentric Celestial Reference System (BCRS) with coordinates $(t, \mathbf{x})$, where t = TCB is determined by a specific form of the metric tensor, constructed under the assumption that the solar-system is isolated and space-time is asymptotically flat. Effects from cosmology or matter outside the solar system are not taken into account. Clearly an ecliptic might be defined as some t = const. Euclidean plane in barycentric spatial coordinates. IAU2000-Resolution B1.3 also specifies the Geocentric Celestial Reference System (GCRS) with coordinates $(T, \mathbf{X})$, where T = TCG by a corresponding geocentric metric tensor, where gravitational effects from external bodies are described as tidal forces. The GCRS is the basic reference system for a description of physical processes that take place in the immediate neighborhood of the Earth, especially for Earth's rotation. Considering precession-nutation in the past usually angles were used whose definitions require two spatial coordinate planes: some Earth's equator and some kind of ecliptic. The definition of an equinox or some obliquity of ecliptic are examples for that. It is without doubts that such concepts are of great value, e.g., for their relations with the seasons and the tropical year. In Capitaine & Soffel (2015) the definition and use of the ecliptic in modern astronomy is recalled.

However, such definitions face serious problems when we consider very high accuracies when effects from relativity are no longer negligible. As mentioned above some BCRS-ecliptic might be introduced and as long as it is independent upon time (i.e., upon TCB) it might be transferred to the GCRS. However, since the coordinate transformation from $(t, \mathbf{x})$ to $(T, \mathbf{X})$ is a 4-dimensional space-time transformation one faces serious problems when one wants to transfer a time dependent BCRS spatial coordinate plane with t = const. into the GCRS (see, e.g., Soffel 2004). For that reason one should avoid the concept of an ecliptic if such high accuracies are considered.

With respect to the accuracies that are presently achieved with VLBI a theoretical VLBI model should have an accuracy of better than 1 ps and it must be based upon Einstein's theory of gravity. The standard model as e.g., described in the IERS Conventions (2010) (Petit & Luzum, 2010) is based upon a consensus model involving publications of Fanselow–Thomas–Treuhaft–Sovers, Shapiro, Hellings–Shadid–Saless, Soffel–Müller–Wu–Xu and Zhu–Groten (see Eubanks, 1991). The paper of Klioner (1991) also had some influence on the material that can be found in the IERS Conventions (2010).

Together with Sergei Kopeikin we have started to work on a new improved and completely documented relativistic VLBI theory. We started with the works by Klioner (1991), Klioner and Kopeikin (1992) and

by Sekido & Fukushima (2006). We checked all calculations, tried to find simpler derivations and started with an exhaustive documentation. As usual the theory is based upon the BCRS and GCRS as the two basic reference systems, e.g., for baseline definitions. The gravitational time delay is now entirely derived by means of the Time-Transfer-Function (TTF). In the frame of this work a very elegant derivation of the Shapiro time delay was derived for a body with arbitrary (time independent) mass- and spin-multipoles moving with a small velocity was found; for details see Soffel & Han (2015). Corrections for parallax and proper motion of the radio source have been discussed. For more details the reader is referred to the living document that can be found under http://astro.geo.tu-dresden.de/RIFA/.

2. RELATED WORK

For theoretical astrometric models beyond the μas-level of accuracy work was done towards a rigorous derivation of the post-linear (BCRS) metric for a system of bodies. The metric in harmonic gauge is written in the form

$$\begin{aligned} g_{00} &= -1 + \frac{2}{c^2}w - \frac{2}{c^4}w^2 + O(c^{-6})\,, \\ g_{0i} &= -\frac{4}{c^3}w^i + \mathcal{O}(c^{-5})\,, \\ g_{ij} &= \delta_{ij}\left(1 + \frac{2}{c^2}w + \frac{2}{c^4}w^2\right) + \frac{4}{c^4}q_{ij} + \mathcal{O}(c^{-5}) \end{aligned} \tag{1}$$

and the potential q_{ij} satisfies the relation ($T^{\mu\nu}$: energy-momentum tensor)

$$\Delta q_{ij} = -w_{,i}w_{,j} - 4\pi G\left(T^{ij} - T^{ss}\delta_{ij}\right)\,. \tag{2}$$

We started to look into the case of a single spherically symmetric body. During the calculation of the exterior field (the Schwarzschild field) one faces expressions that depend upon the internal structure of the body (e.g., its radius R) and one has to prove that all such 'bad expressions' either cancel in virtue of the local equations of motion or can be removed by means of a (harmonic) gauge transformation. If one requires the metric to be continuous at the body's surface then outside one faces an unusual form of the Schwarzschild metric that depends upon R. For more details the reader is referred to Klioner & Soffel (2014).

Finally work has been done on models for the Sun and planets with higher spin multipole models; realistic estimates for the higher spin-moments of solar system bodies have been derived (Panhans & Soffel, 2015). In another work the physics in gravitational fields with higher spin multipole moments has been studied (Meichsner & Soffel, 2015).

Acknowledgements. W.-B. Han was supported by the National Natural Science Foundation of China (NSFC) under grant No. 11273045.

3. REFERENCES

Capitaine, N., Soffel, M., 2015, this volume, pp. 61–64.
Eubanks, T.M. (ed.), 1991, Proc. U.S. Naval Observatory Workshop on Relativistic Models for Use in Space Geodesy, U.S. Naval Observatory, Washington, D.C.
Klioner, S., 1991, In: Proc. AGU Chapman Conference On Geodetic VLBI, W.E. Carter (ed.), NOAA Technical Report NOS 137 NGS 49, pp. 188–192.
Klioner, S., Kopeikin, S., 1992, AJ, 104, pp. 897–914.
Klioner, S., Soffel, M., 2014, Phys. Rev. D, 89, 104056.
Meichsner, J., Soffel, M., 2015, to be published.
Panhans, M., Soffel, M., 2015, Class. Quantum Gravity, in press.
Petit, G., Luzum, B. (eds.), 2010, IERS Conventions (2010), IERS Technical Note 36, Frankfurt am Main: Verlag des Bundesamts für Kartographie und Geodäsie.
Sekido, M., Fukushima, T., 2006, J. Geod., 80, pp. 137–149.
Soffel, M., et al., 2003, AJ, 126, pp. 2687–2706.
Soffel, M., 2004, Proc. Journées 2003 "Systèmes de Référence Spatio-Temporels", St. Petersburg, pp. 330–332.
Soffel, M., Han, W.-B., 2015, Phys. Lett. A, 379(4), pp. 233–236.

GRAVITATIONAL REDSHIFT EXPERIMENT WITH THE SPACE RADIO TELESCOPE RADIOASTRON

D. LITVINOV[1], N. BARTEL[2], K. BELOUSOV[3], M. BIETENHOLZ[4], A. BIRIUKOV[3], A. FIONOV[1], A. GUSEV[1], V. KAUTS[3,5], A. KOVALENKO[6], V. KULAGIN[1], N. PORAIKO[1], V. RUDENKO[1]

[1] Lomonosov Moscow State University, Sternberg Astronomical Institute
Universitetsky pr. 13, 119991 Moscow, Russia
e-mail: litvirq@yandex.ru

[2] York University, Toronto, Ontario M3J 1P3, Canada

[3] Astro Space Center, Lebedev Physical Institute, Profsoyuznaya 84, 117997 Moscow, Russia

[4] Hartebeesthoek Radio Observatory, P.O. Box 443, Krugersdorp 1740, South Africa

[5] Bauman Moscow State Technical University, 2-ya Baumanskaya 5, 105005 Moscow, Russia

[6] Pushchino Radio Astronomy Observatory, 142290 Pushchino, Russia

ABSTRACT. A unique test of general relativity is possible with the space radio telescope RadioAstron. The ultra-stable on-board hydrogen maser frequency standard and the highly eccentric orbit make RadioAstron an ideal instrument for probing the gravitational redshift effect. Large gravitational potential variation, occurring on the time scale of ∼24 hr, causes large variation of the on-board H-maser clock rate, which can be detected via comparison with frequency standards installed at various ground radio astronomical observatories. The experiment requires specific on-board hardware operating modes and support from ground radio telescopes capable of tracking the spacecraft continuously and equipped with 8.4 or 15 GHz receivers. Our preliminary estimates show that ∼30 hr of the space radio telescope's observational time are required to reach $\sim 2 \times 10^{-5}$ accuracy in the test, which would constitute a factor of 10 improvement over the currently achieved best result.

1. INTRODUCTION

According to Einstein's principle of equivalence an electromagnetic wave propagating in a region of space where the gravitational potential is not constant experiences a gravitational frequency shift, $\Delta f_{\rm grav}$, proportional to the gravitational potential difference between the measurement points, ΔU, and the frequency, f, of the wave:

$$\frac{\Delta f_{\rm grav}}{f} = \frac{\Delta U}{c^2}, \tag{1}$$

where c is the speed of light (Misner et al. 1973). Any violation of Eq. (1) in an experiment with two identical atomic frequency standards can be parameterized in the following way:

$$\frac{\Delta f_{\rm grav}}{f} = \frac{\Delta U}{c^2}(1+\varepsilon), \tag{2}$$

where the violation parameter, ε, may depend on element composition of the gravitational field sources and on the kind of frequency standards. It is generally agreed that the best test of Eq. (1) to date was performed in the suborbital Gravity Probe A (GP-A) experiment, which measured $\varepsilon = (0.05 \pm 1.4) \times 10^{-4}$ for two hydrogen masers (Vessot et al. 1980). A similar experiment with RadioAstron, benefitting from a more stable hydrogen maser (H-maser) and longer data acquisition, could tentatively measure ε with an accuracy of $\delta\varepsilon \sim 2 \times 10^{-5}$. Below we outline two approaches to the anticipated experiment and give an account of the technical tests made for it.

2. OUTLINE OF THE EXPERIMENT

In the gravitational redshift experiment with RadioAstron we use microwave radio links to monitor the redshifted frequency of the satellite's on-board H-maser as it moves in the regions with different gravitational potential. The satellite radio payload includes two transmitters at 8.4 and 15 GHz and a

7.2 GHz receiver. The transmitters can be fed with a signal phase-locked either to the on-board H-maser, the 7.2 GHz uplink or a specific mixture of the two (see below). Measuring the frequency of a one-way satellite downlink signal at a ground station we see it shifted by (Vessot & Levine 1979):

$$\Delta f = f\left(-\frac{\dot{D}}{c} - \frac{v_\mathrm{s}^2 - v_\mathrm{e}^2}{2c^2} + \frac{(\mathbf{v}_\mathrm{s}\cdot\mathbf{n})^2 - (\mathbf{v}_\mathrm{e}\cdot\mathbf{n})\cdot(\mathbf{v}_\mathrm{s}\cdot\mathbf{n})}{c^2}\right) + \Delta f_\mathrm{grav} + \Delta f_\mathrm{ion} + \Delta f_\mathrm{trop} + \Delta f_0 + O\left(\frac{v}{c}\right)^3, \quad (3)$$

where $\dot{D}$ is the radial velocity of the spacecraft relative to the ground station, $\mathbf{v}_\mathrm{s}$ and $\mathbf{v}_\mathrm{e}$ are the velocities of the spacecraft and the ground station, $\mathbf{n}$ is a unit vector in the direction opposite to that of signal propagation, Δf_grav is the gravitational redshift, Δf_ion and Δf_trop are the ionospheric and tropospheric shifts, Δf_0 is an unknown frequency offset between the ground-based and space-borne H-masers and each quantity is referred to the geocentric inertial reference frame. Terms of $O\left(\frac{v}{c}\right)^3$ need to be taken into account only if aiming for an experiment accuracy of $\delta\varepsilon \lesssim 10^{-6}$ (Salomon et al. 2001).

The value of Δf_0 could be relatively large for H-masers due to their low intrinsic accuracy. For RadioAstron's H-maser $\Delta f_0/f \sim 10^{-11}$, which makes it impossible to experimentally determine the total value of the gravitational redshift effect $\Delta U/c^2 \sim 7\times10^{-10}$ with an accuracy higher than $\sim 10^{-2}$. However, since the rate of change, or drift, of Δf_0 is typically small ($\sim 1\times10^{-15}$ per day for RadioAstron), the relatively large value of Δf_0 does not prohibit us from conducting a high-accuracy experiment as long as only the variation, but not the total value, of the gravitational redshift effect is to be determined. Then the fundamental limit to the accuracy, $\delta\varepsilon$, is set by the available gravitational potential variation along the orbit, the frequency standard's instability and its drift. For RadioAstron this theoretical limit is 2×10^{-6} if the experiments are performed in the periods of the lowest perigee height ~1,000 km.

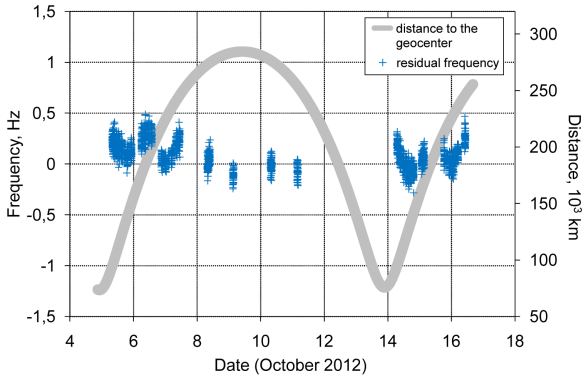

Figure 1: Frequency residuals (observed–predicted) as a function of epoch for the 8.4 GHz link. RMS of residuals: 0.18 Hz; gravitational redshift Δf_grav: 5 to 6 Hz (not plotted).

The principal source of error, when using Eq. (3) directly, is not the on-board H-maser performance but the spacecraft radial velocity uncertainty $\delta\dot{D} \sim 1$ mm/s, which sets the limit to the experiment accuracy $\delta\varepsilon \sim 3\%$ (Fig. 1). Obviously, since the Doppler term cannot be determined sufficiently accurately, the best would be to eliminate it completely from the analysed signal. This is indeed possible if two kinds of radio links are available, a one-way downlink, synchronized to the on-board H-maser, and a two-way phase-locked loop (PLL), synchronized to the ground H-maser. The 1st-order Doppler shift of the two-way link is twice that of the one-way downlink, but the gravitational frequency shift is zero. The signals of these two links can be combined by a radio engineering scheme, first used in GP-A, so that its output fully retains the gravitational contribution but eliminates the 1st-order Doppler term.

For RadioAstron the GP-A compensation scheme is not directly applicable, because 1- and 2-way carrier frequency measurements (Fig. 2) cannot be performed simultaneously. Nevertheless, two modified versions of the Doppler compensation scheme are possible, both of which rely on spacecraft tracking by ground radio telescopes equipped with 8.4 or 15 GHz receivers (Duev et al. 2012). The first option requires switching back and forth between the 1-way ("H-maser") and 2-way ("Coherent") modes of operation (Fig. 2a, b). Interleaving the two synchronization modes results in two sets of gapped 1-way and 2-way frequency measurements, which, after interpolation, allow for direct application of the original GP-A 1st-order Doppler compensation scheme. The approach with interleaved measurements does not

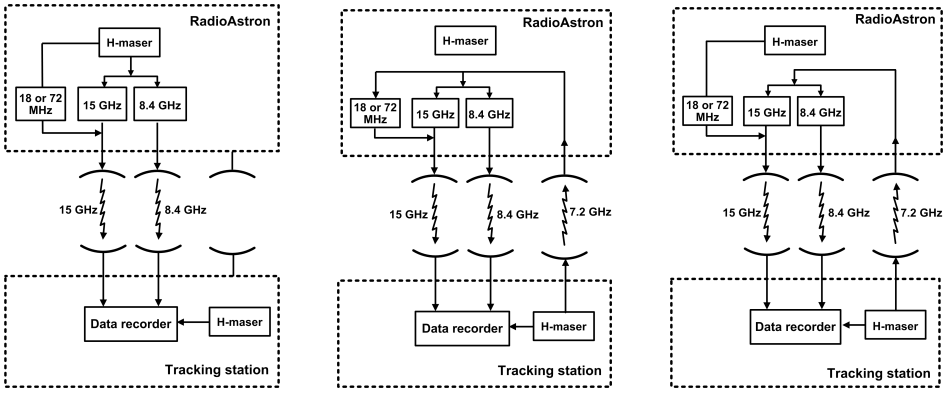

Figure 2: On-board hardware synchronization modes: a) "H-Maser"; b) "Coherent"; c) "Semi-Coherent". Note that the 8.4 GHz tone and the carrier of the 15 GHz data link cannot be synchronized independently.

rely on any features of the signal spectrum, and thus can be realized with telescopes equipped with any type of receiver (8.4 or 15 GHz).

The second approach to Doppler compensation involves recording the 15 GHz data link signal in the "Semi-Coherent" mode of the on-board scientific and radio equipment (Fig. 2c). In this mode the 7.2 GHz uplink tone, the 8.4 GHz downlink tone and the 15 GHz data downlink carrier are phase-locked to the ground H-maser signal, while the modulation frequency of the data downlink is phase-locked to the on-board H-maser signal. This approach also depends on the broadband ($\sim$1 GHz) nature of the QPSK-modulated 15 GHz signal and the possibility of turning its spectrum into a comb-like form by transmitting a predefined periodic data sequence (Fig. 3). It was shown by Biriukov et al. (2014) that different subtones of the resulting spectrum act like separate links of the GP-A scheme and can be organized in software postprocessing into a combination, which is free from the 1st-order Doppler and tropospheric noise terms (the ionospheric term persists).

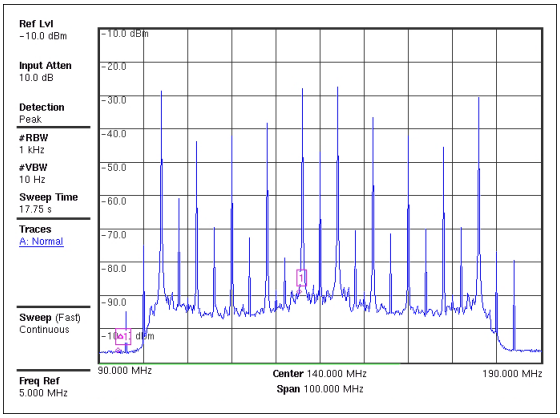

Figure 3: 15 GHz datalink signal spectrum in the "Test-2" 72 MHz mode of the on-board formatter.

Since in Europe only the Effelsberg telescope is equipped with a 15 GHz receiver, most experiments supported by the RadioAstron mission's Pushchino tracking station would use the first approach to Doppler compensation. By contrast, experiments supported by the Green Bank tracking station could use any of the two approaches since the GBT and all VLBA antennas are equipped with 8.4 and 15 GHz receivers and are capable of continuous spacecraft tracking (however, only Hn, NL and, of course, the GBT are located sufficiently close to the Green Bank tracking station to be able to observe RadioAstron during low perigee sessions). A single experiment would be made in two 1-hr sessions, one close to perigee and another close to apogee. The currently predicted RadioAstron orbit allows for 10 to 15 experiments

in 2015 to 2016 with a modulation of the gravitational potential along the orbit of $\Delta U/c^2 \sim 3 \times 10^{-10}$ and 1 to 3 radio telescopes tracking the satellite. With preliminary values for the Allan deviation of $\sim 3 \times 10^{-14}$ at 1,000 s for the 1- and 2-way modes, the accuracy of the experiment could be as high as

$$\delta\varepsilon \sim 2 \times 10^{-5}. \quad (4)$$

3. PRESENT STATUS OF THE EXPERIMENT

Currently the experiment is in its testing phase. Up to now we have checked the operability of the required on-board hardware modes and performed a series of recordings of the satellite downlink signals using regular VLBI equipment at the RadioAstron mission's tracking station in Pushchino. The recovered signal frequencies show good agreement with ordinary frequency measurements performed at the tracking station as part of the mission support (Fig. 4). Their stability (Allan deviation of 6×10^{-14} at 1,000 s) is lower than required to achieve $\delta\varepsilon \lesssim 2 \times 10^{-5}$ but in accord with previous satellite tracking experiments at Pushchino. The recordings obtained from the first RadioAstron tracking test in the 2-way mode by a number of EVN and Asian telescopes exhibit at least 2 times better signal stability and give reason to believe that the above accuracy of the gravitational redshift test can be achieved.

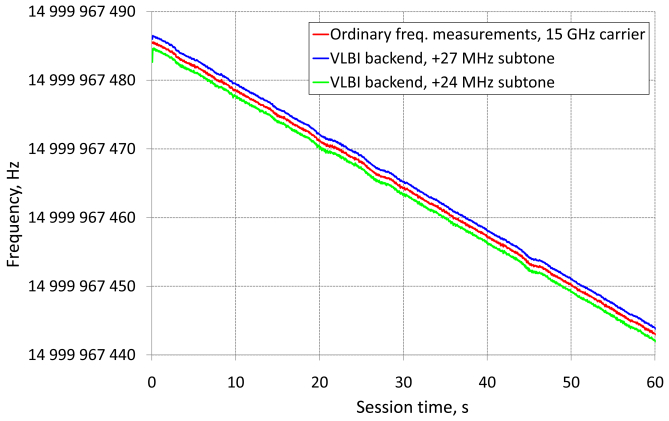

Figure 4: Frequency measurements of the 15 GHz signal subtones in the "Test-2" 18 MHz mode made at the Pushchino tracking station, 2014/08/31 08:20:00 UTC. The carrier frequencies were measured using standard tracking station equipment, the subtone frequencies were recovered from a 2-bit quantization 32 MHz bandwidth recording made by a VLBI backend. Subtone frequencies are offset by ∼24 and ∼27 MHz for easier comparison with the carrier frequency measurements.

Acknowledgements. The RadioAstron project is led by the Astro Space Center of the Lebedev Physical Institute of the Russian Academy of Sciences and the Lavochkin Scientific and Production Association under a contract with the Russian Federal Space Agency, in collaboration with partner organizations in Russia and other countries.

4. REFERENCES

Biriukov A.V., et al., 2014, "Gravitational Redshift Test with the Space Radio Telescope RadioAstron", Astron. Rep., 58, pp. 783–795.

Duev D., et al., 2012, "Spacecraft VLBI and Doppler tracking: algorithms and implementation", A&A, 541, A43.

Misner, C., Thorne, K., Wheeler, J., 1973, Gravitation, San Francisco: Freeman

Salomon, C., et al., 2001, "Cold atoms in space and atomic clocks: ACES", C. R. Acad. Sci. Paris, t. 2, Série IV, p. 1313–1330

Vessot, R.F.C., Levine M., 1979, "A Test of the Equivalence Principle Using a Space-Borne Clock", Gen. Rel. Grav., 10, pp. 181–204.

Vessot, R.F.C., et al., 1980, "Test of Relativistic Gravitation with a Space-Borne Hydrogen Maser", Phys. Rev. Let., 45, pp. 2081–2084.

THE DEFLECTION OF LIGHT INDUCED BY THE SUN'S GRAVITATIONAL FIELD AND MEASURED WITH GEODETIC VLBI

O.A. TITOV[1], A.A. GIRDIUK[2]
[1] Geoscience Australia
PO Box 378, Canberra, ACT 2601, Australia
e-mail: oleg.titov@ga.gov.au
[2] Institute of Applied Astronomy, Russian Academy of Sciences
Kutuzov Quay 10, 191187, Saint-Petersburg, Russia
e-mail: girduik@ipa.nw.ru

ABSTRACT. The Sun's gravitational field deflects the apparent positions of close objects in accordance with the formulae of general relativity. Optical astrometry is used to test the prediction, but only with the stars close to the Sun and only during total Solar eclipses. Geodetic Very Long Baseline Interferometry (VLBI) is capable of measuring the deflection of the light from distant radio sources anytime and across the whole sky. We show that the effect of light deflection is equivalent to the gravitational delay calculated during the reduction of VLBI data. All reference radio sources display an annual circular motion with the magnitude proportional to their ecliptic latitude. In particular, radio sources near the ecliptic pole draw an annual circle with magnitude of 4 mas. This effect could be easily measured with the current precision of the geodetic VLBI data.

1. INTRODUCTION

Very Long Baseline Interferometry (VLBI) is capable of measuring precise group delays - the difference in arrival times of radio waves at two radio telescopes (Schuh & Behrend, 2012) from distant extragalction radio sources (quasars). Accurate positions of these radio sources are obtained with an accuracy of 40 microarcsec (Ma et al., 2009).

Gravitational time delay caused by the Solar gravitational field is calculated during the reduction of geodetic VLBI data (Shapiro, 1964, 1967). The conventional formula for calculating gravitational delay is formulated in terms of the positions of the radio telescopes within the barycentric reference frame of the Solar System (Kopeikin, 1990; Eubanks et al., 1991; Soffel et al., 1991; Klioner, 1991), rather than the baseline length between the radio telescopes.

We propose an alternate gravitational delay formula using a Taylor series expansion. We show that the conventional formula can be split into a sum of several terms, and the major term links the gravitational delay and the well-known formula for the light deflection angle. The light deflection angle can be considered equivalent for all baselines and estimated for each radio source at times of interest. We develop a new approach to probe the formula for the light deflection angle at an arbitrary elongation from the Sun. Finally, estimates of the light deflection for several reference radio sources based on VLBI observations in 1991–2001 are presented.

2. GRAVITATIONAL DELAY VS LIGHT DEFLECTION

The light deflection angle α at an arbitrary elongation θ from the Sun, is given by

$$\alpha = \frac{(\gamma+1)GM}{c^2 r}\frac{\sin\theta}{1-\cos\theta}, \tag{1}$$

where G is the gravitational constant, M is the mass of a gravitational body, c is the speed of light, r is the distance from the Earth to the Sun, γ is the parameter of the Parametrised Post-Newtonian formalism (PPN), θ is the elongation angle (i.e. the angular distance between the Earth and the gravitational body (Shapiro, 1967; Ward, 1970). The conventional gravitational delay is calculated as follows

$$\tau_{grav} = \frac{(\gamma+1)GM}{c^3} \ln \frac{|\vec{r_1}| + (\vec{s}\cdot\vec{r_1})}{|\vec{r_2}| + (\vec{s}\cdot\vec{r_2})}, \tag{2}$$

The VLBI total delay model also comprises a term due to the transformation from the barycentric to the geocentric reference frames.

$$\tau_{coord} = \frac{(\gamma+1)GM}{c^2 r} \frac{(\vec{b}\cdot\vec{s})}{c}. \tag{3}$$

It can be shown that the three formulae are approximately linked as (Titov & Girdiuk, 2015)

$$\tau_{GR} \approx \tau_{grav} + \tau_{coord} = \alpha \frac{b}{c} \sin\varphi \cos A, \tag{4}$$

where angles φ, θ, A are linked by the standard spherical triangle formula

$$\cos\psi = -\cos\varphi\cos\theta - \sin\varphi\sin\theta\cos A, \tag{5}$$

Converting the three dot products with angles φ, ψ, θ (Fig. 1), where

$$(\vec{b}\cdot\vec{s}) = |\vec{b}|\cos\varphi, \quad (\vec{b}\cdot\vec{r_2}) = |\vec{b}||\vec{r_2}|\cos\psi, \quad (\vec{r_2}\cdot\vec{s}) = -|\vec{r_2}|\cos\theta. \tag{6}$$

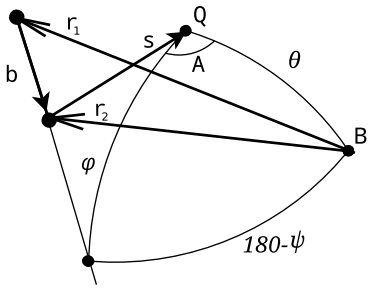

Figure 1: Angles φ, ψ, θ and A, originated by position of gravitational mass (B), quasar (Q) and baseline vector ($\vec{b}$). If the Sun plays the role of the gravitational mass, then, the point B is also the position of the Solar system barycentre.

More accurately, the total contribution of the post-Newtonian (PN) general relativity effect to the total VLBI delay is given by (we recall now $\gamma = 1$ for the case of general relativity)

$$\tau_{GR} \approx \frac{2GMb}{r_2 c^3} \frac{\sin\varphi\sin\theta\cos A}{1-\cos\theta} + \frac{GM}{c^3} \frac{b^2(1-\cos^2\varphi\cos^2\theta)}{r_2^2(1-\cos\theta)} - \frac{GM}{c^3} \frac{b^2\sin^2\varphi\sin^2\theta\cos^2 A}{r_2^2(1-\cos\theta)^2}. \tag{7}$$

The two additional terms appear because the elongation angles θ_1 and θ_2 between the direction to the observed radio source and the centre of the gravitational body, as measure from each radio telescope, are not equivalent. The parallactic effect for a baseline of 6,000 km is about 8 arcsec, and the deflection angles α_1 and α_2 for the "first" and the "second" radio telescope differing. At a large elongation the additional terms are negligible, so in the small angle approximation this effect should be considered.

$$\tau_{GR} = \frac{4GM}{c^2 R_2} \frac{b}{c} \sin\varphi(\cos A - \frac{b}{2R_2}\sin\varphi\cos 2A) = \alpha_2 \cdot \frac{b}{c}\sin\varphi(\cos A - \frac{b}{2R_2}\sin\varphi\cos 2A), \tag{8}$$

where α_2 is the classical deflection angle for light propagated through a gravitation field (Einstein, 1916) for the second station $\alpha_2 = \frac{4GM}{c^2 R_2}$ and $R_2 = r_2\cos\theta_2$.

In an alternative form

$$\tau_{GR} = (\alpha_2 - \frac{GM}{c^2 R_2}\frac{b}{R_2}\frac{\sin\varphi\cos 2A}{\cos A}) \cdot \frac{b}{c}\sin\varphi\cos A = (\alpha_2 + \alpha_2') \cdot \frac{b}{c}\sin\varphi\cos A, \tag{9}$$

where α_2' is the additional deflection angle

$$\alpha_2' = \frac{GM}{c^2 R_2}\frac{b}{R_2}\frac{\sin\varphi\cos 2A}{\cos A}. \tag{10}$$

3. OBSERVATIONAL DATA

We processed the available VLBI data between 1991 and 2001 using the OCCAM software (Titov et al., 2004). A fraction of well-established reference radio sources were assigned as astrometrically unstable, i.e. their coordinates were not fixed. The observational group delays were approximated by the theoretical values, and the O–C (observed minus calculated) differences were used to obtain a set of estimates of the standard daily parameters (Earth orientation, station positions, wet troposphere delays and gradients, etc.) and corrections to the selected radio source coordinates (right ascension and declination) regardless of its elongation from the Sun. The consensus gravitational delay (3) and the coordinate term (4) were not applied for the calibration of the group delay for the radio sources. The ionosphere fluctuations were calibrated in the conventional way, and, as it will be shown later, this makes possible VLBI observations of radio sources in the range of 1°.5 to 3° from the Sun.

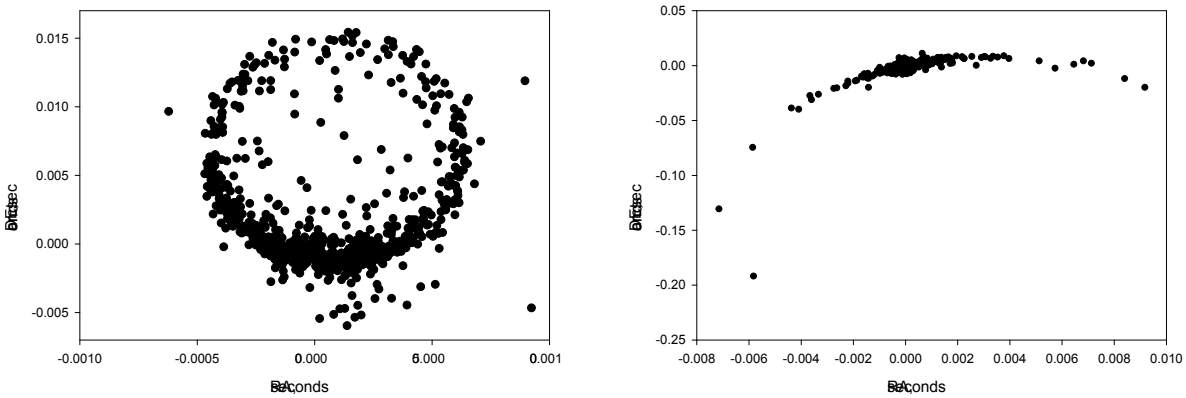

Figure 2: The variations of the coordinates of the radio sources 1606+106 (left) and 0229+131 (right) in 1991–2001. A smaller minimum angle θ for 0229+131 results in larger size of the circle.

We used the Least Squares collocation method to estimate the wet troposphere fluctuations with the OCCAM software. The mutual correlation between observables are introduced in the data adjustment process. The difference between the VLBI estimates of the wet troposphere delays and independent radiometer data is typically within 3–6 mm, or 10–20 ps (Titov & Stanford, 2013). Thus, the impact of the wet troposphere delay on the astrometric light deflection angle estimated near the Sun is negligible.

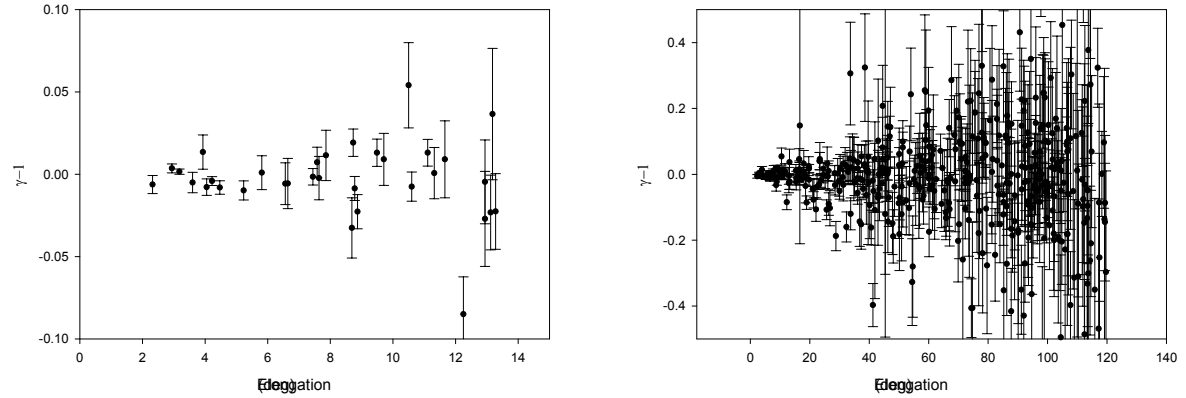

Figure 3: Variations of the daily estimates of the PPN parameter γ for radio source 0229+131 in 1991–2001 at the different scale of angle θ.

Figure 2 shows the variations of the coordinates of two selected radio source over 10 years (1991–2001). Each point on the plot corresponds to a daily position estimated from a single 24-hour session. About 10 annual circles are drawn by each radio source on the plots. The catalogue (non-deflected) positions are at the reference origin, and the total deflection angle is equal to distance to the point from the reference origin. The ecliptic latitude of the four sources are different, therefore, elongation angles vary over different ranges. As a result, the deflection angle does not change essentially for the former radio

sources (the reference origin is in the middle of the ring) with a magnitude about 4 mas. In contrast, for the latter case, the deflection angle varies from zero to $0''.2$ (for the minimum elongation of 3°), and the reference origin lies near the edge of the ring.

The variations of the deflection angle are easily converted with formula (1) to the variations of the PPN parameter γ. Figure 3 shows the variations of the deflection angle as a function of θ for the reference radio source 0229+131 at different scales. This radio source is almost on the ecliptic plane (ecliptic latitude $\epsilon \approx -1^\circ.5$), and the elongation angle is limited by the technical capability of observing near the Sun. On 29 April, 1997 (session code 97APR29XE) the mean elongation angle was $1^\circ.55$, and the measured deflection reached a maximum among all selected radio sources, $\alpha = 0''.3100 \pm 0''.0009$. However, this estimate was obtained from only 7 observations. The best accuracy was achieved on 1 May, 1996 (session code 96MAY01XO) with 122 observations. The deflection angle estimate is $\alpha = 0''.1588 \pm 0''.0002$, and the relative accuracy is 0.0012, in spite of a larger mean elongation angle for this date.

4. CONCLUSION

The effects of general relativity are explicitly contained in both components of the total VLBI delay model – the gravitational and geometric delays. While the former component uses the individual barycentre positions of the radio telescopes to calculate the effect, the latter component is expressed in terms of the baseline between the radio telescopes. Coupling between both parts has not been investigated until now.

The Shapiro effect as measured by radars, and the deflection of light measured with traditional astronomical instruments are considered two independent tests of general relativity. In this paper we show that the total group delay model joins the two tests within one observational technique - geodetic VLBI. The gravitational delay that traditionally originated from the Shapiro effect is linked to the light deflection angle. Therefore, the two approaches, VLBI delay and angular, are absolutely equivalent.

For almost all realistic situations this angle does not depend on the baseline length, thus, a standard geodetic VLBI interferometer acts as a traditional astronomical instrument. In addition, the coordinate term explicitly presented in the conventional geometric delay model ceases to exist because it is compensated by the same effect in the gravitational delay with the opposite sign. Thus, the proposed alternative version of the general relativity contribution to the total VLBI group delay model is free from coordinate effects. Therefore, the two approaches, time delay and angular deflection, are absolutely equivalent.

The final equation of the general relativity contribution also comprises two smaller terms which are significant at very small angular separation between the deflecting body and distant radio source. These terms may be considered as an increment in the light deflection angle due to the additional time delay for propagation of the light from station 1 to station 2. This effect become significant at $\frac{b}{R} > 0.1$.

Acknowledgements. This paper is published with the permission of the CEO, Geoscience Australia.

5. REFERENCES

Einstein, A., 1916, Annalen der Physik, 354, 769.
Eubanks, T.M., Carter, M.S., Josties, F.J., Matsakis, D.N., McCarthy, D.D., 1991, IAU Colloq. 127: Reference Systems, 256.
Klioner, S.A., 1991, In: Proc. of AGU Chapman Conference on Geodetic VLBI: Monitoring Global Change, Washington DC, 188.
Kopeikin, S.M., 1990, Sov. Astron., 34, 5.
Ma, C., Arias, E.F., Bianco, G., et al., 2009, IERS Technical Note 35.
Schuh, H., Behrend, D., 2012, J. Geodyn., 61, 68.
Shapiro, I.I., 1964, Phys. Rev. Lett., 13, 789.
Shapiro, I.I., 1967, Science, 157, 806.
Soffel, M.H., Wu, X., Xu, C., Mueller, J., 1991, AJ, 101, 2306.
Titov, O., Girdiuk, A., 2015, A&A, 574, A128
Titov, O., Stanford, L., 2013, In: 21st EVGA Meeting Proc., Reports of the Finnish Geodetic Institute, 151.
Titov, O., Tesmer, V., Boehm, J., 2004, In: IVS 2004 General Meeting Proc., 267.
Ward, W.R., 1970, ApJ, 162, 345.

TIME AND FREQUENCY TRANSFER WITH A MICROWAVE LINK IN THE ACES/PHARAO MISSION

C. LE PONCIN-LAFITTE[1], P. DELVA[1], F. MEYNADIER[1], C. GUERLIN[1,2], P. WOLF[1]
P. LAURENT[1]
[1] LNE-SYRTE, Observatoire de Paris, CNRS/UPMC
61, Avenue de l'Observatoire, 75014 Paris, France
e-mail: christophe.leponcin@obspm.fr
[2] Laboratoire Kastler-Brossel, ENS, CNRS, Université Pierre et Marie Curie, Paris 6
24 rue Lhomond, 75005 Paris, France

ABSTRACT. The Atomic Clocks Ensemble in Space (ACES/PHARAO mission), which will be installed on board the International Space Station (ISS), uses a dedicated two-way microwave link in order to compare the timescale generated on board with those provided by many ground stations disseminated on the Earth. Phase accuracy and stability of this long range link will have a key role in the success of the ACES/PHARAO experiment. SYRTE laboratory is heavily involved in the design and development of the data processing software: from theoretical modeling and numerical simulations to the development of a software prototype. Our team is working on a wide range of problems that need to be solved in order to achieve high accuracy in (almost) real time. In this article we present some key aspects of the measurement, as well as current status of the software's development.

1. THE ACES-PHARAO MISSION

The ACES/PHARAO mission is an international cooperation of more than 150 people, PI laboratories being SYRTE at Paris Observatory, LKB at ENS, Neuchâtel Observatory, and leading space agencies are the European Space Agency and CNES, the French space agency. Many industries are involved, the main ones being EADS/Astrium, TimeTech and Thales. The payload will be installed on board ISS and will realize in space a timescale of very high stability and accuracy. To reach this goal, the ACES payload includes a cesium atomic clock (PHARAO), an active hydrogen maser (SHM), a GNSS receiver for precise orbit determination, a Frequency Comparison and Distribution Package (FCDP) for local comparison of the on board clocks and generation of the on board timescale. This timescale will be compared to a ground clock network thanks to a dedicated two-way microwave link, using both code-phase and carrier-phase measurement. The main scientific objectives of the mission are 1. to demonstrate the high performance of the atomic clocks ensemble in the space environment and the ability to achieve high stability on space-ground time and frequency transfer, 2. to compare ground clocks at high resolution on a world-wide basis using a link in the microwave domain where the link stability should reach around 0.3 ps after 300 seconds of integration in common view mode and 3. to perform equivalence principle tests. It will be possible to test Local Lorentz Invariance and Local Position Invariance to unprecedent accuracy by doing three types of tests: a test of gravitational red-shift, drift of the fine structure constant and of anisotropy of light.

2. THE MICROWAVE LINK

The MicroWave Link (MWL) will be used for space-ground time and frequency transfer. A time transfer is the ability to synchronize distant clocks, *i.e.* determine the difference of their displayed time for a given coordinate time. The choice of time coordinate defines the notion of simultaneity, which is only conventional. A frequency transfer is the ability to syntonize distant clocks, *i.e.* determine the difference of clock frequencies for a given coordinate time. Here we suppose that all clocks are perfect, their displayed time is exactly their proper time. Proper time τ is given in a metric theory of gravity by the relation

$$c^2 d\tau^2 = -g_{\alpha\beta} dx^\alpha dx^\beta \,, \tag{1}$$

where $g_{\alpha\beta}$ are the components of the metric tensor, c the velocity of light in vacuum, $\{x^\alpha\}$ the coordinates, Einstein summation rule being used.

MWL is composed of three signals of different frequencies: one uplink at frequency $f_1 \simeq 13.5$ GHz, and two downlinks at $f_2 \simeq 14.7$ GHz and $f_3 = 2.2$ GHz. Measurements are done on the carrier itself and on a code which modulates the carrier. The link is asynchronous: a configuration can be chosen by interpolating observables, the so-called Λ-configuration, which minimizes the impact of the space clock orbit error on the determination of the desynchronisation (Duchayne et al., 2009). We define the SYRTE Team (ST) observables by $\Delta\tau = \tau_e - \tau_r$ with τ_e the proper time of emission of the signal and τ_r the proper time of reception. It can be linked to desynchronisation by

$$\tau^s(t_2) - \tau^g(t_2) = \frac{1}{2}\left(\Delta\tau^g_{\rm mo}(\tau^g(t_4^0)) - \Delta\tau^s_{\rm mo}(\tau^s(t_2^0)) + [T_{34} - T_{12}]^g\right) , \quad (2)$$

where t is coordinate time, $\Delta\tau_{\rm mo}$ are the ST observables corrected for the delays in the cable between the clock and the antenna at transmission and at reception, $T_{ij} = t_j - t_i$, $[.]^g$ being the transformation from the coordinate time to the ground clock proper time obtained from Eq. (1). T_{34} and T_{12} are the coordinate time of flight and can be calculated from the known orbits of the clocks, accounting for the tropospheric, ionospheric and Shapiro delays. The observables from the two downlinks can be used to determine the Total Electronic Content (TEC) of the atmosphere along the line-of-sight, in order to correct for the ionospheric delay. The two-way configuration cancels the tropospheric delay, which does not depend on the signal frequency at this level of accuracy. The basic observables of the modem developed by TimeTech (TT observables) are different from the ST observables. At the emitter and the receiver are generated a PPS signal (one Pulse Per Second), a 12.5 PPS (one pulse every 80 ms, the period of measurements), and a periodic signal (either code at 100 MHz or carrier). When received, the periodic signal is mixed with a local oscillator signal not far from the received frequency, and filtered to obtain the low frequency part of the beatnote. The beatnote frequency is around 195 kHz for code and 729 kHz for carrier. The receiver modem records the time of the first ascending zero-phase of the beatnote signal after the 12.5 PPS signal, and it counts the number of ascending zero-phase during one 80 ms sequence. The link between the TT and ST observables is detailed in Delva et al. 2012.

3. DATA ANALYSIS AND SIMULATION

The SYRTE team is developing an independent data analysis software to be able to perform a pre-processing of the raw data and a complete scientific analysis. This software is written in Python language. In order to test it, we wrote also a simulation that generates (noisy) TT observables, as well as theoretical ST observables. This simulation is written in Matlab language, and is as much as possible independent from the data analysis software. Current status of our implementation includes several effects as

- ISS orbitography + ground stations coordinates in ITRF, with transformation into ICRF,
- Clock modeling for ISS & ground stations, with basic noise simulation,
- Time transfer modeling between the two terminals,
- Generation of TimeTech observables, together with theoretical values against which calculated values will be compared.

Current work concerns the modeling of multipath effect and the attitude of ISS and of the ACES-payload. For the multipath, we use a simplified model where the emitted signal finds two paths to reach the receiver : one path goes in straight line from the emitter to receiver, the other one is reflected once somewhere on the path. This second path is heavily attenuated and is considered to be a perturbation of the main signal. We only consider the code signal (as opposed to carrier). For the attitude problem, we are currently implementing some new Python classes linking the attitude of ACES-payload with ITRF.

4. REFERENCES

Duchayne, L., Mercier, F., Wolf, P., 2009, "Orbit determination for next generation space clocks", A&A, 504, pp. 653–661.

Delva, P., Meynadier, F., Wolf, P., Le Poncin-Lafitte, C., Laurent, P., 2012, arXiv:1206.6239.

PARAMETRIC INVARIANCE OF THE RELATIVISTIC COORDINATE PULSAR TIME SCALES

A.E. AVRAMENKO
Lebedev Physical Institute
Moscow, Russia
e-mail: avr@prao.ru

To implement the pulsar time scale corresponding to modern requirements of accuracy and stability, one needs to find coordinated answers to a number of interrelated challenges:

a) the uncertainty of the observed intervals of pulsar time which are determined by the physical conditions that are known very approximately;

b) the extension of barycentric pulsar scales to other observational reference frames (Klioner at al., 2009);

c) parameterization of pulsar scales which suppresses effect of unmodeled timing noise and random residuals deviations.

It is evident that these problems require a precise analytical solution. Our approach, in general, is to find analytical relation of the pulsar time intervals and the physical parameters so that the numerical values of these parameters should be determined and best matched with measured values of the observed intervals. From fitting can be excluded any parameters that can't be obtained directly from observations.

Analytical form of the pulsar time intervals PT, expressed by the rotation parameters of the pulsar, is reduced to Maclaurin power series:

$$PT(P_0, \dot{P}, \ddot{P}) = P_0 N + \frac{1}{2} P_0 \dot{P} N^2 + \frac{1}{6}(P_0^2 \ddot{P} - 2P_0 \dot{P}^2) N^3, \quad N = 1, 2, 3, \ldots \tag{1}$$

The equation of the observed intervals of PT_i in accordance with (2) is:

$$PT_i = (1 + \alpha_i)(P_0^* N + \frac{1}{2} P_0^* \dot{P} N^2 + \frac{1}{6}(P_0^{*2} \ddot{P} - 2P_0^* \dot{P}^2) N^3)_i. \tag{2}$$

Here are: PT_i is the numerical values of the observed intervals obtained from the planetary ephemeris; P_0^*, $\dot{P}$, $\ddot{P}$ are the pulsar rotation parameters obtained by solving equation (2); α_i is divergence of series of the PT_i approximated by the rotation parameters of pulsar.

By parametric approximation of the intervals PT_i (2), the fixed rotation period and its derivatives on the initial epoch, are defined.

It is evident, for any choice of the initial epoch, the value of period is different, taking into account the gap between epochs and the derivatives $\dot{P}$, $\ddot{P}$. The corresponding settings of rotation parameters also satisfy the convergence of the series expansion (2) for any extension in the vicinity specified by the variable $t = P_0^* N$:

$$P(t) = P_0^* + \dot{P}_0 \cdot t + \ddot{P} \cdot t^2; \qquad t = P_0^* N, 1 < N < \infty. \tag{3}$$

where

$$P(t) = P_0^* + \dot{P} \cdot t; \qquad \dot{P} = \dot{P}_0 + \ddot{P} \cdot t.$$

Values of N_i, determined by the equation (2), unlike the ratio (1), are not integer due to random variations in the pulse time of arrival (propagation, error of AT, planetary ephemeris of the Solar system, fitting, etc.). The real values N_i are different from integer value by $\Delta N_i = \dfrac{\Delta\varphi(t)_i}{2\pi}$ determined by the observed pulse phase shift $\Delta\varphi(t)_i = \dfrac{2\pi}{P}\Delta t_i$ within the current period of rotation. Real value $(N_i + \Delta N_i)$ corresponds to the minimum of random variations of the divergence α_i and matches the phase of the observed event to the stable rotation parameters of the pulsar. Random variations of the observed

intervals are limited by nanosecond range, although the scattering of the time of arrival can reach several milliseconds.

According to the principle of relativity (Poincare, 1906), all physical processes occurring in any inertial system under the same conditions, which are defined by the Lorentz transformations, are identical. Logunov (1990) extended the principle of relativity of Poincare without any changes physical entity to the non-inertial reference systems as well.

It has been shown (Avramenko, 2009) that the equation of the pulsar time (2) is form-invariant under coordinate transformations, in which the numerical values of the observed rotation period are coincide in the barycentric and topocentric coordinate systems at the same epochs of the local time. Left part of the equation (2) consists the observed topocentric TT_{obs} or barycentric TB_{obs} intervals. The right part contains the intervals TT_{calc} or TB_{calc}, which are calculated by the observed rotation parameters obtained by approximation of TT_{obs} or TB_{obs}.

Figure 1 compares the intervals of the pulsar time PSR B0809+74 in the barycentric and topocentric coordinate systems. Monotonically growing intervals TT_{obs} and TB_{obs} (left, up) have a cyclical differential variations, due to the orbital motion of the Earth around the Sun (left, down). The quasi-stationary differences $TT_{obs} - TT_{calc}$ and $TB_{obs} - TB_{calc}$ (right) with near zero average confirm precise consistency of intervals PT_{obs} counted by the metric of General relativity (GR) of the numerical ephemeris, and by the metric of Special relativity (SR) of the parameterized intervals, in both topocentric and barycentric coordinate systems. Long-term instability of the parametric pulsar time scales about 10^{-18}–10^{-19} within the 40-year span is several orders better than of the quantum standards.

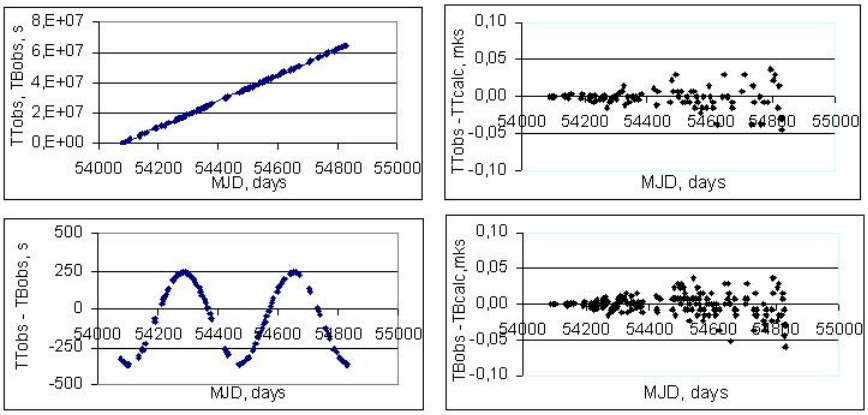

Figure 1: Consistency of the topocentric and barycentric intervals of the PSR B0809+74.

Thus, coordinate pulsar time scales determined by the observed rotation parameters of the pulsar, are the physical implementation of the barycentric dynamical time TDB and terrestrial time TT, expressed by numerical planetary ephemeris of the solar system. Together with reference ICRF-ICRS, to which are oriented Cartesian observational systems and planetary ephemeris, the parametric pulsar scales constitute a single astronomical 4-dimensional reference system based on the periodic radiation of the pulsars and the coordinates of the quasars.

REFERENCES

Avramenko, A.E., 2009, "Form invariance of coordinate pulsar time metrics", Measurement Techniques, 53(5), pp. 525–532.

Klioner, S.A., Capitaine, N., Folkner, W.M., Guinot, B., Huang, T.-Y., Kopeikin, S.M., Pitjeva, E.V., Seidelmann, P.K., Soffel, M.H., 2009, "Units of relativistic time scales and associated quantities", Proc. IAU Symp. 261, pp. 79–84.

Logunov, A.A., 1990, "Lectures in Relativity and Gravitation", Pergamon Press.

Poincare, H., 1906, "Sur la dynamique de l'electron", Rendiconti del Circolo Matematico di Palermo, 21(1), pp. 129–176.

GRAVITATIONAL EFFECTS FROM A SERIES OF IVS R&D VLBI-SESSIONS WITH OBSERVATIONS CLOSE TO THE SUN

R. HEINKELMANN[1], B. SOJA[1], H. SCHUH[1,2]
[1] Helmholtz Centre Potsdam, GFZ German Research Center for Geosciences, Telegrafenberg, 14473 Potsdam, Germany
e-mail: heinkelmann@gfz-potsdam.de
[2] Institute of Geodesy and Geoinformation Science, Technische Universität Berlin, Straße des 17. Juni 135, 10623 Berlin, Germany

ABSTRACT. In 2011 and 2012 the IVS observed twelve VLBI research and development (R&D) sessions that include successful observations as angularly close as 3.9° from the heliocenter. Among others, one purpose of these IVS-R&D sessions was to achieve an improvement in the determination of the PPN parameter γ. Besides, by analyzing this specifiic set of IVS sessions, it was for the first time possible to measure the dispersive effect of the Solar corona with VLBI (Soja et al., 2014). In this work we assess the formal error of the γ-parameter and the contributions of the various terms to the partial derivative of the γ-parameter. Furthermore, we investigate the size of the gravitational delays caused by: (i) Solar monopole field at rest and with approximately linear translation, (ii) rotation of the Solar monopole field, (iii) Solar gravitational field quadrupole expansion, and (iv) Solar higher order term.

1. COMPARISON OF GRAVITATIONAL DELAY MODELS

The current conventional gravitational delay model is based on the *Consensus* model (Eubanks, 1991) and specified by the current IERS Conventions (2010) (Petit & Luzum, 2010). It contains the first and higher order terms of the Solar monopole field at rest. Comments regarding the nomenclature and completeness of the current IERS Conventions: (i) The nomenclature of the unit vector in the direction of the radio source changes from $\vec{K}$ (eqs. 11.1, 11.2) to $\hat{K}$ (after eq. 11.2). (ii) The index used for the gravitating body changes from J (eqs. 11.1 till 11.7) to i (eq. 11.14), before index i was used for the individual antenna. (iii) It is not specified how the position of the gravitating body at the time of closest approach is to be numerically evaluated (e.g. interpolation or linear extrapolation). (iv) *"For observations made very close to the Sun, higher order relativistic time delay effects become increasingly important."* (Petit & Luzum, 2010). It is not specified what "very close to the Sun" numerically means.

The gravitational delay model in the Vienna VLBI Software VieVS (Böhm et al., 2012) equals the conventional model with two exceptions: (i) the time used for the iteration of the position of the gravitating body is different from the time of closest approach and (ii) the higher order term for the Sun is neglected. The time used for the evaluation of the closest approach considers the theoretical travel time from the gravitating body to the receiver. This is only a valid approximation if the gravitating body stays between the source and the baseline and the signal travels very close to the gravitating body. For all other cases the approximation is not valid. In particular it does not consider the case where the gravitating body is situated behind the baseline (as seen from the radio source).

The most complete gravitational delay model, derived by Klioner (1991) and reported in detail in Klioner & Kopejkin (1992), includes all additional terms of the 2PN metric. Compared to the conventional delay model it considers the delay caused by linear translation and rotation of the monopole field and by the expansion of the gravitational field to the quadrupole moment of the Sun. Furthermore, other expressions that are necessary for the derivation, such as the time of closest approach and the higher order term are given with precision higher than the two aforementioned models.

The maximum differences of the main term, the Solar gravitational monopole field at rest, when analysing the twelve IVS-R&D sessions (Soja et al., 2014), are at the level of $1 \cdot 10^{-3}$ ps. For the current precision of standard X/S VLBI group delay observables of about 20 ps the differences are negligible. For the minimum Solar elongation angles involved in the twelve IVS-R&D sessions of 3.9° the maximum absolute value of the higher order term reaches 0.14 ps and that of the quadrupole field term 0.06 ps. The other terms, the Solar translational and rotational terms, are negligible. For the analysis of the twelve

IVS-R&D sessions it follows that it is sufficient to work with one of the three models mentioned above. However, analysing other IVS sessions, where the Sun is situated in opposition and not in conjunction with the observed radio source, the deviations of the gravitational delay model of VieVS can exceed these values. The current minimum Solar elongation angle of IVS is 4°. For smaller elongations the higher order term and also the term due to the quadrupole expansion may become significant.

2. FORMAL ERROR AND PARTIAL DERIVATIVE OF THE γ-PARAMETER

In Heinkelmann & Schuh (2010) we first outlined that the partial derivative of the γ-parameter could be obtained considering the term of the gravitational delay of the Sun alone. For the twelve IVS R&D sessions under investigation we derived and considered the complete γ partial derivative that also involves the terms due to the Lorentz transformation, the Earth gravitational delay, the gravitational delays induced by the other planets and the Moon, and the contributions due to the extensions of the Solar gravitational delay as discussed in the first section. The average size of the contributions to the partial derivative are listed in Table 1. They are valid for the particular geometry of the twelve IVS-R&D sessions only.

The twelve IVS-R&D sessions that were designed to observe close to Sun aimed to improve the determination of the γ-parameter. We estimated two solutions: the first solution includes all observations of the IVS-R&D sessions and for the second solution we disregarded those observations within 15° Solar elongation. The formal error of γ estimated as a global parameter over the twelve sessions increased from 0.00076 to 0.00134 (almost double the size). The formal error when fixing station positions on their catalogue values increased from 0.00136 to 0.00239 if angularly close observations are excluded, indicating that the estimation of γ significantly depends on other parameters as well. Of course, a more reliable estimate of γ can be derived by including much more than twelve IVS sessions (Lambert & Le Poncin-Lafitte, 2009).

Solar monopole field at rest	1
Lorentz transformation	0.3
Earth gravitation	0.01
Planetary and Lunar gravitation	0.0005
Extended Solar gravitational terms	0.00001

Table 1: Mean size of the component's contribution to the γ partial derivative relative to the first component (Solar monopole field at rest).

3. REFERENCES

Böhm, J., Böhm, S., Nilsson, T., Pany, A., Plank, L., Spicakova, H., Teke, K., Schuh, H., 2012, "The new Vienna VLBI software", In: S. Kenyon, M.C. Pacino, U. Marti (eds.) IAG Symposia, 136, pp. 1007–1011, doi: 10.1007/978-3-642-20338-1_126.

Heinkelmann, R., Schuh, H., 2010, "Very long baseline interferometry: accuracy limits and relativistic tests", In: Proc. IAU Symp. 261 "Relativity in Fundamental Astronomy", S.A. Klioner, P.K. Seidelmann, M.H. Soffel (eds.), pp. 286–290, doi: 10.1017/S1743921309990524.

Eubanks, T.M.A., 1991, "A consensus model for relativistic effects in geodetic VLBI", In: Proc. USNO Workshop on Relativistic Models for Use in Space Geodesy, pp. 60–82.

Klioner, S.A., 1991, "General Relativistic Model of VLBI Observables", In: Proc. AGU Chapman Conference on Geodetic VLBI: Monitoring Global Change, 22–26 April 1991, Washington, D.C., USA, NOAA Technical Report, No. 137, NGS 49, pp. 188–202.

Klioner, S.A., Kopejkin, S.M., 1992, "Microarcsecond astrometry in space: relativistic effects and reduction of observations", AJ, 104(2), pp. 897–914.

Lambert, S.B., Le Poncin-Lafitte, C., 2009, "Determining the relativistic parameter γ using very long baseline interferometry", A&A, 499, pp. 331–335.

Petit, G., Luzum, B. (eds.), 2010, IERS Conventions (2010), IERS Technical Note 36, Frankfurt am Main: Verlag des Bundesamts für Kartographie und Geodäsie.

Soja, B., Heinkelmann, R., Schuh, H., 2014, "Probing the solar corona with very long baseline interferometry", Nat. Commun., 5:4166, doi: 10.1038/ncomms5166.

Session 3

SOLAR AND EXTRASOLAR SYSTEMS DYNAMICS

DYNAMIQUE DES SYSTÈMES SOLAIRE ET EXTRA-SOLAIRE

RESONANCES IN THE SOLAR AND EXOPLANETARY SYSTEMS

I. SHEVCHENKO
Pulkovo Observatory
196140 St. Petersburg, Russia
e-mail: iis@gao.spb.ru

Dynamical problems on the orbital resonances, including mean motion resonances (both two-body and three-body ones) and secular resonances, are considered in application to the dynamics of the Solar and exoplanetary systems. The analyzed systems include multiplanetary (those with two or more than two planets) systems and planetary systems of double stars. Theoretical methods and criteria for revealing stability or instability of various planetary configurations are described.

INVESTIGATIONS OF ASTEROIDS IN PULKOVO OBSERVATORY

A.V. DEVYATKIN, D.L. GORSHANOV, V.N. L'VOV, S.D. TSEKMEISTER, S.N. PETROVA, A.A. MARTYUSHEVA, V.Y. SLESARENKO, K.N. NAUMOV, I.A. SOKOVA, E.N. SOKOV, S.V. ZINOVIEV, S.V. KARASHEVICH, A.V. IVANOV, A.Y. LYASHENKO, S.A. RUSOV, V.V. KOUPRIANOV, E.A. BASHAKOVA, A.V. MELNIKOV
Central Astronomical Observatory at Pulkovo of Russian Academy of Sciences
65 Pulkovskoe Sh., 196140, St. Petersburg, Russia
e-mail: adev@gao.spb.ru

ABSTRACT. Observational Astrometry Laboratory and Ephemeris Provision Sector of Pulkovo Observatory carry out a joint multipurpose research on asteroids belonging to various groups. Astrometric and photometric observations are done using ZA–320M and MTM–500M telescopes located at Pulkovo and in Northern Caucasus mountains, correspondingly. We obtain lightcurves that allow us to determine spin parameters and shapes of asteroids. Their color indices and taxonomy classes are derived from wideband filter observations. Improvement of asteroid orbits is achieved by doing positional measurements. Orbital evolution of asteroids is modelled, taking into account also non-gravity forces, including light pressure and Yarkovsky effect. NEAs, as well as binary asteroids, take an important place in our investigations. Quasi-satellites of Venus, Earth, and Mars are new targets of our research, one of the examples being 2012 DA14 that approached Earth in early 2013; many MTM–500M observations of this asteroid were obtained around the date of approach.

1. TELESCOPES

Observational Astrometry Laboratory of Pulkovo Observatory carries out observations with two small robotic telescopes. ZA–320M ($D = 32\,\mathrm{cm}$, $F = 320\,\mathrm{cm}$) is installed at Pulkovo observatory (Saint Petersburg). MTM–500M ($D = 50\,\mathrm{cm}$, $F = 410\,\mathrm{cm}$) is located in Northern Caucasus mountains near Kislovodsk at the altitude of 2070 m. Both telescopes are equipped with CCD cameras and $BVRI$ filters.

2. SOFTWARE

CCD images are processed by Apex II software (Devyatkin et al., 2010) developed at Pulkovo Observatory as an all-purpose astronomical image analysis platform. Apex II automatic asteroid pipeline comprises the following basic steps: calibration (including synthesis and application of dark and flatfield frames and cosmetic correction); sky background flattening; object detection; deblending; centroiding by PSF fitting; flux measurement using aperture, PSF, and optimal techniques; rejection of false detections; matching to reference catalog (USNO–A2, USNO–B1, Tycho–2, HIPPARCOS, UCAC4, 2MASS, XPM, user catalogs); astrometric reduction by a set of standard plate models; matching uncorrelated objects to the list of Solar system bodies (EPOS package is used to provide solar system object ephemerides, see below); report creation in one of the standard formats (e. g. MPC). There is a capability to mark objects and reference stars in a visual manner using the dedicated graphical interface.

To calculate the motion of solar system bodies, we use EPOS software (L'vov, Tsekmeister, 2012), also developed at Pulkovo. The software provides several kinds of celestial mechanics calculations and visualization modes, including ephemerides, $\mathrm{O}-\mathrm{C}$, orbit determination and improvement, and modelling the motion of solar system bodies in the various coordinate systems.

3. ASTEROID INVESTIGATIONS

From our observations, we get astrometric positions of asteroids for improvement of their orbits. Also, we do numerical modelling of orbital evolution of asteroids, taking into account both gravity and non-gravity effects (light pressure, Yarkovsky effect, close approaches to planets). Lightcurves obtained from photometric observations allow us to estimate parameters of rotation of asteroids, while $BVRI$

magnitudes provide their color indices and (in some cases) help us to estimate their taxonomy classes.

We focus on observations of the following types of asteroids: near-Earth asteroids, binary and multiple systems, asteroids named after Pulkovo astronomers, and several other types. We take part in the international campaigns for asteroid observations, like the ground-based follow-up of GAIA mission targets. A new prospective direction of our research are asteroids that are quasi-satellites of inner planets. Some of the recent results for asteroids that approached Earth are shown below.

4. ASTEROID (367943) DUENDE = 2012 DA14

The asteroid had a very close approach (27700 km) to Earth on 15.02.2013. It was a target of GAIA follow-up training observational campaign. We obtained 436 astrometric positions with the average accuracy of $0.''46$ in right ascension and $0.''23$ in declination. Three color indices were estimated from $BVRI$ observations: $B-V = 0.^m86 \pm 0.^m15$, $V-R = 0.^m39 \pm 0.^m04$, $R-I = 0.^m36 \pm 0.^m03$. Based on these values, we estimated the possible Tholen taxonomy class of Duende – either G or C.

Using EPOS, we have modelled the orbital evolution of this asteroid and got some interesting results. Duende orbits the Sun near 1:1 mean motion resonance with Earth and sometimes closely approaches the latter, which changes its orbital parameters. The latest closest approaches were in 2004 and 2013 (see Fig. 1). At the moments of approaches, orbital elements changed abruptly.

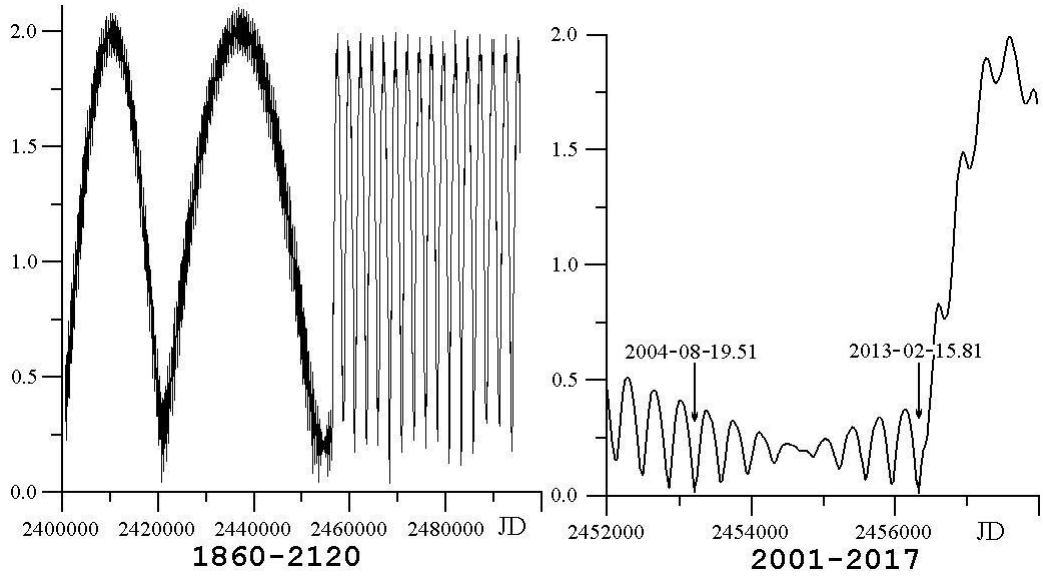

Figure 1: Geocentric distance (in AU) of Duende over 160 years (left) and on a shorter timescale (right). Arrows indicate the moments of closest approaches to Earth.

Moreover, the asteroid even changes the type of its orbit with respect to Earth. Let us use a rotating coordinate system with X axis going from Sun towards Earth. The possible types of Duende trajectory are shown in Fig. 2. However, this result is extremely sensitive to small changes in orbital elements at the initial moment of calculations. When using pre-April 2013 MPC elements, Duende changes the type of its orbit three times from circulating orbit to a horseshoe one and then (possibly) to the one of an Earth's quasi-satellite. Taking a more recent set of elements leads to the asteroid maintaining a circulating orbit, but moving in the opposite direction with respect to Earth and escaping from 1:1 resonance as a result of the 2013 approach.

We obtained two lightcurves for Duende: on February 16 and 19 2013. Each of them is about 10 hours long, which should roughly correspond to one rotation period, considering their shape. Unfortunately, these two fragments do not allow one to reliably determine the period. Comparing with lightcurves observed by other teams reveals a certain degree of coincidence. However, there are also lightcurves not overlapping with ours in time that do not match ours assuming the period of 9 to 11 hours. This is an indication of a quite complex rotation of the asteroid during approach.

We also made an attempt to model the asteroid rotation based solely on our two lightcurves, both

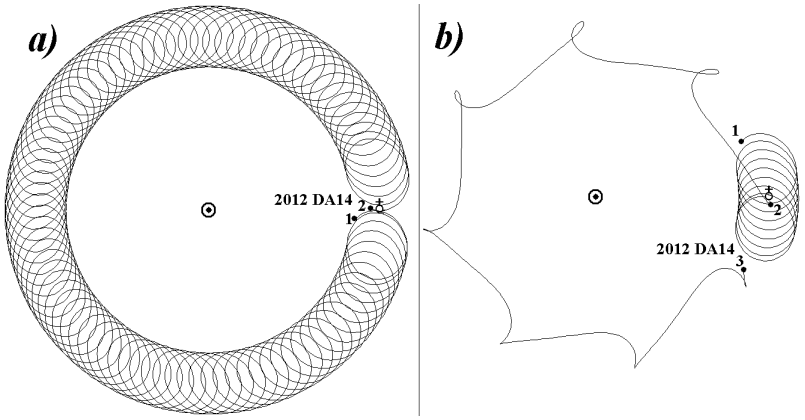

Figure 2: The possible types of Duende trajectory with respect to Earth in the rotating coordinate system: *a)* horseshoe orbit; *b)* quasi-satellite (1–2) and circulating (2–3) orbit.

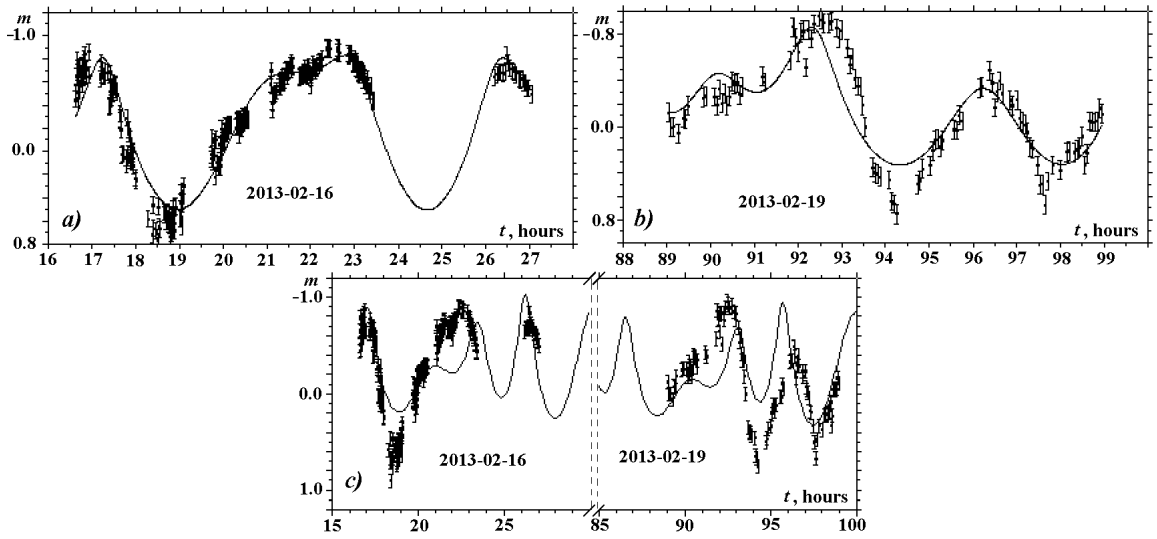

Figure 3: Model lightcurves of Duende (solid lines) superimposed over the observation data from ZA–320M and MTM–500M. *a)* and *b)* two separate datasets; *c)* lightcurve from two combined datasets.

taken separately and combined. The resulting model lightcurves and observed points are shown in Fig. 3. The modelling suggests that the ratio of "photometric" ellipsoid axes is 10:2:1, whereas the ratio of the axes of asteroid body is 4:2:1. Therefore, Duende shape greatly differs from ellipsoid and, possibly, its albedo is non-homogeneous. The axis of rotation of the asteroid has moved by 52° between these two sets of observations. Hence, Duende tumbled near the time of approach. We are currently calculating a model that incorporates all available lightcurves.

5. ASTEROID 2014 HQ124

The asteroid had a 0.0086 AU approach with Earth on 08.06.2014. It was a target of GAIA FUN SSO training campaign as well. Also, there was a sub-campaign for synchronous observations of the asteroid during its close approach for the purpose of triangulation.

We have got 84 astrometric positions from our observations, with an average accuracy of $0\farcs19$ in right ascension and $0\farcs26$ in declination. 18 positions were observed at the planned epochs simultaneously with other observatories. We also obtained lightcurves from these observations. Due to a rapid motion of the asteroid across the sky, the resulting accuracy is very moderate ($\approx 0\fm08$).

6. ASTEROID 2013 TV135

The asteroid had a 0.045 AU approach to Earth on 17.09.2013. Again, it was a training GAIA FUN SSO campaign target. We have obtained 335 astrometric positions from our observations, with an average accuracy of 0.″28 in both right ascension and declination. Furthermore, we have obtained 5 lightcurves. Using their average values, we made an attempt to construct a phase curve of the asteroid and estimate its absolute magnitude and slope parameter ($G = -0.06 \pm 0.03$, $H_R = 18\overset{m}{.}7 \pm 0\overset{m}{.}2$). However, phase angle was too large ($\approx 50°$) to obtain a reliable estimate. Using our lightcurves spanning two weeks, we were able to accurately determine the rotation period of the asteroid: $P = 2\overset{\mathrm{h}}{.}3512 \pm 0\overset{\mathrm{h}}{.}0004$ (see Fig. 4).

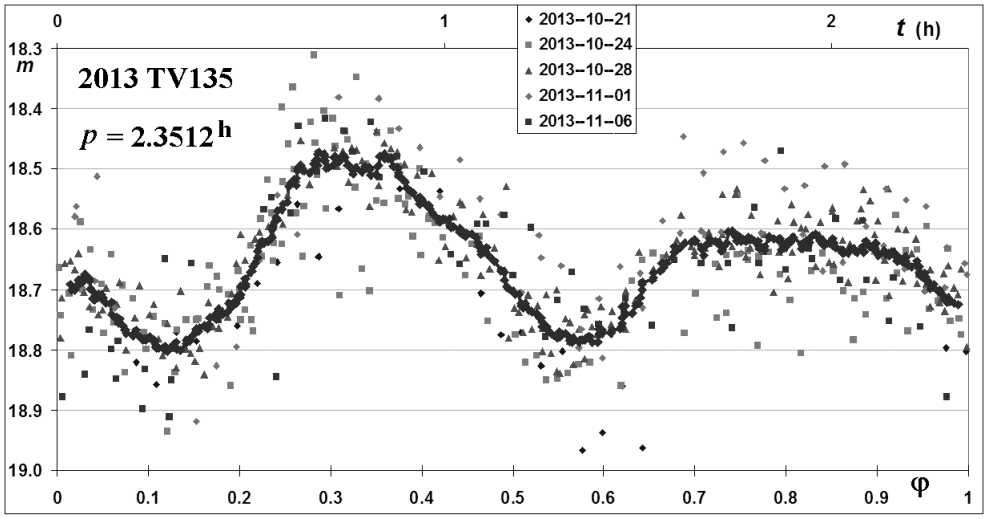

Figure 4: Lightcurve of 2013 TV135 phased with the period of $2\overset{\mathrm{h}}{.}3512$ derived from our observations. It comprises 5 individual fragments obtained on MTM–500M.

7. ASTEROID 251346

The asteroid had a 0.049 AU approach to Earth on 22.01.2014. 120 astrometric positions with an average accuracy of 0.″23 in right ascension and 0.″12 in declination and 4 lightcurves were obtained. Unlike the previous example, here we used the known period $P = 2\overset{\mathrm{h}}{.}718$ determined by other researchers (Hicks, Ebelhar, 2014; Warner, 2014) to combine the separate lightcurves. Our observations confirmed the above value.

8. REFERENCES

Devyatkin, A.V., Gorshanov, D.L., Kouprianov, V.V., Verestchagina, I.A., 2010, "Apex I and Apex II software packages for the reduction of astronomical CCD observations", Solar System Research, 44(1), pp. 68–80.

Hicks, M., Ebelhar, S., 2014, Astronomer's Telegram 5801, http://www.astronomerstelegram.org.

L'vov, V.N. Tsekmeister, S.D., 2012, "The Use of the EPOS Software Package for Research of the Solar System Objects", Solar System Research, 46(2), pp. 177–179.

Warner, B.D., 2014, Minor Planet Bul., 41, pp. 113-124.

EVOLUTION OF EPHEMERIDES EPM OF IAA RAS

E.V. PITJEVA
Institute of Applied astronomy RAS
Kutuzov Quay 10, 191187 St.-Petersburg, Russia
e-mail: evp@ipa.nw.ru

ABSTRACT. The evolution of numerical EPM ephemerides of the IAA RAS from available EPM2004, EPM2008, EPM2011, to the new EPM2014 version is presented briefly. The comparison progress of ephemerides includes: the growing database of different types of observations from classical optical to radio technical of spacecraft from 1913 to 2014, enlarged up to more 800000 measurements; improved dynamical model from mutual perturbations of all planets, the Sun, the Moon, 301 largest asteroids to additional perturbations from of 30 largest trans-neptunian objects (TNO) and perturbations from remaining smaller asteroids and TNO modeled by the two-dimensional asteroid ring and the one-dimensional TNO ring; program software ERA-7 to ERA-8.

1. INTRODUCTION

The EPM ephemerides (**E**phemerides of **P**lanets and the **M**oon) were first created in the 1970s in support of Russian space flight missions and constantly improved at IAA RAS. Several factors influence the progress of planet ephemerides: dynamical models of planet motion; observational data, with the crucial role of spacecraft ranging with their growing accuracy; reduction of observations; updated database of asteroids (masses and orbits); program software; access to ephemerides.

2. DYNAMICAL MODELS

The uncertainty of modern ranging observations is only a few meters, that demands the accuracy of planet positions of at least 12 significant figures, so it is necessary to take into account any significant influencing factors in dynamical models. The dynamical models of planet part of EPM ephemerides have taken into account the following

EPM87 (Krasinsky et al., 1993):

- Mutual perturbations from the major planets, the Sun, the Moon and 5 more massive asteroids;
- the relativistic perturbations.

EPM are based on General Relativity involving the relativistic equations of celestial bodies motion and light propagation, as well as the relativistic time-scales.

EPM98:

- Perturbations from the other 296 asteroids chosen due to their strong perturbations upon Mars and the Earth. The perturbations from 300 asteroids were taken into account starting with DE230 and were implemented in the well-known DE403 ephemerides (Standish et al. 1995). The perturbations from 300 asteroids were taken into account since EPM98 (Pitjeva, 1998).

EPM2000 (Pitjeva, 2001):

- Perturbations due to the solar oblateness J_2, that is currently determined during the processing of high-precision ranging measurements.

EPM2004:

- Perturbation from the massive one-dimensional asteroid ring with the constant mass distribution. The two parameters characterizing the ring (its mass M_r and radius R_r) were included into the set of parameters that were fitted to observations. That approach was proposed by Krasinsky et al.(2001) and implemented in EPM2004 ephemerides (Pitjeva, 2005).

EPM2008 (Pitjeva, 2010):

- Perturbations from the 21 largest Trans-Neptunian Objects (TNO).;

EPM2011 (Pitjeva, 2013):

- Perturbation from a massive ring of TNO in the ecliptic plane with the radius of 43 au.

EPM2013/EPM2014 (Pitjeva & Pitjev, 2014):

- Perturbation from the massive two-dimensional asteroid annulus (R_1 = 2.06 au, R_2 = 3.27 au). The accuracy of estimation of the the mass of the modeled annulus of small asteroids, as well as the accuracy of the total mass of the main asteroid belt increased by 6.3 times as compared to the previous estimates using the one-dimensional asteroid ring;
- perturbations from the 30 largest Trans-Neptunian Objects (TNO).

3. OBSERVATIONS, THEIR REDUCTIONS, PARAMETERS

The observational data set was increased by an order of magnitude as compared to EPM2000 ephemerides, resulting in more 800000 observations, mostly high-precision data from spacecraft. The planetary part of EPM2013/14 ephemerides has been fitted to observations of different types, spanning 1913-2014. Majority of planet observations was taken from the Jet Propulsion Laboratory (JPL) database (http://iau-comm4.jpl.nasa.gov/ plan-eph-data/index.html). 4086 normal points of new spacecraft data were added to the database of EPM2013 including the observations obtained for Odyssey, Mars Reconnaissance Orbiter (MRO), Mars Express (MEX) and Venus Express (VEX) spacecraft, updated ranging data for Cassini (2004-2014) (Hees et al., 2014), as well as 7861 data for Pluto, They are the CCD observations of Pluto obtained in 1950-2013 at Brazilian Pico dos Dias observatory (Benedetti-Rossi et al., 2014), and a new analysis of photographic plates taken at Lowell Observatory from 1931 to 1951 (Buie & Folkner, 2015). These new data were obtained through the courtesy of Folkner (JPL), Fienga (IMCCE), and Benedetti-Rossi (Observatorio Nacional/MCT). The ephemerides of the inner planets are based fully on radiotechnical observations, mostly measurements of time delays.

The processing of observational data was done using proven and reliable techniques with due account for all needed reductions (Standish 1990; Pitjeva 2005, 2013), as well as proper TT-TDB differences (Pitjeva, 2013).

EPM2014 have been oriented to ICRF with the accuracy better than 1 mas by including into the total solution the 321 ICRF-base VLBI measurements of spacecraft (Magellan, Phobos, MGS, Odyssey, Venus Express, Mars Reconnaissance Orbiter, and Cassini) 1989 - 2013 near Venus, Mars, and Saturn.

More than 270 parameters were determined while improving the planetary part of EPM2014 ephemerides. They include, in addition to orbital elements of all planets and 16 satellites of the outer planets, parameters of orientation of ephemerides, parameters of rotation and topography of planets, masses of asteroids. the Earth to Moon ratio, the value $GM_\odot$, many postmodel parameters, etc.

The dynamical models of the EPM ephemerides have been improved significantly. Number of observations used for improvement of ephemerides and their accuracy have increased greatly, and the number of adjusted parameters has grown accordingly.

4. PROGRESS OF EPM EPHEMERIDES

The progress of EPM ephemerides may be shown on any new data not used when fitting the ephemeris parameters. Recently the new MEX data obtained from 2013.01.01 to 2014.05.05 have become available for us due to Fienga. Those data were not used for fitting any EPM ephemerides except EPM2014. The decrease of their residuals (without fitting) computed using EPM2004, EPM2008, EPM2011, EPM2013 ephemerides demonstrates the improvement of the Mars orbit from EPM2004 to EPM2013. Their rms standard deviations are equal to 63, 34, 29, and 20 m for EPM2004, EPM2008, EPM2011, EPM2013, respectively (Fig. 1). After improvement of these observations for the new EPM2014 version, their residuals have decreased to 1.5 m. For EPM2014, the WRMS residuals of ranging for Odyssey, MRO, and VEX spacecraft are 1.2 m, 1.2 m, 3.1 m, respectively.

Orbits of all planets have been improved significantly. In particular, formal uncertainties of orbital elements of all planets have decreased by several times. Especially it is notably for the inner planets and Saturn (Table 1).

Ephemeris	Planet	a [m]	$\sin i \cos\Omega$ [mas]	$\sin i \sin\Omega$ [mas]	$e\cos\pi$ [mas]	$e\sin\pi$ [mas]	λ [mas]
EPM2004	Mercury	0.105	1.654	1.525	0.123	0.099	0.375
EPM2014		0.065	0.7976	0.5545	0.0857	0.0687	0.1536
EPM2004	Venus	0.329	0.567	0.567	0.041	0.043	0.187
EPM2014		0.004	0.00315	0.00255	0.00013	0.00013	0.00312
EPM2004	Earth	0.146	—	—	0.001	0.001	—
EPM2014		0.005	—	—	0.00005	0.00005	—
EPM2004	Mars	0.657	0.003	0.004	0.001	0.001	0.003
EPM2014		0.015	0.00077	0.00082	0.00007	0.00013	0.00039
EPM2004	Jupiter	639	2.410	2.207	1.280	1.170	1.109
EPM2014		347	2.005	1.808	0.128	0.109	0.882
EPM2004	Saturn	4222	3.237	4.085	3.858	2.975	3.474
EPM2014		4.828	0.0807	0.0573	0.00097	0.00035	0.0124
EPM2004	Uranus	38484	4.072	6.143	4.896	3.361	8.818
EPM2014		30033	3.453	4.007	2.849	2.003	3.592
EPM2004	Neptune	478532	4.214	8.600	14.066	18.687	35.163
EPM2014		270479	2.669	5.195	5.546	13.540	12.345
EPM2004	Pluto	3463309	6.899	14.940	82.888	36.700	79.089
EPM2014		563306	0.865	3.312	12.900	8.384	4.870

Table 1: The formal standard deviations of planetary orbital elements adjusted in EPM2004 and EPM2014 ephemerides

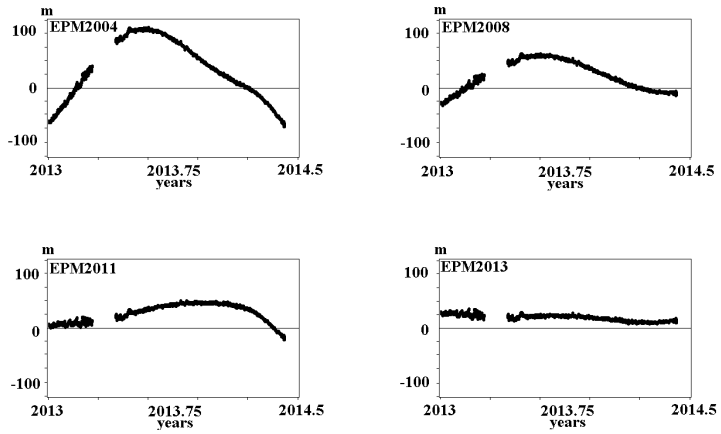

Figure 1: The residuals of one-way ranging for spacecraft MEX from 01.01.2013 to 05.05.2014 (before fitting) computed for EPM2004, EPM2008, EPM2011, EPM2013.

5. SOFTWARE AND ACCESS TO EPM EPHEMERIDES

The software for ephemeris construction has changed radically since 1970's from individual astronomical programs, and the first constrained astronomical programs and program package to complicated program complex ERA (Ephemeris Research in Astronomy) -7 (Krasinsky & Vasilyev, 1997) and ERA-8 (portable across Windows/Linux, 32- and 64-bit) with improved stability, diagnostics, and debugging programs (Pavlov & Skripnichenko, 2014).

The access to EPM ephemerides improved greatly from distribution of files with coordinates and velocities of objects (1970's-1980's), then access to Chebyshev polynomial approximation of object positions (about 2000), to the access package (Calc_Eph), and Standardizing Access to Ephemerides and File

Format Specification developed by the IAU Commission 4 Working Group on Standardizing Access. The formats are: Spacecraft and Planet Kernel (SPK) for the position ephemerides of the Sun, Moon, Earth, other planets, and asteroids; also for the so-called "time ephemerides" containing TT-TDB data; Planetary Constants Kernel (PCK) for lunar orientation (libration angles). PCK and SPK formats are being supported by the IAA in parallel to its original text and binary formats. The files containing polynomial approximation for EPM ephemerides are available from ftp://quasar.ipa.nw.ru/incoming/EPM/.

6. CONCLUSION

The progress in the accuracy of planet ephemerides is due to the improvement of reduction techniques and dynamical models and also to he improvement of quality and growth of quantity of observational data with the crucial role of spacecraft ranging. Expansion of such data on other bodies of the Solar System and on a larger time interval allows to construct more accurate ephemerides and estimate small effects and parameters more precisely.

7. REFERENCES

Benedetti-Rossi, G., Vieira Martins, R., Camargo, J., Assafin, M., Braga-Ribas, F., 2014, "Pluto: improved astrometry from 19 years of observations", A&A, 570, A86.

Buie, M., Folkner, W., 2015, "Astrometry of Pluto from 1930–1951 Observations", AJ, 149, 22.

Hees, A., Folkner, W.M., Jacobson, R.A., Park, R.S., 2014, "Constraints on modified Newtonian dynamics theories from radio tracking data of the Cassini spacecraft", Physical Review D, 89(10), 102002.

Krasinsky, G.A., Pitjeva, E.V., Sveshnikov, M.L., Chunajeva, L.I., 1993, "The motion of major planets from observations 1769–1988 and some astronomical constants", Celest. Mech., 55, pp. 1–23.

Krasinsky, G., Vasyliev, M., 1997, "ERA: knowledge base for ephemeris and dynamic astronomy", Proc. IAU Colloquium 165, pp. 239–244.

Krasinsky, G.A., Pitjeva, E.V., Vasilyev, M.V., Yagudina, E.I., 2002, "Hidden mass in the asteroid belt", Icarus, 158, pp. 98–105.

Pavlov, D.A., Skripnichenko, V.I., 2014, "Preliminary results in implementation of a cross-platform version of the ERA software system", IAA Transactions, No. 30, pp. 32–40. (in Russian)

Pitjeva, E.V., 1998, "The new numerical planet ephemeris EPM98, its comparison with DE403 ephemeris of Jet Propulsion Laboratory of USA", IAA Transaction, 3, pp. 5–23.

Pitjeva, E.V., 2001, "Modern numerical ephemerides of planets and the importance of ranging observations for their creation", Celest. Mech. Dyn. Astr., 80, pp. 249–271.

Pitjeva, E.V., 2005, "High-precision ephemerides of planets – EPM and determinations of some astronomical constants", Solar System Research, 39, pp. 176–186.

Pitjeva, E.V., 2010. "Influence of trans-neptunian objects on motion of major planets and limitation on the total TNO mass from planet and spacecraft", Proc. IAU Symp. 263, D. Lazzaro, D. Prialnik, R. Schulz, J.A. Fernandez (eds.), pp. 93–97.

Pitjeva, E.V., 2013, "Updated IAA RAS Planetary Ephemerides EPM2011 and their use in scientific research", Solar System Research, 47, pp. 386–402.

Pitjeva, E.V., Pitjev, N.P., 2014, "Development of planetary ephemerides EPM and their applications", Celest. Mech. Dyn. Astr., 119, pp. 237–256.

Standish, E.M., Jr., 1990, "The observational basis for JPL's DE200, the planetary ephemerides of the Astronomical Almanac", A&A, 233, pp. 252–271.

Standish, E.M., Newhall, XX, Williams, J.G., Folkner, W.M., 1995, "JPL Planetary and Lunar Ephemerides, DE403/LE403", Interoffice Memorandum 314.10-127.

THE IMPROVEMENT OF THE PLUTO ORBIT USING ADDITIONAL NEW DATA

A. GIRDIUK
Institute of Applied Astronomy RAS
Kutuzov Quay 10, 191187 St. Petersburg, Russia
e-mail: girduik@ipa.nw.ru

ABSTRACT. Observational series of the Pluto dwarf planet have started since 1913. At this moment observations have covered only a third of the Pluto orbit, therefore, the Pluto orbital elements are defined with insufficient accuracy. A growing number of observations leads to the improvement of the accuracy of the orbit determination. The database of the Pluto's observations was expanded with the help of about 350 observations during 1930–1996 obtained at the Pulkovo Observatory, and about 5500 observations (1995–2013) including occultation data from Brazilian colleagues obtained at the European Southern Observatory and the Pico dos Dias Observatory, and the new analyzed 469 historical photographic observations archived at Lowell Observatory. The new cross-platform software ERA-8 has been developed in IAA RAS and has been used for implementation of all mathematical procedures for constructing Pluto orbit. The modern ephemerides (EPM2011, EPM2013, DE430, DE432, INPOP13c) are chosen for comparison of the ephemeris positions: equatorial coordinates and heliocentric distance. The main result of the work – construction of ephemerides EPM2014a is a significant improvement of the Pluto's orbit using additional observations.

1. INTRODUCTION

Prof. George Krasinsky and his group started the development of The Ephemerides of Planets and the Moon (EPM) since 1974, firstly in the Institute of Theoretical Astronomy, then in the Institute of Applied Astronomy of the Russian Academy of Science (IAA RAS). The most complete version of that time, designated EPM87, was created in 1987 (Krasinsky et al., 1993). Its parameters were fit to a wide variety of observational data for the time span XVIII–XX centuries. EPM ephemerides were computed using the program package ERA-7 (ERA: Ephemeris Research in Astronomy) (Krasinsky & Vasilyev, 1997). Pluto ephemerides presented in this paper, was based on the improvement of only Pluto orbit using additional new observations. The corresponding ephemerides are called EPM2014a.

The Pluto was discovered in 1930 (Tombaugh, 1946), but its observational series are available from 1913 due to finding of the Pluto image on old photographic plates. Therefore, only one third part of the Pluto orbit has been covered with observations. As a result, its positions and velocities are known far worse than for other big planets of the Solar system (Pitjeva & Pitjev, 2014). Observational data recently obtained (Assafin et al., 2010; Khrutskaya et al., 2013; Buie & Folkner, 2015; Folkner, 2014; Folkner et al., 2014; Benedetti-Rossi et al., 2014) present a valuable information for making the new ephemeris.

2. THE SURVEY OF THE NEW DATA

The new observations can be divided into two groups represented in Table 1. Figure 1 shows both groups of observations: the photographic plates are on the left plot and the CCD data are on the right plot. The multicolor dots of plots in Fig. 1 mark residuals of the three sorts of photographic plates from Table 1. The CCD observations of Pluto in Table 1 was started from 1995 and are presented on the right side of Fig. 1. All the data were calculated using the ephemerides EPM2014a. The CCD data are far better than photographic ones, but, unfortunately, they cover a very short arc of Pluto orbit.

3. THE CONSTRUCTION OF THE EPHEMERIDES EPM2014A

The modern ephemerides EPM2013 was used as a zero approximation to make the EPM2014a. Only the Pluto orbit was improved for the EPM2014a. The new cross-platform software ERA-8 (Pavlov &

name of observatory	type of data	N observations	time span
digitized Pulkovo (Khrutskaya et al., 2013)	photographic plates	63	1930–1960
USNO/Lowell (Buie & Folkner, 2015)		469	1931–1951
review Pulkovo (Rylkov et al., 1995)		193	1930–1992
Pico dos Dias (PDO) (Benedetti-Rossi et al., 2014)	CCD	5489	1995–2011
USNO/Flagstaff (Folkner et al., 2014)		1197	1995–2013
Table Mountain (TMO) (Folkner, 2014)		695	2001–2013
ESO/La Serena (Assafin et al., 2010)		11	2005–2008

Table 1: Description of the new observations.

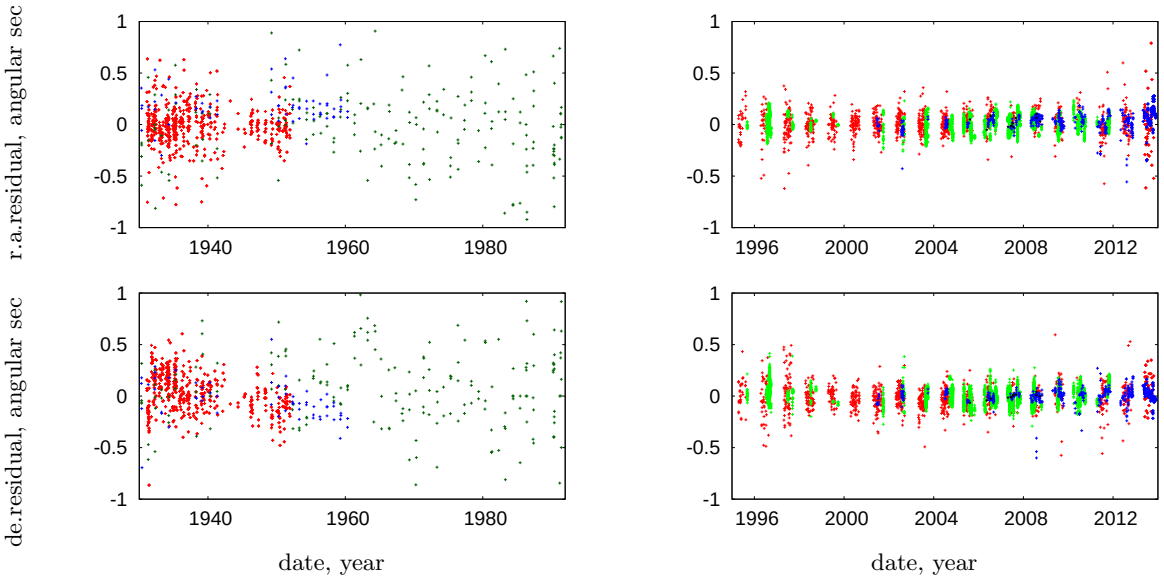

Figure 1: Residuals in right ascension (the upper panel) and declination (the bottom panel) of photographic plates (on the left side): digitized Pulkovo of blue color, USNO/Lowell of red color and review of Pulkovo of green color and CCD observations (on the right side): the PDO of green color, the USNO/Flagstaff of red color and the TMO of blue color, the ESO/La Serena of black color.

	element	EPM2014a	of the EPM2013	of the EPM2014a
1	a	39.713 a.u.	1316.116 km	563.306 km
2	$\sin i \cos \Omega$	0.285	0.816 mas	0.865 mas
3	$\sin i \sin \Omega$	0.276	4.516 mas	3.312 mas
4	$e \cos \pi$	-0.170	27.453 mas	12.900 mas
5	$e \sin \pi$	-0.187	21.417 mas	8.384 mas
6	l	-2.435	13.299 mas	4.870 mas

Table 2: Lagrangian elements.

Skripnichnko, 2014) has been used for implementation of all mathematical procedures of process for constructing Pluto orbit. The six elements of the orbit were derived from this solution. The observations from Table 2 cover only one third part of the Pluto orbit, therefore the standard deviations of the six elements are larger than for the same elements of other planets of the Solar system (Pitjeva & Pitjev, 2014). One of the results, the Lagrangian elements are computed with the EPM2014a for the epoch of 2446600.5 JD, are shown in Table 2. The standard deviations for the elements of the EPM2014a are better than for the EPM2013 (Pitjeva & Pitjev, 2014).

4. THE RESULT OF THE COMPARISON WITH MODERN EPHEMERIDES

Figure 2 illustrates positions differences between independent orbit estimates of EPM2014a ephemeris and EPM2011 and EPM2013 on the left side, as well as differences of orbit estimates for the A test ephemeris and DE430, and for the B test ephemeris and DE432 as a function of time on the right side.

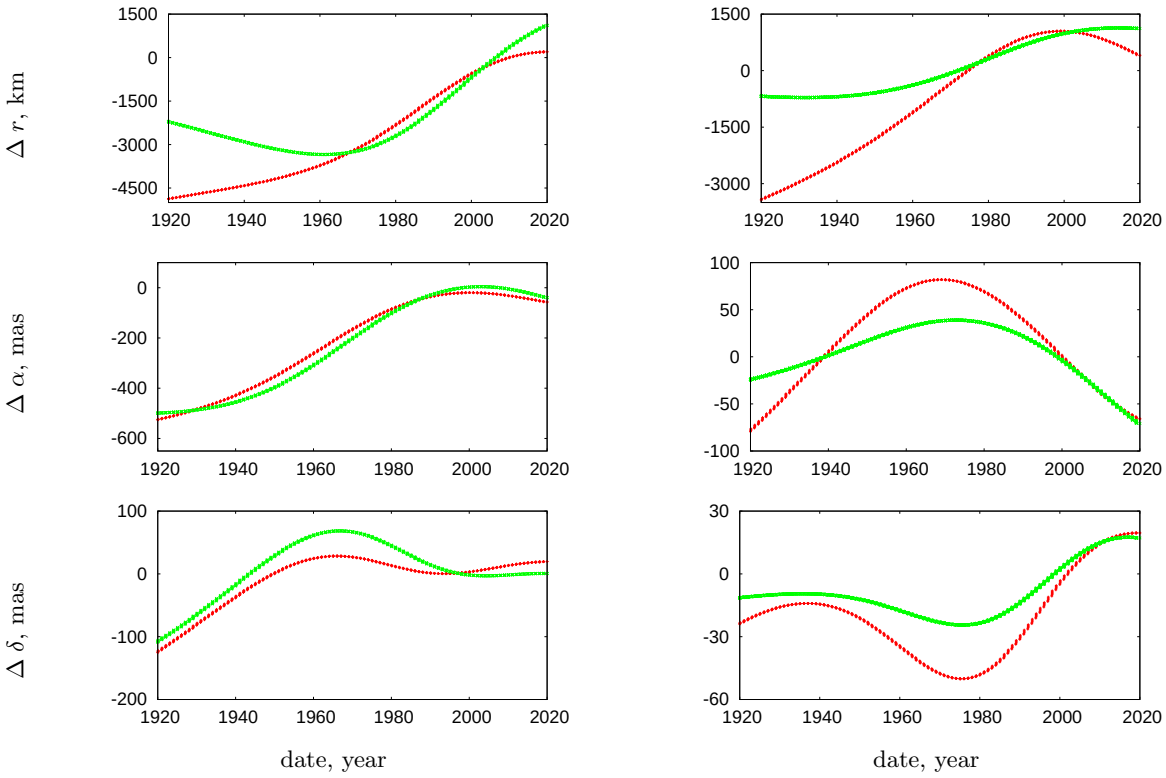

Figure 2: The upper panel is the heliocentric distance in kilometers, the middle panel is right ascension and the bottom — declination differences in milliarcseconds. The left side presents comparison of EPM2014a ephemerides to EPM2011 of red line and to EPM2013 of green line. The right side presents comparison of the A test ephemeris to DE430 of red line and the B test ephemeris to DE432 of green line.

The calculation of differences between equatorial coordinates and radius vectors is a suitable procedure for comparison of ephemerides. The comparison was carried out for several different ephemerides discussed below. At first, the EPM2014a ephemeris was taken, where the full set of Pluto available observations was used. Two test ephemerides were also constructed. The test ephemeris A used for fitting the same set Pluto observations as DE430 including Pulkovo photographic observations and data from the following observatories: the TMO, the PDO, the USNO/Flagstaff. The test ephemeris B used for fitting the same set Pluto observations as DE432, i.e. in addition to observations for the test ephemeris A, the Lowell observations were added.

And finally, the comparison of ephemeris the EPM2014a with modern ephemerides INPOP13c (Fienga et al., 2014) and DE432 is represented in Fig. 3. There are a lot of reasons for existing difference, for example, different data arrays and their weight data, the process of improvement and estimated parameters.

5. CONCLUSION

The data array observations were expanded with the new data up to about 10 thousand observations. The increasing accuracy ephemerides with the addition of new data was demonstrated, particularly, the improvement of ephemerides appears in residual observations. The EPM2014a corresponds to the modern ephemerides EPM2011, EPM2013, DE430, especially, is close to DE432.

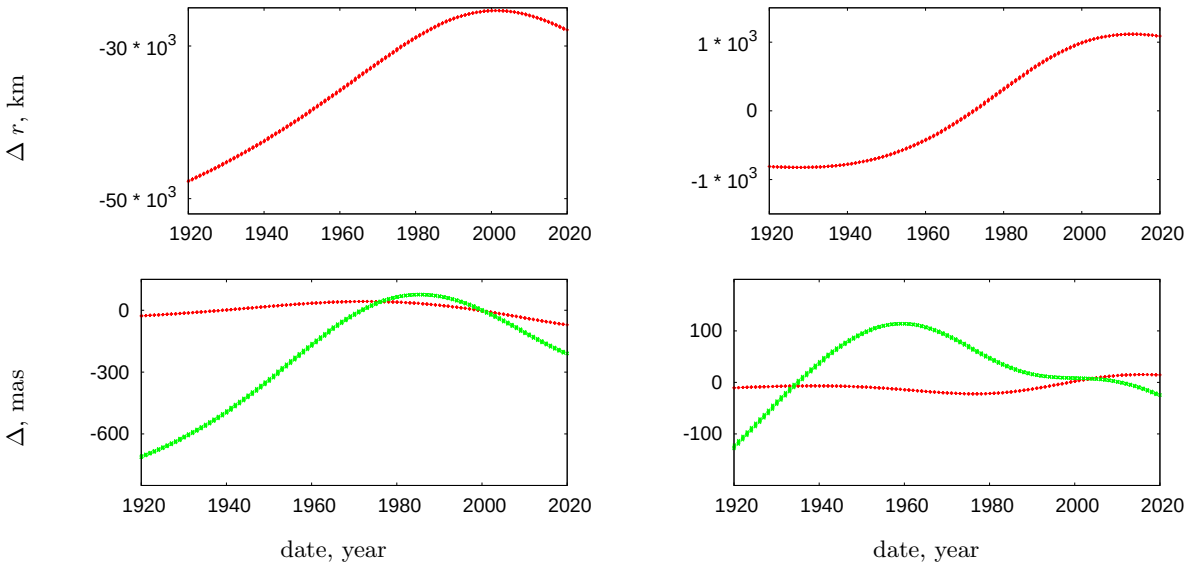

Figure 3: The upper panel is the heliocentric distance in kilometers for difference between EPM2014a and INPOP13c on the left side and DE432 on the right side, the bottom panel left to right is right ascension and declination differences in milliarcsecond and presents comparison of the EPM2014a to DE432 of red line and to INPOP13c of green line.

6. REFERENCES

Assafin, M., et al., 2010, "Precise predictions of stellar occultations by Pluto, Charon, Nix, and Hydra for 2008–2015", A&A, 515, A32.

Benedetti-Rossi, G., Vieira Martins, R., Camargo, J., Assafin, M., Braga-Ribas, F., 2014, "Pluto: improved astrometry from 19 years of observations", A&A, 570, A86.

Buie, M., Folkner, W., 2015, "Astrometry of Pluto from 1930–1951 Observations: the Lampland Plate Collection", AJ, 149(1), 22.

Fienga, A., Manche, H., Laskar, J., Gastineau, M., Verma, A., 2014, "INPOP new release: INPOP13c".

Folkner, W., 2014, "Planetary ephemeris DE432", JPL Interoffice Memorandum, 392R-14-003.

Folkner, W., et al., 2014, JPL Interplanetary Network Progress Report 42–196.

Khrutskaya, E., De Cuyper, J.-P., Kalinin, S., Berezhnoy, A., de Decker, G., 2013, "Positions of Pluto extracted from digitized Pulkovo photographic plates taken in 1930–1960", arXiv:1310.7502.

Krasinsky, G., Pitjeva, E., Sveshnikov, M., Chunajeva, L., 1993, "The motion of major planets from observations 1769–1988 and some astronomical constants", Celest. Mech. Dyn. Astr., 55, pp. 1–23.

Krasinsky, G., Vasyliev, M., 1997, "ERA: knowledge base for ephemeris and dynamic astronomy", IAU Coll. 165, pp. 239-244

Pavlov, D.A., Skripnichenko, V.I., 2014, "Preliminary results in implementation of a cross-platform version of the ERA software system", IAA Transactions, No. 30, pp. 32–40. (in Russian)

Pitjeva, E., Pitjev, N., 2014, "Development of planetary ephemerides EPM and their applications", Celest. Mech. Dyn. Astr., 119, pp. 237–256.

Rylkov, V., Vityazev, V., Dementieva, A., 1995, "Pluto: An analysis of photographic positions obtained with the Pulkovo normal astrograph in 1930–1992", Astron. Astrophys. Trans., 6, pp. 265–281.

Tombaugh, C., 1946, "The Search for the Ninth Planet, Pluto", Leaflet of the Astronomical Society of the Pacific, 5, pp. 73–80.

PHOBOS MASS ESTIMATIONS FROM MEX AND VIKING 1 DATA: INFLUENCE OF DIFFERENT NOISE SOURCES AND ESTIMATION STRATEGIES

M.V. KUDRYASHOVA[1,2], P. ROSENBLATT[1], J.-C. MARTY[3]
[1] Royal Observatory of Belgium
3, av. Circulaire, 1180 Brussels, Belgium
[2] IMCCE/Paris Observatory
77, av. Denfert Rochereau, 75014 Paris, France
[3] CNES/GRGS
18 avenue Edouard Belin, 31401 Toulouse Cedex 9, France
e-mail: mkudryashova@imcce.fr, rosenb@oma.be, Jean-Charles.Marty@cnes.fr

ABSTRACT. The mass of Phobos is an important parameter which, together with second-order gravity field coefficients and libration amplitude, constrains internal structure and nature of the moon. And thus, it needs to be known with high precision. Nevertheless, Phobos mass (GM, more precisely) estimated by different authors based on diverse data-sets and methods, varies by more than their 1-sigma error. The most complete lists of GM values are presented in the works of R. Jacobson (2010) and M. Paetzold et al. (2014) and include the estimations in the interval from $(5.39 \pm 0.03) \cdot 10^5$ (Smith et al., 1995) till $(8.5 \pm 0.7) \cdot 10^5 [\mathrm{m}^3/\mathrm{s}^2]$ (Williams et al., 1988). Furthermore, even the comparison of the estimations coming from the same estimation procedure applied to the consecutive flybys of the same spacecraft (s/c) shows big variations in GMs. The indicated behavior is very pronounced in the GM estimations stemming from the Viking1 flybys in February 1977 (as well as from MEX flybys, though in a smaller amplitude) and in this work we made an attempt to figure out its roots. The errors of Phobos GM estimations depend on the precision of the model (e.g. accuracy of Phobos a priori ephemeris and its a priori GM value) as well as on the radio-tracking measurements quality (noise, coverage, flyby distance). In the present work we are testing the impact of mentioned above error sources by means of simulations. We also consider the effect of the uncertainties in a priori Phobos positions on the GM estimations from real observations. Apparently, the strategy (i.e. splitting real observations in data-arcs, whether they stem from the close approaches of Phobos by spacecraft or from analysis of the s/c orbit evolution around Mars) of the estimations has an impact on the Phobos GM estimation.

1. ANALYSIS OF REAL RADIOSCIENCE DATA

In February 1977 orbiter Viking1 performed several consecutive close encounters (or, flybys) of Phobos. Radio-tracking measurements acquired during those flybys are used here for Phobos GM estimations. Those measurements were originally collected by E. Christensen at JPL and split into data-arcs by G. Balmino at Centre National des Etudes Spatiales (CNES) in such a way that they do not contain any maneuvers inside. Since four out of five data-arcs of G. Balmino contained two flybys and this could affect GM_{PH} estimations, we split them further so that the new arcs have duration 24 hours and contain only one flyby.

In case of Mars Express (MEX), we use the radioscience data acquired during the flybys of Phobos performed by MEX in 2006, 2008 and 2010. The duration of data arcs is about 1.5-2 days depending on the maneuvers performed by the s/c. This means that we try to choose a data-arc which either does not contain any maneuvers or at least does not start/finish with a maneuver.

All the Viking1 and MEX flybys have been processed using the GINS (Géodésie par Intégration Numériques Simultanées) software (Rosenblatt et al., 2008).

The only test done with the real observation is the evaluation of the impact of the a priori Phobos ephemerides error on the GM_{PH}. For this purpose we took ephemerides published by Lainey et al. (2007) and by R. Jacobson (2010) and which differ by about ± 0.5 km at the time interval under consideration (see Fig. 1). Thus, the estimation of GM_{PH} with different a priori ephemerides (under the condition that all the other models/parameters are the same) is equivalent to introduction of upto $\|0.5\|$ km error

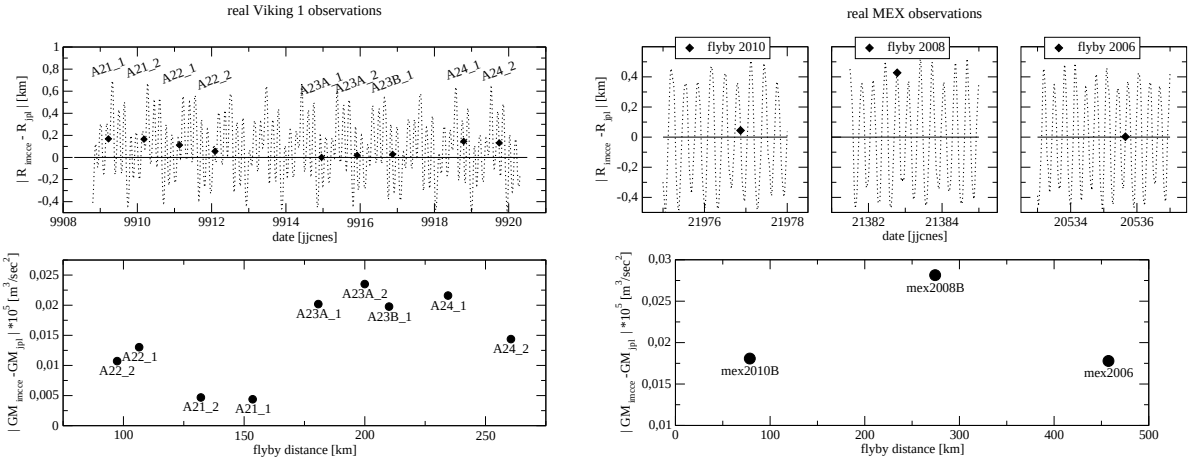

Figure 1: Difference in GM estimations due to the errors in a priori Phobos positioning: a) Viking real radioscience observations; b) the same for MEX. The lower panel represents the absolute value of the differences in the GM estimations, obtained with different a priori ephemerides: $\Delta GM^{JPL}_{IMCCE} = |GM_{IMCCE} - GM_{JPL}|$ versus flyby distance. The upper panels depict the differences in the Mars-Phobos distances given by the above mentioned ephemerides for each flyby. The difference between two ephemerides at the moment of flyby is represented by the diamonds.

into a priori ephemeris. Estimated parameters for both s/c are: initial state vector, Phobos GM and radiation pressure coefficients. Additionally, in case of MEX, we estimated also atmospheric drag, doppler frequency offset, range bias as well as thruster parameters.

In case of Mars Express there is a clear dependence between Phobos GM estimations and a priori ephemerides used: the bigger are the difference in a priori ephemerides (which reaches 0,5 km for the flyby of the year 2008) the bigger are the difference in GM estimations (see Fig. 1). While Viking 1 data doesn't show such kind of dependency.

2. ANALYSIS OF SIMULATED DATA

We used simulations in order to clearly distinguish the impact of each factor on the radioscience observables. Furthermore, in order to avoid any additional source of errors, we simplified our dynamical

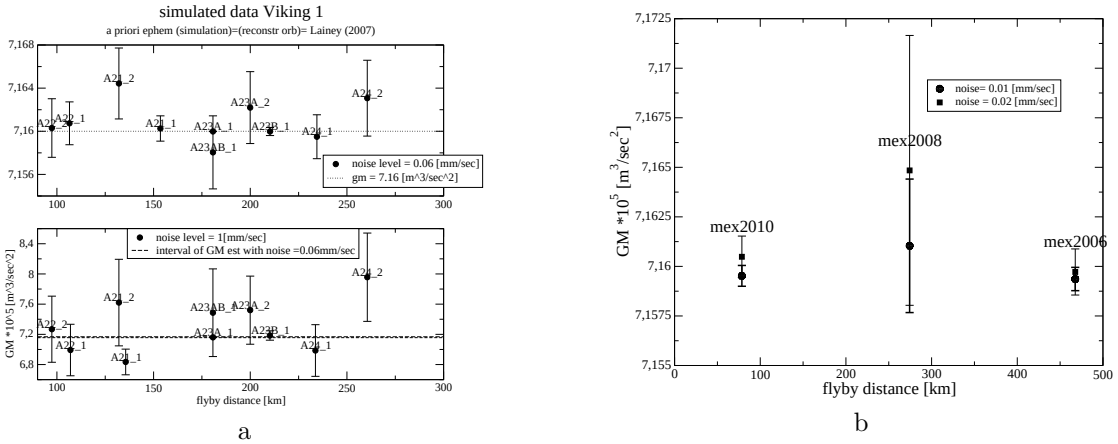

Figure 2: Comparison of GM estimations under different observational noise level. a) Simulated Viking 1 data: upper panel shows GM_{PH} obtained with noise level 0.06 mm/s. The lower panel – the same values obtained under 1 mm/s noise level. The scale on both graphs is essentially different. Thus, the grey dashed line on the latter graph presents the area shown on the upper plot. b) MEX simulated data (noise levels are $\sigma_1^{MEX} = 2 \cdot 10^{-5}$ and $\sigma_2^{MEX} = 1 \cdot 10^{-5}$ m/s).

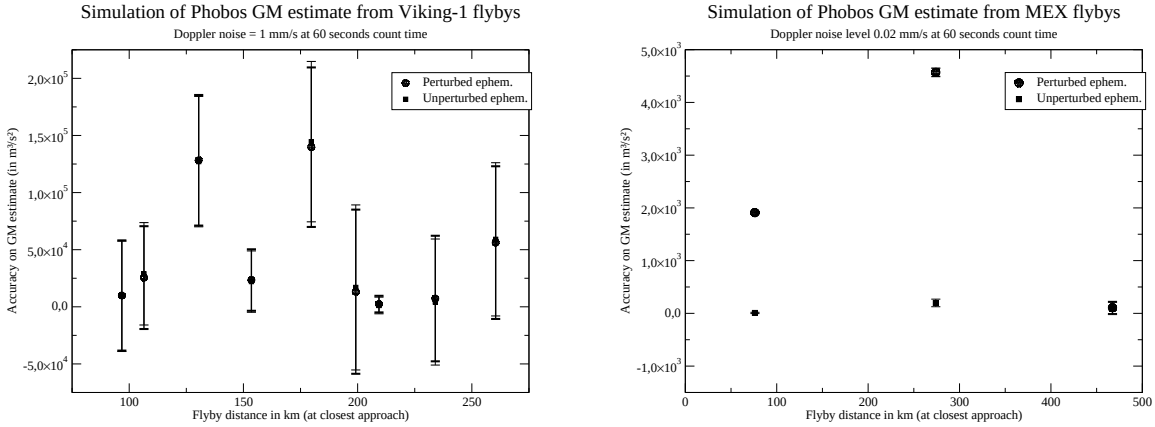

a b

Figure 3: Sensitivity of the GM_{PH} w.r.t. a priori Phobos position (simulated data): left panel – Viking1; right panel – MEX. Squares depict deviation of GM estimations from a nominal GM value ($GM_{nominal} = 7.16 \cdot 10^5 m^3/s^2$) when the orbit have been reconstructed with perturbed Phobos ephemerides; in circles – unperturbed.

model: the radiation pressure (as well as atmospheric drag for MEX) has been fixed to its model value in all our simulations; no maneuver-like accelerations have been introduced neither for the same reason. Therefore, there is no need to estimate these parameters during the subsequent procedure of fitting the model to the simulated observations. Below we present the tests, carried out in this work.

TEST 1: sensitivity of the Phobos GM estimations to the observational/modelling noise

We used several noise levels to simulate MEX/Viking 1 observations and then to reconstruct its orbits. We restore the orbit with the *same* noise level and Phobos ephemeris (IMCCE) as simulations was done. Both, for Viking 1 and MEX simulated observations cover the same time intervals as real data-arcs. For both satellites we suppose that the noise is the only source of errors, and thus, during the subsequent orbit reconstruction process, we estimate only initial state vector and Phobos GM.

TEST 2: impact of errors in a priori Phobos ephemeris on the Phobos GM

Observations have been simulated with the IMCCE a priori Phobos ephemeris and typical X-band/S-band noise level for MEX/Viking1 correspondingly. While the reconstruction of the orbits have been done by using perturbed IMCCE ephemeris (IMCCE Phobos ephemeris to which 1 km error have been added) and the same noise level. In this test, estimated parameters are GM_{PH} and spacecraft initial state vector.

TEST 3: sensitivity of the estimated GM w.r.t. a priori GM value

The main idea of this test is to simulate Doppler observations with certain value of $GM_{PH} = 7.16 \cdot 10^5\,\mathrm{m}^3/\mathrm{s}^2$ and subsequently to reconstruct the orbit by fitting the model with a wrong value $GM = GM_{PH} \pm \Delta GM$. An erroneous value of one of the parameters of dynamical model should produce a certain signal in the post-fit residuals. Therefore, from the analysis of post-fit residuals one can estimate the response of simulated data to the introduced errors in Phobos GM. In this test the data have been simulated with $\sigma^{noise} = 0.0$. During the fitting process we estimate only initial state vector and fix Phobos GM to some deliberately wrong values: $\Delta GM_1^{PH} = 0.5 \cdot 10^5\,\mathrm{m}^3/\mathrm{s}^2$ (i.e. $GM_1^{PH} = 7.66 \cdot 10^5$) and $\Delta GM_2^{PH} = 10^5\,\mathrm{m}^3/\mathrm{s}^2$ (i.e. $GM_2^{PH} = 8.16 \cdot 10^5$).

3. CONCLUSIONS

Accuracy and precision of GM estimations increase with decreasing of the value of the noise for both spacecraft (see Fig. 2).

VIKING1: *observational noise dominates all other considered sources of errors;*

- both simulated and real data show that observational noise prevails inaccuracies in Phobos a priori positions during GM estimation process (see Fig. 1 (a) and Fig. 3 (a), correspondingly);

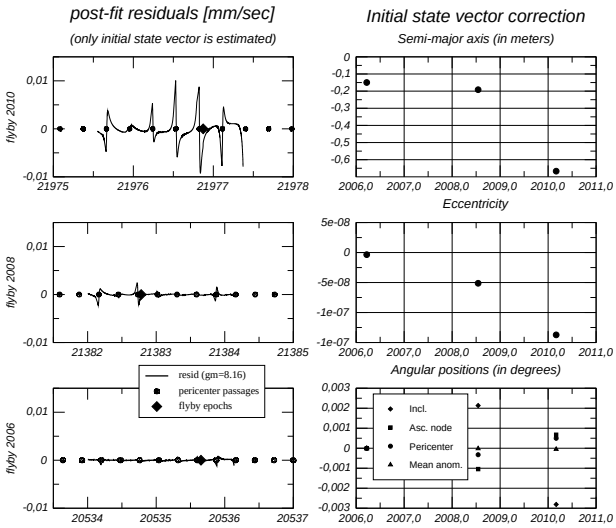

Figure 4: The post-fit doppler residuals after the s/c orbit reconstruction from simulated MEX data. Left-hand panels: Phobos GM in legend is given in $10^5 \mathrm{m}^3/\mathrm{s}^2$ units. Solid line represents post-fit residuals; circles – epochs of pericenter passages by s/c; and in diamonds – the epoch of flyby. Right-hand panels: corrections to the initial state vector.

- the post-fit Doppler residuals are not very sensitive to the errors in GM_{PH}: changes of the spacecraft velocities due to $\Delta GM_{PH} = 10^5[\mathrm{m}^3/\mathrm{s}^2]$ are at the level of 0.06 mm/s which corresponds to the most optimistic estimation of the observational noise level in case of Viking 1.

MEX: *the uncertainties in Phobos a priori position dominate other sources of errors.*

- there is a clear dependence between Phobos GM estimations and a priori ephemerides used (see Fig. 1 (b) and Fig. 3 (b), correspondingly): the bigger the difference in a priori ephemerides (which reaches 0,5 km for the flyby of the year 2008) the bigger the difference in GM estimations;

- Changes of the spacecraft velocities due to $\Delta GM_{PH} = 10^5[\mathrm{m}^3/\mathrm{s}^2]$ could be observed: they are between 0.02 mm/s (flyby in the year 2006 at the distance about 467 km) and 0.2 mm/s (flyby of the year 2010 at the distance about 78 km) while the typical noise level of MEX observations is about 0.02 mm/s (Fig. 4).

Acknowledgements. This work is a part of the European Satellite Partnership Computing Ephemerides (ESPaCE), funded by the European FP7-project.

4. REFERENCES

Jacobson, R.A., 2010, "The orbits and masses of the martian satellites and the libration of Phobos", AJ, 139, pp. 668–679.

Lainey, V., Dehant, V., Pätzold, M., 2007, "First numerical ephemerides of the Martian moons", A&A, 465, pp. 1075–1084.

Pätzold, M., Andert, T., Jacobson, R., Rosenblatt, P., Dehant, V., 2014, "Phobos: Observed bulk properties", Planetary and Space Science, 102, pp. 86–94.

Rosenblatt, P., Lainey, V., Le Maistre, S., Marty, J.C., Dehant, V., Pätzold, M., van Hoolst, T., Häusler, B., 2008, "Accurate Mars Express orbits to improve the determination of the mass and ephemeris of the Martian moons", Planetary and Space Science, 56, pp. 1043–1053.

Smith, D.E., Lemoine, F.G., Zuber, M.T., 1995, "Simultaneous estimation of the masses of Mars, Phobos, and Deimos using spacecraft distant encounters", Geophys. Res. Lett., 22, pp. 2171–2174.

Williams, B.G., Duxbury, T.C., Hildebrand, C.E., 1988, "Improved determination of Phobos and Deimos masses from Viking Fly-Bys", In: Abstracts of the Lunar and Planetary Science Conference, 19, p. 1274.

EXPANSION OF THE HAMILTONIAN OF A PLANETARY SYSTEM INTO THE POISSON SERIES IN ALL ORBITAL ELEMENTS

A.S. PERMINOV, E.D. KUZNETSOV
Ural Federal University
Ekaterinburg, Russia
e-mail: perminov12@yandex.ru; eduard.kuznetsov@urfu.ru

ABSTRACT. The study of planetary systems orbital evolution is one of important problems of celestial mechanics. This work is the first stage in our investigation of this problem. We present algorithm for constructing of a planetary system Hamiltonian expansion into the Poisson series in all orbital elements. The expansion was constructed for a planetary systems with 4 planets. So, we can study orbital evolution of giant-planets of the Solar System and many extrasolar systems also. Estimation accuracy of Hamiltonian expansion is presented in this work.

1. INTRODUCTION

Let us consider planetary system with 4 planets. We need to write its Hamiltonian. For our purpose we can use canonical Jacobi coordinates (Murray, Dermott, 2009). It is hierarchical coordinate system, which is more preferable for investigation of planetary system orbital evolution. A position of each following body is determined relative to a center of inertia of previously including bodies set. We need to know differences of radius vectors in inertial frame. This frame can be barycentric for example. Differences are determined here:

$$|\boldsymbol{\rho}_i - \boldsymbol{\rho}_j| = \mathbf{r}_i - \mathbf{r}_j + \mu \sum_{k=j}^{i-1} \frac{m_k}{\bar{m}_k} \mathbf{r}_k, \tag{1}$$

where numbers i and j satisfy a condition $1 \leq j < i \leq N$; $\boldsymbol{\rho}_k$ is barycentric radius vector of k-th planet, $\mathbf{r}_k$ is Jacobi radius vector of the same planet; μm_k is mass of the planet in items of Sun mass, $\bar{m}_k = 1 + \mu m_1 + \ldots + \mu m_k$, μ is small parameter. Variable μ denotes ratio of sum of planets masses to mass of the Sun. For the Solar system the value of μ can take equal to 0.001.

The Hamiltonian h can be expressed as sum of two terms – undisturbed part and disturbing function (Kholshevnikov et al., 2001), as shown here:

$$h = -\sum_{i=1}^{N} \frac{M_i \kappa_i^2}{2a_i} + \mu \times \frac{Gm_0}{a_0} \Big\{ \sum_{i=2}^{N} \frac{a_0 m_i (2\mathbf{r}_i \mathbf{R}_i + \mu R_i^2)}{r_i \tilde{R}_i (r_i + \tilde{R}_i)} - \sum_{i=1}^{N} \sum_{j=1}^{i-1} \frac{a_0 m_i m_j}{|\boldsymbol{\rho}_i - \boldsymbol{\rho}_j|} \Big\}, \tag{2}$$

where G is gravitational constant, a_0 is any constant of length typical for a planetary system (for example 1 astronomical unit), m_0 is mass of the Sun, M_i is normalized mass, κ_i^2 is gravitational parameter, a_i is semi-major axis; N is number of planets; other quantities are defined below:

$$\mathbf{R}_i = \sum_{k=1}^{i} \frac{m_k}{\bar{m}_k} \mathbf{r}_k, \quad \tilde{R}_i = \sqrt{r_i^2 + 2\mu \mathbf{r}_i \mathbf{R}_i + \mu^2 R_i^2}. \tag{3}$$

The first sum in (2) is undisturbed part of the Hamiltonian. The expression in figure brackets is the disturbing function. Introducing the value of a_0 into account, the disturbing function becomes dimensionless. Double sum in (2) is major part of the disturbing function. The major part describes interaction between planets. Denominator of the major part is defined in expression (1).

We used the second system of Poincare elements for constructing of the Hamiltonian expansion. It allows sufficiently simplifying an angular part of the series expansion. In this case only one angular element – mean longitude is defined.

After that, we get the Hamiltonian of a planetary system in this form:

$$h = h_0 + \sum_{k,n} A_{kn} x^k \cos(ny), \tag{4}$$

where h_0 is undisturbed Hamiltonian, A_{kn} is numerical coefficient, x^k is product of Poincare elements with corresponding degrees, cosine is represent an angular part of the series, ny is linear combination of mean longitudes of planets.

2. AGORITHM

Computer algebra system Piranha is used for expansion of the Hamiltonian. This program was written by Francesco Biscani (Biscani, 2009). Piranha is new specialized system for analytical calculations in celestial mechanics. It is multi-platform C++ program with Python's interface. At this moment Piranha is one of the fastest computer algebra systems. Piranha have various convenient implements for working with series. It allows set limit degree of series truncation, filtering of series items, substitution into series, saving to text files and others. Piranha works with different series types. In particular, supported series types are polynomials with rational numerical coefficients and Poisson series with polynomial coefficients.

Lets consider algorithm of constructing of the Hamiltonian expansion into the Poisson series:

- to be necessary make classical celestial mechanics series, such as x/a, y/a, y/a and r/a, a/r, which are base elements for the Hamiltonian expansion. We need to transform expressions for these expansions from Kepler elements (eccentricity and mean anomaly) to Poincare elements. We can use standart algorithms for it (Sharlier, 1966). Classical expansions in Kepler elements can be obtained using the Kepler processor implemented in Piranha;

- next, using x/a, y/a, z/a series it is possible to take the expansion of scalar product. Series for r_i/r_j ratio is obtained from expansions of r_i/a_i and a_j/r_j;

- inverse absolute value of radius vectors difference in Jacobi frame, which is denoted below as $1/\Delta_{ij}$, can be expanded into a series as follows. Write the definition of $1/\Delta_{ij}$:

$$1/\Delta_{ij} = |\mathbf{r}_i - \mathbf{r}_j|^{-1} = \frac{1}{r_j}\Big(1 + \Big(\frac{r_i}{r_j}\Big)^2 - 2\Big(\frac{r_i}{r_j}\Big)\cos H\Big)^{-\frac{1}{2}} = \frac{1}{r_j}\sum_{n=0}^{\infty}\Big(\frac{r_i}{r_j}\Big)^n P_n(\cos H), \qquad (5)$$

  where P_n is Legendre polynomial of n-th degree, H is angle between vectors $\mathbf{r}_i$ and $\mathbf{r}_j$. In (5) you can see the generating function of Legendre polynomials. So, we can expand $1/\Delta_{ij}$ into Poisson series, using series for $1/r_j$ and r_i/r_j. The series in Legendre polynomials absolutely converges when $|r_i/r_j| < 1$. In our case Legendre polynomials have not inner structure and saved in series as symbol variables. It allows reducing of number of expansion terms, necessary working memory and disk space;

- after that, we can take expansion of the Hamiltonian. Common form of items of the major part expansion up to the second degree of small parameter is shown here:

$$\frac{1}{|\boldsymbol{\rho}_i - \boldsymbol{\rho}_j|} = \frac{1}{\Delta_{ij}}\Big(1 - \frac{2\mu A_{ij} + \mu^2 B_{ij}}{\Delta_{ij}^2}\Big)^{-\frac{1}{2}} = \frac{1}{\Delta_{ij}} - \mu\frac{A_{ij}}{\Delta_{ij}^3} + \mu^2\Big(-\frac{B_{ij}}{\Delta_{ij}^3} + \frac{3}{4}\frac{A_{ij}^2}{\Delta_{ij}^5}\Big) + \ldots, \qquad (6)$$

  and here for items of the second part of the disturbing function:

$$\begin{aligned}\frac{2\mathbf{r}_i\mathbf{R}_i + \mu\mathbf{R}_i^2}{r_i\tilde{R}_i(r_i + \tilde{R}_i)} &= \frac{C_i + \mu D_i}{r_i^3\sqrt{1 + \frac{\mu C_i + \mu^2 D_i}{r_i^2}}\Big(1 + \sqrt{1 + \frac{\mu C_i + \mu^2 D_i}{r_i^2}}\Big)} = \\ &= \frac{C_i}{r_i^3} + \mu\Big(-\frac{3}{2}\frac{C_i^2}{r_i^5} + \frac{1}{2}\frac{D_i}{r_i^3}\Big) + \mu^2\Big(\frac{5}{2}\frac{C_i^3}{r_i^7} - \frac{3}{2}\frac{C_i D_i}{r_i^5}\Big) + \ldots,\end{aligned} \qquad (7)$$

$$A_{ij} = (\mathbf{r}_i - \mathbf{r}_j)\sum_{k=j}^{i-1}\frac{m_k}{\bar{m}_k}\mathbf{r}_k,\ B_{ij} = \Big(\sum_{k=j}^{i-1}\frac{m_k}{\bar{m}_k}\mathbf{r}_k\Big)^2,\ C_i = \mathbf{r}_i\sum_{k=1}^{i-1}\frac{m_k}{\bar{m}_k}\mathbf{r}_k,\ D_i = B_{i1}, \qquad (8)$$

  $1 \le j < i \le N$ in (6) and $2 \le i \le N$ in (7). In our case $N = 4$. So, using series for inverse distances, scalar products and quantities of $1/\Delta_{ij}$ with various degrees, we can construct items of the Hamiltonian expansion. Such quantities as small parameter μ and masses ratio $m_k/\bar{m}_k$ are used as symbol variables in series constructing.

3. RESULTS

Calculations were performed on Quad-core PC with 2600 MHz Core i5 processor and 8 Gb available memory. Computer algebra system Piranha using on Unix-like OS Ubuntu 14. Algorithms for series calculations was written as Python-modules of Piranha.

In the process, Piranha showed a high speed of calculations. Table 1 presents a time of series calculation, a number of its items and estimation accuracy for base series. Parameter n in the first column is a limit of degrees of eccentric and oblique Poincare elements. Results in the last column are correspond to series for $1/\Delta_{ij}$ with maximum degree of Legendre polynomials is equal to 35.

n	series	x/a	y/a	z/a	r/a	a/r	r_i/r_j	$\mathbf{r}_i.\mathbf{r}_j$	$1/\Delta_{ij}$
6	time	0.5^s	0.5^s	0.5^s	0.5^s	0.5^s	0.5^s	1^s	40^s
	items	146	146	216	66	61	847	6282	32628
	accuracy	10^{-8}	10^{-8}	10^{-8}	10^{-9}	10^{-9}	10^{-8}	10^{-7}	$10^{-12} - 10^{-8}$
11	time	12^s	12^s	12^s	19^s	19^s	1^s	56^s	12^m44^s
	items	792	792	2128	303	298	13548	228629	515291
	accuracy	10^{-14}	10^{-14}	10^{-14}	10^{-15}	10^{-15}	10^{-13}	10^{-12}	$10^{-13} - 10^{-9}$

Table 1: Calculation time, number of terms and estimation accuracy for base series.

The value of n is determined by required accuracy of expansion of the disturbing function. Rows which are named 'accuracy' consist relative differences between series expansion and accurate formula. In this work estimation accuracy of base series is determined for the Solar System giant-planets. Indexed values were calculated for all planetary pairs of Solar System. A wide range of values in some cells is obtained various estimations accuracy for planets pairs. The value of $1/\Delta_{ij}$ for the planetary pair "Uranus–Neptune" has the lowest accuracy. The best accuracy gives the planetary pair "Jupiter–Neptune".

The Hamiltonian expansion was constructed to 1 degree of small parameter. Maximum considered degree of eccentric and oblique Poincare elements is 6. Legendre polynomials are considered up to 35 degree.

Precision of the Hamiltonian approximation was calculated for the Solar system and 47 UMa, HD 69830 extrasolar systems also. Kepler elements for the Solar System are taken w.r.t. epoch J2000.0 and correspond to mean ecliptic. Orbital elements, such as semi-major axes, eccentricities and perigee arguments, and planets masses of above extrasolar systems are taken from http://www.exoplanet.eu. Planetary system of star HD 69830 is interesting in that it is compact with orbits eccentricities of the order of 0.1. Estimation accuracy of the series approximation is presented in the Table 2 for all items of the disturbing function. Columns which are named 'accuracy' consist relative differences (absolute values) between series expansion and accurate formula.

	Solar System		47 UMa star system		HD 69830 star system	
	series expansion	accuracy	series expansion	accuracy	series expansion	accuracy
i,j	the major part		the major part		the major part	
1,2	$6.247 \cdot 10^{-2}$	$2 \cdot 10^{-5}$	0.26590	$4 \cdot 10^{-5}$	$1.271 \cdot 10^{-2}$	$1 \cdot 10^{-5}$
1,3	$2.12 \cdot 10^{-3}$	$1 \cdot 10^{-5}$	0.31009	$5 \cdot 10^{-5}$	$5.9438 \cdot 10^{-3}$	$5 \cdot 10^{-7}$
1,4	$1.599 \cdot 10^{-3}$	$2 \cdot 10^{-6}$	–	–	–	–
2,3	$5.72 \cdot 10^{-4}$	$7 \cdot 10^{-6}$	0.08499	$2 \cdot 10^{-5}$	$4.10297 \cdot 10^{-3}$	$4 \cdot 10^{-8}$
2,4	$4.43 \cdot 10^{-4}$	$1 \cdot 10^{-6}$	–	–	–	–
3,4	$1.95 \cdot 10^{-4}$	$1 \cdot 10^{-6}$	–	–	–	–
i	the second part		the second part		the second part	
2	$1.58379 \cdot 10^{-2}$	$4 \cdot 10^{-7}$	0.04968	$7 \cdot 10^{-5}$	$3.01 \cdot 10^{-3}$	$2 \cdot 10^{-5}$
3	$9.5 \cdot 10^{-5}$	$5 \cdot 10^{-6}$	0.02549	$1 \cdot 10^{-5}$	$1.6471 \cdot 10^{-3}$	$7 \cdot 10^{-7}$
4	$7 \cdot 10^{-6}$	$5 \cdot 10^{-6}$	–	–	–	–
	whole disturbing function		whole disturbing function		whole disturbing function	
Σ	$8.526 \cdot 10^{-2}$	$2 \cdot 10^{-5}$	0.63676	$5 \cdot 10^{-5}$	$2.741 \cdot 10^{-2}$	$3 \cdot 10^{-5}$

Table 2: Precision of estimation of the disturbing function.

Table 2 shows that estimation accuracy of the disturbing function expansion is about 10^{-5} for the Solar System and different extrasolar systems. According to expression (2) the disturbing function must be multiplied by small parameter μ. After that, we can get estimation accuracy of the Hamiltonian expansion into series. It is about 10^{-8}.

4. CONCLUSION

We described algorithm for constructing of the Hamiltonian expansion of a planetary system with 4 planets into the Poisson series in all elements. The expansion was made to 6 degree of orbital elements and to 1 degree of small parameter. Estimation accuracy of the disturbing function is presented in this paper. Relative difference between series estimation and accurate formula is about 10^{-5} for the Solar System and extrasolar systems. So, the Poisson series for the Hamiltonian was constructed with precision about 10^{-8}. Now we are constructing the expansion for the Hamiltonian to 11 degree of orbital elements and 2 degree of small parameter.

5. REFERENCES

Biscani, F., 2009, "The Piranha algebraic manipulator", arXiv:0907.2076v1.

Kholshevnikov, K.V., Greb, A.V., Kuznetsov, E.D., 2001, "The expansion of the Hamiltonian of the planetary problem into the Poisson series in all Keplerian elements (theory)", Solar System Research, 35(3), pp. 243–248.

Murray, C.D., Dermott, S.F., 2009, "Solar System dynamics", Cambridge University Press.

Sharlier, K., 1966, "Nebesnaya mekhanika (Celestial Mechanics)", Moscow: Nauka. (in Russian)

LONG TIME DYNAMICAL EVOLUTION OF HIGHLY ELLIPTICAL SATELLITES ORBITS

E.D. KUZNETSOV, P.E. ZAKHAROVA
Ural Federal University
Ekaterinburg, Russia
e-mail: eduard.kuznetsov@urfu.ru

ABSTRACT. Dynamical evolution of objects near Molniya-type orbits is considered. Initial conditions correspond to highly elliptical satellite orbits with eccentricities 0.65 and a critical inclination 63.4°. Semi-major axis is varied near resonant value 26560 km in an interval 500 km. Variations were analyzed for positional orbital elements, an ascending node longitude and an argument of pericenter. Initial conditions determined when orbital elements variations are minimal. These regions can be used as orbits for safe stationing satellites which finish work on Molniya-type orbits. The study of dynamical evolution on long time intervals was performed on the basis of the results of numerical simulation. The model of disturbing forces taken into account the main perturbing factors. Time interval was up to 24 yr. Area-to-mass ratio varied from small values corresponding to satellites to big ones corresponding to space debris.

1. INTRODUCTION

Region of high-elliptical orbits (HEO) has a very complex dynamics. Both active and passive objects are moved on HEO. There is a problem of protecting active satellites from space debris. It requires high-accuracy propagation of HEO objects motion. These objects have a long-term evolution of eccentricities and inclinations due to the Lidov–Kozai resonance (Lidov, 1962; Kozai, 1962). There are secular perturbations of semi-major axes due to the atmospheric drag. The Poynting–Robertson effect also leads to secular perturbations of semi-major axes for objects with area-to-mass ratio (AMR) more than 1 m^2/kg (Kuznetsov et al., 2012). The dynamical evolution of high AMR objects in the Molniya-type orbits was studied by (Sun et al., 2013). In this paper, a vicinity of Molniya orbit is considered. A stochastic trajectory formation due to objects passage through high-order resonance zones was considered.

We present both analytical and a numerical results for locations and sizes of high-order resonance regions in the vicinity of Molniya-type orbits. Secular perturbations of the semi-major axes of the orbits are estimated in the vicinity of the resonance zones. A long-time orbital evolution is investigated for HEO orbits and orbits surrounding these regions. AMR values are variable. Capture and escape from resonance, as well as a passage through resonance, is considered to be an orbital evolution.

2. ANALYTICAL APPROXIMATION

The frequencies of the perturbations caused by the effect of sectoral and tesseral harmonics of the Earth's gravitational potential are a linear combinations of the mean motion of a satellite n_M, angular velocities of pericenter motion n_g and node motion n_Ω of it's orbit, and angular velocity of the Earth ω.

Following Allan (1967a, 1967b), we form the frequencies

$$\nu_1 = p(n_M + n_\Omega + n_g) - q\omega, \qquad \nu_2 = p(n_M + n_g) + q(n_\Omega - \omega), \qquad \nu_3 = pn_M + q(n_g + n_\Omega - \omega) \quad (1)$$

of three critical arguments

$$\Phi_1 = p(M+\Omega+g) - q\omega t = \nu_1 t, \quad \Phi_2 = p(M+g) + q(\Omega - \omega t) = \nu_2 t, \quad \Phi_3 = pM + q(g+\Omega-\omega t) = \nu_3 t, \ (2)$$

where M is the mean anomaly, Ω is the longitude of the ascending node, g is the argument of the pericenter, and p, q are an integers.

The condition $\nu_1 \approx 0$ corresponds to the resonance p:q between the satellite's mean motion n_M and the Earth's angular velocity ω. This condition represents the n-resonance. The condition $\nu_2 \approx 0$ corresponds to an i-resonance under which the position of the ascending node of the orbit repeats periodically in a

rotating coordinate system. The condition $\nu_3 \approx 0$ corresponds to an e-resonance at which the position of the line of apsides is considered.

Analytical estimations were obtained for locations and sizes of resonance regions. Mean motions n_M, n_g, n_Ω were calculated taking into account the secular perturbations from the Earth's oblateness $\dot{\bar{M}}_{J_2}$, $\dot{\bar{g}}_{J_2}$, $\dot{\bar{\Omega}}_{J_2}$ (Beutler, 2005), the Moon's attraction $\dot{\bar{M}}_L$, $\dot{\bar{g}}_L$, $\dot{\bar{\Omega}}_L$, the Sun's attraction $\dot{\bar{M}}_S$, $\dot{\bar{g}}_S$, $\dot{\bar{\Omega}}_S$ (Timoshkova and Kholshevnikov, 1974).

$$n_M = \sqrt{\frac{\varkappa^2}{a^3}} + \dot{\bar{M}}_{J_2} + \dot{\bar{M}}_L + \dot{\bar{M}}_S, \qquad n_g = \dot{\bar{g}}_{J_2} + \dot{\bar{g}}_L + \dot{\bar{g}}_S, \qquad n_\Omega = \dot{\bar{\Omega}}_{J_2} + \dot{\bar{\Omega}}_L + \dot{\bar{\Omega}}_S. \tag{3}$$

Where $\varkappa^2$ is the Earth's gravitational parameter and a is a semi-major axis of an orbit,

$$\dot{\bar{\Omega}}_{J_2} = -\frac{3}{2} J_2 n \left(\frac{r_e}{a}\right)^2 \frac{\cos i}{(1-e^2)^2}, \qquad \dot{\bar{\Omega}}' = -\frac{3}{16} n \frac{m'}{m_\oplus} \left(\frac{a}{a'}\right)^3 \frac{2+3e^2}{(1-e^2)^{1/2}} (2 - 3\sin^2 i') \cos i,$$

$$\dot{\bar{g}}_{J_2} = \frac{3}{4} J_2 n \left(\frac{r_e}{a}\right)^2 \frac{5\cos^2 i - 1}{(1-e^2)^2}, \qquad \dot{\bar{g}}' = \frac{3}{16} n \frac{m'}{m_\oplus} \left(\frac{a}{a'}\right)^3 \frac{4 - 5\sin^2 i + e^2}{(1-e^2)^{1/2}} (2 - 3\sin^2 i'),$$

$$\dot{\bar{M}}_{J_2} = \frac{3}{4} J_2 n \left(\frac{r_e}{a}\right)^2 \frac{3\cos^2 i - 1}{(1-e^2)^{3/2}}, \qquad \dot{\bar{M}}' = \frac{1}{16} \frac{m'}{m_\oplus} \left(\frac{a}{a'}\right)^3 (8 + 15e^2)(2 - 3\sin^2 i')(2 - 3\sin^2 i).$$

Where J_2 is the second zonal harmonic coefficient, n is the two-body mean motion, r_e is the mean equatorial radius of the Earth, i and e are the inclination and eccentricity of satellite's orbit, $m_\oplus$ is the Earth's mass, m', a' and i' are the mass, semi-major axis and inclination of perturbing body orbit (the Moon or the Sun).

Expansions of perturbing functions coincide for outer body attraction and solar radiation pressure. These expansions are differed by notations and limits of summation only. We used expansion for solar attraction to take into account solar radiation perturbations. The Sun's mass was reduced on

$$\mu = -\frac{1}{f} b \gamma P_0 r_S^2. \tag{4}$$

Where μ is the Sun's mass reduction (Polyakhova and Timoshkova, 1984), f is the gravitational constant, b is the reflection coefficient of the satellite surface, γ is AMR, $P_0 = 4.56 \cdot 10^{-6}$ kg m^{-1} s^{-2} is the solar pressure, r_S is the distance from the Earth to the Sun.

We estimated values of the semi-major axis corresponding to the n-, i- and e-resonances from the conditions $\nu_1 = 0$, $\nu_2 = 0$, and the $\nu_3 = 0$ in the vicinity of Molniya-type orbits. Initial conditions corresponded to high-elliptical orbits with an eccentricity 0.65 and critical inclination 63.4°. Semi-major axis values varied from 26000 km to 27100 km. There were 17 high-order resonance relations p:q between mean motion of angular orbital elements and the Earth's angular velocity: $16 \leqslant |p| \leqslant 25$, $33 \leqslant |q| \leqslant 49$, orders of the resonances are $49 \leqslant |p| + |q| \leqslant 74$ in this region.

3. NUMERICAL SIMULATION

The study of orbital evolution on long time intervals was performed based on the results of numerical simulations conducted using "A Numerical Model of the Motion of Artificial Earth's Satellites" developed by the Research Institute of Applied Mathematics and Mechanics of the Tomsk State University (Bordovitsyna et al., 2007). The model of disturbing forces accounts the nonsphericity of the gravitational field of the Earth (model EGM96, harmonics up to the 27$^{\text{th}}$ order and degree inclusive), the attraction of the Moon and the Sun, the tides in the Earth's body, the direct radiation pressure, taking into account the shadow of the Earth (the reflection coefficient of the satellite surface $b = 1.44$), the Poynting–Robertson effect, and the atmospheric drag. The integration of motion equations was carried out using the Everhart's method of the 19$^{\text{th}}$ order.

Initial conditions as mentioned above correspond to high-elliptical orbits with an eccentricity $e_0 = 0.65$ and critical inclination $i_0 = 63.4°$. Initial semi-major axes a_0 values are consistent with a resonant conditions arisen from the analytical approximation. The initial value of the argument of the pericenter g_0 was 270°. The initial values of the longitude of the ascending node Ω_0 are 0°, 90°, 180°, and 270°.

This coincides with initial values of a solar angle $\varphi_0 = \Omega_0 + g_0 = 270°$, $0°$, $90°$, and $180°$. AMRs tried were equal to 0.02, 0.2, and 2 m^2/kg. Period of integration is 24 years.

4. DYNAMICAL EVOLUTION IN A REGION NEAR THE 22:45 RESONANCE

We present dynamical evolution using the example of the 22:45 resonance. Qualitative evolution for the rest 16 high-order resonances is the same.

Semi-major axis evolution depends on the solar angle weakly when AMR is 0.02 m^2/kg and it corresponds a satellite. The evolution of e, i, and g for Molniya-type orbits depend on the orientation of the orbital plane significantly. Maximal magnitudes of oscillations are reached when the initial solar angle $\varphi_0 = 0°$. The magnitudes of oscillations are minimal at $\varphi_0 = 180°$. The argument of the pericenter has a libration near the initial value of $g_0 = 270°$ due to the initial critical inclination $i_0 = 63.4°$.

Object has temporary captures into i- and e-resonance due to the long-term evolution of eccentricity and inclination of it's orbit. Libration of critical argument Φ corresponds to resonant motion. Object has capture into resonance and escape from resonance due to the long-term evolution of eccentricity and inclination of it's orbit when mean value of semi-major axis is saved almost constant. Secular perturbations of semi-major axis is approximately to -5 m/year due to the Pointing–Robertson effect.

When AMR is 2 m^2/kg, it corresponds a space debris. Increase of AMR leads to increase of magnitude of short-periodic perturbations. There are captures into n-resonance when mean value of semi-major axis is equal to resonant value one. After 12 years the mean value of the semi-major axis is became less the resonant value due to the Poynting–Robertson effect. Secular decrease in the semi-major axis, which, for a spherically symmetrical satellite with AMR = 2 m^2/kg near the 22:45 resonance region, equals approximately -0.5 km/year. Numerical simulation shows that this effect weakens slightly, in resonance regions. Under the Poynting–Robertson effect objects pass through the regions of high-order resonances.

5. STOCHASTIC TRAJECTORIES FORMATION

The Poynting–Robertson effect results in a secular decrease in the semi-major axis of a spherically symmetrical satellite (Smirnov et al., 2001). The secular perturbations of the semi-major axis lead to formation weak stochastic trajectories. We described the stochastic properties of the motion based on an analysis of the integrated autocorrelation function (IACF) $\mathcal{A}$ (Wytrzyszczak et al., 2007).

The IACF $\mathcal{A}$ asymptotically approaches unity for constant time series. For a uniform time series representing a periodic sine function, $\mathcal{A} = 0.5$. For other periodic and quasi-periodic time series, $\mathcal{A}$ approaches a finite value close to 0.5. For chaotic trajectories, $\mathcal{A}$ asymptotically approaches zero with a speed proportional to the inverse of the exponential decay time.

Figure 1 shows the IACF $\mathcal{A}$ for the semi-major axis a. Initial value of semi-major axis a_0 is 26162 km, AMR is 0.02 m^2/kg. The IACF $\mathcal{A}$ is asymptotically decreasing to 0.02 for all the solar angles. The dynamical evolution has chaotic properties for all initial values of the solar angle.

6. CONCLUSION

The Poynting–Robertson effect results in a secular decrease in the semi-major axis of a spherically symmetrical satellite. Secular decrease in the semi-major axis is approximately -0.5 km/year for an object near-resonance 22:45 region with AMR = 2 m^2/kg. In resonance regions the effect weakens slightly. Reliable estimates of secular perturbations of the semi-major axis were obtained from the numerical simulation. Under the Poynting–Robertson effect objects pass through the regions of high-order resonances. The Poynting–Robertson effect and secular perturbations of the semi-major axis lead to formation weak stochastic trajectories.

Acknowledgements. This research was supported by the Ministry of Education and Science of the Russian Federation (unique project identifier RFMEFI59114X0003) and the Russian Foundation for Basic Researches (grant 13-02-00026a).

7. REFERENCES

Allan, R.R., 1967a, "Resonance effects due to the longitude dependence of the gravitational field of a rotating primary", Planet. Space Sci., 15, pp. 53–76.

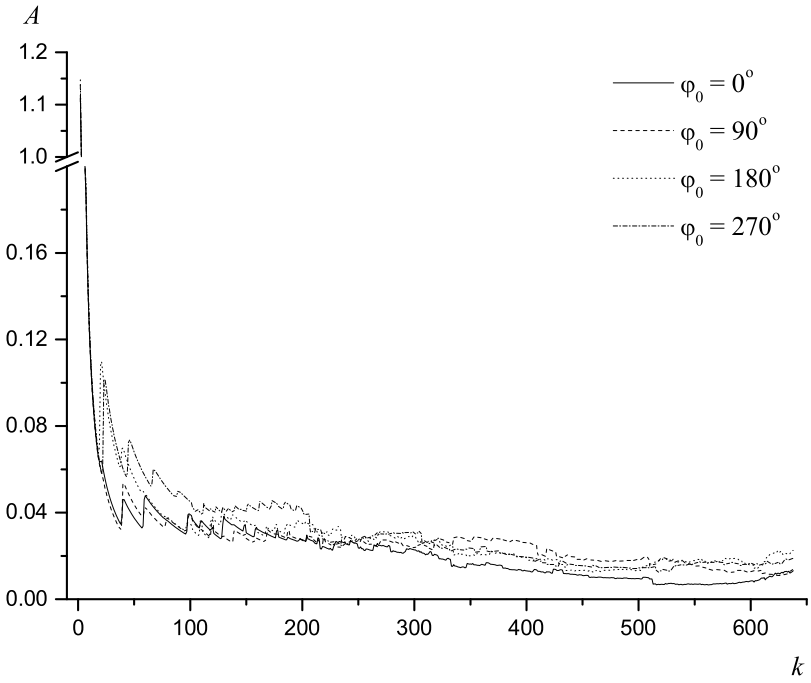

Figure 1: The integrated autocorrelation function $\mathcal{A}$ for the semi-major axis a.

Allan, R.R., 1967b, "Satellites resonance with the longitude-dependent gravity. ii. effects involving the eccentricity", Planet. Space Sci., 15, pp. 1829–1845.

Beutler, G., 2005, "Methods of Celestial Mechanics", Vol. 2, Springer-Verlag, Berlin, Heidelberg.

Bordovitsyna, T.V., Baturin, A.P., Avdyushev, V.A., Kulikova, P.V., 2007, "Numerical model of motion for earth artificial satellite", Izv. Vyssh. Uchebn. Zaved., Fiz., 50, pp. 60–65. (in Russian)

Kozai, Y., 1962, "Secular perturbations of asteroids with high inclination and eccentricity", AJ, 67, pp. 591–598.

Kuznetsov, E.D., Zakharova, P.E., Glamazda, D.V., Shagabutdinov, A.I., Kudryavtsev, S.O., 2012, "Light pressure effect on the orbital evolution of objects moving in the neighborhood of low-order resonances", Solar System Research, 46, pp. 442–449.

Lidov, M.L., 1962, "The evolution of orbits of artificial satellites of planets under the action of gravitational perturbations of external bodies", Planet. Space Sci., 9, pp. 719–759.

Polyakhova, Y.N., Timoshkova, Y.I., 1984, "Quasicircular equatorial orbits of artificial earth satellites with allowance for light pressure", USSR Report Space (JPRS-USP-84-003), Jun., 71 (Transl. from Vestn. Leningr. Univ.: Mat., Mekh., Astron. (USSR), No. 1, Jan. 1984, pp. 100–106).

Smirnov, M.A., Mikisha, A.M., Novikova, E.S., and Rykhlova, L.V., 2001, "Secular variations of semimajor axis of debris particles near GEO due to solar radiation pressure", Proc. of the Third European Conf. On Space Debris, ESA SP-473, pp. 403–406.

Sun, R.-Y., Zhao, C.-Y., Zhang, M.-J., Hou, Y.-G., 2013, "Dynamical evolution of high area-to-mass ratio objects in Molniya orbits", Adv. Sp. Res., 51, pp. 2136–2144.

Timoshkova, E.I., Kholshevnikov, K.V., 1974, "On effects of the sun and moon on the motion of a satellite of a planet", Trudy Astronomicheskoj Observatorii Leningrad, 30, pp. 141–156 (Uchenye Zapiski Leningr. Un-ta, No. 373, Seriya Matem. Nauk, Vyp. 50). (in Russian)

Wytrzyszczak, I., Breiter, S., Borczyk, W., 2007, "Regular and chaotic motion of high altitude satellites", Adv. Sp. Res., 40, pp. 134–142.

PLANNED LLR STATION IN RUSSIA AND ITS IMPACT ON THE LUNAR EPHEMERIS ACCURACY

M.V. VASILYEV[1], E.I. YAGUDINA[1], J.-M. TORRE[2], D. FERAUDY[2]
[1] Institute of Applied Astronomy of the Russian Academy of Sciences
10, Kutuzov quay, 191187, St. Petersburg, Russia
e-mail: eiya@ipa.nw.ru, mvv@ipa.nw.ru
[2] Geoazur/Observatoire de la Cote d'Azur
2130 Route de l'Observatoire, Saint-Vallier-de Thiey,France
e-mail: torre@oca.eu,feraudy@geoazur.unice.fr

ABSTRACT. Precise modern Lunar Ephemerides (DE/LE, USA; INPOP serias, France and EPM-ERA IAA, Russia) are based only on LLR (Lunar Laser Ranging) observations obtained at sixth LLR ground stations during 1969-2013 years. At present there are only four stations active: Grasse(Cerga), McDonald, Apache Point (Apollo) and Matera (Italy). To improve the accuracy of lunar ephemerides the new stations are necessary. Now exist two projects of new LLR stations: Altay (Russia) and Hartebeesthoek in South Africa (1m telescope). La Silla (Chilli) station is very promising but now only under theoretical consideration. In the paper, the impact of a installation of new LLR device on the 3.12 m telescope at Altay station Siberia, Russia is considered. To check the actuality of the project it should be shown, in particular, that the accuracy of the lunar ephemeris will visibly increase. The only way to prove that fact now is the numerical simulation.

1. INTRODUCTION

During about 45 years only LLR observations form the basis for modern Lunar ephemerides. About 18700 LLR observations (normal points, NP) have been obtained during the interval 1970–2013, which were used for obtaining the geodynamical and selenodynamical parameters and improving Lunar ephemeris. Improving the accuracy of LLR observations from 30 cm (1970) to several millimeters (2010-Apache Point station) required new and more sophisticated theories of orbital and rotational Moon motion. Now there are only 3 active stations at the Earth and the construction of new stations with modern lunar laser devices located at different points at the Earth can significantly improve the precision of Lunar ephemeris. One of such projects which is being realized in Russia (Altay station, Siberia region) is the main subject of our paper. The coordinates of the station are: 52N latitude, 82E longitude, H=385 m. The 3.12-meter telescope of the Altay Optical Laser Center will be used for LLR observations. The suggested accuracy of LLR observations (NP) is about 3 mm. The meteorological conditions are: 1400 clear nights hours, 240 nights per year. The main project participants are: OJC Research-and Production Corporation "Precision Systems and Instruments", VNIIFTRI and IAA RAS, the Russian Academy of Sciences. As it was mentioned above, the only way to prove the increase of the accuracy of Lunar ephemeris due to the new LLR station is numerical simulation.

2. NUMERICAL SIMULATION AND RESULTS

The main problem to perform reliable simulation is to create a plausible observational program for the planned LLR station for some time interval. We have analyzed LLR observations at operational LLR stations and made statistical distributions depending on a number of parameters. Three plots of such distributions are presented in Furure 1: reflectors distribution, elevation of the Moon distribution and distribution of real observations per day for every station. We tried to find some regularities that could be the basis for our numerical simulation. But as can be seen on these plots, there is no regularity or uniformity required. So, our conclusion was to use the observational program of real and most precise Apache Point and Grasse(Cerga) LLR stations as the basis to create simulated LLR measurements. Longitude-depended shift and other limitations were taken into account to transfer the observational program from the real LLR Apache Point or Grasse(Cerga) station to simulated the Altay one. Spe-

cial SW was developed to simulate LLR observations and to estimate the adjusted parameters using both real and simulated LLR measurements within the frame of ERA system (Ephemeris Research in Astronomy)(Krasinsky, Vasilyev, 1996).

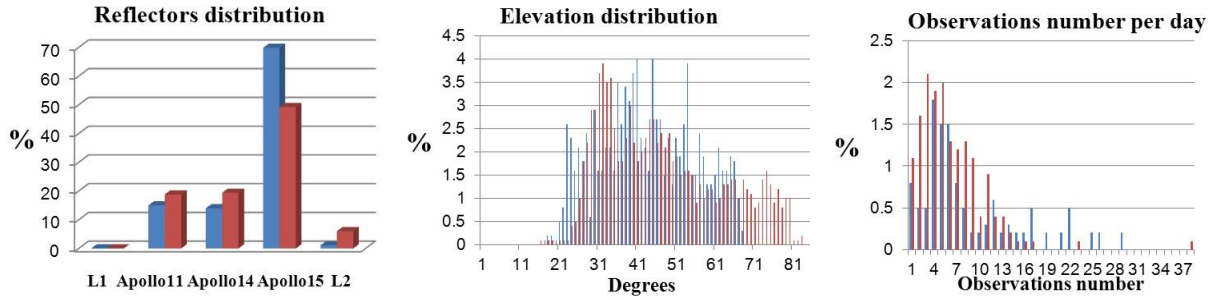

Figure 1: Reflectors distribution, Moon elevation distribution, and distribution of real observations per day.

The last version of the lunar ephemeris EPM-ERA2012 which is used for numerical simulation was described in (Vasilyev, Yagudina, 2014). Several scenarios of simulations have been used to show the result of the impact of the simulated observations at the new Altay station:

I.1.18700 real observations (1970–2013 years) + the simulated observations from 2006 till 2013 at the Altay station just as it was observed at the Apache (Apollo) and the Grasse(Cerga) stations (in simulation-"Apache 2006", "Cerga2006").

I.2. 18700 real observations (1970–2013 years) + the simulated observations from 2006 (-1 month shift) till 2013 at the Altay station just as it was observed at Apache Point and Grasse(Cerga) stations (in simulation — "Apache 2006shift", "Cerga2006shift").

II. 18700 real observations (1970–2013 years) + the simulated observations from 2008 till 2013 at the Altay station just as it was observed at the Apache Point and Grasse(Cerga) stations (in simulation — "Apache 2008", "Cerga2008").

III. 18700 real observations (1970–2013 years) + the simulated observations from 2012 till 2013 at the Altay station just as it was observed at the Apache Point and Grasse(Cerga) stations (in simulation — "Apache 2012", "Cerga2012").

The impact on parameter's accuracy of the "Apache 2006" and the "Cerga2006" scenarios are presented in Fig. 2. Here are shown the visible improvement of the parameters under consideration depending on the reference station. It shall be noted that a more intense observational program generated from the Apache Point one gives more promising results. These parameters are: initial coordinates and velocity of the Moon (1–6), Libration angles and theirs derivatives (7–12), the coordinates of the ground stations(23-40) and reflectors (13–22), Lag of the Moon (60), Lag of the Earth (54) and other parameters (totally 67 parameters).

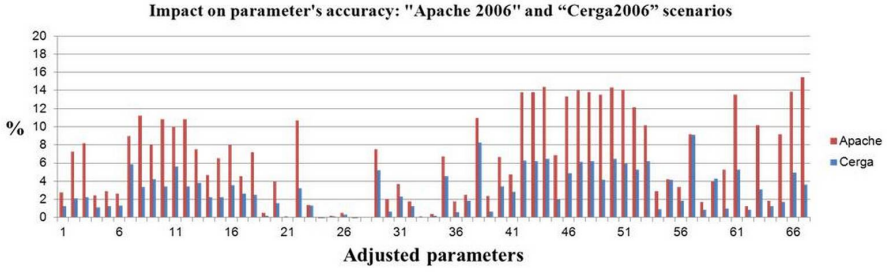

Figure 2: Adjusted parameters.

Next three plots are shown in Fig. 3. Here are presented three graphs for "Lag of the Moon", "Lag of the Earth" and "K_2 Moon" — Love number of the Moon which demonstrate the accuracy vs. observation interval for these adjusted parameters. In case of the Apache Point based scenario we have observed accuracy growth (the improvement is 14 percent for K_2, while at the same time for Grasse(Cerga)

scenario improvement is rather small and almost the same vs years). It demonstrates the importance of intensive observation program for the Altay station, because its geographical positions are closer to Grasse(Cerga) station than to Apache Point one. One additional remark: two last points on each graphs show the simulation precision.

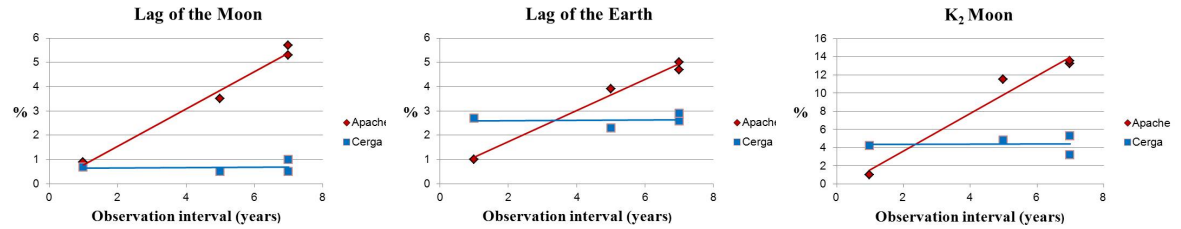

Figure 3: Improvement of the parameters vs observational interval.

3. COMPARISON WITH LA SILLA

There is another project, connected with the probable installation of LLR device at 3.6 m telescope at La Silla station. It would be interesting to compare the conditions at the two stations. The SHELLI (Southern Hemisphere Lunar Laser Instrumentation) project is located at ESO, La Silla, Chile (29 N-latitude, 70 W-longitude, H=2400m). It is a twin of the Apache Point in terms of quality and regularity of the produced data. Meteorological conditions: ESO, bordering the southern extremity of the Atacama desert in Chile.

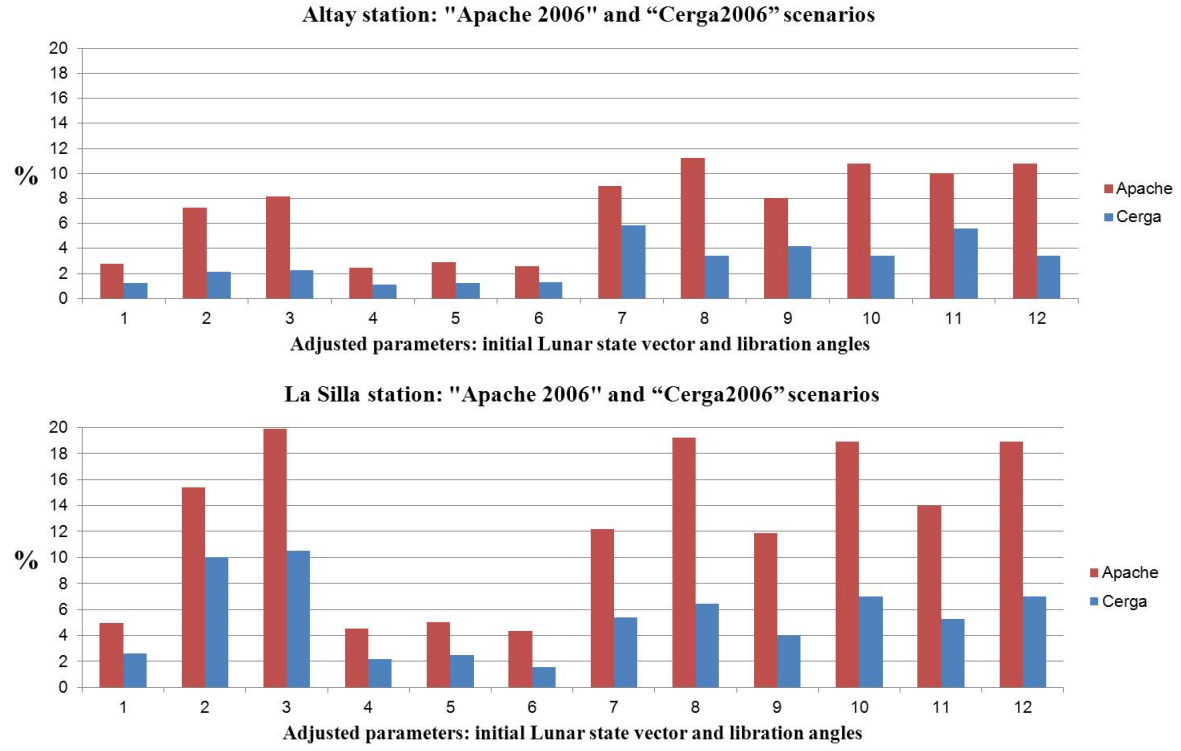

Figure 4: Comparison of the improvement of the parameters for the Altay and the La Silla stations.

The probable participants: ESO, Geoazur(OCA), INSU. In Table 1. the geographical and meteorological data for different stations (real and planned Altay and La Silla stations) are shown to compare observational conditions at the stations. Figure 5 demonstrates that Altay station is not located in the best conditions as compare with the Grasse(Cerga) and Apache Point stations: elevation of the Moon is lower than at the Apache Point and Grasse(Cerga) stations. As for meteorological conditions (2400 m La Silla and 385 m Altay!) are also guaranteed more observational nights at La Silla station.

Station	Latitude	Longitude	Altitude, m	Telescope
Apache	33 N	254 W	2788	3.5m
Cerga	45 N	7 W	1270	1.54m
Altay	51 N	82 E	385	3.12m
La Silla	29 S	70 W	2400	3.6m

Table 1: Geographical and meteorological conditions at different stations (comparison).

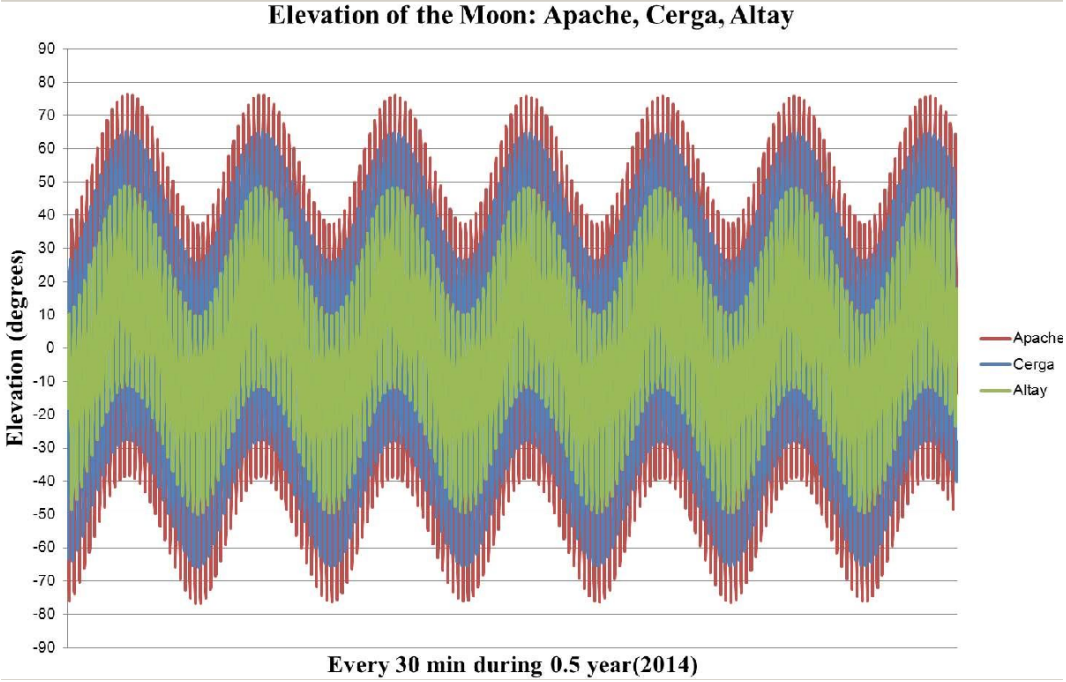

Figure 5: Elevation of the Moon at 3 stations: Apache Point, Grasse(Cerga), and Altay.

4. CONCLUSION

1. According to our simulations new Russian LLR observations will provide visible accuracy improvement of the Lunar ephemeris and corresponding physical models: about 2–16% depending on the adjusted parameters.

2. Simulation SW was developed estimating the impact of the new LLR stations on the accuracy of Lunar ephemeris.

3. Russian LLR station has observational limitations due to geographical position. Thus,its observational program should be very intense to provide the impact comparable with other modern LLR stations. The results obtained are in good agreement with the similar work in the field (Fienga, et al., 2014).

4. Russian LLR station can make significant contribution into the common world database of LLR data.

5. REFERENCES

Krasinsky, G.A., Vasiliev, M.V., 1996, "ERA: knowledge base for Ephemeris and dynamical astronomy", In: Proc. IAU Colloquium 165, Poznan, Poland, pp. 239–244.

Fienga, A., Courde, C., Torre, J-M., Manche, H., Murphy, T., Mieller, J., Laskar, J., Bouquillon, S., Biskupek, L., Hofmann, F., Capitaine, N., Rambaux, N., 2014, "Interest of a new Lunar laser instrumentation on the ESO NTT Telescope", arXiv:1405.0473v1.

Vasilyev, M.V., Yagudina, E.I., 2014, "Russian Lunar Ephemeris EPM-ERA 2012", Solar Syst. Res., 48(2), pp. 158–165 .

MEASURES OF THE EARTH OBLIQUITY DURING THE 1701 WINTER SOLSTICE AT THE CLEMENTINE MERIDIAN LINE IN ROME

A.H. ANDREI[1,2,3,4], C. SIGISMONDI[1,3,5,6], V. REGOLI[6]
[1] Observatório Nacional/MCTI
Rua Gal. José Cristino 77, Rio de Janeiro, RJ CEP 20921-400, Brasil
e-mail: oat1@ov.ufrj.br
[2] SYRTE, Observatoire de Paris, CNRS/UPMC
Avenue de l'Observatoire 61, Paris 75014, France
[3] Observatório do Valongo/UFRJ
Ladeira do Pedro Antônio 43, Rio de Janeiro, RJ CEP 20080-090, Brasil
[4] Osservatorio Astrofisico di Torino/INAF
Strada Osservatorio 20, Pino Torinese, TO 10025, Italia
[5] Istituto Tecnico Industriale Galileo Ferraris
Via Conte Verde 51, Roma CAP 00185, Italia
e-mail: costantino.sigismondi@gmail.com
[6] Pontifical Athenaeum Regina Apostolorum
Via degli Aldobrandeschi 190, Roma CAP 00163, Italia

ABSTRACT. The great meridian line in the Basilica of Santa Maria degli Angeli in Rome was built in 1701/1702 with the scope of measuring the obliquity of the Earth's orbit in the following eight centuries, upon the will of Pope Clement XI. During the winter solstice of 1701 the first measurements of the obliquity were taken by Francesco Bianchini. He was the astronomer who designed the meridian line, upgrading the similar instrument realized by Giandomenico Cassini in San Petronio, Bononia. The accuracy of the data is discussed from the point of view of the use of the pinhole.

1. THE ASTROMETRIC PINHOLE

All ancient meridian lines have been re-measured after some decades of duty, in order to verify their alignment and the position of the pinhole. These instruments have been built to measure the variation of the obliquity along the centuries, and the need of a re-calibration was part of the observational duties. The Cassini meridian line in San Petronio, Bologna, made in 1655 was revised in 1695 by the same astronomer Giandomenico Cassini. Similarly Leonardo Ximenes in 1761 restored the meridian line in Santa Maria del Fiore in Florence, made by Paolo del Pozzo Toscanelli in 1475. The great Clementine gnomon of Santa Maria degli Angeli in Rome, completed by Francesco Bianchini in 1702, was studied and remeasured by Anders Celsius in 1734 and Ruggero G. Boscovich in 1750. They found the deviation of the azimuth from the true North, respectively of $2'$ (1734) and $4'30''$ (1750). Our measurements of 2006 (Sigismondi, 2013), used the Polaris transits technique, yielding $4'28''.8 \pm 0.6''$, in agreement with the measurements made by Boscovich.

In the recognitions of Cassini and Ximenes the main issue was the movement of the pinhole with respect to the original position.

This was due to the fact that the pinhole in Bologna was on the roof, and in Florence was in the dome of the church: both positions were subjected to motions of the buildings due to thermal response, winds and settling of the walls.

For this reason Francesco Bianchini chosen the basilica of Santa Maria degli Angeli in Rome to build the meridian line upon the will of Pope Clement XI (1700–1721): this church was built by Michelangelo in the original roman hall of the Diocletian baths, a 1500 years old structure, with no more settling ongoing.

2. RESULTS

On Figure 1 we can see that the center of the Sun has $c \sim 67.6$ in remarkable agreement with the IMCCE/Observatoire de Paris ephemeris for the day — z=34°.0548, equivalent to c=67.590. Bianchini could measure the nearest arcsecond by drawing both the locations of the Southern and the Northern limbs of the Sun.

Figure 1: The image of the Sun is projected through a pinhole on the floor moving up on September 2^{nd} 2014.

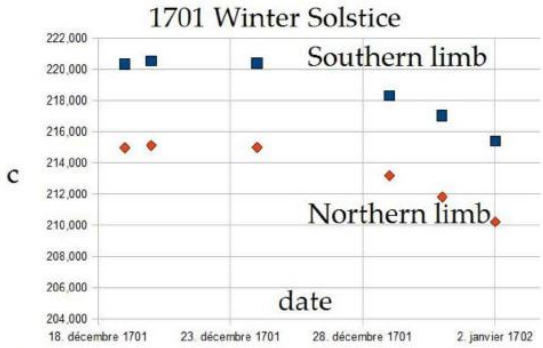

Figure 2: Graphical representation of the data in the letter of Francesco Bianchini to Pope Clement XI.

On Figure 2 the quadratical fit with the Southern limb yields 22.17 December for the solstice, and 21.94 December. The average gives the solstice at 22.06 December 1701 at 00:26 UT. For the same solstice, the IMCCE ephemeris give 21 December at 23:35.

The same quadratic fit yields for the extreme positions of the two limbs of the Sun at the solstice time: Southern 220.597 and Northern 215.228.

Correspondingly the unperturbed center of the solstitial Sun has declination $\delta = 23°28'48''$, being $41°54'11''.2$ the latitude of the pinhole.

Thus the observed mean Obliquity can be derived as $\epsilon = 23°28'54''.3$.

This is in excellent agreement with modern calculations for the mean obliquity in 1702.0. Laskar method gives $\epsilon = 23°28'40''.9$, whereas Duffet-Smith method gives $\epsilon = 23°28'58''.6$.

3. REFERENCES

Sigismondi, C., 2013, "The astrometric recognition of the Solar Clementine Gnomon (1702)", Intern. J. of Modern Physics, Conference Series, vol. 23, 454.

LOCAL TESTS OF GENERAL RELATIVITY WITH GAIA AND SOLAR SYSTEM OBJECTS

D. HESTROFFER[1], P. DAVID[1], A. HEES[2,1], C. LE PONCIN-LAFITTE[3]
[1] IMCCE, Paris Observatory, UPMC, univ. Lille1, CNRS
77 av. Denfert-Rochereau, F-75014 Paris
e-mail: hestro@imcce.fr
[2] Department of mathematics, Rhodes University, RSA
[3] SYRTE, Observatoire de Paris, CNRS/UPMC, Paris, France

ABSTRACT. The Gaia mission has been launched by ESA on 2013 December, 19. It aims to survey, in addition to stars, a large number of solar system objects (SSO). Hence, Gaia will provide during its 5 years mission high precision astrometry in an absolute reference frame of about 300 000 asteroids, including many Near-Earth Objects. The very precise orbits Gaia will provide, will enable to determine simultaneously the solar J_2 and the PPN parameter beta and other parameters for testing the GR. Improvement from combining Gaia and radar data are also expected.

1. INTRODUCTION

The Gaia space mission is an ESA astrometric mission of the Horizon 2000+ programme provides Europe with a successor to Hipparcos/Tycho, with many huge improvements. The number of stars observed and catalogued, in addition to the precision of the measures – astrometric, photometric, and spectroscopic – complemented by some imaging capabilities, make it more than a Hipparcos-II. In this respect, the Gaia satellite and telescope will observe a large number of Solar System Objects (SSO) during the 5 years mission duration, down to magnitude $V \approx G \leq 20.5$, as presented in e.g. Hestroffer & Tanga (2014) and Mignard et al. (2007). Given the astrometric precision involved—at the sub-mas level—relativistic effects have to be taken into account in the data reduction and analysis. This was already the case in the Hipparcos mission, also for the Solar System objects (Hestroffer & Morando 1995, Hestroffer 1997), and is now also mandatory at all stages of the reduction pipeline within the Gaia mission. A group, REMAT, within the Gaia DPAC Data Processing and Analysis Consortium, is providing RElativity Models And Testings. In this framework tests of Genaral Relativity (GR) can be performed by measuring the Parameterised Post-Newtonian (PPN) parameters, and more exactly their possible deviation from the canonical value of the GR theory. This is done for instance from the astrometry of stars and a measure of the light deflection through parameter γ (e.g. Mignard & Klioner 2010; Raison et al. 2010), but also by a test of the quadrupole effect around Jupiter and the GAREX experiment (Crosta & Mignard 2006; Le Poncin-Lafitte & Teyssandier 2008), and last, from the orbit of solar system objects. We will present in the following some aspects of the scientific outcome of Gaia within the Solar System for deriving the PPN β, together with the Solar quadrupole J_2 and other parameters, and prospective for testing GR or other alternative theory.

2. MISSION AND EXPECTED RESULTS

There are some obvious advantages to use astrometry from space, of high precision and accuracy, with a single instrument and data reduction performed directly in a fundamental stellar catalogue. All these are provided by the Gaia satellite, telescope and mission. On the other hand the programmatic of the Gaia observations is not adapted to SSO, but imposed by the scanning law of the satellite. Since most of Gaia asteroids are well known objects, we will be able to derive orbit improvements from ordinary least squares techniques involving only Gaia observations within the DPAC consortium. We can then perform a variance analysis of the system of equations' inversion and get the formal precisions of all unknown parameters estimation.

The astrometric precision is—depending on the target's magnitude—of the order of 1 mas and better. Given such unprecedented astrometric precision available for the observations of Solar System, big

improvements are expected in orbit refinement, so that small effects and perturbations on the orbits can be detected, dynamical or physical parameters estimated such as mass of asteroids (Mouret et al. 2007), and models tested. In particular, small additional acceleration due to GR is affecting all orbits of SSOs, and mostly this of eccentric orbits close to the Sun. Thus Near Earth Objects (asteroids and comets) are particularly good test particles for the purpose of testing the General Relativity in the Solar System. It is well known that both the Sun quadrupole J_2 and GR imply an advance of the perihelion of the orbit that can hardly be separated from the observation of one single target, such as Mercury, alone. Gaia will provide observations of bout 2000 NEOs and will yield a simultaneous determination of both J_2 and PPN β. The order of precision obtained 10^{-4} for β, 10^{-8} for J_2, are not much better than current estimates but completely independent of other modelling (Nordvedt, Sun interior, ...) or assumption on one of the parameters. Besides of these test of GR combined with the measure of Sun dynamical flattening, one will be able to test a possible variation of the gravitational constant. Moreover, since all SSO positions will be derived directly in the optical ICRF realised by the Gaia QSOs, a direct link between the dynamical and kinematical non-rotating frames will be established. This will put the ecliptic and equinox within the ICRF, and also test a possible rotation rate at the μas/year level (Hestroffer 2010).

3. PROSPECTIVE

The influence of the Lense-Thirring drag is tested. It mimics precession from Solar J_2 and can account to 7% of the value so determined (Folkner et al. 2014); the perihelion precession can reach 2.8 mas/cy in the case of NEA 2000 BD_{19} ($a = 0.876$ AU; $e = 0.895$), similar to the one from PPN β. Besides, other framework can be considered such as post-Einsteinian gravity, MOND, SME (Hees et al. 2014, and references therein). Some improvements can hence be expected in several ways:

- observing more objects down to magnitude $V \leq 21$. This is considered because the limitation in magnitude is not imposed by the telescope and instruments sensitivity, but by the data downlink to Earth. Going to fainter magnitude has his cost of operations but shows some benefits particularly for testing the GR.
- one year mission extension. Such extension can be decided by ESA at later stages of the mission. Increasing the time span has obvious advantages for deriving orbits' precession and their secular effects, making angles and longitudes on the orbit vary quadratically with time. Combined with the push in limiting magnitude, a gain of factor 2 can be expected.
- complementary ground-based observations for a few targets. Only measures of high precision and with high accuracy can be considered here, these are already obtained by radar techniques at Arecibo (Margot & Giorgini 2010) and will span about two decades.

4. REFERENCES

Crosta, M.-T., Mignard, F., 2006, "Microarcsecond light bending by Jupiter", CQGr, 23, pp. 4853–4871.

Folkner, W., et al., 2014, "The Planetary and Lunar Ephemerides DE430 and DE431", IPN Progress Report 42-196, pp. 1–81.

Hees, A., et al., 2014, "Tests of gravitation at Solar System scale beyond PPN formalism", In: Proc. Journées 2013 "Systèmes de Référence Spatio-Temporels", N. Capitaine (ed.), pp. 241–244.

Hestroffer, D., Morando, B., 1995, "Observations of minor planets by Hipparcos", P&SS, 43, pp. 817–820.

Hestroffer, D., 1997, "The HIPPARCOS Solar System Objects Annexes", ESA SP-402, pp. 35–40.

Hestroffer, D., et al., 2010, "Gaia and the asteroids: Local test of GR", IAU Symp. 261, pp. 325–330.

Hestroffer, D., Tanga, P., 2014, "New frontiers on small bodies from the Gaia mission", In: COSPAR Conf., 2–10 August 2014, Moscow, Russia. Abstract B0.4-20-14.

Le Poncin-Lafitte, C., Teyssandier, P., 2008, "Influence of mass multipole moments on the deflection of a light ray by an isolated axisymmetric body", Physical Review D, 77, 044029.

Margot J.-L., Giorgini, J.D., 2010, "Probing general relativity with radar astrometry in the inner solar system", IAU Symp. 261, pp. 183–188.

Mignard, F., et al., 2007, "The Gaia Mission: Expected Applications to Asteroid Science", EM&P, 101, pp. 97–125.

Mignard, F., Klioner, S., 2010, "Gaia: Relativistic modelling and testing", IAU Symp. 261, pp. 306–314.

Raison, F., et al., 2010, "Implementation of the Global Parameters Determination in Gaia's Astrometric Solution (AGIS)", ASP Conf. series, 434, pp. 386–389.

STATISTICAL INVERSION METHOD FOR BINARY ASTEROIDS ORBIT DETERMINATION

I.D. KOVALENKO[1], D. HESTROFFER[1], A. DORESSOUNDIRAM[2], N.V. EMELYANOV[3]
R.S. STOICA[1,4]
[1] IMCCE, Observatoire de Paris, CNRS/UPMC
77 Av. Denfert Rochereau, F-75014 Paris, France
e-mail: ikovalenko@imcce.fr
[2] LESIA, Observatoire de Paris, CNRS
5, place Jules Janssen, F-92195 Meudon
e-mail: alain.doressoundiram@obspm.fr
[3] Sternberg Astronomical Institute
13 Universitetskij prospect, 119899 Moscow, Russia
e-mail: emelia@sai.msu.su
[4] Université Lille 1, Laboratoire Paul Painlevé
59655 Villeneuve d'Ascq Cedex, France
e-mail: radu.stoica@math.univ-lille1.fr

ABSTRACT. We focus on the study of binary asteroids, which are common in the Solar system from its inner to its outer regions. These objects provide fundamental physical parameters such as mass and density, and hence clues about the early Solar System. The present method of orbit calculation for resolved binaries is based on Markov Chain Monte-Carlo statistical inversion technique. In particular, we use the Metropolis-Hastings algorithm combined the Thiele-Innes equation for sampling orbital elements through the sampling of observations. The method requires a minimum of four observations, made at the same tangent plane; it is of particular interest for initial orbit determination. The observations are sampled within their observational errors with an assumed distribution. The sampling predicts the whole region of possible orbits, including the one that is most probable.

1. STATISTICAL INVERSION PROBLEM

The statistical ranging method using Markov-Chain Monte-Carlo for asteroid heliocentric orbit determination has been investigated by, for example, Oszkiewicz et al. (2009) and Virtanen et al. (2001). We use the similar approach for binary asteroids to determine relative orbit.

The N astrometric observations at times $t = (t_1, ..., t_N)$ are related to the theoretical positions through the observational equation:

$$\varphi = \psi(X) + \varepsilon\,,$$

where $\varphi = (\rho_1, \theta_1; ...; \rho_N, \theta_N)$ is a set of N observations, presented by relative distance and angle, $\psi(X)$ is a computed sky-plane positions, $X = (a, e, i, \Omega, \omega, T, P)$ is the vector of orbital elements (semi-major axis, eccentricity, inclination, longitude if the ascending node, argument of periapcsis, the time of perihelion passage) and the period respectively, and $\varepsilon = (\varepsilon_{\rho 1}, \varepsilon_{\theta 1}; ...; \varepsilon_{\rho N}, \varepsilon_{\theta N})$ is the vector of observational errors.

Applying the Bayesian statistics the *a posteriori* probability density of the binary asteroid orbital parameters can be estimated from the *a priori* and the noise probability density. Using the Bayes' theorem

$$p(X|\varphi) = \frac{p(X)p(\varphi|X)}{p(\varphi)}$$

and following the statistical inversion theory, the *a posteriori* probability density of the orbit elements is related to the *a priori* and noise probability densities:

$$p(X|\varphi) \propto p(X)p_\varepsilon\,,$$

where the likelihood function coincides with the noise probability density $p_\varepsilon = p(\varphi|X) = exp(-\frac{1}{2}\varepsilon^T\Lambda^{-1}\varepsilon)$, $\varepsilon = \varphi - \psi(X)$, and Λ is the covariance matrix $2N \times 2N$ for the observational errors.

The *a priori* probability density can be expressed as $p(X) = exp[-U(X)]$, where $U(X)$ includes the distributions of each parameter. The final *a posteriori* orbital parameters probability density function:

$$p(X|\varphi) \propto exp[-\frac{1}{2}\varepsilon^T \Lambda^{-1} \varepsilon - U(X)] \,.$$

2. MARKOV CHAIN MONTE-CARLO METHOD

The Metropolis-Hastings algorithm, based on the Markov Chain Monte-Carlo method, has been used for sampling parameters X. First, from the whole set of N observations we select four observations on the same tangent plane; this is necessary and sufficient for binary asteroid relative orbit determination using the Thiele-Innes method. Then, the corresponding relative distance ρ and angle θ which sampled. For each iteration we introduce the proposal densities for the set of four observations, correspond to the Gaussian distribution of observational errors. They are centred around the last accepted sampling. We denote the proposal set of 4 positions S' and last accepted S_t.

We generate proposal positions $(\rho_i'; \theta_i'), i = 1, 2, 3, 4$ for the four chosen observation data with the proposal densities

$$(\rho_i' \propto G(\rho_i^t; \sigma(\rho_i); \theta' \propto G(\theta_i^t; \sigma(\theta_i)) \,.$$

Then from the four positions sampled we calculate an orbit X' using Thiele-Innes method, and check the solution to all observations. The new candidate orbital elements and system mass are rejected or accepted according to acceptance criteria:

$$a = \frac{p(X'|\varphi)p(S_t, S')J_t}{p(X_t|\varphi)p(S', S_t)J'} \,,$$

where J' and J_t are the determinants of the Jacobian matrix from (ρ, θ) coordinates to parameters X for the candidate and the last accepted sample. The Jacobians are defined as (Oszkiewicz et al., 2009):

$$J = \left| \frac{\partial S}{\partial X} \right| \,.$$

We use the symmetric p.d.f.s $p(S_t, S')$ and $p(S', S_t)$, therefore

$$a = \frac{p(X'|\varphi)J_t}{p(X_t|\varphi)J'} \,.$$

If $a \geq 1$ we accept the candidate elements, then $X_{t+1} = X'$. If $a < 1$ we accept the candidate elements with a probability equal to a, or $X_{t+1} = X_t$ with a probability equal to $1 - a$. This process is repeated until the stationary a posteriori density is reached. The algorithm is run for a large number of iterations until the entire possible orbital-element space is mapped.

Acknowledgements. This work is supported by Labex ESEP (ANR No. 2011-LABX-030).

3. REFERENCES

Oszkiewicz, D., Muinonen, K., Virtanen, J., Granvik, M., 2009, "Asteroid orbital ranging using Markov-Chain Monte Carlo", Meteoritics & Planetary Science, 44, pp. 1897–1904.

Virtanen, J., Muinonen, K., Bowell, E., 2001, "Statistical Ranging of Asteroid Orbits", Icarus, 154, pp. 412–431.

DIAGRAMS OF STABILITY OF CIRCUMBINARY PLANETARY SYSTEMS

E. POPOVA
Pulkovo Observatory
196140 St. Petersburg, Russia
e-mail: m02pea@gmail.com

The stability diagrams in the "pericentric distance – eccentricity" plane of initial data are built and analysed for Kepler-38, Kepler-47, and PH1. This completes a survey of stability of the known up to now circumbinary planetary systems, initiated by Popova and Shevchenko (ApJ, 769, 152, 2013), where the analysis was performed for Kepler-16, 34, and 35. In the diagrams, the planets appear to be "embedded" in the fractal chaos border; however, I make an attempt to measure the "distance" to the chaos border in a physically consistent way. The obtained distances are compared to those given by the widely used numerical-experimental criterion by Holman and Wiegert (1999), who employed smooth polynomial approximations to describe the border. I identify the resonance cells, hosting the planets.

Results of this study will appear in Proceedings of IAU Symposium 310 "Complex planetary systems".

METHOD OF DETERMINING THE SMALL BODIES ORBITS IN THE SOLAR SYSTEM BASED ON AN EXHAUSTIVE SEARCH OF ORBITAL PLANES

D.E. VAVILOV, Y.D. MEDVEDEV
Institute of Applied Astronomy of Russian Academy of Science
Kutuzova emb. 10, 191187 St.-Petersburg, Russia
e-mail: dj_vil@bk.ru, medvedev@ipa.nw.ru

ABSTRACT. A universal method of determining the orbits of newly discovered small bodies in the Solar System using their positional observations has been developed. In this method we avoid determining the topocentric distances of an object by iterations. Instead the different orbital planes of object's motion are considered and the most appropriate one is chosen as a first approximation for the differential method of improving orbit. Criterion for choosing the most appropriate plane is the least rms of the observations. For each considered plane the topocentric distances are calculated and the two reference observations are chosen. The orbits for each plane are calculated using the method of determining orbital elements by two heliocentric positions and times.

1. INTRODUCTION

Newly discovered asteroids that have short observational arcs and few observations pose a special problem in orbit determination. Gauss developed his method for orbit determination about 2 ages ago but it uses only 3 observations. Nowadays generally the amount of asteroid's observations more than tree even at the first day of observing this object. Also the iterations used in this method sometimes can diverge of tend to inappropriate or strange result (e.g. topocentric distances less than zero).

Usually the problem of calculating small body orbits can be divided into two stages: determining the Keplerian imperturbation orbit; improving the orbit by differential method taking significant perturbations into account.

Let's there are $n \geq 3$ positional observations of a body: points in time t_j, right ascensions α_j and declinations δ_j $(j = \overline{(1,n)})$. Then, unit vectors $\underline{\mathbf{L}}_j$ pointing to the body in the topocentric equatorial coordinate system have the following form: $\underline{\mathbf{L}}_j = (\cos\alpha_j \cdot \cos\delta_j, \sin\alpha_j \cdot \cos\delta_j, \sin\delta_j), \quad (j = \overline{(1,n)})$

The relationship between the heliocentric and topocentric vectors of the celestial body positions is determined by the equations:

$$\underline{\mathbf{X}}_j = \rho_j \cdot \underline{\mathbf{L}}_j + \underline{\mathbf{E}}_j, \quad (j = \overline{(1,n)}) \tag{1}$$

where $\underline{\mathbf{X}}_j$ are the heliocentric vectors of the celestial body positions, ρ_j are the topocentric distances, and $\underline{\mathbf{E}}_j$ are the heliocentric vectors of the observer's position. Note that $\underline{\mathbf{E}}_j$ can be calculated by some planet ephemerid (e.g. DE431, INPOP13c or EPM 2013).

The unknown variables in the equation system (1) are topocentric distances ρ_j and 6 orbital parameters (vectors $\underline{\mathbf{X}}_j$ are functions of orbital parameters). Consequently we have $3n$ equations and $6 + n$ unknown variables. In order to find the orbit one should solve this nonlinear system. Generally this system is solved using iterations that can can diverge of tend to inappropriate or strange result especially in cases of short observation arc and few observations.

2. DESCRIPTION OF THE PROPOSED METHOD

In this method we want to avoid using iteration in the solving of system (1). Note that topocentric distances can be considered as functions of observation and only two orbital elements: inclination i and longitude of the ascending node Ω (as lengths of vector sections $\underline{\mathbf{L}}_j$ pointing from the observer to the object till the intersection with the plane).

Our main idea is find the first approximation for the differential method. We propose the following scheme. We do exhaustive search of orbital planes and for each plane we do the following (Bondarenko et al., 2014):

1. Calculate topocentric distances ρ_j
2. Take aberration corrections into account
3. Choose two reference observations (generally the first and the last ones)
4. Determine the orbit using the method of determining orbital elements based on two heliocentric positions and times
5. Calculate rms $\sigma = \sqrt{\frac{1}{2n}\sum_{j=0}^{n}(\alpha_j - \alpha_j^c)^2\cos^2\delta_j + (\delta_j - \delta_j^c)^2}$, where α_j^c and δ_j^c are the calculated equatorial coordinates of the celestial body.

Then we consider the orbit, which associated with the least σ, as the most appropriate one and use it as a first approximation of the orbit.

The advantage of this approach is that we always obtain some approximation that we can try to improve.

3. RESULTS

The efficiency of the technique was verified with 34 new celestial objects published in the Minor Planet Center circulars between September 17–29, 2010, and May 24 – June 3, 2011. This method found satisfying first approximations of orbits, which were improved by differential method, for all considered asteroids. On the other hand using the classical Gauss method, we failed to determine preliminary orbits for 11 asteroids that could be further improved using the differential method. In nine cases the epochs of observations were represented as two groups separated by a fairly long time interval. For one asteroid the accuracy of the mean observation was not well enough. And in one case a problem with the convergence of iterations in the determination of geocentric distances arose while calculating the orbit. The values of geocentric distances for this asteroid obtained using the Gauss method turned out to be negative.

4. REFERENCES

Bondarenko, Yu.S., Vavilov, D.E., Medvedev, Yu.D., 2014, "Method of Determining the Orbits of the Small Bodies in the Solar System Based on an Exhaustive Search of Orbital Planes", Solar System Research, 48(3), pp. 212–216.

Sub-Session on the IAU/IAG Joint Working Group "Theory of Earth Rotation"

Sous-Session sur le Groupe de travail UAI/AIG "Théorie de la rotation de la Terre"

REPORT ON ACTIVITIES OF THE IAU/IAG JOINT WORKING GROUP ON THEORY OF EARTH ROTATION

J.M. FERRÁNDIZ[1], R.S. GROSS[2]
[1] Dept. Applied Mathematics, University of Alicante
PO Box 99, E-03080 Alicante, Spain
e-mail: jm.ferrandiz@ua.es
[2] Jet Propulsion Laboratory, California Institute of Technology
Pasadena, USA
e-mail: richard.s.gross@jpl.nasa.gov

ABSTRACT. This report of progress on the activities of the IAU/IAG Joint Working Group on Theory of Earth Rotation (JWG_ThER) has a twofold purpose. First, providing a short introduction to the JWG_ThER dedicated sub-session, recalling the purpose, structure and operation of the JWG and the main activities developed so far. Second, summarizing the discussion scheduled at the end of the sub-session after the presentation of the reports, by giving a brief account of the topics submitted by the Chairs of the JWG and its three Sub Working Groups as well as the argumentations and the reached agreements.

1. INTRODUCTION

Purpose. The International Association of Geodesy (IAG) and the International Astronomical Union (IAU) set up a new Joint Working Group on Theory of Earth Rotation in April 2013. The purpose of this JWG is promoting the development of theories of Earth rotation that are fully consistent and that agree with observations and provide predictions of the EOP (Earth Orientation Parameters) with the accuracy required to meet the needs of the near future as recommended by, e.g., GGOS, the Global Geodetic Observing System of the IAG. Let us recall that GGOS accuracy and stability goals are 1 mm in position and 0.1 mm/yr in velocity on global scales for the reference frame realizations, especially the ITRF (International Terrestrial Reference Frame) – see, e.g., Plag and Pearlman, 2009; Plag et al., 2009. The accuracy in position corresponds roughly to 30 μas and 3 μas/yr in the angles measured from the Earth's centre.

Desired Outcomes.

- Contribute to improving the accuracy of Precession-Nutation and UTPM (Universal Time, Polar Motion) theoretical models by proposing both new models or additional corrections to existing models.
- Clarify the issue of consistency among conventional EOP, their definitions in various theoretical approaches, and their practical determination.
- Establish guidelines or requirements for future theoretical developments with improved accuracy.

The overall goals of the JWG cannot be achieved within only two years and the first term should be used to develop a solid concept of how to reach its aims. Reports must be concluded and presented at the next General Assemblies of IAU and IAG to be held in 2015.

Structure. The structure of this JWG follows the characteristics of the current set of EOP as well as the fields of specialization of researchers. The people in charge are: José M. Ferrándiz (Chair, mainly IAU) and Richard Gross (Vice-Chair, mainly IAG). The WG is structured in three Sub-Working Groups (SWG):

1. Precession/Nutation (Chair[1]: Juan Getino)

2. Polar Motion and UT1 (Chair: Aleksander Brzeziński)

3. Numerical Solutions and Validation (Chair: Robert Heinkelmann)

SWG 3 is dedicated to numerical theories and solutions, relativity and new concepts and validation by comparisons among theories and observational series.

Each SWG is entrusted with its own tasks and goals. The three SWG should work in parallel for the sake of efficiency and they should be coordinated and linked together as closely as the needs of consistency demand. The JWG is intended on an open basis and the cooperation of non-members is welcome. All people interested in Earth rotation are invited to contribute; it suffices contacting directly any of the chair–persons or visiting the JWG web site hosted by the Institution of the Chair (University of Alicante, Spain), at `http://web.ua.es/en/wgther`. That site contains the full terms of reference (ToR), member lists and a brief account of the activities to be described in the next section, including the corresponding memorandums and presentations.

2. PREVIOUS ACTIVITIES AND MEETINGS

The JWG serves as a forum for the exchange of ideas and information on the contemporary and prospected future advances in the theory of Earth rotation, resulting from the activity of its ordinary or correspondent members and the community of researchers interested in this matter. A selection of the investigations carried out recently in different aspects of Earth rotation is collected in the reports of each SWG, therefore we do not reiterate them here.

At the initial stages of operation some invited talks introducing the JWG and its goals were delivered at conferences of special relevance for our subject, namely the *IAG Scientific Assembly* (Potsdam, September 2013) and shortly afterwards the *Journées 2013 Systèmes de Référence Spatio-Temporels* (JSR2013, Paris, September 2013) – Ferrándiz and Gross, 2014a, 2014b. Besides, a number of business or science meetings of opportunity were organized on occasion of those two and of later conferences, generally open to their attendants. Among the main scientific topics discussed at the JSR2013 splinter meeting, we can remark:

- The need of agreeing on a common background among the three SWG to encompass the development of the tasks of each SWG and keep the main issue of consistency.

- The convenience of preparing a first catalogue of potential sources of inconsistency among theory and the series of EOP determined from the data obtained by the various observational techniques. Inconsistencies may result from many causes: differences among reference systems used in theories and data analyses, realizations of frames, geophysical models, etc. Assessing their magnitudes would help to ascertain which effects may be not negligible at the pursued accuracy level.

- Revising Earth models used in different theoretical approaches to EOP since they exhibit large variations. Some possibilities, as adopting triaxial models or taking into account other new geophysical effects, should be addressed in future.

- Studying further and testing new effects or corrections to nutations proposed in the last few years.

- Considering the role of theoretical predictions in a scenario in which observational accuracy goes ahead of theory, etc.

An additional presentation dedicated to the JWG_ThER scope and its initial activities was performed at the *AGU Fall Meeting 2013* held in San Francisco, December 2013 (Ferrándiz and Gross, 2013).

The issues of accuracy and consistency of EOP and the relationships between theory and observations were addressed in a talk made at the *8th General Meeting of the IVS* (International VLBI Service) held in Shanghai from 2-9 March 2014 (Ferrándiz et al., 2014a) Other activities of the JWG on Theory of Earth Rotation which took place at that meeting are:

A - JWG business meeting. The Chair and Vice-Chair of the JWG and the Chair of SWG3 got together with the President and Past-President of IAU C19 (Ferrándiz, Gross, Heinkelmann, Huang, Schuh, respectively) and had an informal business meeting to discuss about the agenda. It was agreed: The Splinter Meeting scheduled at the EGU 2014 would provide an opportunity to each SWG Chair

[1]Due to some health problems of J. Getino, A. Escapa is temporarily acting as Co–Chair of Sub–WG1.

to make a presentation concerning his SWG (Ferrándiz et al., 2014b; Brzeziński, 2014; Getino, 2014; Heinkelmann, 2014) and it would help to organize its work according to the ToRs. The only SWG Chair attending the IVS GM was Heinkelmann, who also supported the idea, so Getino and Brzeziński were invited to do it. The next milestone to be considered were the Journées 2014, that would take place half year later. It was expected that reports of progress of all the SWG could be presented in this conference too, that usually gathers many experts on various Earth rotation topics.

B - Participation in the Analysis Workshop. The SWG3 Chair contributed to the discussion with a short presentation during the IVS Analysis Workshop (Heinkelmann et al., 2014b). A keen discussion started immediately following the presentation. It mainly was about the interpretation of the GGOS goals for accuracy (1 mm, 0.1 mm/year), whether the accuracy applies on the session or on the reference frame level and about how these accuracy goals are forwarded to the linking EOP. The significance of the EOP quality reported by IERS (International Earth Rotation Service) was seriously questioned. A number of topics and questions concerning the numerical determination of EOP by VLBI and the effects of Earth rotation theory on VLBI was addressed and was forwarded to the VLBI community by making the presentation available on the website of the IVS Analysis Coordinator, which was under development.

Finally, the aforesaid Splinter Meeting of the IAU/IAG JGW_ThER (SPM1.49) took place at the General Assembly of the European Geosciences Union (EGU) held in Vienna in April 2014. It was open to all interested EGU attendants and timely announced by means of an IERS message (No. 247). It was intended for the presentation of reports of progress on the activities of the three SWG and the whole JWG as well as for discussion. Its agenda was very similar to the one of this dedicated sub-session at the JSR 2014 and the presentations made by Getino, Brzeziński, and Heinkelmann are posted on the JWG web site, as well as a poster that summarize them. Links to all of them are provided in the References section.

3. DISCUSSION

The Sub-Session on the "IAU/IAG Joint Working Group on Theory of Earth Rotation" ended with a general discussion according to the program. It was organized around a block of five questions posed by the JWG Chair, after consulting the Chairs of the Sub-Working Groups:

1. *Should the scope of SWG1 and SWG2 be split based on geophysical/astronomical mechanisms rather than solely by frequency?*

   The previous agreement of the Chairs of both SWGs was ratified: Astronomical components of polar motion associated with the multipole structure of the Earth's inertia tensor, having amplitudes as large as 0.1 mas, should be included in the scope of SWG1 *Precession/Nutation*; but geophysical effects in nutation, primarily the Free Core Nutation and S1 tidal signals that have amplitudes as large as 0.5 mas, should be included in the scope of SWG2 *Polar Motion and UT1*. Of course, SWG1 and SWG2 will continue to work together to coordinate their activities and ensure consistency of their results.

   The next two questions were put forward by the Chair of SWG1, and the respective technical details are provided in his report.

2. *Should the JWG recommend that the IAU2000A nutation theory be corrected to be fully consistent with the IAU2006 precession theory?*

   It was agreed that a Group of Experts be formed to study this issue and make a proposal.

3. *Should the JWG recommend a terminology to be used to make clear the different IAU2000A nutation and IAU2006 precession theories being used with or without consistency corrections?*

   It was agreed that suggestions concerning the terminology would be solicited from the community.

4. *Why are models behind data in terms of accuracy? What are the remaining key limiting factors in of Earth rotation modeling? Should model validation be done using "official" series or is it sufficient to use individual solutions? Should the JWG recommend that EOP be determined as part of a joint determination of ITRF, ICRF, and EOP?*

   Because of time constraints, there was no real discussion of these topics, raised by the Chair of SWG3 as well as the next.

5. *How should the individual improvements to the theory of the Earth's rotation that have been obtained so far be integrated into a consistent theoretical framework?*

   It was agreed that this should be a topic of discussion at future meetings of the JWG.

Finally, it was suggested that the JWG start email discussions of its work in order to increase participation in its activities. Meetings-of-opportunity should still be held at the major conferences (EGU, AGU, IAG, IUGG) but since not everyone can attend these, it would be beneficial if JWG discussions could also be conducted by email.

Acknowledgements. JMF acknowledges partial support of the University of Alicante and of the Spanish government under grant AYA2010-22039-C02-01 from Ministerio de Economía y Competitividad (MINECO). The work of RSG described in this paper was performed at the Jet Propulsion Laboratory, California Institute of Technology, under contract with the National Aeronautics and Space Administration. Support for that work was provided by the Earth Surface and Interior Focus Area of NASA's Science Mission Directorate.

4. REFERENCES

Brzeziński, A., 2014, "Report on activities of the IAU/IAG Joint Working Group on Theory of Earth Rotation, Sub-WG 2 "Polar motion and UT1", presented at SPM1.49, EGU 2014, available at `http://web.ua.es/en/wgther/documentos/report-of-swg-2.pdf`.

Ferrándiz, J.M., Gross, R.S., 2013, "The IAU/IAG Joint Working Group on Theory of Earth Rotation: scope and initial activities", American Geophysical Union, Fall Meeting 2013, #G11C-07, available at `\tthttp://web.ua.es/en/wgther/documentos/agupresentation2013.pdf`.

Ferrándiz, J.M., Gross, R.S., 2014a, "The New IAU/IAG Joint Working Group on Theory of Earth Rotation", In: IAG Symposia, 143, in print.

Ferrándiz, J.M., Gross, R.S., 2014b, "The goal of the IAU/IAG Joint Working Group on the Theory of Earth rotation", In: Proceedings of the Journées 2013 Systèmes de Référence Spatio-Temporels, N. Capitaine (ed.), Observatoire de Paris, pp. 139–143.

Ferrándiz, J.M., Gross, R.S., Heinkelmann, R., Schuh, H., 2014a, "On the IAU/IAG Joint Working Group on the Theory of Earth Rotation", 8th IVS General Meeting, available at `http://web.ua.es/en/wgther/documentos/ivs-gm2014.pdf`

Ferrándiz, J.M., Gross, R.S., Getino, J., Brzeziński, A., Heinkelmann, R., 2014b, "Report of activities of the IAU/IAG Joint Working Group on Theory of Earth rotation", EGU General Assembly 2014, poster #EGU2014-7932, available at `http://web.ua.es/en/wgther/documentos/poster-jwg-ther-egu14.pdf`.

Getino, J., 2014, "Report on activities of the SWG 1 Precession and Nutation", presented at SPM1.49, EGU 2014, available at `http://web.ua.es/en/wgther/documentos/report-of-swg1.pdf`

Heinkelmann, R., 2014, "Report on activities of the SWG 3 Numerical Solutions and Validation", presented at SPM1.49, EGU 2014, available at `http://web.ua.es/en/wgther/documentos/report-of-swg3.pdf`.

Heinkelmann, R., Ferrándiz, J.M., Gross, R.S., Schuh, H., 2014, "IAU/IAG Joint Working Group on the Theory of Earth Rotation", IVS Analysis Workshop, available at `http://web.ua.es/en/wgther/documentos/ivs-analysis.pdf`.

Plag, H.-P., Gross, R., Rothacher, M., 2009, Global Geodetic Observing System for Geohazards and Global Change. Geosciences, BRGM's journal for a sustainable Earth, 9, 96–103.

Plag, H.-P., Pearlman, M. (eds.), 2009, Global Geodetic Observing System: Meeting the Requirements of a Global Society on a Changing Planet in 2020, Springer–Verlag, Berlin–Heidelberg.

REPORT ON ACTIVITIES OF THE SUB-WORKING GROUP 1 "PRECESSION/NUTATION" OF THE IAU/IAG JOINT WORKING GROUP ON THEORY OF EARTH ROTATION

J. GETINO[1], A. ESCAPA[2,3]
[1] Department of Applied Mathematics, University of Valladolid
E-47011 Valladolid, Spain
e-mail: Getino@maf.uva.es
[2] Department of Applied Mathematics, University of Alicante
PO Box 99, E-03080 Alicante, Spain
[3] Department of Mechanical, Informatics, and Aerospace Engineering, University of León
E-24071 León, Spain

ABSTRACT. This is the mid–term report of the Sub-WG1 of the IAU/IAG Joint Working Group on Theory of Earth Rotation (JWG_ThER). The main objectives are (1) to provide some feasible enhancements of current precession/nutation model; (2) to give a list of potential future improvements of that model provided by the contributors of the subgroup, and (3) to raise out some open questions which should be discussed within the JWG_ThER.

1. INTRODUCTION

This contribution[1] is a continuation of the former report (Getino 2014) of the activities of the subgroup presented at EGU 2014 meeting, held in Vienna in April 2014. Here, we focus on some potential actions that could be undertaken in a relatively short term, having in mind the proximity of next General Assemblies of the International Association of Geodesy (IAG GA, 22 June 2015, Prague) and the International Astronomical Union (IAU GA, 2 August 2015, Honolulu).

In particular, we propose feasible enhancements of the current precession/nutation models by completing the changes needed to get full consistency between the new precession theory and the nutation one, and by clarifying the nomenclature to the users. As it is well known both issues are of paramount importance for the objectives of JWG_ThER (e.g., Ferrándiz & Gross 2015).

Besides, we address future improvements of the models. They account for different effects that provide contributions above or near the 10 μas level and might play a role for observational demands, geophysical interpretation, or better consistency. However, it seems quite unlikely that they can be incorporated in an immediate future, since they could entail a change in the basic Earth model considered in IAU2000A nutation.

2. CURRENT PRECESSION/NUTATION MODEL

The XXIVth IAU GA (Manchester 2000) resolution B1.6 adopted a new IAU precession–nutation model (Mathews et al. 2002, MHB2000), fully implemented through IAU 2000A model and IAU 2000B for users needing lower accuracy. The nutational part of the theory represents a clear improvement over the IAU 1980 nutation model, whereas the precessional one is basically that of IAU 1976, updated with corrections to precession rates. It was the cause for an encouraging of the development of new expressions for precession consistent with the IAU 2000A. Finally, this task was accomplished in the XXVIth IAU GA (Prague 2006) where the solution by Capitaine et al. (2003, P03) was adopted as IAU precession model by Resolution B1.

At the highest levels of precision the matching of P03 precession theory with IAU 2000A nutational part is not direct. Some nutation terms must be corrected to keep consistency (Capitaine & Wallace 2006), due to changes of some relevant parameters derived from P03. The main adjustments are due to the inclusion of J_2 rate and to the change in the value of the obliquity ε_0, both considered in P03.

[1] Due to some health problems of J. Getino, A. Escapa is temporarily acting as Co–Chair of Sub-WG1.

The first one contributes to Poisson terms (mixed secular) in nutation both in longitude ψ and obliquity ε (Capitaine & Wallace 2006, Escapa et al. 2014). In addition, it also originates some out of phase terms (Escapa et al. 2015). Numerically some of those contributions are relevant at 1 μas level. Both of them are shown in Tables 1 & 2. As it can be seen the adjustments worked out in both investigations (Table 1) shows a high level of agreement in spite of the different methods used to derive those contributions.

Argument					Period	$t\,d\psi$ (μas/cJ)		$t\,d\varepsilon$ (μas/cJ)	
l_M	l_S	F	D	Ω	Days	CW2006	EGFB2015	CW2006	EGFB2015
+0	+0	+0	+0	+1	-6793.48	47.8	48.0	-25.6	-25.6
+0	+0	+0	+0	+2	-3396.74	-0.6	-0.6	–	–
+0	+0	+2	-2	+2	182.63	3.7	3.5	-1.6	-1.5
+0	+0	+2	+0	+2	13.66	0.6	0.6	–	–

Table 1: Contributions due to J_2 rate (mixed secular). CW2006 and EGFB2015 mean Capitaine & Wallace (2006) and Escapa et al. (2015), respectively. Those contributions less than 0.5 (μas/cJ) are completed with –.

Argument					Period	$d\psi$ (μas)		$d\varepsilon$ (μas)	
l_M	l_S	F	D	Ω	Days	CW2006	EGFB2015	CW2006	EGFB2015
+0	+0	+0	+0	+1	-6793.48	NC	-1.4	NC	-0.8

Table 2: Contributions due to J_2 rate (out of phase terms, nutations). The abbreviations are the same as in Table 1, NC meaning not considered.

The second adjustment affects nutations in longitude through a scale factor $\sin\varepsilon_0$ accounted by Capitaine & Wallace (2006) and also computed in Escapa et al. (2015). Besides it also influences all the reference rigid Earth nutation amplitudes in longitude and obliquity (Escapa et al. 2015), via the orbital functions $B(\varepsilon_0)$ introduced by Kinoshita (1977). For brevity, we refer to the first as 'global rescaling' and to the later as 'consistency of rigid solution'. Those contributions, at the 1 μas level, are displayed in Tables 3 & 4. Again the effects worked out in both researches (Table 3) provide identical values.

Argument					Period	$d\psi$ (μas)	
l_M	l_S	F	D	Ω	Days	CW2006	EGFB2015
+0	+0	+0	+0	+1	-6793.48	-8.1	-8.1
+0	+0	+2	-2	+2	182.63	-0.6	-0.6

Table 3: Contributions due to change in the value of the obliquity ε_0 (global reescaling). The abbreviations are the same as in Table 1.

Let us remark that the adjustments related to the change of the reference rigid Earth nutations (Table 4) are of the same order of magnitude than those due to the global rescaling. Hence, a consistent treatment of the change in the value of the obliquity ε_0 should lead to consider the total corrections (μas, t in cJ)

$$d\psi = (-15.6 - 8.1t)\sin\Omega,\ d\varepsilon = 0.8\cos\Omega, \tag{1}$$

rather than only those displayed in Table 3.

Some of the adjustments due to changes of the precession theory, those from Capitaine & Wallace (2006), are considered in the current IERS Conventions (2010). However, there is no explicit mention in any IAU resolution about the inclusion of those adjustments, which are necessary to ensure compatibility between P03 and MHB2000.

In this way we face with two combinations: (1) P03 (precession, IAU 2006) + MHB2000 (nutation, IAU 2000A) and (2) P03 (precession, IAU 2006) + MHB2000 (nutation, IAU 2000A) + adjustments to MHB2000 (Capitaine & Wallace 2006).

As it was pointed by Urban & Kaplan (2011) this fact has also originated the use of different terminology for designating the same model depending on the source. For example, IERS Conventions (2010)

Argument					Period	$d\psi$ (μas)	$d\varepsilon$ (μas)	$t\,d\psi$ (μas/cJ)	$t\,d\varepsilon$ (μas/cJ)
l_M	l_S	F	D	Ω	Days	EGFB2015			
+0	+0	+0	+0	+1	-6793.48	-7.5	0.8	-8.1	–
+0	+0	+2	-2	+2	182.63	0.5	–	–	–

Table 4: Contributions due to change in the value of the obliquity ε_0 (consistency of rigid solution). The abbreviations are the same as in Table 1. None of these contributions are present in Capitaine & Wallace (2006).

designates (1) as IAU 2006/2000A and (2) as IAU 2006/2000A$_{\rm R06}$. Standards of Fundamental Astronomy (SOFA, e.g., Hohenkerk 2012) uses IAU 2006/2000A (suffix "00A") for (1) and IAU 2006/2000A (suffix "06A") (2). Explanatory Supplement to the Astronomical Almanac (2013) names (1) as IAU 2006/2000A and (2) as IAU 2006/2000A$_{\rm R}$. Therefore, there is a clear need of uniformizing the terminology.

3. FUTURE IMPROVEMENTS OF THE MODEL

After the adoption of IAU2000 model, scientific contributions related to Sub-WG1 issues have focused mainly on new second order effects. These effects comprise terms arising from crossing first order contributions in the perturbation sense (mathematical), and also not modeled (or ill modeled) terms whose magnitude is small (physical). They provide corrections of the order of some tens of μas (or more) whose consideration is nowadays necessary.

Next, we outline the topics contributed by some ordinary and correspondents members of this subgroup. Regrettably, the limitation of space does not allow us to provide full explanations on them. We encourage the interested readers to look up the extended mid–term report (Getino & Escapa 2014) available on-line, as well as the papers reported by the contributors in this issue. There, they will find more details on these topics and a list of the proper references. For brevity, it is just indicated the name of the sender, although some works are the result of their cooperation with other colleagues.

- J. Souchay: Proposes to study the influence of the Moon when considering it as a triaxial, not pointlike object; (proposal) to study the precession–nutation in primary ages of the solar system, when the Moon was considerably closer to the Earth.
- C. Huang: Earth nutation and its coupling with the magnetic field; new theory of Earth rotational modes (application to Free Core Nutation); a generalized theory of the figure of the Earth interior.
- J. Müller: Nutation determined from only Lunar Laser Ranging (LLR) data.
- J. Vondrák: Geophysical excitation of nutations by numerical integration of Brzeziński's broad–band Liouville equations.
- Y. Barkin: Study of the perturbed rotational motion of the Earth caused by the weak variation of the mass geometry and the angular momentum of the relative motion of the planet particles.
- V. Dehant & M. Folgueira: Topographic coupling at core-mantle boundary in rotation and orientation changes of planets.
- A. Brzeziński: (JWG_ThER organizational proposal) Convenience of splitting up the scope of Sub-WG1 and Sub-WG2 based on geophysical mechanism: the geophysical excitations of nutations (long period) should be considered by Sub-WG2, while modeling the librations (astronomical) in polar motion by Sub-WG1; atmospheric and oceanic excitation of the Free Core Nutation estimated from recent geophysical models; on estimation of the high frequency geophysical signals in Earth rotation by complex demodulation.
- A. Escapa: Direct effects of the rotation of the inner core; influence of the triaxiality on the Earth rotational motion.
- J. Getino: New perturbation technique to integrate higher orders in the Earth rotation theory.
- J. M. Ferrándiz: Nutation and precession couplings (consistency) due to second order and tidal effects of the non–rigid Earth.

4. DISCUSSION

Accordingly to the former sections some questions arise in a natural way. They were opened to the discussion by Sub-WG1 members and, in general, to all JWG_ThER (Ferrándiz & Gross 2015). On the one hand, there are three questions related with the adjustments to IAU 2000A (nutation) induced by IAU 2006 (precession), which could be addressed in a relatively short term:

1. *Should the current numerical values of the adjustments to MHB2000 nutations (Capitaine & Wallace 2006) be completed (see Section 2)?*
2. *Should combination of P03 (precession, IAU 2006) + MHB2000 (nutation, IAU 2000A) + adjustments to MHB2000 be officially supported by IAU/IAG JWG_ThER through some action?*
3. *Should IAU/IAG JWG_ThER suggest or recommend a clear terminology for the models/algorithms in use, e.g., Urban & Kaplan (2012), etc.?*

On the second one, there are some questions related with the future improvement of the current nutation/precession model. However, the integration of described effects (Section 3) into a single consistent theory presents a complex scenery, which requires deeper considerations, for example:

1. *Could IAU2000A basic (symmetric) Earth model be preserved or should we move to another more sophisticated model?*
2. *How to homogenize their theoretical analysis to "plug" them into a global model?*
3. *How much of this task can be carried out in the current term of the JWG_ThER?*

Acknowledgements. We thank the contributions to this report made by the Sub-WG1 members Y. Barkin, Russia; V. Dehant, Belgium; J. Ferrándiz, Spain; M. Folgueira, Spain; CL. Huang, China; J. Müeller, Germany; J. Souchay, France, and J. Vondrák, Czech Republic; the correspondent members G. Kaplan, USA and S. Urban, USA, and the chair of Sub-WG2 A. Brzeziński, Poland.

The autors' work has been partially supported by the Spanish government under MINECO projects AYA201022039-C02-01, AYA2010-22039-C02-02, and the Generalitat Valenciana, project GV/2014/072.

5. REFERENCES

Capitaine, N., Wallace, P.T., Chapront, J., 2003, "Expressions for IAU 2000 precession quantities", A&A, 412, pp. 567–586.

Capitaine, N., Wallace, P.T., 2006, "High precision methods for locating the celestial intermediate pole and origin", A&A, 450, pp. 855–872.

Escapa, A., Getino, J., Ferrándiz, J., Baenas, T., 2014, On the changes of the IAU 2000 nutation theory stemming from IAU 2006 precession theory, Proceedings of the Journées 2013 Systèmes de Référence Spatio-Temporels, N. Capitaine (ed.), Observatoire de Paris, pp. 148–151.

Explanatory Supplement to the Astronomical Almanac, 3rd edition, 2013, S.E. Urban, P.K. Seidelmann (eds.), University Science Books.

Ferrándiz, J.M., Gross, R.S., 2015, "Report on Activities of the IAU/IAG Joint Working Group on Theory of Earth Rotation", this volume, pp. 127–130.

Getino, J., 2014, "Report on activities of the SWG 1 Precession and Nutation", presented at SPM1.49, EGU 2014, available at `http://web.ua.es/en/wgther/presentations.html`.

Getino, J., Escapa, A., 2014, "Extended mid-term report on activities of the SWG 1 Precession and Nutation", available at `http://web.ua.es/en/wgther/presentations.html`.

Hohenkerk, C.Y., 2012, "SOFA and the algorithms for transformations between time scales & between reference systems", Proc. Journées 2011 Systèmes de référence spatio-temporels, H. Schuh, S. Böhm, T. Nilsson, N. Capitaine (eds.), Vienna University of Technology, pp. 21–24.

IERS Conventions, 2010, G. Petit, B. Luzum (eds.), IERS Technical Note 36.

Kinoshita, H., 1977, "Theory of the rotation of the rigid Earth", Celest. Mech. Dyn. Astr., 15, pp. 277–326.

Mathews, P.M., Herring, T.A., Buffett, B.A., 2002, "Modeling of nutation and precession: new nutation series for nonrigid Earth and insights into the Earth's interior", J. Geophys. Res., 107(B4), 2068.

Urban, S.E. & Kaplan, G. H., 2012, "Nomenclature for the current precession and nutation models", Proc. Journées 2011 Systèmes de r éférence spatio-temporels, H. Schuh, S. Böhm, T. Nilsson, N. Capitaine (eds.), Vienna University of Technology, pp. 270–271.

REPORT ON ACTIVITIES OF THE SUB-WORKING GROUP 2 "POLAR MOTION AND UT1" OF THE IAU/IAG JOINT WORKING GROUP ON THEORY OF EARTH ROTATION

A. BRZEZIŃSKI[1,2]
[1] Inst. of Geodesy and Geodetic Astronomy, Warsaw University of Technology, Warsaw, Poland
[2] Space Research Centre, Polish Academy of Sciences, Warsaw, Poland
e-mail: alek@cbk.waw.pl

ABSTRACT. This is the mid-term report of the Sub-WG2. The main objectives are (1) to summarize the status of the current theories of Earth rotation focusing on variations with long and diurnal periods, and on modeling of geophysical excitations; (2) to point out some unsolved problems which should be discussed by the Sub-WG2.

1. INTRODUCTION

The purpose of this report is to define the framework for discussion of the S-WG2. We start from description of the definitions and current conventions regarding polar motion and UT1, and end up with proposal of splitting up the scope of considerations between S-WG1 and S-WG2. Section 3 is devoted to the review of the theory of polar motion, giving the list of simplifying assumptions and defining the improvements of the theory which should be done first. We also mention some selected recent publications contributing to the progress in the theory. The last part of report is devoted to the subject of geophysical excitation. Due to the limited space of the paper, we give only a brief review of the current situation and point out some problems which should be considered by the S-WG2.

2. POLAR MOTION AND UT1 VARIATION, DEFINITIONS AND CONVENTIONS

According to the classical definition, a change of direction of the Earth's rotation axis with respect to the Earth-fixed reference system is called *polar motion* while a change with respect to the space-fixed reference system is called *nutation*. The *universal time UT1* is a parameter used to measure the angular speed of rotation. However, according to the current convention the reference pole for polar motion and nutation is not the instantaneous rotation pole but the conventional pole called the *Conventional Intermediate Pole* (CIP). Also UT1 expresses the rotation rate about the CIP axis. The equatorial component of rotation is split up into polar motion and nutation based on the frequencies of perturbations (IERS Conventions, 2010) – all perturbations with space-referred periods longer than 2 days are treated as nutation and all other as polar motion. Hence, the frequency domain of nutation, expressed in the celestial system, is the interval $(-0.5\Omega, +0.5\Omega)$, where Ω denotes the mean angular frequency of diurnal sidereal rotation. The frequency domain of polar motion, expressed in the terrestrial system, is $(-\infty, -1.5\Omega) \cup (-0.5\Omega, +\infty)$ therefore polar motion comprises both the low-frequency and the high-frequency components.

To the first order, the time variations of the terrestrial coordinates of the CIP are related to those of the instantaneous rotation pole by a simple differential relationship, therefore the equation of polar motion can be transformed to the form using the reported parameters as variables.

As far as we are interested in the scientific aspects of Earth rotation, a more adequate decomposition into polar motion and nutation is based on the excitation mechanism:

- astronomical effects (due to the lunisolar and planetary torques upon the rotating Earth) are considered as nutation;
- geophysical effects (due to the mass and angular momentum exchanges between the solid Earth and its liquid envelopes) are considered as polar motion.

Our proposal to the WG Chairs and members is to follow the last decomposition in the discussion of the WG, that means

- astronomical components of polar motion, which are associated with the multipole structure of the Earth's inertia tensor (size up to 0.1 mas), should be considered by the S-WG1 "Precession/nutation";
- geophysical effects in nutation, mainly the FCN and S1 signals (size up to 0.5 mas), should be considered by the S-WG2 "Polar motion and UT1"; see the next section.

3. THEORY OF POLAR MOTION AND UT1 VARIATION

Long periods. The investigations of polar motion and UT1 variation are usually based on the linear equations of Earth rotation, developed originally by Munk and MacDonald (1960) who introduced the perturbation scheme into the Liouville equations. Later on, Wahr (1982, 1983, 2005) derived a more general linear equations of motion based on the earlier models of Hough (1895), Dahlen (1976), and Smith and Dahlen (1981). Gross (2007, 2015) recomputed the coefficients of the equations of Wahr using the most up-to-date values of geodetic and geophysical constants. He proposed a hybrid theory in which: 1) the body tide Love number k_2 has been replaced with a wobble-effective Love number k_w computed from normal mode theory in order to more accurately model the structure of the core and the deformation of the crust and mantle; and 2) the theoretical Chandler wobble frequency has been replaced with its observed value in order to account for the effects of mantle anelasticity since no adequate theory of these effects currently exists.

The linear equations of Earth rotation are expressed by the excitation variables: h_ℓ which are components of the relative angular momentum vector $\vec{h} = [h_1\ h_2\ h_3]^T$ defining the motion term of excitation, and $c_{\ell j}$ – the incremental components of the Earth's inertia tensor defining the mass term of excitation, and by the rotational variables m_ℓ related to the rotation vector $\vec{\omega} = \Omega\,[m_1\ m_2\ 1{+}m_3]^T$. Gross (2015) summarized the simplifying assumptions underlying the linearized theory of Earth rotation as follows

- the perturbing excitations are small with $h_\ell(t) \ll \Omega C$ and $c_{\ell j}(t) \ll C$, where C denotes the principal axial moment of inertia of the whole Earth;
- the rotational response of the Earth is small with $m_\ell(t) \ll 1$;
- the induced relative angular momentum of the core is linearly related to changes in the rotation of the solid Earth;
- the induced deformations of the mantle, crust, and oceans are linearly related to the changes in rotation;
- the rotating terrestrial reference frame is the Tisserand mean-mantle frame;
- the oceans stay in equilibrium as the rotation changes;
- the core is uncoupled from the mantle;
- the crust, mantle, and core are axisymmetric;
- the rotational variations occur on time scales much longer than a day;
- the coupling between the components of rotation introduced by a non-uniform ocean are negligibly small and hence can be ignored to first order;
- the difference in the oceanic Love number for the two components of polar motion is negligibly small and hence to first order can be replaced by a mean oceanic Love number for the wobble.

With the current accuracy of determination of the Earth orientation parameters, which is at the level of 0.05 mas corresponding to 1.5 mm, some of those simplifications are no more adequate. Gross (2015) proposed the following improvements of the theory of Earth rotation to be considered first

- the theory should describe the rotation of a triaxial body with a fluid core;
- the theory should account for the non-equilibrium response of the oceans which is particularly important at the fortnightly period.

Several promising advances in modeling Earth rotation, which are along those guidelines, have been reported recently. We should mention here the three papers by Wei Chen and his co-workers: 1) Chen and Shen (2010) have developed a theory of the Earth's rotation that accounts for the triaxiality of the mantle and core, the anelasticity of the mantle, and dissipation in the oceans; 2) Chen et al. (2013a) attempted to improve the polar motion theory by developing refined frequency-dependent transfer functions with the most recent models for ocean tides, the Earth's rheology, and core-mantle coupling; in the associated paper, Chen et al. (2013b) applied the frequency-dependent transfer function to compare the geophysical excitations derived from various global atmospheric, oceanic, and hydrological models.

Other interesting recent contribution is by Bizouard and Zotov (2013) who have developed a theory of the Earth's rotation that accounts for the triaxiality of the Earth and includes the effect of asymmetric, but still equilibrium, oceans.

Diurnal periods, the free core nutation resonance. Sasao and Wahr (1981) showed that diurnal atmospheric and oceanic loading of the Earth's surface provide an efficient excitation mechanism of the free core nutation (FCN) signal. They developed dynamical model of diurnal excitation including both the FCN and the Chandler wobble (CW) resonances. A new dynamical model of the excitation of nutation by geophysical fluids has been recently published by Koot and de Viron (2011). The corresponding dimensionless response coefficients a_p, a_w appearing in the broad-band Liouville equation of polar motion (Brzeziński, 1994), expressing how sensitive is the FCN mode relative the CW mode to the excitation by the mass and motion terms of the atmospheric and oceanic angular momenta, are the following:

Sasao and Wahr (1981): $a_p = 9.509 \times 10^{-2}$, $a_w = 5.489 \times 10^{-4}$;
Koot and de Viron (2011): $a_p = 9.200 \times 10^{-2}$, $a_w = 2.628 \times 10^{-4}$.

The difference of the two estimates of the pressure term coefficient a_p is small, at the level of 3%, and much larger in case of the wind term coefficient. The new value of a_w is about two times smaller than the old one. Note, however, that the contribution of the wind term has been usually considered small and neglected in the FCN excitation studies.

Geophysical excitation functions. The influence of geophysical fluids, the atmosphere, the oceans and the land hydrosphere, is a dominant source of the excitation of polar motion and plays an important role in driving variations in UT1; see Gross (2007) for review. Hence modeling the dynamics of geophysical fluids and comparison with the observed polar motion and UT1 is of crucial importance for understanding variability of Earth rotation at time scales from subdaily to decadal. The global atmospheric, oceanic and hydrological angular momentum (AAM, OAM, and HAM, respectively) data have been estimated and made available for the users by the International Earth Rotation Service (IERS) and its special bureaus.

The AAM series have been estimated by several meteorological agencies on regular basis since almost 3 decades, and some of the series begin around 1950. Particularly important are the multidecadal reanalysis series offering several advantages over the routine operational series. As a rule, the sampling interval of AAM is 6 hours that enables studies of excitation at periods from daily to decadal.

The first OAM series were computed in the middle of 1990-ties, but only recently three OAM series have been updated on regular basis. Two of them are produced by the Jet Propulsion Laboratory, USA, with daily sampling, and one by the GeoForschungsZentrum (GFZ) Potsdam, Germany, with 6-hourly sampling.

Several HAM series based on different hydrology models have been published so far. Only one HAM series, estimated by the GFZ, has been regularly updated and made available for users via the IERS website. Note however that in contrast to AAM and OAM, the contribution from HAM is expected to be important only at seasonal and lower frequencies.

Adding OAM improved in most cases the agreement with the observed (geodetic) excitation of polar motion. Unfortunately, there are still large differences between the HAM models, therefore combining HAM with AAM and OAM at seasonal frequencies is still far from being conclusive.

The mass redistribution within the surficial geophysical fluids can also be estimated from the time variations of gravity measured by the satellite experiment GRACE. Hence, the GRACE-based "gravimetric" excitation function can be considered as an equivalent of the mass term of AAM+OAM+HAM. That makes it useful for studying excitation of polar motion, where the contribution from the mass term is dominant. However, the low time resolution of GRACE data (1 month) and the limited period of data (from 2002 up to now), impose a frequency limit on its application for the excitation studies. Also various estimates of the GRACE-based excitation series are still not fully consistent with each other and do not close the seasonal excitation balance of polar motion.

4. DISCUSSION

Here we attempt to list some important problems which should be addressed in the discussion of S-WG2:

- Improving excitation balance of the seasonal variations, particularly in polar motion. That includes also improvements of the estimation of geophysical and gravimetric excitation functions.
- Explaining the excitation mechanism of the free signals in Earth rotation, the free core nutation FCN and the Chandler wobble CW; that includes also improvement of the FCN and CW parameters.
- Estimation of the contribution of diurnal and subdiurnal atmospheric tides to polar motion, UT1 and nutation, particularly modeling of the S_1 tide.

- Improvement of the model of the ocean tide contributions to all 3 components of Earth rotation, polar motion, UT1 and precession/nutation.

Additional problems, put forward by Wei Chen and Jim Ray, concern the differences between the terrestrial system (ITRS) and its realization (ITRF):

- the ITRF is geocentric in a long-term average sense (CF frame) whereas the ITRS is instantaneously geocentric, following the resolutions of the IAU and IUGG;
- the ITRS is also geocentric in the general relativistic sense and the appropriate timescale (TCG) and SI units are recommended by the Unions. However, for very practical reasons, times related to terrestrial time TT (e.g., UTC) are used by all geodetic analysts.

We should add here that also equations of motion which are used in practice are all derived under the assumption that the underlying Cartesian system is instantaneously geocentric.

Acknowledgements. I thank the following members and corresponding members of the S-WG2 who contributed to this report: Ch. Bizouard, France; B. Chao, Taipei; W. Chen, China; R. Gross, USA; W. Kosek and J. Nastula, Poland; J. Ray, USA; M. Schindelegger, Austria. The Local Organizing Committee of the Journées 2014 is acknowledged for the free accommodation and waiving the registration fee. This work and participation in the conference was supported by the Polish national science foundation NCN under grant No. DEC-2012/05/B/ST10/02132.

5. REFERENCES

Bizouard, C., Zotov, L., 2013, "Asymmetric effects on polar motion", Cel. Mech. Dyn. Astron., 116(2), pp. 195–212.

Brzeziński, A., 1994, "Polar motion excitation by variations of the effective angular momentum function, II: extended model", manuscripta geodaetica, 19, pp. 157–171.

Chen, W., Shen, W., 2010, "New estimates of the inertia tensor and rotation of the triaxial nonrigid Earth", J. Geophys. Res., 115, B12419, doi:10.1029/2009JB007094.

Chen, W., Ray, J., Li, J., Huang, C., Shen, S., 2013a, "Polar motion excitations for an Earth model with frequency-dependent responses: 1. A refined theory with insight into the Earth's rheology and core-mantle coupling", J. Geophys. Res.: Solid Earth, 118(9), pp. 4975–4994, doi:10.1002/jgrb.50314.

Chen, W., Ray, J., Shen, S., Huang, C., 2013b, "Polar motion excitations for an Earth model with frequency-dependent responses: 2. Numerical tests of the meteorological excitations", J. Geophys. Res.: Solid Earth, 118(9), pp. 4995–5007, doi:10.1002/jgrb.50313.

Dahlen, F.A., 1976, "The passive influence of the oceans upon the rotation of the Earth", Geophys. J. Roy. Astr. Soc., 46, pp. 363–406.

Gross, R.S., 2007, "Earth rotation variations – long period", In: Herring T.A. (ed.), Physical Geodesy: Treatise on Geophysics, Vol. 3, Elsevier, Oxford, pp. 239–294.

Gross, R.S., 2015, "Theory of Earth rotation variations", In: N. Sneeuw (ed.), IAG Symposia, 142, in press.

Hough, S.S., 1895, "The oscillations of a rotating ellipsoidal shell containing fluid", Phil. Trans. R. Soc. London A, 186, pp. 469–506.

IERS Conventions, 2010, G. Petit, B. Luzum (eds.), IERS Technical Note 36, Frankfurt am Main: Verlag des Bundesamts für Kartographie und Geodäsie.

Koot, L., de Viron, O., 2011, "Atmospheric contributions to nutations and implications for the estimation of deep Earth's properties from nutation observations", Geophys. J. Int., 185, pp. 1255–1265.

Sasao, T., Wahr, J., 1981, "An excitation mechanism for the free 'core nutation' ", Geophys. J. Roy. Astr. Soc., 64, 729–746.

Smith, M.L., Dahlen, F.A., 1981. "The period and Q of the Chandler wobble", Geophys. J. Roy. Astr. Soc., 64, 223–281.

Wahr, J.M., 1982, "The effects of the atmosphere and oceans on the Earth's wobble – I. Theory", Geophys. J. Roy. Astr. Soc., 70, pp. 349–372.

Wahr, J.M., 1983, "The effects of the atmosphere and oceans on the Earth's wobble and on the seasonal variations in the length of day - I. Results", Geophys. J. Roy. Astr. Soc., 74, 451–487.

Wahr, J.M., 2005, "Polar motion models: Angular momentum approach", In: Forcing of Polar Motion in the Chandler Frequency Band: A Contribution to Understanding Interannual Climate Change, H.-P. Plag, B.F. Chao, R. S. Gross, T. van Dam (eds). Cahiers du Centre Européen de Géodynamique et de Séismologie vol. 24, Luxembourg, 89–102.

REPORT ON ACTIVITIES OF THE SUB-WORKING GROUP 3 "NUMERICAL SOLUTIONS AND VALIDATION" OF THE IAU/IAG JOINT WORKING GROUP ON THEORY OF EARTH ROTATION

R. HEINKELMANN
Helmholtz Centre Potsdam, GFZ German Research Center for Geosciences
Telegrafenberg, 14473 Potsdam, Germany
e-mail: heinkelmann@gfz-potsdam.de

ABSTRACT. In this report I briefly summarize the latest activities of the Sub Working Group 3: Numerical Solutions & Validation members under the IAU/IAG Joint Working Group on Theory of Earth Rotation. I present a list of selected publications and point out unsolved problems that could be addressed by the Sub Working Group.

1. THE SUB WORKING GROUP

Sub Working Group 3 on Numerical Solutions & Validation consists of 18 members chaired by R. Heinkelmann. The communication among the Sub Working Groups is ensured by cross - Sub Working Group members. Those members are printed in bold fonts in Table 1.

Chao, B.F.	Taipei	**Gross, R.**	USA	**Rogister, Y.**	France
Chen, W.	China	**Huang, C.-L.**	China	Sansaturio, M.E.	Spain
Dehant, V.	Belgium	Luzum, B.	USA	**Schuh, H.**	Germany
Ferrándiz, J.	Spain	Malkin, Z.	Russia	**Seitz, F.**	Germany
Gambis, D.	France	Navarro, J.F.	Spain	Thomas, M.	Germany
Gerlach, E.	Germany	**Ray, J.**	USA	**Wang, Q.J.**	China

Table 1: Members of the Sub Working Group 3: Numerical Solution & Validation. The members in bold characters are members in other Sub Working Groups as well.

2. STATUS OF THE NUMERICAL SOLUTIONS AND VALIDATIONS

The results from numerical solutions suffer from simplifications of solid Earth models, from incomplete consideration of the interactions of the spheres of the Earth system or from neglecting of certain coupling mechanisms between some of the solid Earth components. In addition, there are computational limitations and limitations through the neglected relativistic background. There are various groups working on improving numerical solutions of Earth rotation. Recent progress has been obtained in particular through the following activities:

- inclusion of more realistic non-rigid Earth models such as elastic Earth models (Getino & Ferrándiz, 1995), two layer Earth models (Getino, 1995; Getino, et al., 2000, Getino & Ferrándiz, 2001, Ferrándiz, et al., 2004) or three layer Earth models (Escapa, et al., 2001), and the symbolic processor for the Earth rotation theory (Navarro & Ferrándiz, 2002),
- development of refined numerical methods such as the application of the Galerkin method for the determination of a new multiple layer spectral method (Huang & Zhang, 2015),
- coupling of certain solid Earth components, e.g. core-mantle boundary (Huang, et al., 2011; Malkin, 2013) or inner core boundary (Dehant, et al., 2013),
- interaction of spheres of the Earth system, e.g. coupled atmosphere-ocean angular momentum (Seitz & Thomas, 2012), and the
- formulation of Earth rotation in a consistent relativistic setting (Klioner, et al., 2010; Gerlach, et al., 2012).

Validation of Earth rotation theory can be achieved by comparison with results obtained from space geodetic techniques. The determination of Earth Orientation Parameters (EOP) is based on the analysis of observations of the space geodetic techniques that are combined applying various procedures. Since the two last International Terrestrial Reference Frames (ITRF) the conventional EOP are determined together with the ITRF, currently IERS 08 C04 together with ITRF2008 (Altamimi, et al., 2011), what ensures the consistency among those products. The TRF coordinate model allows for a simple determination of a position at an epoch inside the data time span. Without a significant loss of quality it can also be used for the extrapolation to the outside of the data time span. Different from that, the EOP are treated as time series with a sampling of usually one day. Consequently, the EOP have to be predicted or updated and between the part that is determined together with ITRF and the updates the consistency has to be ensured. The consistency with the International Celestial Reference Frame (ICRF) is only indirectly achieved via the VLBI observations that enter the ITRF and EOP computations. Within the multi-technique combination, so far no special attention has been paid on the consistency with ICRF. The VLBI observations are adjusted together with other observations that refer to other space segments, for example to satellite orbits. The ICRF and those space segments do not necessarily have the same orientation giving rise to inconsistencies.

For the quality of the validation using space geodetic techniques the consistency among the techniques and among the reference frames is of highest importance. Various studies have been carried out to assess the level of consistency among the conventional reference frames and the EOP, e.g. Malkin (2012); Heinkelmann et al., (2015a, 2015b). Progress in the validation of the IAU 2006/2000 precession-nutation has been achieved in particular through comparison with VLBI data (Capitaine, et al., 2009; Capitaine, et al., 2012; Malkin, 2014b). The validation shows that the values of the celestial pole offset and the main nutation terms require correction.

In the current situation the theoretical results are believed to be less precise than the observational results from space geodetic techniques. Besides the abovementioned limitations this is partly due to the fact that some of the observed effects are free modes that can not be rigorously predicted, e.g. the free core nutation (FCN). The current IAU2006/2000 precession-nutation model includes only an empirical model for FCN[1]. This model needs to be updated and the updates have to be made consistent with the original model that was derived from the data used for the creation of ITRF2008 and IERS 08 C04. As an alternative to the deterministic model, FCN can be described by stochastic models, e.g. by time series models (Brzeziński & Kosek, 2004). The other way around there are predicted motions that have not yet been observed, e.g. the free inner core nutation (FICN; Lambert, et al., 2013; Malkin, 2014a). The confirmation of the FICN through observations would probably help the theoretical developments significantly. As a consequence, model parameters are compared to or fitted to observations. Hence, improvements of the observations of the space geodetic techniques do not necessarily help to improve the theory of Earth rotation. The quality of reduction of space geodetic observations by applying the models of Earth rotation lags behind the quality of the observations and prohibits further progress in the analysis.

3. REFERENCES

Altamimi, Z., Collilieux, X., Métivier, L., 2011, "ITRF2008: an improved solution of the international terrestrial reference frame", J. Geod., 85, pp. 457–473.

Brzeziński, A., Kosek, W., 2004, "Free core nutation: stochastic modelling versus predictability", In: Proc. Journées 2003 Systèmes de référence spatio-temporels 2003, A. Finkelstein, N. Capitaine (eds.), Institute of Applied Astronomy, St. Petersburg, pp. 99–106.

Capitaine, N., Mathews, P.M., Dehant, V., Wallace, P.T., Lambert, S.B., 2009, "On the IAU 2000/2006 precession-nutation and comparison with other models and VLBI observations", Celest. Mech. Dyn. Astr., 103, pp. 179–190.

Capitaine, N., Lambert, S.B., Yao K., Liu J., 2012, "Evaluation of the accuracy of the IAU 2006/2000 precession-nutation", JD7 Space-time reference systems for future research, 28th IAU GA, Bejing, China, August 2012,
`http://referencesystems.info/uploads/3/0/3/0/3030024/capitaine_6.07.pdf`.

Dehant, V., Lambert, S.B., Koot, L., Trinh, A., Folgueira, M., 2013, "Recent advances in applications of geodetic VLBI to geophysics", In: IVS 2012 General Meeting Proc., D. Behrend, K.D. Baver (eds.),

[1] `http://syrte.obspm.fr/~lambert/fcn/`

NASA/CP-2012-217504, http://ivscc.gsfc.nasa.gov/publications/gm2012/.
Escapa, A., Getino, J., Ferrándiz, J.M., 2001, "Canonical approach to the free nutations of a three-layer Earth model", J. Geophys. Res., 106(B6), pp. 11,387–11,397.
Ferrándiz, J.M., Navarro, J.F., Escapa, A., Getino, J., 2004, "Precession of the nonrigid earth: effect of the fluid outer core", AJ, 128, pp. 1407–1411.
Gerlach, E., Klioner, S.A., Soffel, M.H., 2012, "A new numerical theory of Earth rotation", JD7 Space-time reference systems for future research, 28th IAU GA, Bejing, August 2012, http://referencesystems.info/uploads/3/0/3/0/3030024/2012_jd7.pdf.
Getino, J., Ferrándiz, J.M., 1995, "On the effect of the mantle elasticity on the Earth's rotation", Celest. Mech. Dyn. Astr., 61, pp. 117–180.
Getino, J., Ferrándiz, J.M., 2001, "Forced nutations of a two layer Earth model", MNRAS, 322, pp. 785–799.
Getino, J., 1995, "Forced nutations of a rigid mantle-liquid core earth model in canonical formulation", Geophys. J. Int., 122, pp. 803–814.
Getino, J., Escapa, A., Miguel, D., 2000, "General theory of the rotation of the non-rigid Earth at the second order. I. The rigid model in Andoyer variables", AJ, 139, pp. 1916–1934.
Heinkelmann, R., Karbon, M., Nilsson, T., Raposo-Pulido, V., Soja, B., Schuh H., 2015a, "Reference frame-induced errors in VLBI Earth orientation determinations", In: IAG Symposia, 143, in print.
Heinkelmann, R., Belda-Palazón, S., Ferrándiz, J.M., Schuh, H., 2015b, "The consistency of the current conventional celestial and terrestrial reference frames and the conventional EOP series", this volume, pp. 224–225.
Huang, C.-L., Dehant, V., Liao, X.-H., Van Hoolst, T., Rochester, M.G., 2011, "On the coupling between magnetic field and nutation in a numerical integration approach", J. Geophys. Res., 116, B03403, doi: 10.1029/2010JB007713.
Huang, C.-L., Zhang, M., 2015, "Do we need various assumptions to get a good FCN?", this volume, pp. 206–210.
Klioner, S.A., Gerlach, E., Soffel, M.H., 2010, "Relativistic aspects of rotational motion of celestial bodies", In: Proc. IAU Symp. 261 "Relativity in Fundamental Astronomy", S.A. Klioner, P.K. Seidelman, M.H. Soffel (eds.), doi:10.1017/S174392130999024X.
Lambert, S.B., Rosat, S., Cui, X., Rogister, Y., Bizouard, C., 2013, "A search for the free inner core nutation in VLBI data", In: IVS 2012 General Meeting Proc., D. Behrend, K.D. Baver (eds.), NASA/CP-2012-217504, http://ivscc.gsfc.nasa.gov/publications/gm2012/.
Malkin, Z., 2012, "Connecting terrestrial to celestial reference frames", JD7 Space-time reference systems for future research, 28th IAU GA, Bejing, China, August 2012, http://www.referencesystems.info/uploads/3/0/3/0/3030024/malkin-jd7-systems.pdf.
Malkin, Z., 2013, "Free core nutation and geomagnetic jerks", J. Geodyn., 72, pp. 53–58.
Malkin, Z., 2014a, "On detection of the free inner core nutation from VLBI data", Proc. Journées 2013 "Systèmes de Référence Spatio-Temporels", N. Capitaine (ed.), Observatoire de Paris, pp. 224–225.
Malkin, Z., 2014b, "On the accuracy of the theory of precession and nutation", Astron. Rep., 58(6), pp. 415–425.
Navarro, J.F., Ferrándiz, J.M., 2002, "A new symbolic processor for the Earth rotation theory", Celest. Mech. Dyn. Astr., 82, pp. 243–263.
Seitz, F., Thomas, M., 2012, "Simulation, prediction and analysis of Earth rotation parameters with a dynamic Earth system model", In: Proc. Journées Systèmes de référence spatio-temporels 2011, H. Schuh, S. Böhm, T. Nilsson, N. Capitaine (eds.), Vienna University of Technology, Vienna, pp. 109–112.

Session 4

EARTH'S ROTATION AND GEODYNAMICS

ROTATION DE LA TERRE ET GÉODYNAMIQUE

THE GLOBAL S_1 TIDE AND EARTH'S NUTATION

M. SCHINDELEGGER[1], J. BÖHM[1], D.A. SALSTEIN[2]
[1] Department of Geodesy and Geoinformation, Vienna University of Technology
27-29 Gußhausstraße, A-1040 Wien, Austria
e-mail: michael.schindelegger@tuwien.ac.at, johannes.boehm@tuwien.ac.at,
[2] Atmospheric and Environmental Research, Inc.
131 Hartwell Avenue, Lexington, MA 02421-3126, USA
e-mail: dsalstei@aer.com

ABSTRACT. Diurnal S_1 tidal atmospheric oscillations induced by the cyclic heating of air masses through solar radiation elicit a small contribution to Earth's prograde annual nutation at a level of 100 μas (microarcseconds). Previously published estimates of this Sun-synchronous perturbation based on angular momentum series from global geophysical fluid models have however diverged, and within the present conventional nutation theory, the effect has been instead accounted for in an empirical manner based on analyzing residual spectra of observed celestial pole offsets. This study constitutes a first, tentative reassessment of the S_1 signal in nutation by resorting to modern-day atmospheric reanalyses as well as available hydrodynamic solutions for diurnal oceanic angular momentum changes that are driven by daily air pressure variations at the water surface. We elucidate the global character of the S_1 tide with particular regard to Earth rotation variations and investigate to which extent atmospheric and oceanic excitation terms from various sources can be superimposed. The combined influence of the principal diurnal tide on Earth's nutation, associated with both atmosphere and ocean dynamics, is found to yield a sound agreement with its observational evidence from geodetic VLBI (Very Long Baseline Interferometry) measurements.

1. INTRODUCTION

Describing Earth's orientation in space is a multidisciplinary topic that has attracted the interest of astronomers, geophysicists, and geodesists alike. The currently most accurate model of precession-nutation, i.e. the spatial motion of a conventional reference axis relative to a quasi-inertial system, has been elaborated by Mathews et al. (2002, MHB for short) as a semianalytical theory built upon both a comprehensive model for nutational motions of a non-rigid Earth as well as the assistance of VLBI observations to constrain basic Earth parameters by means of a least-squares fit. Additional effects of external geophysical fluids, such as those from gravitationally-forced ocean tides, have been accounted for in an a priori fashion or via iterative adjustment based on well-established values of oceanic angular momentum (OAM). By analogy, Mathews et al. (2002) anticipated diurnal radiational tides in the atmosphere to evoke small seasonal nutations; though—given the lack of adequate atmospheric angular momentum (AAM) estimates at that time—the authors were left incapable of constructing proper theoretical estimates of the atmosphere-induced nutations to match their observational evidence in VLBI data. As a result, particularly pronounced residuals at the order of 100 μas were registered at the prograde annual nutation frequency and ascribed to the forcing of the principal diurnal S_1 wave. Opting for an empirical but still accurate representation of this anomaly in their model, Mathews et al. (2002) subtracted the S_1 contribution from their observational data prior to adjustment and superimposed the very same values as postfit corrections to the final nutation series.

In keeping with one of the earlier fundamental recommendations (Fedorov and Smith, 1980) of the International Astronomical Union (IAU), it is still desirable to eschew a purely empirical account of the S_1 residual as in MHB's case and replace it by an unambiguous explanation in terms of angular momentum estimates from geophysical fluid models. While several studies have pursued this idea, including Brzeziński et al. (2004) or Brzeziński (2011), a sufficiently good agreement with MHB's postfit correction term has not been documented yet. This mismatch prompts the conclusion that the diurnal AAM/OAM estimates deduced from global numerical atmosphere-ocean models were of subpar quality and that a renewed consideration of the S_1 signal in nutation from the viewpoint of up-to-date geophysical fluid

models is warranted. The present paper serves as a preparatory text for such a thorough investigation (Schindelegger et al., 2015) and is conceptualized to recall the nature of the global radiational S_1 tide, to assemble estimates of its impact on nutation from published and newly probed sources, and to present some initial explorations on the likely consensus between geophysical and geodetic excitation quantities at the prograde annual frequency.

2. THE ATMOSPHERIC S_1 TIDE

Solar tides in the atmosphere are ubiquitous oscillations occurring in all types of surface and vertical parameters at frequencies that evenly divide into a mean 24-hour day. Decomposition of the principal diurnal (24-hour, S_1) tide from a global domain to Fourier space reveals pronounced Sun-synchronous or so-called "migrating" waves, whose thermal forcing mechanisms through incoming solar radiation are now well understood (Hagan et al., 2003). To first order, the migrating S_1 component in surface variables is a downward-propagated, linear response of tropospheric layers to the heating associated with infrared absorption by water vapor. Figure 1, conceived as a sample climatology of diurnal surface pressure variations, reflects the Sun-locked mode both by a circular phase advancement and a persistent pressure high of about 60 Pa in the equatorial Pacific. Obvious land/ocean modulations of S_1 and local peak amplitudes of up to 180 Pa testify to the presence of additional, non-Sun-synchronous waves, which are known to be forced by latent heat release mostly in the tropics and sensible heat flux from the ground to atmospheric layers aloft.

Solutions for the mean S_1 pressure tide (as in Fig. 1) and its pronounced seasonal modulations are however by no means concordant when compared across different atmospheric analysis systems and globally distributed in situ observations (Schindelegger and Ray, 2014). Much of the difficulties in modeling the

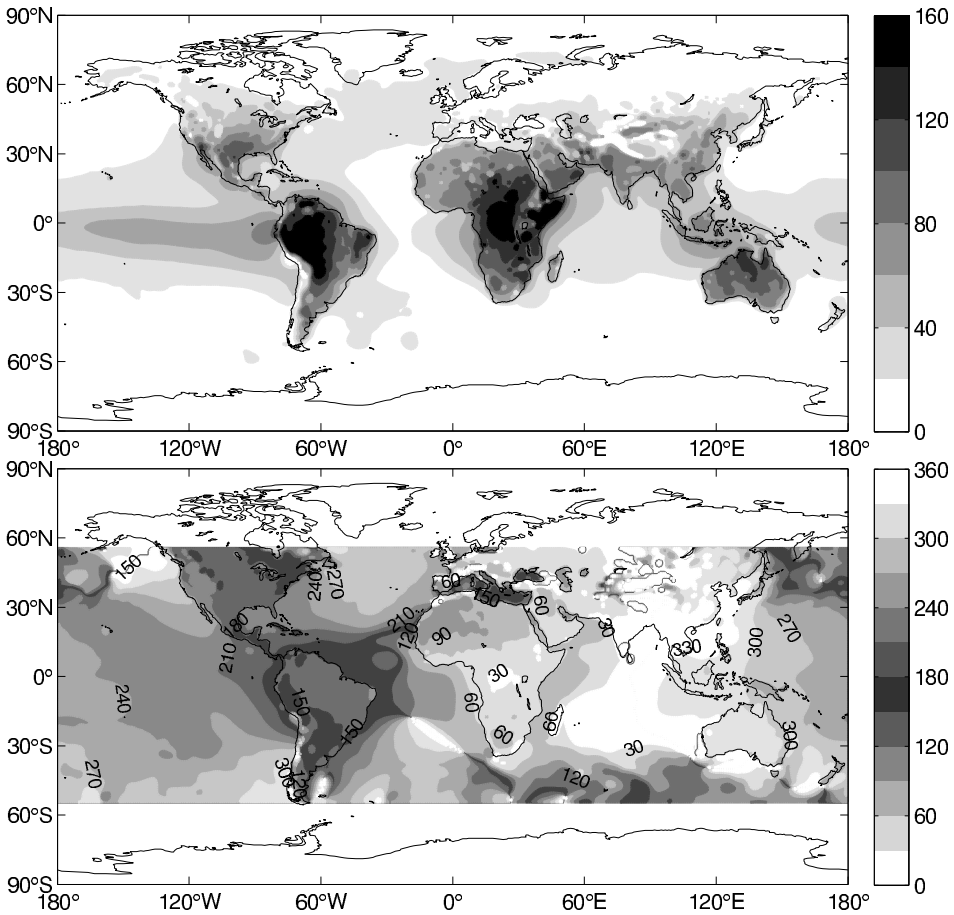

Figure 1: Long-term averages of diurnal air pressure tide amplitudes (Pa, upper panel) and corresponding Greenwich phase lags (deg, lower panel) as deduced from 10 years of ERA-Interim 3-hourly forecast data.

Name	Source	Generation	Fixation	Resolution (km)
NCEP R1	NCEP	1	1995	210
NCEP R2	NCEP	1	1995	210
ERA-40	ECMWF	2	2001	125
JRA-25	JMA	2	2002	120
MERRA	NASA GMAO	3	2004	60
CFSR	NCEP	3	2004	40
ERA-Interim	ECMWF	3	2006	80

Abbreviations: NCEP (National Centers for Environmental Prediction), ECMWF (European Centre for Medium-Range Weather Forecasts), ERA (ECMWF Reanalysis), JRA-25 (Japanese 25-year Reanalysis), JMA (Japan Meteorological Agency), MERRA (Modern Era-Retrospective Analysis for Research and Applications), GMAO (Global Modeling and Assimilation Office), CFSR (NCEP Climate Forecast System Reanalysis).

Table 1: Compilation of available atmospheric reanalyses, including information about the meteorological agency, a "generation" or age index as assigned by the climate data community (at https://climatedataguide.ucar.edu/), the fixation or freezing date of the agency's operational model, as well as the horizontal resolution.

diurnal cycle in numerical weather prediction models relate to the existence of peak diurnal oscillations on subgrid scales as well as uncertainties attached to the daily variations in tropical convection. Mass (i.e. pressure) term estimates of the S_1 effect in nutation have thus varied considerably, handicapped also by a small signal-to-noise ratios as a result of cancellation phenomena between regional pressure maxima. By contrast, the vertically-integrated wind portion of AAM exceeds the retrograde diurnal pressure term by a factor of seven, allowing for a rather unambiguous representation of it in different atmospheric models (Koot and de Viron, 2011).

A proper assessment of seasonal variations in nutation forced by pressure and wind AAM imposes the requirement of a stable, long-term atmospheric dataset, in which possible systematics associated with frequent model updates have been eliminated. So-called "reanalyses", built upon "frozen" versions of the operational assimilation and analysis models of specific weather agencies, largely comply with this condition and have thus become the preferred means to investigate the diurnal atmospheric forcing of nutation amplitudes. Table 1 provides an overview of currently available reanalysis datasets, sorted by a qualitative generation (age) index which roughly mirrors the models' improvements in terms of physics, discretization, input data, and assimilation technique.

Most of the hitherto published S_1 estimates in nutation are based on NCEP's first-generation reanalysis R1, whose formulation and admittedly coarse resolution ($2.5^\circ \times 2.5^\circ$ output grids) date back to 1995. Bizouard et al. (1998) and later Brzeziński et al. (2004) used the R1 data for a first comprehensive examination of the entire atmosphere-induced nutation spectrum, while Koot and de Viron (2011) included additional AAM series from NCEP R2 and ERA-40 (Table 1) and could demonstrate a fair agreement with the results from NCEP R1. However, with the exception of ERA-Interim being probed by Brzeziński (2011), the latest, third-generation set of reanalyses has not been mapped to nutation, although such an effort should, in principle, benefit from the afore-noted model advances over the last decade. The present paper is conceived as a provisional attempt to fill this gap, using 10 years of 3-hourly AAM series (2004.0–2013.12) for MERRA and ERA-Interim (henceforth ERA). Pressure term series were inferred from a combination of analysis and forecast fields at a horizontal resolution of 0.5° (ERA) and 1.25° (MERRA), whereas the wind term integrals were computed from isobaric level data at 2.0° (ERA) and 1.25° (MERRA) latitude-longitude intervals.

Viable procedures translating AAM functions to seasonal perturbations of nutation have been described in Bizouard et al. (1998) and Koot and de Viron (2011) and usually involve an initial demodulation of the terrestrial time series to the celestial frame, low-pass filtering, an adjustment of in- and out-of-phase components referred to the fundamental arguments of nutation, as well as scaling to actual rotational variations by aid of separate transfer functions for pressure and wind terms. Here, we follow Bizouard et al. (1998)'s approach but replace their sophisticated spectral estimator by a simple least-squares fit of in- and out-of-phase terms. Mean S_1 nutation values of ERA/MERRA including three-fold formal errors are displayed in Fig. 2 together with the estimates for NCEP R1, NCEP R2, and ERA-40 from Koot and de Viron (2011). The agreement between both third-generation results is excellent and within 30 μas of the predictions from earlier reanalyses. A moderate amplitude reduction observable

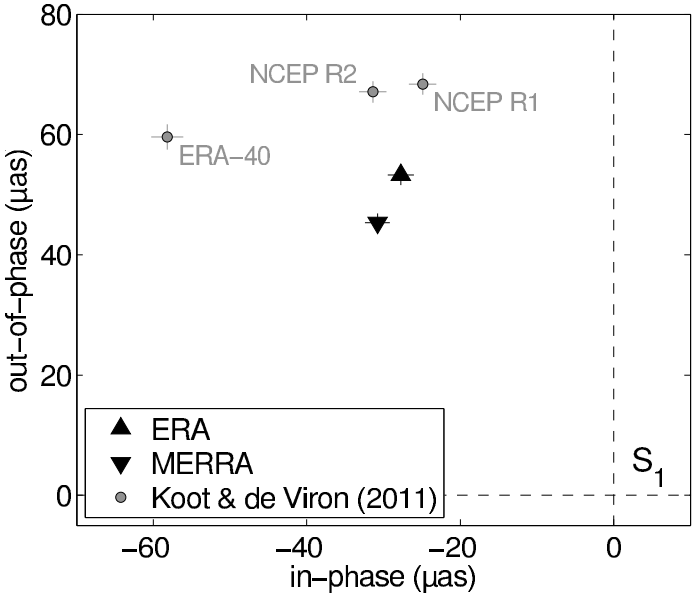

Figure 2: Total (pressure + wind) atmospheric contribution to the prograde annual nutation (S_1) obtained from ERA and MERRA during 2004.0–2013.12 in comparison to the estimates from Koot and de Viron (2011) from earlier generation models for the period 1979.0-2002.7.

Model	Resolution	Atmospheric forcing	in-phase (μas)	out-of-phase (μas)
FES2012	5–75 km	ECMWF operational (mean field)	−11.7	51.9
Ray & Egbert	0.25°	ECMWF operational (mean field)	11.6	62.3
CLIO	1.5°	NCEP R1 (time-variable)	8.0	57.0
OMCT	1.875°	ERA-Interim (time-variable)	−29.4	30.3

Model abbreviations and references: FES (Finite Element Solution, Carrère et al., 2012), Ray and Egbert (2004), CLIO (Coupled Large-Scale Ice-Ocean model, de Viron et al., 2004), OMCT (Ocean Model for Circulation and Tides, mapped to nutation by Brzeziński et al., 2012).

Table 2: Compilation of ocean models that provide a hydrodynamic S_1 solution from forward integration using either a constant forcing or time-variable atmospheric data. FES2012 and the model of Ray and Egbert (2004) are barotropic formulations, whereas CLIO and OMCT are baroclinic models.

for ERA and MERRA likely relates to the use of 3-hourly atmospheric data which resolve semi- and ter-diurnal solar tides and are thus void of folding effects as present in the 6-hourly AAM series of Koot and de Viron (2011). The analysis window of this reference study (1979.0-2002.7) is however disjoint from the one employed here, and a more admissible comparison between the various reanalyses will require a retrospective extension of the ERA/MERRA series by at least one decade.

3. THE OCEANIC S_1 TIDE

As evident from Fig. 2, the atmospheric contribution to the prograde annual nutation is at the level of 60 μas and therefore not the solitary explanation for the S_1 residual in VLBI data (about 100 μas; cf. Section 1). A second substantial geophysical driving arises from the small S_1 ocean tide, which is an "anomalous" phenomenon inasmuch as its gravitational excitation is minor as against the effect of pressure loading associated with the diurnal atmospheric tide (Ray and Egbert, 2004). Nonetheless, the spatial pattern of this "meteorological" ocean tide resembles those of gravitational diurnal tides, including large magnitude oscillations ($>$ 15 mm) in the Gulf of Alaska, the Okhotsk Sea, the Indian Ocean, and the shallow Arafura Sea; cf. the amplitude chart of a modern-day S_1 representation in Fig. 3.

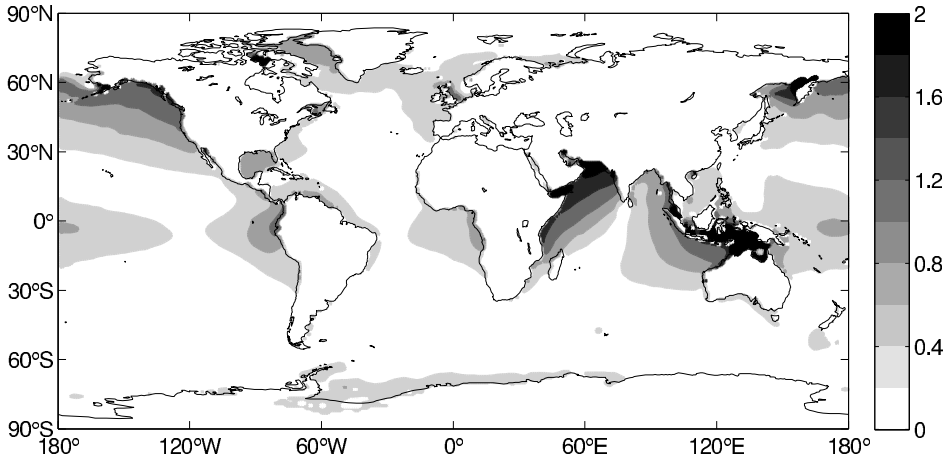

Figure 3: Tidal heights (cm) of the radiational S_1 tide in the global ocean as predicted by the FES2012 model (Carrère et al., 2012) based on a data-free hydrodynamic forward integration forced by a 10-year pressure tide mean from 3-hourly ECMWF operational data.

Accurate determinations of the oceanic S_1 tide originate from hydrodynamic time-stepping models forced by strictly harmonic or time-variable atmospheric pressure (and occasionally wind) data containing the diurnal cycle. A brief tabulation of relevant modeling efforts of that kind is given in Table 2 with emphasis on the model resolution and the respective nutation estimates. Two of the considered numerical solvers (FES, Ray and Egbert) are barotropic (2D) formulations and were rendered to nutation estimates in the frame of this study following the same procedure as in Section 2, whereas CLIO and OMCT results have been extracted from the publications referenced in Table 2. With the exception of OMCT, in- and out-of-phase components of all models agree reasonably well, although the CLIO estimates might be fortuitous, considering that a low-resolution baroclinic (3D) formulation has been used to model a barotropic response characterized by small-scale oscillations.

Given the close inter-model agreement documented for the atmospherically-driven prograde annual nutation (Fig. 2) as well as the barotropic oceanic contribution (FES, Ray and Egbert), a superposition of both effects seems to be warranted. However, such an attempt violates requirements of dynamical consistency, since the forcing climatologies of the hydrodynamic models are different from those inherent to ERA and MERRA. To some extent, these restrictions are weakened by the fact that our pressure tide solutions share strong similarities with those of FES and the Ray model, as evidenced for instance by a global RMS difference of only 4 Pa (average over all pelagic points equatorward of 60°). Moreover, if converted to in- and out-of-phase components of prograde annual nutation, the pressure tide maps of especially the Ray model yield excitation values (-33.9 μas in-phase, 22.7 μas out-of-phase) that conform to the mass term results from reanalyses (e.g. -30.4 μas in-phase, 15.0 μas out-of-phase for MERRA). Bearing in mind this level of inconsistency, combined nutation estimates from both AAM and OAM comply well with the S_1 residual from VLBI observations (Table 3). In particular, oceanic excitation values from Ray and Egbert (2004) superimposed to either ERA or MERRA match the observation to within 10 μas, surpassing the rather approximate agreement noted in predecessor studies (Brzeziński et al., 2004, 2012).

4. DISCUSSION AND OUTLOOK

Present-day determinations of the global S_1 tide in atmospheric and oceanic models have been mapped to nutation signals and were found to yield an accurate account of the empirical prograde annual correction term of the current IAU nutation model (Mathews et al., 2002). This balance is tentative, though, since (a) no allowance has been made for insufficiencies of the MHB model regarding small secondary prograde annual nutations, such as those elicited by mantle anelasticity or the gravitational S_1 ocean tide; (b) only a mean atmospheric contribution has been inferred from 10 years of reanalysis data without exploring the temporal variability of pressure and wind effects over a longer time span; and (c) inconsistencies have been incurred in adding up atmospheric and oceanic excitation estimates from different sources.

	ERA-Interim nutation (μas)		MERRA nutation (μas)	
Model Combination	in-phase	out-of-phase	in-phase	out-of-phase
Atmosphere-only	-27.8	53.3	-30.8	45.3
Atmosphere + FES2012	-39.5	105.2	-42.5	97.2
Atmosphere + Ray and Egbert	-16.2	115.6	-19.2	107.6
VLBI estimate (MHB)	-10.4	108.2	-10.4	108.2

Table 3: Combined effect of atmosphere and oceans on the prograde annual nutation, taking into account ERA and MERRA as well as the two barotropic ocean models cited in Table 2. All estimates given with respect to the fundamental arguments of nutation.

Resolving the latter issue will require the development of a medium-resolution, barotropic time-stepping model in the fashion of Ray and Egbert (2004) which can be forced by the pressure tide solutions of ERA and MERRA, either as long-term averages or as constantly updated "real-time" fields. Extensions of the utilized set of reanalyses, both in time (back to 1994) and by a third state-of-the-art model in the form of CFSR are envisaged and will likely contribute to a more comprehensive picture of the global S_1 tide and its impact on nutation.

Acknowledgements. This study was carried out within project I1479 of the Austrian Science Fund. David Salstein was supported by the US National Science Foundation under Grant ATM-0913780.

5. REFERENCES

Bizouard, C., Brzeziński, A., Petrov, S., 1998, "Diurnal atmospheric forcing and temporal variations of the nutation amplitudes", J. Geod., 72(10), pp. 561–577.

Brzeziński, A., 2011, "Diurnal excitation of Earth rotation estimated from recent geophysical models", In: N. Capitaine (ed.) Proc. of the Journées 2010 "Systèmes de Référence Spatio-Temporels", Observatoire de Paris, pp. 131–136.

Brzeziński, A., Ponte, R.M., Ali, A.H., 2004, "Nontidal oceanic excitation of nutation and diurnal/semidiurnal polar motion revisited", J. Geophys. Res., 109, B11407, doi: 10.1029/2004JB003054.

Brzeziński, A., Dobslaw, H., Thomas, M., Ślusarczyk, Ł., 2012, "Subdiurnal atmospheric and oceanic excitation of Earth rotation estimated from 3-hourly AAM and OAM data", Geophys. Res. Abstracts, 14, Poster presentation at EGU General Assembly 2012, EGU2012-10530.

Carrère, L., Lyard, F., Cancet, M., Guillot, A., Roblou, L., 2012, "FES2012: A new global tidal model taking advantage of nearly 20 years of altimetry", In Proc. of "20 Years of Progress in Radar Altimetry", Venice, 2012.

de Viron, O., Boy, J.-P., Goosse, H., 2004, "Geodetic effects of the ocean response to atmospheric forcing in an ocean general circulation model", J. Geophys. Res., 109, B03411, doi:10.1029/2003JB002837.

Fedorov, E.P., Smith, M.L., (eds.), 1980, "Nutation and the Earth's Rotation", In: Proc. IAU Symp. 78, Kiev, 1977.

Hagan, M.E., Forbes, J.M., Richmond, A., 2003, "Atmospheric tides", In: J. Holton, J. Pyle, J. Curry (eds.) Encyclopedia of Atmospheric Sciences, 1st ed., Academic Press, pp. 159–165.

Koot, L., de Viron, O., 2011, "Atmospheric contributions to nutations and implications for the estimation of deep Earth's properties from nutation observations", Geophys. J. Int., 185, pp. 1255–1265, doi: 10.1111/j.1365-246X.2011.05026.x.

Mathews, P.M., Herring, T.A., Buffett, B.A., 2002, "Modeling of nutation and precession: New nutation series for nonrigid Earth and insights into the Earth's interior", J. Geophys. Res., 107, B4, 2068, doi: 10.1029/2001JB000390.

Ray, R.D., Egbert, G.D., 2004, "The global S_1 tide", J. Phys. Oceanogr., 34, pp. 1922–1935.

Schindelegger, M., Ray, R.D., 2014, "Surface pressure tide climatologies deduced from a quality-controlled network of barometric observations", Mon. Weather Rev., 142(12), pp. 4872–4889.

Schindelegger, M., et al., 2015, "Earth's nutation and the global S_1 tide", in preparation.

REFINEMENTS ON PRECESSION, NUTATION, AND WOBBLE OF THE EARTH.

V. DEHANT[1], M. FOLGUEIRA[2], M. PUICA[2], T. VAN HOOLST[1]
[1] Royal Observatory of Belgium
avenue Circulaire 3, B1180 Brussels, Belgium
e-mail: v.dehant@oma.be
[2] Universidad Complutense de Madrid, Spain

ABSTRACT Most of the essential elements of the theory of nutation of the nonrigid Earth have been presented in the IAU adopted model MHB2000 (Mathews et al., 2002) considering an ellipsoidal rotating Earth, with a solid inner core, a liquid outer core, and an ellipsoidal inelastic mantle, and with a magnetic field. However in the meantime, the observed nutation amplitudes have been redetermined with a better precision. A number of relatively small significant effects have to be taken into account before one can expect to have a theoretical framework that can yield numerical results matching the precession and nutation observations. The adopted model already accounts for the existence of a geomagnetic field passing through the mantle and the fluid core regions and beyond. The model MHB2000 considers an electromagnetic torque generated by this field when the core and the mantle are moving relative to each other, which can in turn affect some nutation amplitudes (both in phase and out-of-phase) to the extent of a few hundreds of microarcsecond (μas), playing thus a significant role. The paper revisits the last adopted model in order to incorporate potential additional coupling effects at the core-mantle boundary, that can be at an observable level, such as the existence of a non-hydrostatic core-mantle boundary topography, the viscosity of the liquid core, the existence of stratification in the core, the existence of boundary layers at both sides of the core-mantle boundary.

1. STARTING FROM OBSERVATIONS AND THE IAU2000 ADOPTED NUTATION MODEL

Nutation observations are performed using Very Long Baseline Interferometry (VLBI). The performance of the VLBI antenna networks used for these observations has increased during the recent years, allowing a higher-precision determination of the nutation amplitudes. Figure 1 shows the residuals in milliarcsecond (mas) as a function of time between the nutation observations and the theoretical nutation amplitude as

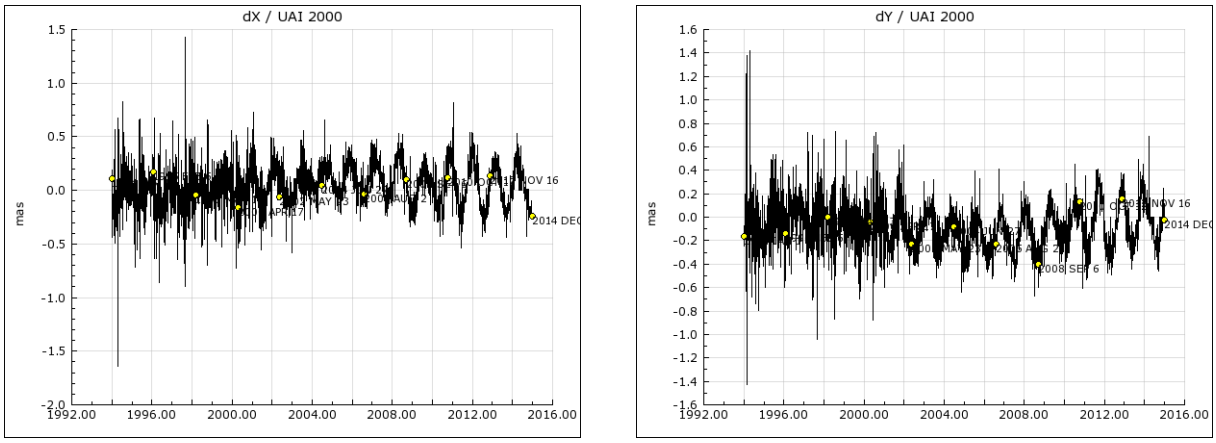

Figure 1: Residuals between nutation observations and the IAU2000 nutation model (dX,dY), as determined from the IERS EOP Product Center website http://hpiers.obspm.fr.

adopted by the IAU and IUGG in 2000 and 2003. These residuals are mainly due to the Free Core Nutation (FCN), a free mode excited by the atmosphere. The FCN amplitude cannot be precisely determined due to the poor knowledge of its excitation however an estimation can be obtained from the observations themselves. Even after subtraction of the effect of the FCN free mode contribution (as determined by the IERS) on the nutation in the time domain, there are still contributions at the level of a few tens of μas in the main nutation amplitudes. These residuals are presently not believed to be due to imperfection in the rigid Earth precession and nutation theory, accounting not only for the luni-solar direct effect on the Earth but as well for the direct and indirect of the planets. Starting from recent observed nutation series, Koot et al. (2010) have redetermined new estimations for the coupling constants at the CMB (core-mantle boundary) and at the ICB (inner core boundary) that are not explained by the presently adopted MHB2000 nutation model. This paper provides potential explanations considering additional coupling mechanisms at the CMB (core-mantle boundary).

2. IMPROVEMENT IN COUPLING MECHANISMS AT CORE-MANTLE BOUNDARY

There are several coupling mechanisms that have to be considered to explain the observed coupling constant at the CMB: (1) the classical ellipsoidal pressure-gravitational torque, already considered in MHB2000 nutation model, (2) the electromagnetic torque, also considered in MHB2000, (3) the viscous torque, and (4) the topographic torque. These coupling mechanisms are discussed below.

First we examine the constraints that we can use for further interpreting the coupling constants in terms of physics at the CMB. If we want to compute the electromagnetic torque acting at the CMB, we need to know the initial magnetic field and the outer core electrical conductivity as well as the lower mantle conductivity. The mantle is composed of silicates but a thin boundary layer at the bottom of the mantle (typically 200 m thickness) may still have a large conductivity possibly due to contamination with iron from the core. The electrical conductivity σ in that layer must of course be lower than the iron alloy conductivity (or equal to it in an extreme case), determined from laboratory experiments to be at the level of $\sigma = 5\ 10^{-5}\ Sm^{-1}$ (Stacey and Anderson, 2001). The electrical conductivity inside the mantle can be considered to be with typical values like $\sigma = 10\ Sm^{-1}$, $\sigma = 10^{-4}\ Sm^{-1}$, and $\sigma = 5\ 10^{-5}\ Sm^{-1}$. The poloidal magnetic field component at the CMB can be computed from downward continuation of the observed value at the Earth surface. This provides a typical value for the mean amplitude, the so-called RMS of the magnetic field, at the level of 0.3 mT, far below the amplitudes expected from the nutation data. Indeed, Koot et al. (2010) have deduced the coupling constants at the CMB from VLBI data as explained in the previous paragraph and have used these values in order to show that if one considers electromagnetic coupling only, the RMS of the radial magnetic field at the CMB must be 0.7 mT or larger, depending on the electrical conductivity considered for the bottom of the mantle.

In order to compute the viscous torque at the CMB we need to know the viscosity of the outer core fluid. Laboratory experiments and *ab initio* computations suggest that the molecular viscosity is at the level of $10^{-6}\ m^2s^{-1}$ and the eddy viscosity is at the level of $10^{-4}\ m^2s^{-1}$ (Buffett and Christensen, 2007). Koot et al. (2010) show that, in order to allow for lower values of the magnetic field at the CMB, in agreement with the value deduced from the surface magnetic field, we would need values for the viscosity of the core at the level of $10^{-2}\ m^2s^{-1}$, far too large with respect to the values that are admissible as mentioned above. The viscous coupling at the CMB is shown to be negligible for reasonable values of the core viscosity and other mechanisms must be considered to explain the observed coupling constant and to impose a decrease of the large magnetic field amplitude inferred when other coupling mechanisms are ignored.

The question is then how to explain this large electromagnetic coupling at the CMB if the viscous torque is disregarded? One explanation has been recently provided by Buffet (2012) considering the results of laboratory experiments published by Pozzo et al. (2012a, 2012b). These later authors have shown that the thermal conductivity of liquid iron under the conditions in the Earth's core is several times higher than previous estimates. This has the consequence that the heat carried by conduction in this layer is increased; less heat is thus available to drive convection in the core, which decreases the electrical resistance. In the induction equation for the induced field at the CMB, there is thus more generation than loss in the magnetic field balance equation (Buffett, 2012).

Another explanation can be found in considering that the only constraints on the core magnetic field that we have from the surface magnetic field observations are for the degrees lower than 13. But smaller scales contributions are unknown. In that consideration, nutation suggests that most of the energy of

the magnetic field at the CMB comes from these.

Alternatively, the inclusion of topographic coupling may also reduce the need of a large electromagnetic field. We know from seismology that the core-mantle boundary topography is at the km level. The liquid pressure at the CMB on this topography induces a pressure torque able to transfer angular momentum from the core to the mantle. This phenomena is well known for explaining decadal variations of Earth rotation (Hide, 1977). At the nutation diurnal timescale, it is difficult and challenging to compute, but the topographic torque cannot be ruled out to explain the coupling constants determined from nutation observations. Wu and Wahr (1997) have used seismic value for the topography at the CMB and have computed the effect on nutations. They have shown that the effects on the retrograde annual nutation can be at the milliarcsecond level and that for some topography wavelength there are amplifications of the contributions. While Wu and Wahr (1997) used a numerical technique, Puica et al. (2014) examine the approach and equations and further study them using an analytical approach. Aiming at obtaining the torque and the associated effects on nutation, the following strategy must be used: (1) establish the motion equations and boundary conditions in the fluid; (2) compute analytically/numerically the solutions; (3) obtain the dynamic pressure as a function of the physical parameters; and (4) determine the topographic torque. With this strategy, Puica et al. (2014) show that the amplifications can exist due to resonances with inertial waves in the rotating fluid core and that some of the resonances as determined from their approach can be found near the main nutations. Though, these conclusions may change in the presence of an inner core.

Lastly, one can consider that there are chemical interactions between the core and the mantle (Buffett, 2010). In this approach, the core is considered to be stratified. The motions in the liquid core are then almost parallel to the constant density surfaces; there are only small changes in density; and the resulting buoyancy forces are weak. However, in the presence of a topography at the CMB, the vertical component of the motion in the fluid core can be important, the density field in a stratified fluid is disturbed and a buoyancy force arises, lowering the required strength of the radial magnetic field, as we wanted.

3. CONCLUSIONS

From our above discussion we can conclude that the existence of a topography of the CMB may provide a coupling mechanism between the core and the mantle for explaining nutation contributions and that contributions from some of the wavelenghts of the CMB topography may be larger than others due to resonance effects with inertial waves or due to large topography amplitudes. However other mechanisms can also be invoked such as the existence of a core stratification that enables buoyancy force to arise, lowering the required strength of the radial magnetic field in the electromagnetic coupling, or the existence of smaller scales in the magnetic field amplitude contributing largely to the electromagnetic torque, or even an increase of the electromagnetic torque arising from a decrease in electrical resistance consequently from the fact that the thermal conductivity of liquid iron under the conditions in Earth's core can be several times higher than previous estimates.

4. REFERENCES

Buffett, B., Christensen, U., 2007, "Magnetic and viscous coupling at the core-mantle boundary: Inferences from observations of the Earth's nutations", Geophys. J. Int., 171(1), pp. 145–152, DOI: 10.1111/j.1365-246X.2007.03543.x.

Buffett, B., 2010, "Chemical stratification at the top of Earth's core: Constraints from observations of nutations", Earth and Planetary Science Letters, 296(3-4), pp. 367–372, DOI: 10.1016/j.epsl.2010.05.020.

Buffett, B., 2012, "Geomagnetism under scrutiny", Nature, 485(7398), pp. 319–320, DOI: 10.1038/485319a.

Hide, R., 1977, "Towards a theory of irregular variations in the length of the day and core-mantle coupling", Philosophical Transactions of the Royal Society (London), Series A, 284(1326), pp. 547–554, DOI: 10.1098/rsta.1977.0030.

Koot, L., Dumberry, M., Rivoldini, A., de Viron, O., Dehant, V., 2010, "Constraints on the coupling at the core-mantle and inner core boundaries inferred from nutation observations", Geophys. J. Int., 182, pp 1279–1294, DOI: 10.1111/j.1365-246X.2010.04711.x.

Mathews, P.M., Herring, T.A., Buffett, B.A., 2002, "Modeling of nutation and precession: new nutation series for nonrigid Earth and insights into the Earth's interior", J. Geophys. Res., 107(B4), 2068, DOI: 10.1029/2001JB000390.

Pozzo, M., Davies, C., Gubbins, D., Alfè, D., 2012a, "Transport properties for liquid silicon-oxygen-iron mixtures at Earth's core conditions", Physical Review B, 87(1), 014110, DOI: 10.1103/PhysRevB.87.014110.

Pozzo, M., Davies, C., Gubbins, D., Alfè, D., 2012b, "Thermal and electrical conductivity of iron at Earth's core conditions", Nature, 485(7398), pp. 355–358, DOI: 10.1038/nature11031.

Puica, M., Dehant, V., Folgueira, M., Trinh, A., Van Hoolst, T., 2014, "Analytic computation of the total topographic torque at the Core-Mantle-Boundary and its impact on nutations and on tidal length of day variations", A&A, in preparation.

Stacey, F.D., Anderson, O.L., 2001, " Electrical and thermal conductivities of Fe-Ni-Si alloy under core conditions", Physics of the Earth and Planetary Interiors, 124(3-4), pp. 153–162, DOI: 10.1016/S0031-9201(01)00186-8.

Wu, X., Wahr J.M., 1997, "Effects of non-hydrostatic core-mantle boundary topography and core dynamics on Earth rotation", Geophys. J. Int., 128, pp. 18–42.

POSSIBLE IMPROVEMENT OF THE IAU 2006 PRECESSION BASED ON RECENT PROGRESS

J.-C. LIU[1], N. CAPITAINE[2]
[1] School of Astronomy and Space Science, Nanjing University
163 Xianlin Avenue, 210046 Nanjing, China
e-mail: jcliu@nju.edu.cn
[2] SYRTE, Observatoire de Paris, CNRS, UPMC
61, avenue de l'Observatoire, 75014 Paris, France
e-mail: n.capitaine@obspm.fr

ABSTRACT. We aim to investigate the possibility of improving the IAU 2006 precession model after more than 10 years since its publication based on new solutions of the Earth-Moon Barycenter (EMB) motion, new theoretical contribution to the precession rates, and the revised J_2 long-term variation obtained from the Satellite Laser Ranging (SLR). We use these upgraded models and follow the same procedure as that followed by Capitaine et al. (2003) to provide the IAU 2006 precession expressions. The revised precession expressions for the ecliptic are derived by fitting the new analytical planetary theory VSOP2013 to the JPL numerical ephemerides DE422. For solving the precession of the equator, more realistic Earth model including the J_2 quadratic variation and precession rate at initial epoch are applied in the integration of equations. The quadratic and cubic terms in the revised precession quantity $\psi_{\rm A}$ differs from IAU 2006 quite significantly. The statistics of the VLBI celestial pole offsets (1979–2014) and least squares fits with different empirical models show that the revised precession is slightly more consistent with the VLBI observations but the improvement relative to the IAU model is not convincing.

1. INTRODUCTION

The current precession model is the IAU 2006 model (Capitaine et al. 2003). The precession of the ecliptic was derived by fitting the analytical ephemerides VSOP87 to the long term ephemerides DE406 over 2000 years. The IAU 2006 precession of the equator is a dynamically consistent solution. The basic precession quantities $\psi_{\rm A}$ and $\omega_{\rm A}$ were derived by solving the dynamical equations using improved ecliptic precession, integration constants provided by IAU 2000 with a careful consideration of the perturbing effects, and the best non-rigid Earth model available at that time. The linear change in J_2 was considered, which contributes -14 mas t in the theoretical precession rate in longitude, and is responsible for about -7 mas cy^{-2} in the final polynomial expression of $\psi_{\rm A}$. The uncertainty of J_2 rate, which is expected to be of about 20%, is the main limiting factor for the accuracy of the precession in longitude.

This paper reports on our effort to develop upgraded precession solutions with application of new scientific progresses during the last ten years. The methods used are mainly based on Capitaine et al. (2003) and our results are compared with IAU 2006 model and VLBI observations

2. IMPROVING THE PRECESSION OF THE ECLIPTIC

The precession of the ecliptic is defined as the secular part of the ecliptic pole motion in the initial reference system, which is described by the parameters $P_{\rm A}$ and $Q_{\rm A}$. We use the new analytical planetary solution VSOP2013 developed by Simon et al. (2013) to improve the precession of the ecliptic. VSOP2013 solution provides the elliptic elements, including p and q (equivalent to $P_{\rm A}$ and $Q_{\rm A}$), for the eight planets in the form of Poisson series, the secular parts of p and q for EMB representing the precession of the ecliptic. It is more accurate by a factor of 5 with respect to VSOP2000. On the other hand the improved DE422 numerical ephemerides are used as observational material to confine the secular motion of the ecliptic as provided by VSOP2013. Figure 1 shows the difference between DE422 and VSOP2013 for the EMB motion represented by $P_{\rm A}$ and $Q_{\rm A}$ in the dynamical ecliptic frame over 20 centuries.

The 250-day sampling series of (t, Δp, Δq) in sense of [DE422−VSOP2013] between J1000 and J3000 are fitted to the fifth order polynomials. The resulting coefficients of constant terms p_0 and q_0 are used

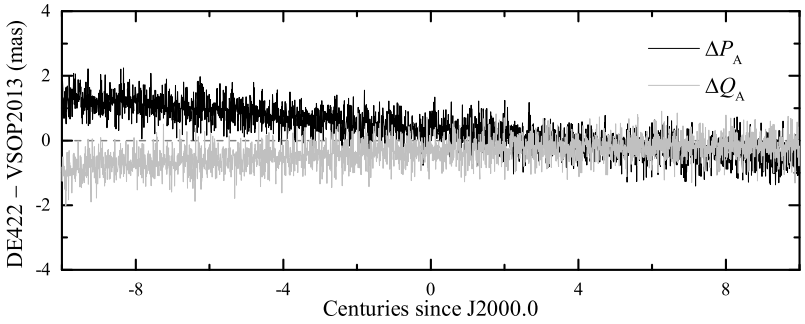

Figure 1: The difference $\Delta P_{\rm A}$ and $\Delta Q_{\rm A}$, for $P_{\rm A}$ and $Q_{\rm A}$, in sense of [DE422−VSOP2013] over 20 centuries.

to improve the rotation angles while the coefficients of $t^1 - t^5$ terms are added to corresponding secular terms given by VSOP2013. Table 1 gives the final ecliptic precession quantities $P_{\rm A}$ and $Q_{\rm A}$ derived from VSOP2013 fitted to DE422. The major discrepancies between the revised and the IAU 2006 precession of the ecliptic are at the order of several tens of microarcseconds per century in the linear terms , while the second-order term differs less than $20\,\mu{\rm as\,cy}^{-2}$, which can be considered as negligible.

	unit	t^1	t^2	t^3	t^4	t^5
$P_{\rm A}$	$''$	4.19903	0.19401	-2.23533×10^{-4}	-1.03944×10^{-6}	2.15694×10^{-9}
$\Delta P_{\rm A}$	μas	-65	18	1	-0.1	0.01
$Q_{\rm A}$	$''$	-46.81099	0.05102	5.21368×10^{-4}	-5.5808×10^{-7}	-1.2059×10^{-9}
$\Delta Q_{\rm A}$	μas	28	-11	-3	0.1	0.02

Table 1: Precession quantities of the ecliptic derived from VSOP2013 and DE422 ephemerides and comparison with the IAU 2006 precession model. $\Delta P_{\rm A}$ and $\Delta Q_{\rm A}$ are calculated in sense of [revised − IAU 2006].

3. IMPROVING THE PRECESSION OF THE EQUATOR BASED ON RECENT PROGRESS

The solutions for the precession of the equator are derived by solving the differential equations. The classical 7(8)-degree Runge-Kutta-Fehlberg method was used to derive the discrete points (250-day step over 2000 years centered on J2000.0) for basic quantities $\psi_{\rm A}$, $\omega_{\rm A}$ and secondary quantities $\epsilon_{\rm A}$, $\chi_{\rm A}$ and $p_{\rm A}$, then the polynomial expressions are obtained from least squares fit.

The Earth model used in precession computation is reflected in the theoretical expressions for the precession rates r_ψ and r_ϵ with respect to the moving ecliptic where the complete list for the theoretical contributions are provided in Table 3 of Capitaine et al. (2003). The progress in precession rates, within our knowledge, include following terms: 1. Revised nonlinear terms in longitude $-960\,\mu{\rm as\,cy}^{-1}$ and in obliquity $+340\,\mu{\rm as\,cy}^{-1}$ (Capitaine et al. 2005); 2. Determination of the J_2 long-term variation based on satellite laser ranging (SLR, Cheng et al. 2013). This will be discussed in detail in the following. 3. The contribution of tidal Poisson terms on non-rigid Earth rotation (Folgueira et al. 2007). This contributes $88\,\mu{\rm as\,cy}^{-1}$ to the precession rate in obliquity; 4. The effect of second-order torque on precession rate in obliquity (Lambert & Mathews 2008). The value was found to be $-1840\,\mu{\rm as\,cy}^{-1}$; 5. The effect from Galactic aberration (Liu et al. 2012). The systematic effect in precession rates caused by Galactic aberration is at the order of $10\,\mu{\rm as\,cy}^{-1}$.

Generally the long-term trend in J_2 has been approximated by a negative linear drift. Cheng & Tapley (2004) has found from 28-year SLR observational data (1976-2004) a secular decrease of J_2 with a rate $-2.75\times10^{-9}\,{\rm cy}^{-1}$, which is close to the value used in the IAU model. More recently, Cheng et al. (2013) reported the updated feature in J_2 based on the time series of 30-day SLR estimate of J_2 between 1976 and 2012. Figure 2 shows the variation of J_2. Straight lines and parabola are used as empirical models to interpret the long-term variations in the observations. The estimated linear trend with the data earlier than 1996 (green solid line) is $-3.04\pm0.32\times10^{-9}\,{\rm cy}^{-1}$, but a much smaller value $-0.67\pm0.19\times10^{-9}\,{\rm cy}^{-1}$ can be found if more recent data between 1996 and 2012 are involved (red solid line). This shows that

the deceleration in J_2 variation is significant; therefore the J_2 variation can be described by a sum of a linear term and a parabola fitted to LSR data (black curve):

$$J_2 = 1.08263582 \times 10^{-3} - 0.53191 \times 10^{-9}\, t + 1.08490 \times 10^{-8}\, t^2. \quad (1)$$

Consequently the contribution of J_2 variation to the precession rate in longitude is $-2\,482\,\mu\mathrm{as}\,t^2 + 50629\,\mu\mathrm{as}\,t^3$.

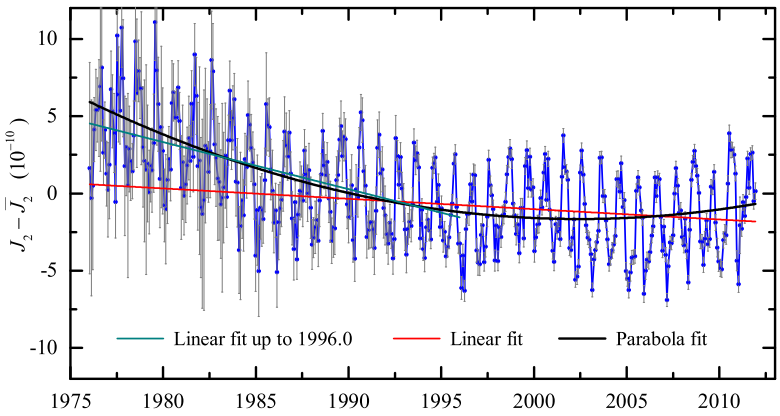

Figure 2: 30-day estimates of J_2 values from SLR and its long term variation. The constant $\bar{J}_2$ is the mean value for J_2, which equals 0.0010826359797. The original data is provided by Cheng et al. (2013).

The integration constants r_0 and u_0 at J2000.0 for precession rates in longitude and obliquity are crucial for solving the precessional equations. The precession corrections that are consistent with the updated non-linear terms are given by Capitaine et al. (2005). Taking the spurious contributions (Capitaine et al. 2003) into consideration, we obtain the integration constants r_0 and u_0:

$$r_0 = 5038''.482040; \quad u_0 = -0''.025754. \quad (2)$$

By using (1) the updated ecliptic precession in Table 1, (2) additional theoretical contributions to the precession rates, and (3) integration constants in Eq. (2), we obtain the precession of the equator by solving differential equations. The basic precession quantities are:

$$\begin{aligned} \psi_\mathrm{A} &= 5038''.482040\,t - 1''.0732414\,t^2 + 0''.01573401\,t^3 + 0''.000127135\,t^4 - 0''.0000001020\,t^5 \\ \omega_\mathrm{A} &= \epsilon_0 - 0''.025754\,t + 0''.0512625\,t^2 - 0''.0077249\,t^3 - 0''.000000267\,t^4 + 0''.000000267\,t^5, \end{aligned} \quad (3)$$

with $\epsilon_0 = 84381''.406$. The differences between the revised solution and IAU 2006 precession of the equator are:

$$\Delta\psi_\mathrm{A} = 532\,t + 5765\,t^2 + 16874\,t^3 - 6\,t^4 - 0.01\,t^5; \quad \Delta\omega_\mathrm{A} = -1\,t + 0.3\,t^2 + 0.1\,t^3 + 0.1\,t^4 - 0.07\,t^5, \quad (4)$$

where the units of the coefficients are μas and t is in Julian centuries from J2000.0. The largest difference in the quadratic and cubic terms for ψ_A are induced by using the updated empirical model for J_2 variation.

4. COMPARISON WITH VLBI CELESTIAL POLE OFFSETS

The observed differences with respect to the IAU-model-predicted CIP positions are reported as "celestial pole offsets" dX and dY. We try to investigate the accuracy of the revised precession model using the best available VLBI data over 1979-2013. The time series for celestial pole offsets are derived with respect to the revised and IAU 2006 precession respectively. The free core nutation has been removed with the empirical model. For each dX and dY time series we calculated the Weighted Mean (WM) value and the Weighted Root Mean Square (WRMS) which can be used to indicate the overall consistency between the theoretical predictions and observations. Table 2 shows that the smaller WM and WRMS of the offsets can be found when the revised precession model has been applied to calculate the CIP location.

For the dX component, the revised precession appears to be more consistent with VLBI observations than the current IAU 2006 precession as the WM decrease about 72% refer to the IAU one. Regarding the dY component, the WM and WRMS relative to the revised solution are close to the value for the IAU model.

		IAU 2006	revised			IAU 2006	revised
WM	dX	0.0467	0.0130	WRMS	dX	0.1349	0.1261
	dY	−0.0565	−0.0561		dY	0.1442	0.1441

Table 2: Weight Mean (WM) and Weighted Mean Root Square (WRMS) of the celestial pole offsets related to the revised and the IAU 2006 precession models. The unit is mas.

To interpret the residuals between VLBI observations and two precession solutions, we have used parabola and straight line plus 18.6-year nutation for the least squares fit. The results show that the longer time span of VLBI data reduced the coefficients of the quadratic model especially for the t^2 term compared to the results in Capitaine et al. (2009). However it is difficult to discriminate which model is more appropriate to interpret the physical reason for the overall residuals because the WRMS relative to both IAU and the revised precession are reduced by approximately the same level and the coupling between linear/quadratic and linear/18.6-year terms are significant.

5. DISCUSSION

In this work we have investigated the possibility of improving the IAU 2006 precession (Capitaine et al. 2003) model with recent progress in the last decade. The revised solution developed in this paper are based on recent improvements in EMB motion and theories in precession rates. However we recommend to retain the current IAU model for the following reasons: (1) The changes in the precession of the ecliptic is negligible; (2) The J_2 variation can still be approximated by empirical model but not predicted by geophysical theories; (3) Improvement of the revised solution is not very convincing from the comparison with VLBI; (4) The precession model itself is a secular phenomenon over thousands of years: 10 years of progress seems not sufficient to change the standard of the model. More detailed analysis will be carried out by the authors in the near future.

6. REFERENCES

Capitaine, N., Wallace, P.T., Chapront, J., 2003, "Expressions for IAU 2000 precession quantities", A&A, 412, pp. 567–586.

Capitaine, N., Wallace, P.T., Chapront, J., 2005, "Improvement of the IAU 2000 precession model", A&A, 432, pp. 355–367.

Capitaine, N., Mathews, P.M., Dehant, V., Wallace, P.T., Lambert, S.B., 2009, "On the IAU 2000/2006 precession nutation and comparison with other models and VLBI observations", Celest. Mech. Dyn. Astr., 103, pp. 179–190.

Cheng, M.K., Tapley, B.D., 2004, "Variations in the Earth's oblateness during past 28 years", J. Geophys. Res., 109, B009402

Cheng, M., Tapley, B.D., Ries, J.C., 2013, "Deceleration in the Earth's oblateness", J. Geophys. Res., 118, pp. 740–747.

Folgueira, M., Dehant, V., Lambert, S.B., Rambaux, N., 2007, "Impact of tidal Poisson terms on nonrigid Earth rotation", A&A, 469, pp. 1197–1202.

Lambert, S.B., Mathews, P.M., 2008, "Second-order torque on the tidal redistribution and the Earth's rotation", A&A, 481, pp. 882–884.

Liu, J.-C., Capitaine, N., Lambert, S.B., Malkin, Z., Zhu, Z., 2012, "Systematic effect of the Galactic aberration on the ICRS realization and the Earth orientation parameters", A&A, 548, A50.

Simon, J.-L., Francou, G., Fienga, A., Manche, H., 2013, "New analytical planetary theories VSOP2013 and TOP2013", 557, A49.

TOWARDS NEW NUTATION THEORY

V.E. ZHAROV
Lomonosov Moscow State University, Sternberg State Astronomical Institute
Universitetskij prospekt, 13, Moscow 119991
e-mail: vladzh2007@yandex.ru

ABSTRACT. Time series of the Earth orientation parameters (EOP) were calculated. The ARIADNA software was used to analyze the corrections of the nutation angles. Main feature is un-modeled motion of the CIP in the GCRS that is known as the free core nutation (FCN). In contrast from theory the FCN motion is complex motion. Hypothesis of reason of this complex motion is based on amplitude modulation of the excitation that is connected with the atmospheric tide ψ_1.

1. INTRODUCTION

The extremely high precision with which the orientation of the Earth in space can now be measured by the space geodetic methods gives an opportunity to test new hypothesis to improve the conventional nutation theory. Nutation that is the motion of the Celestial Intermediate Pole (CIP) in the inertial reference frame is excited by the nearly diurnal forcing. The nutation is retrograde motion of CIP, and the retrograde terms have frequencies which are less than -1 cycles per siderial day.

The main reason of nutation motion is the lunisolar gravitational torque on the Earth's equatorial bulge. The effect of the atmosphere in diurnal frequency band is much smaller. Nevertheless the atmosphere has a non negligible effect on nutation, in particular on the prograde and retrograde annual nutation (Zharov, Gambis, 1996; Zharov, 1997).

According the IERS Conventions (2010) (Petit, Luzum, 2010) the transformation to relate the International Terrestrial Reference System (ITRS) and the Geocentric Celestial Reference System (GCRS) at the date of the observation include the precession-nutation theory IAU2000/2006 (Capitaine, Wallace, 2006). The theory determines the coordinates of the CIP in the GCRS or "celestial pole offsets" denoted as X and Y. Corrections δX and δY to the X and Y coordinates are estimated from the VLBI observations and include mainly the contribution of the Free Core Nutation (FCN).

In this work we calculate the corrections to the celestial pole offsets and formulate the hypothesis to explain the FCN term by amplitude modulation of the atmospheric tide ψ_1.

2. SOLUTION DESCRIPTION

Very Long Baseline Interferometry (VLBI) technique is used by the IERS for production of the Earth orientation parameters (EOP) that include corrections δX and δY to the X and Y coordinates.

In this work the software ARIADNA was used for estimation of the EOP for period 1984–2013. Method that used is based on the equinox-based transformation matrix for precession-nutation. The matrix $Q(t)$ that transforms from the true equinox and equator of date system to the GCRS composed of the classical nutation matrix, the precession matrix including four rotations, and a separate rotation matrix for the frame biases. New series of the nutation angles δX and δY were calculated for preparation of our suggestion to improve the nutation theory.

Corrections δX and δY are shown on Fig. 1. To emphasize effect of the FCN the original values were smoothed with period 430 days. Solution gsf2014a was used to compare our results.

According theory the FCN is a free retrograde diurnal motion of the Earth's rotation axis with respect to the Earth. It is caused by the interaction of the mantle and the fluid, ellipsoidal core as it rotates. Frequency of the FCN is determined by the mantle and the core parameters and equal to $f = -1.002324$ (corresponding period is $P = -430.23$ days). Due to unknown time-varying excitation and damping, a FCN model was not included in the IAU 2000A nutation model. As a result the FCN as un-modeled motion of the CIP in the GCRS at the 0.1–0.3 mas level still exists after the IAU 2006/2000A model has been taken into account.

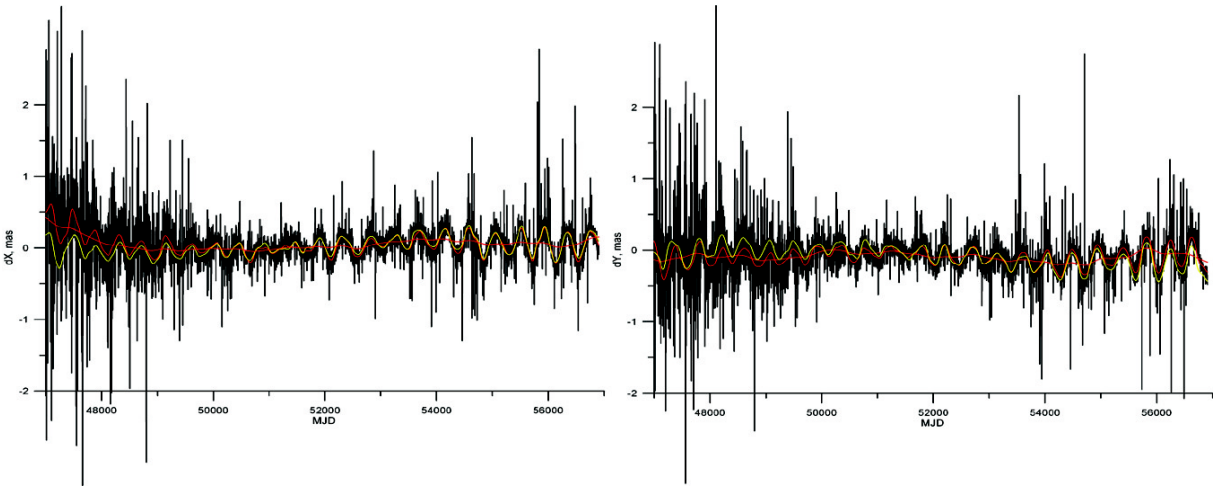

Figure 1: Corrections δX and δY (black line). Smoothed values δX, δY from my (red line) and from gsf2014a solutions (yellow line).

Spectral density of the complex value $\delta X + i\delta Y$ is shown on Fig. 2. Main features of the spectrum are the wide peak corresponding the FCN with maximum value of term with period equal to - 440 days and peaks with periods in range from -3200 to -8200 days and from 5200 to 8200 days. Short length of time series of $\delta X + i\delta Y$ can not allow to reach more higher spectral resolution and can explain unsufficient accuracy of the IAU 2006/2000A model for low frequencies.

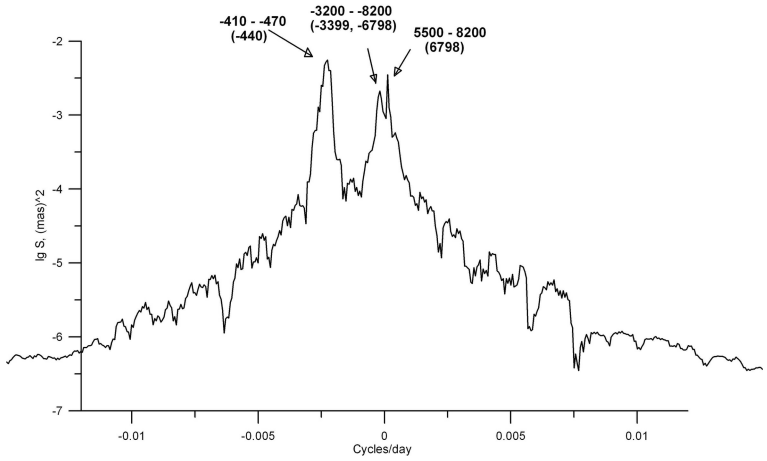

Figure 2: Spectral density of the complex value $\delta X + i\delta Y$.

But explanation of the FCN peak is not obvious. According theory only narrow line with the FCN frequency has to be in spectrum of $\delta X + i\delta Y$. Excitation of the FCN is connected with the atmospheric tide ψ_1 that is one of tidal terms and results from semi-annual modulation of the thermal S_1 tide (Zharov, 1997) (Fig. 3).

Broadening of the FCN spectral line can be connected with amplitude modulation of the tidal term ψ_1. If amplitude A of an signal

$$a(t) = A\cos(\omega_0 t + \varphi)$$

is function of time:

$$A(t) = A_0 + \Delta A\cos(\Omega t + \gamma)$$

then

$$a(t) = A_0\cos(\omega_0 t + \varphi) + \frac{MA_0}{2}\cos[(\omega_0 + \Omega)t + (\varphi + \gamma)] + \frac{MA_0}{2}\cos[(\omega_0 - \Omega)t + (\varphi - \gamma)], \quad M = \frac{\Delta A}{A_0},$$

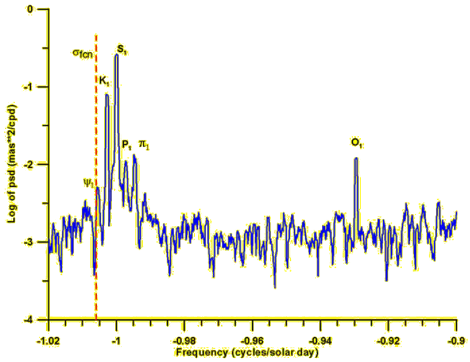

Figure 3: Spectral density of atmospheric pressure term around the FCN frequency.

or amplitude modulation of sinusoidal signal leads to appearance of two additional spectral terms with the same amplitude. If frequency of modulation Ω much less then frequency ω_0 ($\Omega \ll \omega_0$) then we can observe broadening of the spectral line ω_0 (Fig. 4) if spectral resolution is not enough.

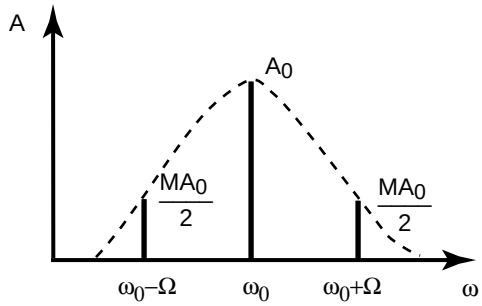

Figure 4: Broadening of the spectral line due to amplitude modulation of sinusoidal signal.

From Fig. 2 we have $f_{FCN} = -1.002273 (P = -440)$ and sideband frequencies are -1.002439 and -1.002127). It means that frequency modulation is in the range $(0.000146 \div 0.000166)$ or period modulation is close to 18.5 years.

To test this result the corrections δX and δY were written as sum of four terms:

$$a(t) = \sum_{i=1}^{4} [D_i \cos(\omega_i t) + F_i \sin(\omega_i t)] = \sum_{i=1}^{4} A_i \cos(\omega_i t + \gamma_i), \quad \omega_i = 2\pi f_i.$$

Then function $a(t)$ was fitted at first to δX and then to δY by variation both amplitudes of sine and cosine terms and their frequencies. Initial values of amplitudes and frequencies are necessary to start procedure of fitting. Results are shown on Fig. 5.

In contrast to accepted value of the FCN period ($P = -430.23$ days) the fitting procedure gives period 417.3 and 415.8 days for δX and δY and two sideband frequencies. Low frequency term is close to main nutation harmonic with period 18.6 years.

3. CONCLUSIONS

Series of the celestial pole offsets corrections δX and δY of 30-years duration were obtained and used for comparison with the IAU 2000/2006 nutation series. Spectral density of the complex value $\delta X + i\delta Y$ was calculated. Main feature of the spectrum is the wide peak corresponding the FCN frequency. One of possible explanation of broadening of the FCN spectral line is amplitude modulation of the tidal term ψ_1 that can excite the FCN. Period of modulation signal is close to 18.5 years. Question that can be asked "Is the FCN frequency splitting arise due to modulation by main nutation harmonic with period 18.6 years?" is nevetheless open.

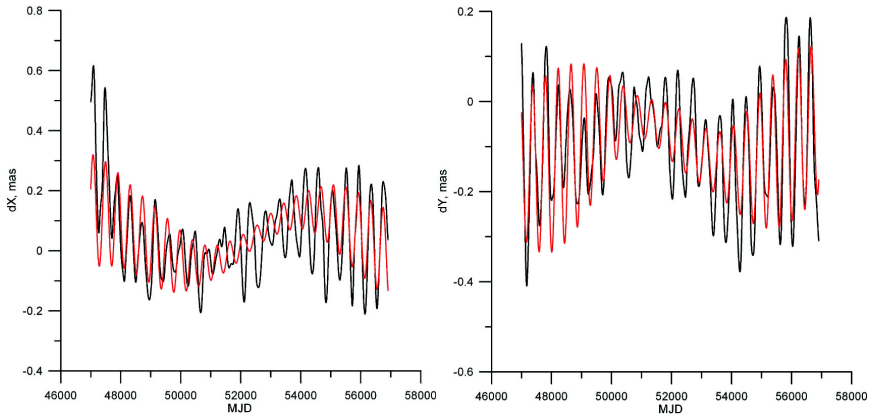

$$dX(t) = \sum_{i=1}^{4} A_i \cos(2\pi f_i t + \varphi_i) \quad dY(t) = \sum_{i=1}^{4} B_i \cos(2\pi f_i t + \gamma_i)$$

A	$P = 1/f$	φ	B	$P = 1/f$	γ
0.09	7275.44	2.23	0.06	6838.33	165.60
0.01	493.72	-69.49	0.09	446.43	99.30
0.12	417.26	-91.98	0.09	415.80	-18.87
0.09	406.67	-35.48	0.06	405.37	39.60

Figure 5: Smoothed corrections δX and δY (black line) and model of the FCN (red line).

Acknowledgements. This work was supported by the RFBR grant 14-02-00735.

4. REFERENCES

Capitaine, N., Wallace, P.T., 2006, "High precision methods for locating the celestial intermediate pole and origin", A&A, 450, pp. 855–872, doi:10.1051/0004-6361:20054550.

Petit, G., Luzum, B. (eds.), 2010, IERS Conventions (2010), IERS Technical Note 36, Frankfurt am Main, Germany: Verlag des Bundesamtes für Kartographie und Geodäsie.

Zharov, V.E., Gambis, D., 1996, "Atmospheric tides and rotation of the Earth", J. of Geodesy, 70, pp. 321–326.

Zharov, V.E., 1997, "Rotation of the Earth and atmospheric tides", Solar System Research, 31, pp. 501–506.

LUNAR INFLUENCE ON EQUATORIAL ATMOSPHERIC ANGULAR MOMENTUM

C. BIZOUARD[1], L. ZOTOV[2], N. SIDORENKOV[3]
[1] SYRTE, Observatoire de Paris, CNRS/UPMC
61, avenue de l'Observatoire, 75014 Paris, France
e-mail: christian.bizouard@obsm.fr
[2] Sternberg Astronomical Institute of Moscow State University
Moscow, Russia
e-mail: wolftempus@gmail.com
[3] Hydrometeorological Centre of Russia / Global Atmospheric Circulation Laboratory
Moscow, Russia
e-mail: sidorenkov@mecom.ru

ABSTRACT This study investigates the relationship between the equatorial atmospheric angular momentum oscillation in the non-rotating frame and lunar tidal potential. Between 2 and 30 days, the corresponding equatorial component is mostly constituted of prograde circular motions, especially of a harmonic at 13.6 days, and of a weekly broad band variation. A simple equilibrium tide model explains the 13.6-day pressure term as result of the O_1 lunar tide; the tidal lunar origin of the whole band from 2 to 30 days is attested by specific features, not occurring for seasonal band dominated by the solar thermal effect.

1. INTRODUCTION

The Equatorial Atmospheric Angular Momentum (EAM) displays prominent quasi-diurnal clockwise variations at 24 h (S_1), 24.07 h (P_1) and 23.93 h (K_1), commonly interpreted as the effect of diurnal solar thermal heating (24 h) subject to a yearly amplitude modulation (Bizouard et al., 1998). It also presents a minor but sharp 25.82-hour peak (Brzeziński et al., 2002) evasively attributed to the O_1 lunar tesseral tide, considering the absence of thermal processes at this frequency. This paper deepens the insight into this signal by an analysis of equatorial AAM variations from 2 to 30 days in the non-rotating frame.

2. BASIC DEFINITIONS

Let H_i be the Cartesian components of the Atmospheric Angular Momentum vector in the Terrestrial Reference Frame (TRF), $C = 8.0370\,10^{37}$ kg m^2 the mean axial moment of inertia, $A = 8.0101\,10^{37}$ kg m^2 the mean equatorial moment of inertia, $\Omega = 2\pi\,1.002738$ rad/day the mean stellar angular frequency. At sub-secular time scales, polar motion (and by extension nutation) are commonly investigated by the linear Liouville equations, where the equatorial excitation of any surface fluid layer maps into a non-dimensional terrestrial quantity $\chi = \chi_1 + i\chi_2$ of the angular momentum of this layer with $\chi_1 = H_1/((C-A)\Omega)$, $\chi_2 = H_2/((C-A)\Omega)$. The χ_i are called Equatorial Angular Momentum Functions (EAMF) and are composed of two terms: i) the first, produced by the rotation of the air mass distribution, can be computed from surface pressure data, and is usually called *pressure term*; ii) the second, caused by the winds, is proportional to the relative angular momentum of the atmosphere, and might be denoted as *wind term* (Barnes et al., 1983). Note that, in order to account for Earth's non-rigidity in the Liouville equations, the AMF have to be multiplied by appropriate coefficients close to 1, yielding the so-called Effective EAMF. Brzeziński (1994) introduced the concept of Celestial Equatorial Angular Momentum (CEAM) defined by

$$\chi' = -\chi e^{i\theta(t)}\,, \tag{1}$$

where $\theta(t) = \theta(TAI_0) + \Omega(TAI - TAI_0)$ is the uniformly varying rotation angle with TAI_0 being a conventionally chosen instant of TAI (IERS Conventions, 2010). Whereas the diurnal band is squeezed in a frequency band around 24 h in the TRF, the corresponding periodicities of the CEAM stretch

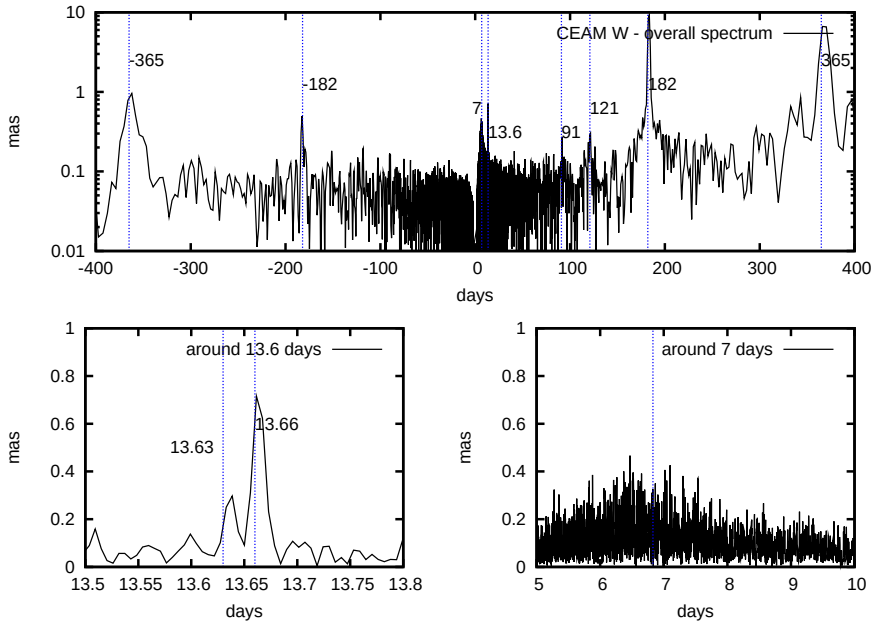

Figure 1: Amplitude spectrum of the wind term of the Celestial Angular Momentum over the period 1949-2012. Data source: NCEP/NCAR.

from 2 days to several years with respect to the non-rotating reference frame: any diurnal component of frequency $\sigma = -\Omega + \sigma'$ with $\sigma' \ll \Omega$ is mapped to a long periodic celestial component of frequency σ'.

3. ANALYSIS OF THE CEAM

Using 6-hourly EAMF estimates from the reanalysis model of NCEP/NCAR (National Center for Environmental Prediction / National Center of Atmospheric Research) over the period 1949−2013, as provided by the Global Geophysical Fluids Center of the IERS (SBA, 2014), we computed the associated CEAM according to (1) for both pressure and wind terms. Prior to demodulation, we removed the long term components (periods larger than 2 days) of the AAM. After application of (1), a low band pass filter was used to eliminate residual diurnal/sub-diurnal signal content and to obtain the celestial excitation limited to periods larger than 2 days, corresponding to the precession-nutation frequency band.

The complex Fourier spectrum of the obtained wind term of CEAM is displayed in Fig. 1 (pressure term presents the same spectral peaks with lower amplitude). Casting aside the peaks with periods above 100 days widely characterised by numerous studies, we focus on the rapid band of the CEAM between 2 days and 30 days, of which the spectral zoom clearly unveils a harmonic at +13.6 days (25.8 h in the TRF) and a broad band peak around +7 days (28 h in the TRF).

After applying an appropriate high band pass filter, this band is isolated in time domain and shown over 130 days (from MJD 50000 to MJD 50130) in Fig. 2 for both wind terms in X and Y components as well as the full Non Inverted Barometer (NIB) pressure terms. It is remarkable that, for X and Y coordinates, wind and pressure terms are evidently proportional. Throughout the period 1949−2014 correlations amount to 0.57 for both X components and Y components and linear regression gives $\chi'_w \sim 2.1\chi'_p$. The detected proportionality appears to be a feature of the short term CEAM from 2 days to 1 month; it does not extend to the complementary spectral bands, ranging from 1 month to several years, where correlations between pressure and wind terms drop to 0.1. Another striking feature distinguishing the 2−30 day band from other parts of the spectrum is the fact that contributions of Northern and Southern hemisphere to the wind terms have synchronous variations, as evidenced by Fig. 2.

The torque that the atmosphere exerts on the solid Earth is composed of the bulge torque $\vec{\Gamma}_b$ acting on the equatorial bulge because of pressure and gravitational forces, and of a local torque $\vec{\Gamma}_l$ caused by pressure on the local topography as well as the friction drag on Earth's surface. In the non-rotating frame we have the following complex quantities: $H'_{w/p}$ for the equatorial wind/pressure term, Γ'_l for the local torque, Γ'_b for the bulge torque, Γ'_{ext} for the external gravitational torque on the atmosphere. As shown

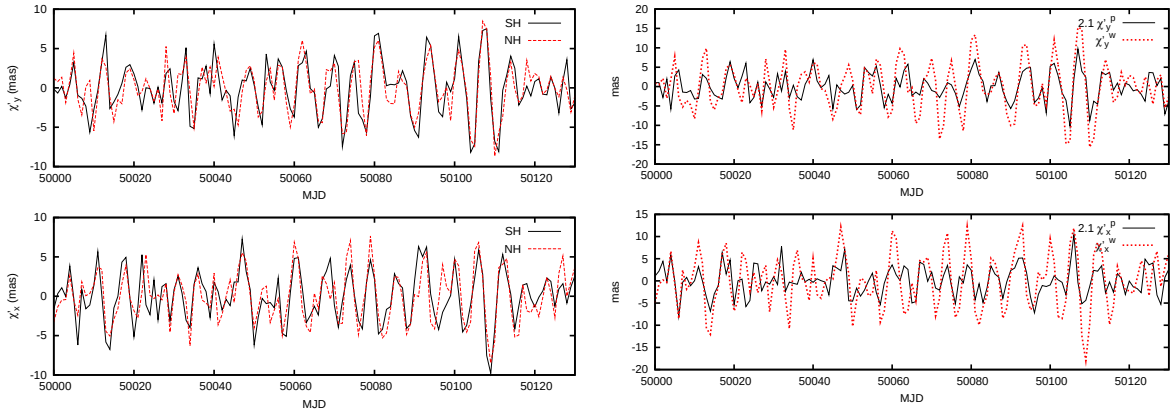

Figure 2: Left panel: contributions of the Southern Hemisphere (SH) and Northern Hemisphere (NH) to the wind term in χ'_X (bottom) and χ'_Y (top) for the 2−30 day band. Right panel: components X and Y of the Celestial Atmospheric Angular Momentum for wind term χ_w and NIB pressure term χ_p multiplied by 2.1 (linear regression coefficient from 1949 to 2014) computed from CEAM series after eliminating long term periods above 1 month. Time series over 130 days commencing at MJD 50000 (10/10, 1995).

in (Bizouard et al., 2014), law of the angular momentum allows to established in frequency domain that

$$1 - \frac{\sigma'}{\Omega} - \frac{\sigma'}{\Omega}\frac{\hat{H}'_w}{\hat{H}'_p} = \frac{-\hat{\Gamma}'_l + \hat{\Gamma}'_{ext}}{\hat{\Gamma}'_b} \ , \tag{2}$$

where the sign " ˆ " corresponds to the Fourier transform. If the residual torque $-\hat{\Gamma}'_l + \hat{\Gamma}'_{ext}$ is much smaller than the bulge torque Γ'_b then

$$\hat{H}'_w \approx \frac{\Omega - \sigma'}{\sigma'}\hat{H}'_p \ . \tag{3}$$

For positive angular frequencies σ' of the filtered CEAM, with periods from 2 days to 1 month, we have $1/30\,\Omega \leq \sigma' \leq 1/2\,\Omega$ (the retrograde part of the spectrum is much smaller); so, according to (3) pressure and wind terms become almost proportional. This is in contrast with the seasonal band (S_1 in the TRF) where the smallness of the local torque with respect to the bulge torque is not satisfied (Marcus et al., 2004). Considering for the lunar tidal band a typical magnitude of $|\chi'_p| \sim 0.2$ mas (see fit of section 4), the bulge torque magnitude, given by $|\Gamma'_b| = \Omega^2(C-A)|\chi'_p|$ (Marcus et al., 2004), amounts to $\sim 1.5\,10^{18}$ Nm. According to (Bizouard and Lambert, 2001), the diurnal external torque Γ'_{ext} is at most $\sim 10^{17}$ Nm, which is at least 10 times smaller than the equatorial bulge torque $\Omega|H'_p|$. Hence, as far as the local torque does not exceed the order of magnitude of the external torque, the above condition holds.

4. TIDAL ORIGIN OF THE 13.6-DAY TERM AND QUASI-WEEKLY BAND

The most natural hypothesis for the origin of the 13.66 day peak is the diurnal tidal wave O_1 determined by the Delaunay argument $2(F+\overline{\Omega})$ in the non-rotating frame, with $F = \overline{\omega} + l$ being the sum of the perigee argument $\overline{\omega}$ and the mean anomaly l, and $\overline{\Omega}$ being the longitude of the ascending node of the Moon on the ecliptic plane. As expected from tidal theory, the main peak is accompanied by a side-lobe at 13.63 days having the argument $2F + \overline{\Omega}$. These two components differ by the frequency $\overline{\Omega}$ of the displacement of the ascending node of the Moon, that is 1/18.6 cpy (cycles/year). The fact that we observe both of these peaks in CEAM substantiates the tesseral lunar influence on CEAM, in particular on the wind component. The celestial oscillations of arguments $\Phi_1 = 2F + 2\overline{\Omega}$ (13.66 days) and $\Phi_2 = 2F + \overline{\Omega}$ (13.63 days) are fitted by a least-squares method to the model $\chi' = \sum_{j=1}^{2}(m_c^j + i m_s^j)e^{i(\phi_j + \pi/2)}$. For the period 1949−2013 we obtain

$$\begin{aligned}
\chi'^{IB}_p[mas] &= (0.05 - i0.02)\, e^{i(\phi_1+\pi/2)} + (0.02 - i0.00)\, e^{i(\phi_2+\pi/2)} \\
\chi'^{NIB}_p[mas] &= (0.17 - i0.06)\, e^{i(\phi_1+\pi/2)} + (0.06 - i0.01)\, e^{i(\phi_2+\pi/2)} \\
\chi'_w[mas] &= (0.73 - i0.04)\, e^{i(\phi_1+\pi/2)} + (0.23 - i0.01)\, e^{i(\phi_2+\pi/2)}
\end{aligned} \tag{4}$$

The m_s terms are small relatively to m_c, except for the IB term. Disregarding the IB solution, the harmonic coefficients are therefore almost in phase with the tidal wave of argument $\phi_i+\pi/2$, confirming the proportionality of wind and pressure terms at this period and supporting their common tidal gravitational cause. The ratio $\chi'_w/\chi'^{NIB}_p = H'_w/H'_p \sim 4$ for both tidal frequencies does not match the numerical value of the condition (3), namely $H'_w/H'_p = 13.6 - 1 \sim 13$. On the other hand the ratio $\chi'_w/\chi'^{IB}_p \approx 14$ much better fits the expected ratio of 12.6, as if the effective pressure term around the O_1 frequency was the one restricted to continents and a static IB ocean. This is quite peculiar, since an IB response of the oceans is generally observed above 10 days but not at diurnal periods in the TRF.

The mere consideration that the tidal O_1 oscillation is at equilibrium accounts for both the amplitude and the phase of the NIB pressure term (Bizouard et al., 2014). If the hydrostatic assumption is true for surface pressure, tidal winds do not blow at Earth's surface, but at high altitudes. As tidal lunar variation of the horizontal wind have never been indeed reported in the low troposphere, tidal winds do not produce any notable friction torque. On the other hand, a tesseral tidal pressure field exerts a torque on the bulge but cannot contribute to the topographic torque, which results from spherical harmonics of degree higher than 3 (Bizouard, 2014). Thus the tidal atmospheric circulation does not contribute significantly to the local torque, in accordance with condition (3), and it accounts for the proportionality of χ'_w and χ'_p.

The broad band peak between 5 and 8 days is much more powerful than the thin peaks around 13.6 days, showing episodes with an amplitude of 10 mas. Some studies like (Brzeziński et al., 2002) attribute this weekly signal to the retrograde Rossby-Haurwitz atmospheric normal mode Ψ^1_1, having in the TRF the geometry of a spherical harmonic $\cos(\phi)e^{i\lambda}$ (ϕ is the latitude, λ is the longitude) propagating to the west. In the non-rotating frame, this resonant mode propagates from the west to the east as the Moon, and with an averaged period of ~ 7 days it could be amplified at planetary scale by the minor lunar tides around 7.09 days at least 100 times smaller than O_1. Moreover, at quasi-weekly periods ($\sigma'/\Omega \approx 1/7$) the ratio $\chi'_w/\chi'^{NIB}_p \approx 5.8$ fits the condition (3) reading $H'_w/H'_p \approx 7 - 1 = 6$, and is thus valid for the full pressure term in contrast to what is observed at 13.6 days.

5. CONCLUSION

Our quintessential conclusion is as follows: from 2 to 30 days in the CRF (24.8 h to 48 h in the TRF) the retrograde equatorial atmospheric angular momentum variations are triggered by the Moon. In order to observe a possible effect on nutation, improvements of the VLBI/GNSS data processing as well as optimized observation schedules are required.

6. REFERENCES

Barnes, R.T.H., Hide, R., White, A.A., Wilson, C.A., 1983, "Atmospheric angular momentum fluctuations, length-of-day changes and polar motion", Proc. R. Soc. London A ,387, pp. 31–73.

Bizouard, C., Brzeziński A., Petrov, S., 1998, "Diurnal atmospheric forcing and temporal variations of the nutation amplitudes", J. Geodesy, 72, pp. 561–577.

Bizouard, C., Lambert, S., 2001, "Lunisolar torque on the atmosphere and Earth's rotation", Planetary and Space Science, 50(3), pp. 323–333.

Bizouard, C., 2014, "Le mouvement du pôle de l'heure au siècle", PAF, 284 pp.

Bizouard, C., Zotov, L., Sidorenkov, N., 2014, "Lunar influence on equatorial angular momentum", J. Geophys. Res.: Atmosphere, 119, pp. 11,920–11,931, DOI: 10.1002/2014JD022240.

Brzeziński, A., 1994, "Polar motion excitation by variations of the effective angular momentum function, II: Extended model", Manuscripta Geodaetica, 19, 157–171.

Brzeziński, A., Bizouard, C., Petrov, S., 2002, "Influence of the atmosphere on Earth rotation: what new can be learnt from the recent atmospheric angular momentum estimates?" Surv. Geophys., 23, pp. 33–69.

IERS Conventions, 2010, G. Petit, B. Luzum (eds.), IERS Technical Note 36, Frankfurt am Main: Verlag des Bundesamts für Kartographie und Geodäsie.

Marcus, S., de Viron, O., Dickey, J., 2004, "Atmospheric contributions to Earth Nutation: Geodetic constraints and limitations of the torque approach", Atmospheric sciences, 61, pp. 352–356.

SBA, 2014, website of the IERS Special Bureau for the Atmosphere `http://ftp.aer.com/pub/anon_collaborations/sba/`.

ESTIMATION OF NUTATION RATES FROM COMBINATION OF RING LASER AND VLBI DATA

M. TERCJAK[1], J. BÖHM[2], A. BRZEZIŃSKI[1,3], A. GEBAUER[4], T. KLÜGEL[5], U. SCHREIBER[4], M. SCHINDELEGGER[2]
[1] Warsaw University of Technology
Plac Politechniki 1, 00-661 Warsaw, Poland
e-mail: m.tercjak@gik.pw.edu.pl
[2] Vienna University of Technology, Austria
[3] Space Research Centre, Polish Academy of Sciences, Warsaw, Poland
[4] Forschungseinrichtung Satellitengeodäsie Technische Universität München, Germany
[5] Bundesamt für Kartographie und Geodäsie, Geodätisches Observatorium Wettzell, Germany

ABSTRACT. Ring laser gyroscopes (RLG) are instruments measuring inertial rotations locally and in real-time without the need for an external reference system. They are sensitive to variations in the instantaneous rotation vector, therefore they are considered as a potential complement to space geodetic techniques for studying Earth rotation. In this work we examine the usability of ring laser observations for estimation of nutation rates. We investigate possibilities of computing those parameters from only one ring laser and we simulate the usage of several instruments. We also combine simulated RLG observations with actual Very Long Baseline Interferometry VLBI data and compare them with real Wettzell RLG data. Our results attest to the theoretical possibility of estimating nutation rates, albeit with a number of restrictive assumptions.

1. MOTIVATION AND ASSUMPTIONS

Ring laser gyroscopes are instruments which present a dynamical approach to the determination of Earth rotation parameters. They enable measuring Earth rotation on the surface of the Earth, as they are sensitive to variations in the instantaneous rotation vector. They are considered as a potential complement to space geodetic techniques in studying Earth rotation. To date many experiments have been conducted in order to investigate possible advantages of combining ring laser observations and data from space geodetic techniques, especially from Very Long Baseline Interferometry. The majority of those experiments concern polar motion and universal time (UT1) variations. In this work we examine the potential usage of ring laser observations for estimating nutation rates simulating two weeks of ring laser observations and checking the conditions under which such an estimation is possible. Our work is divided into three parts. The first part concerns the determination of nutation rates from ring laser data only, in the second part we address a combined solution with VLBI data, and in the last part we compare our results obtained from simulated RLG observations with those from real Wettzell data.

The conducted simulation is based on the relative Sagnac frequency equation (Nilsson et al., 2012):

$$\Delta S = \cot\varphi(m_x \cos\lambda + m_y \sin\lambda) + m_z + \Delta S_{\text{tilt}} + \Delta S_{\text{instr}}, \tag{1}$$

where φ and λ are latitude and longitude of the instrument, ΔS_{tilt}, ΔS_{instr} are errors caused by tilts and instrumental imperfections, and m_x, m_y, m_z are dimensionless parameters defining perturbations of the instantaneous rotation vector $\vec{\omega} = \Omega_0[m_x\ m_y\ 1+m_z]^T$ (with Ω_0 denoting the mean angular speed of rotation). Hence m_x, m_y describe polar motion of the Instantaneous Rotation Pole (IRP), which relates to the motion of the Celestial Intermediate Pole (CIP) via (Cerveira et al., 2009):

$$m_x = \frac{1}{\Omega_0}(\Omega_0 x_p - \dot{y}_p + (\dot{X} + d\dot{X})\sin\theta - (\dot{Y} + d\dot{Y})\cos\theta), \tag{2}$$

$$m_y = \frac{1}{\Omega_0}(-\Omega_0 y_p - \dot{x}_p + (\dot{X} + d\dot{X})\cos\theta + (\dot{Y} + d\dot{Y})\sin\theta), \tag{3}$$

where θ denotes the Earth rotation angle, x_p and $-y_p$ are terrestrial components of the CIP, describing polar motion (PM), $X$and Y are coordinates of the CIP in Geocentric Celestial Reference System (GCRS),

dX, dY are the celestial pole offsets describing the celestial perturbation of the CIP, that is nutation, and the dot represents the time derivative. Variations of the axial component of the instantaneous rotation vector are expressed by (Nilsson et al., 2012):

$$m_z = 1.0027 d\dot{U}T1, \tag{4}$$

where dUT1 = UT1 − UTC (with UTC denoting the coordinated universal time) and 1.0027 is the proportionality factor between the solar and the sidereal time scales.

The design matrix A is constructed assuming one value of the nutation offset rates $d\dot{X}$, $d\dot{Y}$ and one value of the instrumental error per day as unknowns. The right-hand side vector is $L = \Delta S_{\text{obs}} - \Delta S_{\text{comp}}$ + random noise. For ΔS_{obs} we use values obtained with PM and dUT1 from the C04 08 EOP series, taking into account ocean tides, and with nutation from the IAU 2006/2000 model (X, Y) and offsets (dX, dY) from the C04 08 series. ΔS_{comp} is derived the same way, with the exception of excluding nutation offsets from the C04 08 series. The random noise is generated by a random multiplication with a prescribed accuracy level. The weighting matrix P contains σ^{-2} on the diagonal with $\sigma = 10^{-11}$, since it turned out that the accuracy level 10^{-8} suggested in (Nilsson et al., 2012) is not adequate to our task. To obtain satisfactory results we had to increase the accuracy level by three orders of magnitude. The first day of observations is assumed to be September 15, 2011, as it is the first day of a two-week campaign of continuous VLBI sessions CONT11.

The first question we are looking for an answer is how many instruments do we need. For this end we estimate nutation rates assuming the use of one to six instruments, located regularly over the world. The locations of RLG are assumed in the same places as the existing VLBI stations: Wettzell, Hobart, Fortaleza, Kokee, Badary and Syowa. First we assume one RLG in Wettzell, then two (Wettzell and Hobart), then three (Wettzell, Hobart and Fortaleza), and so on. The second problem we want to investigate is the potential advantage of a combination of RLG and VLBI data. For this purpose we process CONT11 sessions using the VieVS software (Böhm et al., 2012) following (Nilsson et al., 2012), and then combine simulated RLG data with VLBI observations on the normal equation level. As there are no common parameters for both techniques the new normal equation matrix and the right-hand side vector are prepared as follows:

$$N_{\text{new}} = \begin{bmatrix} N_{\text{VLBI}} & 0 \\ 0 & N_{\text{RLG}} \end{bmatrix} \text{ and } L_{new} = \begin{bmatrix} L_{\text{VLBI}} \\ L_{\text{RLG}} \end{bmatrix}, \tag{5}$$

and taking into account constraints, i.e. nutation rates = nutation finite differences

$$N_C = \begin{bmatrix} N_{\text{new}} & C^T \\ C & 0 \end{bmatrix} \text{ and } L_C = \begin{bmatrix} L_{\text{new}} \\ 0 \end{bmatrix}. \tag{6}$$

For our combination we use simulations based on one, three and six instruments, starting with the present-day accuracy level of 10^{-8} and followed by refinement to 10^{-9}, 10^{-10} and 10^{-11}. The last part of the procedure consists in a comparison of our simulated RLG observations with real data, from the Geodetic Observatory Wettzell. At this stage we simulate observations for one instrument only located at Wettzell, assuming the present-day accuracy level of 10^{-8} and a time span of 24 days (May 1–25, 2010).

2. RESULTS

Results of the first part, i.e. dX and dY rates derived under the assumptions of using of one to six RLG, are shown in Fig. 1, and the corresponding RMS errors of residuals are summarized in Table 1.

The graphical results are compared with a model time series taken to be nutation rates as computed based on the C04 08 series. It can be seen that for one and two devices the results are less consistent with the model as those obtained from three and more RLG. This observation conforms with the results

	1	2	3	4	5	6
$d\dot{X}$	0.5407	0.2480	0.0601	0.0555	0.0466	0.0450
$d\dot{Y}$	0.4634	0.3654	0.1237	0.1195	0.1373	0.1243

Table 1: RMSs of the residuals with respect to the number of used ring lasers. Values in 10^{-7}mas/s.

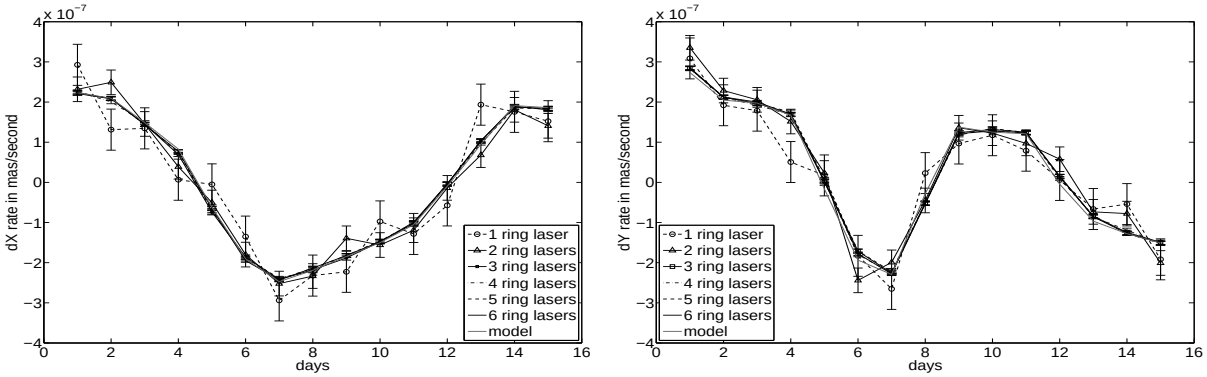

Figure 1: Nutation rates in X and Y, from RLG observations depending on the number of instruments.

of Nilsson et al. (2012), who concluded that for estimation of the complete Earth rotation vector at least three ring lasers with different orientations would be needed.

Results for the combined solution are shown in Fig. 2. It turns out again, that the present-day accuracy level of RLGs is not sufficient for our task. For a level of 10^{-8} there is no difference if we have one or more instruments, the combination does not provide a satisfactory solution. Similarities with the expected model curve emerge with $\sigma = 10^{-9}$ and are further enhanced for the case of refined accuracy level. As apparent from Figs. 2a and 2b the differences between values obtained from one RLG and from three and six are not so large if we use 10^{-9}, but when assuming 10^{-10} the differences are considerable (Figs. 2c and 2d). This might again suggest that one instrument is not enough, even for a combined solution, but it also shows that the present-day accuracy level is not adequate for the task.

After analyzing simulated data, we estimate nutation rates based on real RLG data from the Wettzell instrument. We use the same algorithm, but for ΔS_{obs} we take real observations, after accounting for

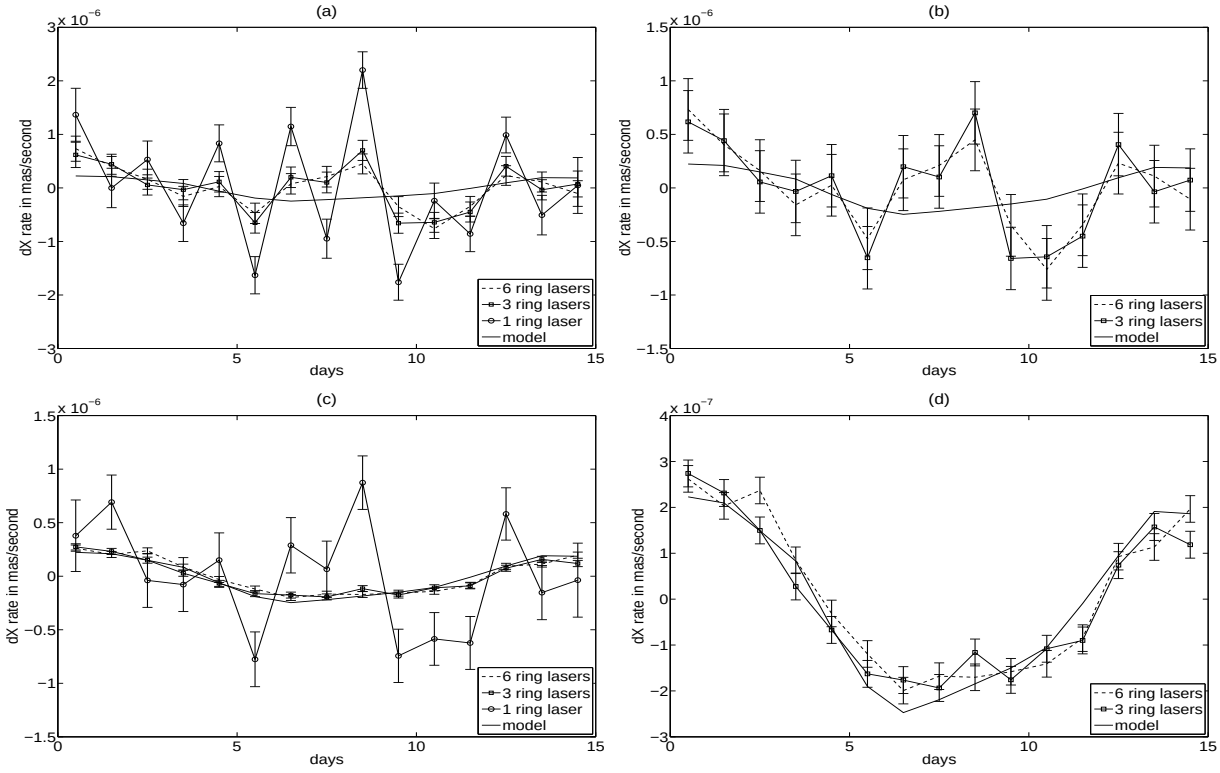

Figure 2: Nutation rates from VLBI and RLG combined solution. Plots (a) and (b) show results for an assumed RLG accuracy level of 10^{-9}, and (c) and (d) for 10^{-10}. Note the different scales.

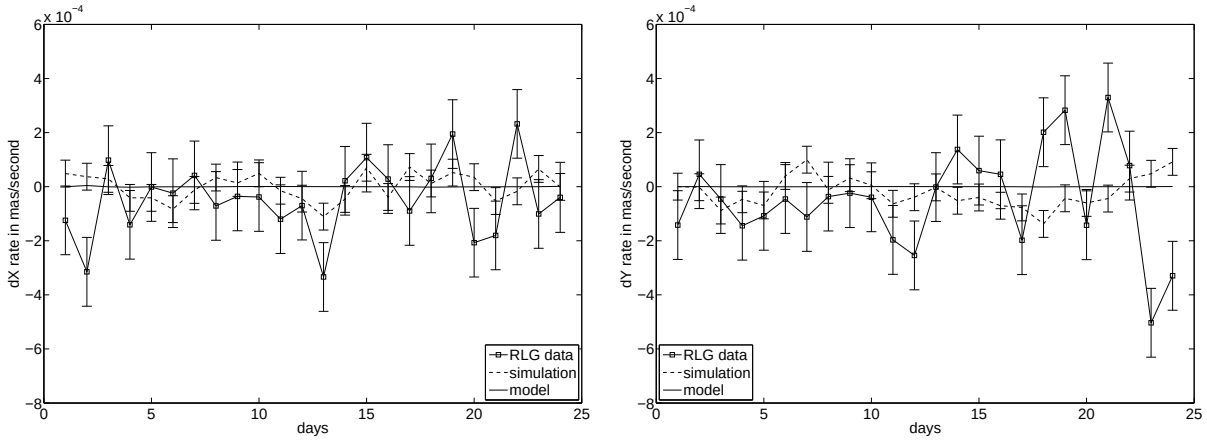

Figure 3: Comparison of results from simulated and real Wettzell RLG data. The solid line with square markers shows results obtained based on real data and the dashed one – based on simulated observations.

tilt corrections. Figure 3 shows that the results from simulated observation, though not satisfactory, nevertheless better agree with the model than the results based on real data. This might indicate that in our investigation we assume a too simple model for the Sagnac frequency or that we did not take into account some important local effects.

3. CONCLUSIONS

We demonstrated that the estimation of nutation rates from ring laser observations is possible. A comparison of our simulations with real ring laser data showed that the recent accuracy is not sufficient to detect nutation rates in the time series. In order to improve VLBI measurements of nutation rates at least three RLG instruments and an accuracy level three orders of magnitude higher than nowadays are required. This is hard to achieve as shown by Schreiber et al. (2011). Moreover it should be mentioned that we used a very simple model of relative Sagnac frequency and did not take into account any local effects and we considered only the geometrical aspect associated with the localization of instruments. This discouraging conclusion is not surprising, as the ring laser is not very sensitive to nutations, and it was never considered to measure nutation rates at all. In this context it should also be stressed that one instrument measuring one component is compared with a global set of radio telescopes. However, the ring laser yields valuable Earth rotation data in the terrestrial frame, as it is the only instrument measuring polar motion of the rotation axis without the need of conventions. Recent improvements in the long term stability of the ring laser are promising that investigations of this topic should be continued.

Acknowledgements. This work was supported by the Polish national science foundation (NCN) under grant No. 2012/05/B/ST10/02132. The first author express her thanks to the International Association of Geodesy for Young Scientists Travel Award and the Local Organizing Committee for free accommodation and waiving the registration fee.

4. REFERENCES

Cerveira, P.J.M., Böhm, J., Schuh, H., Klügel, T., Velikoseltsev, A., Schreiber, U., Brzeziński, A., 2009, "Earth rotation observed by very long baseline interferometry and ring laser", Pure Appl Geophys., 166, pp. 1499–1517.

Nilsson, T., Böhm, J., Schuh, H., Schreiber, U., Gebauer, A., Klügel, T., 2012, "Combining VLBI and ring laser observations for determination of high frequency earth rotation variation", Journal of Geodynamics, 62, pp. 69–73.

Böhm, J., Böhm, S., Nilsson, T., Pany, A., Plank, L., Spicakova, H., Teke, K., Schuh, H., 2012, "The new Vienna VLBI Software VieVS", In: IAG Symposia, 136, pp. 1007–1011.

Schreiber, K.U., Klügel, T., Wells, J.-P.R., Hurst, R.B., Gebauer, A., 2011, "How to Detect the Chandler and the Annual Wobble of the Earth with a Large Ring Laser Gyroscope", Phys. Rev. Lett., 107, 173904.

ON APPLICATION OF THE COMPLEX DEMODULATION FOR MONITORING EARTH ROTATION: ANALYSIS OF THE NUTATION AND LONG PERIODIC UT1 DATA ESTIMATED BY VieVS CD

A. BRZEZIŃSKI[1,2], A. WIELGOSZ[2], S. BÖHM[3]
[1] Inst. of Geodesy and Geodetic Astronomy, Warsaw University of Technology, Warsaw, Poland
[2] Space Research Centre, Polish Academy of Sciences, Warsaw, Poland
[3] Department of Geodesy and Geoinformation, Vienna Univ. of Technology, Vienna, Austria
e-mail: alek@cbk.waw.pl

ABSTRACT. In the recent work (Böhm et al., J. Geodynamics, 62(2012), 56–68) we demonstrated the application of the complex demodulation (CD) technique for VLBI estimation of the Earth orientation parameters (EOP). This technique enables simultaneous determination of the long period components of polar motion (x,y), universal time (dUT1=UT1−UTC) and nutation (celestial pole offsets dX,dY) as well as the high frequency (diurnal, semidiurnal, ...) components of polar motion and dUT1. In this work we perform analysis of the retrograde diurnal component of polar motion and the low frequency component of dUT1 estimated by the VieVS CD software. By comparison to the results based on the celestial pole offsets and dUT1 series from the combined solutions IVS and IERS we demonstrate consistency of the CD parametrization with the standard approach.

1. INTRODUCTION

The complex demodulation (CD) technique enables simultaneous determination of the long period components of polar motion (x,y), universal time (dUT1=UT1−UTC) and nutation (celestial pole offsets dX,dY) as well as the high frequency (diurnal, semidiurnal, ...) components of polar motion and dUT1 (Brzeziński, 2012). The algorithm of complex demodulation was implemented by Böhm et al. (2012) into a dedicated version of the Vienna Very Long Baseline Interferometry (VLBI) Software VieVS. They processed around 3700 geodetic 24-h observing sessions over 1984.0–2010.5 and estimated simultaneously the time series of the long periodic components of the Earth Orientation Parameters (EOP) and of diurnal, semidiurnal, terdiurnal and quarterdiurnal components of polar motion and dUT1.

The high frequency components of EOP estimated by Böhm et al. (2012) were analyzed by Brzeziński and Böhm (2012). The analysis reported here concerns the low frequency components of EOP estimated by the use of the VieVS CD algorithm. The purpose is twofold. First, we want to demonstrate that the long periodic components of EOP estimated with the use of CD parametrization are consistent with those obtained by the use of standard parametrization. Second, we like to show that the diurnal retrograde component of polar motion demodulated by CD is equivalent to the standard time series of the celestial pole offsets.

The results concerning low frequency polar motion were reported by Brzeziński et al. (2014). Here we confine attention to the results based on the nutation and dUT1 series.

2. DATA DESCRIPTION AND ANALYSIS

The following parametrization of polar motion (PM) and universal time (UT1) has been applied by Böhm et al. (2012) for complex demodulation of VLBI data

$$\begin{bmatrix} x(t) \\ y(t) \end{bmatrix} = \sum_{\ell=-N}^{N} \left\{ \begin{bmatrix} x_\ell(t) \\ y_\ell(t) \end{bmatrix} \cos(\ell\phi) + \begin{bmatrix} y_\ell(t) \\ -x_\ell(t) \end{bmatrix} \sin(\ell\phi) \right\}, \tag{1}$$

$$d\mathrm{UT1}(t) = \sum_{\ell=0}^{N} \left[u^c_\ell(t) \cos(\ell\phi) + u^s_\ell(t) \sin(\ell\phi) \right], \tag{2}$$

where x, y are the reported coordinates of polar motion, dUT1=UT1−UTC is the difference of UT1 and the uniform time scale UTC, ϕ =GMST+π, GMST stands for Greenwich Mean Sidereal Time and $x_\ell(t)$,

$y_\ell(t)$, $u^s_\ell(t)$, $u^c_\ell(t)$ are assumed to be slowly varying functions of time t. When estimated from VLBI data, these time dependent amplitudes are treated as constant during one 24-hour session. We also assume that the argument ϕ is a linear function of time $\phi = \Omega t + \phi_\circ$, where Ω denotes the mean angular velocity of diurnal sidereal rotation (equal 2π rad/sidereal day $= 7\,292\,115 \times 10^{-11}$ rad/s) and $\phi_\circ$ is a constant phase referred to the initial epoch $t = 0$. Let us make the following remarks:

- the terms $\ell = 0$ of the expansion (1)–(2) are the long periodic components of PM and UT1 estimated in standard adjustment;
- the terms $\ell = \pm 1, \pm 2, \pm 3, \pm 4, \ldots$, express quasi diurnal, semidiurnal, terdiurnal, quarterdiurnal, ..., variations in PM (retrograde/prograde for $-/+$) and in UT1;
- the $\ell = -1$ term of the expansion (1) gives an equivalent representation of the celestial pole offsets dX, dY, in a sense that $[x_{-1}(t), -y_{-1}(t)] = [dX(t), dY(t)]$ in the first order approximation.

Böhm et al. (2012) performed VLBI data processing over 1984.0–2010.5 based on the complex demodulation model described by equations (1)–(2) with $N = 4$. In the following analysis we will use the diurnal retrograde component of polar motion $[x_{-1}(t), -y_{-1}(t)]$ representing nutation, and the low frequency of dUT1, $u^c_0(t)$. As an external reference we use the nutation $[dX(t), dY(t)]$ and dUT1(t) series from the following two combined solutions

- IVS 13q2X (http://ivscc.gsfc.nasa.gov) which is based on VLBI technique only;
- IERS C04 (www.iers.org) which is a combined solution from all space geodetic techniques, nevertheless the computations of nutation and UT1 series rely also basically on VLBI measurements.

All three time series have been reduced and analyzed in the same way.

Nutation component. We estimated corrections to the precession (1-st order polynomial) and 6 largest components of nutation – 18.6 yr, 9.3 yr, 1 yr, 0.5 yr and 13.7 d. As there is a strong interference between the FCN signal and the retrograde annual nutation, we removed the FCN empirical model recommended by the IERS Conventions (2010) prior to the least-squares adjustment of the nutation harmonics. The nutation series, after removal of the estimated corrections to the conventional precession-nutation model and adding back the FCN empirical model, are compared in Fig. 1. The estimated corrections to the forced nutation terms are illustrated by the phasor diagrams in Fig. 2.

From Fig. 1 it can be seen that the early nutation data is noisy and contains variability which is not consistent with the rest of the series. When the data analysis does not include weighting it is recommended to remove data prior to 1990. But also after 1990 the reduction of noise level and of difference between the three series with time is clearly seen. We can conclude that when considering the residual nutation signal in time domain, the VieVS CD series is consistent with both the IVS and IERS combination series.

The estimated corrections of the forced nutation terms, shown in Fig. 2, based on the VieVS CD series are also consistent with those derived from the IVS and IERS series. The largest corrections are to the main term of nutation with period of 18.6 years. The amplitude of the VieVS CD correction term ($\approx$50 μas) is between the result of IVS ($\approx$60 μas) and IERS ($\approx$40 μas), while the difference of phase is about 30° with respect to IVS and up to 60° with respect to IERS. The other correction terms do not exceed the level of 20μas; the difference of results based on VieVS and the two combined solutions is generally not larger than the difference of results from the two combined series.

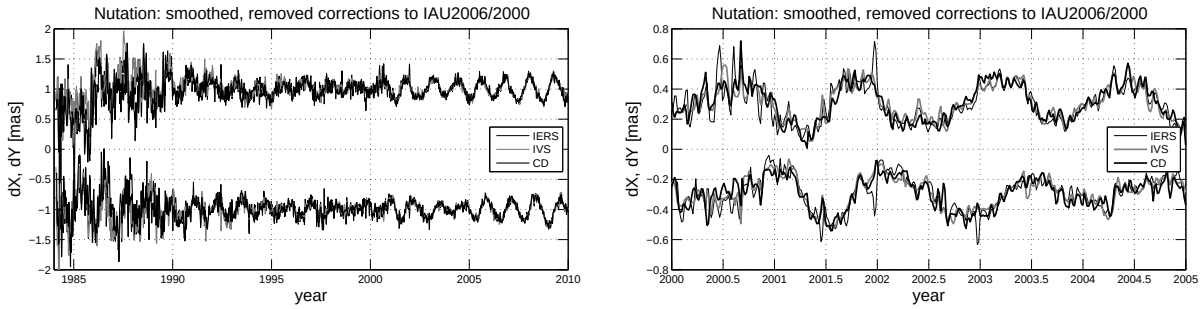

Figure 1: Nutation component (PM with $\ell = -1$) estimated by VieVS CD after applying empirical corrections to the conventional precession-nutation model and a weak smoothing (left) and its zoom (right). The VieVS CD series is compared to the combined solutions IVS 13q2X and IERS C04.

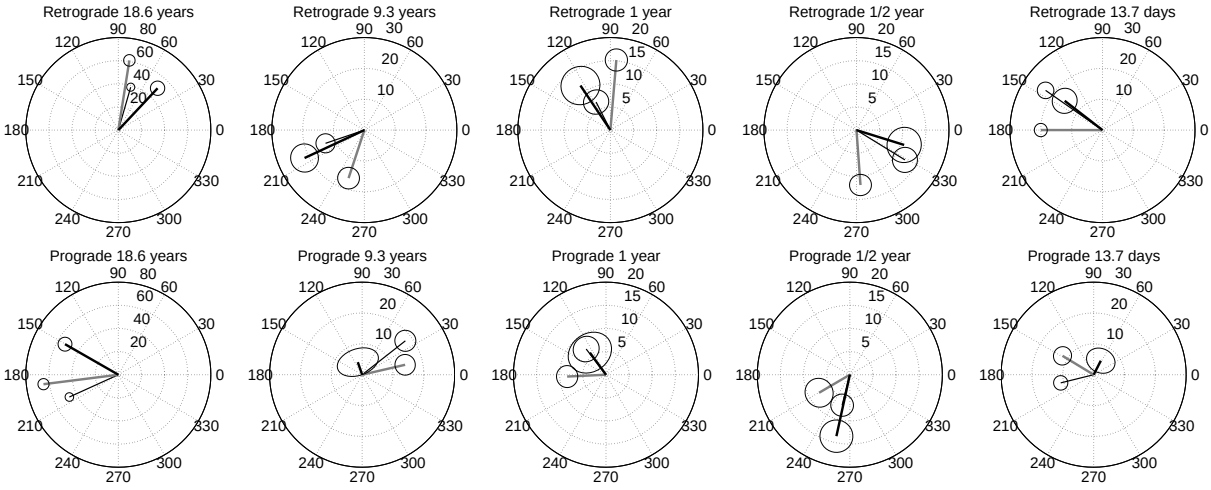

Figure 2: Estimated corrections to the selected nutation terms of the conventional model with standard deviations of estimates shown as ellipses. Reference precession/nutation model: IAU 2000/2006, units: microarcseconds, input time series: CD VieVS – thick black, IVS 13q2X – thick gray, and IERS C04 – thin black, period of analysis: 1984.0–2010.5.

Low frequency component of UT1. Comparison of the low frequency component of dUT1 is shown in Fig. 3. We started from adding back the leap seconds and removing the model of variation due to the zonal tides (IERS Conventions, 2010). The three curves are very similar. The only difference is in the error bars which are larger in case of VieVS CD, particularly in the first part of data. Next, we estimated by the weighted least-squares adjustment the model comprising the 4-th degree polynomial and the sum of harmonics with periods of 11.2, 2, 1, 1/2 and 1/3 years.

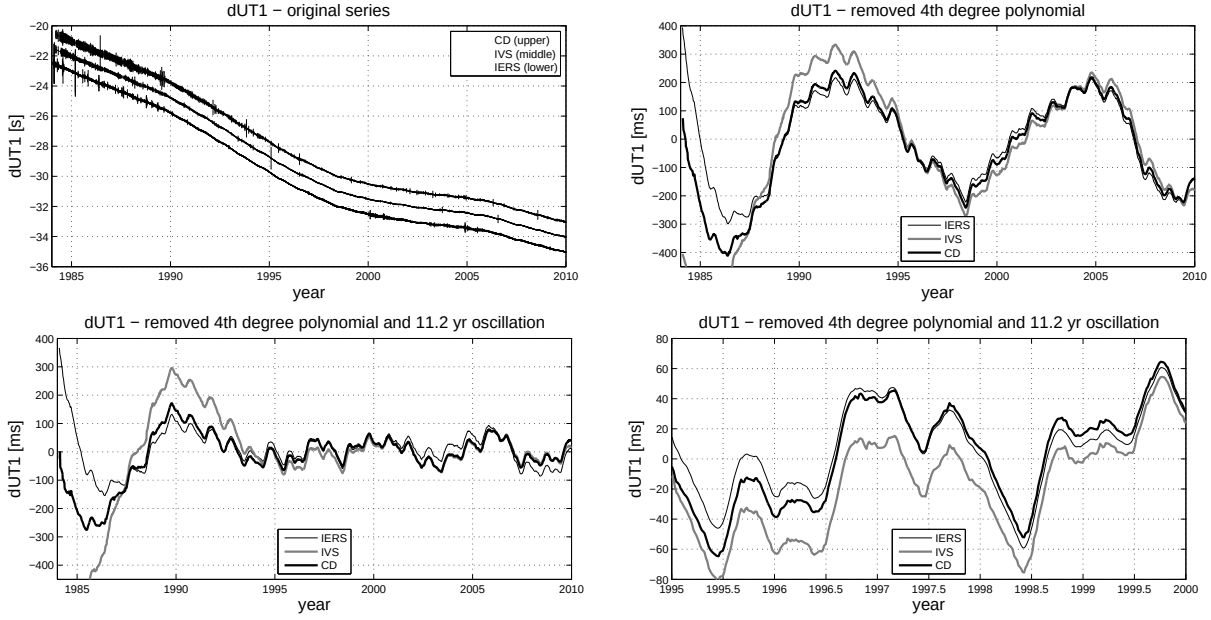

Figure 3: Low frequency component of dUT1: original series with the error bars after adding back the leap seconds and removal of the conventional tidal model (top left), after additional removal of the 4th order polynomial (top right) and the 11.2-year sinusoid (bottom left), and its zoom (bottom right).

From the comparison shown in Fig. 3 it can be seen that there is a good agreement of dUT1 data at seasonal and subseasonal frequencies. The difference is in the long periodic behavior. One reason of that can be the decrease of formal errors with time causing that the estimation of the model depends heavily on the recent data. It is particularly well seen in the left lower plot where the large decadal variability still

exists prior to 1995. Another reason is the high correlation of errors between the estimated coefficients of the polynomial and 11.2-yr sinusoid. Clearly, a more refined model is needed for representing the long periodic variation in dUT1.

An excellent agreement is also found from comparison of the harmonic terms of the model (Fig. 4), with a higher consistency between results from VieVS CD and IVS.

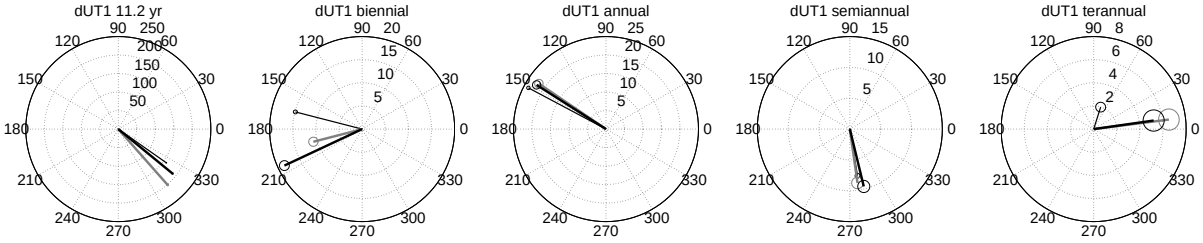

Figure 4: Estimated parameters of the periodical components of dUT1 with standard deviations of estimates shown as ellipses. Units: milliseconds, input time series: CD VieVS – thick black, IVS 13q2X – thick gray, and IERS C04 – thin black (cf. Fig. 3), period of analysis: 1984.0–2010.5.

3. SUMMARY AND CONCLUSIONS

The complex demodulation algorithm is an efficient tool for extracting the high frequency signals in Earth rotation from the VLBI observations. Its application to the EOP determination by other space geodetic techniques is also possible. Here we perform analysis of the retrograde diurnal component of polar motion and of the low frequency component of dUT1 estimated by the VieVS CD software (Böhm et al., 2012). Results have been compared to those based on the celestial pole offsets and dUT1 series from the combined solutions IVS and IERS in order to check the consistency of the CD parametrization with the standard approach.

When considering the residual nutation signal in time domain, the VieVS CD series is found to be consistent with both the IVS and IERS combination series. The differences between series are larger for early data and decrease with time reaching very low level after 2005. The estimated corrections of the forced nutation terms based on the VieVS CD series are also consistent with those derived from the IVS and IERS series in a sense that the difference is not larger than the difference of results from the two combination series.

Comparison of the low frequency component of dUT1 shows a good agreement of the three curves at seasonal and subseasonal frequencies. The differences of the long periodic variation could be attributed to inadequate modeling. An excellent agreement is found for the parameters of the harmonic terms of the model, particularly between those from VieVS CD and IVS.

Acknowledgements. The Local Organizing Committee of the Journées 2014 is acknowledged for the free accommodation and waiving the registration fee. This work and participation of A.B. in the conference was supported by the Polish national science foundation NCN under grant No. DEC-2012/05/B/ST10/02132.

4. REFERENCES

Böhm, S., Brzeziński, A., Schuh, H., 2012, "Complex demodulation in VLBI estimation of high frequency Earth rotation components", J. Geodynamics, 62, pp. 56–68, doi: 10.1016/j.jog.2011.10.002.

Brzeziński, A., 2012, "On estimation of high frequency geophysical signals in Earth rotation by complex demodulation", J. Geodynamics, 62, pp. 74–82, doi: 10.1016/j.jog.2012.01.008.

Brzeziński, A., Böhm, S., 2012, "Analysis of the high frequency components of Earth rotation demodulated from VLBI data", In: Proc. Journées 2011 Systèmes de Référence Spatio-Temporels, H. Schuh, S. Böhm, T. Nilsson, N. Capitaine (eds.), Observatoire de Paris, pp. 132–135.

Brzeziński, A., Wielgosz A, Böhm, S., 2014, "On application of the complex demodulation procedure for VLBI data analysis: consistency check with the standard approach using the long periodic EOP components", Geophys. Research Abstracts, Vol. 16, EGU2014-15198, EGU General Assembly 2014.

IERS Conventions, 2010, G. Petit, B. Luzum (eds.), IERS Technical Note 36, Frankfurt am Main: Verlag des Bundesamts für Kartographie und Geodäsie.

EFFECTS OF THE TIDAL MASS REDISTRIBUTION ON THE EARTH ROTATION

T. BAENAS[1], J.M. FERRÁNDIZ[1], A. ESCAPA[1,2], J. GETINO[3]
[1] Department of Applied Mathematics, University of Alicante
PO Box 99, E-03080 Alicante, Spain
e-mail: tomas.baenas@ua.es
[2] Department of Mechanical, Informatics and Aerospace Engineering, University of León
E-24071 León, Spain
[3] Department of Applied Mathematics, University of Valladolid
E-47011 Valladolid, Spain

ABSTRACT. The effects of the tidal mass redistributions on the Earth precession and nutations are revisited, under various hypothesis on the elastic response of the Earth and using the Hamiltonian approach. New non-negligible secular and periodic contributions have been found.

1. INTRODUCTION

The gravitational action of the Moon and the Sun on the deformable Earth perturbs its state by inducing in it a mass redistribution. In turn, such mass redistribution produces a variation of the gravitational energy of the system, leading to an additional term commonly referred to as *redistribution tidal potential*. In this regard, Moon and Sun are viewed as perturbed bodies. The effects of that redistribution potential on the forced rotational motion of the Earth figure axis have been previously discussed by Souchay and Folgueira (2000), Escapa et al. (2004), Ferrándiz et al. (2012) and Baenas (2014), within a Hamiltonian framework. Another approach to the problem, based in the SOS equations (Sasao et al. 1980), can be found in Lambert and Mathews (2006).

The Hamiltonian treatment of the elastic Earth follows the classic ideas by Love (1911) and assumes that the variation of the Earth's gravitational potential due to its tidal mass redistribution is proportional to the perturbing potential – Getino and Ferrándiz (1990, 1991, 1995), Kubo (1991), Escapa (2011). However, that proportionality can be modeled in various ways, adapted to different rheological hypothesis and different levels of mathematical complexity. A first, simplified model consists in considering a sole, global constant, within the Love's number approach (Munk and MacDonald 1960), to determine the additional gravitational potential at the deformed Earth surface. Besides, this simplified elastic behaviour has been profusely used to search the effects of the associated changes of the inertia tensor and kinetic energy on the Earth's rotation – which are indeed larger than those due to the incremental potential. However, it is only compatible with a rheological Earth model which is also simplified, the non-perturbed state being a non-rotating sphere (Wahr 1981).

Before introducing a more general elastic response in the analytical modeling, a rheological model based in Wahr (1981) can be considered as a first step. In such a situation closer to reality, the non-perturbed state is assumed to be ellipsoidal and rotating. The Earth's elastic response, seen, e.g., in the redistribution tidal potential, is described by means of a set of Love's numbers, which can depend on the order m of the spherical harmonics in the geopotential expansion and on the excitation frequencies as well. They form a set of complex numbers in the general case corresponding to some anelastic behaviour in the response, a case included, e.g., in the IERS Conventions 2010 (Petit and Luzum 2010). We denote those numbers by

$$\bar{k}_{2m} = \left|\bar{k}_{2m}\right| e^{i\varepsilon_{2m}}. \tag{1}$$

From a dynamical point of view, that hypothesis requires an *ab initio* reconstruction of the rotation theory (Baenas 2014), in which the expression of the redistribution energy potential is given by the sum

(over p and q, both representing either Moon or Sun) of terms of the form

$$\begin{aligned} V_{t;p,q} &= \frac{a_E^5}{r^3 r'^3} G m_p m_q \left\{ \left|\bar{k}_{20}\right| \cos\varepsilon_{20} \mathscr{C}_{20}(\eta,\alpha)\, \mathscr{C}'_{20}(\eta',\alpha') \right. \\ &+ \left|\bar{k}_{21}\right| \frac{1}{3} \left[\mathscr{C}_{21}(\eta,\alpha)\, \mathscr{C}'_{21}(\eta',\alpha'-\varepsilon_{21}) + \mathscr{S}_{21}(\eta,\alpha)\, \mathscr{S}'_{21}(\eta',\alpha'-\varepsilon_{21}) \right] \\ &+ \left. \left|\bar{k}_{22}\right| \frac{1}{12} \left[\mathscr{C}_{22}(\eta,\alpha)\, \mathscr{C}'_{22}\left(\eta',\alpha'-\frac{\varepsilon_{22}}{2}\right) + \mathscr{S}_{22}(\eta,\alpha)\, \mathscr{S}'_{22}\left(\eta',\alpha'-\frac{\varepsilon_{22}}{2}\right) \right] \right\}, \end{aligned} \tag{2}$$

where $\mathscr{C}_{2j}$, $\mathscr{S}_{2j}$ and $\mathscr{C}'_{2j}$, $\mathscr{S}'_{2j}$, stand for the second degree real surface spherical harmonics, related to perturbed bodies (unmarked) and perturbing ones (with $'$) respectively, and relative to the terrestrial frame, (r,η,α) being the spherical coordinates – radial distance, colatitude and longitude. The symbol G denotes the gravitational constant; a_E is a conventional mean Earth's radius and m_p, m_q stands for the masses.

2. ANALYTICAL MODELING

An Andoyer-like set of canonical variables is used to describe the rotation linking the non-rotating system $OXYZ$ (an ecliptic frame) and the terrestrial one $Oxyz$ (a Tisserand mean system, Munk and MacDonald 1960, Escapa et al. this vol.), where O represents the Earth's barycenter. The canonical coordinates and conjugated momenta are denoted by $p = (\lambda,\mu,\nu)$, $q = (\Lambda, M, N)$, where M is the angular momentum modulus and Λ and N its projections on to the Z and z axes, respectively. The spherical harmonics in (2) must be expressed in terms of the spherical harmonics referred to the $OXYZ$ system, in which the orbital motions of Moon and Sun are provided by convenient ephemeris. The final expansion takes the form of a so-called *Poisson series* depending on the Andoyer variables and the fundamental arguments of nutation, denoted by (Kinoshita 1977)

$$\Theta_j = m_{1j} l + m_{2j} l' + m_{3j} F + m_{4j} D + m_{5j} \Omega. \tag{3}$$

Here l, l', F, D and Ω are the Delaunay variables of Moon and Sun. The subindex j stands for the 5-tuple of integers m_{ij}, so it can be used to indicate the functional dependence of $n_j = d\Theta_j/dt$. The coordinate λ and the auxiliary angle I (defined by $\cos I = \Lambda/M$) describe the motion of the Earth's angular momentum axis in the space system. The figure axis motion is given by the Euler's angles ψ, θ (longitude and obliquity), which are related to the Andoyer variables by the expansions (Kinoshita 1977)

$$\psi = \lambda + \sigma \frac{\sin\mu}{\sin I} + O(\sigma^2), \;\; \theta = I + \sigma\cos\mu + O(\sigma^2), \tag{4}$$

which are accurate enough since the auxiliary angle σ (defined by $\cos\sigma = N/M$) has a magnitude about 10^{-6} rad, of the order of polar motion (Kinoshita 1977).

The Lie-Hori canonical perturbation method (Hori 1966) is used to tackle the evolution of the system with Hamiltonian $H = H_0 + H_1$, where the unperturbed part, $H_0 = T_0$, is the kinetic energy for a non-spherical symmetric rigid Earth (Kinoshita 1977) and the perturbed one is $H_1 = T_t + V_t$, in which T_t stands for the redistribution kinetic energy (Kubo 1991, Getino and Ferrándiz 1990, 1995) and V_t for the redistribution potential energy (2). Due to the linearity of the perturbation equations at the first order, the effects of T_t and V_t can be studied separately, and analytical expressions can be obtained for each component of the rotational motion of the Earth's figure axis (Baenas 2014).

The contribution of the mass redistribution to the precessional motion, denoted by δn_λ and δn_I, comes from the additional secular component of the Hamiltonian and can be determined from the variation of the velocities $n^*_\lambda = d\lambda^*/dt$ and $n^*_I = dI^*/dt$. Similar additive terms for the nutations, $\triangle\psi$ and $\triangle\theta$ are obtained taking into account (4) and the perturbation equations.

The solution to the precession rates caused by the Earth's mass redistribution can be expressed as

$$\begin{aligned} \delta n_\lambda &= -\frac{1}{\sin I^*} \frac{1}{CH_d} \sum_{p,q}^{M,S} \sum_{\substack{i,j \\ \tau\Theta_i - \epsilon\Theta_j = 0}} \sum_{\tau,\epsilon}^{\pm 1} \sum_{m}^{0,1,2} \left|\bar{\kappa}_{2m,j;p}\right| k_q T^{(n_\lambda)}_{ijpq,m}(\tau,\epsilon) \cos\varepsilon_{2m,j}, \\ \delta n_I &= -\frac{1}{\sin I^*} \frac{1}{CH_d} \sum_{p,q}^{M,S} \sum_{\substack{i,j \\ \tau\Theta_i - \epsilon\Theta_j = 0}} \sum_{\tau,\epsilon}^{\pm 1} \sum_{m}^{0,1,2} \left|\bar{\kappa}_{2m,j;p}\right| k_q T^{(n_I)}_{ijpq,m}(\tau,\epsilon) \sin\varepsilon_{2m,j}, \end{aligned} \tag{5}$$

where the functions $T^{(-)}_{ijpq,m}(\tau,\epsilon)$ depend on the auxiliary variable I and on the orbital solutions through the Kinoshita's (1977) B_i, C_i and D_i functions and are given by

$$\begin{aligned} T^{(n_\lambda)}_{ijpq,m}(\tau,\epsilon) &= \frac{9}{4}\frac{\partial B_{i;p}}{\partial I}B_{j;q}\delta_{m0} + 3\frac{\partial C_{i;p}}{\partial I}C_{j;q}\delta_{m1} + \frac{3}{4}\frac{\partial D_{i;p}}{\partial I^*}D_{j;q}\delta_{m2}, \\ T^{(n_I)}_{ijpq,m}(\tau,\epsilon) &= \tau m_{5i}\left(\frac{9}{4}B_{i;p}B_{j;q}\delta_{m0} - 3C_{i;p}C_{j;q}\delta_{m1} - \frac{3}{4}D_{i;p}D_{j;q}\delta_{m2}\right). \end{aligned} \quad (6)$$

The complex parameter $\bar{\kappa}_{2m,j;p}$ is a generalization of the constant defined by Kubo (1991)

$$\bar{\kappa}_{2m,j;p} = \frac{1}{3}\bar{k}_{2m;j}m_p a_E^2\left(\frac{a_E}{a_p}\right)^3,$$

where subindex j points to the dependence on the orbital (or excitation) frequencies n_j. The constant k_q is the one defined by Kinoshita (1977), $H_d = 1 - A/C$ is the Earth's dynamical ellipticity, A and C being the equatorial and polar Earth's principal moments of inertia, and δ_{mk} is the Kronecker delta.

These analytical formulas show that the nonzero contribution to the precessional rate in obliquity, δn_I, is a purely anelastic effect, as it only stands for complex values of the Love's numbers (with any $\varepsilon_{2m,j} \neq 0$), what is in accordance with Lambert and Mathews (2006).

3. RESULTS

It can be shown analytically (Escapa et al. 2004, Baenas 2014) that in the case of the simplified Earth's elastic response, with $\bar{k}_{2m} = k \in \mathbb{R}$, the effects of the different harmonic contributions of the redistribution potential cancel each other out in all cases: precession velocities and nutation terms. When more general rheological models for the Earth's mantle elasticity are considered, there appear non-negligible secular and periodic contributions to the motion of the Earth's figure axis.

For the evaluation of the analytical solutions, the frequency dependent complex Love's numbers have been taken from IERS Conventions 2010. Table 1 shows the results for the contributions to the precession rates, including separately the additive terms coming from the well-known harmonic contributions of the perturbing tidal potential: zonal, tesseral and sectorial, denoted respectively by B, C and D. In the zonal part, the permanent tide contribution, B_0, is computed separately. This particular term must be included or removed, depending on the dynamical model considered for the rigid part of the Earth's inertia tensor ("zero tide" or a "tide free" according to IERS Conventions 2010 terminology).

	Zonal		Tesseral	Sectorial	Total
	B_0	$B - B_0$	C	D	
δn_λ	43.7900	−4.1389	−60.6554	27.0102	6.0059
δn_I	0.0000	-0.0118	0.1209	0.6656	0.7748

Table 1: Contribution of the mass redistribution to the precessional rates (unit 1 mas/cJ).

Table 2 displays only the in-phase amplitudes of the main nutation terms. They are computed from analytical expressions that extend (5) and correspond to the non-vanishing combinations $\tau\Theta_i - \epsilon\Theta_j$ ($\tau, \epsilon = \pm 1$) of the fundamental arguments of nutation (3), where Θ_i stands for the perturbed bodies and Θ_j for the perturbing ones. For the sake of briefness, the contributions B_0, $B - B_0$, C and D have not been shown separately in Table 2. The out-of-phase contributions are smaller in magnitude.

The numerical results show a significant influence of the frequency dependence of the Love's numbers. This effect is mainly due to the existence of the free core nutation (FCN) resonance processes in the diurnal band.

Considering the complete mass redistribution contribution, kinetic and potential energies, the differences with respect to the simplified elastic model reach significant values: about 6 mas/cJ for the velocity of precession in longitude, 0.8 mas/cJ for the velocity of precession in obliquity, 140 μas in the amplitude of the nutation in longitude with period of 13.66 days, and 50 μas in the amplitude of the nutation in obliquity for the same component.

Finally it can be noted that the analytical formulation allows the inclusion of different rheological models, which can be considered as a numerical input for the rotation solution, in a similar way than the orbital motion of the perturbing bodies.

Argument					Period	T_t		V_t	
l	l'	F	D	Ω	days	$\Delta\psi$	$\Delta\theta$	$\Delta\psi$	$\Delta\theta$
+0	+0	+0	+0	+1	−6793.48	+933.35	−274.99	+5.4095	−11.5748
+0	+0	+0	+0	+2	−3396.74	−18.00	+6.55	−1.0599	+0.5897
+0	+1	+0	+0	+0	365.26	−43.06	−58.19	+0.1294	−0.1903
+0	−1	+2	−2	+2	365.25	+19.71	−6.69	+0.0025	−0.0033
+0	+0	+2	−2	+2	182.63	−2338.50	+844.09	+1.8798	−0.9666
+0	+1	+2	−2	+2	121.75	−138.48	+50.26	+0.0282	−0.0150
+1	+0	+0	+0	+0	27.55	+21.65	−311.39	+0.0938	+0.0037
+0	+0	+2	+0	+2	13.66	−5537.17	+2043.26	−0.2686	+0.1373
+0	+0	+2	+0	+1	13.63	−1134.83	+349.43	−0.0027	+0.0157
+1	+0	+2	+0	+2	9.13	−1101.47	+408.67	+0.0372	−0.0186

Table 2: Contribution of the mass redistribution to the figure axis nutations (unit 1 μas).

Acknowledgements. This work has been partially supported by the Spanish government through the MINECO projects I+D+I AYA201022039-C02-01, AYA2010-22039-C02-02 and by the Generalitat Valenciana project GV/2014/072.

4. REFERENCES

Baenas, T., 2014, "Contribuciones al estudio analítico del movimiento de rotación de una Tierra deformable", PhD thesis, University of Alicante.

Escapa, A., Getino, J., Ferrándiz, J.M., 2004, "On the effect of the redistribution tidal potential on the rotation of the non-rigid Earth", Proceeding Journeés 2004. Paris, 20–22 Sep., pp. 70–73.

Escapa, A., 2011, "Corrections stemming from the non-osculating character of the Andoyer variables used in the description of rotation of the elastic Earth", Celest. Mech. Dyn. Astr., 110, pp. 99–142.

Ferrándiz, J.M., Baenas, T., Escapa, A., 2012, "Effect of the potential due to lunisolar deformations on the Earth precession", 2012 EGU General Assembly.

Getino, J., Ferrándiz, J.M., 1990, "A Hamiltonian theory for an elastic Earth: Canonical variables and kinetic energy", Celest. Mech. Dyn. Astron., 51, pp. 303-326.

Getino, J., Ferrándiz, J.M., 1991, "A Hamiltonian theory for an elastic Earth: First order analytical integration", Celest. Mech. Dyn. Astron., 49, pp. 35–65.

Getino, J., Ferrándiz, J.M., 1995, "On the effect of the mantle elasticity on the Earth's rotation", Celest. Mech. Dyn. Astr., 61, pp. 117–180.

Hori, G.I., 1966, "Theory of general perturbations with unspecified canonical variables", Publ. Astron. Soc. Jpn., 18, pp. 287–296.

Kinoshita, H., 1977, "Theory of the rotation of the rigid Earth", Celest. Mech. Dyn. Astr., 15, pp. 277–326.

Kubo, Y., 1991, "Solution to the rotation of the elastic Earth by method of rigid dynamics", Celest. Mech. Dyn. Astr., 50, pp. 165–187.

Lambert, S.B., Mathews, P.M., 2006, "Second-order torque on the tidal redistribution and the Earth's rotation", A&A, 453, pp. 363–369.

Love, A.E.H., 1911, "Some problems of Geodynamics", Cambridge University Press.

Munk, W.K., MacDonald, G.J.F., 1960, "The rotation of the Earth: a geophysical discussion", Cambridge University Press.

Petit, G., Luzum, B. (eds.), 2010, IERS Conventions (2010), IERS Technical Note 36, Frankfurt am Main: Verlag des Bundesamts für Kartographie und Geodäsie.

Sasao, T., Okubo, S., Saito, M., 1980, "A Simple Theory on Dynamical Effects of Stratified Fluid Core upon Nutational Motion of the Earth", Proc. IAU Symp. 78, E.P. Fedorov, M.L. Smith, P.L. Bender (eds.), pp. 165–183.

Souchay, J., Folgueira, M., 2000, "The effect of zonal tides on the dynamical ellipticity of the Earth and its influence on the nutation", Earth, Moon and Planets, 81(3), pp. 201–216.

Wahr, J.M., 1981, "Body tides on an elliptical, rotating, elastic and oceanless Earth", Geophys. J. R. Astr. Soc., 64, pp. 677–703.

NEW HIGH-PRECISION EARTH AND MOON ROTATION SERIES AT LONG TIME INTERVALS

V.V. PASHKEVICH
Central (Pulkovo) Astronomical Observatory of RAS
Pulkovskoe shosse, 65/1, 196140, St. Petersburg, Russia
e-mail: pashvladvit@yandex.ru

ABSTRACT. Dynamics of the rotational motion of the Earth and Moon is investigated numerically at a long time intervals. In our previous studies (Pashkevich, 2013), (Pashkevich and Eroshkin, 2011) the high-precision Rigid Earth Rotation Series (designated RERS2013) and Moon Rotation Series (designated MRS2011) were constructed. RERS2013 are dynamically adequate to the JPL DE422/LE422 (Folkner, 2011) ephemeris over 2000 and 6000 years and include about 4113 periodical terms (without attempt to estimate new sub-diurnal and diurnal periodical terms). MRS2011 are dynamically adequate to the JPL DE406/LE406 (Standish, 1998) ephemeris over 418, 2000 and 6000 years and include about 1520 periodical terms. The main aims of present research are improvement of the Rigid Earth Rotation Series RERS2013 and Moon Rotation Series MRS2011, and as a result of the construction of the new high-precision Rigid Earth Rotation Series RERS2014 dynamically adequate to the JPL DE422/LE422 ephemeris over 2000 years and Moon Rotation Series MRS2014 dynamically adequate to the JPL DE422/LE422 ephemeris over 6000 years. The elaboration of RERS2013 is carried out by means recalculation of sub-diurnal and diurnal periodical terms. Improve the accuracy of the series MRS2011 is obtained by using the JPL DE422/LE422 ephemeris.

1. INTRODUCTION

The aims of the present research are construction of the improved high-precision Rigid Earth Rotation Series RERS2014 (with including new sub-diurnal and diurnal periodical terms) and the high-precision Moon Rotation Series MRS2014 dynamically adequate to the JPL DE422/LE422 ephemeris, over 2000 and 6000 years, respectively. The numerical solution of the problem is obtained by solving the Lagrange differential equations of the second kind for the rigid Earth rotation with respect to the fixed ecliptic and equinox of epoch J2000 (Pashkevich, 2013). The orbital motions of the disturbing celestial bodies are defined by the DE422/LE422 ephemeris. The mathematical model of the problem is described in detail in the papers (Eroshkin and Pashkevich, 1997), (Pashkevich and Eroshkin, 2011), (Eroshkin, Pashkevich and Brzeziński, 2002) and (Pashkevich, 2013). The discrepancies between the high-precision numerical solutions and the semi-analytical solutions for the rigid Earth and the Moon rotation problems with respect to the fixed ecliptic of epoch J2000 are investigated by the iterative algorithm, which used the least-squares method and the spectral analysis methods (Pashkevich and Eroshkin, 2005, 2010). Comparison of the new Series RERS2014 and MRS2014 with the previous solution RERS2013 (Pashkevich, 2013) and MRS2011 (Pashkevich and Eroshkin, 2011), respectively is carried out. The rigid Earth rotation problem is solved for the relativistic (kinematical) case in which the geodetic perturbations (the most essential relativistic perturbations) in the Earth rotation are taken into account. Investigation of the Moon rotation problem is carried out only for the newtonian (dynamical) case.

2. ALGORITHMS AND RESULTS

The results of the numerical solutions of the problem are compared with the semi-analytical solutions of the studied body rotation (RERS2013 for the Earth or MRS2011 for the Moon). The residuals of these comparison are studied by means *the iterative algorithm:*

1. Numerical solution of the studied body rotation (the rigid Earth or Moon) is implemented with the quadruple precision of calculations. The initial conditions are computed by the semi-analytical solution of the studied body rotation (RERS2013 for the Earth or MRS2011 for the Moon). Discrepancies between the numerical solution and the semi-analytical solution are obtained over all investigation time interval

with 0.1 day spacing in Euler angles (1) for the Earth case or with 1 day spacing in the perturbing terms of the physical librations (2) for the Moon case. The expressions for these discrepancies are as follows

$$\left.\begin{aligned}
\Delta\psi &= \sum_{k=0}^{8}\psi_k t^k + \sum_{j=1}^{4113}\sum_{k=0}^{4}[\psi_{Sjk}\sin(\nu_{j0}+\nu_{j1}t) + \psi_{Cjk}\cos(\nu_{j0}+\nu_{j1}t)]t^k \\
\Delta\theta &= \sum_{k=0}^{8}\theta_k t^k + \sum_{j=1}^{4113}\sum_{k=0}^{4}[\theta_{Sjk}\sin(\nu_{j0}+\nu_{j1}t) + \theta_{Cjk}\cos(\nu_{j0}+\nu_{j1}t)]t^k \\
\Delta\phi &= \sum_{k=0}^{8}\phi_k t^k + \sum_{j=1}^{4113}\sum_{k=0}^{4}[\phi_{Sjk}\sin(\nu_{j0}+\nu_{j1}t) + \phi_{Cjk}\cos(\nu_{j0}+\nu_{j1}t)]t^k
\end{aligned}\right\}, \tag{1}$$

$$\left.\begin{aligned}
\Delta\tau &= \sum_{j=1}^{1520}\sum_{k=0}^{3}[\tau_{Sjk}\sin(\nu_{j0}+\nu_{j1}t) + \tau_{Cjk}\cos(\nu_{j0}+\nu_{j1}t)]t^k \\
\Delta\varrho &= \sum_{j=1}^{1520}\sum_{k=0}^{3}[\varrho_{Sjk}\sin(\nu_{j0}+\nu_{j1}t) + \varrho_{Cjk}\cos(\nu_{j0}+\nu_{j1}t)]t^k \\
\Delta I\sigma &= I\sum_{j=1}^{1520}\sum_{k=0}^{3}[\sigma_{Sjk}\sin(\nu_{j0}+\nu_{j1}t) + \sigma_{Cjk}\cos(\nu_{j0}+\nu_{j1}t)]t^k
\end{aligned}\right\}, \tag{2}$$

where ψ is the longitude of the ascending node of the Earth's dynamical equator on the fixed ecliptic J2000; θ is the angle of the inclination of the Earth's dynamical equator to the fixed ecliptic J2000; ϕ is the proper rotation angle of the Earth between the ascending node of the Earth's dynamical equator and the principal axis of the minimum moment of inertia; τ, ϱ and σ are the perturbing terms of the physical librations of the Moon for the fixed ecliptic of epoch J2000 in the longitude, in the inclination and in the node longitude, respectively; ν_{j0}, ν_{j1} are the phases and the frequencies of the corresponding semi-analytical solutions, respectively; t is the time in the Julian days; ψ_k, θ_k, ϕ_k are the coefficients of the secular terms; $\psi_{Sjk}, \theta_{Sjk}, \phi_{Sjk}, \psi_{Cjk}, \theta_{Cjk}, \phi_{Cjk}, \tau_{Sjk}, \varrho_{Sjk}, \sigma_{Sjk}, \tau_{Cjk}, \varrho_{Cjk}, \sigma_{Cjk}$ are the coefficients of the periodic and Poisson terms.

2. Investigation of the discrepancies is carried out by the least squares method (LSQ) and by the spectral analysis (SA) method (Pashkevich and Eroshkin, 2005, 2010). The sets of the frequencies of the semi-analytical solutions are used without change. Only the coefficients of the systematical terms, the coefficients of the periodical terms and the coefficients of the Poisson terms are improved. The systematic, periodic and Poisson terms representing the new high-precision studied body rotation series (RERS2014$_i$ for the Earth or MRS2014$_i$ for the Moon (where i is the number of iteration)) are determined:

$$\left.\begin{aligned}
\psi_{\mathrm{RERS2014}_i} &= \Delta\psi_{i-1} + \psi_{\mathrm{RERS2014}_{i-1}} \\
\theta_{\mathrm{RERS2014}_i} &= \Delta\theta_{i-1} + \theta_{\mathrm{RERS2014}_{i-1}} \\
\phi_{\mathrm{RERS2014}_i} &= \Delta\phi_{i-1} + \phi_{\mathrm{RERS2014}_{i-1}}
\end{aligned}\right\}, \quad \left.\begin{aligned}
\tau_{\mathrm{MRS2014}_i} &= \Delta\tau_{i-1} + \tau_{\mathrm{MRS2014}_{i-1}} \\
\varrho_{\mathrm{MRS2014}_i} &= \Delta\varrho_{i-1} + \varrho_{\mathrm{MRS2014}_{i-1}} \\
\sigma_{\mathrm{MRS2014}_i} &= \Delta\sigma_{i-1} + \sigma_{\mathrm{MRS2014}_{i-1}}
\end{aligned}\right\}, \tag{3}$$

where $\psi_{\mathrm{RERS2014}_0} = \psi_{\mathrm{RERS2013}}$, $\theta_{\mathrm{RERS2014}_0} = \theta_{\mathrm{RERS2013}}$, $\phi_{\mathrm{RERS2014}_0} = \phi_{\mathrm{RERS2013}}$, $\tau_{\mathrm{MRS2014}_0} = \tau_{\mathrm{MRS2011}}$, $\varrho_{\mathrm{MRS2014}_0} = \varrho_{\mathrm{MRS2011}}$ and $\sigma_{\mathrm{MRS2014}_0} = \sigma_{\mathrm{MRS2011}}$.

3. Numerical solution of the studied body rotation is constructed anew with the new initial conditions, which are calculated by RERS2014$_i$ (for the Earth) or MRS2014$_i$ (for the Moon).

4. Steps 2 and 3 are repeated till the assumed convergence level of the discrepancies between the new numerical solution and the new semi-analytical solution (RERS2014i for the Earth or MRS2014i for the Moon) has been achieved.

The investigation of the rigid Earth rotation over 2000 years time interval is carried out with used DE422/LE422 ephemeris. The discrepancies between the numerical solutions and semi-analytical series RERS2013 are depicted in Fig. 1 black color. The convergence level was achieved after application of the second iteration of the iterative algorithm. So, the process of the iterative algorithm was finished at this

step. As a result, the Rigid Earth Rotation Series RERS2014 was constructed, which include new recalculated the sub-diurnal and diurnal periodical terms and is dynamically adequate to the DE422/LE422 ephemeris over 2000 years. The discrepancies between the new numerical solutions and the semi-analytical solutions of RERS2014-2 do not surpass 3 μas over 2000 years for $\Delta\psi$ and $\Delta\phi$ and do not surpass 1 μas over 2000 years for $\Delta\theta$ (presented in Fig. 1 grey color).

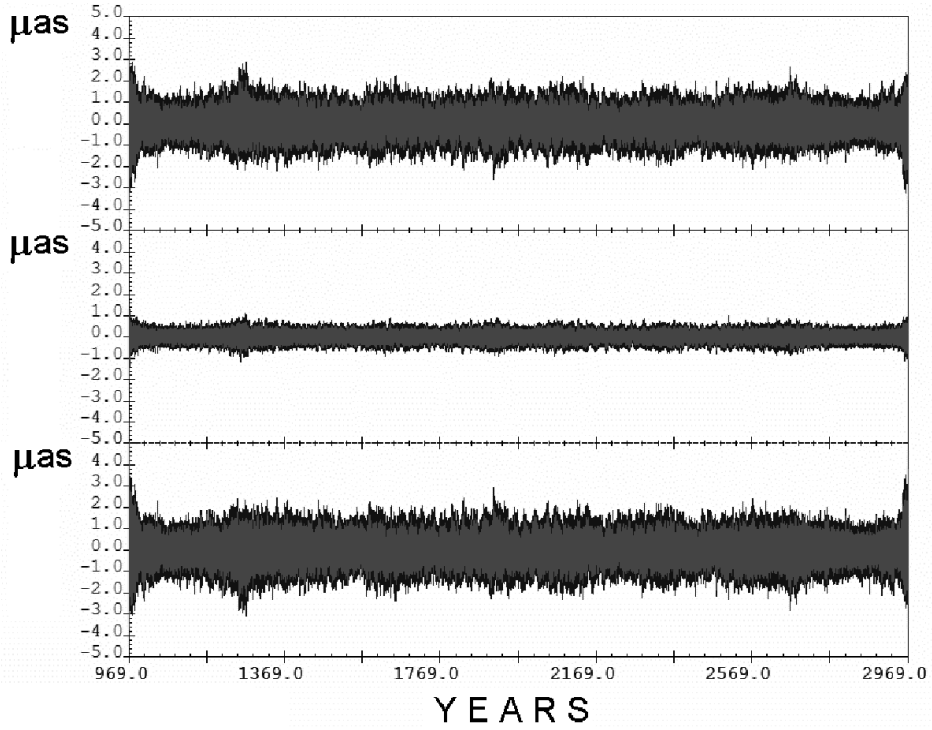

Figure 1: Discrepancies between the numerical and RERS2013 solutions of the Earth rotation (black) and between new numerical and RERS2014-2 solutions of the Earth rotation (grey).

The investigation of the Moon rotation over 6000 years time interval is carried out with used DE422/LE422 ephemeris. The discrepancies between the numerical solutions and semi-analytical series MRS2011 (dynamically adequate to the DE406/LE406 ephemeris) are depicted in Fig. 2 black color. The convergence level was achieved after application of the first iteration of the iterative algorithm. So, the process of the iterative algorithm was finished at this step. As a result, the Moon Rotation Series MRS2014 was constructed, which is dynamically adequate to the DE422/LE422 ephemeris over 6000 years. The discrepancies between the new numerical solutions and the semi-analytical solutions of MRS2014-1 do not surpass 8 arc seconds over 6000 years for $\Delta I\sigma$, do not surpass 4 arc seconds over 6000 years for $\Delta\varrho$ and do not surpass 0.6 arc seconds over 6000 years for $\Delta\tau$ (presented in Fig. 2 grey color).

Thus, the result of the comparison on 2000 years for the Earth case and 6000 years for the Moon case demonstrates a good consistency of new RERS2014 and MRS2014 series, respectively, with the DE422/LE422 ephemeris.

3. CONCLUSION

The new improved high-precision Rigid Earth Rotation Series RERS2014 (with including new sub-diurnal and diurnal periodical terms) dynamically adequate to the DE422/LE422 ephemeris over 2000 years have been constructed. RERS2014 include about 4113 periodical terms. The residuals between the numerical solution and RERS2014 do not surpass 3 μas over 2000 years.

The new high-precision Moon Rotation Series MRS2014 dynamically adequate to the DE422/LE422 ephemeris over 6000 years have been constructed. MRS2014 include about 1520 periodical terms. The residuals between the numerical solution and MRS2014 do not surpass 8 arc seconds over 6000 years, It means a good consistency of the MRS2014 series with the DE422/LE422 ephemeris.

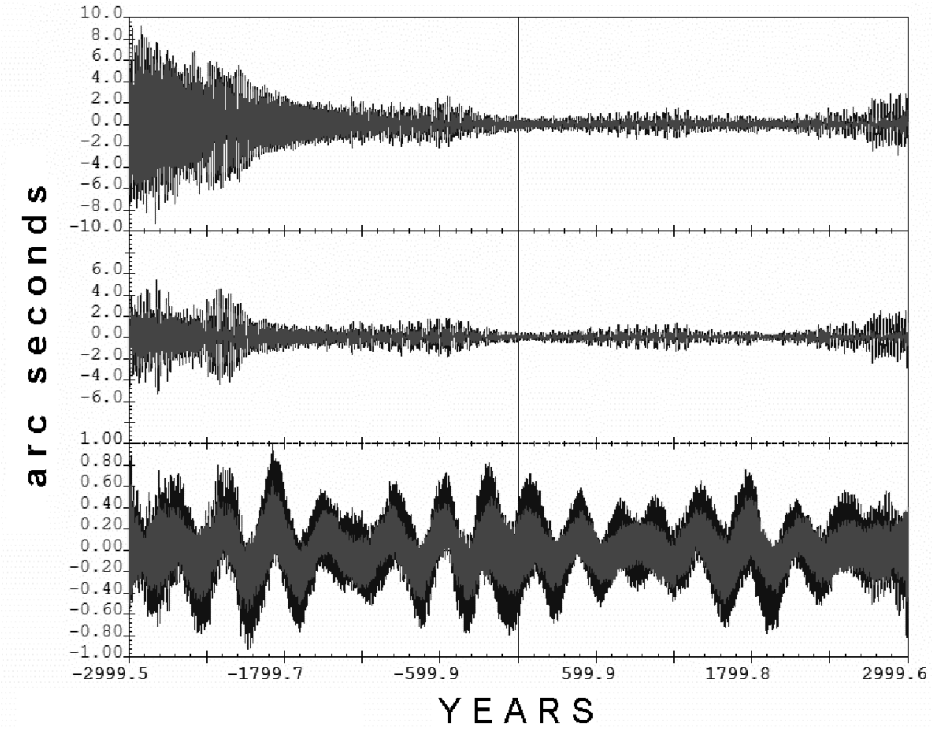

Figure 2: Discrepancies between the numerical and MRS2011 solutions of the Moon rotation (black) and between new numerical and MRS2014-1 solutions of the Moon rotation (grey).

Acknowledgements. The investigation was carried out at the Central (Pulkovo) Astronomical Observatory of the Russian Academy of Science and the Space Research Centre of the Polish Academy of Science, under a financial support of the Cooperation between the Polish and Russian Academies of Sciences, Theme No 34 and the Polish national science foundation NCN under grant No. DEC-2012/05/B/ST10/02132.

4. REFERENCES

Eroshkin, G.I., Pashkevich, V.V., 1997, "Numerical Simulation of the Rotational Motion of the Earth and Moon", In: Dynamics and Astrometry of Natural and Artificial Celestial Bodies, IAU Colloquium 165, I.M. Wytrzyszczak, J.H. Lieske, R.A. Feldman (eds.), Kluwer, Dordrecht, pp. 275–280.

Eroshkin, G.I., Pashkevich, V.V., Brzeziński, A., 2002, "Extension of the high-precision numerical theory of the rigid Earth rotation to the case of a long time interval", Artificial Satellites, 37(4), pp. 169–183.

Folkner, W.F., 2011, "JPL Planetary and Lunar Ephemerides: Export Information", Pasadena, CA: JPL, http://iau-comm4.jpl.nasa.gov/README.html.

Pashkevich, V.V., Eroshkin, G.I., 2005, "Choice of the optimal spectral analysis scheme for the investigation of the Earth rotation problem", in Proc. Journées 2005 "Systèmes de référence spatio-temporels", Warsaw, Poland, 19–21 September, A. Brzeziński, N. Capitaine, B. Kołaczek (eds.), pp. 105–109.

Pashkevich, V.V., Eroshkin, G.I., 2010, "Application of the spectral analysis for modeling the rotations of the Moon", Artificial Satellites, 45(4), pp. 153–162, doi: 10.2478/v10018-011-0004-4.

Pashkevich, V.V., Eroshkin, G.I., 2011, "Construction of the numerical and semi-analytical solutions of the Moon rotation", In: Proc. Journées 2011 "Systèmes de référence spatio-temporels", Vienna, 19–21 September, H. Schuh, S. Böhm, T. Nilsson, N. Capitaine (eds.), pp. 205–208.

Pashkevich, V.V., 2013, "Construction of the numerical and semi-analytical solutions of the rigid Earth rotation at a long time intervals", Artificial Satellites, 48(1), pp. 25–37, doi: 10.2478/arsa-2013-0003.

Standish, E.M., 1998, "JPL Planetary and Lunar Ephemerides, DE405/LE405", JPL IOM 312.F-98-048.

NUMERICAL–ANALYTICAL MODELING OF THE EARTH'S POLE OSCILLATIONS

Y.G. MARKOV, A.S. FILIPPOVA
Moscow Aviation Institute
Volokolamskoe shosse, 4, Moscow, 125080, Russia
e-mail: filippova.alex@gmail.com

ABSTRACT. For the purpose of more accurate forecasting the oscillatory process of the Earth pole in time periods with significant anomalies (irregular deviations) a numerical-analytical approach is presented for the combined modeling of the interdependent dynamical processes - the oscillatory-rotational motion of the Earth and the time dependant coefficients of the geopotential. The oscillations of the inertia tensor components of the Earth depend on various factors such as mechanical and physical parameters of the planet, the motions of the tide-generating bodies and observed large scale natural events. Time variations of these and some other factors affect the Earth orientation parameters. The generalization of the previously researched mathematical model of Chandler and annual oscillations of the Earth pole is being held with the use of celestial mechanics methods and the mathematical description of the Earth gravitational field's temporal variations. The latter makes possible to improve the forecast precision of the Earth pole trajectory. Also the more precise model is to have small number of parameters and to agree with the previously developed one (to have the same structural features and to have a correspondence between the averaged dynamical parameters and the parameters of the basic model).

1. INTRODUCTION

To achieve the characteristics of a high-accuracy forecast of oscillations of the Earth's pole, interdependent dynamic processes are considered, namely, rotary-oscillatory motions of the Earth and time-varying coefficients of the planetary geopotential. Oscillations of the Earth's inertia tensor components depend on many factors, e.g., the mechanical and physical parameters of the planet, the motion of tide-generating bodies, and observed large-scale natural phenomena. Time variations in these and other factors have an effect on the parameters of the Earth's rotation. In connection with this, joint simulation of the oscillatory motion of the Earth's pole and time variations in geopotential coefficients having an effect on parameters of the rotating geoid is of scientific and practical interest.

We described the rotational motions of the deformable Earth and the oscillations of the Earth's pole using a simplified mechanical model for the viscoelastic rigid body of the Earth. To take into account gravitational-tidal effects, we assumed the Earth to be axially symmetric and two-layered, i.e., consisting of a rigid (spherical) core and a viscoelastic mantle. We could have used some more complex model. However, employing anymore complex figure for the Earth is not justified, since we cannot determine the geometrical and physical parameters of the Earth with the required accuracy and completeness via a statistical processing of indirect data from seismic measurements. We adhere to the idea that the complexity of a model must strictly correspond to the problem formulated and to the accuracy of the data used. To construct a model for the polar oscillations, we can determine a small number of some mean (integrated) characteristics of the inertia tensor. Comparison with measurements and further analysis indicate that our simplifications are justified (Akulenko, et al., 2012).

2. MATHEMATICAL MODEL OF THE EARTH'S POLE MOTION

It is convenient to represent the trajectory of the Earth's pole as an ensemble of an irregular trend (drift containing secular and low-frequency component with periods of six years and longer) and polhode (trajectory of the pole motion around the middle position) expressed in terms of the amplitude a and phase ψ of the pole motion. Then, the pole coordinates have the form

$$x_p = c_x + a\cos\psi, \quad y_p = c_y + a\sin\psi. \tag{1}$$

When moving around the middle position, the pole describes a helical curve that is obtained as the sum of two main components: the Chandler wobble with a period of $2\pi/N \simeq 433$ days and the annual nutation. The choice of the parameters a and ψ turns out to be more convenient for describing the fluctuations of the main components of the modulation motion of the pole.

It is well known (Akulenko, et al., 2007) that the amplitude and phase of the Chandler component of the oscillatory process of the pole are very sensitive to different disturbing factors, in particular, to those possessing irregular properties (gravitational, oceanic, atmospheric, and, probably, others). It is natural to associate the mechanism of these actions with weak perturbations of the inertia tensor. The Earth's figure is a dynamic geoid figure due to variations in the inertia tensor; at the same time, it creates an additional time-dependent perturbing potential $\delta W(t)$. The largest summand from the expansion of the potential δW is the perturbation from the second harmonic δW_2:

$$\delta W_2 = \frac{fm_E R_E^2}{r^3}\Delta\bar{Y}_2(\theta,\varphi), \tag{2}$$

$$\Delta\bar{Y}_2 = \delta c_{20}\bar{P}_{20}(\cos\theta) + [\delta c_{21}\cos\varphi + \delta s_{21}\sin\varphi]\bar{P}_{21}(\cos\theta) + [\delta c_{22}\cos 2\varphi + \delta s_{22}\sin 2\varphi]\bar{P}_{22}(\cos\theta)$$

where θ, φ and r are spherical coordinates; R_E is the average radius of the Earth ($R_E \simeq 6.38\times10^6$ m); and $fm_E = 3.98600442\times10^{14} m^3 s^{-2}$. The change in the normalized spherical function $\Delta\bar{Y}_2(\theta,\varphi)$ is expressed in terms of second order coefficients of the geopotential expansion and $\bar{P}_{2m}(\cos\theta)$ are normalized adjoint Legendre functions.

Differential equations for the amplitude and phase of the modulation motion of the Earth's pole can be obtained from the dynamic Euler-Liouville equations of the Earth's motion with respect to the center of masses:

$$\begin{aligned}
\dot{a} &= \frac{2m_E R_E^2}{A^*} r_0 \left[c_{22}^* \left(1 - \frac{C^*}{B^*}\right) + \delta c_{22}\right] a\sin 2\psi + [\mu_p\cos\psi + \mu_q\sin\psi]\,,\\
\dot{\psi} &= -N_q\cos^2\psi - N_p\sin^2\psi + a^{-1}\left[\mu_q\cos\psi - \mu_p\sin\psi\right].
\end{aligned} \tag{3}$$

Here A^*, B^*, C^* are effective principal central moments of inertia with allowance for deformations of the "frozen" figure of the Earth; $c_{2m} = c_{2m}^* + \delta c_{2m}$, $s_{2m} = s_{2m}^* + \delta s_{2m}$ are second order coefficients of the potential expansion into a series in terms of spherical functions; r_0 is the average velocity of axial rotation of the Earth; and variable coefficients

$$N_p = \frac{C^* - B^* + \delta C - \delta B}{A^* + \delta A} r_0, \quad N_q = \frac{C^* - A^* + \delta C - \delta A}{B^* + \delta B} r_0$$

are close quantities determining the frequency of Chandler oscillations of the pole. The quantities μ_p and μ_q are determined by gravitation-tidal moments of forces from the Sun and the Moon. The average frequency of free nutation N^*, according to solution (3), is $\sqrt{N_p^* N_q^*}$. Variation in the frequency of Chandler oscillations (free nutation frequency) is a function of the dynamic compression of the geoid and variation in the axial moment of inertia:

$$N \cong N^* + \delta N, \quad \delta N = -F(\delta C, \delta c_{20}). \tag{4}$$

Then, for the amplitude a_{ch} and phase ψ_{ch} of the Chandler oscillation, we obtain the expressions

$$\begin{aligned}
a_{ch} &= a_{ch}^0 + a_{ch}^{var}\left(t, \frac{\pi}{N}\right),\\
\psi_{ch} &= \psi_{ch}^0 - N^* t + \int F(\delta C, \delta c_{20})dt + \psi_{ch}^{var}\left(t, \frac{\pi}{N}\right),
\end{aligned} \tag{5}$$

where a_{ch}^0, ψ_{ch}^0 are the average value of the amplitude and constant phase shift and a_{ch}^{var}, ψ_{ch}^{var} are summands depending on the sectorial c_{22} and other coefficients; they express the ellipticity of the Chandler component trajectory with a very small eccentricity.

As follows from the results of the numerical simulation, the parameters of the perturbed Chandler oscillation can be found from variations in the geopotential coefficient c_{20}. As an example, Fig. 1 presents the variation in the perturbed Chandler oscillation frequency $\Delta\dot{\psi} - N^*$ and variations in the second zonal harmonic δc_{20} according to SLR (Satellite Laser Ranging) data (Cheng and Tapley, 2004).

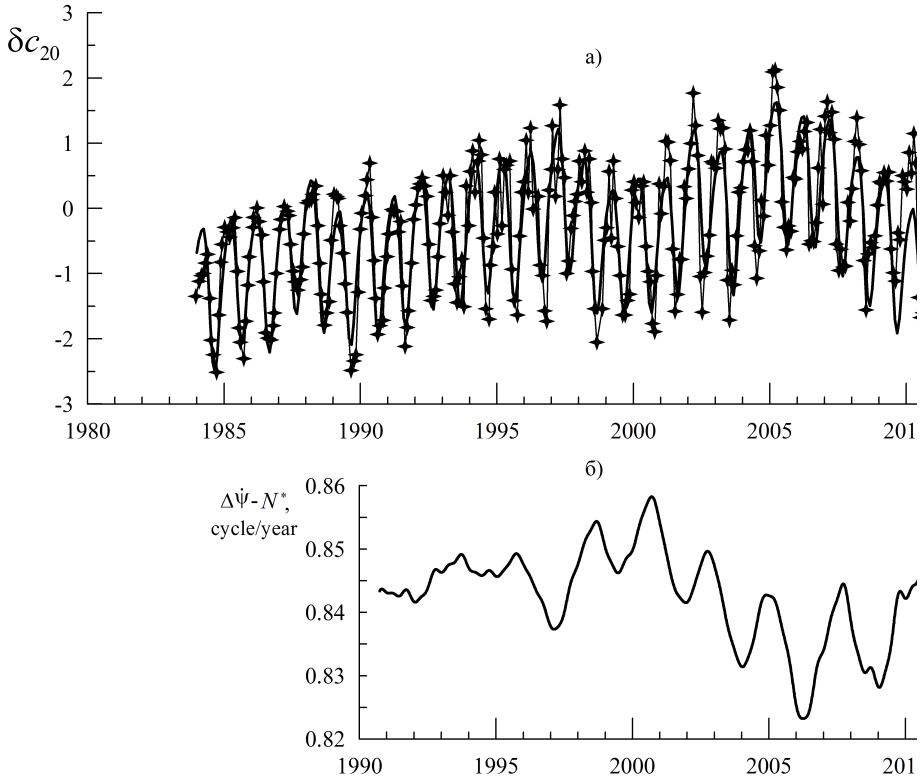

Figure 1: (a) Interpolation of variations in the second zonal harmonic δc_{20} of the geopotential on the time interval of 1984-2008 and a forecast for six years (2009-2014): the stars joined with a thin solid line are the SLR measurement data and the contrast solid line is the constructed curve. (b) Variation in the frequency $\Delta\dot{\psi}$ of the perturbed Chandler oscillation of the Earth's pole constructed in the course of the numerical simulation (1990-2014).

For coordinates of the Earth's pole (neglecting the difference in the amplitudes of the main components $\tilde{a}_{ch,h} \approx a^{p,q}_{ch,h}$), we obtain the final expressions:

$$\begin{aligned} x_p &= c_x + \tilde{a}_{ch}\cos\left(\psi^0_{ch} - N^*t + \delta\psi + \Delta\psi\right) + a_h\cos(\psi^0_h + \nu_h t + \chi), \\ y_p &= c_y + \tilde{a}_{ch}\sin\left(\psi^0_{ch} - N^*t + \delta\psi + \Delta\psi + \varepsilon\right) + a_h\sin(\psi^0_h + \nu_h t), \\ \delta\psi &= \int F(\delta C, \delta c_{20})dt. \end{aligned} \tag{6}$$

Here, $\tilde{a}_{ch}$ is the resulting amplitude of the Chandler oscillation; ε and χ are the phase shifts in x_p and y_p for the Chandler and annual oscillations, respectively; and ν_h is the annual oscillation frequency.

Figure 2 presents the results of the numerical simulation of the Earth's pole motion according to the basic model (Akulenko, et al., 2012) and model (6). The plot shows an interpolation on a long time interval (from 1990 up to and including 2012) and a forecast for 2013 and 2014 for the oscillatory process in coordinates of the Earth's pole according to two models - the basic model and the refined one (6) in comparison with highly accurate IERS data.

In addition, Fig. 2 yields residuals between IERS data and theoretical curves. The corresponding root-mean-square deviations calculated on the interpolation interval for the basic model (σ^*_x, σ^*_y, σ^*_{xy}) and model (6) (σ_x, σ_y, σ_{xy}) are given in milli arcseconds:

$$\begin{aligned} &\sigma^*_x = 44.30672865, \quad \sigma^*_y = 43.32902488, \quad \sigma^*_{xy} = 61.97169186, \\ &\sigma_x = 24.14765269, \quad \sigma_y = 20.25418818, \quad \sigma_{xy} = 31.51731698. \end{aligned} \tag{7}$$

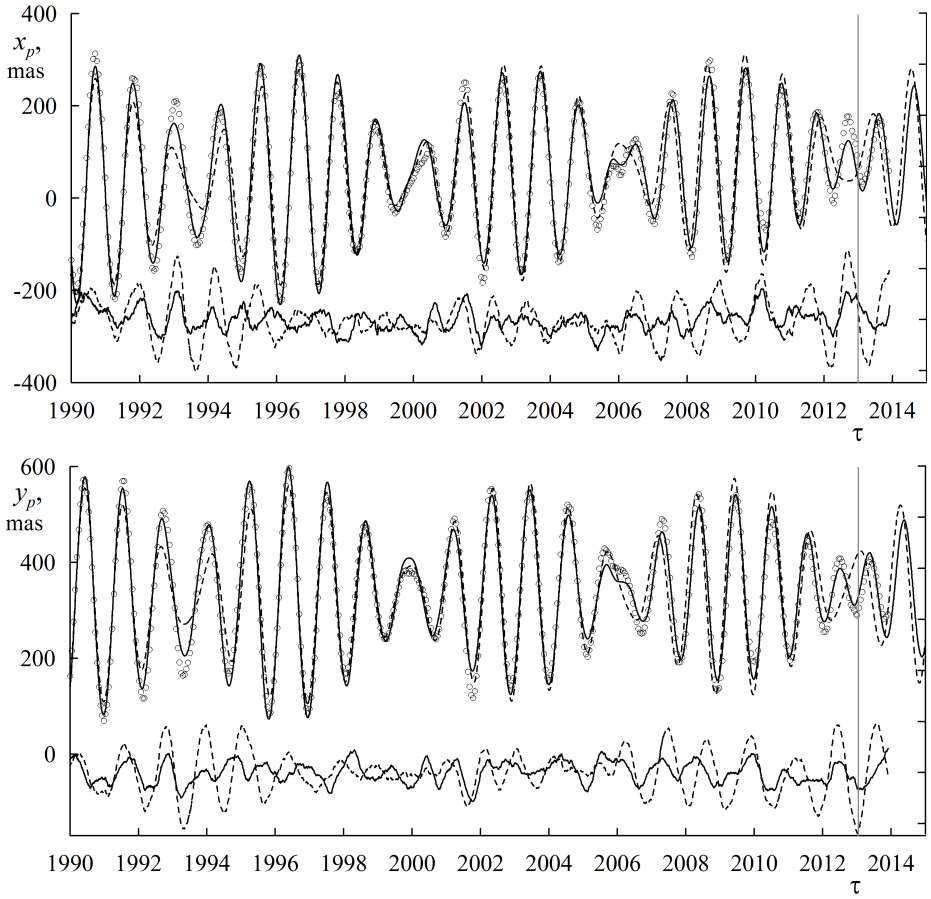

Figure 2: (a) Interpolation on the time interval from 1990 up to and including 2012 and forecast for 2013 and 2014 for the oscillatory process of the Earth's pole coordinates according to the basic (dashed line) and refined (solid curve) models in comparison with highly accurate IERS observation and measurement data (discrete points). Residuals (given below the basic plots), differences between IERS data and theoretical curves constructed according to the basic (dashed line) and refined (solid curve) models.

Based on the obtained interpolation results and forecast of pole oscillations, one can conclude that joint simulation of dynamic processes (taking into account time variations of the geopotential) allows one to refine the analytical model and improve the forecast for the pole motion trajectory.

Acknowledgements. This work was supported in the framework of the basic part of the state task by the Ministry of Education and Science of the Russian Federation (project no. 721).

3. REFERENCES

Akulenko, L.D., Klimov, D.M., Markov, Yu.G., Perepelkin, V.V., 2012, "Oscillatory-rotational processes in the Earth motion about the center of mass: Interpolation and forecast", Mechancs of Solids, 47(6), pp. 601–621, doi: 10.3103/S0025654412060015.

Akulenko, L.D., Kumakshev, S.A., Markov, Yu.G., Rykhlova, L.V., 2007, "Analysis of multifrequency effects in oscillations of the Earth's pole", Astron. Rep., 51(5), pp. 421–427, doi: 10.1134/S1063772907050083.

Cheng, M., Tapley, B.D., 2004, "Variations in the Earth's oblateness during the past 28 years", J. Geophys. Res.(Solid Earth), 109, B09402, doi: 10.1029/2004JB003028.

COMPARISON OF POLAR MOTION EXCITATION FUNCTIONS COMPUTED FROM DIFFERENT SETS OF GRAVIMETRIC COEFFICIENTS

J. NASTULA[1], M. WIŃSKA[2], M. BIRYŁO[3]
[1] Space Research Center Polish Academy of Sciences
Bartycka 18A, 00-716 Warsaw, POLAND
e-mail: nastula@cbk.waw.pl
[2] Warsaw University of Technology, Faculty of Civil Engeneering
Al. Armii Ludowej 16, 00-637 Warsaw, POLAND
e-mail: m.winska@il.pw.edu.pl
[3] University of Warmia and Mazury in Olsztyn
ul. Michala Oczapowskiego 2, 10-719 Olsztyn POLAND
e-mail: monika.sienkiewicz@uwm.edu.pl

ABSTRACT. Since its launch in February, the Gravity Recovery and Climate Experiment (GRACE) has been source of data of temporal changes in Earth's gravity field. These gravity fields can be used to determine the changing mass field of the Earth caused by redistribution of the geophysical fluids, and from that excitations of polar motion. The so-called Level 2 gravity field product are available, in the form of changes in the coefficients: C_{nm}, S_{nm}. Since 2002 until the present time there are still attempts to better process these data. In this study we estimate gravimetric excitation of polar motion using a recent series of C_{21}, S_{21} coefficients. In our calculations we use several series developed by different centers. Firstly, we compare these gravimetric functions with each other. Then we examine the compatibility of these functions with hydrological signal in observed geodetic excitation function. We focus on seasonal and subseasonal time scales. The main purpose is to explore which from these several solutions are closed to observation.

1. RESULTS AND ANALYSIS

In recent years many studies on the impact of land hydrology and Hydrological Angular Momentum (HAM) on the polar motion were carried on (Shuanggen et al., 2010; Brzeziński et al., 2009; Chen and Wilson, 2005; Nastula et al., 2007; Seoane et al., 2009).
Investigations of influence of HAM on the polar motion in different part of spectra show that consideration of the HAM data not improve significantly an agreement of the geophysical excitation of polar motion (atmosphere, oceans and hydrology) with geodetic excitation function GAM (Brzeziński et al., 2009; Chen and Wilson, 2005; Nastula and Kolaczek, 2005; Nastula et al., 2011; Shuanggen et al., 2010).

Here gravimetric HAM functions were estimated from several gravimetric monthly GRACE/CHAMP solution data: ITG-GRACE2010 gravity field model, DMT-1 (DEOS Mass Transport Model), AIUB - multi - annual mean gravity field GRACE03S, Tongji - GRACE monthly solution from the Tongji University, ULUX - monthly CHAMP solution from the university of Luxembourg, CNES/GRGS solution determined by a combined analysis of LAGEOS and GRACE observations, from GRACE monthly solutions from the three processing centers CSR, GFZ and JPL from RL05 series, from GRACE weekly solutions: GFZ Release 05 and from SLR solution obtained from the analysis SLR data to five geodetic satellites LAGEOS 1 and 2, Starlette, Stella and Ajisai. The gravimetric data are available in ICGEM - International Center for Global Gravity Field Model.
The gravimetric HAM functions were computed from harmonic coefficients of the Earth gravity field, based on formulae (Chen and Wilson, 2005):

$$\begin{bmatrix}\chi_1^{mass}\\ \chi_2^{mass}\end{bmatrix} = -\frac{1}{(1+k_2')\sqrt{\frac{3}{5}}\frac{C-A}{1.098R_e^2M}}\begin{bmatrix}\Delta C_{21}\\ \Delta S_{21}\end{bmatrix} \quad (1)$$

where M and R_e are the mass and mean radius of the Earth, respectively, C and A are the Earth's principal moments of inertia, is the degree–2 Love number (-0.301) accounting for elastic deformational effects on gravitational change. ΔC_{21}, ΔS_{21} are Stokes coefficients of the gravity field.
The gravimetric excitation functions of polar motion (HAM) were compared with the so-called geodetic residuals series G-A-O computed by removing atmospheric (Atmospheric Angular Momentum-AAM) and oceanic (Oceanic Angular Momentum-OAM) contributions from the GAM series (Nastula et al., 2011). In this study we used the geodetic time series estimated by the International Earth Rotation and Reference System Service (IERS) from C04 series of the pole coordinates (Bizouard and Gambis, 2009). The atmospheric excitation function AAM were derived from time series of NCEP/NCAR reanalysis data (Salstein et al. 1993). The oceanic excitation function OAM including bottom pressure and currents term were computed on the basis of ECCO-JPL ocean model (Gross et al. 2003).

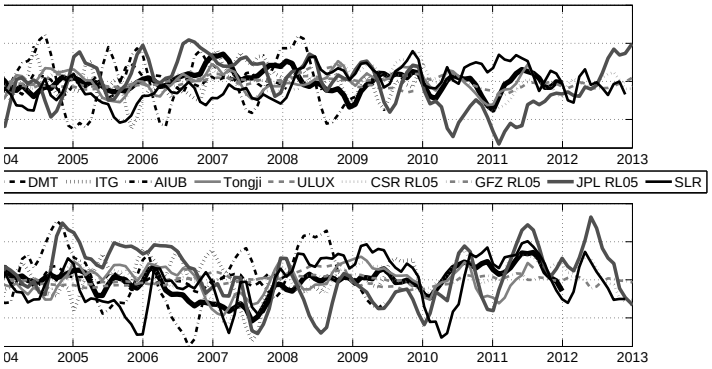

(a) Gravimetric excitation functions vs. GAO (30 days step)

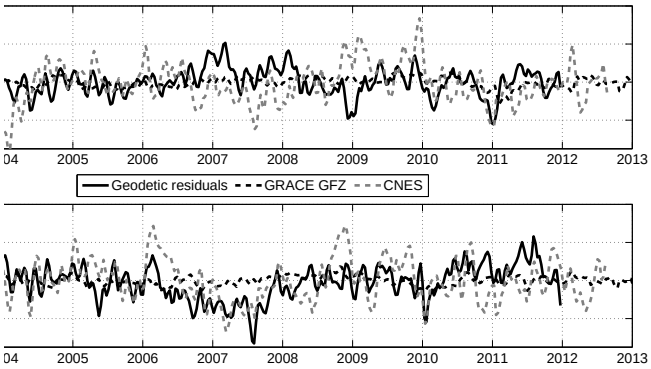

(b) Gravimetric excitation functions vs. GAO (10 days step)

Figure 1: Comparison of components of the gravimetric excitation functions, χ_1 and χ_2, of polar motion from different gravimetric data and of the geodetic residuals G-A-O being the difference between the geodetic excitation function and sum of the atmospheric and oceanic excitation function of polar motion. All the data were smoothed with a step of 30 days (top panel) and 10 days (bottom panel), FWHM=60 (top panel) and FWHM=20 (bottom panel). The 365.25, 180.0 and 120.0 days oscillations were removed from the time series.

Comparison of the equatorial components of the gravimetric excitation polar motion functions (monthly and 10 days sampling) with the geodetic residuals excitation function G-A-O are shown in Fig. 1. Tables 1 compares variances of the series. One can see that gravimetric excitation functions are not consistent with each other and with geodetic residuals. However, the agreement between geodetic residuals and gravimetric excitation function determined from CNES/GRGS data is quite good, especially for χ_2 equatorial component of polar motion. Next the comparison of the geodetic residuals and the HAM were carried out in two ways: through the determination of annual oscillation parameters (see Table 3) and the computation of correlation coefficients of non-seasonal variations of the series obtained subtracting a seasonal signals model (365 days, 181 days, 121, days) from the time series (Table 2), using LSQ method (Brzeziński et al., 2009). The correlation coefficients, computed for non-seasonal variations of all considered gravimetric time series, indicated generally better agreement between χ_2 component than χ_1 of

Variances of HAM		
Excitation functions	$\chi_1[mas^2]$	$\chi_2[mas^2]$
G-A-O	28.3	57.1
DMT	11.9	9.1
ITG	95.8	104.0
AIUB	179.7	221.7
Tongji	29.9	51.3
ULUX	28.1	11.3
GRACE CSR	33.0	60.8
GRACE GFZ	6.9	4.6
GRACE JPL	166.3	211.1
SLR	65.8	145.5
GFZ (10 days)	8.5	6.4
CNES (10 days)	121.6	119.09

Table 1: Variances of global geodetic and gravimetric excitation functions of polar motion; geodetic residuals are calculated as differences between GAM (C04 series) and sum of AAM (NCEP/NCAR model were used) and OAM (ECCO model were used).

Correlation coefficients Geodetic residuals vs. HAM		
Geodetic residuals vs.	χ_1	χ_2
CSR RL05 (monthly)	0.24	0.69
GFZ RL05 (monthly)	0.30	0.37
JPL RL05 (monthly)	0.25	0.29
ITG (monthly)	0.24	0.14
DMT (monthly)	0.02	0.26
AIUB (monthly)	0.18	0.15
SLR (monthly)	0.10	0.46
ULUX (monthly)	0.33	0.00
Tongji (monthly)	0.35	0.60
CNES (10 days)	0.30	0.52
GRACE GFZ (10 days)	0.24	0.26

Table 2: Correlation coefficients between global geodetic and gravimetric excitation functions of polar motion calculated after removing annual signals from time series; geodetic residuals are calculated as differences between GAM (C04 series) and sum of AAM (NCEP/NCAR model were used) and OAM (ECCO model were used); statistical significance $p = 0.3$.

Data	Prograde annual		Retrograde annual	
	Amplitude	Phase	Amplitude	Phase
ULUX	14.5	-53.9	14.9	128.9
Tongji	1.8	11.7	4.0	139.6
ITG	4.2	-60.1	8.5	-100.9
SLR	15.0	-89.3	18.3	-118.7
DMT	0.4	-3.6	2.9	72.0
CNES 10 days	2.6	-171.0	3.2	-74.4
AIUB	10.9	-76.6	4.4	-61.3
CSR RL05	2.8	-2.0	3.1	138.7
GFZ RL05	3.6	-14.3	4.5	130.2
JPL RL05	4.6	-5.8	5.9	11.2
GFZ Weekly	3.7	-27.5	4.8	137.7
G-A-O	6.4	-53.5	3.5	120.8

Table 3: Amplitudes and phases of the of the prograde and retrograde annaul oscillations of the residuals of the geodetic excitation function (G-A-O) and of the different gravimetric excitation functions by using Last Square Method. The fitted and removed from the time series data model comprises the order polynomial and a sum of complex sinusoids with periods 365.25, 180.0, 120.0 days. Analysis is done over the period 2003.0 to 2009.5.

these gravimetric excitation functions (see Table 2). The highest value, equal to 0.69, of the correlation coefficient was reached, when to estimate of gravimetric computation the CSR RL05 data were used. Amplitudes and phases of these annual oscillations are presented in Table 3. It can be concluded, that the annual oscillations of the gravimetric excitation functions have different amplitudes and phases, furthermore, only ITG function is close to the geodetic residuals in prograde oscillations and only GRACE GFZ RL05 and GRACE CSR RL05 vectors are close to the geodetic residuals in retrograde oscillations.

2. CONCLUSIONS

GRACE is a powerful tool to determine time-variable geophysical mass fields, and in particular that of the changing land-based hydrology, which is estimated otherwise only with complex hydrological models. We found that these gravimetric-hydrological excitation functions, obtained by the several processing

centers, still differ significantly. One difference is that a greater degree of smoothness is exhibited by GFZ than the other products. Analyses show that the use of these new data to compare with GAO does not bring significant new results from to previous studies (Seoane et al., 2009, 2011; Nastula et al., 2011), though confirms the current extent of the differences among the series. The best agreement between gravimetric-hydrological excitation functions and geodetic residuals was obtained for the χ_2 component of gravimetric excitation function computed from the CSR, Tongji and CNES data series, and this may be due to some positive attributes in the processing, like its increased background resolution.

Acknowledgements. This work was supported by the National Science Centre contracts 2012/07/N/ST10/03275 and 2012/05/B/ST10/02132.

3. REFERENCES

Bizouard, C., Gambis, D., 2009, "The combined solution C04 for Earth orientation parameters consistent with international terrestrial reference frame 2005", In: H. Drewes (ed.), Geodetic Reference Frames, Proc. IAG Symp., Munich, Germany, October 9-14, 2006, Springer, Berlin, pp. 265–270.

Brzeziński, A., Nastula, J., Kołaczek B., 2009, "Seasonal excitation of polar motion estimated from recent geophysical models and observations", J. Geodyn., 48, pp. 235–240.

Chen, J.-L., Wilson, C.R., 2005, "Hydrological excitation of polar motion, 1993–2002", J. Geophys. Int. 160, pp. 833–839, doi: 10.1111/j.1365-246X.2005.02522.x.

Nastula, J., Kołaczek, B., 2005, "Analysis of Hydrological Excitation of Polar Motion", In: Proc. Workshop: Forcing of polar motion in the Chandler frequency band, a contribution to understanding interannual climate variations. Centre Europeen de Geodynamique et de Seismolgie, Luxembourg, pp. 149–154.

Nastula, J., Ponte, R.M., Salstein, D.A., 2007, "Comparison of polar motion excitation series derived from GRACE and from analyses of geophysical fluids", Geophys. Res. Lett., 34, L11306, doi: 10.1029/2006GL028983.

Nastula, J., Paśnicka, M., Kołaczek, B., 2011, "Comparison of the geophysical excitations of polar motion from the period: 1980.0–2009.0", Acta Geophysica, 59(3), pp. 561–577, doi: 10.2478/s11600-011-0008-2.

Salstein, D.A., Kann, D.M., Miller, A.J., Rosen, R.D., 1993, "The subbureau for atmospheric angular momentum of the international Earth rotation service: A meteorological data center with geodetic applications", Bull. Am. Meteor. Soc. 74, pp. 67–80, doi: 10.1175/1520-0477(1993)074<0067:TSBFAA>2.0.CO;2.

Seoane, L., Nastula, J., Bizouard, C., Gambis, D., 2009, "The use of gravimetric data from GRACE mission in the understanding of polar motion variations", Geophys. J. Int., 178(2), pp. 614–622, doi: 10.1111/j.1365-246X.2009.04181.x.

Shuanggen, J., Chambers, D.P., Tapley, B.D., 2010, "Hydrological and oceanic effects on polar motion from GRACE and models", J. Geophys. Res., 115, B02403, doi: 10.1029/2009JB006635.

GEOMAGNETIC EXCITATION OF NUTATION

C. RON, J. VONDRÁK
Astronomical Institute, Academy of Sciences of Czech Republic
Boční II, 14100 Prague 4, Czech Republic
e-mail: ron@asu.cas.cz, vondrak@ig.cas.cz

ABSTRACT. We tested the hypothesis of Malkin (2013), who demonstrated that the observed changes of Free Core Nutation parameters (phase, amplitude) occur near the epochs of geomagnetic jerks. We found that if the numerical integration of Brzeziński broad-band Liouville equations of atmospheric/oceanic excitations is re-initialized at the epochs of geomagnetic jerks, the agreement between the integrated and observed celestial pole offsets is improved (Vondrák & Ron, 2014). Nevertheless, this approach assumes that the influence of geomagnetic jerks leads to a stepwise change in the position of celestial pole, which is physically not acceptable. Therefore we introduce a simple continuous excitation function that hypothetically describes the influence of geomagnetic jerks, and leads to rapid but continuous changes of pole position. The results of numerical integration of atmospheric/oceanic excitations and this newly introduced excitation are then compared with the observed celestial pole offsets, and prove that the agreement is improved significantly.

1. INTRODUCTION

Atmospheric and oceanic excitations play dominant role in polar motion and rotational velocity of the Earth. Thanks to the precise P/N model IAU2000/2006, small but non-negligible effects can be seen also in the observed celestial pole offsets (CPO), i.e. in nutation. These effects are caused by quasi-diurnal changes of angular momentum functions of the geophysical fluids (atmosphere, oceans, hydrology, ...).

In our previous study (Vondrák & Ron, 2014) we found that atmospheric/oceanic effects do not explain the observed CPO completely. The integrated excitations in celestial reference frame (CRF) in comparison with the observed CPO became out-of-phased after some period. We suppose that additional excitations have effect. In Ron et al. (2014) we tested additional events at epochs of strong earthquakes, jumps in observed data (Chapanov et al., 2014) and geomagnetic jerks (GMJ) shown in Malkin (2013). Geomagnetic jerks (or secular geomagnetic variation impulses) are relatively sudden changes in the second derivative of the Earth's magnetic field with respect to time (Olsen & Mandea, 2007). The re-initialization of the integration in the dates of these events was used in Vondrák & Ron (2014) and the best agreement has been found for the GMJ epochs. But the re-initialization of integration leads to a stepwise change in the position of celestial pole, which is not acceptable from the physical point of view.

Here we present a slightly modified approach by adding a simple continuous excitation function near GMJ epochs.

2. USED PROCEDURE

The excitations of the Earth rotation in the celestial reference frame (nutation) by atmosphere and ocean were studied using Brzeziński's broad-band Liouville equations (Brzeziński, 1994)

$$\ddot{P} - i(\sigma'_C + \sigma'_f)\dot{P} - \sigma'_C\sigma'_f P = -\sigma_C \left\{ \sigma'_f(\chi'_p + \chi'_w) + \sigma'_C(a_p\chi'_p + a_w\chi'_w) + i[(1+a_p)\dot{\chi}'_p + (1+a_w)\dot{\chi}'_w] \right\}, \quad (1)$$

where $P = dX + idY$ is excited motion of Earth's spin axis in celestial frame, σ'_C, σ'_f are the complex Chandler and free core nutation frequencies in CRF, respectively, σ_C in TRF. $a_p = 9.200 \times 10^{-2}$, $a_w = 2.628 \times 10^{-4}$ are dimensionless constants (Koot & de Viron, 2011). χ'_p and χ'_w are the angular momentum excitation functions (pressure and wind) expressed in CRF.

To be able to integrate the system we need initial values P_0, $\dot{P}_0$ constrained so that the free Chandlerian term (with quasi-diurnal period in celestial frame) vanishes. The initial values are closely connected to the phase and amplitude of the integrated series. The final choice of P_0 was made by repeating integration

with different values P_0 to fit the integrated series to VLBI observations so that reaches a minimum rms differences. The Runge-Kutta 4th order integration in 6-hour steps has been used to solve Eq. (1).

Procedure of searching the additional excitations. We tested several functions (an impulse, step-wise, ...) and found the double ramp function of a triangle shape as the best one. The central epochs of additional excitations around GMJ epochs have been fixed at 1991.0, 1994.0, 1999.0, 2003.5, 2004.7, and 2007.5. GMJs last typically several months so we fixed the length of excitation to 200 days. The complex amplitudes of the excitations were then estimated to lead to the best rms fit to observed CPO. In Vondrák & Ron (2014) we also tested if the excitations is preceding, delaying or corresponding to the GMJ epochs and the best agreement was found for the epochs of GMJ. The found additional excitations are shown in Fig. 1.

3. USED DATA AND RESULTS

Celestial pole offsets. We took the CPO from the last IVS combined solution `ivs14X1q.eoxy` covering the interval 1989.0-2014.0. dX and dY are given in unequally spaced intervals. We cleaned the data by removing outliers (CPO > 1mas) and then the empirical Sun-synchronous correction of IAU2000 nutation model has been added in order to be the observed CPO comparable with the atmospheric contribution. The series were filtered to retain only periods between 60 and 6000 days and interpolated at regular 10-day intervals.

Atmospheric angular momentum. There are two sources of atmospheric angular momentum (AAM) data

- European Center for Medium-Range Weather Forecasts (ECMWF), ERA40
- Atmospheric and Environmental Research, USA, NCEP/NCAR reanalysis

Our previous study based on AAM/OAM function of European meteorological Center ECMWF ERA40 and on the ocean model OMCT showed not so good agreement in comparison with the NCEP/NCAR series. No model of oceanic angular momentum driven by NCEP atmosphere is available for the whole studied period. But the pressure term with inverted barometer (IB) correction implies a simple model of oceanic response on the pressure changes. The series of AAM χ (complex values) were transformed from the terrestrial frame to the celestial frame by using the complex decomposition at retrograde diurnal frequency $\chi' = -\chi e^{i\Phi}$, Φ is the Greenwich sidereal time. Because we are interested in the long-periodic motion (comparable with nutation), we applied the smoothing to remove periods shorter than 10 days and calculated their time derivatives needed for integration. The series of AAM pressure term with IB correction transformed in this way are shown in Fig. 1.

The celestial pole offsets from IVS corrected for the sun-synchronous correction was then compared with geophysically excited motion of celestial pole obtained by numerical integration of Eq. (1). To obtain the best fit to CPO values, the integration was repeated with different initial values for the first interval,

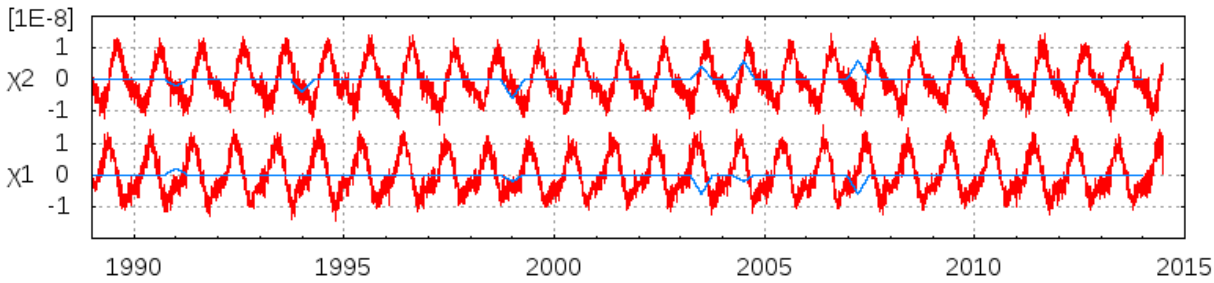

Figure 1: The AAM pressure term with IB correction in CRF (red line) and the found additional excitations at epochs of geomagnetic jerks (blue triangles).

i.e., from the beginning of the series in 1989 up to the first epoch of geomagnetic jerk 1991 and then were searched the complex values of the additional excitations for each interval between the successive geomagnetic jerks.

The integrated celestial pole offsets obtained with NCEP excitations with the inverted barometer correction and the solution with additional excitations in GMJ epochs are graphically depicted in Fig. 2.

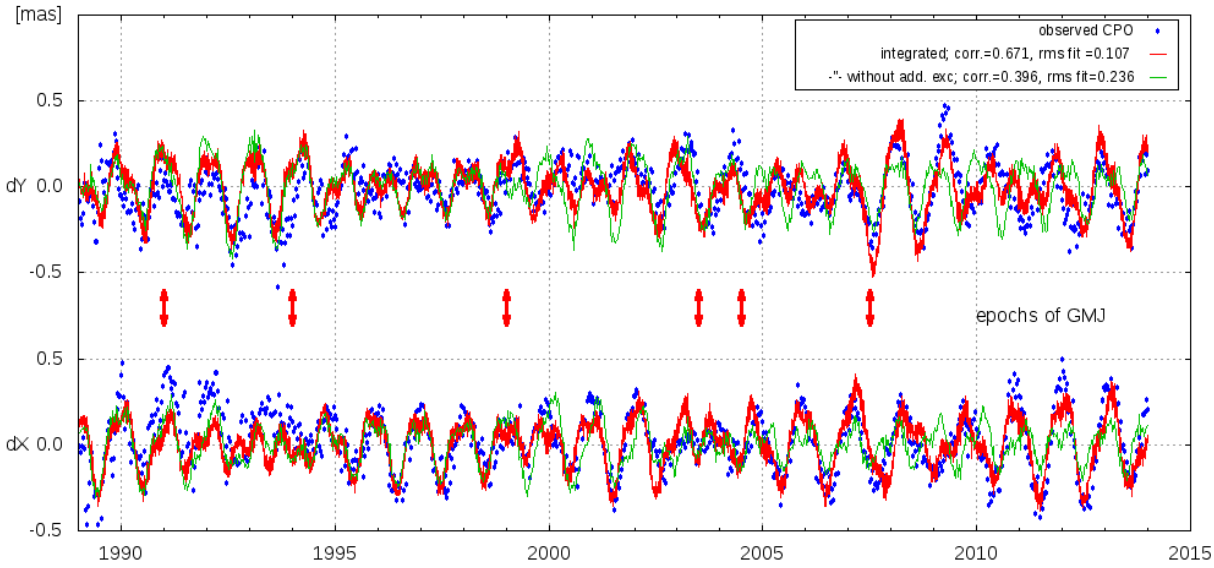

Figure 2: Observed (dots) and integrated celestial pole offsets. The green line corresponds to the solution of AAM with IB correction and the red line corresponds to the solution with additional excitations in GMJ epochs.

Series	without add. exc.		with add. exc.	
	rms [mas]	corr.	rms[mas]	corr.
NCEP with IB	0.236	0.396	0.107	0.671

Table 1: The rms fit and the correlation between integrated and observed celestial pole offsets with and without additional excitations.

In the process of searching the best rms fit we used the procedure of wavelet based semblance analysis (Cooper & Cowan, 2008) to compare the integrated and observed series of celestial pole offsets. The semblance measure $S = \cos(\theta)$, where θ is a local phase between the real and imaginary part of the cross wavelet transform, can reach the values between $< -1, +1 >$. The value $+1$ means correlated, 0 uncorrelated and -1 inversely correlated series, respectively. An example of the value of semblance and its multiplication by an amplitude of the cross-wavelet power (marked as 'Dot product') is shown at Fig. 3. The y-axis shows the width of the studied window in years. The improvement due to the application of the additional excitation is then clearly seen in the figure.

4. CONCLUSIONS

Geophysical excitations can yield significant contribution to nutation, of the order of 0.1mas. NCEP solution with the inverted barometer correction leads to better agreement than ERA solution. The influence of motion (wind) terms is one order of magnitude smaller than that of matter (pressure) terms. The application of schematic additional excitations at epochs of geomagnetic jerks improve the agreement of integrated celestial pole position with VLBI observations. The interpretation of the physical nature of the GMJ effect on nutation requires more study in future.

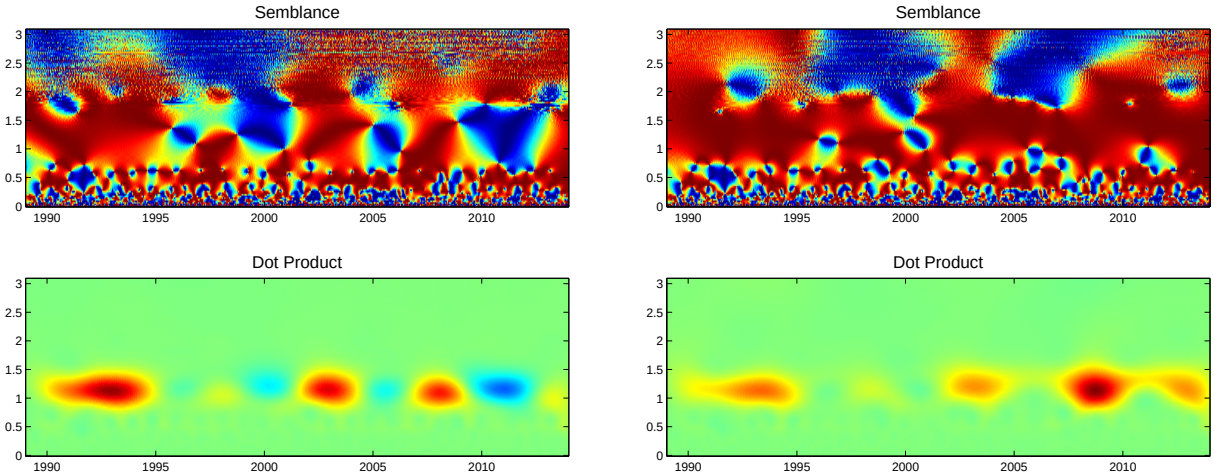

Figure 3: The wavelet semblance analysis of the the observed and integrated series of CPO (here Y axis only) without (left) and with the additional excitation at GMJ epochs (right). White (bright red in online version) color corresponds to a semblance +1 (correlated), black (dark blue in online version) to a semblance -1 (inversely correlated), gray (green in online version) to a semblance 0 (uncorrelated).

Acknowledgements. This research was financially supported by the grant No. 13-15943S "Geophysical excitations in the motion of Earth's axis of rotation", awarded by the Grant Agency of the Czech Republic.

5. REFERENCES

Brzeziński, A., 1994, "Polar motion excitation by variations of the effective angular momentum function: II. Extended Model", Manuscripta Geodaetica, 19, pp. 157–171.

Chapanov, Ya., Vondrák, J., Ron, C., Pachalieva, R., 2014, "Natural and systematic polar motion jumps", Proc. Journées 2013 Systèmes de référence spatio-temporels, N. Capitaine (ed.), Observatoire de Paris, pp. 193–196.

Cooper, G.R.J., Cowan, D.R., 2008, "Comparing time series using wavelet-based semblance analysis", Computers & Geosciences, 34, pp. 95–102.

Olsen, N., Mandea M., 2007, "Investigation of a secular variation impulse using satellite data: The 2003 geomagnetic jerk". Earth and Planetary Science Letters, 255, pp. 94–105.

Malkin, Z., 2013, "Free core nutation and the geomagnetic jerks", J. Geodyn., 72, pp. 53–58

Ron, C., Vondrák, J., Chapanov, Ya., 2014, "Free core nutation – possible causes of changes of its phase and amplitude", Proc. Journées 2013 Systèmes de référence spatio-temporels, N. Capitaine (ed.), Observatoire de Paris, pp. 164–167.

Vondrák, J., Ron, C., 2014, "Geophysical excitation of nutation – comparison of different models", Acta Geodyn. Geomater., 11, pp. 193–200.

THE CHANDLER WOBBLE OF THE POLES AND ITS AMPLITUDE MODULATION

N. SIDORENKOV
Hydrometcentre of Russian Federation
B. Predtechensky pereulok, 11–13, Moscow 123242, Russia
e-mail: sidorenkov@mecom.ru

ABSTRACT. It is shown that the period of the Chandler wobble of the poles (CWP) is a combined oscillation caused by three periodic processes experienced by the Earth: (a) lunisolar tides, (b) the precession of the orbit of the Earth's monthly revolution around the barycenter of the Earth - Moon system, and (c) the motion of the perigee of this orbit. The addition of the 1.20 - year Chandler wobble to sidereal, anomalistic, and synodic lunar yearly forcing gives rise slow periodic variations in the CWP amplitude with periods of 32 to 51 years.

1. INTRODUCTION

It is well known that the Earth and the Moon revolve around their center of mass (barycenter) with a sidereal period of 27.3 days. The orbit of the Earth's center of mass (geocenter) is geometrically similar to the Moon's orbit, but the orbit size is roughly 1/81 as large as that of the latter. The geocenter is, on average, 4671 km away from the barycenter. In the Earth's rotation around the barycenter, all its constituent particles trace the same nonconcentric orbits and undergo the same centrifugal accelerations as the orbit and acceleration of the geocenter. The Moon attracts different particles of the Earth with a different force. The difference between the attractive and centrifugal forces acting on a particle is called the tidal force. The rotation of the Earth-Moon system around the Sun (Fig. 1) leads to solar tides. The total lunisolar tides vary with a period of 355 days (13 sidereal or 12 synodic months). This period is known as the lunar or tidal year.

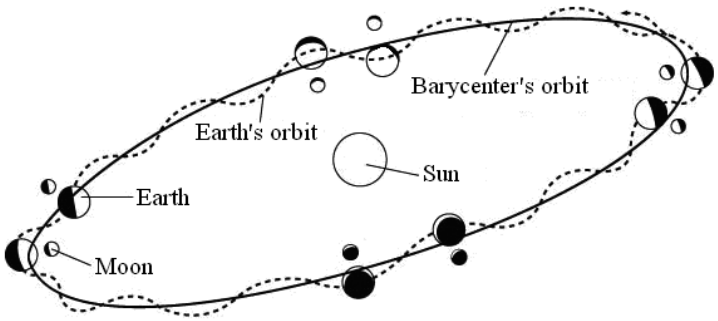

Figure 1: Revolution of the Earth-Moon system around the Sun.

It is well known that the lunar nodes precess westward around the ecliptic, completing a revolution in 18.6 years. Lunar perigee moves eastward, completing a revolution in 8.85 years. Because of these opposite motions, a node meets a perigee in exactly in 6 years.

2. QUASI-BIENNIAL OSCILLATION

In my books (Sidorenkov, 2002, 2009) it was shown that the Earth, the ocean, and the atmosphere exhibit consistent oscillations, influencing each other, i.e., joint oscillations initiated by tides occur in the

Earth-ocean-atmosphere system. Visual manifestations of these oscillations include the wobble of the Earth's poles, El Nino and La Nina in the ocean, and the Southern Oscillation and the quasi-biennial oscillation in the atmosphere.

The wobble of the poles is the movement of the Earth's daily rotation axis inside of the Earth's body.

The quasi-biennial oscillation (QBO) is a quasiperiodic oscillation of the equatorial zonal wind between easterlies and westerlies in the tropical stratosphere with a mean period of 28 months.

Figure 2 shows power spectra of the pole coordinate x (top) and the QBO indices (bottom). A surprising feature is that the spectrum of QBO indices is similar with a factor of 2 to that of the pole's coordinates x and y. If the horizontal-axis scale in the spectrum of the pole's coordinates is doubled as shown in Fig. 2, then all the details in the spectrum of QBO indices coincide with those in the polar motion spectrum; that is the oscillation in the polar motion is reflected as the doubled-period QBO in the atmosphere. In the equatorial stratosphere, the duration of the all the Earth's polar motion cycles is doubled.

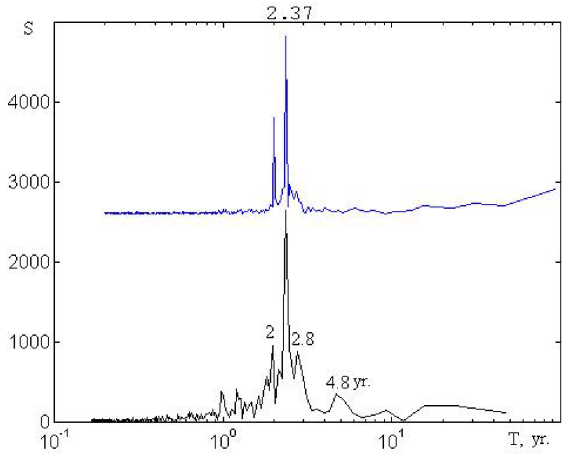

Figure 2: Power spectra of the pole coordinate x (top) and the QBO indices (bottom). To demonstrate the curves' similarity, the pole's curve was transformed as follows: $T = 2T_0$ and $S = 30S_0 + 2600$, where T_0 and S_0 are the actual values of the periods T and spectral densities S, respectively.

These facts testify that the Chandler wobble of the poles and the QBO cyclicity of the stratospheric winds are likely to have the common mechanism of excitation that is due to the geodynamic processes in the Sun-Earth-Moon system. The mechanism of QBO excitation is associated with the absorption of lunisolar tidal waves in the equatorial stratosphere. The QBO period is equal to a linear combination of the frequencies corresponding to the doubled periods of the tidal year (0.97 year), of the node regression (18.6 years), and of the perigee motion (8.85 years) of the Earth's monthly orbit:

$$\frac{1}{2}\left(\frac{1}{0.97} - \frac{1}{8.85} - \frac{1}{18.61}\right) = \frac{1}{2.3}$$

In other words, the quasi-biennial oscillation of the wind direction in the equatorial stratosphere is a combined oscillation caused by three periodic geodynamic processes experienced by the atmosphere: lunisolar tides, the precession of the orbit of the Earth's monthly revolution around the barycenter of the Earth-Moon system, and the motion of the perigee of this orbit.

3. CHANDLER WOBBLE OF THE POLES

The wobble of the Earth's poles and the QBO in the atmosphere have similar spectra (with the ratio of the periods being 1:2) (Sidorenkov, 2002, 2009). The period of the Chandler wobble of the poles (CWP) is believed to differ from the Euler period of 305 days because of the elastic properties of the Earth. However, it is physically unlikely that both QBO and CWP are caused by the features of the Earth's internal structure. A natural assumption is that QBO and CWP have a single cause, namely, the features of the Earth's monthly revolution in the Earth-Moon system and the revolution of this system around the Sun. The wobble forcing with a solar year period of 365.24 days is modulated by the precession of

the Earth's monthly orbit with a period of 18.61 years and by the motion of its perigee with a period of 8.85 years. Finally, the resulting solar annual forcing generates polar wobbles with a Chandler period of 1.20 year:

$$\frac{1}{2}\left(\frac{1}{1.0} - (\frac{1}{8.85} + \frac{1}{18.61})\right) = \frac{1}{1.2}$$

The amplitude modulation of CWP is clearly exhibited with a period about 40 years. It is known that the AAM and OAM functions are capable to account for about 90 % of the required CWP excitation. This excitation is believed to occur at the fundamental frequency of the climate system forcing with a period of 365.24 days. However, it was shown in the author's most recent works that, in addition to this basic forcing, the climate system experiences additional forcing caused by cloud amount variations with lunar-year periods (http://geoastro.ru). Climatic characteristics and the equatorial component of the atmospheric angular momentum h2 were found to oscillate with a period of 355 days (Sidorenkov, 2009; Sidorenkov and Sumerova, 2012a, 2012b). The wobble forcing with a lunar year period of 355 days (13 tropical months) is modulated by the precession of the Earth's monthly orbit with a period of 18.61 years and by the motion of its perigee with a period of 8.85 years. Finally, the resulting "lunar tropical year" forcing generates polar wobble with a period of 1.16 year:

$$\left(\frac{1}{355.18days/365.24(days/yr)} - (\frac{1}{8.85} + \frac{1}{18.61})\right) = \frac{1}{1.1606yr}$$

Interference of the 1.20-year Chandler oscillation and the 1.16-year oscillation leads to beats, i.e., to periodic variations in the polar wobble amplitude with a period of 35.3 years:

$$\left(\frac{1}{1.16} - \frac{1}{1.2}\right) = \frac{1}{35.3}$$

Similarly, the lunar synodic year (12 synodic months) must excite polar wobble with a period of 1.1574 year:

$$\left(\frac{1}{354.37days/365.24(days/yr)} - (\frac{1}{8.85} + \frac{1}{18.61})\right) = \frac{1}{1.1574yr}$$

Interference of this excitation and CWP generates beats with a period of 32.6 years.

The "lunar anomalistic" annual (13 anomalistic months) excitation can generate polar wobble with a period of 1.172 year:

$$\left(\frac{1}{358.21days/365.24(days/yr)} - (\frac{1}{8.85} + \frac{1}{18.61})\right) = \frac{1}{1.172yr}$$

Interference of this wobble with CWP can generate beats with a period of 50.9 years:

$$\left(\frac{1}{1.172} - \frac{1}{1.2}\right) = \frac{1}{50.9}$$

Thus, interference of CWP (1.20-year period) with these moon-caused oscillations gives rise to beats, i.e., to slow periodic variations in the CWP amplitude with periods of 32 to 51 years. They are observed in reality.

4. REFERENCES

Sidorenkov, N.S., 2002, "Physics of the Earth's Rotation Instabilities", Moscow: Nauka, 384 pp. (in Russian)

Sidorenkov, N.S., 2009, "The interaction between Earth's rotation and geophysical processes", Wiley-VCH Verlag GmbH and Co. KGaA, Weinheim.

Sidorenkov, N.S., Sumerova, K.A., 2012a, "Temperature Fluctuation Beats as a Reason for the Anomalously Hot Summer of 2010 in the European Part of Russia", Russian Meteorology and Hydrology, 37(6), pp. 411–420.

Sidorenkov, N.S., Sumerova, K.A., 2012b, "Geodynamic causes of decade changes in climate", Proc. Hydrometeorological Center of Russia, Vol. 348, pp. 195–214.

PREDICTION OF THE CHANDLER WOBBLE

L.V. ZOTOV[1,2], C. BIZOUARD[3],
[1] Sternberg Astronomical Institute of Moscow State University, Laboratory of Gravimetry
Universitetski pr., 13, Moscow, 119992, Russia
e-mail: tempus@sai.msu.ru
[2] National Research University Higher School of Economics
20, Myasnitskaya Ulitsa, Moscow, 101000, Russia
[3] SYRTE, Observatoire de Paris, CNRS/UPMC
61, Avenue de l'Observatoire, 75014, Paris, France

ABSTRACT. Chandler wobble amplitude have been decreasing in 2010s as in 1930s. We try to predict its future behaviour through prediction of its complex envelope. The excitation of the Chandler wobble (ChW) reconstructed by Panteleev's filter was also analized. The equation for the complex envelope propagation through the Euler-Liouville equation was derived. Similarities with the climate change characteristics are discussed.

1. INTRODUCTION

Chandler wobble (ChW) is one of the crucial component of the Earth's polar motion (PM). It was discovered in 1891 by Seth Carlo Chandler, astronomer and economist, who manually processed more than 33000 astronomical observations in order to detect variations of latitude. The period of ChW, now estimated as 433 days (Vicente and Wilson, 1997; Liu et al., 2007), was a great surprise for astronomers, for they expected a free wobble of 305-day period corresponding to a rigid oblate Earth. The annual PM was also discovered by Chandler. Since, Newcomb and others modified the rigid Earth theory to take into account the non-rigidity of the Earth: mantle elasticity, presence of fluid parts like the oceans and the core. This allows to get a theoretical Chandler period consistent with observations. Actually the free wobble concept, where no forcing is required, does not exactly hold any more. Some small excitation is required to maintain resonant ChW, because of its damping having a relaxation time between 20 and 100 years. To model the pole path described in the geographic equatorial plane by the complex coordinate $p(t) = x(t) - iy(t)$, we use the linear Liouville equation (Munk, MacDonald, 1960; Lambeck, 1980)

$$\frac{i}{\sigma_c}\frac{dp(t)}{dt} + p(t) = \chi(t), \tag{1}$$

where the complex Chandler angular frequency $\sigma_c = 2\pi f_c(1 + i/2Q)$ depends on the real Chandler frequency $f_c = 0.8435$ yr^{-1} and the quality factor $40 < Q < 200$, which empirically determines the damping (in this work we use the value $Q = 100$); $\chi(t) = \chi_1(t) + i\chi_2(t)$ is the complex equatorial excitation function.

It is well known, that ChW amplitude has been changing in $\sim$ 150-years period of observations, and has even completely decayed in 1930s (Fig. 1, left). Several interpretations were proposed: the first one suggests two near-by frequencies of ChW (see Guo et al., 2005), which produce the beating effect. But this concept contradicts the only one resonant frequency f_c of equation (1). Another school proposes that random variations of hydro-atmospheric excitation are responsible for ChW changes (Gross, 2000; Brzeziński et al., 2012).

The analysis of atmospheric angular momentum AAM and oceanic angular momentum OAM for the recent 60 years proves that at f_c the changes of currents and ocean bottom pressure, from one side, and winds and atmospheric pressure, from another side, is sufficient to maintain ChW. However, AAM and OAM spectra do not show any prominent feature at Ch. freq. (Fig. 1, right) and behave like white noise there. Indeed the main AAM and OAM modes are at annual, ter-annual, semi-annual, and tidal frequencies (mainly diurnal and semi-diurnal). Since resonant motion does not require much forcing, sometimes it is also proposed that the side-lobe of the near-by annual mode, evident in AAM and OAM spectra, and causing 365-day PM, can also force 433-day ChW. It means that the current theory

understands ChW and its amplitude changes as a random process at resonant frequency, given by linear equation (1) and maintained by small stochastic oscillations in the ocean and atmosphere (see Chao and Chung, 2012).

On the other hand, work of (Sidorenkov, 2009) suggests a non-linear interrelation between ChW and planetary oscillation modes, such as El Nino Southern Oscillation (ENSO) and quasi-biannual oscillations (QBO), for these latter present some super-harmonics of the ChW period.

In our work we analyse the complex ChW envelope within the framework of classical equation (1) in order to predict it for next decades. The method we use to extract ChW and its excitation is explained in (Zotov, Bizouard, 2012). The results are presented in the next section.

2. CHANDLER WOBBLE ENVELOPE

To extract ChW the Panteleev's filter and Complex Singular Spectrum Analysis (CSSA) can be used (Zotov, Bizouard, 2012). They allow to extract ChW component in a very narrow prograde frequency band. Both methods of processing give very similar results. The x-component of the obtained signal is presented in Fig. 1, left. The y-component of purely prograde ChW is similar, but shifted by $\pi/2$ (109 days). The red rectangle displays the region, where the filtering edge effects can be neglected. One of the most prominent feature of ChW envelope (obtained by Gabor transform) is its decrease around 1930s, at the beginning of the interval, 1840s, and at the end, 2010s (edge effects should be negligible for CSSA). Another variation of amplitude with a 40-year period and minima around 1890, 1930, 1970, is superimposed on the first one (see Nastula et al., 1993).

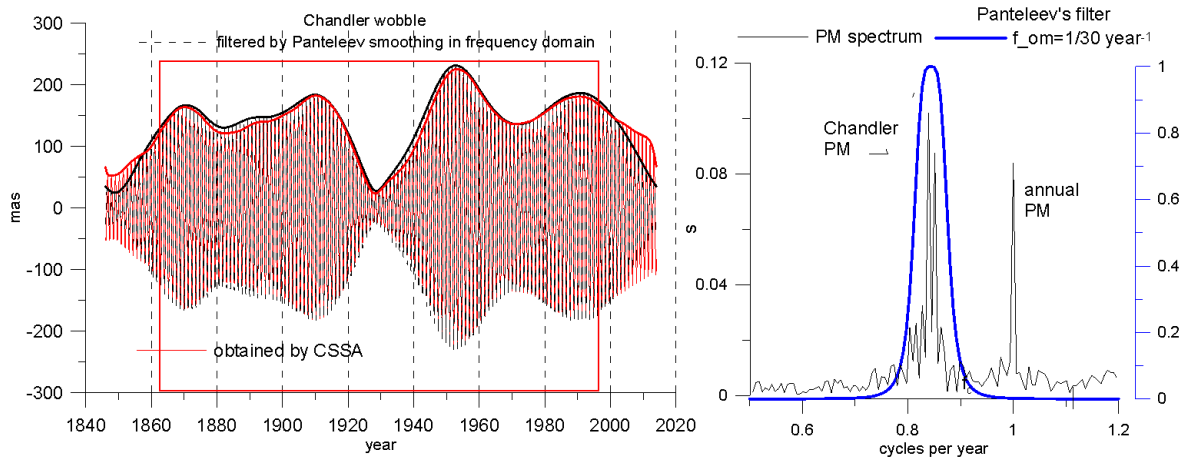

Figure 1: Chandler wobble obtained by CSSA and Panteleev's filter, and its envelope (left). Complex PM spectrum (module) around Chandler frequency and Panteleev's filter frequency response (right).

In Figure 1, right, the PM spectrum in the ChW frequency band and Panteleev's filter transfer function are represented. The filter does not allow annual and other non-chandlerian frequencies to pass. The ChW component is centred around f_c, but it is not just one line, corresponding to one harmonic. The ChW line is split into two frequency components, it also has side-lobes. It means that the oscillation is not purely harmonic, but has modulation (beating). Fourier analysis represents the signal as a set of harmonics of given amplitudes and phases with infinite time extent. At the same time, we can represent ChW by one harmonic with the circular frequency $\omega_c = 2\pi f_c$ and complex amplitude $C(t)$ according to

$$p(t) = C(t)\exp\{i\omega_c t\} = A(t)\exp\{i\phi(t)t\}\exp\{i\omega_c t\}, \tag{2}$$

or through $A(t) = |C(t)|$, $\phi(t) = Arg\{C(t)\}$ – real instantaneous amplitude and phase. They completely describe ChW behaviour, but in a different way from the spectrum in Fig. 1, right. The real envelope $E(t)$ and phase $\theta(t)$ of the excitation at Chandler frequency

$$\chi(t) = E(t)\exp\{i\theta(t)t\}\exp\{i\omega_c t\} \tag{3}$$

can be related to $A(t), \phi(t)$ through the expression

$$E(t)\frac{\exp\{i\theta(t)t\}}{\exp\{i\phi(t)t\}} = \frac{i}{\sigma_c}\left(\frac{dA(t)}{dt} + i\frac{d\phi(t)}{dt}A(t)\right) + \left(1 - \frac{\omega_c}{\sigma_c}\right)A(t), \tag{4}$$

obtained by substitution of representations (2), (3) into (1). For example, if $A(t) = \sin(2\pi t/T_{mod})$, where T_{mod} is the period of ChW modulation, let's say 40 years, the main term of excitation amplitude $E(t)$ would be proportional to $|\dot{A}(t)| = |\cos(2\pi t/T_{mod})|$ i.e. it would have period of 20 years.

We modelled the ChW envelope $A(t)$ from Fig. 1, obtained by Panteleev's filter, using non-linear least squares method (NLSM). The estimates for the mean and two harmonics are given in Table 1. Using this simple model of envelope we made a prediction until 2045, shown in Fig. 2, left, whereby the ChW amplitude reaches its minimum now (2015) and will start to increase soon.

	Period, years	Amplitude, mas	Phase (for epoch 1880), deg
80-year component	83.44	42.6	40.8
40-year component	42.0	54.6	−101.5
mean	–	134.8	–

Table 1: The components of ChW envelope, obtained by NLSM.

The phase of ChW $\phi(t)$ is shown in Fig. 2, right. It has a jump by π in 1930s. It was also modelled and predicted, but the phase prediction is much more uncertain than the amplitude's one. It is possible that the next phase jump will accompany the present-day ChW amplitude decrease.

We reconstructed the Chandler excitation by the corrective filtering method, presented in (Zotov, Bizouard, 2012). Its envelope $E(t)$ was compared to those one, reconstructed using eq. (4) from $C(t)$. It is very important to include ChW phase $\phi(t)$ information into this reconstruction. The results presented in Fig. 3 for both methods completely match each other.

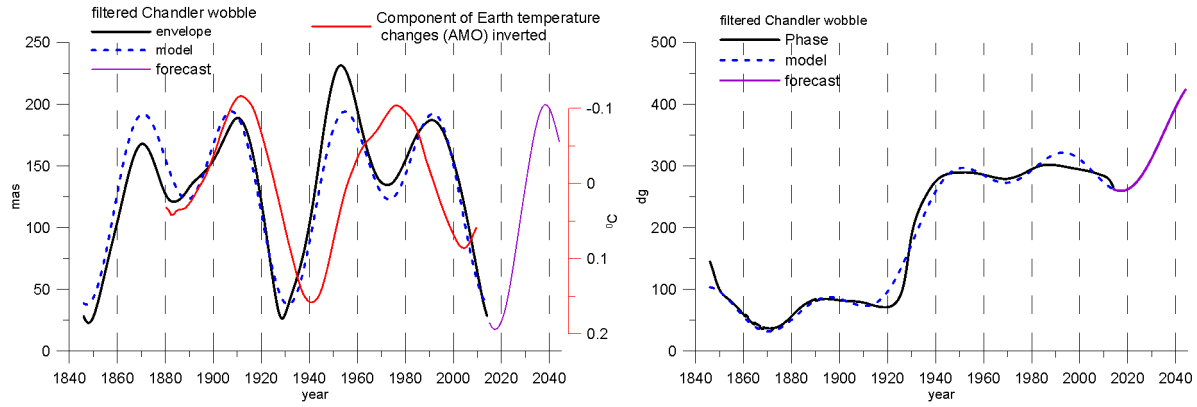

Figure 2: ChW envelope $A(t)$ (left) and phase $\phi(t)$ (right), their models, and forecasts, compared to the Earth temperature changes component.

3. DISCUSSION AND CONCLUSION

We modelled ChW amplitude and phase by a very simple harmonic model and predicted them for thirty years in the future. Our epoch is probably the one of the ChW amplitude minimum, as predicted by (Nastula et al., 1993), and reminiscent the minimum observed in 1930s. The complex ChW envelope $C(t)$ completely describes its amplitude and phase changes and is an alternative for the spectrum representation, given in Fig. 1, right. The equation (4) allows to obtain Chandler excitation envelope $E(t)$, given ChW's one $C(t)$.

In (Zotov, Bizouard, 2012) it was proposed, that 20-years modulation of ChW excitation could be caused by the Moon orbital precession. We prove this modulation of the envelope using eq. (4), Fig. 3.

In (Zotov, 2013) it was shown, that Earth climate, in particular global mean temperature GMT and global mean sea level GMSL have similar 20-years oscillations. In addition, the first principal component

extracted from GMT by means of multichannel SSA, also shown in Fig. 2, has ∼60-year period with maxima in 1880, 1940, and 2000s, coinciding with the minima of the Chandler wobble amplitude.

While the Chandler wobble is mostly produced by the hydro-atmospheric excitations, it has some non-random, periodic changes in amplitude and phase. In particular, ChW have minima in 1840s, 1930s, and 2010s, what is very similar to temperature changes on Earth usually attributed to the Multidecadal Atlantic Oscillation (MAO). If ChW amplitude changes could be related to the changes of Earth's climate characteristics, then such events, as Hiatus, pause of Global warming observed in 2000s, and present-day absence of El Nino/La Nina could be potentially predicted based on the Earth rotation.

Another possible explanation of ChW variations could be that its main excitation acts not exactly at the frequency f_c, but at one of the near-by frequencies $f_c \pm 1/T_{mod}$, providing ChW modulation with period T_{mod}. The phase jump by π (Fig. 2, right) could be related to the excitation frequency migration from one side of f_c to another. But this is a subject of another study.

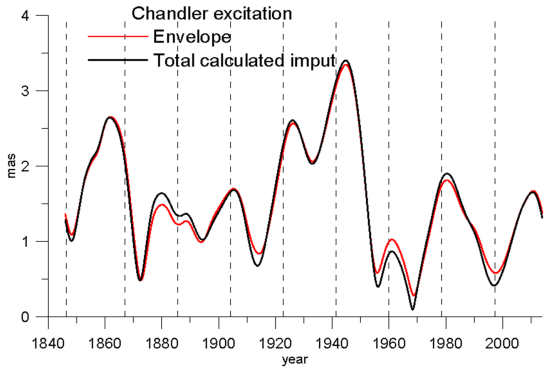

Figure 3: Comparison of ChW geodetic excitation derived in (Zotov, Bizouard, 2012) and through the equation (4).

Acknowledgements. First author is indebted to Paris Observatory for supporting this work (2 month position). This work is also supported by the RFBI grants N 12-02-31184, and N 15-05-02340.

4. REFERENCES

Brzeziński, A., Dobslaw, H., et al., 2012, "Geophysical Excitation of the Chandler Wobble Revisited", In: IAG Symposia, 136, pp. 499–505.

Chao, B.F. Chung, W.-Y., 2012, "Amplitude and phase variations of Earth's Chandler wobble under continual excitation", J. of Geodynamics, 62, pp. 35–39.

Gross, R., 2000, "The excitation of the Chandler wobble", Geophys. Res. Lett., 27(15), pp. 2329-2332.

Guo, J.Y., Greiner-Mai, H., et al., 2005, "On the double-peak spectrum of the Chandler wobble", J. of Geodesy, 78(11-12), pp. 654–659.

Liu, L., Hsu, H., Grafarend, E.W., 2007, "Normal Morlet wavelet transform and its application to the Earth's polar motion", J. Geophys. Res., 112, B08401.

Lambeck, K., 1980, "The Earth's Variable Rotation: Geophysical Causes and Consequences", Cambridge Univ. Press.

Munk, W., MacDonald, G., 1960, "The rotation of the Earth", Cambridge Univ. Press.

Nastula, J., Korsun, A., et al., 1993, "Variations of the Chandler and annual wobbles of polar motion in 1846–1988 and their prediction", Manuscripta Geodaetica, 18, pp. 131–135.

Sidorenkov, N.S., 2009, "The Interaction Between Earth's Rotation and Geophysical Processes", Wiley-VCH Verlag, Weinheim.

Vicente, R.O., Wilson, C.R., 1997, "On the variability of the Chandler frequency", J. Geophys. Res., 102(B9), pp. 20439–20445.

Zotov, L.V., 2013, "Sea Level And Global Earth Temperature Changes have common oscillations", Odessa Astronomical Publications, 26(2), pp. 289–291.

Zotov, L.V., Bizouard, C., 2012, "On modulations of the Chandler wobble excitation", J. of Geodynamics, 62, pp. 30–34.

OPERATIVE EOP ACTIVITIES IN VNIIFTRI

S.L. PASYNOK, I.V. BEZMENOV, M.B. KAUFMAN
National Research Institute for Physical-Technical and Radio Engineering Measurements
141570, VNIIFTRI, Mendeleevo, Moscow Reg., RUSSIA
e-mail: pasynok@vniiftri.ru, bezmenov@vniiftri.ru

ABSTRACT. VNIIFTRI as the Russian Main Metrological Center of Time, Frequencies and Earth Rotation Service carried out the EOP activities for many years. The brief information about these activities is presented.

1. INTRODUCTION

VNIIFTRI as the Russian Main Metrological Center of Time, Frequencies and Earth Rotation Service carried out the rapid EOP processing based on GNSS, VLBI and SLR observations for many years.

VNIIFTRI takes participation in GNSS and SLR observations of IGS and ILRS too.

The EOP activities at VNIIFTRI can be grouped in four basic topics:
1) Processing GNSS, SLR and VLBI observation data for EOP evaluation;
2) Combination of EOP series for evaluation of reference EOP values;
3) Combination of GLONASS satellites orbit/clock;
4) Providing GNSS and SLR observations at five metrological sites acting under the auspices of Federal Agency on Technical Regulating of Metrology(ROSSTANDART).

The processing of GNSS, SLR and VLBI observations is currently executed with the help of modern application program packages such as BERNESE GPS software (Dach et al., 2006; Dach & Walser, 2014), OCCAM software (Titov et al., 2006) and VieVS software (Boehm et al., 2009) that were properly adapted to the rapid service mode.

Combining daily EOP are calculated in Russian Main Metrological Center by means the combination of the eight independent individual EOP series provided by four Russian analysis centers.

The orbit/clock combination is carried out by means of the software which has been recently developed in VNIIFTRI.

GNSS observations on the five metrological sites are carried out permanently and hourly files are formed. The results of observations are collected in Russian Main Metrological Center in hourly mode. SLR observations are carried out at Mendeleevo and Irkutsk.

More detailed information one can find in the following sections.

2. GNSS, SLR AND VLBI DATA PROCESSING FOR EOP EVALUATION

Processing of measurements by phase GPS in VNIIFTRI has been started in 1999. Today EOP from GPS are obtained by processing of measurements on a Russian network, which includes approximately 35 GNSS receivers of the various organizations and departments(RSA , RAS, ROSSTANDART and others). Processing is carried out with the help of a program package BERNESE 5.0 (IAUB).

The actual algorithm was entered in 2006 (see Kaufman & Pasynok (2010)). It is based on the so-called method of Precise Point Positioning (PPP).

From 2004 EOP evaluations from VLBI technique are carried out with the help of software package OCCAM, specially adapted to the rapid service mode. In 2011 we began to process of new series of VLBI data using VieVS software developed at the Institute of Geodesy and Geophysics (IGG), Vienna University of Technology. According to requirements of rapid calculations (quick automatic processing without participation of operator), the special control program was written by Kaufman and Pasynok. No changes were made in VieVS blocks when developing the control program. Its task is receiving, processing and sending data without manual interaction. The details can be found in Kaufman & Pasynok (2012). Now VLBI observations are processed in VNIIFTRI with the help of OCCAM and VieVS packages.

Using of SLR observations of the Lageos-1 and Lageos-2 has been started in 1995. Processing was carried out with the help of a program package ITALAS (IAA). But the facilities and ideas which were realized in this program many years ago are not allowed to evaluate EOP with accuracy what is required now. So, using of this program for EOP evaluation in VNIIFTRI were stopped.

The preparation for renewal of regular operative calculations of EOP based on results of SLR measurements is conducted. As a base software product the BERNESE 5.2 is chosen. The additional blocks considering features of laser observations and program are developed by E. Tsyba and M. Kaufman and one can find the details in Tsyba & Kaufman (2015).

3. OPERATIVE AND RAPID COMBINATION OF EOP SERIES

Rapid combination of EOP for evaluation of reference EOP values has been started in VNIIFTRI at 1955. The form of bulletins and processing methods were changing in process of development of new methods of measurements and improvement of technics. D.Yu. Belocerkovskii and M.B. Kaufman were that scientists who were leading this work in VNIIFTRI.

Now the eight independent series are used for EOP combination (see Table 1). The method of combination which was developed and implemented by M. Kaufman in 2006 is used.

	Analysis centers of Russian EOPPC	Observation technics	Values
1	MMC NSTF (VNIIFTRI)	GPS	$X, Y, UT1$
2	MMC NSTF (VNIIFTRI)	VLBI	$X, Y, UT1, d\psi, d\varepsilon$
3	IAA RAS	SLR	$X, Y, UT1$
4	IAA RAS	GPS	$X, Y, UT1$
5	IAA RAS	VLBI	$X, Y, UT1, d\psi, d\varepsilon$
6	SVOEVP (from 1.07.13)	GPS/GLONASS	$X, Y, UT1$
7	MCC RSA	SLR	X, Y
8	IAC RSA	GPS	X, Y

Table 1: Separate series which are used for combination in 2013.

The $UT1 - UTC$ values of separate series which are used for combination are shown on Fig. 1.

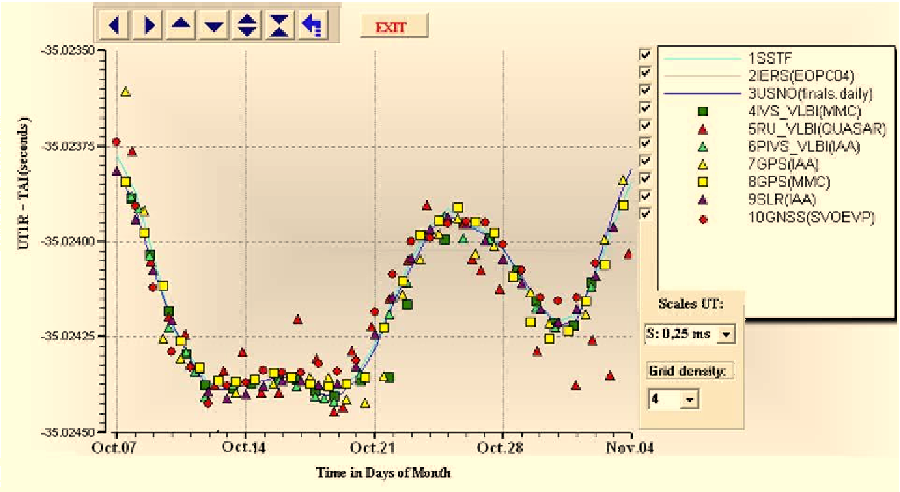

Figure 1: $UT1 - UTC$ values of separate series which are used for combination.

The basic stages of the method of combination processing according to Kaufman & Pasynok (2010) are:

— excluding of systematical errors;

— evaluation of average values EOP;

— prediction;
— estimation of accuracy;
— generation of bulletins with the target data.

The average of smoothed MMC series number 1 and 2 are used as a basis of Russian EOP system. For other series the regular amendments are estimated by exponential smoothing of EOP deviations of every series from basis values. After taking these amendments into account the averages of EOP values are formed using the weights which are calculated according to accuracy estimation for previous calendar year.

Calculations are conducted by three cycles:

— operative (ultra-rapid) values for the last day and predictions for the following of 30 days are evaluated every day;

— every Thursday saved measurements for the last calendar week are processed, the systematic errors of independent individual series are recalculated and the rapid values are evaluated;

— five weeks after end of the calendar month all saved measurements are processed and final values are evaluated.

Such mode of calculations allows quickly, though with limited accuracy to provide the current EOP values and prediction, and then to refine them as far as new observation data become avialable. So, during calculation of operative and rapid EOP values only the limited set of the observations is used. In particular, VLBI data are not used for calculation of operative EOP values, since results of their measurements are accessible with a delay of few days.

The RMS values for estimation based on internal convergence are counted up under the formula:

$$m_C = \left(\frac{\sum_j p_j \nu_j^2}{\sum p_j} \right)$$

where:

j is the numbers of individual EOP series listed in Table 1;

ν_j is deviations of individual daily EOP values from combined one;

p_j is the weights of individual EOP values.

Operative bulletin Q is issued daily at 6h UTC. It contains the values EOP for last day and the prediction data for next 30 days.

The bulletins are accessible only in electronic form ($ftp.vniiftri.ru/Out\_data/Bul\_rus\_Q/$).

Rapid Bulletin A is issued every Thursday. It contains daily values EOP(RU) for the last calendar week and the forecast for 7 next weeks. One release within each month contains finals values EOP(RU) in addition.

Bulletins A are accessible in electronic form ($ftp.vniiftri.ru/Out\_data/Bul\_rus\_A/$) and in printed one (disseminated on requests mark@imvp.ru).

4. COMBINATION OF GLONASS SATELLITES ORBIT/CLOCK

An algorithm and a program for GLONASS satellites orbits combination were developed. The calculations by this program as well as calculations of the coordinate differences for GNSS antennas in VNIIFTRI (Mendeleevo, Moscow reg.) and the North-Eastern branch of VNIIFTRI (Irkutsk) using different orbits and clock corrections are provided. Some theoretical estimates for RMS in satellites coordinate reference values determination were derived. It is shown that under condition when RMSs in satellite coordinates estimation provided by separate Analytic Centers during a long time interval are commensurable the RMS of reference values is no greater than RMS of satellite coordinates estimated by any of the Analytic Centers. The main program window is shown on Fig. 2.

The details one can be find in paper Bezmenov and Pasynok (2015).

5. PROVIDING OF THE GNSS AND SLR OBSERVATIONS AT THE ROSSTANDART SITES

The providing GNSS and SLR observations at five metrological sites acts under the auspices of Federal Agency on Technical Regulating of Metrology(ROSSTANDART). These sites are situated in VNIIFTRI (Mendeleevo, Moscow reg.) and its branches: North-Eastern (Irkutsk), Far Eastern (Khabarovsk) and

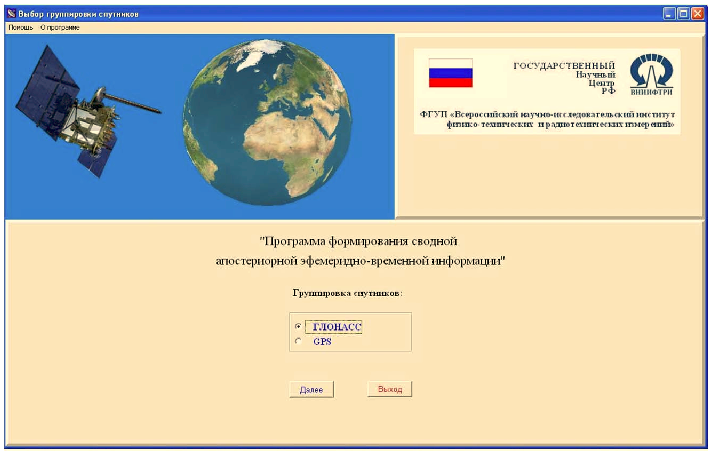

Figure 2: The main window of GLONASS satellites orbit\clock combination program.

Kamchatskii (Petropavlovsk-Kamchstskii). One site is situated in SNIIM (Novosibirsk). The SLR equipment had only 2 sites: Mendeleevo and Irkutsk.

The results of GNSS observations are accumulated in VNIIFTRI in hourly mode and are used for rapid EOP evaluation.

The direct results of SLR observations are transferred into IAC RSA and further in ILRS. Details can be found in Ignatenko et al.(2012) and Ignatenko & Zhestkov (2012).

6. CONCLUSIONS

The main directions of EOP activities in VNIIFTRI as the Russian Main Metrological Center of Time, Frequencies and Earth Rotation Service are presented. More information one can find by anonymous access on addresses ftp.vniiftri.ru and www.vniiftri.ru.

7. REFERENCES

Bezmenov, I., Pasynok, S., 2015, "GLONASS orbit/clock combination in VNIIFTRI", this volume, pp. 215–216.

Boehm, J., Spicakova, H., Plank L., Teke, K., Pany, A., Wresnik, J., Englich, S., Nilsson, T., Schuh, H., Hobiger, T., Ichikawa, R., Koyama, Y., Gotoh, T., Kubooka, T., Otsubo, T., 2009, "Plans for the Vienna VLBI Software VieVS", Proc. 19th European VLBI for Geodesy and Astrometry Working Meeting, 24–25 March 2009, Bordeaux, G. Bourda, P. Charlot, A. Collioud (eds.), pp. 161–164.

Dach, R., Hugentobler, U., Fridez, P., Meindl, M. (eds.), 2006, Bernese GPS Software. Version 5.0.

Dach, R., Walser, P., 2014, "Bernese GNSS Software Version 5.2. Tutorial. Processing Example. Introductory Course. Terminal Session", September 2014.

Ignatenko, I, Palchikov, V., Zhestkov, A., 2012, "New generation of the SLR station Mendeleevo", Mitteilungen des Bundesamtes fuer Kartographie und Geodaesie, 48, pp. 363–365.

Ignatenko, I.Yu., Zhestkov, A.G., 2012, "Metrological support of SLR measurements", WLPTN2012 Conference
`http://www.ipa.nw.ru/conference/wpltn2012/docs/25/1300%20ignatenko.pdf`.

Kaufman, M., Pasynok, S., 2010, "Russian state time and Earth rotation service: observation, EOP series, prediction", Artificial Satellites, 45(2), pp. 81–86.

Kaufman, M., Pasynok, S., 2012, "Rapid EOP calculations using VieVS software", In: Proc. Journées 2011 "Earth rotation, reference systems,and celestial mechanics: Synergies of geodesy and astronomy", 19–21 September 2011, Vienna, Austria, pp. 129–131.

Titov, O., Tesmer, V., Boehm, J., 2006, "OCCAM 6.2. User's guide".

Tsyba, E., Kaufman, M., 2015, "Improvement of the software BERNESE for calculation of the Earth rotation parameters from satellite laser ranging observations of Lageos 1 and Lageos 2 in the Main Metrological Center of the State Time and Frequency Service", this volume, pp. 235–236.

DO WE NEED VARIOUS ASSUMPTIONS TO GET A GOOD FCN?

C.L. HUANG, M. ZHANG
Key Laboratory of Planetary Sciences, Shanghai Astronomical Observatory, CAS
80 Nandan Road, Shanghai 200030, China
e-mail: clhuang@shao.ac.cn

ABSTRACT. Free core nutation (FCN) is a rotational modes of the Earth with fluid core. All traditional theoretical methods produce FCN period near 460 sidereal days with PREM Earth model, while precise observations (VLBI + SG tides) say it is approximately 430 days. In order to fill this big gap, astronomers and geophysicists give various assumptions, e.g., increasing core-mantle-boundary (CMB) flattening by about 5%, a strong coupling between nutation and geomagnetic field near CMB, viscous coupling, or topographical coupling cross CMB, etc. Do we really need these unproved assumptions? or is it only the problem of these traditional theoretical methods themselves? Earth models (e.g., PREM) provide accurate and robust profiles of physical parameters, like density and Lame parameters, but their radial derivatives, which are also used in all traditional methods to calculate normal modes (e.g., FCN), nutation and tides of non-rigid Earth theoretically, are not so trustable as the parameters themselves. Moreover, the truncation of the expansion series of displacement vector and stress tensor in traditional methods is also of question. A new stratified spectral method is proposed and applied to the computation of normal modes, to avoid these problems. Our primary result of the FCN period is 435 ± 3 sidereal days.

1. KEY QUESTION TO THE STUDY OF FCN

Free core nutation (FCN) is a rotational mode of the Earth with fluid outer core (FOC), as the rotating axes of the FOC and that of the mantle do not coincide. The period of FCN reflects and depends on the physical parameters and dynamics of the FOC, mantle and especially that near core-mantle-boundary (CMB). Moreover, FCN influences strongly the retrograde annual (–1yr.) nutation due to their resonance. Therefore, FCN is key parameter in the study of the Earth rotation and the physics of the Earth interior.

Almost all calculated FCN periods from traditional theoretical approaches are near 460 days (e.g., Dehant & Defraigne, 1997; Huang et al., 2001; Rogister, 2001; Mathews et al., 2002; Crossley & Rochester, 2014) with a one-dimensional Earth model like PREM (Dziewonski & Anderson, 1981), while modern precise observations from VLBI and superconductivity tidal gravimetry produce FCN period near 430 days with precision of less than one day (e.g., Malkin, 2007; Cui et al., 2014). Their difference of approximate 30 days is significant large comparing with the observation precision. Although some studies discover that the FCN period may vary in the past three decades, its variation is still less than 3 days and much smaller than the 30 days gap.

In order to fill this big gap, astronomers and geophysicists give various assumptions. The earliest and easiest assumption is to increase the flattening of core-mantle-boundary (CMB) by about 5% (see e.g., Newburg et al., 1990; Huang, 1999) from that calculated from hydro-static-equilibrium Earth by Clairaut equation and PREM Earth model, i.e., increasing the difference between the polar radii and the equatorial radii by about 500 meters.

Another mechanism proposes a strong coupling between nutation and geomagnetic field near CMB. In the original work of Rochester & Smylie (1965), the equatorial components of the electromagnetic torque act on the mantle is calculated rigorously and the electromagnetic damping of the Chandler wobble is first quantitatively investigated, and it is shown that the electromagnetic core-mantle coupling fails by several orders of magnitude either to generate or to damp the Chandler wobble. Following the same way of this work, Buffett et al. (2002) discuss the effect of this coupling on nutation and FCN and show that this coupling can explain the gap of FCN period. However, Huang et al. (2011) argue that, even using the same values of the electro-magnetic parameters near CMB as used by Buffett et al. (2002), the contribution of this coupling to FCN period is one order of magnitude smaller than required.

There are also some other assumptions proposed to interpret this big gap of FCN period. They are viscous coupling (e.g., Mathews & Guo, 2005; Buffett, 2010, and topographical coupling (Wu & Wahr,

1997; Dehant et al., 2014), etc.

Do we really need these unproved assumptions? or is it only the problem of these traditional theoretical methods themselves? We propose an independent approach here to study FCN and show that we do not need these assumptions and our primary result of FCN period is 435 ± 3 sidereal days, very close to the observation.

2. THEORETICAL APPROACH

As usual, we start from the dynamic equation for infinitesimal elastic-gravitational motion for a rotating, slightly elliptical Earth is given as, in a steadily rotating reference frame with constant speed Ω_0, (Smith, 1974; or Dahlen & Tromp (1998) for more information):

$$\rho D_t^2 \mathbf{s} + 2\rho \mathbf{\Omega_0} \times D_t \mathbf{s} = -\rho \mathbf{\Omega_0} \times (\mathbf{\Omega_0} \times \mathbf{s}) + \nabla \cdot \mathbf{T}^e - \nabla(\gamma \nabla \cdot \mathbf{s}) - \rho \nabla \phi_1 - \rho \mathbf{s} \cdot \nabla \nabla \phi + \nabla \cdot [\gamma (\nabla \mathbf{s})^T], \quad (1)$$

where γ is the equilibrium pressure, and ϕ_1 is the incremental gravitational potential induced by the mass redistribution due to deformation. The stress tensor $\mathbf{T}^e$ is the incremental stress with respect to the reference stress, $\mathbf{T}^{ref.} = -\gamma \mathbf{I}$ where $\mathbf{I}$ is the identity tensor, and is related to the displacement field by two Lamé parameters (λ, μ) for an isotropic medium as

$$\mathbf{T}^e = \lambda(\nabla \cdot \mathbf{s})\mathbf{I} + \mu[\nabla \mathbf{s} + (\nabla \mathbf{s})^T] \quad (2)$$

where rigidity $\mu = 0$ in a liquid part of the Earth.

There is not magnetic field (or Lorentz torque) nor viscosity involved here. The boundary conditions cross various kinds of boundaries are the same as usual (Smith, 1974; or Huang, 2001; for more information) and not presented here.

In order to solve these sets of equations, one can use direct numerical integration approach or other approaches. We propose here another new stratified spectral method (SSM), as well as a linear operator method (LOM) instead of generalized spherical harmonics (GSH).

The main idea of this SSM is to divide the Earth model into several subdomains (for example, solid inner core, fluid outer core and mantle) and to apply spectral method (Galerkin method or collocation method) on each subdomain. We will discuss and one-dimension example to show this method.

Global spectral method uses a single representation of an unknown function $u(x)$ through out the whole domain via a truncated series expansion, for instance,

$$u(x) \approx u_N(x) = \sum_{n=0}^{N} c_n \phi_n(x), \quad (3)$$

where $\phi_n(x)$ are the basis functions and c_n are their coefficients. This series is then submitted into a differential (or integral) equation like Eq. (1) which is abbreviated as

$$L[\sum_{n=0}^{N} c_n \phi_n(x)] = d \quad (4)$$

L is a linear operator. This equation can be solved by Galerkin method, collocation method or other spectral method.

Using Galerkin method the above equation turns into a group equations

$$\int_V \psi_j(x) L[\sum_{n=0}^{N} c_n \phi_n(x)] dx = d \quad (5)$$

where $\psi_j(x)$ is the trial functions. For a complex Earth model, a global domain resolves into K subdomains. In the $k^{th.}$ subdomain, the unkown function $u^{(k)}(x)$ is

$$u^{(k)}(x) \approx \sum_{n=0}^{N} c_n^{(k)} \phi_n^{(k)}(x), \quad (6)$$

where $\phi_n^{(k)}(x)$ are the basis functions of the $k^{th\cdot}$ subdomain and $c_n^{(k)}$ are their coefficients. We us polynomial functions of radii (r) as the basis functions, i.e. $r^1, r^2, r^3, ..., r^n$. So Eq. (5) turns into K groups of equations:

$$\int_{V^{(k)}} \psi_j^{(k)}(x) L^{(k)} [\sum_{n=0}^{N} c_n^{(k)} \phi_n^{(k)}(x)] dx = d^{(k)} \tag{7}$$

where $\psi_j^{(k)}(x)$ are the trial functions in the $k^{th\cdot}$ subdomain, and $L^{(k)}$ is its corresponding linear operator. Eq. (7) will create a $K(N+1) \times K(N+1)$ matrix. Suppose that there are M boundary conditions:

$$B_i [\sum_{k=1}^{K} u^{(k)}(x)] = 0, \quad i = 1 \cdots M \tag{8}$$

We use Tau method to combine these boundary conditions with Eq. (7). The detail process of this SSM and Tau method will be presented in another paper.

3. EARTH MODEL AND ELLIPTICITY PROFILE

We adopt PREM as input Earth model. The Earth is divided by solid inner core (1 subdomain), fluid outer core (1 subdomain), and mantle (10 subdomains, including crust, but without ocean). The Earth is treated as hydro-static equilibrium. The ellipticity (ϵ) profile interior is derived from Clairaut equation with precision of $o(\epsilon^1)$ and plotted in Fig. 1, which is identical as what was used in Huang et al. (2001). The ellipticity of CMB ($r = 3480km$) is $\epsilon_{cmb} = 0.00254656$.

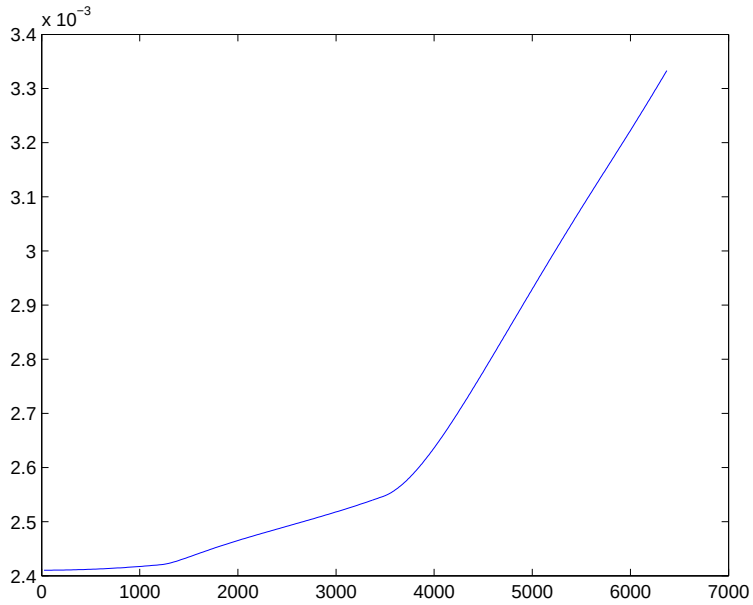

Figure 1: Ellipticity profile of hydro-static equilibrium Earth. x-axis is radii in km.

4. PRIMARY RESULT OF FCN AND DISCUSSION

The displacement field is truncated in following chain $\mathbf{s} \approx \mathbf{T}_1^1 + \mathbf{S}_2^1 + \mathbf{T}_3^1$. The polynomial (basis) functions of radii is truncated at $N = 4$ and the result is well converged.

Our preliminary result of the FCN period is 435 ± 3 sidereal days without any unproved assumptions (e.g., increasing core-mantle-boundary (CMB) flattening by about 5%, a strong coupling between nutation and geomagnetic field near CMB, viscous coupling, or topographical coupling etc.). It is very close to the observed one (about 430 days).

The following question is: How can this SSM get better result of FCN than other approaches? or, what is the essential difference among these approaches? or is it only the problem of these traditional theoretical approaches themselves? Earth models (e.g., PREM) provide accurate and robust profiles of physical parameters, like density and Lame parameters, but their radial derivatives, which are also used in all traditional methods to calculate normal modes (e.g., FCN), nutation and tides of non-rigid Earth theoretically, are not so trustable as the parameters themselves.

As in this SSM approach, physical parameters (density and Lame parameters) from a given Earth model are needed as input, however, their radial derivatives (like $\partial_r \rho$) which are also used in all other traditional approaches are not needed in this SSM approach. A numerical experiment to test the influence of the uncertainty of Earth model on nutation has been made (Huang & Zhang, 2014) and show that the uncertainty in the radial derivatives of the material density near CMB ($\partial_r \rho_{cmb}$) do have large influence on the calculated result of FCN period, although this experiment investigated only the factor of $\partial_r \rho_{cmb}$, and in this numerical experiment, the change of $\partial_r \rho_{cmb}$ is somewhat arbitrary or even not consistent with PREM model. This experiment, at least, provides us a hint that the uncertainty of $\partial_r \rho_{cmb}$ in an input Earth model may be a problem. Unfortunately, PREM model does not give the information of its precision nor accuracy.

Moreover, the truncation of the expansion series of displacement vector and stress tensor in traditional methods is also of question. All these possibilities need to be further studied.

Acknowledgements. This work was supported by the National Natural Science Foundation of China (11373058/11073044/11133004) and Shanghai Key Laboratory of Space Navigation and Position Techniques.

5. REFERENCES

Buffett, B.A., Mathews, P.M., Herring, T.A., 2002, "Modeling of nutation and precession: Effects of electromagnetic coupling", J. Geophys. Res., 107(B4), 2070, doi:10.1029/2000JB000056.

Buffett, B.A., 2010, "Tidal dissipation and the strength of the Earth's internal magnetic field", Nature, 468, pp. 952–955, doi:10.1038/nature09643.

Crossley, D.J., Rochester, M.G., 2014, "A new description of Earth's wobble modes using Clairaut coordinates 2: Results and inferences on the core mode spectrum", Geophys. J. Int., 198, pp. 1890–1905.

Cui, X.M., Sun, H.P, Xu, J.Q., Zhou, J.C., Zhou, H.W., 2014, "Temporal variation of the period of free core nutation from VLBI and superconducting gravity data", Chinese J. Geophys., 57(2), pp. 384–391. (in Chinese)

Dahlen, F.A., Tromp, J., 1998, "Theoretical global seismology", Princeton University Press, Princeton, New Jewsey.

Dehant, V., Defraigne, P., 1997, "New transfer functions formulations of a non-rigid Earth", J. Geophys. Res., 102, pp. 27659–27688.

Dehant, V., Puica, M., Folgueira, M., Trinh, A., Van Hoolst, T., 2014, "Topographic Coupling at Core-Mantle Boundary in Rotation and Orientation Changes of the Earth", AGU Fall Meeting 2014, San Francisco, USA, G13A-0527.

Dziewonski, A.M., Anderson, D.L., 1981, "Preliminary reference Earth model", Physics of the Earth and Planetary Interiors, pp. 297–356.

Huang, C.L., 1999, "A study of the non-rigid Earth nutation with ocean and atmosphere in second order of ellpticity", PhD. dissertation, Shanghai Astronomical Observatory, China.

Huang, C.L., 2001, "The scalar boundary conditions for the motion of the elastic Earth to second order in ellipticity", Earth, Moon, and Planets, 84(3), pp. 125–141.

Huang, C.L., Jin, W.J., Liao, X.H., 2001, "A new nutation model of a non-rigid Earth with ocean and atmosphere", Geophys. J. Int., 146, pp. 126–133.

Huang, C.L., Dehant, V., Liao, X.H., Van Hoolst, T., Rochester, M.G., 2011, "On the coupling between magnetic field and nutation in a numerical integration approach", J. Geophys. Res., 116, B03403, doi:10.1029/2010JB007713.

Huang, C.L., Zhang, M., 2014, "A numerical experiment to test the influence of the uncertainty of Earth model on nutation", AGU Fall Meeting 2014, San Francisco, USA, G13A-0517.

Malkin, Z.M., 2007, "Empiric models of the Earth's free core nutation", Solar System Research, 41(6), pp. 492–497.

Mathews, P.M., Guo, J.Y., 2005, "Viscoelectromagnetic coupling in precession-nutation theory". J. Geophys. Res., 110, B02402, DOI: 10.1029/2003JB002915.

Neuberg, J., Hinderer, J., Ziirn, W., 1990, "On the complex eigenfrequency of the "nearly diurnal free wobble" and its geophysical interpretation", In: Variations in Earth Rotation, Geophys. Monogr. Ser., vol. 59, D.D. McCarthy and W.E. Carter (eds.), Am. Geophys. Un., Washington, DC., pp. 11–16.

Rochester, M.G., Smylie, D.E., 1965, "Geomagnetic core-mantle coupling and the Chandler wobble", Geophys. J. R. Astr. Soc., 10, pp. 289–315.

Rogister, Y., 2001, "On the diurnal and nearly diurnal free modes of the Earth", Geophys. J. Int., 144, pp. 459–470.

Smith M.L., 1974, "The scalar equations of infinitesimal elastic-gravitational motion for a rotating, slightly elliptical Earth", Geophys. J. R. Astr. Soc., 37, pp. 491–526.

Wu, X.P., Wahr, J., 1997, "Effects of non-hydrostatic core-mantle boundary topography and core dynamics on Earth rotation", Geophys. J. Int., 128, pp. 18–42.

DEFORMATION OF THE SOUTH-EASTERN BALTIC SHIELD FROM GNSS OBSERVATIONS

V.L. GORSHKOV[1], S.D. PETROV[2], N.V. SHCHERBAKOVA[1], S.S. SMIRNOV[1,2], A.V. MOHNATKIN[1,2], D.A. TROFIMOV[2], T.V. GUSEVA[3], V.P. PEREDERIN[3], N.K. ROSENBERG[3]
[1] Pulkovo Observatory
196140 St. Petersburg, Russia
[2] St. Petersburg State University
199034 St. Petersburg, Russia
[3] Schmidt Institute of Physics of the Earth of the Russian Academy of Sciences
123995 Moscow, Russia
e-mail: vigor@gao.spb.ru

ABSTRACT. The Pulkovo observatory is situated in a unique geological setting. Within only 300 kilometres from Northern Karelian Isthmus to a few kilometres south from the observatory the Archean, Paleo and Neoproterozoic, Cambrian, Ordovician, Devonian, and Carboniferous rocks are sequentially surfacing. Thus these 300 kilometres in distance correspond to 3 billion years in geologic time. The city of St. Petersburg marks a transition zone from the Baltic Shield to the East European Platform, and the observatory is built on the Baltic Klint that in turn marks a transition from Ediacaran to Devonian. Such a rich geological constitution of the region summons a need for geodynamical studies. The authors have recently gathered the GNSS observations available in the region from 1993 until present, including those made by the authors, with permanent and high quality field GNSS stations. These measurements were processed with the GIPSY software using the PPP strategy. The resulting coordinates were then adjusted for atmospheric loading corrections, and station velocities were computed. The station velocities were then used for estimation of the regional deformation field. The resulting deformation field shows a weak meridional compression and possibly a slow counterclockwise rotation of the Baltic shield with respect to the East European platform.

1. INTRODUCTION

Both the Baltic shield and the East European platform are traditionally considered as parts of one rigid Eurasian plate. Both are cratons or blocks of the ancient continental lithosphere but if the East European platform is covered by a thick layer of sedimentary rocks, the Baltic shield mostly consists of the Archean or Proterozoic rocks of igneous origin. The transition region between the two landmasses had been until recently considered seismically quiet. An interest to the region from geodynamical point of view was recently motivated by the 2004 Kaliningrad earthquake (Assinovskaya et al., 2011). The Baltic shield is also subject to the ongoing glacial isostatic adjustment (GIA). There were a few GNSS campaigns conducted in the region for the GIA investigations which concerned vertical lithospheric motions (Kierulf et al., 2014). The present study concentrates on possible horizontal movements of the regional GNSS stations. This work is a continuation of a previous study by Gorshkov et al. (2012) that did reveal a possible horizontal motion of the Baltic shield with respect to the East European platform.

The transition zone between Baltic shield and East European platform is known as the Polkanov flexure zone (Svetov and Sviridenko, 1991). The recent geological studies also suggest that this flexure zone may be subject to a stress and hence exhibit deformations. A possible mechanism of these deformation may be a layer of sediments on the East European platform that creates a load to the south of the flexure zone in contrast with the sediment free Baltic shield to the north from the flexure zone. This spatially variable load may produce both vertical and horizontal crustal motions in the border region.

Recently, there is a growing number of permanent GNSS-stations being installed and run in the region by various organizations. A few field campaigns were conducted as well. Unfortunately, not all of the stations are installed in view of proper geodetic standards. Some of them are known to be mounted on the roofs of buildings or on the steel posts so that their achievable accuracies can be restricted.

Nevertheless, there are still a substantial number of stations properly mounted that can be analysed in view of computing their velocities and regional deformations. Thus, an attempt to gather all available regional GNSS measurements and to process them in a unique framework was endeavoured as described below.

2. DATA PROCESSING

A database of GNSS observations was gathered by the authors currently including RINEX files for 38 permanent and field stations for the period from 1993 till present. Four of the permanent GNSS stations as well as all field ones were run by the authors. The rest of the data were provided by the courtesy of other organizations.

All the measurements were processed by use of the GIPSY-OASIS 6.3 software within a unique framework by the Precise Point Positioning (PPP) technique. The solution was formed with absolute antennae calibrations, IGb08 orbit and clock corrections, VMF1GRID tropospheric corrections, IERS Earth orientation parameters and solid Earth tides, GOT4.8 ocean loads, GOT4.8ac geocenter mode, and IMLS atmospheric loading corrections. As a result of the analysis the geodetic latitudes and longitudes of the stations were estimated for each diurnal series of observations.

The resulting station coordinate time series were edited for outliers as well as for jumps due to stations maintenance, changes of antennae etc. Some of the field station coordinate time series were apparently too short in time to produce a reliable velocity estimates and were excluded from the analysis. The permanent stations in the vicinity of St. Petersburg have for the present short observational history (2–3 years). At last the observations of SUUR and TORE stations were used only after relocation of these stations in 2011 year because their previous data yield considerably different velocity vector.

As a next step, a linear trend (weighted for field stations) was fitted to each of the station coordinate time series and the station velocities were computed. The ITRF 2008 plate motion model (Altamimi et al., 2012) was subtracted from the computed station velocities. Thus, the horizontal velocities for 33 stations were obtained. These velocity vectors were then used to compute the deformations with an algorithm based on (Teza et al., 2008).

3. RESULTS AND DISCUSSION

The velocities for all stations used in the analysis are shown in Fig. 1. Figure 2 is a close up of the former showing the velocities of stations in the vicinity of St. Petersburg.

The borderline between the Baltic shield and the East European platform is known to lie along the southern shores of Gulf of Finland and Ladoga lake. The main feature of the residual velocity field is slightly different average directions of the station velocities to the north from that borderline (the northern stations) and those to the south (the southern stations). It can be seen from the Figure that the southern stations tend to move more to the south than the northern ones. In other words there exists a slight clockwise rotation of the East European platform with respect to the Baltic shield.

A few exceptions to this tendency can also be seen from Figs. 1 and 2. Stations SEST, VASO and GORN in the north-western St. Petersburg are slowly moving in direction totaly different from that of the majority of the stations. Possible reasons for that peculiar movement are unknown and need further study. Nevertheless, in spite of these few exceptions the relative motion is clearly seen from Figs. 1 and 2.

Figure 3 shows a regional deformation map. It can be seen from the Figure that deformations generally reflect the velocities. Thus, the direction change of the residual station motions along the flexure zone produces a contraction along that same zone up to three nanostrains per year. This contraction is directed from south-east to north-west. A small expansion can also be seen from the Figure in a perpendicular direction, that is from south-west to north-east.

All of the above suggests that the Polkanov flexure zone, or the transition region between the Baltic shield and the East European platform is clearly geodynamically active. One can also conjecture that there is a possible counterclockwise rotation of the Baltic shield with respect to the East European platform, but this needs further studies.

In order to verify the above relative motion conjecture the algorithm of Teze et al. (2008) of deformation estimation should be developed further to include the rotation effects. In other words, a new algorithm should estimate the regional deformations together with the angular velocity components of a specific region, say the Baltic shield. This will be a subject for a further study.

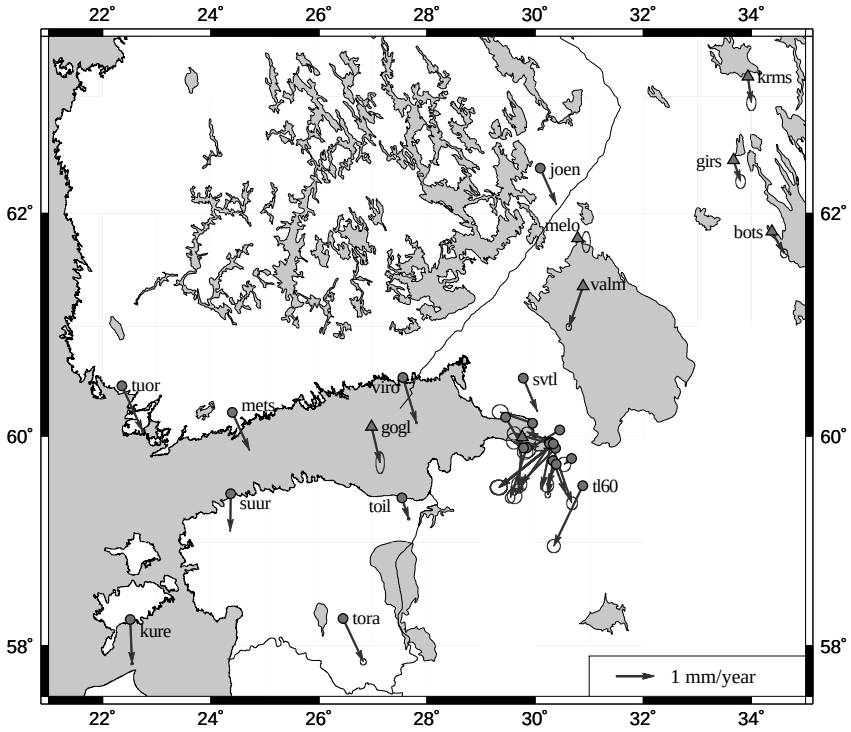

Figure 1: Residual horizontal station velocities. Permanent stations denoted with circles, field stations denoted with triangles, formal errors indicated with ellipses.

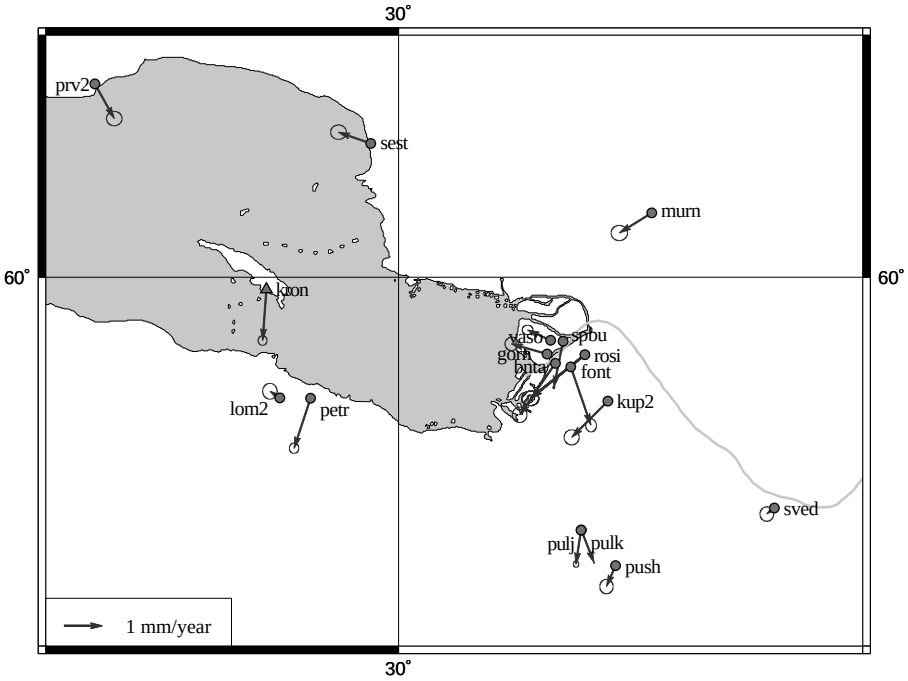

Figure 2: Residual horizontal station velocities, a close up. Permanent stations denoted with circles, field stations denoted with triangles, formal errors indicated with ellipses.

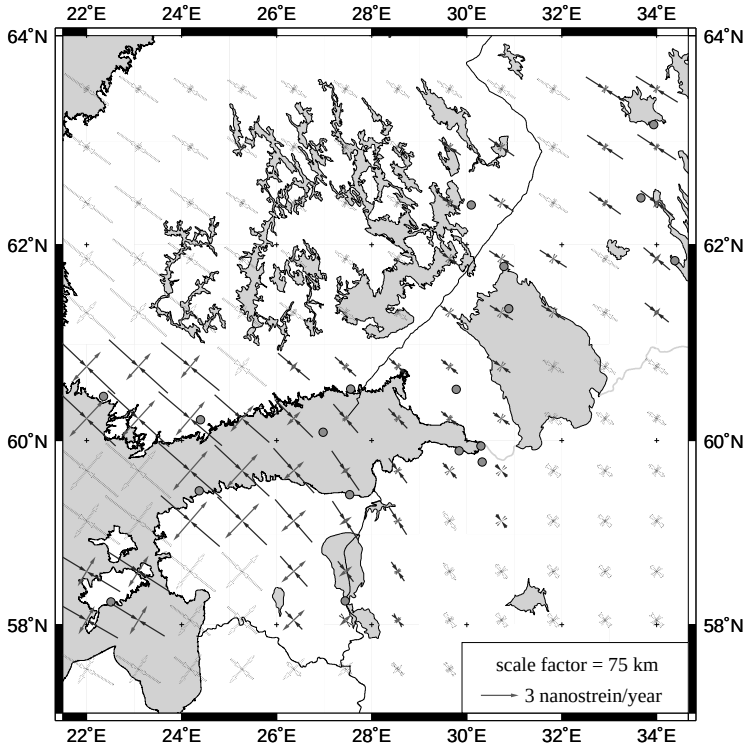

Figure 3: Horizontal deformations estimated from horizontal station velocities.

4. REFERENCES

Altamimi, Z. Métivier, L., Collileux, X., 2012, "ITRF2008 plate motion model", J. Geophys. Res., 117, B07402.

Assinovskaya, B., Shchukin, Ju., Gorshkov, V., Shcherbakova, N., 2011, "On recent geodynamics of the Eastern Baltic Sea region", Baltica, 24(2), pp. 61–70.

Gorshkov, V.L., Smirnov, S.S., Scherbakova, N.V., 2012, "Load effects in GNSS observations in regional geodynamical stadies", Vestnik SPbSU, Series 1, Issue 2, pp. 148–156. (in Russian)

Kierulf, H.P., Steffen, H., Simpson, M.J.R., Lidberg, M, Wu, P., Wang, H., 2014, "A GPS velocity field for Fennoscandia and a consistent comparison to glacial isostatic adjustment models", J. Geophys. Res., 119(8), pp. 6613–6629.

Svetov, A.P., Sviridenko, L.P., 1991, "Sutural zone magmatism of the Baltic Shield", Leningrad: Nauka. (in Russian)

Teza, G., Pesci, A., Galgaro, A., 2008, "Grid_strain and grid_strain3: Software packages for strain field computation in 2D and 3D environments", Computers & Geosciences, 34, pp. 1142–1153.

GLONASS ORBIT/CLOCK COMBINATION IN VNIIFTRI

I.V. BEZMENOV, S.L. PASYNOK
National Research Institute for Physical-Technical and Radio Engineering Measurements
141570, VNIIFTRI, Mendeleevo, Moscow Region, Russia
e-mail: bezmenov@vniiftri.ru, pasynok@vniiftri.ru

ABSTRACT. An algorithm and a program for GLONASS satellites orbit/clock combination based on daily precise orbits submitted by several Analytic Centers were developed. Some theoretical estimates for combine orbit positions RMS were derived. It was shown that under condition that RMS of satellite orbits provided by the Analytic Centers during a long time interval are commensurable the RMS of combine orbit positions is no greater than RMS of other satellite positions estimated by any of the Analytic Centers.

1. INTRODUCTION

An idea of the weighted average orbit/clock combination for GPS and GLONASS satellite constellations by mathematical processing of calculation results obtained by individual Analytic Centers goes back to Beutler et al. (1995) and Kouba et al. (1995). Since 1993 and to the present IGS issues Sp3-files with official values of coordinates and clock corrections of GPS satellites. Since 2004 up to now the combined orbits and clock corrections of GLONASS satellites are formed under the auspices of IGS by the Data-processing center of National administration of oceanic and atmospheric researches and National geodetic service of the USA (NOAA/NGS).
The purpose of this paper is to demonstrate our own activity in VNIIFTRI in orbit/clock combining and some theoretical results in this scope as well.

2. RESULTS

By now an algorithm and software were developed in VNIIFTRI for production of the combined orbits and clock corrections for GLONASS satellites. Main functions of the software are as follows:
∘ production of combined GLONASS orbits and clock corrections on base of data sets provided by individual Centers;
∘ outliers detection in satellite orbit/clock data sets as they determined by each Center and elimination if needed appropriate epochs for each satellite and for each Center from further combination process;
∘ the detection and elimination of "bad" satellites from combination process;
∘ application orbital dynamics with calculation of long arc (1, 3, 5, 7 days) orbits to obtain some statistical characteristics of combined orbits;
∘ producing report files of two types:
1) SP3-files with combined orbits and clock corrections for GLONASS satellites (daily);
2) Sum-files of reports for the 8th day period with transformation parameters, statistical, accuracy and orbital characteristics for each satellites and each Center (weekly).

Comparison results of GLONASS orbits defined by the Centers with the IGL combined orbits for the period from 2011.01.29 to 2011.02.05 are presented in Fig. 1.

Let us denote:
N_{Cent} – number of Centers, N_{Sat} – number of satellites, N_{Epo} – number of epochs in a day,
$\boldsymbol{x}^j_{i,k,n}$ – position of j-th satellite as it was estimated by i-th Center in k-th day at n-th epoch.
$\Delta\boldsymbol{x}^j_{i,k,n}$ – residual vector: $\Delta\boldsymbol{x}^j_{i,k,n} = \boldsymbol{x}^j_{exect,k,n} - \boldsymbol{x}^j_{i,k,n}$, where $\boldsymbol{x}^j_{exect,k,n}$ is the exact solution (unknown).
Then the main theoretical result of this paper is the following (Bezmenov and Pasynok, 2015):

THEOREM. *Let the following conditions be satisfied*

1. RMS calculated for the period in N days for each of the Centers, asymptotically (at N sufficiently large) are equal to each other.

2. In k-th day and n-th epoch the position vector for combined orbit of j-th satellite represents a weighted average (with weights $W_{i,k}$) of satellite's positions as determined by the Centers:

$\boldsymbol{x}^j_{Comb,k,n} = \sum_{i=1}^{N_{Cent}} W_{i,k} \cdot \boldsymbol{x}^j_{i,k,n}; n = 1, ..., N_{Epo}, j = 1, ..., N_{Sat},$

3. The weights $W_{i,k}$ are related for each k with residual mean squared

$RMS_{i,k} = \left(\frac{1}{3N_{Epo}N_{Sat}} \sum_{j=1}^{N_{Sat}} \sum_{n=1}^{N_{Epo}} \|\boldsymbol{x}^j_{i,k,n}\| \right)^{1/2}$ *by monotonously decreasing dependence.*

Then RMS for the combined orbit calculated for the period in N days is no greater then RMS for each of the Centers.

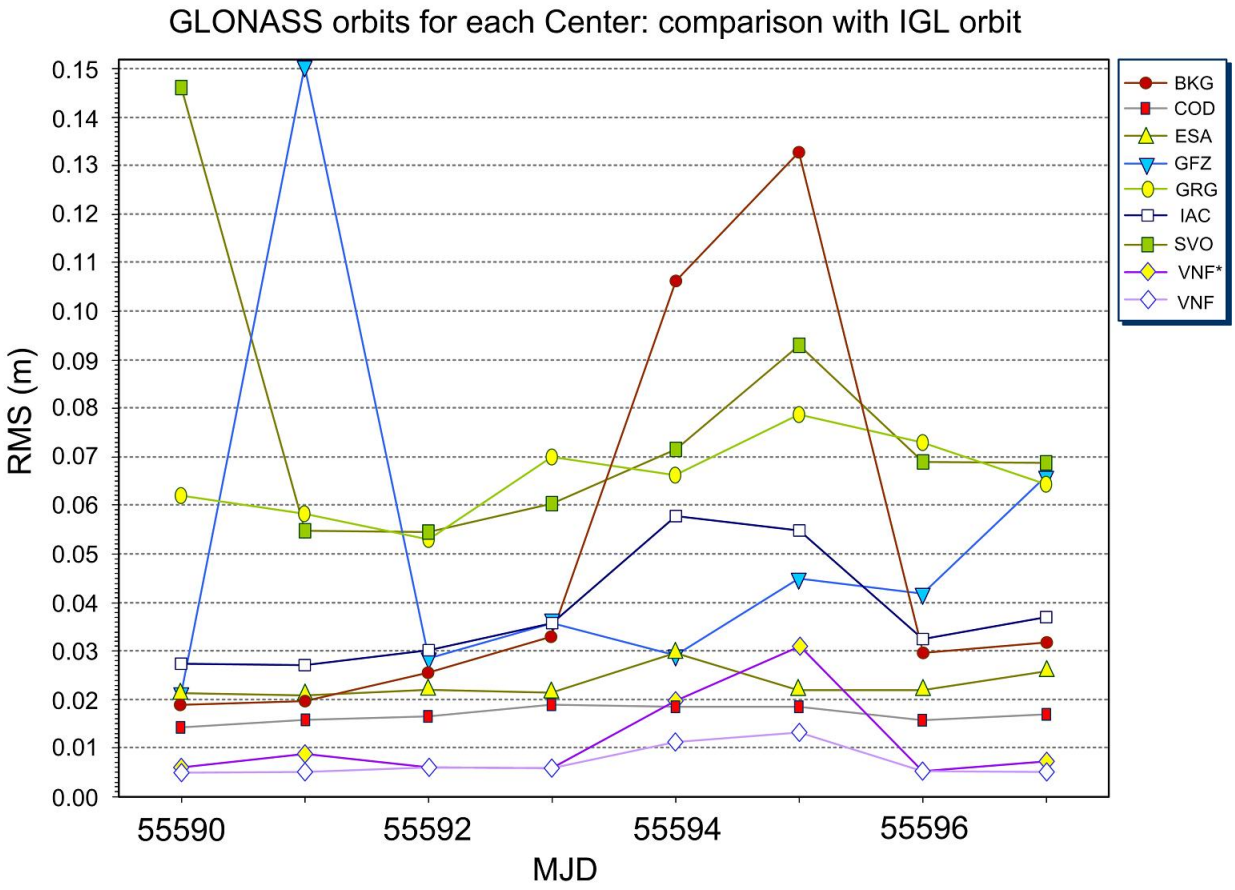

Figure 1: The abbreviation (excepting VNF, SVO) is commonly-accepted in IGS. VNF – final combined orbits of VNIIFTRI; VNF* – preliminary combined orbits of VNIIFTRI (before elimination of "bad" satellites); SVO – abbreviation of High-precision ephemeris and time correction estimation system (HETCES/SVOEVP), RF.

3. REFERENCES

Beutler, G., Kouba, J., Springer, T., 1995, "Combining the orbits of the IGS. Analysis Centers", Bull. Geod., 69, pp. 200–222.

Bezmenov, I., Pasynok, S., 2015, "GLONASS satellites orbit/clock combination", Measurement Techniques, No. 3, in print.

Kouba, J., Mireault, Y., Lahaye, F., 1995, "1994 IGS Orbit/Clock Combination and Evaluation", Appendix I of the Analysis Coordinator Report, International GPS Service for Geodynamics (IGS) 1994 Annual Report, pp. 70–94.

IRREGULAR PHENOMENA IN THE EARTH POLE OSCILLATION PROCESS AND TEMPORAL VARIATIONS OF GEOPOTENTIAL

V.V. BONDARENKO, V.V. PEREPELKIN
Moscow Aviation Institute
125993, Volokolamskoe shosse, 4, Moscow, Russia
e-mail: vadimkin1@yandex.ru

ABSTRACT. The observed irregular effects in the oscillatory process of the Earth Pole are of significant variability. They may be caused by the hydrosphere oscillations as well as the perturbations associated with the process of excitation and maintenance of the main oscillations components. Previously while carrying out the modeling of the Earth orientation parameters (EOP) in short time intervals (interyear periods) the tidal coefficients correction procedure, which took into account high-frequency unstable fluctuations with small amplitudes, was considered alongside with the regular model components. Such a short-period variations caused by geophysical processes don't make a significant influence on the quasi-periodical Earth motion and can be presented in the model as the additional components - residuals. According to the modeling results and the processing of the high-precise series of the IERS observations in the oscillation process of the Earth Pole "irregular effects" can be defined, that are associated with intrayear variation of the main oscillation components. That sort of effects that are registered by IERS, are significantly different than the ones in earlier researches. They are presented as "anomalous" fluctuations of the Earth Pole coordinates, which have a negative impact on the interpolation and prognosis of the mathematical model.

1. INTRODUCTION

It is well known that the observed irregular phenomena in the Earth Pole oscillation process are very variety. Based on the results of simulation and the processing of high-precise series of the IERS observations "irregular effects" in the Earth Pole oscillation process are extracted that are connected with within-annual variability of parameters of the main oscillation components. The abrupt changes in the oscillation phase in the middle of 1974 and in the end of 2005 – beginning of 2006 non-forecasting in the frames of the first approximation model are of significant interest. The trajectory of the Pole motion according to the IERS observation data and the theoretic interpolation curves on time interval of the Pole abnormal behavior in 2005–2006 are presented on Fig. 1.

These indicated in the IERS data phenomena are the "abnormal" fluctuations of the Earth Pole coordinates which are connected with the variation of the geodynamical parameters and they make a negative impact on the interpolation and forecast precision of the first approximation mathematical model. A numerical-analytical modeling of the Earth Pole motion shows that root-mean-square deviation of main model extrapolation of the Pole motion on the time intervals after the abnormal phenomena of 2006 year is increased considerably that corresponds to essential decreasing of the model precision.

2. MODELLING OF THE EARTH POLE MOTION

The construction of numerical-analytical model of the Earth Pole oscillation that allows to increase the precision of trajectory forecast in periods of considerable abnormalities is based on analysis of variations of the Earth gravitational field and the Earth rotation parameters (Markov et al., 2014). Figure 1 shows the plot of phase variation $\psi^{var}(\tau)$ of the Earth Pole motion that constructed on the IERS observation data on time interval from 1970 till 2011 years in the comparison with the variations of the Pole motion phase according to interpolations of two models (the main one and the refined one) on time intervals from 1990 till 2011 years. The residuals between the observed and calculated values of the phase are shown in the bottom of the plot.

The parameters of main component of the Pole oscillations on the forecast interval are assumed to be equal to its fixed values in the end of interpolation interval. The precision of annual forecast of the

refined model is higher than the forecast precision of main model during the abnormal fluctuations in the Pole oscillation process. But the precision of main model is higher when Chandler and annual oscillation characteristics are stable. The comparable short period of the Pole stable behavior was observed from 2004 till the middle of 2005. The average precisions of annual forecast of the Pole motion that is calculated by main and refined models are 1.66 m and 1.50 m correspondingly.

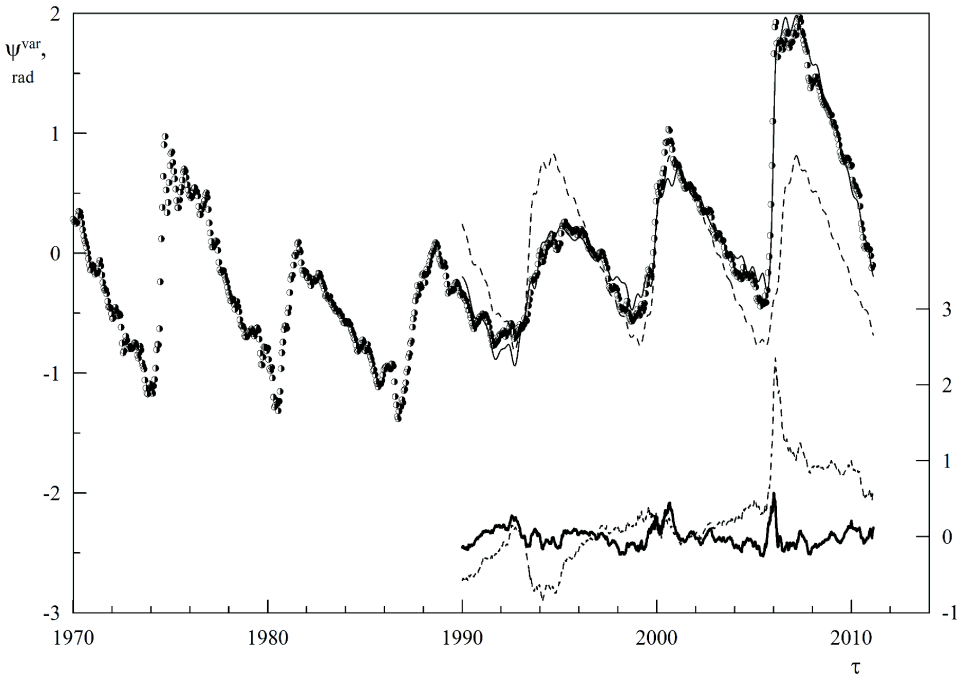

Figure 1: Variations in the phase $\psi^{var}(\tau)$ of the Earth's pole motion (upper plot) according to IERS observation data on pole coordinates on the time interval from 1970 to 2011 (discrete points) in comparison with phase variations in the pole motion according to two compared models: basic (dashed line) and refined (solid curve) models on a 23-year time interval (from 1990 to 2011). Residuals (lower plot), differences between the observed and calculated values of the phase according to the basic (dashed line) and refined (solid curve) models.

3. REFERENCES

Markov, Yu.G., Perepelkin, V.V., Krylov, S.S., 2014, "Time variations of geopotential coefficients in the structure of the oscillatory process of the Earth's pole", Doklady Physics, 59(11), pp. 544–549.

ON THE MINIMIZATION PROPERTIES OF TISSERAND SYSTEMS

A. ESCAPA[1,2], T. BAENAS[1], J.M. FERRÁNDIZ[1], J. GETINO[3]
[1] Department of Applied Mathematics, University of Alicante
PO Box 99, E-03080 Alicante, Spain
e-mail: Alberto.Escapa@ua.es
[2] Department of Mechanical, Informatics and Aerospace Engineering, University of León
E-24071 León, Spain
[3] Department of Applied Mathematics, University of Valladolid
E-47011 Valladolid, Spain

ABSTRACT. Tisserand systems are a useful concept to model the rotation of deformable sets of particles. They can be characterized by means of three alternative conditions related with the angular momentum and kinetic energy of the set. In this note, we revisit the issue providing a new proof of the equivalence between some of these defining conditions. In addition, we determine the time evolution of Tisserand systems in a clear way.

1. TISSERAND SYSTEMS. EQUIVALENT CONDITIONS

When a discrete or continuous collection of material particles $\mathcal{S}$ experience relative displacements, it is no possible to define unambiguously a rotational motion of the system – or *non-rigid body*. The usual solution is to assign to $\mathcal{S}$ a certain reference system $Oxyz$ with origin in the body barycenter O and linked to it in some prescribed way (the "body axes"). By doing so, the rotation of the system of particles is identified with the rotation of the body axes with respect to some inertial, or quasi–inertial, reference system $OXYZ$ (the "fixed axes"). This rotation admits a precise mathematical definition.

There are different possibilities to connect the body axes $Oxyz$ with the considered set of particles (Munk & McDonald 1960). From the point of view of simplifying the equations of motion, a convenient method is using the so–called *Tisserand systems* (Tisserand 1891).

To introduce Tisserand systems, let us write the absolute velocity (relative to $OXYZ$,) of a particle of $\mathcal{S}$ with position $\vec{x_i}$ and mass m_i as

$$\vec{V_i} = \vec{\omega} \times \vec{x_i} + \vec{v}_i(\vec{\omega}). \tag{1}$$

The vector $\vec{\omega}$ is common for the set $\mathcal{S}$ and, at this stage, arbitrary. In contrast $\vec{v}_i(\vec{\omega})$, the deformation or residual velocity (Moritz & Mueller 1987), depends on each particle i and the choice of $\vec{\omega}$.

Tisserand systems can be defined by any of the following conditions that fix $\vec{\omega}$ to a certain value $\vec{\omega_T}$:

(a) The angular momentum of $\mathcal{S}$

$$\vec{L} = \sum_{i \in \mathcal{S}} m_i \left(\vec{x}_i \times \vec{V}_i \right) \tag{2}$$

can be expressed as $\vec{L} = \mathbb{I}\,\vec{\omega_T}$ (Tisserand 1891), where $\mathbb{I}$ is the matrix of inertia of $\mathcal{S}$.

(b) The kinetic energy of $\mathcal{S}$ associated to the deformation velocity

$$\mathcal{T}_{\rm def}(\vec{\omega_T}) = \frac{1}{2} \sum_{i \in \mathcal{S}} m_i (\vec{v}_i(\vec{\omega_T}))^2 \tag{3}$$

is minimum (Jeffreys 1976).

(c) The *relative* angular momentum of $\mathcal{S}$ related with the deformation velocity

$$\vec{h}(\vec{\omega_T}) = \sum_{i \in \mathcal{S}} m_i \left[\vec{x}_i \times \vec{v}_i(\vec{\omega_T}) \right] \tag{4}$$

is the null vector (Tisserand 1891).

The former characterizations turn out to be equivalent, that is to say, (a) ⇒ (b), (b) ⇒ (c), and (c) ⇒ (a). The second and third implications are detailed, to some extent, in the existing literature (e.g., Moritz & Mueller 1987). Let us focus on the first one.

From Eqs. (1) and (3), the deformation kinetic energy can be written as (Escapa 2011)

$$\mathcal{T}_{\rm def}\left(\vec{\omega}\right) = \mathcal{T} - \vec{L}\vec{\omega} \ + \frac{1}{2}\vec{\omega}\,\mathsf{I}\,\vec{\omega}, \tag{5}$$

where $\mathcal{T}$ is the kinetic energy of $\mathcal{S}$. Hence, for an arbitrary vector $\vec{\lambda}$ different from $\vec{0}$, we have

$$\mathcal{T}_{\rm def}\left(\vec{\omega}+\vec{\lambda}\right) = \mathcal{T}_{\rm def}\left(\vec{\omega}\right) - \vec{L}\ \vec{\lambda} + \vec{\lambda}\,\mathsf{I}\,\vec{\omega} + \frac{1}{2}\vec{\lambda}\,\mathsf{I}\,\vec{\lambda}. \tag{6}$$

If we consider condition (a), defining the angular momentum of the system $\vec{L}$, in Eq. (6), we get

$$\mathcal{T}_{\rm def}\left(\vec{\omega}_T+\vec{\lambda}\right) - \mathcal{T}_{\rm def}\left(\vec{\omega}_T\right) = \frac{1}{2}\vec{\lambda}\,\mathsf{I}\,\vec{\lambda}. \tag{7}$$

Since the matrix of inertia is definite positive, we have that

$$\frac{1}{2}\vec{\lambda}\,\mathsf{I}\,\vec{\lambda} > 0,\ \ \vec{\lambda}\in\mathbb{R}^3,\ \ \vec{\lambda}\neq\vec{0}. \tag{8}$$

Therefore, Eq. (7) implies that $\mathcal{T}_{\rm def}\left(\vec{\omega}\right)$ takes its minimum at $\vec{\omega}_T$, i.e., condition (b).

2. TIME EVOLUTION OF TISSERAND SYSTEMS

The angular velocity $\vec{\omega}_T$, considered as a known function of time, determines the rotational kinematics of the body axes, but not its orientation in a univocal manner (Tisserand 1891). Specifically, from the components of $\vec{\omega}_T$ in the $OXYZ$ system, we can construct the skew–symmetric matrix

$$\mathsf{\Sigma}_T(t) = \begin{pmatrix} 0 & -\omega_{TZ}(t) & \omega_{TY}(t) \\ \omega_{TZ}(t) & 0 & -\omega_{TX}(t) \\ -\omega_{TY}(t) & \omega_{TX}(t) & 0 \end{pmatrix}. \tag{9}$$

It allows defining a rotation matrix $\mathsf{R}(t)$ that brings the $OXYZ$ system to the body axes through (Wintner 1941)

$$\mathsf{\Sigma}_T(t) = \frac{d\mathsf{R}^t}{dt}\mathsf{R}, \tag{10}$$

where the superscript t denotes the transpose of a matrix. The solution of this linear differential equation is given by

$$\mathsf{R}(t) = \mathsf{R}\left(t_0\right)\exp\left(-\int_{t_0}^{t}\mathsf{\Sigma}_T(s)ds\right), \tag{11}$$

$\mathsf{R}\left(t_0\right)$ providing the numerical value of $\mathsf{R}(t)$ at the epoch t_0.

In this way, besides any of the conditions (a), (b), or (c), the specification of a particular Tisserand system requires providing explicitly the initial orientation of the body axes relative to $OXYZ$.

Acknowledgements. This work has been partially supported by the Generalitat Valenciana project GV/2014/072, and the Spanish government under MINECO projects I+D+I AYA201022039-C02-01, AYA2010-22039-C02-02.

3. REFERENCES

Escapa, A., 2011, Celest. Mech. Dyn. Astr., 110, pp. 99–142
Jeffreys, H., 1976, "The Earth", Cambridge University Press.
Moritz, H., Mueller, I., 1987, "Earth Rotation", NY: Frederic Ungar.
Tisserand, F.F., 1891, "Traité de Mécanique Céleste", Vol. 2, Paris: Gauthier–Villars.
Wintner, A., 1941, "The Analytical Foundations of Celestial Mechanics", Princeton University Press.

POLE TIDE TRIGGERING OF SEISMICITY

V.L. GORSHKOV
Pulkovo observatory
St. Petersburg 196140, Russia
e-mail: vigor@gao.spb.ru

ABSTRACT. The influence of the pole tide (PT) on intensity of seismic process is searched on base of Harvard Centroid-moment tensors catalogue (CMT). The normal and shear stresses excited by PT were calculated for each earthquake (EQ) from CMT (32.3 thousands of EQ events after for- and aftershock declustering). There was revealed that there are two maxima of PT influence on weak (less 5.5 magnitudes) thrust-slip EQ near the both extrema (min and max) of shear stress. This influence has 95 % level of statistical significance by Schuster and χ^2 criteria and could explain the 0.6-year periodicity in seismic intensity spectrum. The PT influence on seismicity becomes negligible when PT variations decrease up to 100 mas. This could explain 6–7 years periodicity in seismic intensity spectrum.

1. MOTIVATION

There is periodicity of EQ intensity in PT frequency band (0.6, 1.2 and 6–7 years). The most obvious excitation factor of these EQ intensity variations is PT. But excited stress variations in the crust by PT are less 1 kPa while lunisolar tide (LST) stress variations achieve 5 kPa. Why PT can trigger EQ but it is almost impossible to reveal EQ triggering by more power LST? First of all PT is significantly powerful than LST in above-mentioned frequency band while LST is the most powerful near 0.5–1 day periodicity. Secondly the failure time t_n is depend on energy of seismic event and t_n = 1–10 years for magnitude M = 3.5–5.5 (Sadovsky, Pisarenko, 1991). That is to say preparation time t_n for weak EQ coincides with frequency band of PT induced stress variations. Thus LST are added to stress accumulation process in fault zone as powerful high-frequency noise while PT acts as systematic, nearly synchronous component for a weak EQ. At last some confirmation of the PT influence on seismic process can be found in the next papers (Levin, Sasorova, 2002; Shen, et al., 2007).

2. DATA AND METHOD

There were used 32264 EQ events from CMT (1976–2014) to search the trace of PT in seismicity after declustering for strong EQ with $M_w > 7.2$: $\Delta d(km) = 1.2exp(0.8M_w - 1.0)$ and $\Delta t(days) = 1.2exp(0.8M_w - 2.9)$. The normal and shear stresses were calculated by (Zhu, 2013):

$$\sigma_n = \sigma_n^0 \sin^2 \delta \tau_s = \tau_s^0 \sin\delta\cos\psi + 0.5\sigma_n^0 \sin 2\delta \sin\psi,$$

where $\sigma_n^0 = \tau_{\theta\theta}\cos^2\alpha + \tau_{\lambda\lambda}\sin^2\alpha + \tau_{\theta\lambda}\sin 2\alpha$, $\tau_s^0 = 0.5(\tau_{\lambda\lambda} - \tau_{\theta\theta})\sin 2\alpha + \tau_{\theta\lambda}\cos 2\alpha$, and α, δ, ψ are strike, dip and rake angles of EQ fault plane, $\tau_{\theta\theta}, \tau_{\lambda\lambda}, \tau_{\theta\lambda}$ are element of induced by PT stress tensor. In view of free surface boundary condition (Melchior, 1978) the rest of tensor elements are equal to zero.

Phases of σ_n and τ_s were estimated for each EQ as a part between its previous and following max/min values in EQ coordinate point. EQ number N_ψ was counted in 30° phase boxes for next faulting type of EQ: normal ($-120° < \psi < -60°$), thrust ($60° < \psi < 120°$), strike-slip ($0° <\mid \psi \mid< 30°, 150° <\mid \psi \mid< 180°$) and the rest – oblique strike-slip. Schuster (1897) and χ^2 statistic tests were used for assessment of significance of phase concentration near some particular phase. Null hypothesis on random distribution of phase is rejected if probability $p_s = exp(-R^2/N_\psi) < p_{0.05}$ for Schuster and $\chi^2 > \chi^2_{0.95} = 18.307$ for χ^2 statistic test, where $R^2 = C^2 + S^2, C = \sum_{i=1}^{N_\psi}\cos\beta_i, S = \sum_{i=1}^{N_\psi}\sin\beta_i$.

3. RESULTS AND CONCLUSIONS

Approximately 90% of EQ events are indifferent to variations of Pole. The rest of events (10%) nearly repeat time variations of Pole. It is remarkable that 10% events in CMT have magnitude $M_w < 5.3$.

What are these events? PT has an influence with 95% confidence level on seismic intensity only for thrust-slip EQ with magnitude $M_w < 5.3$ ($p_s = 0.028, \chi^2 = 18.7$). Other faulting type EQ are indifferent to PT influence according to used statistic.

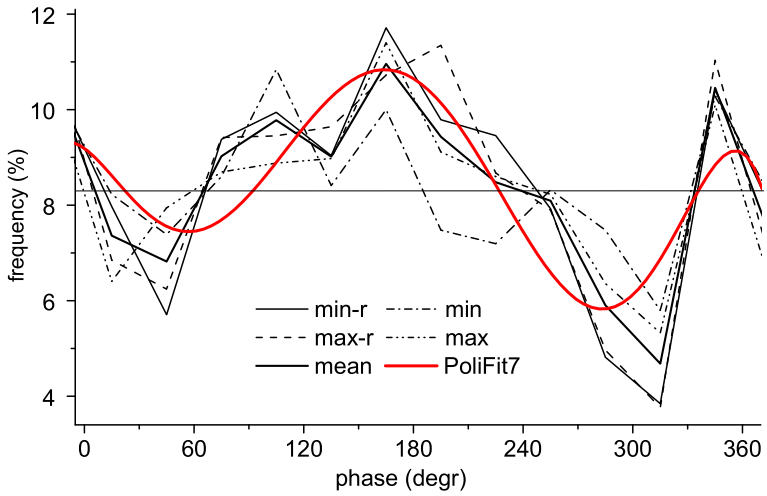

Figure 1: Various variants of frequency distribution of shear stress phases of thrust EQ. Straight line (8.3%) corresponds to even distribution of phase. Smooth red line is polynomial fitting of 'mean' line.

There are two maxima of PT influence on thrust EQ near both extrema (min and max) of shear stress (Fig. 1). This result could explain the 0.6-year periodicity in seismic intensity. The PT influence on seismicity when Pole variation damping (less than 100 *mas*, r in Fig. 1 denotes the data without this EQ events) becomes actually noise as it was checked by independent estimations of χ^2 and p_s. Therefore the PT is the most probable reason of 6–7 years periodicity in seismic intensity.

So we may conclude:

- Pole tide influence on seismic intensity is revealed only for thrust type of EQ with 95% reliability.
- This influence falls with rise of magnitude M and vanishes for $M_w > 5.5$.
- There are two maxima of this influence approximately coinciding with both extreme of shear stresses. This result could explain 0.6-year spectral peak in seismic intensity.
- Pole tide influence on seismic intensity for time of Pole wobble damping (< 100 *mas*) is actually noise. This could explain 6–7 year periodicity in seismic process.

4. REFERENCES

Levin, B., Sasorova, E., 2002, "On the 6-Year Tsunami Periodicity in the Pacific", Izvestiya, Physics of the Solid Earth, 38(12), pp. 1030–1038.

Melchior, P., 1978, "The tides of the planet Earth". New York: Pergamon press, 608 pp.

Sadovsky, M.A., Pisarenko, V.F., 1991, "Seismic process and the block medium", Moscow: Nauka, 96 pp. (in Russian)

Schuster, A., 1897, "On lunar and solar periodicities of earthquake", Proc. R. Soc. London, 61, pp. 455–465.

Shen, Z.-K., et al., 2007, "Pole-Tide Modulation of Slow Slip Events at Circum-Pacific Subduction Zones", Geophys. J. Int., 53(3), pp. 617–621.

Zhu, P.P., 2013, "Normal and shear stresses acting on arbitrarily oriented faults, earthquake energy, crustal GPE change and the coefficient of friction", J. Seismol., 17, pp. 985–1000, doi: 10.1007/s10950-013-9367-2.

ESTIMATING THE PERIOD AND Q OF THE CHANDLER WOBBLE FROM OBSERVATIONS AND MODELS OF ITS EXCITATION

R. GROSS[1], J. NASTULA[2]
[1] Jet Propulsion Laboratory, Caltech
4800 Oak Grove Drive, Pasadena, CA 91109, USA
e-mail: richard.gross@jpl.nasa.gov
[2] Space Research Center PAS
Bartycka 18a 00-716 Warsaw, Poland
e-mail: nastula@cbk.waw.pl

Any irregularly shaped solid body rotating about some axis that is not aligned with its figure axis will freely wobble as it rotates. For the Earth, this free wobble is known as the Chandler wobble in honor of S.C. Chandler, Jr. who first observed it in 1891. Unlike the forced wobbles of the Earth, such as the annual wobble, whose periods are the same as the periods of the forcing mechanisms, the period of the free Chandler wobble is a function of the internal structure and rheology of the Earth, and its decay time constant, or quality factor Q, is a function of the dissipation mechanism(s), like mantle anelasticity, that are acting to dampen it. Improved estimates of the period and Q of the Chandler wobble can therefore be used to improve our understanding of these properties of the Earth. Here, estimates of the period and Q of the Chandler wobble are obtained by finding those values that minimize the power within the Chandler band of the difference between observed and modeled polar motion excitation spanning 1962–2010. Atmosphere, ocean, and hydrology models are used to model the excitation caused by both mass and motion variations within these global geophysical fluids. Direct observations of the excitation caused by mass variations as determined from GRACE time varying gravitational field measurements are also used. The resulting estimates of the period and Q of the Chandler wobble will be presented along with a discussion of the robustness of the estimates.

THE CONSISTENCY OF THE CURRENT CONVENTIONAL CELESTIAL AND TERRESTRIAL REFERENCE FRAMES AND THE CONVENTIONAL EOP SERIES

R. HEINKELMANN[1], S. BELDA-PALAZÓN[2,1], J.M. FERRÁNDIZ[2], H. SCHUH[1,3]
[1] Helmholtz Centre Potsdam, GFZ German Research Center for Geosciences
Telegrafenberg, 14473 Potsdam, Germany
e-mail: heinkelmann@gfz-potsdam.de
[2] University of Alicante, Departamento de Matematica Aplicada
Road San Vicente del Raspeig, 03690 San Vicente del Raspeig - Alicante, Spain
[3] Institute of Geodesy and Geoinformation Science, Technische Universität Berlin
Straße des 17. Juni 135, 10623 Berlin, Germany

ABSTRACT. For applications in Earth sciences, navigation, and astronomy the celestial (ICRF) and terrestrial (ITRF) reference frames as well as the orientation among them, the Earth orientation parameters (EOP), have to be consistent at the level of 1 mm and 0.1 mm/yr (GGOS recommendations). We assess the effect of unmodeled geophysical signals in the regularized coordinates and the sensitivity with respect to different a priori EOP and celestial reference frames. The EOP are determined using the same VLBI data but with station coordinates fixed on different TRFs. The conclusion is that within the time span of data incorporated into ITRF2008 (Altamimi, et al., 2011) the ITRF2008 and the IERS 08 C04 are consistent. This consistency involves that non-linear station motion such as unmodelled geophysical signals partly affect the IERS 08 C04 EOP. There are small but not negligible inconsistencies between the conventional celestial reference frame, ICRF2 (Fey, et al., 2009), the ITRF2008 and the conventional EOP that are quantified by comparing VTRF2008 (Böckmann, et al., 2010) and ITRF2008.

1. CONSIDERATION OF UNMODELLED GEOPHYSICAL SIGNALS

The regularized coordinate model of ITRF provides for each station a position at the catalogue epoch (for ITRF2008 it is 2005.0) and a linear velocity. As specified by IERS Conventions, most of the known significant station displacements are considered for the reduction of the observations of the space geodetic techniques, but not all. The atmospheric pressure loading is for example disregarded. For our investigations, we have to fix station coordinates on their catalogue values in order to assess the level of inconsistency of the catalogue. The fixation of station coordinates on catalogue values causes shifts and drifts of EOP of which y_{pol} is most significant: shift $\approx 30\mu$as, drift $\approx 3\mu$as/yr . The root mean square (rms) of the pole coordinates and dUT1 (ERP) increases significantly when station coordinates are estimated. The IERS 08 C04 EOP are adjusted together with ITRF2008 station coordinates and are thus consistent with the linear station velocity model. Consequently, if station coordinates are adjusted, the EOP differ from IERS 08 C04 causing larger rms.

2. SENSITIVITY TO A PRIORI EOP AND RADIO SOURCE COORDINATES

Here we assess how much the estimated EOP depend on the a priori information about the EOP and the radio source coordinates. Therefore we test radio source coordinates from ICRF-Ext.2 (Fey, et al., 2004) as an alternative to ICRF2. As an alternative to IERS 08 C04 we introduce EOP from USNO finals or celestial pole offsets from IAU2006/2000A models. Taking coordinates from the various radio source catalogues causes insignificant weighted mean differences of the EOP up to about 14 μas. The rms of EOP w.r.t. ICRF-Ext.2 is generally larger than w.r.t. ICRF2. Significantly different celestial pole offsets can be found, if the a priori values are taken from IAU models that do not contain the free core nutation (FCN) component. If including a FCN model the weighted mean difference drops to 10 μas.

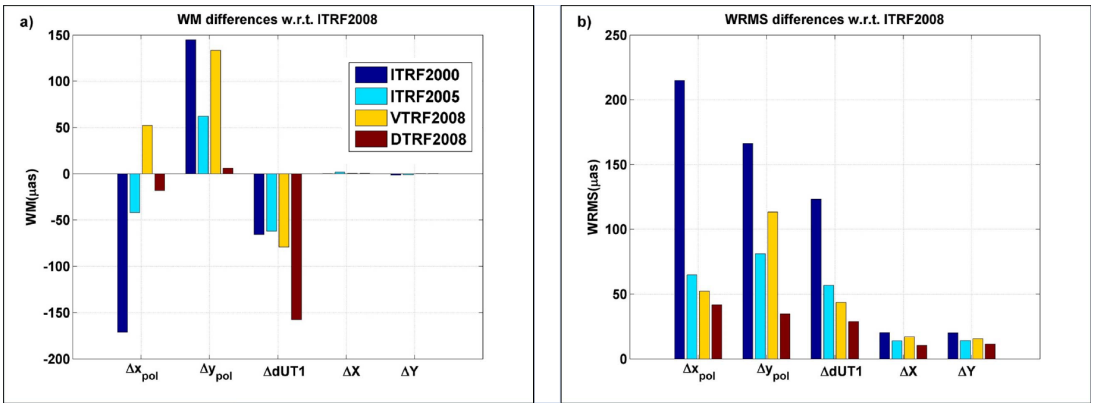

Figure 1: EOP differences caused by the TRF.

3. EOP DIFFERENCES USING DIFFERENT TRF

The predecessors of ITRF2008, ITRF2000 (Altamimi, et al., 2002) and ITRF2005 (Altamimi, et al., 2007) have been used to conserve the orientation of ITRF using no net rotation conditions (NNR): ITRF2005 was NNR constrained to ITRF2000, and ITRF2008 to ITRF2005. If the NNR would work perfectly, we could expect almost no change of the orientation of those frames and consequently no change of the attached EOP even if just the VLBI subset of stations was used. The weighted mean differences of ERP are at the level of about 50 μas and weighted rms are about 60-80 μas comparing ITRF2008 with ITRF2005 (Fig. 1).

The VLBI contribution to ITRF2008, VTRF2008, has been used as the terrestrial reference frame for the creation of the conventional celestial reference frame, ICRF2. During creation of the ITRF2008 and the conventional EOP, the IERS 08 C04, no explicit care has been taken for consistency with ICRF2. It is thus possible to assess the consistency of ICRF2, IERS 08 C04, and ITRF2008 by comparing VTRF2008 and ITRF2008. Fixing coordinates on the VLBI-only frame results in large shifts and drifts of the ERP, in particular of $y_{pol} \approx -38.8\mu$as and $\dot{y}_{pol} \approx -18.6\mu$as/yr.

DTRF2008 (Seitz, et al., 2012) is based on the same input data as ITRF2008 but presents an alternative combination approach. Thus, we would expect very small differences to ITRF2008. Comparing the EOP, however, we find a large shift of $dUT1 \approx -170\mu$as.

Acknowledgements. We thank the Spanish MINECO by partially supporting SB and JMF through grant AYA2010-22039-C02-01. S. Belda-Palazón has been visiting GFZ during creation of the paper.

4. REFERENCES

Altamimi, Z., Sillard, P., Boucher, C., 2002, "ITRF2000: A new release of the International Terrestrial Reference Frame for earth science applications", J. Geophys. Res., 107(B10), 2214, doi: 10.1029/2001JB000561.

Altamimi, Z., Collilieux, X., Legrand, J., Garayt, B., Boucher, C., 2007, "ITRF2005: A new release of the International Terrestrial Reference Frame based on time series of station positions and Earth Orientation Parameters", J. Geophys. Res., 112(B9), 401, doi: 10.1029/2007JB004949.

Altamimi, Z., Collilieux, X., Métivier, L., 2011, "ITRF2008: an improved solution of the international terrestrial reference frame", J. Geod., 85, pp. 457–473.

Böckmann, S., Artz, T., Nothnagel, A., 2010, "VLBI terrestrial reference frame contributions to ITRF2008", J. Geod., 84, pp. 201–219.

Fey, A.L., Ma, C., Arias, E.F., Charlot, P., Feissel-Vernier, M., Gontier, A.-M., Jacobs, C.S., Li, J., MacMillan, D.S., 2004, "The second extension of the International Celestial Reference Frame", AJ, 127, pp. 3587–3608.

Fey, A.L., Gordon, D., Jacobs, C.S. (eds.), 2009, "The second realization of the International Celestial Reference Frame by Very Long Baseline Interferometry", IERS Technical Note 35, Verlag des Bundesamts für Kartographie und Geodäsie, Frankfurt am Main.

Seitz, M., Angermann, D., Bloßfeld, M., Drewes, H., Gerstl, M., 2012, "The 2008 DGFI realization of the ITRS: DTRF2008", J. Geod., 86, pp. 1097–1123.

APPLICATION OF THE TITIUS-BODE LAW IN EARTHQUAKE STUDY

H. HU[1], Z. MALKIN[2,3], R. WANG[1]
[1] Yunnan Observatory, Chinese Academy of Sciences
Kunming 650011, P.R. China
e-mail: huhui@mail.ynao.ac.cn
[2] Pulkovo Observatory
St. Petersburg 196140, Russia
[3] St. Petersburg State University,
Universitetskii Pr. 28, St. Petersburg 198504, Russia
e-mail: malkin@gao.spb.ru

ABSTRACT. This article introduces application of the commensurability revealed by Titius-Bode Law in earthquake (EQ) prediction study. The results show that occurrence of the most of the world's major earthquakes is not accidental, and they occurred at the commensurable points of time axis. As an example, both EQ 7.0 in Lushan, China on 2013–04–20 and EQ 8.2 in Iquique, Chile on 2014–04–01 occurred at their commensurable epochs. This provides an important scientific basis for the prediction of major EQ, which will occur in the area in future.

1. INTRODUCTION

In the ITRF model, station motion is described by the piecewise linear model. However, the actual station motion is more complicated and includes other effects such as seasonal and irregular position variations as well as jumps and exponential relaxation after large earthquake (EQ). So, the studies on the EQs time distribution and prediction is of large importance for the assessment of the ITRF stability.

During recent years huge EQs frequently occurred and made surprise attacks on many places of the globe, especially in the south and east of Asian, and the seismic belt around the Pacific Ocean. Since the EQ 9.0 occurred in Sumatra in 2004, then the EQ 8.0 in Chile in 2010, the EQ 9.0 in Honshu in 2011, the EQ 8.2 in Chile in 2014, etc. They caused strong impact to the expecting continued developing economy and the tranquility of human society of the world. Frequent exceptional strong disasters of EQs remind that we must strengthen our research on cause of formation, mechanism, prediction and forecast of the EQs, and achieve the goal of advancing the development of Earth science and mitigation of seismic disasters.

We have therefore in-depth studied the commensurability revealed by Titius-Bode law. Based on many years' research and development of Titius-Bode law, we compiled a FORTRAN program, which we used to analyze major EQs in the world since 1900. We found that most of the world's major earthquake occurred at their commensurable points of time axis (Hu et al., 2013). Both EQ 7.0 in Lushan, China on 2013–04–20 and EQ 8.2 in Iquique, Chile on 2014–04–01 occurred at their commensurable points of time axis. This once again proves the universality of the commensurability.

2. TITIUS-BODE LAW AND ITS EXPANSION

Titius-Bode law in its classical formulation has the following form:

$$a_n = 0.4 + 0.32 \times 2^{n-2} \,, \tag{1}$$

which can be also expressed as

$$\beta = \frac{a_{n+1}}{a_n} \,, \tag{2}$$

where a_n is the distance of the planet n from to the Sun in astronomical units, n is the order number of the planet, and β is the commensurable value for the planets in the solar system (Zhang et al. 1980).

Weng Wenbo (Weng, 1981) pointed out that the commensurability is one of the orders in the natural world. The equation (2) brings light to the distribution law of the matter in a space region, and for time domain the commensurability can be expressed as (Weng, 1981)

$$\Delta X = \frac{X_{i+\Delta i} - X_i}{K} \ , \tag{3}$$

where K is an integer constant. If the above relation is tenable, then the data set $\{X_i\}$ is commensurable. ΔX is the commensurable value of the data set $\{X_i\}$, and $X_i, X_{i+\Delta i} \in \{X_i\}$. The subscript Δi is the difference between the sequential numbers of the two arbitrary data in the data set $\{X_i\}$. In our practical analysis and computation $\Delta i \equiv 1$ (Weng, 1981).

3. PREDICTION ON THE LUSHAN EQ 7.0 IN CHINA OF 2013 AND THE IQUIQUE EQ 8.2 IN CHILE OF 2014

An EQ 7.0 occurred in Lushan, China on 2013–04–20. We point out that the expanding time points in its time axis are the time point when a future EQs may occur (Hu et al.,2013). In the paper we analyzed the commensurability of the EQs in the Sichuan–Yunnan region since 1900.0 and obtained its commensurable value to be 2.44 years. The previous EQ of M≥7.0 is the Wenchuan EQ 8.0 occurred on 2008–05–12, i.e. 2008.36, so

$$2013{-}04{-}20 = 2008.36 + 2.44 \times 2 = 2013.31 = 2013{-}03{-}29 + 22 \text{ days} \ .$$

It occurred just at the commensurable point equal to two times of its time axis. Its absolute error is 22 days, and its relative error is 0.03.

An EQ 8.2 in Iquique, northern Chile, occurred on 2014–04–01. In the paper (Hu et al., 2013) we have also analyzed the EQs in south-central Chile and found that its commensurable value is equal to 0.59 years. For strict scientific purposes, the EQ events we selected are expanded to include northern Chile, and obtained their commensurable value to be still equal to 0.59 year. The previous EQ 8.0 in Chile occurred on 2010–02–27, i.e. 2010.15, so

$$2014{-}04{-}01 = 2010.15 + 0.59 \times 7 = 2014.28 = 2014{-}04{-}12 - 11 \text{ days} \ .$$

It occurred just at the commensurable point equal to seven times of its time axis. Its absolute error is 11 days, and its relative error is 0.05.

4. CONCLUDING REMARKS

Previous research has shown that Titius-Bode law not only is applicable for the planets of the solar system, but is also applicable for satellites of Jupiter, Saturn, Uranus, etc., only their concrete expressions have different forms (Zhang et al., 1980). Titius-Bode law itself brings to light the distribution law of the matter in a space region, and the expanding Titius-Bode law reveals the time law of the occurrence of the events in a specified space region. It can be seen that the commensurability is present in various natural phenomena and has universality. Therefore, astronomical achievements not only provide service to astronomical developments, but also to other scientific research, such as applied geoscience. It is helpful to study the complicated relationships among various matters, and thus merits further in-depth research.

5. REFERENCES

Hu, H., Han, Y., Su, Y., Wang, R., 2013, "Commensurability of Earthquake Occurrence", Journal of Asian Earth Sciences, 70-71, pp. 27–34.

Weng, W.B., 1981, "Commensurability", Acta Geophysical Sinica, 24(4), pp. 151–154. (in Chinese)

Zhang, Y., et al. (eds.), 1980, "Encyclopaedia of China: Astronomy", Beijing, Encyclopaedia of China Press, pp. 375. (in Chinese)

PERIODICAL REGULARITIES OF POLAR MOTION IN THE PULKOVO LATITUDE VARIATIONS

N.O. MILLER
Pulkovo Observatory
Pulkovskoe Sh. 65, St. Petersburg 196140, Russia
e-mail: natm@gao.spb.ru

ABSTRACT. The work studies the main component of Polar Motion, obtained from variations in the Pulkovo latitude. We employed different methods of analysis of time series: Singular spectral analysis, and Fourier and Hilbert transforms. Six components in the interval of 1.1–1.3 year were found by . The first two components possess repeated structural features well apparent during the periods of 1850–1930 and 1930–2010 in the time variations of phase and amplitude.

1. DECOMPOSITION SSA

A detailed study of Pulkovo combined time series of latitude Phi (1840.4–2014.0) was carried out in this work. The rate of sampling is 0.1 yr. The latitude observations at Pulkovo began in 1840. The latitude variations obtained from X.I. Peters's observations with Ertel vertical circle by A.A. Ivanov and from V.J. Struve's observations with Repsold transit instrument in the first vertical by B.Wanah were used to develop a time series Phi (1840–1848) (Miller & Prudnikova, 2010). The latitude variations obtained observations with ZTF-135 were used to develop a time series Phi (1904–1941, 1948–2006). In addition, the longest records of pole coordinates (IERS C01) for 1846–2009 and 2010–2014 (IERS C04) were used. Measurements of the Pulkovo latitude Phixy were calculated by the IERS time series of pole coordinates. The Singular Spectrum Analyses (SSA) method (Vityazev et al., 2010) was used for the investigation time series Phi, Phixy. The variations of amplitude and a phase of the CW and annual components were calculated with the help of Hilbert transform.

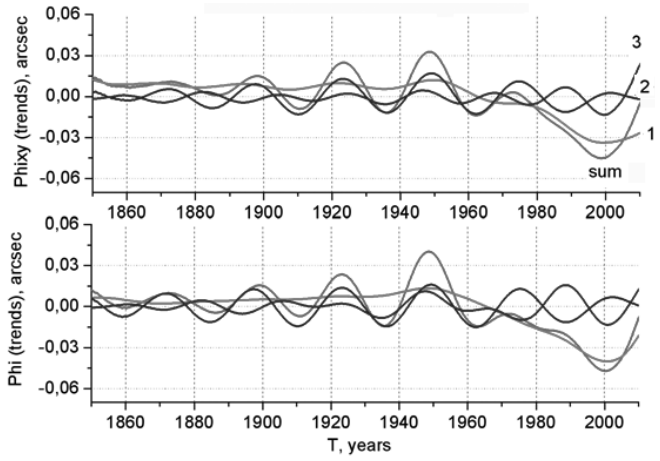

Figure 1: The comparison of the decomposition SSA of the trends Phi and Phixy.

We obtained by SSA the following main components of the polar motion: trend (1.96%), Chandler (63.67%) and annual (19.62%) wobbles. The sum reconstruction of the main components contributes 90% for Phixy time series and 85% for Phi. Results of research for 1840–2009 are shown in (Miller, 2011).

The new SSA decomposition affords interesting comparison of non-linear trends in the Phi with the trends Phixy. Results of research are shown in Fig. 1.

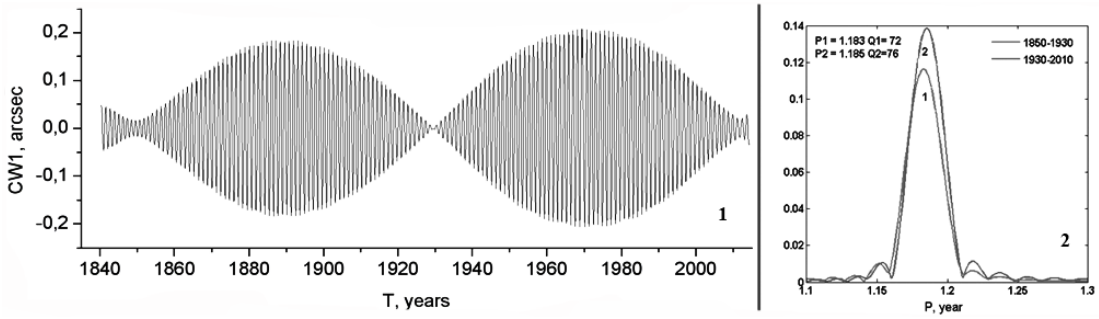

Figure 2: 1: the CW1 - main CW component, 2: spectra of CW signal computed for both intervals.

Six initial components were obtained at the Chandler wobble (CW) frequency using the SSA. The main CW component: CW1 is the sum of the first two initial components, which makes contribution 52.9%, and the sum of other four initial components CW2 makes 10.77% (CW=CW1+CW2). The first component CW1 has two intervals of similar behavior, 1850–1930 and 1930–2010 (Fig. 2 (1)). Fig. 2 (2) presents spectra of CW signal computed for both intervals. From these plots one can clearly see that the CW amplitude variations are similar for both intervals. This result can provide an evidence of a new CW period of 80(0.2) yr (Malkin & Miller, 2010).

The residual series (14%) were found after exclusion of all components described above. The residual series are well approximated by a random process. This means that the bulk of regular components are already excluded.

2. CONCLUSION

1 The full research of fine structure of pole movement obtained by SSA is presented on the scheme by the time series variations in the Pulkovo latitude (1840–2014).

2 We have found two epochs when the CW amplitude decreased near 1850 and 2010, which are also accompanied by a large phase jump, similar to well known event in 1930s. This result can provide an evidence of a new CW period of 80(0.2) yr. Unfortunately, we can't finally confirm this result as both periods of the phase disturbances described in this example are located at the edges of the interval of the studied time series.

3 The CW parameters (P = 1.183, 1.185 yr, A = 0.18, 0.21", Q = 72, 76) were calculated for each of the two spans: 1850–1930 and 1930–2010 separately. Moreover, calculations were carried out across the width of the spectral line separately for the two intervals with a known constant phase.

4 The periods of 11, 16, 20, 29, 44 years were found in the amplitude of the second component of the CW2 after 1900.

5 There is increase of the amplitude by 0.03" and phase by 45 deg during 174 years in annual fluctuation.

6 The main trend has peculiarities of behavior after 1980.

3. REFERENCES

Malkin, Z., Miller, N., 2010, "Chandler wobble: two more large phase jumps revealed", Earth Planets and Space, 62, pp. 943–947.

Miller, N., 2011, "Chandler Wobble in Variations of the Pulkovo Latitude for 170 Years", Solar System Research, 45(4), pp. 342–353.

Miller, N., Prudnikova, E., 2010,"Early Pulkovo Latitude Observations", Kinemat. Fiz. Nebesn. Tel, 27(1), pp. 40–52.

Vityazev, V., Miller, N., Prudnikova, E., 2010, "Singular Spectrum Analysis in Astrometry and Geodynamics", AIP Conf. Proc., 1283, pp. 319–328.

CONT14 — HIGH-FREQUENCY EARTH ROTATIONS VARIATIONS FROM VLBI OBSERVATIONS

E.A. SKURIKHINA, A.V. IPATOV, S.G. SMOLENTSEV, S.L. KURDUBOV,
I.S. GAYAZOV, A.A. DIYAKOV, V.V. OLIFIROV
Institute of Applied Astronomy of RAS
Kutuzov Quay 10, 191187 St.-Petersburg, Russia
e-mail: sea@ipa.nw.ru, ipatov@ipa.nw.ru

ABSTRACT. Results of data processing of CONT14 15 day campaign of continuous VLBI sessions with a network of 17 globally distributed stations in May 2014 with participation of two stations of Russian QUASAR network stations Badary and Zelenchukskaya are presented. Preliminary analysis results on EOP precision, baseline length precision are discussed. The observed intraday variations EOP are compared with a tidal model and with results of previous CONT campaigns. Troposphere parameters are compared with ones obtained with GPS technique.

CONT14 is a campaign of continuous VLBI sessions was held from 6-th till 20-th of May 2014. At the global VLBI network from 17 stations with the goal to acquire state-of-the-art VLBI data and continuous to study high frequency (sub-daily) Earth Orientation Parameters (EOP). The data was correlated using BONN correlator.

Secondary treatment program CONT14 observation was carried out using a software package OCCAM / GROSS. In the calculation of diurnal EOP 15 daily sessions were combined into one 15-day session (consisting of 23040 scans and 287,275 delays), which has been processed using a package OCCAM/GROSS using the forward run of the Kalman filter to estimate the stochastic parameters. As stochastic parameters are considered EOP (pole coordinates and universal time), the date, time, wet component of the tropospheric delay at the zenith (WZD). The behavior of stochastic parameters of simulated random walk process. Otherness from standard treatment mode is shown in Table 1.

Solution type	Parametrization
EOP service solution (daily EOP)	constant parameters: X_{pol}, Y_{pol}, $dUT1$, X_c, Y_c stochastic parameters : WZD, $clock$ A-priory spectral density for EOP: 100 mas^2
Intraday EOP solution (X_{pol}, Y_{pol}, $dUT1$)	constant parameters: X_c, Y_c stochastic parameters : X_{pol}, Y_{pol}, $dUT1$, WZD, $clock$ A-priory variance for EOP: 1 mas^2 A-priory EOP spectral density : 1 mas^2 a day

Table 1: Distinction these solution from EOP service solution.

Diurnal variation of X_{pol}, Y_{pol} and $dUT1$ were compared with the model of diurnal variations of EOP recommended by IERS Conventions (2010) (designed here as "model"), RMS (X_{pol} – model) = 188 μas, RMS (Y_{pol} – model) = 159 μas, RMS ($dUT1$ – model)= 19 μs.

The value of Tropospheric Total Zenith Delay (TZD) obtained during CONT14 from VLBI are in a good agreement with date obtained from GPS observations. For example we show s here the picture for Badary station with TZD from VLBI and GPS data. The results of TZD comparison for all stations for CONT14 are in the Table 2. At the row 2 given Number of points, at the row 3 and 4 - RMS and bias for the differences of TZD from VLBI and GPS.

We are planning to continue the data analysis with QUASAR software and careful analysis of obtained series of intraday EOP and tropospheric parameters intraday variations.

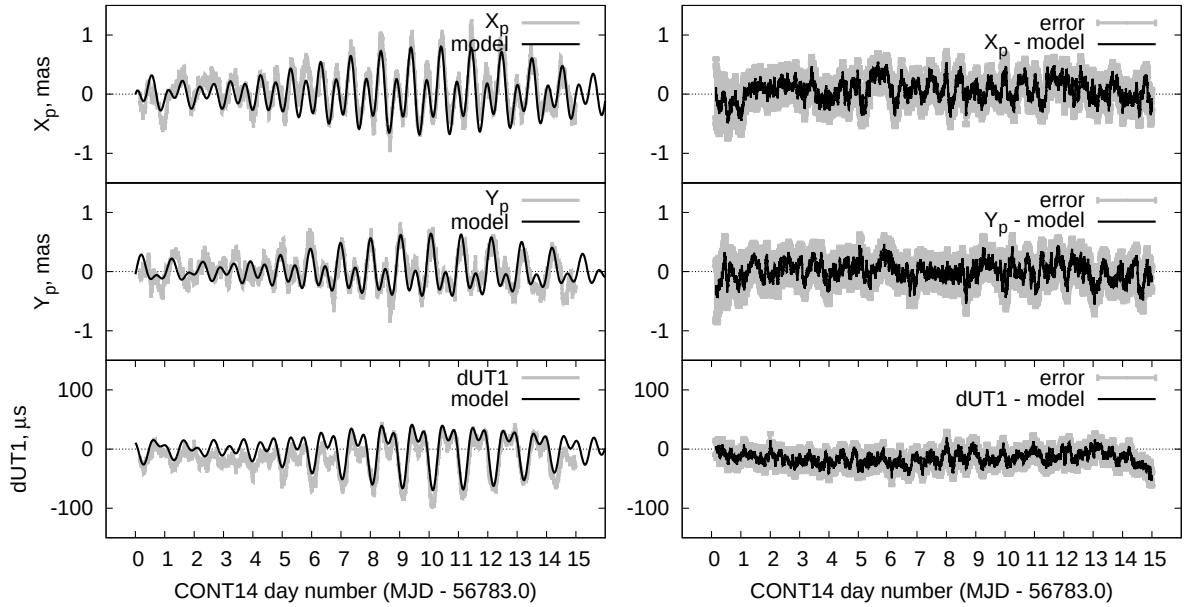

Figure 1: EOP intraday variations from CONT14. At the right side presented X_{pol}, Y_{pol}, $dUT1$ estimated from VLBI in comparison with IERS model intraday EOP variations, at the left side – corresponding differences and errorbars.

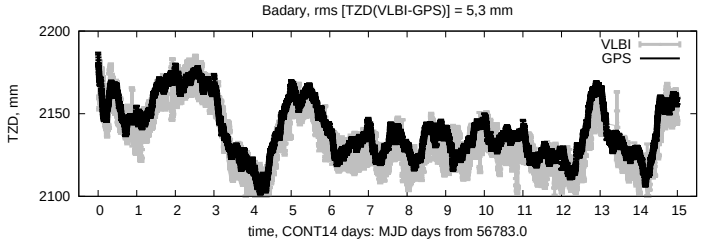

Figure 2: Example of TZD: TZD from VLBI and GPS observations during CONT14 company for Badary station.

Station	Number if point	RMS, mm	bias, mm
Badary	430	2.3	-5.1
Fortaleza	276	3.0	4.1
Hartrao	353	2.7	4.7
Hobart26	340	1.4	-0.1
Hobart12	354	2.3	-10.1
Kokee	390	1.6	0.8
Matera	362	1.5	-3.5
Ny Alezund	367	1.8	-3.8
Onsala	390	1.6	-0.3
Tsukuba	527	1.9	-5.6
Westford	464	2.1	-4.9
Wettzell	434	1.8	0.5
Zelenchukskaya	398	3.1	-8.1
Yarragadee	349	4.2	-11.9
Yebes	429	4.2	-14.3

Table 2: Comparison of TZD from VLBI and GPS observations during CONT14 (for stations in Ny Ålesund and Yebes used for comparison data of USNO GPS Analysis Center (AC), for other stations – CODE GPS AC.

TRIAXIAL EARTH'S ROTATION: CHANDLER WOBBLE, FREE CORE NUTATION AND DIURNAL POLAR MOTION

R. SUN[1], W.-B. SHEN[1,2]
[1] Key Laboratory of Geospace Environment and Geodesy, School of Geodesy and Geomatics, Wuhan University, Wuhan, China
[2] State Key Laboratory of Information Engineering in Surveying, Mapping and Remote Sensing, Wuhan University, Wuhan 430079, China
e-mail: wbshen@sgg.whu.edu.cn

In this study, we formulate two-layered triaxial Earth rotation theory, focusing on the influence of the triaxiality on the Chandler wobble (CW), free core nutation (FCN) and diurnal polar motion. We estimate the frequencies of the normal modes CW and FCN, and results show that though the influence of two-layer triaxiality on the CW and FCN frequencies are very small, there appear some new natures. The response of the Earth's polar motion to the excitation consists of two parts. One is in response to the same frequency excitation and the other is in response to the opposite frequency excitation. For an Earth model with triaxial mantle and core, both of these two parts have four resonant frequencies rather than two that are suggested by rotational symmetric Earth model. However, due to the small strength of these new resonances, the effects of these resonances are only significant when the excitation frequencies are very near to these resonance frequencies. In addition, compared to the biaxial case, the influences of the triaxiality on the prograde and retrograde diurnal polar motions excited by ocean tide component K_1 are estimated as -1.4μas and -0.9μas respectively, which should be taken into account in theory. This study is supported by National 973 Project China (grant No. 2013CB733305), NSFC (grant Nos. 41174011, 41210006, 41128003, 41021061).

PROBABILISTIC APPROACH TO DESCRIBING THE CHANDLER WOBBLE: THE ROLE OF THE OCEAN

I.Y. TSURKIS, M.S. KUCHAI, E.A. SPIRIDONOV, S.V. SINYUKHINA
Schmidt Institute of Physics of the Earth
B. Gruzinskaya Str, 10 , 123995 Moscow, Russia
e-mail: sp287@mail.ru

ABSTRACT. The atmospheric component of polar motion can be treated as the anisotropic Markov process with discrete time, and the torque exerted by the atmosphere on the solid Earth, as the white noise. The efficiency of the atmospheric mechanism in the excitation of the Chandler wobble (CW) is estimated in the context of the probabilistic model. It was shown, that one can interprets the oceanic perturbation as a stationary anisotropic random process characterized by the correlation time less than 100 day. The probabilistic approach to the description of the CW is expanded to the case of anisotropic random load. The polar motion is treated as a two-dimensional Markov process, i.e. the solution of the Liouville equation with discrete time. With a sufficiently large time step, the polar motion can be considered as an isotropic process irrespective of the particular ratio between the eigenvalues of the diffusion matrix. Thus, it is demonstrated that the observed variations in amplitude can be explained in the context of the probabilistic approach without hypothesizing the isotropy of the random load.

1. INTRODUCTION

The probabilistic approach to describing the Chandler wobble (CW) was suggested by Arato and Kolmogorov (Arato et al., 1962). The authors of the quoted paper assumed that the moment of forces causing CW is a stationary random process with a small (compared to the length T of the time series of the observations) correlation time τ_{cor}. Then, the CW itself can be considered as a diffusion Markov process with discrete time, in which the sampling interval should satisfy the condition $\Delta \gg \tau_{cor}$. In (Tsurkis et al., 2009) it was shown that the probabilistic model is consistent with the observations. Besides, the authors of the quoted work obtained the estimates for τ_{cor} and coefficient of diffusion d:

$$\tau_{cor} < 100 \text{ days}, \tag{1}$$

$$d = 1.1 \cdot 10^{-16} \ldots 1.8 \cdot 10^{-16} \text{rad}^2/\text{day}. \tag{2}$$

Studying the processes that are responsible for CW is an equally important task. The polar motion is caused by a few factors, among which the impact exerted on the solid Earth by the ocean and atmosphere is perhaps most important (Gross et al., 2003). The analysis of the oceanic angular momentum data is carried out in (Tsurkis et al., 2012). The present communication relies on the results obtained in the quoted paper.

2. STATEMENT OF THE PROBLEM

The oceanic component of CW is described by the linearized Liouville equation::

$$\frac{d}{dt}x_1 + \frac{1}{2Q}\frac{d}{dt}x_2 + \omega x_2 = f_1, \quad \frac{d}{dt}x_2 - \frac{1}{2Q}\frac{d}{dt}x_1 - \omega x_1 = f_2,$$

Here $x_k, k = 1, 2$ are the dimensionless coordinates of the pole; Q is the Q-factor (at the frequencies of the order of the Chandler frequency $\omega \approx 0,0145$ day^{-1}), $f_k = M_k/(\Omega C)$, M_k are components of the torque that acts on the solid Earth from the ocean, Ω is the average frequency of the Earth's rotation, C is the axial moment of inertia of the Earth. In the probabilistic approach, f_k are random functions of time. We hypothesize that loading $\big(f_1(t), f_2(t)\big)$ is a stationary normal random process with correlation time τ_{cor}, which is small compared to the length of the time series of the observations. In other words,

$$M\big(f_1(t_1), f_1(t_2)\big) = F_{11}\delta(t_2 - t_1), \quad M\big(f_2(t_1), f_2(t_2)\big) = F_{22}\delta(t_2 - t_1);$$

$$M\big(f_1(t_1), f_2(t_2)\big) = F_{12}\delta(t_2 - t_1), \tag{3}$$

where F_{11}, F_{22}, F_{12} are the components of non-negative symmetric matrix.

$$\mathbf{F} = \begin{pmatrix} F_{11} & F_{12} \\ F_{12} & F_{22} \end{pmatrix}.$$

Our aim is to test the statistical hypothesis (3) and to estimate the correlation time τ_{cor} and the parameters characterizing matrix $\mathbf{F}$: the coefficient of diffusion a and anisotropy constant κ

$$a(\mathbf{F}) = \mathrm{Tr}\mathbf{F} = F_{11} + F_{12}, \qquad \kappa(\mathbf{F}) = 1 - F_2/F_1,$$

where F_1 and $F_2 \le F_1$ are eigenvalues of matrix $\mathbf{F}$. We do not assume that $F_2 = F_1$.

3. DATA

We used the time series of the oceanic excitation functions $\chi_k(t)$, $k = 1, 2$ for the period from January 1, 1980 to March 27, 2003 provided by the IERS (http://www.iers.org). The IERS data are referred to the Cartesian coordinates whose axes and are located in the equatorial plane and axis x_1 is oriented along the projection of the Greenwich meridian onto this plane. Components M_1 and M_2 of the torque that acts on the solid Earth from the ocean are

$$M_1 = \omega C\big(\Omega - \chi_2 - \dot{\chi}_1\big), \qquad M_2 = -\omega C\left(\Omega\chi_1 - \dot{\chi}_2\right),$$

where $\Omega 2\pi/\mathrm{day}$ is the average frequency of the Earth's rotation, $C = 7.04 \times 10^{37}$ kg·m^2 is the axial moment of inertia of the Earth, $\omega \approx 0.0145$ day^{-1} is the frequency of free nutation (Chandler frequency). The method for calculating the excitation functions $\chi_1(t)$ and $\chi_2(t)$ is described in (Gross et al, 2003).

4. RESULTS

1. The data studied are in accordance with the main hypothesis; the estimation for the correlation time coincides with (1).

2. With probability $P > 0.92$, parameters a and κ belong to the intervals:

$$a = 1.3 \cdot 10^{-17} \ldots\ 2.2 \cdot 10^{-17}\mathrm{rad}^2/\mathrm{day}, \quad \kappa = 0.06 \ldots 0.65. \tag{4}$$

One can see that confidence interval for the anisotropy constant entirely lies in the positive area; therefore, the random load acting on the solid Earth from the ocean is anisotropic with probability > 0.92.

3. Comparing (4) and (1), we see that $a \sim 0.1d$; so if the polar motion were entirely excited by the ocean, the amplitude would be on average about $\sqrt{a/d} \sim 1/3$ of the observed value. But if we subtract the oceanic torque from the angular momentum acting on the Earth's rotation axis, the mathematical expectation of the CW amplitude insignificantly decreases (by about 5%). This is due to the fact that the average CW amplitude as a function of the diffusion coefficient is not linear but it scales as a square root function.

5. REFERENCES

Arato, M., Kolmogorov, A.N., Sinai, Ya.G., 1962, "On estimation of parameters of complex stationary Gaussian processes", Dokl. Akad. Nauk, 146(4), pp. 747–750. (in Russian)

Gross, R., Fukumori, I., Menemenlis, D., 2003, "Atmospheric and oceanic excitation of the Earth's wobbles during 1980–2000", J. Geophys. Res., 2003, 108(B8), 2370.

Tsurkis, I.Ya., Spiridonov E.A., 2009, "On the applicability of the mathematical apparatus of Markovian processes to the description of the Chandler wobble", Izvestiya, Physics of the Solid Earth, 45(4), pp. 273–286.

Tsurkis, I.Ya., Kuchay, M.S., 2012, "Probabilistic analysis of the data on the oceanic angular momentum from January 1, 1980 to March 27, 2003", Geofizicheskie issledovaniya, 13(2), pp. 66–84. (in Russian)

IMPROVEMENT OF THE SOFTWARE BERNESE FOR SLR DATA PROCESSING IN THE MAIN METROLOGICAL CENTRE OF THE STATE TIME AND FREQUENCY SERVICE

E.N. TSYBA, M.B. KAUFMAN
National Research Institute for Physical-Technical and Radio Engineering Measurements
141570, VNIIFTRI, Mendeleevo, Moscow Region, Russia
e-mail: tsyba_e_n@mail.ru

ABSTRACT. Preparatory works for resuming operational calculations of the Earth rotation parameters based on the results of satellite laser ranging data processing (LAGEOS 1, LAGEOS 2) are to be completed in the Main Metrology Centre Of The State Time And Frequency Service (VNIIFTRI) in 2014. For this purpose BERNESE 5.2 software (Dach & Walser, 2014) was chosen as a base software which has been used for many years in the Main Metrological Centre of the State Time and Frequency Service to process phase observations of GLONASS and GPS satellites. Although in the BERNESE 5.2 software announced presentation the possibility of the SLR data processing is declared, it has not been fully implemented. In particular there is no such an essential element as corrective action (as input or resulting parameters) in the local time scale ("time bias"), etc. Therefore, additional program blocks have been developed and integrated into the BERNESE 5.2 software environment. The program blocks are written in Perl and Matlab program languages and can be used both for Windows and Linux, 32-bit and 64-bit platforms.

1. INTRODUCTION

In 2010 at VNIIFTRI a program development for SLR measurements processing was started under the supervision of leading researcher M. B. Kaufman to calculate Earth rotation parameters. The program was developed on the base of BERNESE software. The authors of the work developed and implemented algorithm and calculation technique for determination of ERP from SLR observations, and also individual software elements enabling to calculate and then to include Range-bias (Rb) and Time-bias (Tb) corrections in measurements files. Also a software module was developed to provide preliminary analysis and screening of rough measurements.

2. RESULTS

At this time ILRS Network includes around 40 stations. The measurements of 33 are used for ERP calculation. The list of stations which measurements are used for ERP calculation is shown in Table 1.

Nowadays the program is operating in experimental conditions and the first results have been obtained:

- the influence of Rb and Tb on the observations carried out on station MDVL is shown in Fig. 1;
- Figure 2 shows the residuals between calculated pole coordinate (Xp, Yp) and IERS for 2013.

3. CONCLUSIONS

The conclusions are:

- the programme for Earth Rotation Parameters (ERP) calculation has been developed;
- the accuracy of the obtained results is close to one of the IERS.

In order to integrate the programme into the service activity the only thing left to do is to overcome a series of technical issues.

Monument	Location Name, Country	Monument	Location Name, Country
1873	Simeiz, Ukraine	7405	Concepcion, Chile
1879	Altay, Russia	7406	San Juan, Argentina
1884	Riga, Latvia	7501	Hartebeesthoek, South Africa
8834	Wettzell, Germany	7810	Zimmerwald, Switzerland
1893	Katzively, Ukraine	7821	Shanghai, China
7080	McDonald Observatory, Texas	7824	San Fernando, Spain
7090	Yarragadee, Australia	7825	Mt Stromlo, Australia
7105	Greenbelt, Maryland	7838	Simosato, Japan
7110	Monument Peak, California	7839	Graz, Austria
7119	Haleakala, Hawaii	7840	Herstmonceux, United Kingdom
7124	Tahiti, French Polynesia	7841	Potsdam, Germany
7237	Changchun, China	7845	Grasse, France
7249	Beijing, China	7941	Matera, Italy
7308	Koganei, Japan(CRL)	1874	Mendeleevo, Russia
7328	Koganei, Japan		

Table 1: List of ILRS station which measurements were used for ERP calculation.

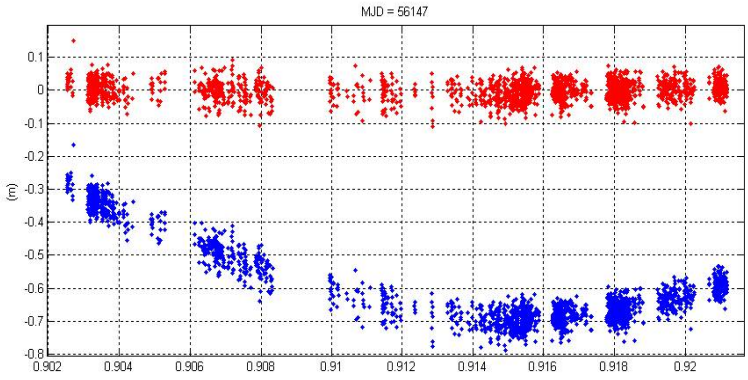

Figure 1: Influence of Rb and Tb on laser satellite measurement (station MDVL).

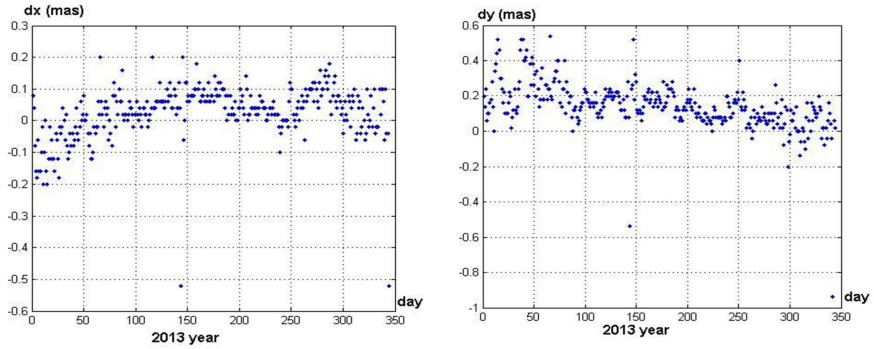

Figure 2: Residuals between calculated pole coordinate values (Xp, Yp) and IERS data.

4. REFERENCES

Dach, R., Walser, P., 2014, "Bernese GNSS Software Version 5.2. Tutorial. Processing Example. Introductory Course. Terminal Session", September 2014.

Session 5

ASTRONOMICAL ALMANACS AND SOFTWARE

ALMANACHS ET LOGICIELS ASTRONOMIQUES

THE FUTURE OF ALMANAC SERVICES — AN HMNAO PERSPECTIVE

S.A. BELL, S.G. NELMES, P.S. PREMA, J.A. WHITTAKER
H.M. Nautical Almanac Office
UK Hydrographic Office, Taunton, TA1 2DN, United Kingdom
e-mail: {Steve.Bell, Susan.Nelmes, Paresh.Prema, James.Whittaker}@ukho.gov.uk

ABSTRACT. This talk will explore the means for delivering almanac data currently under consideration by HM Nautical Almanac Office in the near to medium future. While there will be a need to continue printed almanacs, almanac data must be available in a variety of forms ranging from paper almanacs to traditional web services through to applications for mobile devices and smartphones. The supply of data using applications may call for a different philosophy in supplying ephemeris data, one that differentiates between an application that calls on a web server for its data and one that has built-in ephemerides. These ephemerides need to be of a reasonably high precision while maintaining a modest machine footprint. These services also need to provide a wide range of applications ranging from traditional sunrise/set data though to more specialized services such as celestial navigation. The work necessary to meet these goals involves efficient programming, intuitive user interfaces, compact and efficient ephemerides and a suitable range of tools to meet the user's needs.

1. HISTORY

An almanac is a list of forthcoming events, be they meteorological or astronomical, usually occurring in the coming year. A calendar is the most obvious form of almanac giving information on days of the week and the day of the week on which a particular date falls. The origin of the word almanac is unclear. It may come from the Greek word "almenichiaka" which means calendar or possibly from an Arab word "al-manach" meaning to count. The latter may also be translated as climate and the natural change in weather patterns over the year. The first documented use of the word is by Roger Bacon in 1267.

Almanacs have a long history, perhaps dating back as far as the second millennium BCE. These almanacs originated in western Asia and include hemerologies and parapegma. Hemerologies, from the Greek word hemera meaning "day", can be composed of lists showing favourable and unfavourable days for various activities. An example of such a work is the Babylonian Almanac dating back to 1100-800 BCE.

Parapegma, using an inscribed stone and movable pegs inserted into the holes within the stone, were used to indicate days of the month in ancient Greece. Ptolemy, in the second century, wrote a treatise on the motions of the fixed stars which was underpinned by a parapegma listing the dates of seasonal weather changes, the first and last appearances of stars and constellations at both sunrise and sunset as well as solstices organized on a yearly basis.

The almanac can also be linked to Babylonian astronomy where tables of planetary periods were used to make predictions of lunar and planetary phenomena. In the medieval Islamic world, similar results were obtained with the Zij, the Persian word for cord, tabulating parameters used for calculating the position of the Sun, Moon and planets. Another example of an almanac of that period is the Calendarium Cracoviense, Poland's oldest known print, which was first produced in 1474 by Kasper Staube. It was an astronomical wall calendar which listed church holidays and astronomical data as well as planetary oppositions and conjunctions and included the optimum days for bloodletting!

The "modern" almanac, which started to appear in the second half of the 16^{th} century, differs from all of the ones described here by the fact that the positions of celestial bodies are given directly with no further computation. These almanacs were produced in English by such individuals as Anthony Askham, Thomas Buckminster, John Dade and Gabriel Frende. These publications were very popular, selling in numbers second only to the Bible. Examples of what we now recognize as traditional almanacs started with *La Connaissance des Temps ou calendrier et éphémérides du lever & coucher du Soleil, de la lune & des autres planètes* by Picard in 1679, the *Astronomische Ephemeriden* by Hell in 1757, *The Nautical Almanac and Astronomical Ephemeris* by Maskelyne in 1767 and the *Berliner Astronomisches Jahrbuch*

by Bode in 1776. Most of these publications are still available today although in certain cases their titles have changed and their contents are very different.

It is interesting to note that even GPS uses an almanac to transmit data to the constellation of satellites. In the same way that the Babylonian Almanac provided data to find celestial bodies, the almanac for the GPS satellites contains information on the orbit of each satellite, an ionospheric model for predicting orbit decay and the necessary information to relate GPS time to UTC.

2. EXAMPLES OF HMNAO SERVICES

For the purposes of this talk, I will use the products and services of HM Nautical Almanac Office (HMNAO) as an example. The office is composed of six staff based at the UK Hydrographic Office (UKHO) in Taunton, England generating publications and services for a wide range of customers, both commercial and scientific and including the general public.The publication side of HMNAO's work involves several annual almanacs including *The Nautical Almanac*, *The Astronomical Almanac*, *Astronomical Phenomena*, *The Star Almanac for Land Surveyors* and *The UK Air Almanac*. The first three are joint publications with the Nautical Almanac Office of the US Naval Observatory (USNO). The UK Air Almanac is available as an online publication only. Other publications available on a five year time scale are *Navpac and Compact Data*, *Rapid Sight Reduction Tables for Navigation* and *Planetary and Lunar Coordinates* available on a twenty year cycle. Volume 1 of *Rapid Sight Reduction Tables for Navigation* is also jointly produced with the USNO. The web services operating under the URL http://astro.ukho.gov.uk can be broken down into several different sub-sites as described below.

The first are dynamical services, providing data "on the fly" i.e. as a direct response to user input. Websurf is HMNAO's source of data which provides information on rise/set data for the Sun, Moon and planets, twilight timings, transit times, altitudes and azimuths at a specific time, azimuths of objects at specific altitudes, altitudes of objects at specific azimuths, solstices and equinoxes, moon phases, crescent moon visibility and prayer times for the Islamic community. We also provide topocentric almanac data for the Sun, Moon and planets, generating right ascensions, declinations, azimuths, altitudes, distances, magnitudes, semi-diameters and visibilities. Locations can be specified in a variety of formats including databases of locations and postcodes, manual entry of latitude and longitude and location entry and refinement using *Googlemaps*. Output is generally provided in ascii and/or pdf format but other formats are under consideration.

Crescent moon visibility information is available through a public participation project initially run in collaboration with the Institute of Physics called Crescent MoonWatch. This web site provides information of the global visibility of the crescent moon over the first three days of each lunation. It then allows observers to record their sightings of the crescent moon allowing HMNAO to use these data to improve their predictions of the new crescent moon. This site is of use to the Islamic community whose calendar is still dependent on the sighting of the new crescent moon. The information supplied by HMNAO is unbiased and is independent of any religious grouping. Warnings of the impending new moon can be sent out to users who sign up for this information.

Eclipses Online is HMNAO's eclipse resource and is designed for those wishing to visualise the progress of an eclipse for a specific location. In conjunction with the US Naval Observatory, HMNAO have provided a canon of eclipses based on software used in the production of *The Astronomical Almanac*. It can be seen as a replacement for the *USNO Eclipse Circulars* published by the USNO. This canon provides global and local circumstances, animations and eclipse panoramas for partial, annular, total and hybrid solar eclipses in the period 1501 CE to 2100 CE. Pre-generated animations for a gazetteer of around 1500 locations are provided for those locations in the eclipse footprint. This site comprises around 300,000 animated gif files in addition to many thousands of static graphics files. Similarly, global circumstances of penumbral, partial and total lunar eclipses are available for the same period.

HMNAO can also provide information on ground illumination. This is usually generated for a 24-hour period and displayed for a variety of cloud obscurations, indicating when photopic, mesopic and scotopic vision is likely. This information can be used in connection with Police investigations and legal cases as well as maritime applications particularly in twilight and moonlight. Although this work is not currently available as a web application, it could be easily be made available. An animated ground illumination diagram is presented in this talk for the north-west Indian Ocean region. The ground illumination is represented by colour contours and the altitudes of the Sun and Moon are represented by individual line contours.

3. CURRENT PRACTICE

Paper almanacs are usually annual publications which tend to be somewhat expensive to produce when compared with their digital counterparts. Their availability should be widespread if not global but in certain cases this may be limited by the use of distributor chains. They are usually geocentric, giving data in specific reference planes, systems, timescales and coordinate systems. However, topocentric data can easily be produced for defined locations on the Earth's surface. They can require a certain amount of expertise in order to make full use of them. Their main advantage is that they are a book and everyone knows how to use a book. They do not require specific electronic devices to read them. They are archival by nature, their storage does not require technology that may become obsolete in the passage of time and are well suited for long term storage e.g. libraries. Sadly library capacity is fast becoming a dwindling resource. Almanacs do not lend themselves well to electronic publication formats as they contain large amounts of tabular data formatted in very specific ways.

Web services need internet access. They provide flexibility in the sense that topocentric data can easily be generated as opposed to traditional paper almanacs. These services are dynamic by their very nature. They are useless without appropriate connection to the internet i.e. by wireless, broadband or mobile telephony. Web services tend to be generated around specific services and therefore tend to be somewhat inflexible. Web services can provide large amounts of data or give access to large amounts of data i.e. large ephemerides and extensive databases. Some services are ephemeral in their own right as they can be taken down or moved with little or no notice leaving potential users with little more than a dead link.

To use HMNAO as an example once again, there are five annual paper publications and three paper publications produced over a longer production cycle. *The Nautical Almanac* is also available as an e-publication, principally to the maritime community, being part of a product range using a customised pdf viewer reading encrypted files and licensing system. *Navpac and Compact Data* includes a software package for Windows PC's called *Navpac* which provides a means of reducing astronomical sights made with a sextant to generate a position at sea. This provides organisations such as the Royal Navy with a backup solution should GNSS signals be jammed or otherwise interfered with. Another hybrid product is *AsA Online*, the web companion to *The Astronomical Almanac*. This web site provides functionally not easily provided in book form e.g. mapping of phenomena and a means of reporting information within the publication year after the book has gone to press.

4. NEXT GENERATION DATA SERVICES

It is difficult to see how paper publications can change significantly with the exception of layout and content. Publications that are used in the teaching of such topics as celestial navigation may benefit from additional material but it is wise to retain the layout described in the teaching material. Customers may not be best pleased with unexpected changes to books as it may incur significant costs in training processes and modifications to material.

Web services are potentially in a continuous state of change reflecting new technologies, techniques and hardware capabilities. One area that is yet to be fully explored by most almanac offices is that of SOAP / REST servers. Here a request is sent to the web server for a particular type of data. The information is sent back to the requesting server along with a description of the formatting of that data. It is then up to the requesting server to not only interpret that data but also to layout the data in a form specific to that users requirement, This has the advantage to the user of customising the appearance of the data rather than going to a web site and accepting the formatting of that web site. Other areas where new technologies have made their mark is the selection of locations as input to a topocentric calculation. The most obvious is the use of *Googlemaps* in conjunction with location sensitive software.

Mobile applications are a major growth area. These generally fall into two categories, one is an application running solely on the mobile device itself. The other is an application that uses the device's internet connections to access databases on a web server somewhere. Typically, a self-contained application needs a compact ephemeris perhaps with an accuracy of around one arcsecond. This requires the generation of ephemerides specifically designed for their small footprint, rapid evaluation and reasonable timespans. The output of the application makes full use of the display facilities of the mobile device as well as the location and orientation sensors on the device. It is also possible to use the camera facilities on such devices to provide augmented or mediated reality. A live direct view of a physical scene can have sound, video or graphical data added to the scene.

5. FUTURE SERVICES

Development of web services and mobile applications are likely to be the main area of progress and much will depend on changes in technologies and software. It is also likely that the means by which material is disseminated will change. For instance, one area might be more flexible licensing of data to make the creation of new products simpler. This will mean that derived products from generated data from the almanac offices may provide commercial opportunities for not only the almanac offices themselves but other entrepreneurial entities downstream from the offices. Repackaging of data with other forms of commercial data such as that already described for electronic version *The Nautical Almanac* may become much more widespread. Disseminating data via such outlets as *YouTube* will become more popular, especially where animations and data visualisations are concerned. Indeed the embedding of almanac data into social media such as *Facebook* and *Twitter* will become more pervasive.

On the subject of the visualisation of data, HMNAO are looking at the use of different map projections for the phenomenological presentation of data. This may involve the use of unusual and little used map projections such as the Peirce quincuncial projection (Taylor & Bell, 2013). This map projection requires considerable computation but provides a projection well suited to showing global or all-sky data particularly in the polar regions with relatively little distortion. As it renders a sphere as a square, it can be tiled in all directions. Another possibility in this area is the use of *Blender*, an open source 3-D graphics authoring tool. This is an extensive package capable of many tasks but for our purposes it can turn a static crescent moon visibility diagram into a one that the observer can fly around. This may have applications for the presentation of solar eclipse data, allowing the viewer to fly along the track of totality or indeed explore the obscuration of the Sun in the rest of the eclipse footprint.

The influence of external factors on almanacs will remain an issue. An upcoming example is the decision on whether or not to drop leap seconds which will be made by the International Telecommunications Union in late 2015. If the decision is to drop leap seconds, this will be a major impetus to switch from UT1-based almanacs to ones using UTC as the time system. Some offices already supply such data, but it will mean that all almanac offices will have to take a more proactive role in assisting their customers with the prediction of UT1-UTC differences and how that affects the data they publish. Paper almanacs will find these issues harder to deal with than their electronic counterparts.

The future of almanacs and indeed almanac offices probably lies in the provision of electronic data via the web and, more likely, through mobile applications. The future of paper publications is perhaps more limited but will remain a necessity for emergency applications and archival purposes. This will mean that almanac offices and the skills of their staff will migrate towards a more software focused approach. What will not change is the requirement for the fundamental skill set of their staff to be retained and enhanced.

6. REFERENCES

Taylor, D.B., Bell, S.A., 2013, "Astronomical applications of the quincuncial map projection", Astronomy & Geophysics, 54, pp. 13–15.

REWORK OF THE ERA SOFTWARE SYSTEM: ERA-8

D.A. PAVLOV, V.I. SKRIPNICHENKO
Institute of Applied Astronomy RAS
nab. Kutuzova 10, St. Petersburg 191187, Russia
e-mail: dpavlov@ipa.nw.ru

ABSTRACT. The software system that has been powering many products of the IAA during decades has undergone a major rework. ERA has capabilities for: processing tables of observations of different kinds, fitting parameters to observations, integrating equations of motion of the Solar system bodies. ERA comprises a domain-specific language called SLON, tailored for astronomical tasks. SLON provides a convenient syntax for reductions of observations, choosing of IAU standards to use, applying rules for filtering observations or selecting parameters for fitting. Also, ERA includes a table editor and a graph plotter. ERA-8 has a number of improvements over previous versions such as: integration of the Solar system and TT − TDB with arbitrary number of asteroids; option to use different ephemeris (including DE and INPOP); integrator with 80-bit floating point. The code of ERA-8 has been completely rewritten from Pascal to C (for numerical computations) and Racket (for running SLON programs and managing data). ERA-8 is portable across major operating systems. The format of tables in ERA-8 is based on SQLite. The SPICE format has been chosen as the main format for ephemeris in ERA-8.

1. INTRODUCTION

This paper describes a rework of a software system ERA that has been in usage and constant development for at least 25 years (Krasinsky et al., 1989; Krasinsky, Vasilyev, 1997; Krasinsky, Vasilyev, 2006). ERA stands for "Ephemeris Research in Astronomy". Its main applications are: production of the fundamental ephemeris of the Solar System bodies EPM (Pitjeva, Pitjev, 2014); numerical motion theories of natural satellites (Poroshina et al., 2013); astronomical yearbooks (Glebova et al., 2013); various fundamental research related to the dynamics of the Solar System (Pitjeva, Pitjev, 2013).

The core of the ERA system is the implementation of a domain-specific language called SLON. Most tasks that are being done within the system are put in the form of a program code in the SLON language. Most astronomical data (observations, parameters of models, etc) is being kept in the form of tables.

The main objective of the rework was keeping the existing abilities (most notably, ability to run a lot of existing SLON programs and read existing tables) while improving the portability, manageability, stability, scalability, and extensibility of the system. Also, some new functionality was added during the process.

2. BRIEF DESCRIPTION OF THE SYSTEM

The system can be presented as consisting of two parts: the scientific part and the technical part.

The scientific part is the following set of astronomical algorithms, exposed to the user as native constructs of the SLON language:

– Reductions of astronomical observations (optical, radar ranging, laser ranging). That includes implementation of IERS Conventions (2010) for: precession and nutation models, IERS EOP corrections, solid tide models, tectonic plate models, tropospheric delay models, relativistic corrections, and other models;

– Analytical theories for satellites of outer planets and rotation of Mars; coefficients of gravitational potential of Earth, Moon and planets, other known models of Solar system bodies;

– Gauss-Everhart numerical integrator. Reworked implementation is based on (Avdyushev, 2010);

– Equations of forces for integrating the motion of: asteroids, satellite systems, whole Solar system including lunar libration (Vasilyev, Yagudina, 2014);

– Calculation of partial derivatives of astronomical observables with respect to different parameters, such as: orbital elements of Earth or observed body, station coordinates, initial position and libration

angles (for Moon), rotation parameters (for Mars), solar corona parameters, masses of perturbing bodies, and many others;

– Weighted least squares method for determining the corrections to the parameters.

The technical part consists of the following components, merged into an integrated environment:

– SLON language parser and interpreter (compiler in the reworked implementation);
– Text editor for the SLON programs;
– Graph plotter;
– Access to numerical theories of celestial bodies presented in the form of Chebyshev expansions;
– Math library;
– Viewer and editor of tables with special support for astronomical data.

3. REWORK OF THE SYSTEM

Change of programming platform. Previous versions of the system were implemented almost entirely in Pascal, with limited usage of some in-house languages for system configuration. With long-term plans of making the system workable on different hardware and software environments, a different programming language and platform has to be chosen. The choice was: C for intense numerical work; Racket (`http://racket-lang.org`) for parsing and compiling SLON programs, dealing with input and output data, and building a graphical user interface.

Racket is a programming language and an open-source platform with reach feature set:

– automatic memory management with a garbage collector;
– high-performance virtual machine (VM) with Just-in-time (JIT) compiler to native code;
– portability over all variants of Windows, Linux, and Mac, including cross-platform graphic widgets;
– support for imperative, functional, and object-oriented programming styles;
– sophisticated packaging and documenting system;
– foreign function interface to C modules;
– support of Unicode, threading, extended precision (80-bit) arithmetics, Web development;
– (important for scientific programming) interactive mode, graph plotter;
– decent documentation and strong community.

In addition, Racket has arguably the most advanced macro system and other tools for creation of domain-specific languages (DSLs). While SLON is a quite complicated DSL, it was not a problem to write a parser that translate SLON constructs into Racket's syntax objects, thus making SLON language native to Racket VM, and taking full advantage of the VM's facilities, including the JIT compiler.

Transition to Racket resulted in a significant shrink of ERA's code base. Memory manager written in Pascal in 1980-s, with Soviet BESM-6 hardware in mind, is gone and superseded by Racket's generational garbage collector "3m". Custom parser generator, created for ERA around the same time, is replaced with Racket's implementation of `lex` and `yacc`. ERA's graph plotting module has been substituted by Racket's `plot` library. Finally, there was no need to reimplement an IDE for SLON in ERA-8: any domain-specific language implemented in Racket becomes native to Racket's IDE, DrRacket. Users are able to edit, compile, run, and even debug SLON programs in DrRacket directly.

Finally, automatic memory management allowed to revoke some limits for input data, inherent to previous versions of the ERA system: number of simultaneously integrated bodies, number of attributes size of SLON programs, number of arguments to SLON actors, etc.

Format of table data files. SQLite (`http://sqlite.org`) format has been chosen for storing the tabular data in ERA-8, instead of some custom binary format with custom program interface for access. SQLite library took the responsibility for disk I/O, simultaneous access, and caching of input and output data of the system. Old format is supported in ERA-8 in read-only mode.

Format of ephemeris data files. In previous versions of ERA, a special binary format was developed to store and distribute the numerical theories. ERA-8, though, has switched to another format (Hilton et al., 2014) known as the format used by the SPICE library of NASA NAIF. That format (actually, two formats used to store differend kinds of data: SPK and PCK) has been recently accepted as the main format for fundamental ephemeris among the producers (IAA RAS, NAS JPL, IMCCE). Some extensions were made to guarantee lossless conversion of IAA ephemeris to the new format. Old format is still supported in ERA-8 for backward compatibility.

4. NEW RESULTS OBTAINED WITH ERA-8

TT − TDB integration. The revocation of limit on the number of simultaneously integrated objects allowed to integrate TT − TDB difference in ERA-8 with arbitrary number of bodies. Currently, 322 most massive asteroids are accounted for in the integration of TT − TDB in ERA-8 (together with the Sun, the Moon and all the planets). The equations of integration were taken from (Klioner et al., 2010). The resulting TT − TDB differences are available in the form of an SPK file as part of EPM2011 ephemeris and are close to DE430. Figure 1 shows the difference between EPM2011 TT − TDB and DE430 TT − TDB in nanoseconds over a timespan of 400 years.

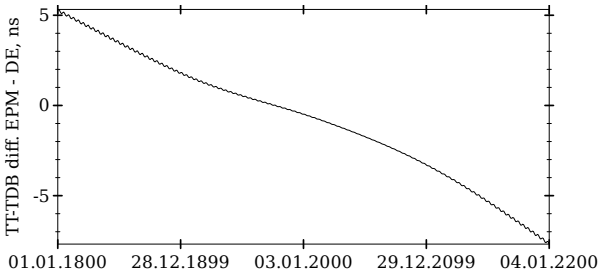

Figure 1: Difference of TT − TDB between EPM2011 and DE430, years 1800–2200.

Cassini range measurements. New Cassini ranging data available from NASA JPL (Hees et al., 2014) made it possible to improve the orbital parameters of Saturn significantly. Figure 2 shows the initial two-way O-C (obtained with EPM2011) for Cassini ranging measurements and residual errors. The RMS for the two-way residuals is about 40 m.

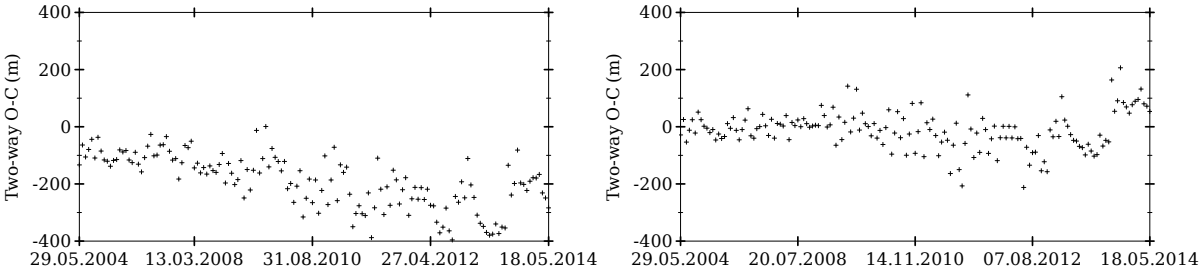

Figure 2: O-C for Cassini measurements before the corrections to Saturn orbit (left) and after (right).

Improvement of the orbit of Pluto. Processing of some observations of Pluto not used previously in the EPM ephemeris was done with ERA-8. More than 8000 observations have been processed, and that resulted into the standard deviations of orbital parameters of Pluto reduced roughly in half. See (Girdiuk, 2015) for the description of this work.

Web site for ephemeris access. Racket platform and its rich libraries for Web development have allowed to expose a piece of ERA-8 facilities as a website (`http://ephemeris.ipa.nw.ru`). The website allows users to calculate ephemeris tables for Sun, Moon, planets, and natural satellites. A number of options is available for: choosing the coordinate system (equatorial, ecliptical, horizontal); choosing the equator (mean J2000, mean of the date, true of the date); choosing the type of the coordinates (Cartesian or spherical); specifying the location of the observer; formatting the output data. The users are also free to choose the planetary theory (EPM, DE, INPOP in different versions) and the theory for natural satellites. All the ephemeris data used by the site is stored as SPICE files.

5. CONCLUSION AND PLANS FOR NEAR FUTURE

ERA-8 has moved to a more advanced software platform while keeping backward compatibility to the previous versions of ERA. Also, the system took a step to new environments, such as Linux desktops and

web servers. The program code has become more transparent, manageable, and flexible, and as a result, new features can be added more quickly.

ERA-8 will definitely benefit from embracing the SOFA library (`http://iausofa.org`) as the implementation of the IERS Conventions (2010). SOFA is to be included into ERA-8 in early 2015.

The next version of the EPM ephemeris—EPM2014—is being prepared with ERA-8, and so is the next issue of the Astronomical Yearbook (2016).

In 2015, ERA-8 will be freely available to users (as WinERA currently is) from the IAA's web site.

Acknowledgements. Authors are indebted to Elena Pitjeva, Eleonora Yagudina, Mikhail Sveshnikov, Sergei Kurdubov, and numerous other colleagues from the Institute of Applied Astronomy who provided a lot of help and support to make the new version of the software possible.

Authors would like to thank Matthew Flatt for help in dealing with obstacles during porting the system to the Racket platform, and Mikhail Filonenko for adding 80-bit floating point arithmetics into the Racket VM.

William Folkner has kindly provided a lot of information crucial to bringing the quality of ERA-8 close to NASA JPL products, particularly with regard to the SPICE format support and processing of Cassini range measurements.

6. REFERENCES

Avdyushev, V., 2010, "Gauss – Everhart Integrator", Computational technologies, 15, pp. 31–46. (in Russian)

Girdiuk, A., 2015, "The improvement of the Pluto orbit using additional new data", this volume, pp. 96–99.

Glebova, N., Lukashova, M., Sveshnikov, M., Skripnichenko, V., 2013, "2014 Astronomical Yearbook", Institute of Applied Astronomy RAS. (in Russian)

Hilton, J., Acton, C., Arlot, J.-E., Bell, S., Capitaine, N., Fienga, A., Folkner, W., Gastineau, M., Pavlov, D., Pitjeva, E., Skripnichenko, V., Wallace, P., 2014, "Report of the IAU Commission 4 Working Group on standardizing access to ephemerides and file format specification", In: Proc. Journées 2013 "Systèmes de Référence Spatio-Temporels", N. Capitaine (ed.), Observatoire de Paris, pp. 265–266.

Hees, A., Folkner, W., Jacobson, R., Park, R., 2014, "Constraints on modified Newtonian dynamics theories from radio tracking data of the Cassini spacecraft", Physical Review D, 89, 102002.

IERS Conventions, 2010, G. Petit, B. Luzum (eds.), IERS Technical Note 36., Frankfurt am Main: Verlag des Bundesamts für Kartographie und Geodäsie.

Klioner, S., Gerlach, E., Soffel, M., 2010, "Relativistic aspects of rotational motion of celestial bodies", Proc. IAU Symp 165, pp. 112–123.

Krasinsky, G., Novikov, F., Scripnichenko, V., 1989, "Problem Oriented Language for Ephemeris Astronomy and its Realisation in the System ERA", Celest. Mech. Dyn. Astr., 45, pp. 219–229.

Krasinsky, G., Vasilyev, M., 1997, "Era: Knowledge Base for Ephemeris and Dynamical Astronomy", Dynamics and Astrometry of Natural and Artificial Celestial Bodies, IAU Coll. 165, pp. 239–244.

Krasinsky, G., Vasilyev, M., 2006, "ERA-7. Knowledge Base and Programming System for Dynamical Astronomy: Manual", Institute of Applied Astronomy RAS.

Pitjeva, E., Pitjev, N., 2013, "Constraints on dark matter in the solar system", Astronomy Letters, 39, pp. 141–149.

Pitjeva, E., Pitjev, N., 2014, "Development of planetary ephemerides EPM and their applications", Celest. Mech. Dyn. Astr., 119, pp. 237–256.

Poroshina, A., Zamarashkina, M., Kosmdamianskiy, G., 2012, "Construction of the numerical motion theories for the main satellites of Mars, Jupiter, Saturn and Uranus in IAA RAS", Trudy IPA RAN, 26, pp. 75–87. (in Russian)

Vasilyev, M., Yagudina, E., 2014, "Russian lunar ephemeris EPM-ERA 2012", Solar System Research, 48, pp. 158–165.

THE SOFTWARE IDA FOR INVESTIGATION OF ASTEROID DYNAMICS AND ITS USE FOR STUDY OF SOME ASTEROID MOTION

T. GALUSHINA, L. BYKOVA, O. LETNER, A. BATURIN
Tomsk State University
36, Lenina St., Tomsk 634050, Russia
e-mail: volna@sibmail.com

This work is devoted to description of the application suite IDA that is designed for investigation of dynamics and probability orbital evolution of asteroids. IDA allows to predict asteroid motion, to reveal close encounters, possible collisions and orbital resonance with planets, to estimate impact probability, to demonstrate asteroid and planets motion on a computer screen and to solve some additional problems. The features of the suite are multifunctionality, high efficiency and a convenient interface. The application suite IDA consists of following subsystems: subsystem "Assol" which allows to study orbital evolution of the nominal orbit and to demonstrate the asteroid and planets motion on a computer screen; subsystem "Observations" which intended to asteroid orbit fitting to positional observations and construction of initial probability domain with non-linear methods; subsystem "Distribution" which developed for the visualization of distribution of observations along an asteroid orbit; subsystem "Clones ensemble" which allows to construct an initial probability domain with the linear method; subsystem "Evolution" which designed for the study of the orbital evolution of an ensemble of asteroid clones; subsystem "Megno" which intended to estimate of predictability time of asteroid motion by means of average MEGNO parameter. The results of the motion investigation of the asteroid 2012 MF7 are given to demonstrate use of the application suite. This object has nonzero collision probability with the Earth in 2046.

ASTROMETRY AND NUMERICAL METHODS FOR THE SOLAR HELIOMETER AT OBSERVATÓRIO NACIONAL IN BRASIL

A.H. ANDREI[1,2,3,4], S.C. BOSCARDIN[1], J.L. PENNA[1], C. SIGISMONDI[5], E. REIS NETO[6], V.A. D'ÁVILA[7]
[1] Observatório Nacional/MCTI
Rua Gal. José Cristino 77, Rio de Janeiro, RJ CEP 20921-400, Brasil
e-mail: oat1@ov.ufrj.br
[2] SYRTE/Observatoire de Paris
Avenue de l'Observatoire 61, Paris 75014, France
[3] Observatório do Valongo/UFRJ
Ladeira do Pedro Antônio 43, Rio de Janeiro, RJ CEP 20080-090, Brasil
[4] Osservatorio Astrofisico di Torino/INAF
Strada Osservatorio 20, Pino Torinese, TO 10025, Italia
[5] Sapienza Università di Roma
Piazzale Aldo Moro 5, Roma 00185, Italia
[6] Museu de Astronomia e Ciências Afins/MCTI
Rua Gal. José Cristino 77, Rio de Janeiro, RJ CEP 20921-400, Brasil
[7] Universidade Estadual do Rio de Janeiro
Rua São Francisco Xavier 524, Rio de Janeiro, RJ CEP 20550-900, Brasil

ABSTRACT. Started its regular, daily operational phase in 2011, the results so far obtained show that the Heliometer from Observatorio Nacional (O.N.) fulfilled its planed performance of single measurement to the level of few tens of mas, freely pivoting around the heliolatitudes without systematic deviations or error enhancement. Such fruition led to evaluate high order terms that are commonly neglected in other solar astrometric observations. Namely, these are: the constancy of the basic heliometric angle, the dependence to meteorological and pointing conditions, the second order terms for diurnal aberration and parallax, the accounting of the Earth's ellipticity of the orbit, and the second order atmospheric refraction. We present and discuss these astrometric additions that are seldom required on ground base astronomic programs.

1. THE HELIOMETER OF O.N. — MAIN CONCEPTS

The heliometric method is one of the most successful techniques to measure small variations of angles. Its principle has been used for the latest space borne astrometric missions, aiming to milliarcsecond precision. The angle to be measured is small (the variation of the solar diameter) confronted with the corresponding linear displacement at the focal plane, thus an error on the linear measurement is smaller by orders of magnitude over the angular variation that is being measured.

At Observatorio Nacional a primary parabolic mirror was bissected to form an angular heliometer. The displacement of the images is produced by rotating the two half-mirrors along a line perpendicular to the line of cut. The heliometric mirror is all made of CCZ-HS, a ceramic material with very low thermal expansion coefficient ($0.2 \times 10^{-7}/°\mathrm{C}$). The two half mirrors are immobilized, in relation to each other, by means of an external ring, all resting over an optical plate. Its cell guarantees the mechanical and geometrical stability for the entire set. This niche is also made in CCZ. The surface quality of the optical plate and the mirrors is better than $\lambda/12$ and $\lambda/20$, respectively. A mask at the top of the cell has been designed to keep the two half mirrors blocked in place and also to assure that the entrance pupil has a symmetric shape, regularizing the PSF. The tube of the telescope is made of carbon fiber. This material, as well as extremely rigid, has very low coefficient of thermal expansion. It is mounted inside a stainless steel truss support and can rotate around its axis. In order to eliminate the secondary mirror the CCD chip was removed apart from the camera electronics and installed directly in the focal plane. Each half-mirror is tilted of an angle slightly greater than 0.135° in order to displace the images relatively to each other by one solar diameter approximately. In this way we will have the opposite limbs

of the Sun almost in tangency in the focal plane at the perihelion (D'Ávila et al., 2010).

The plate scale can be instantaneously known by timing the solar movement over the detector, removing the out-of-focus dependence for the linear distance between two points. No dependence to meteorogical conditions was found examining the results during the first full year of observations (2011), against troposphere and upper atmosphere temperature, pressure, and wind (Andrei et al., 2013a).

The general view of the heliometer and the hemi-mirrors are shown in Fig. 1.

Figure 1: The Heliometer developed at Observatório Nacional/MCTI. The hemi-mirrors and containing cell are shown in the side detail.

2. ASTROMETRIC CORRECTIONS

The corrections for Refraction and Annual Parallax follow what is usually done for precision astrometry. And in particular for the treatment of the Solar Astrolabe observations. Their effects are large (∼arcsec) but taken care of. However there are smaller terms which are usually discarded. But that had to be considered for the $\sim 0.01''$ Heliometer precision.

Aberration. Annual and diurnal effects are opposite for Solar observations. The net effect owes more to the translation velocity. It is given by the difference of two opposite points on the equatorial limb, that is $30'$. The maximum correction is $0.04''$.

Diurnal Parallax. Maximum effect is when for the Sun in perihelion and observed at lowest (in our case z=50°). The difference between the geometric and observing distance amounts to a correction of $0.02''$.

Diurnal Parallax Hourly Variation. The variation of the Solar diameter between aphelion and perihelion is of $16.01''$, with a quasi-sinusoidal modulation. It hence translates to a maximum hourly correction of $0.05''$/hour.

Refraction second order terms. Taking into account the third order terms in the tan expansion of the refraction series, and deriving the maximum difference, which refers to a vertical diameter, the correction attains to $0.02''$.

All these corrections are fully implemented in the program of treatment of the Heliometer mean results (Andrei et al., 2013b).

3. REFERENCES

Andrei, A.H., D'Ávila, V.A., Reis Neto, E.R., et al., 2013a, "Development and first year results from the Heliometer of Observatório Nacional", In: Proc. IAU Symp. 294, 481.

Andrei, A.H., Sigismondi, C., Reis Neto, E.R., et al., 2013b, "The Heliometer of Rio de Janeiro in Operation — 2010 to 2013", arXiv:1307.0548.

D'Ávila, V., Reis Neto, E., Penna, J., et al., 2010, "The development of the Heliometer of the Observatório Nacional", In: Proc. IAU Symp. 264, 487.

SINCOM — THE NEW PROGRAM PACKAGE FOR COMBINED PROCESSING OF SPACE GEODETIC OBSERVATIONS

O.A. BRATTSEVA, I.S. GAYAZOV, S.L. KURDUBOV, V.V. SUVORKIN
Institute of Applied Astronomy of Russian Academy of Sciences
191187, Kutuzova emb. 10, Saint Petersburg, Russian Federation
e-mail: olga-brat@yandex.ru

ABSTRACT. The software SINCom realizing the combination of standardized SINEX-files is introduced. The program package is meant to work in the following two modes: a combined solution within one observational technique on the appointed time interval and an inter-technique combination of daily SINEX-files. The realization of stations velocities estimation is recounted. The mathematical model, algorithms and the special task-forming language are presented. The main features of developed software and the arising problems are discussed. The problem-oriented aspects and the requirements for the content of incoming SINEX-files are viewed. The extensive plans of the SINCom use to obtaining TRF combined solution are considered. The first experimental results of single-technique combination for VLBI, GPS and SLR observations are presented.

1. INTRODUCTION

The SINCom software package is developed for combined processing of different space geodesy observations. The main purpose of the software package is estimating EOPs and positions of stations carrying out observations by modern space geodesy techniques. As each technique has some advantages and weaknesses, more reliable estimation can be attained when combining all observational data. The international standardized SINEX format[1] is chosen as the basic form for solution representation.

2. SOFTWARE DESCRIPTION

The SINEX combine processing allows obtaining two types of solutions (Fig. 1):

— combined solution including observations of different techniques related to the same epoch ("vertical" scheme). The final solution provides more precise EOPs. Further iterative improvement of satellite orbit parameters is also possible

— single-technique combination ("horizontal" scheme) of daily solutions. The final solution can be used to obtain weekly solutions based on global networks observations.

The program SINCom analyzes input files and sorts the parameters in accordance with identification of type of parameter. The quadruple of fields in the SOLUTION blocks: Site Code, Point Code, Parameter Type and Solution ID (for local parameters) forms unique name of a variable. The MATRIX Row/Column Number correspond to the Estimated Parameters Index in the SOLUTION block. To guarantee solvability of the combined system we can apply free-network constraints (no-net-rotation and no-net-translation) and also eliminate or fix some parameters.

SINCom source code was written using Fortran 90 programming language. The LINPACK[2] mathematical library was widely used when developing the program. The program runs in batch mode under MS Windows XP or higher. User interface is implemented by means of special task-forming language.

When the program runs the following steps are executed:

— read the task using special language and input files;

— analyse task and SINEX files containing initial solutions;

— categorize common and local unknowns using SINEX parameter definition;

— adapt solution epochs;

— transform a priori values;

— combine normal systems using stacking technique (Thaller, 2008);

[1] http://www.iers.org/IERS/EN/Organization/AnalysisCoordinator/SinexFormat/sinex.html
[2] http://www.netlib.org/linpack/

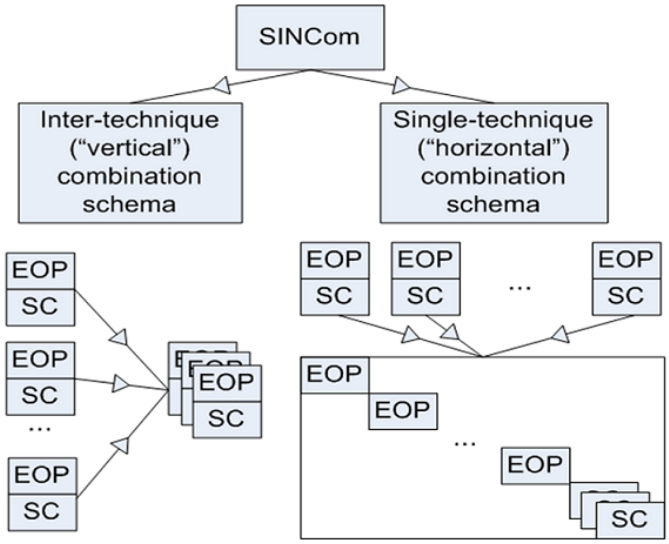

Figure 1: SINCom flowchart.

— apply free-network constraints, fix parameters (Thaller, 2008);
— solve the combined normal system;
— create resulting SINEX file.

For sufficient solutions amount estimation of station velocities is available. Free network constraint should be also applied toward the stations velocities.

3. COMBINATION RESULTS

The horizontal combination scheme was applied to the SINEX files got from SLR observations during 2012–2013 years. Coordinates of SLR stations of the QUASAR network (SVEL, ZELL, BADL) and their velocities were estimated. The results are presented in the article (Gayazov et al., 2013).

4. REFERENCES

Gayazov, I., Rets, Ya., Brattseva, O., 2013, "Improvement of Geocentric Coordinates of SLR Stations at the "Quasar" Network Observatories", IAA Transactions, No. 27, pp. 408–413. (in Russian)

Thaller, D., 2008, "Inter-technique combination based on homogeneous normal equation systems including station coordinates, Earth orientation and troposphere parameters", Scientific Technical Report STR08/15, Deutsches GeoForschungsZentrum.

RUSSIAN ASTRONOMICAL EPHEMERIS EDITIONS AND SOFTWARE

N.I. GLEBOVA, M.V. LUKASHOVA, G.A. NETSVETAEVA, M.L. SVESHNIKOV, V.I. SKRIPNICHENKO
Institute of Applied Astronomy of RAS
Saint-Petersburg, Russia
e-mail: lmv@ipa.nw.ru

ABSTRACT. Institute of Applied Astronomy has published "The Astronomical Yearbook", "The Nautical Astronomical Yearbook", "The Nautical Astronomical Almanac" biennial. Ephemerides are calculated according to resolutions of GA IAU of 2000-2006. The EPM domestic theory of movement of the Solar system bodies is used in Russian astronomical ephemeris editions and software since 2009 according to the recommendations of the conference CTNS-2007. Along with printing the astronomical software are elaborated. "The Personal Astronomical Yearbook" (PersAY) allows the user to solve tasks of calculation of ephemerides for any moment in various time scales, and for any position of the observer on a terrestrial surface. System of the removed access the "Scturman" is developed also intended to solve some the navigating tasks.

1. EPHEMERIDES HARD COPY

Institute of Applied Astronomy of RAS has published "The Astronomical Yearbook" (AY) since 1921, "The Nautical Astronomical Yearbook" (NAY) since 1930, "The Nautical Astronomical Almanac" (NAA-2) biennial since 2001. The latest resolutions of IAU have essentially changed theoretical basis ephemeris calculations. They were deal with new IAU2006/2000 precession-nutation models of rotation of the Earth and new concept of a sidereal time. The system ICRS was entered, which is based on VLBI observations of extragalactic radio sources and extended on optical area by catalogues HIPPARCOS and FK6. Relativistic definitions of coordinate systems and time scales were redefined more exactly. During 2003–2007 according to these resolutions the reform of theoretical and computing base of AY was completed and beginning from the issue AY for 2008, all relevant resolutions of IAU have been implemented in all ephemerides. In 2007 EPM2004 lunar and planetary ephemerides is accepted as the national standard fundamental ephemerides by the resolution of All-Russian conference "Coordinate, time and navigational support" (CTNS-2007) and are used in our ephemerides. At present all ephemerides in AY are referred to the "classical conception of equinox" system. Besides the parameters for reduction to new system are also given. All calculations are work out on the basis of ERA multifunctional software system.

Despite of lower accuracy navigation ephemerides ($0.1'$) for unification of creation of editions NAY is prepared on the same theoretical and technological basis as AY. For ships at long-run sailing new navigating manual has worked out. The biennial NAA-2 includes the star charts, examples for the determination of the compass' correction and the position of a ship by the Sun and stars. Fixing position plotter for laying off line of position (L.O.P.) is also given. The NAA-2 contains the explanation both in Russian and English.

A part of published in AY data and the natural satellites ephemerides are located on a site http://www.ipa.nw.ru/PAGE/EDITION/RUS/rusnew.htm.

2. THE SHTURMAN

Besides system of the removed access the "Shturman" was developed. It intended to solve some the navigating tasks described in NAA-2. The system calculates positions of navigating stars and solves the task of the determination of the position of a ship, and the task of correction of a compass from observations of the Sun and stars. The solving of tasks is carried out in accordance with the accepted in these editions accuracy ($0.1'$). 21 examples are accessible to the decision in the Internet' system now.

The solution report of task is output, and therefore the system can be considered and as the manual. The system is accessible on a site http://shturman.ipa.nw.ru (in Russian). However the system possesses a number of lacks. It is the fixed accuracy of the decision, a small set of examples, dependence on the Internet, etc.

3. THE PERSAY

The electronic versions are developed for two editions. The important stage of reform of AY is creation of "The Personal Astronomical Yearbook" (PersAY). Program system PersAY covers the basic types ephemerides published in AY and also provides possibility to calculate topocentric ephemerides, which it is necessary for observers. The system enables to calculate the data for four types of tasks (different package sections): ephemerides, astronomical events, planetary configurations, daily ephemerides.

Calculations in system PersAY are carried out as well as in AY with accuracy $0.01''$ for fundamental ephemerides. Except EPM2004 in PersAY also it is possible to calculate by means of DE405/LE405 theory to make comparison with others ephemeris editions. In general it is possible the choice of equatorial, horizontal, ecliptic, apparent and mean coordinates and various types of equinox. As objects it can be chosen the Sun, the Moon, any major planet, star from any catalogue. The set of time scales covers all used in ephemeris. The important feature of system PersAY is presence of the detailed description of all used algorithms allows receiving objective information about accuracy calculated ephemerides. The system can be considered as electronic version AY. The demo version of system PersAY with interval of ephemerides 2010–2012 is available via FTP from the Internet ftp://quasar.ipa.nw.ru/pub/PERSAY/persay.zip. The time intervals of validity of the system makes 2010–2015, 2016–2020.

4. THE NAVIGATOR

At present, the off-line electronic version of nautical ephemeris software package for the decision of the basic tasks by definition of a place of a ship on observations of celestial bodies is worked out. The system should provide the decision of following basic astronavigation tasks:

1. planning and definition of conditions of observation (selection of objects, the moments of rising/setting and the culminations of stars and so on);
2. equalization and a reduction of the measured heights and azimuths of celestial bodies;
3. definition of a site of a ship with an estimation of accuracy of the decision on any method of improvement of computed places or direct;
4. definition of compass correction in the various ways;
5. the decision of a problem should be accompanied by the report on standard templates;
6. the system should include the graphic means preparation, carrying out and processing of observation;
7. the system should contain the help block (school) and the contextual help;
8. the results of calculations should be registered (archive).

Navigation astronomy still keeps the value though against satellite navigation and inertial navigating systems. And the compass correction as total influence of a terrestrial and ship magnetic field on a compass reading is defined while only by astronomical methods.

5. CONCLUSION

The reform of ephemeris editions of IAA of RAS has led to complete theoretical identity in Russian astronomical yearbooks and software package, thus providing the ephemeris support of astronomical studies and solution of astronavigation tasks at modern level. Existence of electronic versions of yearbooks does not mean the end of the editions at hard copies. The electronic version should facilitate access to ephemerides, including input data at the computing equipment. The astronavigation software package help to user will help the user to process easier observation of astronavigation bodies.

REPORT OF THE IAU COMMISSION 4 WORKING GROUP ON STANDARDIZING ACCESS TO EPHEMERIDES AND FILE FORMAT SPECIFICATION: UPDATE SEPTEMBER 2014

J.L. HILTON[1], C. ACTON[2], J.-E. ARLOT[2], S.A. BELL[2], N. CAPITAINE[2], A. FIENGA[2], W.M. FOLKNER[2], M. GASTINEAU[2], D. PAVLOV[2], E.V. PITJEVA[2], V.I. SKRIPNICHENKO[2], P. WALLACE[2]
[1] U.S. Naval Observatory
3450 Massachusetts Ave. NW, Washington, DC 20392, USA
e-mail: james.hilton@usno.navy.mil
[2] Affiliations, addresses, and e-mail address of co-authors are available upon request

ABSTRACT. The IAU Commission 4 Working Group on Standardizing Access to Ephemerides recommends the use of the Spacecraft and Planet Kernel (SPK) file format to provide a uniform format for the position ephemerides of planets and other natural solar system bodies. The Working Group also recommends the use of the binary Planetary Constants Kernel (PCK) format ephemeris file for the orientation of a body. It further recommends supporting data be stored in a text PCK. Since the previous report:

- Some minor changes have been made to the formats for:
  - the coordinate time ephemeris
  - data types 20: Chebyshev Polynomials (Velocity Only) and 120: Chebyshev Polynomials (TCB:Velocity Only)
- the working group's final report is currently undergoing review by the Navigation and Ancillary Information Facility (NAIF) of NASA's Jet Propulsion Laboratory (JPL) to assure it correctly describes these file formats.

1. RECOMMENDATIONS

To provide a uniform format for the position ephemerides of planets and other natural solar system bodies, the International Astronomical Union (IAU) Commission 4: Ephemerides Working Group on Standardizing Access to Ephemerides recommends:

1. The use of the Spacecraft and Planet Kernel (SPK) file format.
2. The use of the binary Planetary Constants Kernel (PCK) format ephemeris file for the orientation of a body.
3. Supporting data on the ephemerides, such as values of parameters, whether they are fixed or adjusted, and their uncertainties, are stored in a text PCK kernel.

2. INTRODUCTION

These file formats were developed for and are used by the SPICE system, developed by the Navigation and Ancillary Information Facility (NAIF) of NASA's Jet Propulsion Laboratory (JPL).

Most users will want to use either the SPICE toolkit or CALCEPH, developed by the Institut de mécanique céleste de calcul des éphémérides (IMCCE), to access ephemerides stored in these formats. The SPICE toolkit is available at

`http://naif.jpl.nasa.gov/naif/toolkit.html`,

and CALCEPH is available at

`http://www.imcce.fr/inpop/calceph/index.php`.

Some users, such as ephemeris developers, may want to access the ephemeris files directly or construct ephemeris files in these formats using their own software. For those readers that require a detailed specification of the file formats, it is available in the full version of this report online at the IAU Commission 4: Ephemerides (or its successor) web site.

3. TEXT PCK KERNELS

Most of the supporting data consist of a limited number of single values or small vectors and matrices that are easily stored as text. Text PCK kernels are ASCII files so they may be modified by text editors and can also be ported between computer systems, even when the systems have different file systems and file formats.

Parameter values are associated with name strings using a "keyword = value" format. These name strings, together with their associated values, are called "kernel variables". Kernel variables may consist of arrays of values such as

```
NAME = ( VALUE1, VALUE2, ... )
```

where `NAME` is a case sensitive string, no longer than 32 characters. The values on the right hand side may be integer or floating point numeric values or strings.

4. RECENT CHANGES MADE TO THE SPK AND BINARY PCK FORMATS

Coordinate time scales are now designated by three NAIF identification numbers.

- 1 000 000 001: TT – TDB data are stored in the X-coordinate,
- 1 000 000 002: TCG – TCB data are stored in the Y-coordinate,
- 1 000 000 003: TT – TDB data are stored in the X-coordinate and TCG – TCB data are stored in the Y-coordinate.

5. CURRENT STATUS

The IAU Commission 4 Working Group on Standardizing Access to Ephemerides and File Format Specification recommends the use of the SPICE Toolkit's SPK kernel format for the positional ephemerides of solar system bodies, the SPICE Toolkit's binary PCK for the orientation ephemeris of the Moon, and the text PCK format for the storage of other data useful for the application of these ephemerides.

To assure that the specification of the portions of these kernels of interest to users comply with the SPICE Toolkit, the detailed final report is currently being reviewed by NAIF. Once the detailed report is approved, it will be made available at the IAU Commission 4 or comparable web site and a summary report will be submitted for publication.

Acknowledgements. The working group acknowledges the participation and help of NAIF in adapting SPICE to meet the requirements of all the groups participating in this working group. Nat Bachman of NAIF is providing help in reviewing the full report to assure the specification of the file formats is correct.

SOFA & ASTROMETRY

C.Y. HOHENKERK, Chair IAU SOFA Board
HM Nautical Almanac Office
UK Hydrographic Office, Taunton, TA1 2DN, United Kingdom
e-mail: Catherine.Hohenkerk@ukho.gov.uk

ABSTRACT. The International Astronomical Union's (IAU) Standards of Fundamental Astronomy (SOFA) software library has in the last year introduced a tranche of 32 new routines dealing with the subject area "astrometry". This poster provides a guide to enable users to get to grips easily with the various routines for the transformations between ICRS, ICRS astrometric, GCRS, Celestial Intermediate and observed positions of stars, together with their underlying routines for proper motion, parallax, aberration, light deflection and refraction. A summary of the current status of SOFA is also included.

1. INTRODUCTION

The tenth release (2013 December 2) of the IAU SOFA software included 32 new routines addressing Astrometry. The topic concerns the chain of transformations that link star catalog positions in the International Celestial Reference System (ICRS) with the observed direction for terrestrial and space observers. The intermediate systems include the Barycentric Celestial Reference System (BCRS), the Geocentric Celestial Reference System (GCRS), the Celestial Intermediate Reference System (CIRS), the Terrestrial Intermediate Reference System (TIRS) and the International Terrestrial Reference System (ITRS). For the typical case of a terrestrial observer the supported star positions are catalog places, astrometric ICRS $[\alpha, \delta]$, intermediate $[\alpha, \delta]$, and both topocentric (unrefracted) and observed $[\alpha, \delta]$, $[h, \delta]$ and [azimuth, altitude].

SOFA provides a simple text-based manual, containing the comments from the start of the routines, and a detailed "cookbook", *SOFA Tools for Astrometry*, which explains the software in a tutorial style. Also, there is *SOFA Tools at a Glance*, a two-page summary.

For anyone wishing to transform star positions from one system to another there are several key things about these routines and some initial decisions that have to be made. This paper gives an overview.

Note that the names of Fortran subprograms have the form `iau_NAME` while for ANSI C the function names are `iauName`. Here, for clarity, individual routines are referred to simply as `NAME`.

2. SOFA'S ASTROMETRY ROUTINES

The astrometry routines are divided into two categories and three types. This gives users the combination of ease of use as well as the ability to make their specific choices. The two categories are:

- Routines that include '13' in the name (for example `ATCI13`) require the least number of arguments and are the most convenient, as they call other SOFA routines internally to use currently adopted models, *e.g.* the `PNM06A` routine for the IAU 2006/2000A precession-nutation matrix .
- The routines without any digits in the names, which through additional arguments allow the user to provide explicit values that are independent of SOFA, such as JPL Earth coordinates.

The three types of routine, starting with the most basic, are:

1. The core astrometry routines that transform between the ICRS and the GCRS. These are `PMPX` for space motion and parallax, `AB` for aberration and the light deflection routine `LD`. There are two further light deflection routines `LDSUN` and `LDN`. Both use `LD`, where `LDSUN` assumes just the Sun is the deflection body, and this is used in SOFA's '13' routines, and `LDN` allows for N bodies. There is also an approximate routine for refraction `REFCO` and a routine `PVTOB` which takes a terrestrial observer's WGS84 longitude, latitude and height and forms the observer's position in the CIRS.
2. The `AP` routines. These routines supply the star-independent data, for example the position and velocity of the Earth. The next two letters of the name indicates the start reference system and

where the observer is located (geocentric, terrestrial, or space); for example `APCG` indicates 'celestial' (ICRS) and a geocentric observer, while `APIO` indicates the CIRS and a terrestrial observer.

3. The `AT` routines. These are the top-level routines, where the following letters indicates which systems the transformation is between. The letters are **C** for celestial, **I** for intermediate and **O** for observed *e.g.* `ATOC13` is the transformation of an **o**bserved place to an ICRS astrometric place.

   - The `AT...Q...` (quick) routines are for efficient processing of many stars for the same circumstances and require the star-independent data being already generated via an `AP` routine.
   - The `AT` routines with `N` or `Z` at the end of the name allow for multiple light-deflecting bodies and zero parallax and proper motion, respectively.

3. ACCURACY AND USER CHOICES

Estimates of the achieved accuracy are given in the cookbook. Care is taken to ensure that transformations and their inverses match to high precision. Where this is not achievable simply through rigor (by the use of vector methods for example) iteration is used. Without refraction, the inversions are self-consistent to better than 1 μas all over the celestial sphere.

The '13' routines use the IAU 2006/IAU 2000A precession-nutation models and this limits the accuracy to about 1 mas, mainly because of the (unmodeled) free core nutation and, in time, precession error. If the `EPV00` routine is used for the Earth ephemeris, as it is in the '13' routines, then errors in the aberration predictions of up to 5 μas can occur.

Over much of the sky, SOFA's predictions of light deflection by the Sun are accurate to 1 μas. Close to the Sun the errors may approach the 0.5 mas level. The routine `ATCIQN` allows for cases of other solar system bodies such as at Jupiter's limb where the deflection can be over 16 mas.

Having an understanding of the categories and types of routine together with some key aspects helps the user decide which are the required routines to deliver the positions needed. In particular,

1. between which systems the transformation operates, *e.g.* **O**bserved (ITRS) to **C**elestial (ICRS);
2. the location of the observer, *e.g.* geocentric, terrestrial, or in space;
3. the accuracy goals;
4. whether using SOFA's supplied parameters via the '13' routines or user supplied parameters;
5. whether processing many star positions for the same circumstances and therefore able to use one of the `Q` routines.

4. SOFA USAGE

Each month, SOFA's website at `http://www.iausofa.org` typically receives over 1500 unique visitors with, at present, 720 registered users. The 9th release (9a: 2012 July - 2013 November) has been downloaded 5769 times, while 10b, released in February 2014, has been downloaded 1662 times. There are currently now 220 routines, 59 of which are canonical, delivering IAU Standards.

All SOFA cookbooks are downloadable from `http://www.iausofa.org/cookbooks.html`, including *SOFA Astrometry Tools* (Fortran `sofa_ast_f.pdf and ANSI C sofa_ast_c.pdf versions`) and *SOFA Tools at a Glance* (`sofa_ast_summary.pdf`).

Acknowledgements. The SOFA project is possible due to the collaborative effort and hard work of the members of the Board: John Bangert, United States Naval Observatory (retired), Steven Bell, HM Nautical Almanac Office, UKHO, UK, Nicole Capitaine, Observatoire de Paris, France, William Folkner, Jet Propulsion Laboratory, US, Catherine Hohenkerk, HM Nautical Almanac Office (Chair), UK, Jinling Li, Shanghai Astronomical Observatory, China, Brian Luzum, United States Naval Observatory (IERS), Zinovy Malkin, Pulkovo Observatory, St Petersburg, Russia, Jeffrey Percival, University of Wisconsin, US, Scott Ransom, National Radio Astronomy Observatory, US and Patrick Wallace, RAL Space (retired), UK. Thanks are due to the Board for their oversight and in particular to Patrick Wallace, who continues to produce the source code and Steven Bell who manages the website. Thanks are also due to the institutes of Board members and to the United Kingdom Hydrographic Office for hosting the website.

ALMANAC SERVICES FOR CELESTIAL NAVIGATION

S.G. NELMES, J.A.WHITTAKER
HM Nautical Almanac Office
UK Hydrographic Office, Taunton, TA1 2DN
e-mail: susan.nelmes@ukho.gov.uk, james.whittaker@ukho.gov.uk

ABSTRACT. Celestial navigation remains a vitally important back up to Global Navigation Satellite Systems (GNSS) and relies on the use of almanac services. HM Nautical Almanac Office (HMNAO) provides a number of these services. The printed book, *The Nautical Almanac*, produced yearly and now available as an electronic publication, is continuously being improved, making use of the latest ideas and ephemerides to provide the user with their required data.

HMNAO also produces *NavPac*, a software package that assists the user in calculating their position as well as providing additional navigational and astronomical tools. A new version of *NavPac* will be released in 2015 that will improve the user experience. The development of applications for mobile devices is also being considered.

HMNAO continues to combine the latest improvements and theories of astrometry with the creation of books and software that best meet the needs of celestial navigation users.

1. PUBLICATIONS AND SOFTWARE

HMNAO produces a variety of publications and software and a number of these provide almanac services for use in assisting celestial navigation:

- The traditional printed book, *The Nautical Almanac*, published yearly, provides the ultimate backup for determining position at sea in the case of GNSS failure. It contains tabulations of the Sun, Moon, navigational planets and stars as well as the other necessary tables, diagrams, forms and information for celestial navigation. These include interpolation and altitude correction tables, pole star tables, diagrams and notes for the identification of stars and planets and information on standard times around the world. A concise set of sight reduction tables and a sight reduction form are also included and allow *The Nautical Almanac* to be used as a stand alone book for celestial navigation calculations.

- The recently introduced electronic version of *The Nautical Almanac*, containing identical data, tables, diagrams, forms and information to the printed book, allows for increased ease of use, distribution and portability.

- The software package, *NavPac*, provides the user with a means for automatically carrying out all the calculations necessary for celestial navigation as well as providing a number of additional navigational and astronomical tools. The automation provided saves time and reduces human errors.

- *Compact Data*, a printed book, accompanies *NavPac* and provides navigators and astronomers with simple and efficient methods for calculating the positions of the Sun, Moon, navigational planets and stars over several years to a consistent precision with the aid of a pocket calculator, personal computer or laptop.

- Other celestial navigation products include *Rapid Sight Reduction Tables for Navigation*, providing the altitude and azimuth for a range of declinations as well as of the seven stars most suitable for finding your position with a sextant.

- Looking ahead, the development of applications for mobile devices to assist the user with celestial navigation is also being considered, providing yet another alternative.

2. COLLABORATION WITH USNO

The Nautical Almanac, and its electronic version, are produced in collaboration with the Astronomical Applications Department at the United States Naval Observatory. The combined expertise at the two offices provides further assurance of the accuracy of the data and information.

3. EPHEMERIDES AND IAU RESOLUTIONS

The current edition of *The Nautical Almanac* and its electronic version, as well as the upcoming new release of *NavPac and Compact Data*, are all based on the DE430/LE430 ephemerides provided by the Jet Propulsion Laboratory and all include the latest IAU resolutions, keeping the data in line with the latest improvements and theories of astrometry. In particular the 2012 IAU resolution regarding the redefinition of the astronomical unit is applied throughout these publications and the 2000 and 2006 IAU resolutions concerning nutation and precession are implemented through the use of the latest IAU SOFA software collection.

4. IMPROVED USER INTERFACE FOR NAVPAC

An updated version of the celestial navigation software package produced by HMNAO, *NavPac*, is due to be released in early 2015. This version will incorporate a new interface that will provide an improved user experience making the software easier and more intuitive to use while still retaining all the current features and tools.

5. ADDITIONAL TOOLS WITHIN NAVPAC

The NavPac software, as well as providing an automated version of the calculations that a navigator would carry out using data from *The Nautical Almanac*, provides additional tools. These include a FindIt application that allows for easy planning and identification of celestial objects using a graphical interface, calculation of rise, set and transit times and a tool for calculating great circle and rhumb line tracks.

6. CONTINUOUS IMPROVEMENT

HMNAO are always looking to improve the various products. The upcoming 2016 edition of *The Nautical Almanac* and its electronic version will include a new section on Polar Phenomena. This will allow the user to approximate the durations of sunlight, moonlight and twilight at very high latitudes throughout the year.

7. USER FEEDBACK

HMNAO welcomes feedback from the varied users of the almanac services, including navies and commercial shipping from around the world. Members of HMNAO have travelled aboard ships and attended celestial navigation training given to navies in order to gain an important insight into how the publications and software are used in practice and to listen to the opinions of mariners who use them. This feedback is helpful in the continuous improvement of the products.

EROS — AUTOMATED SOFTWARE SYSTEM FOR EPHEMERIS CALCULATION AND ESTIMATION OF PROBABILITY DOMAIN

P. SKRIPNICHENKO[1], T. GALUSHINA[2], M. LOGINOVA[2]
[1] Ural Federal University
Shevchenko Str., 14 "A" – 30/2, Yekaterinburg 620075, Russia
e-mail: savl-silverheart@rambler.ru
[2] Tomsk State University
36 Lenina Str., Tomsk 634050, Russia
e-mail: volna@sibmail.com

This work is devoted to the description of the software EROS (Ephemeris Research and Observation Services), which is being developed both by the astronomy department of Ural Federal University and Tomsk State University. This software provides the ephemeris support for the positional observations. The most interesting feature of the software is an automatization of all the processes preparation for observations – from the determination of the night duration to the ephemeris calculation and forming of a program observation schedule. The accuracy of ephemeris calculation mostly depends on initial data precision that defined from errors of observations which used to determination of orbital elements. In the case if object has a small number of observations which spread at short arc of orbit there is a real necessity to calculate not only at nominal orbit but probability domain both. In this paper under review ephemeris we will be understand a field on the celestial sphere which calculated based on the probability domain. Our software EROS has a relevant functional for estimation of review ephemeris. This work contains description of software system and results of the program using.

GNSS PROCESSING IN INSTITUTE OF APPLIED ASTRONOMY RAS

V.V. SUVORKIN, S.L. KURDUBOV, I.S. GAYAZOV
Institute of Applied Astronomy RAS
Kutuzov emb. 10, St. Petersburg 191187, Russia
e-mail: suvorkin@ipa.nw.ru

ABSTRACT. GPS processing at Institute of Applied Astronomy (IAA) of Russian Academy of Sciences runs from year 2000. For many years it has been based on the software package GRAPE which processed triple differenced GPS observations. At February 2014 GRAPE and service programs were replaced by a newly developed software package.

1. INTRODUCTION

In 2011 we started developing a new software for undifferenced GLONASS and GPS measurements processing (Gayazov et al., 2013). The main application of this software is daily EOP estimation. Updated at February 2014 IAA GNSS EOP Service provides daily estimates of Xp, Yp, Xp_rate, Yp_rate and LOD based on 24h data from about 50 sites within IGS network with 12h delay. It also estimates orbital parameters, troposphere delay, atmospheric gradients and clock biases of stations and satellites.

2. PROCESSING STRATEGY AND RESULTS

The processing strategy mainly corresponds to IERS and IGS recommendations. Working scheme is shown on Fig. 1.

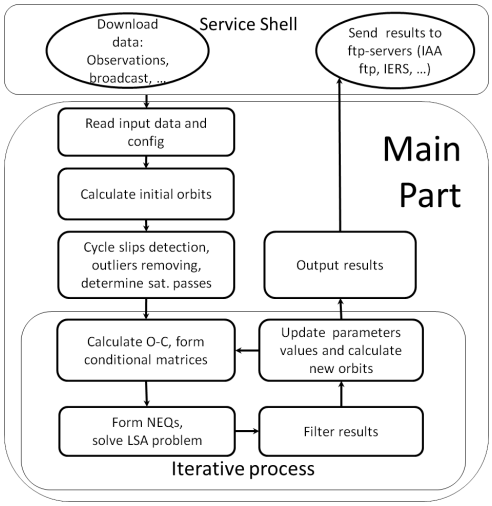

Figure 1: Scheme of GNSS-processing.

Key processing details:

- Data preprocessing: Melbourne-Wubbena combinations of code and phase measurements for cycle slip detection, outliers removing and forming satellite passes.
- Basic Observables: zero-differenced phase and code ionosphere-free combinations corrected by P1-C1 satellite code biases (cc2noncc); we use all measurements from daily RINEX-files with 30 seconds sampling rate.

- Sites coordinates: IGb08 reference frame coordinates and velocities; displacements: solid tides, ocean loading, pole tide loading (IERS 2010).
- Geometric model: receivers antennas eccentricities, absolute receiver and satellite (to CoM) antennas phase centres, elevation-dependent and azimuth-dependent corrections with accordance to absolute model IGS08.atx; wind-up effect.
- Signal propagation: troposphere total ZPD with GMF (IERS) mapping function, horizontal north and east gradients as linear trends with Herring mapping function.
- Relativistic: path range effect (Shapiro delay) and satellite clock corrections.
- Solar system bodies ephemeris: DE421.
- Terrestrial to Celestial frame transformations: IAU 2000A model, subdaily polar motion libration.
- Orbit modelling: GPS, GLONASS; EGM2008-based conventional (IERS 2010) static Geopotential model (truncated to degree and order 12) and tidal corrections; IAU 2000A precession-nutation model, Post-Newtonian relativistic corrections (Schwarzschild metric); empirical Solar radiation pressure model (Gayazov, 2002): a priori + 3 estimated parameters; numerical integration by DINCH integrator (single-step correction-prediction integration with Chebyshev approximation).
- Solution method: segmented Least Squares for two groups of parameters: daily polynomial and every-epoch (30s sampling); no a priory or continuity constraints; float ambiguities with no fixing.

In EOP Service regime we process about 50 stations. On the table 1 and 2 there are some results to show products quality.

Parameter	Accuracy
Satellite orbits (compared to IGS)	25–60 mm (RMS)
Troposphere ZPD (compared to IGS)	1.7–1.9 mm (RMS), 1.3–1.4 mm (St. dev.)
Clock biases (compared to IGS)	80–100 ps (RMS), 25–35 ps (St. dev.)

Table 1: IAA GNSS EOP Service products quality.

Time span, MJD	Xp, μas	Yp, μas	LOD, μs
56659.50 to 56688.50	39	48	10
56690.50 to 56716.50	59	59	16
56718.50 to 56747.50	60	62	14
56749.50 to 56777.50	50	50	15
56779.50 to 56808.50	57	50	9
56810.50 to 56838.50	42	48	17
56840.50 to 56869.50	38	55	11

Table 2: EOP RMS agreement with IERS Bulletins B 313–319.

The accuracy level of our products almost matches to those from other worldwide GNSS-analysis centers. We are going to improve it by introducing a new SRP model (12 parameters and without a priory model) which is under testing at the present time. Also we intend to implement models of yaw-attitudes, Earth albedo, atmospheric loading and 2nd order ionosphere effects. We are going to extend IAA GNSS Service products by weekly station coordinates solutions and SINEX-format output for further combinations within IAA Analysis Center.

3. REFERENCES

Gayazov, I.S., 2002, "Parametrization of the Solar Radiation Pressure model for GPS satellites", IAA Transactions, No. 8, "Celestial Mechanics", pp. 77–78.

Gayazov, I.S., Suvorkin, V.V., Kurdubov, S.L., Pshenkin, V.S., 2013, "A new version of software package GRAPE for GNSS phase measurements processing", IAA Transactions, No. 27, pp. 414–418.